# Radiosensitizing effect of AGuIX® in Head and Neck Squamous Cell Carcinoma (HNSCC) : from cellular uptake to subcellular damage

Stéphanie Simonet

N° d'ordre NNT : 2018LYSE1042

**THESE de DOCTORAT DE L'UNIVERSITE DE LYON**

Opérée au sein de

**L'Université Claude Bernard Lyon 1**

**Ecole Doctorale Interdisciplinaire Sciences-Santé** N° 205

**Spécialité de doctorat** : **Radiobiologie**

**Discipline** : Biologie Cellulaire et Oncologie

Soutenue publiquement le 26/03/2018, par :

**Stephanie SIMONET**

---

# Radiosensitizing effect of AGuIX® in Head and Neck Squamous Cell Carcinoma (HNSCC): from cellular uptake to subcellular damage

---

Devant le jury composé de :

| | |
|---|---|
| **Professeur Laurent CHARLET** – Université Grenoble-Alpes | Rapporteur |
| **Professeur Stéphane ROUX** – Université Franche-Comté | Rapporteur |
| **Docteur Cécile SICARD-ROSELLI** – Université Paris-Sud | Rapportrice |
| **Docteur Hélène ELLEAUME**– Université Grenoble-Alpes | Examinatrice |
| **Professeur Léa PAYEN** – Université Lyon 1 | Examinatrice |
| **Professeur Claire RODRIGUEZ-LAFRASSE** – Université Lyon 1 | Invitée |
| **Professeur Olivier TILLEMENT** - Université Lyon 1 | Invité |
| | |
| **Docteur Dominique ARDAIL** – Université Lyon 1 | Directeur de thèse |
| **Docteur Walid RACHIDI** – Université Grenoble-Alpes | Co-directeur de thèse |

## Abstract

Head and Neck Squamous Cell Carcinoma is ranked among the top ten deadliest cancers due to its high radioresistance and recurrence. One radiosensitizing strategy is the use of high-Z metal nanoparticles. In this study, ultrasmall gadolinium-based nanoparticles, AGuIX®, were used for their potential as a radiosensitizing agent. The objectives of this work were to determine the radiosensitizing conditions of AGuIX® in an HNSCC cell model, their localization after uptake, and the biological consequences generated at the subcellular level after the combined treatment. A preliminary proteomic approach was initiated in order to identify potential molecular targets involved in radiosensitization.

The treatment of SQ20B cells with 0.8mM Gd for 24h resulted in a dose enhancement factor (DEF) of 1.3. AGuIX® were predominantly localized in lysosomes. The overproduction of radical oxygen species following AGuIX® + radiation was intimately involved in the radiosensitization, although largely subdued by the high level of endogenous antioxidant defenses. Autophagy was specifically triggered after the combined treatment, while other irradiation-induced cell deaths remained unchanged. The number of complex, residual double strand breaks (DSBs) was specifically increased with AGuIX® combined to radiation. Lastly, our preliminary proteomic analysis allowed the isolation of potential molecular targets with great promise. Collectively, it seems that the radiosensitizing effect observed in this work may result from a combination of events.

Future work is required to understand the mechanisms linking lysosomes-entrapped AGuIX® with the upregulation of autophagic cell death after radiation.

**Keywords**: Head and Neck Squamous Cell Carcinoma (HNSCC); ionizing radiation; nanomedicine; radiosensitizing strategies; nanoparticles; AGuIX®; Radical Oxygen Species (ROS)

## Résumé

Les cancers des Voies Aérodigestives Supérieures sont classés parmi les dix cancers les plus agressifs du fait de leur radioresistance intrinsèque et leur forte probabilité de récurrence. L'objectif de ce travail a été d'étudier le potentiel radiosensibilisant de nanoparticules à base de gadolinium, AGuIX®, sur un modèle cellulaire de cancer des VADS. Après avoir déterminé et validé les conditions optimales de radiosensibilisation de notre modèle par les AGuIX®, leur localisation après internalisation ainsi que les conséquences biologiques générées à l'échelle subcellulaire ont été successivement étudiées. Enfin, une approche préliminaire protéomique a été initiée afin d'identifier des cibles moléculaires potentielles impliquées dans cette radiosensibilisation.

Le traitement des cellules SQ20B avec 0.8mM Gd pendant 24h se sont révélées être optimales avec un DEF (dose enhancement factor) de 1.3. Les AGuIX® sont localisées presque exclusivement dans les lysosomes après internalisation. La radiosensibilisation est liée à une surproduction de radicaux libres oxygénés, minimisée toutefois par des défenses antioxydantes endogènes élevées. Le traitement combiné (AGuIX®+ irradiation) déclenche spécifiquement la mort cellulaire autophagique et s'accompagne d'une augmentation significative du nombre de cassures double brins résiduelles complexes. L'étude protéomique préliminaire a permis d'identifier une cible moléculaire potentiellement impliquée dans cette radiosensibilisation (la ribonucléotide réductase), cible qui fera l'objet d'une suite à ce travail. De plus, la prochaine étape sera de comprendre les mécanismes qui relient les AGuIX® internalisées dans les lysosomes avec l'augmentation de la mort cellulaire autophagique après irradiation.

**Mots clés**: Cancers des Voies Aéro-Digestives Supérieurs (VADS); irradiation ionisante; nanomédicine; stratégie radiosensibilisante; nanoparticules; AGuIX®; Radicaux Libres Oxygénés (RLO)

# UNIVERSITE CLAUDE BERNARD - LYON 1

| | |
|---|---|
| **Président de l'Université** | **M. le Professeur Frédéric FLEURY** |
| Président du Conseil Académique | M. le Professeur Hamda BEN HADID |
| Vice-président du Conseil d'Administration | M. le Professeur Didier REVEL |
| Vice-président du Conseil Formation et Vie Universitaire | M. le Professeur Philippe CHEVALIER |
| Vice-président de la Commission Recherche | M. Fabrice VALLÉE |
| Directrice Générale des Services | Mme Dominique MARCHAND |

## *COMPOSANTES SANTE*

| | |
|---|---|
| Faculté de Médecine Lyon Est – Claude Bernard | Directeur : M. le Professeur G.RODE |
| Faculté de Médecine et de Maïeutique Lyon Sud – Charles Mérieux | Directeur : Mme la Professeure C. BURILLON |
| Faculté d'Odontologie | Directeur : M. le Professeur D. BOURGEOIS |
| Institut des Sciences Pharmaceutiques et Biologiques | Directeur : Mme la Professeure C. VINCIGUERRA |
| Institut des Sciences et Techniques de la Réadaptation | Directeur : M. X. PERROT |
| Département de formation et Centre de Recherche en Biologie Humaine | Directeur : Mme la Professeure A-M. SCHOTT |

## *COMPOSANTES ET DEPARTEMENTS DE SCIENCES ET TECHNOLOGIE*

| | |
|---|---|
| Faculté des Sciences et Technologies | Directeur : M. F. DE MARCHI |
| Département Biologie | Directeur : M. le Professeur F. THEVENARD |
| Département Chimie Biochimie | Directeur : Mme C. FELIX |
| Département GEP | Directeur : M. Hassan HAMMOURI |
| Département Informatique | Directeur : M. le Professeur S. AKKOUCHE |
| Département Mathématiques | Directeur : M. le Professeur G. TOMANOV |
| Département Mécanique | Directeur : M. le Professeur H. BEN HADID |
| Département Physique | Directeur : M. le Professeur J-C PLENET |
| UFR Sciences et Techniques des Activités Physiques et Sportives | Directeur : M. Y.VANPOULLE |
| Observatoire des Sciences de l'Univers de Lyon | Directeur : M. B. GUIDERDONI |
| Polytech Lyon | Directeur : M. le Professeur E.PERRIN |
| Ecole Supérieure de Chimie Physique Electronique | Directeur : M. G. PIGNAULT |
| Institut Universitaire de Technologie de Lyon 1 | Directeur : M. le Professeur C. VITON |
| Ecole Supérieure du Professorat et de l'Education | Directeur : M. le Professeur A. MOUGNIOTTE |
| Institut de Science Financière et d'Assurances | Directeur : M. N. LEBOISNE |

# Table of Contents

# List of Figures

**Bibliography Review**

**Materials & Methods**

**Results & Discussion**

*Chapter I: Characterization of the radiosensitizing effect of AGuIX®*

# List of Tables

**Bibliography Review**



**Materials & Methods**



**Results & Discussion**

*Chapter I: Characterization of the radiosensitizing effect of AGuIX®*

*Chapter II: Study of the Oxidative Stress Induced by the combined treatment of AGuIX® + I.R. and its functional consequences on mitochondria*



*Chapter IV: Study of the DNA-damage induced by AGuIX® combined with radiation*



*Chapter V: Preliminary results of the proteomic study of 0mM Gd 10Gy versus 0.8mM Gd 10Gy at T=24H after I.R.*

# List of Abbreviations

•NO: nitric oxide
5-FU: Fluorouracil
8-oxo-G: 8-oxo-guanine
ADP: Adenosine Diphosphate
AgNPs: silver nanoparticles
AGuIX®: Activation and Guidance of Irradiation by X-ray
AKT (PKB): Protein Kinase B
ANSM: Agence National de Sécurité du Médicament et des produits de santé
APAF1: Apoptotic Peptidase Activating Factor 1
ATM: Ataxia Telangectasia Mutated
ATP: Adenosine Triphosphate
ATR: Ataxia Telangectasia mutated and Rad3 related
AuNPs: Gold nanoparticles
Bax: Bcl2 Associated X
BCA: Bicinchonic Acid
Bcl-2: B-cell lymphoma 2
Bcl-Xl: B-cell lymphoma-extra large
BER: Base Excision Repair
BSO : L-buthionine sulfoximine
CD95: Cluster of Differentiation 95
Cdc2: Cell-division cycle protein 2
CDKs: Cyclin-Dependent Kinases
CHKs: Checkpoint Kinases
CL: Cardiolipin
cROS: cytosolic Reactive Oxygen Species
CSCs: Cancer Stem Cells
CT: Computed Tomography
CTLA-4: Cytotoxic T-lymphocyte-associated Protein 4
Cya5.5: cyanine 5.5
D: Dose
DAPI: 4',6'-diamidino-2-phenylindole
DAVID: Database for Annotation, Visualization, and Integrated Discovery
DD: Death Domain
DEF: Dose Enhancement Fraction
del mtDNA: deleted mitochondrial DNA
DISC: Death Inducing Signaling Complex
DLS: Dynamic Light Scattering
DMEM : Dulbecco's Modified Eagle Medium
DMF : Dimethylfumarate
DMSO: Dimethyl sulfoxide
DNA: Deoxyribnucleic acid
DNA-PK: DNA-dependent Protein Kinase
DOTA: 1,4,7,10-tetraazacyclododecane-1,4,7,10-tetraacetic acid
DOTAREM: gadoterate muglumine
DR5: Death Receptor 5
DSBs: Double-Strand Breaks
DTPA: Diethylenetriaminepentaacetic acid
dTTP: desoxythymide triphosphate
EBR: Enhanced Biological Response
EcOG: Eastern Cooperative Oncology Group
EDTA: Ethylenediaminetetraacetic acid
EDTA-$Na_2$: Disodium ethylenediaminetetraacetate dihydrate
EGFR: Epidermal Growth Factor Receptor
EPR: Enhanced Permeability Retention
ER: Endoplasmic Reticulum
ERK: Extracellular signal-Regulated Kinases
ETC: Electron Transport Chain
FADD: Fas-Associated Death Domain
FCS: Fetal Calf Serum
FDA: Federal Drug Administration
FFF: Flattening Filter Free
FITC: Fluorescein isothiocyanate
FOXO3a: Forkhead box protein O3

FPG: FormamidoPyrimidine [fapy]-DNA Glycosylase
GBM: Glioblastoma Multiforme
GBNs: Gadolinium-Based Nanoparticles
G-CSF: Granulocyte-Colony-Stimulating Factor
Gd: Gadolinium
$Gd_2O_3$: Gadolinium oxide
GPX: Glutathione Peroxidase
GRX: Glutaredoxin
GSH: Reduced glutathione
GSH: Glutathione
GSSG: Oxidized glutathione
Gy: Gray
$H_2O_2$: hydrogen peroxide
HBSS: Hank's Balanced Salt Solution
HCl: Hydrochloric acid
HIF-1α: Hypoxia-Inducible Factor 1α
HNSCC: Head and Neck Squamous Cell Carcinoma
HO•: Hydroxyl
$HO_2^{\bullet}$: Perhydroxyl
HPLC MS/MS: High-performance Liquid Chromatography-Mass spectrometry
HPV: Human Papillomavirus
HR: Homologous Recombination
I.R.: Ionizing Radiation
ICP-AES: Inductively Coupled Plasma-Atomic Emission Spectrometry
ICP-OES: Inductively Coupled Plasma-Optical Emission Spectrometry
IgG1: Immunoglobulin G1
IgG2a: Immunoglobulin G2a
IMRT: Intensity-Modulated Radiation Therapy
IPA: Ingenuity Pathway Analysis
IV: intravenous
JAK: Janus kinase
JC-1: 5',5', 6, 6'-tetrachloro-1, 1', 3, 3'-tetraethylbenzimidazolycarbocyanine iodide
JNK: c-Jun N-terminal Kinase
k**eV**/M**eV**: kilo electron-volt (energy unit)
L: Ligand
LAMP-2: Lysosomal-Associated Membrane Protein-2
LC3: microtubule-associated protein 1A/1B-Ligh chain 3
LET: Linear Energy Transfer
M: Metal
mAb: monoclonal antibody
MAPK: Mitogen-Activated Protein kinases
MDA: Malondialdehyde
MDM2:human Murine Double Minute 2
MDT: Maximum Dose Tolerated
$MgCl_2$: Magnesium chloride
MHC: Major Histocompatibility Complex
ML: complex Metal/Ligand
MMP: Matrix metalloprotease
MnSOD (SOD2): superoxide dismutase Mn-dependent
mPTP: mitochondrial Permeability Transition Pore
MRI: Magnetic Resonance Imaging
mROS: mitochondrial Reactive Oxygen Species
mtDNA : mitochondrial DNA
mTOR: Mammalian Target Of Rapamycin
MTT: 3-(4,5-dimethylthiazol-2-yl)-2,5-diphenyltetrazolium bromide
NAC: N-acetyl Cysteine
NaCl: Sodium chloride
NADPH: Nicotinamide adenine Dinucleotide Phosphate
NaI: Sodium Iodide
nanoLC MS/MS
NaOH: Sodium hydroxide
nDNA : nuclear DNA
NEM: N-ethylmaleimide
NER: Nucleotide Excision Repair
NFκB: Nuclear Factor-kappa B
NHEJ: Non-Homologous End-Joining

NHP: Non-Human Primates
NOS: Nitric Oxide Synthase
NOX: NADPH Oxydase
NOXA: Latin for damage
NPs: Nanoparticles
NSCLC: Non-Small-Cell Lung Cancer
$O_2^{\bullet -}$: Superoxide anion
$ONOO^-$: Peroxynitrite anion
P.I.: Propidium Iodide
PARP: Poly(ADP-Ribose) Polymerase
PBS : Phosphate-Buffered Saline
PCR: Polymerase Chain Reaction
PD-L1: Programmed Death-Ligand 1
PE : Plating Efficiency
Pep: Peptide
PFA: Paraformaldehyde
pg: picogram
PI3K: Phosphatidylinositol-3-Kinase
PLGA: Poly(Lactic-co-Glycolic Acid)
PRDX : Peroxiredoxins
PTEN: Phosphatase and TENsin homolog
PUMA: p53 upregulated modulator of apoptosis
QDs: Quantum Dots
$R^{\bullet}$: organic radicals
RAD 51: Recombinase RAD51
RIP: Receptor-Interacting Protein
$RO_2\bullet$: alkoxy radical
$RO_2^{\bullet}$: peroxyl radicals
ROOH : hydroperoxides
ROS: Reactive Oxygen Species
RT: Radiation Therapy; RT: Room Temperature
S : Survival
SAPKs: Stress-Activated Protein Kinases
SC: Spectral Count
SCC: Specific Spectral Count
SDS: Sodium Dodecyl Sulfate
SER: Sensitivity Enhancement Ratio
$SF_{4Gy}$ : Survival Fraction at 4Gy
SIRT1: Sirtuin 1
SPIONS: SuperParamagnetic Iron Oxide Nanoparticles
SR-DUV: Super resolution-deep ultraviolet
SSBs: Single-Strand Breaks
STAT: Signal Transducer and Activator of Transcription
TCF4: Transcription Factor 4
TEM: Transmission Electron Microscope
TGF-β: Transforming Growth Factor β
TiONts: Titanate Nanotubes
TKI: Tyrosine Kinase Inhibitors
TNF-α: Tumor Necrosis Factor-α
tot mtDNA: total mitochondrial DNA
Tris-HCl: Tris hydrochloride
UPR: Unfolded Protein Response
VEGF: Vascular Endothelial Growth Factor
VMAT: Volumetric Modulated Arc Therapy
WSC: Weighted Spectral Count
γGLU-GLU: Gamma glutamyl-glutamic acid

# General Introduction

Head and Neck cancer belongs to one of the most prevalent cancers with the majority of cases representing squamous cell carcinoma (SCC) arising in the stratified epithelium of the oral cavity, pharynx, and larynx (Leemans *et al*, 2011). This group of cancer is known under the common name of Head and Neck Squamous Cell Carcinoma (HNSCC), and is ranked among the ten deadliest cancer worldwide due to its high radioresistance and recurrence, which in turn leads to a 5-year survival rate less than 50%. The annual incidence of HNSCC is around 600,000 new cases, frequently presented as locally advanced disease and accounts for 350 000 deaths worldwide per year (Siegel *et al.*, 2016). HNSCC therefore represents an important health concern. Current treatment of HNSCC patients is based on the stage and anatomic location, independent of the underlying biology, and consists in surgery, chemotherapy, radiotherapy, or a combination of these different cancer treatments. Although advancements in the therapeutic options, (in the delivery as well as in the supportive care), have moderately improved the quality of life for patients, the risk of regional and distant relapse is still high. Indeed, patients with recurrent or metastatic HNSCC present an enhanced morbidity and a poor prognosis, with a median survival of ten months (Sacco and Cohen, 2015). Thus, besides gaining insight into the molecular principles that control the high incidence of local recurrence and distant metastasis, the development of more effective and less toxic therapeutic modalities for the management of HNSCC is needed and mandatory. Radiation therapy remains a crucial treatment modality, but rates of therapeutic success are still unacceptable. The different mechanisms that contribute to the radioresistance phenomena in HNSCC are numerous and complex, thus explaining why many promising therapies have often failed during their evaluation in clinical trials.

In the vision of the development of new radiosensitizing strategies (increasing the dose delivered to the tumor while sparing the healthy surrounding tissues), the field of nanotechnology/nanomedicine is quite attractive and shows great promise. Indeed, nanoparticles (NPs) composed of high-Z atoms, such as metallic (gold, platinum) and oxide (hafnium, gadolinium) nanoparticles (NPs) have been proposed as potential nanodrugs to amplify radiation-based therapies (Hainfeld *et al.*, 2008; Porcel *et al.*, 2010; Le Duc *et al.*, 2014). These are being presented as new compounds able to improve both expected aspects of innovative radiation-based therapies: specificity and efficiency. Results obtained with various types of NPs showed that they can specifically increase the radiosensitivity of tumor cells. Among these, gadolinium-based nanoparticles (GdBNs) have been designed, which can act as multimodal agents and improve not only the therapeutic index of the treatment, but also Magnetic Resonance Imaging (MRI) performance (theranostics) (Sancey *et al*., 2014). In this study, we will use GdBNs named AGuIX® (**A**ctivation and **G**uidance of **I**rradiation by **X**-rays) nanoparticles, which are ultrasmall (2-5 nm hydrodynamic diameter) gadolinium-based nanoparticles. These nanoparticles are characterized by their high colloidal stability and good Gd chelation, an absence of *in vivo* toxicity, a high EPR effect (which means that they will preferentially accumulate in tumors due to the tumor's leaky vasculature, which will in turn increase the local dose inside the tumor while sparing the healthy surrounding tissues), a good

biocompatibility after IV injection, a facilitated renal excretion, and their potential use as a contrast agent for M.R.I., making AGuIX® a promising theranostic agent (Sancey *et al*., 2014).

Although many groups have shown early evidence of the radiosensitizing potential of AGuIX®, little is known about the subcellular mechanisms leading to the radiosensitization. Up to now, a significant number of *in vitro* demonstrations of the radiosensitizing effect of GBNs have been reported following different experimental conditions. These experimental conditions varied in terms of the energy of irradiation from keV to MeV, different concentrations of nanoparticles (from 0.1 to 1 mM), and times of incubation (from 1h to 24h), different types of tumor cell lines, as well as the nature of the irradiation (photons, neutrons or ions) (Sancey *et al.*, 2014). Indeed, several *in vitro* studies have demonstrated the radiosensitizing effect of AGuIX® nanoparticles combined to photon irradiation in glioblastoma cells (Štefančíková *et al.*, 2016; Štefančíková *et al.*, 2014), cervical carcinoma HeLa cells (Luchette *et al.*, 2014), HNSCC (Miladi *et al.*, 2015), and prostate cancer cells (K. Butterworth, personal communication). Apart from the work of Miladi *et al.* where the involvement of mitotic catastrophe and late apoptosis were demonstrated in HNSCC (Miladi *et al.*, 2015), little is known about the subcellular effects of these GBNs, the organelles involved in their radiosensitizing effect, as well as the connection between the physical, chemical, and biological effects of GBNs. Moreover, although GBNs were never found to be localized within nuclei (Rima *et al.*, 2013), γ-H2AX or 53BP1 foci have been generally quantified to reflect DNA double-strand breaks (DSBs) and contradictory results have been reported with the same GBNs in different cell lines. While an increase of residual DSBs have been demonstrated in HNSCC, 1h after treatment with GBNs combined to radiation (Miladi *et al.*, 2015), opposite results have been reported with AGuIX® in glioblastoma (Štefančíková *et al.*, 2016).

Given the variety of experimental conditions and cells involved in the studies mentioned above, as well as for other high-Z NPs, it seems impossible that all induce the same cellular response. Moreover, in the direction of a better understanding of the radiosensitization process, the clonogenic survival curve assay cannot be the only way to probe the cellular responses which therefore should be investigated in more details. This work has been undertaken with AGuIX® containing DOTAGA as a macrocyclic $Gd^{3+}$ chelate which is a more stable and better chelator (Mignot *et al.*, 2013) compared to the acyclic ligand DTPA that could release toxic gadolinium (Rogosnitzky *et al.*, 2016).

Despite AGuIX®'s potential to induce radiosensitization in cancer cells, there are several challenges towards their clinical translation which has, to date, led to only a few clinical trials being undertaken (NCT02820454: NANO-RAD and NCT03308607: NANOCOL).

The first objective of this work was to determine the radiosensitizing conditions of AGuIX® in an HNSCC cellular model, SQ20B J.L. cells. Their subcellular localization was studied by time-lapse confocal microscopy. The mechanism leading to the radiosensitization with the

combined treatment of AGuIX® treatment + ionizing radiation was then studied in terms of: (1) ROS production and the oxidative cellular state, (2) the types of cell deaths involved and (3) the potential resulting DNA-damage. At last, a proteomic approach was initiated in order to reveal potential targets and/or subcellular pathways involved after the combined treatment. This work was therefore expected to better understand the mechanisms of action mediating the biological effects of this new formulation of AGuIX®, and the potential subcellular targets in cells in order to move towards clinical applications in a more robust way.

# Bibliography Review

# Chapter I. Head and Neck Squamous Cell Carcinoma

## *1. Generalities, Facts, and Statistics*

Head and Neck Squamous Cell Carcinoma (HNSCC) is a very heterogeneous disease with different sites as well as different histological characteristics. HNSCC represents all cancers arising from the epithelium mucosa of the oral cavity, oropharynx, laryngopharynx, and larynx.

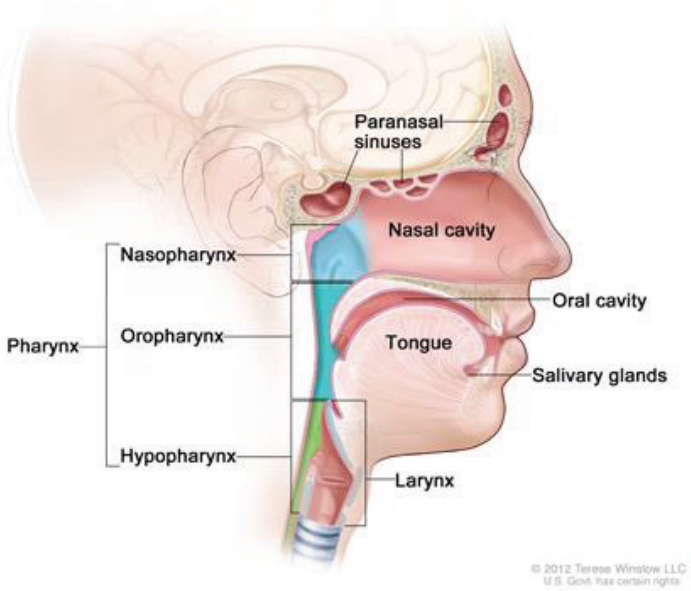


Figure 1: HNSCC sites.

HNSCC represents a major worldwide health concern as it represents 12% of all malignancies and is ranked as the eighth deadliest cancer. 650 000 new cases are diagnosed each year and over 320 000 individuals die every year, ranking this type of cancer eighth according to the World Health Organization. In France, it is the ranked the fourth most common type of cancer and the fifth cause of cancer mortality. This type of cancer is known to be caused by alcohol consumption, tobacco use, and more recently, the infection by the Epstein-Barr virus and human papillomavirus (HPV) have also been found to be linked to this type of cancer. HNSCC can be treated via surgery when possible, chemotherapy, radiotherapy, or a combination of these different treatments, radiotherapy remaining the most frequently used. However, improvements in survival rates for patients remain low as 5-year survival of patients is still under 50% which is unacceptable. This bad prognostic is mostly due to the resistance of the tumors to radiotherapy as well as its recurrence. It is therefore mandatory to further investigate more efficient treatment options. (Jemal *et al.*, 2007; Boyle and Levin, 2008)

HNSCC are classified under the TNM system (T= size of primary tumor, N= degree of spread to regional lymph nodes; M= presence of distant metastasis). However, as previously

mentioned, HNSCC tumors being very heterogeneous, this system lacks biological and molecular markers, which leads to the same treatment for malignancies that are significantly different. This might, in part, explain the low survival rates while the recurrence is high.

## 2. *Frequently dysregulated pathways in HNSCC*

In order to find more efficient treatments, much research has been focused on the understanding of the molecular networks involved in head and neck carcinogenesis. Two classes of genes are present in cells: oncogenes and tumor suppressor genes. It was shown that for many cancer types, carcinogenesis mostly comes from an imbalance where oncogenes will be overexpressed and therefore will promote cell proliferation (Hanahan and Weinberg, 2011). Genetic and epigenetic alterations observed in HNSCC show a loss of tumor suppressor function and aberrant gene and protein expression making HNSCC a particularly radio-resistant type of cancer with a bad prognosis (Molinolo *et al.*, 2010).

Genetic and epigenetic alterations observed in HNSCC include alterations leading to dysplegia (abnormality of development, alteration in size, shape, and organization of cells) (9p21, 3p21, 17p13), carcinoma *in situ* and invasive tumors (Forastiere *et al.*, 2001, Califano *et al.*, 1996). Several known tumor suppressor genes have been highlighted in HNSCC including p16 and $p14^{ARF}$. Loss of the chromosomal region 9p21 is found in 70-80% of dysplastic lesions of the oral mucosa, which together with the inactivation of the remaining alleles of p16 and $p14^{ARF}$ by promoter hypermethylation, represent one of the earliest and most frequent events in HNSCC progression (Molinolo *et al.,* 2009; Forastiere *et al.,* 2001; Califano *et al.* 1996).

One of the characteristics of cancer cells is their ability to replicate endlessly. In HNSCC, it has been shown that this proliferative property is linked to the genetic and epigenetic inactivation of p16, the mutation of p53 and an enhanced activity of telomerase (Todd *et al.*, 2002). The inactivation of p16 in HNSCC tumors allows cells to bypass the "replicative stress-induced senescence", while the enhanced telomerase activity prevents the shortening of the telomeres and the consequent generation of signals from uncapped telomeres that impinge on p53 and other molecules involved in the DNA-damage response (Collado *et al.*, 2007; Molinolo *et al.*, 2009).

Nearly 50% of HNSCC cases have mutations in the p53 tumor suppressor gene (Poeta *et al.*, 2007; Boyle *et al.*, 1993). p53 can halt the cell's progress in the cell-cycle if it detects DNA-damage and therefore can trigger apoptosis if the detected DNA damage is not repaired. However, this tumor suppressor gene is often mutated in most human cancers. Therefore, in HNSCC, mutations rendering p53 inactive are associated with tumor progression and decreased overall survival (Poeta *et al.*, 2007). If p53 does not present point mutations, it can also be inactivated by its ubiquitin-dependent degradation (Molinolo *et al.*, 2009; Vousden and Lane, 2007). Infection by HPV will also bring in a new mechanism in which p53 is inactivated and is unable to play its tumor suppressor role. The following can therefore be

responsible for a reduced activity of p53 including: the infection with HPV16 and/or HPV18, the overexpression of MDM2, or the inactivation of $p14^{ARF}$ (Molinolo *et al.*, 2009; Vousden and Lane, 2007). This therefore leads to further accumulate unchecked alterations due to inappropriate cellular response to DNA damage.

Aberrant gene and protein expression in HNSCC include members of the Wnt and Notch family which have been shown to be involved in tumor progression of HNSCC (Leethanakul *et al.*, 2000). Altered expression of genes involved in cell signaling, gene transcription, cell cycle regulation, oncogenesis, tumor suppression, differentiation, motility and invasion have also been reported in HNSCC (Leethanakul *et al.*, 2000, Alevizos *et al.*, 2001). Frequently upregulated genes include the matrix metalloprotease (MMP) family members, such as MMP-1, MMP-3, MMP-10, and MMP-12, pro-angiogenic chemokines, including IL8 (CXCL8) and Gro-α (CXCL1) whereas down-regulated genes include KRT4, MAL, SPINK5, and TGM3 (Ye *et al*, 2008; Ziober *et al.*, 2006). Using proteomics analysis, several dysregulated, over- or under-expressed, proteins in HNSCC were identified such as heat shock proteins HSP60 and HSP27, calgranulin B, myosin, tropomyosin, and galectin 1 in tongue carcinoma tissues (He *et al.*, 2004).

The Epidermal Growth Factor Receptor (EGFR) is overexpressed in 80-90% of all HNSCC tumors (Grandis and Tweardy, 1993). Overexpression of EGFR represents an independent prognostic marker and can correlate with increased tumor size, increased radioresistance, and increased risk of occurrence (Grandis and Tweardy, 1993; Ang *et al.* 2002; Gupta *et al.*, 2002). This overexpression is due to gene amplification with more than 12 copies per cell found in HNSCC (Temam *et al*., 2007). Examples of pathways activated via EGFR includes the Ras/Raf/mitogen protein kinase (MAPK), the transducer and activator transcription (STAT), and the phosphatidylinositol-3-kinase (PI3K)/AKT/mammalian target of rapamycin (mTOR) pathway, all these leading to the malignant growth and metastatic potential of HNSCC (Molinolo *et al.*, 2009). The over-expression of EGFR and its consequences will be further discussed in the paragraph entitled targeted therapies.

Another factor in HNSCC cancer growth is the aberrant activity of the transcription factor NFκB. NFκB was shown to be, in part responsible in the treatment resistance of HNSCC tumors as its dysregulation promotes tumor angiogenesis and metastasis, and suppresses the pro-apoptotic potential of chemotherapeutic drugs and radiotherapy (Karin *et al.*, 2005; Nakanishi and Toi, 2005). In HNSCC, the expression and activity of NFκB is often upregulated, and its protein level increases gradually from pre-malignant lesions to invasive cancer (Ondrey *et al.*, 1999, Mishra et al., 2006; Sawhney *et al.*, 2007; Bindhu *et al.*, 2006), which suggests that NFκB signaling plays an important role at the early stages of HNSCC carcinogenesis. In fact, NFκB promotes the expression of the anti-apoptotic protein Bcl-2 in HNSCC (Jordan *et al.*, 1996).

In summary, as described above, several dysregulated signaling pathways in HNSCC were highlighted that could have a therapeutic interest as diagnostic markers and/or potential therapeutic targets including:

- ✓ the activation of the signal transducer and activator of transcription (STAT) proteins
- ✓ the Wnt protein family
- ✓ the transforming growth factor-β (TGF-β) (dual role in carcinogenesis: acts as a potent tumor suppressor during the early stages while it would promote tumor growth at later stages) (Prime *et al.*, 2004)
- ✓ the aberrant function of the phosphatidylinositol 3-kinase (PI3Ks), PTEN, AKT and mTOR signaling network

All these frequently dysregulated pathways are summarized in Figure 2. (Molinolo *et al.*, 2009)

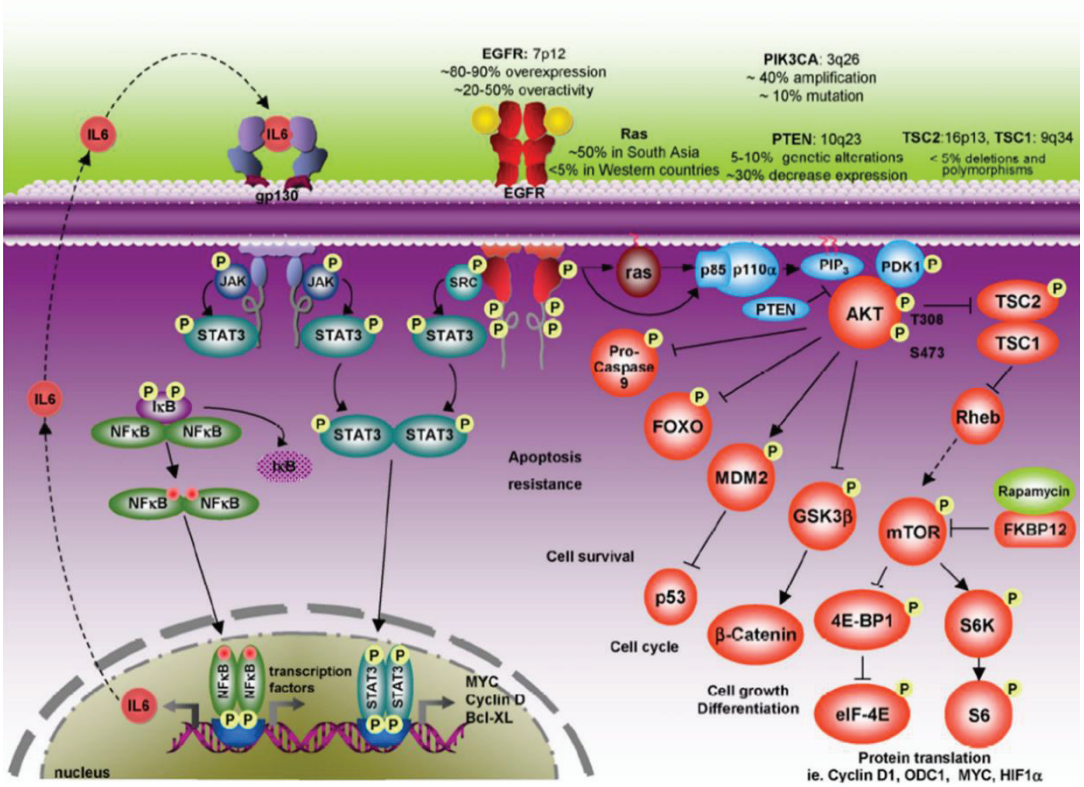


Figure 2: Frequently dysregulated pathways in HNSCC (Molinolo *et al.*, 2009).

## 3. *Treatments options in HNSCC*

The treatment options chosen will depend on several factors including the type and stage of the cancer, the possible side effects, and the patient's overall health.

### 3.1. Surgery

Surgery is the oldest type of cancer therapy and remains one of the most effective treatments as it removes the cancerous tumor and some surrounding healthy tissue (in order to make sure that no cancer is left). Surgery in cancer treatment can take multiple forms:

- Laser technology: can be used to treat early-stage tumors, especially when it was found in the larynx.
- Excision (most commonly used) which removes the tumor as well as a small part of the surrounding healthy tissue.
- Lymph node dissection or neck dissection: when the cancer has spread
- When cancer has spread in a large part and therefore requires major tissue removal (*i.e*. removal of the jaw, skin, pharynx, or tongue), reconstructive (plastic) surgery can be performed in order to replace the missing tissue. This allows the patient to recover his/her appearance as well as the function of the affected area.

Often, one surgery is not sufficient and the patient will be further treated with chemo and/or radiotherapy in order to destroy the remaining cancerous cells.

Although surgery might be thought of as the therapy with the most "positive" outcome, there are still several side effects dependent on the location and type that cannot be ignored in particular: temporary or permanent loss of normal voice, impaired speech, hearing loss, difficulty in chewing and swallowing, swelling of mouth and throat area, difficulty breathing and facial disfigurement. Also, if total laryngectomy, patients may have decreased functioning of the thyroid gland (which will need to be managed).

### 3.2. Chemotherapy

Chemotherapy is defined as the use of drugs to destroy cancer cells, usually by stopping the cancer cell's ability to grow and divide. However, one of its major drawbacks is that the majority of the drugs used in chemotherapy do not specifically target cancer cells but all cells that divide rapidly. Systemic chemotherapy, usually delivered by IV injection or swallowing of a pill or capsule, gets into the bloodstream to reach cancer cells throughout the body. Side effects of chemotherapy include fatigue, risk of injection, nausea and vomiting, hair loss, loss of appetite, and diarrhea.

Depending on the administered mode of chemotherapy, we can define four different types of chemotherapies including simultaneous, adjuvant, palliative, or inductive neoadjuvant chemotherapy.

**Induction chemotherapy** is employed as the primary treatment for cancer therapy that will be followed by another approach such as surgery or radiotherapy. Such a treatment allows to give a first evaluation of the tumor's response to treatment: if a patient responds to inductive

chemotherapy, it means that the tumor is sensitive to the treatment and therefore, the next step will be radiotherapy. If not, there is a probability of non-response to radiotherapy which will direct towards surgery. The use of cisplatin in combination with taxanes and Fluorouracil (5-FU) seemed up to now to be most efficient (Vermorken *et al.*, 2007; Qin *et al.*, 2012). However, it appears that this type of approach does not result in a significant increase in the time of survival nor in the locoregional control of the tumor.

**Simultaneous or concomitant chemotherapy** uses chemotherapeutic agents in combination with radiotherapy. The chemotherapy treatment can be used as mono-therapy where cisplatin is mostly used, whereas in poly-chemotherapeutic treatments, the combination of platin salts (cisplatin or carboplatin) with 5-FU are commonly used. Concomitant chemotherapy has shown benefits compared to radiotherapy alone (Pignon *et al.*, 2009). Concomitant chemotherapy allows the preservation of healthy organs with a decrease of laryngectomies for example (Forastière *et al.*, 2003) as well as an increased survival that is significant when comparing to patients treated with radiotherapy alone (+ 6% at 5 years) (Pignon *et al.*, 2009).

**Adjuvant chemotherapy** allows for the treatment of residual tumors by chemotherapy +/- radiotherapy after surgery and/or following a radiotherapy treatment. Two studies showed a better efficacy of adjuvant chemotherapy used with radiotherapy after surgery including a better locoregional control and a significant increase of the 5-year survival of patients (Bernier *et al.*, 2004; Cooper *et al.*, 2004).

With **palliative chemotherapy**, the aim is a little different than other types of chemotherapy, as the main goal is to increase the patients' life with a particular attention in improving the patients' quality of life. In this case, mono- or multiple-therapies are mostly used, including treatment with methotrexate, platin salts, 5-FU, taxanes, or anti-EGRF antibody.

Platinum derivatives are the most widely used and effective drugs in HNSCC. Cisplatin, a planar heavy-metal complex, targets DNA and will form different kinds of DNA adducts including 1,2-intrastrand cross-links, inter-strand cross-links, monofunctional adducts, or protein-DNA cross-links. A study showed including 288 patients with recurring and metastasized HNSCC, showed that monotherapy of cisplatin had an average remission rate of 28% (Al-Sarraf, 1987). Another agent under the same category is carboplatin. Although this molecule showed a more favorable nephrotoxic, ototoxic, and emetogenic profile, it was more myelotoxic (Canetta *et al.*, 1985). However, higher concentrations of carboplatin, compared to cisplatin, are needed to have the same effect on DNA.

Methotrexate is another compound used in HNSCC showing promising results as it blocked tumor growth. It blocks the formation of tetrahydrofolic acid because of its high affinity for

dihydrofolic acid reductase, a co-enzyme for C1-metabolism during the synthesis in the G1 phase (Hoffmann, 2012).

5-FU, developed by Heidelberger *et al.*, exists since 1957 following an observation that the uracil base was used more often in tumoral DNA synthesis. It is believed that following intra-cellular nucleotide metabolism, 5-FU blocks the key enzyme, thymidylate synthase, which leads to a reduction of desoxythymide triphosphate (dTTP), a preliminary product of DNA synthesis(Sommer and Santi, 1974). In addition, it appears that it acts on RNA synthesis by blocking it (Hoffmann, 2012). If used as a monotherapy in HNSCC, 5-FU only improved remission rate by 15% which is rather low (Al-Sarraf, 1987). Therefore, a combination with cisplatin is important to observe important therapeutic benefits (Armand and Couteau, 1995).

Mitomycin C is an antibiotic used as a chemotherapeutic agent. This drug inserts itself between the two strands of DNA therefore causing irreversible damage triggering cytotoxic signaling cascades. It can either be used as a monotherapy or in combination with 5-FU. It can also be used in combination with radiotherapy and it will increase the outcome compared to radiotherapy alone (Budach *et al.*, 2005).

Taxanes (paclitaxel, docetaxel) are also employed for their cytostatic properties. Taxanes will block cell division and therefore tumor growth by inhibiting the spindle apparatus. Docetaxel monotherapy in HNSCC has a good response rate of 42% (Dreyfuss *et al.*, 1996). Promising remission rates were obtained when combining taxanes with 5-FU and a platin, salt but toxicity can be an issue when administered as induction therapy (Posner *et al.*, 2007, Vermorken *et al.*, 2007).

Other chemotherapeutic drugs used in HNSCC include bleomycin, which binds specifically to guanine and cleaves single and double strands of DNA (Muller and Zahn, 1976); vincristine, which binds to tubulin and therefore inhibits the polymerization to microtubule therefore inducing the cell the a metaphasic arrest (Madoc-Jones and Mauro, 1968). Last, other more rarely used compounds include ifosfamide, gemcitabine, pemetrexed and oral etoposide… (Hoffmann, 2012)

Table 1 shows selected milestones in the history of chemotherapy specifically for the treatment of HNSCC while Table 2 shows FDA-approved chemotherapeutic agents for the treatment of HNSCC.

| Year (Study) | Advances |
|---|---|
| 1965 (Rosenberg *et al.*) | Michigan State University researchers discover platinum-based compounds can impact cell division (precursor to cisplatin). |
| 1970 (Ansfield *et al.*) | Trials at University of Wisconsin demonstrate increased survival with 5-FU-based concurrent chemoradiation in advanced oral/oropharyngeal HNSCC. |
| 1977 (Wittes *et al.*) | Memorial Sloan Kettering reports "major response" rate of 30% in recurrent HNSCC patients receiving platinum-based chemotherapy. |
| 1982 (Kish *et al.*) | Trials at Wayne State University show improved survival with combination 5-FU/cisplatin therapy compared with single-agent therapy in advanced HNSCC. |
| 1991 (VA Laryngeal Cancer Group) | Induction chemotherapy followed by radiation shown to be equivalent to surgery followed by radiation in advanced laryngeal cancer, allowing for "organ preservation." |
| 2004 (RTOG 9501 and EORTC 22931 trials) | Improved locoregional control demonstrated in high-risk patients receiving postoperative concurrent chemoradiation. |
| 2006 (Bonner *et al.*) | Cetuximab-based chemoradiation is superior to radiotherapy alone, becoming the first targeted therapy used in HNSCC. |
| 2016 (KEYNOTE-012 and CheckMate 141 trials) | Efficacy of immune checkpoint inhibitors pembrolizumab and nivolumab demonstrated in recurrent/metastatic HNSCC. |

*5-FU= 5-fluoracil; CheckMate 141 = Trial of Nivolumab vs. Therapy of Investigator's Choice in Recurrent or Metastatic Head and Neck Carcinoma; EORTC = European Organization for Research and Treatment of Cancer; KEYNOTE-012 = Study of Pembrolizumab (MK-3475) in Participants With Advanced Solid Tumors; HNSCC = head and neck squamous cell carcinoma; RTOG = Radiation Therapy Oncology Group; VA = Veteran Affairs.*

Table 1: Selected milestones in the history of chemotherapy for HNSCC (Blasco *et al.*, 2017)

| Agent | Mechanism | Year of Approval | Indication | Important Trials |
|---|---|---|---|---|
| Methotrexate | Antimetabolite | 1959 | Advanced HNSCC | Hertz *et al.*, 1956 |
| Hydroxyurea | Inhibits DNA synthesis | 1967 | Concurrent chemoradiation in locally advanced HNSCC | Argiris *et al.*, 2003 |
| Bleomycin | Induces DNA damage | 1973 | Advanced HNSCC | Ichikawa, 1968 |
| Cetuximab | EGFR inhibitor | 2006 | Concurrent chemoradiation in locally advanced HNSCC; combination chemotherapy in recurrent/metastatic HNSCC | Bonner *et al.*, 2006, Vermoken *et al.*, 2008 |
| TPF | Combination chemotherapy | 2006 | Induction in unresectable locally advanced HNSCC | Vermoken *et al.*, 2007, Posner *et al.*, 2007 |
| Pembrolizumab | PD-1 inhibitor | 2016 | Recurrent/metastatic HNSCC | Seiwert *et al.*, 2016 |
| Nivolumab | PD-1 inhibitor | 2016 | Platinum-refractory recurrent/metastatic HNSCC | Ferris *et al.*, 2016 |

*EGFR = epidermal growth factor receptor; HNSCC = head and neck squamous cell carcinoma; PD-1 = programmed death protein 1; TPF = docetaxel/displatin/5-fluorouracil.*

Table 2: Food and Drug Administration-Approved Systemic Agents in the treatment of HNSCC (Blasco *et al.*, 2017).

Further discussion on cetuximab, a targeted therapy and chemotherapeutic drug frequently used in HNSCC will be discussed later in a dedicated paragraph.

### 3.3. Radiotherapy

Radiation therapy is the use of high-energy X-rays or other particles to destroy cancer cells. A radiotherapy treatment plan is established which usually consists of a specific number of treatments given over a set period of time. Radiotherapy treatment plan in HNSCC consists of 2Gy irradiation 5 times a week for 7 weeks, for a total dose of 70Gy. In the case of HNSCC, radiotherapy can be the unique treatment or it can be used as adjuvant therapy, for example after surgery in order to destroy the remaining cancerous cells which were not removed by the surgery.

The most common type of radiotherapy used is external-beam radiation therapy (radiation delivered by a machine outside of the body). Radiotherapy has majorly improved since its invention and a specific type of external-beam radiation therapy is intensity-modulated radiation therapy (IMRT) which uses advanced technology to accurately direct the beams of radiation at the tumor while minimizing the field to the healthy tissues.

Side effects of radiotherapy are numerous and include tooth decay, short- or long-term pain or difficulty swallowing, changes in voice because of swelling and scarring, loss of appetite, redness or skin irritation in the treated area, fatigue, nausea, hearing loss … In order to reduce these side effects, new techniques and protocols to improved radiotherapy

protocols have been proposed including accelerated fractioning, hyperfractionation, intensity-modulated radiation therapy (IMRT), volumetric modulated arc therapy (VMAT), or tomotherapy.

- ✓ **Accelerated fractioning**: the dose of radiation treatment is delivered on a shorter period of time, so that cancer cells have less time to repair radiation-induced damages.

- ✓ **Hyperfractionation**: the dose of radiation is delivered in fraction throughout the day in order to reduce the amount of radiation received at once, therefore allowing healthy cells to better recover, while limiting the time for cancer cells to recover. This will indeed limit the late side effects caused by radiotherapy. This type of therapy showed a better overall 5-year survival in patients following their treatment (8% gain) but without improving the locoregional control (Bourhis *et al.*, 2006)

- ✓ **Intensity-modulated radiation therapy (IMRT)**: This irradiation mode allows for a more precise radiation dose to the 3-D shape of the tumor by modulating the intensity of the radiation in multiple small volumes. It also allows higher radiation doses to be focused to regions within the tumor while minimizing the dose to surrounding normal critical structures. Treatment is carefully planned by using 3-D computed tomography (CT) or magnetic resonance (MRI) images of the patient in conjunction with computerized dose calculations to determine the dose intensity pattern that will best conform to the tumor shape. Typically, combinations of multiple intensity-modulated fields coming from different beam directions produce a custom radiation dose that maximizes tumor dose while also minimizing the dose to adjacent healthy tissues. Toxicity due to the treatment is reduced, even when the doses are increased. This type of radiation is mostly used to treat prostate cancer, head and neck, and the central nervous system. It can also be used in breast cancer, thyroid, lung, gastrointestinal, gynecologic malignancies and certain types of sarcomas, and can also be beneficial for treating pediatric malignancies.

- ✓ **Volumetric modulated arc therapy (VMAT)**: Advanced form of IMRT, delivers a precisely-sculpted 3D dose distribution with a 360-degree rotation of the gantry in a single or multi-arc treatment. VMAT can deliver the total dose to the tumor in a 360-degree rotation in less than two minutes.

- ✓ **Tomotherapy**: Type of IMRT, also called helical tomotherapy. The radiation is focused on the tumor from many different directions as the accelerator is coupled to a scanner in order to visualize the tumor “in real-time”. This enables the delivery of a high dose to the tumor, by always doing a maximum to spare the healthy tissue in proximity.

However, radiotherapy alone still results in poor local control and survival owing to the radio-resistance of HNSCC tumors which leads to their recurrence.

The interaction of X-ray with matter will be further discussed in the next chapter which is specific to radiotherapy.

### 3.4. Targeted therapies

Novel therapies giving alternatives to chemotherapy and/or radiotherapy are arising to mainly counter the many side effects that patients face when receiving such treatments as well as improve their quality of life. Chemotherapy and radiotherapy, although much progress has been done, do not only target tumor cells but can also cause damage to healthy cells. Therefore, increasing interest was focused on targeted therapies. These therapies are called as such because the molecule used specifically targets a certain molecule/target of the cancer cell. Several examples exist targeting different pathways and will be developed in the following paragraphs.

A special focus, because more commonly used in HNSCC, is the development of a monoclonal antibody against the **E**pidermal **G**rowth **F**actor **R**eceptor (EGFR) which is Cetuximab, and was approved for use by the FDA in 2006.

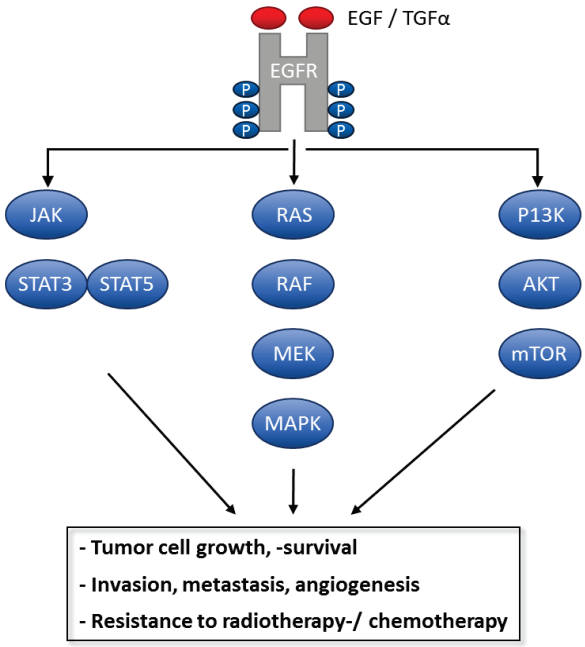


Figure 3: Signaling pathways activated following ligand binding of EGFR. (Hoffmann, 2012)

As can be observed in Figure 3, following ligand binding to the EGFR, intracellular and nuclear cellular signaling cascades are activated, which leads to a conformational change and auto-phosphorylation of EGFR. This is followed by the consecutive activation of signaling pathways leading to tumor-cell proliferation, survival, and metastasis. Inhibition of this ligand binding or receptor phosphorylation has been a new therapeutic approach in HNSCC (Hoffmann, 2012).

### *3.4.1 Development of drugs (monoclonal antibodies) targeting the overexpression of EGFR*

The overexpression of EGFR is one of the main causes for decreased overall survival due to its role in cancer cell survival. The epidermal growth-factor receptor has many roles including proliferation, differentiation, anti-apoptotic signaling, angiogenesis, and metastasis. Expression of EGFR is found in 90% of HNSCC cancer cases, and it is used as an independent prognostic marker as high expression is associated with increased tumor size, decreased radiation sensitivity, and increased risk of recurrence.

After studying the overexpression of EGFR as a potential target to specifically target tumors, two main categories of molecules of key importance were identified (Figure 4):

- Monoclonal antibodies (i.e. cetuximab, panitumumab)
- Tyrosine kinase inhibitors (i.e. gefitinib and erlotinib)

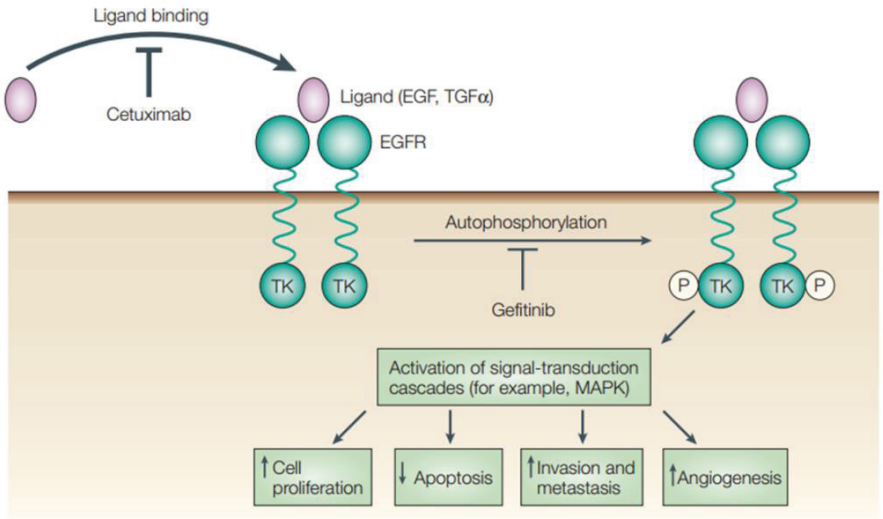


Figure 4: Mechanism of action of cetuximab (monoclonal antibody) or gefinib (tyrosine kinase inhibitor) (Graham *et al.*, 2004).

#### *3.4.1.1 Cetuximab*

Cetuximab is a chimeric (human/mouse) monoclonal antibody against EGFR that received FDA approval for recurrent and metastatic HNSCC, as well as for locally advanced HNSCC. Many clinical trials were put in place in order to see the effects and the possibilities of bettering cancer therapy using cetuximab. One of the pioneering studies was done in patients with locally advanced HNSCC without a primary surgical treatment option, where two treatments were compared: cetuximab combined with radiotherapy versus radiotherapy alone. When comparing radiotherapy alone to radiotherapy + cetuximab, an increase in the

median survival time by 19.7 months (49.0 vs. 29.3 months) was observed for I.R. + cetuximab. An increase in the median time to loco-regional failure by 9.5 months (24.4 vs, 14.9 months) was also observed (Hoffmann, 2012; Bonner *et al.*, 2006; Bonner *et al.*, 2010). No benefits were seen for patients at the T4 or N0 stage, those who had a poor Karnosfsky index, nor for those who were over 65 years of age (Hoffmann, 2012). Several Phase III trials are underway to study the interaction of radiotherapy with cetuximab (RTOG-0920; GORTEC2007-01, and GORTEC2007-02).

Following the many clinical trials, cetuximab/Erbitux® + radiation therapy was registered for the treatment of patients with advanced HNSCC in 2006, and in 2008, it was also approved in combination with first-line chemotherapy for patients with recurrent/metastatic HNSCC. In summary, Erbitux® (cetuximab) can be prescribed with radiation therapy for the initial treatment of certain types of locally or regionally advanced head and neck cancer. Erbitux® can also be used in combination with platinum-based chemotherapy with 5-FU for patients whose tumor has returned in the same location or spread to other parts of the body. Additionally, Erbitux® is approved for the use alone to treat patients whose tumor has returned in the same location or spread to other parts of the body and whose disease has progressed following platinum-based chemotherapy[1].

A couple of other monoclonal antibodies were developed including matuzumab, a humanized EMD72000, a version of IgG1 with an elongated half-life (Bier *et al.*, 2001), panitumumab and zalutumumab, which are two completely humanized antibodies, IgG2a and IgG1 respectively. All four antibodies bind to the EGFR with a higher affinity than the endogenous ligands, which therefore prevents the dimerization, internalization, and auto-phosphorylation. Preclinical studies have shown an inhibition of the proliferation and the induction of apoptosis in the tumor. Also, some interest has been turned towards the combination of anti-EGFR antibodies with taxanes (Hoffmann, 2012).

However, one problem still remains, and that is the : intrinsic and acquired drug resistance. According to Boeckx *et al.* (2013), “many HNSCC tumors remain nonresponsive to EGFR targeting agents, as the response rate with such agents, as for instance cetuximab as a single agent, is consistently lower than 15%”. Possible mechanisms of resistance to EGFR-targeted therapy in HNSCC are illustrated in Figure 5.

[1] https://www.erbitux.com/

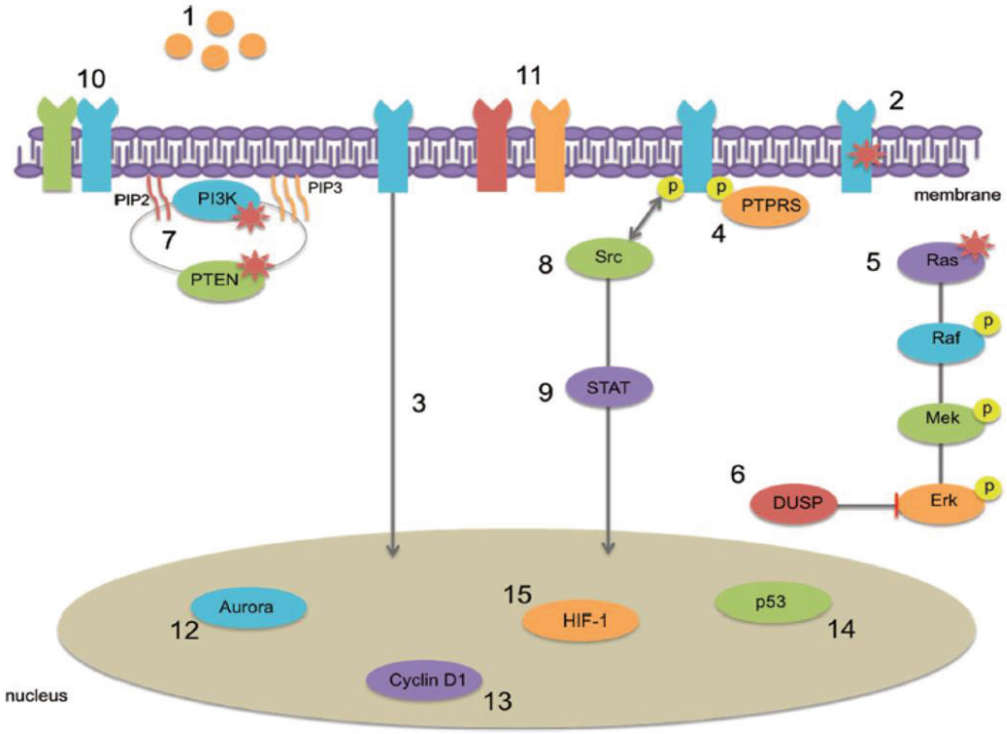


Figure 5: Possible mechanisms of resistance to EGFR-targeted therapy in HNSCC described: (**1**) overexpression of ligands, (**2**) activating mutations in EGFR, (**3**) translocation of EGFR to the nucleus, (**4**) loss of PTPRS, (**5**) activating Ras mutations, (**6**) downregulation of DUSP, (**7**) activating mutations in PIK3CA or inactivating mutation in PTEN, (**8**) activation of Src kinases, (**9**) dysregulation of the STAT pathway, (**10**) heterodimerization with other ErbB family members, (**11**) parallel signaling of other receptors, IGF-1R or MET, (**12**) overexpression of the Aurora kinase A and B, (**13**) deregulation of cyclin D1 or the A870G polymorphism, (**14**) loss of functional p53, and (**15**) activation of HIF-1 signaling. (Boeckx *et al.,* 2013).

### *3.4.2 Anti-angiogenesis*

In HNSCC, it was shown that a correlation exists between tumoral VEGF (**V**ascular **E**ndothelial **G**rowth **F**actor) expression and tumor stage, vascular invasion, and survival. Therefore, antibodies against VEGF are being developed (bevacizumab, Avastin®), as well as tyrosine kinase inhibitors that attack intracellularly at the receptor domain (sunitinib/sorafenib). (Hoffmann, 2012)

### *3.4.3 Signaling cascade inhibition*

#### *3.4.3.1 Tyrosine kinase inhibitors (TKIs)*

It was shown that one main reason for resistance to drugs targeting EGFR was due to a mutation such as EGFRvIII, which appears to be responsible for the constitutive activation of the downstream signaling cascade. In order to overcome this resistance, new possibilities targeting downstream signaling cascades have been shed to light. One such approach is

targeting the EGFR-associated tyrosine kinase. Table 3 summarizes selected clinical studies using TKI for HNSCC treatment.

| Study, phase | Number of patients | Characteristics tumor | Dosage | Result |
|---|---|---|---|---|
| | | ***Gefitinib- selective EGFR inhibitor-*** | | |
| Cohen *et al.*, 2005<br>II, monotherapy | 70 | Recurrent/metastatic | 250mg/d | OR 1.4%, PR 1, SD 23, OS 5.5 mo |
| Kirby *et al.* 2006<br>II, monotherapy | 47 | Recurrent/metastatic | 500mg/d | OR 4.3%, PR 4, SD 13, OS 4.3 mo |
| Stewart *et al.* 2009<br>III, monotherapy | 486 | Recurrent | 250-500mg/d | OS 5.6-6.0 mo |
| | | ***Erlotinib- selective EGFR inhibitor-*** | | |
| Siu *et al.* 2007,<br>I/II, combination therapy + cisplatin | 51 | Recurrent/metastatic | 100mg/d + Cisplatin (75mg/m2 3 w-1) | CR 1, PR 8, OS 7.9 mo |
| Soulieres *et al.* 2004<br>II, monotherapy | 115 | Recurrent/metastatic | 150mg/d | OR 21%, PR 5, SD 44, OS 6.0 mo |
| | | ***Lapatinib-dual tyrosine kinase inhibitor (EGFR, HEP2)-*** | | |
| Abidoye *et al.* 2006,<br>II, monotherapy | 42 | Recurrent/metastatic with (A) or without (B) previous EGFR inhibitor | 1500ng.d | A: SD= 37%; TTP= 1.6 mo<br>B: SD= 20%; TTP= 1.7 mo |
| | | ***Sorafenib-multi-kinase inhibitor-*** | | |
| Williamson *et al.* 2010<br>II, monotherapy | 41 | Recurrent/metastatic | 2x400mg/d | PR 1, OS 9.0 mo |

Table 3: Selected clinical studies with TKI for HNSCC treatment (Hoffmann, 2012)

#### *3.4.3.2 mTOR and other signaling molecules*

Sirolimus/rapamycine (Rapamune®) inhibits a number of cytokine-mediated signal transduction pathways via the complexation of the mTOR protein, a 282 kDa phosphoinositide 3-kinase often activated in HNSCC. The deactivation of mTOR prevents mTOR-dependent cell metabolism which in turn disrupts the cell cycle and inhibits cell growth. Even though sirolimus is a novel treatment approach, studies in HNSCC are currently limited to Phase I trials (Cohen *et al.*, 2011; Hoffmann, 2012). Rapamycin derivatives, such as everolimus, temsirolimus and forolimus, are potent mTOR inhibitors that are more stable and soluble than rapamycin which would therefore make them more attractive. Early clinical studies of these agents as monotherapy or in combination with chemotherapy and chemo-radiotherapy have been initiated (Hoffmann, 2012).

Other therapeutic points of attack targeting the tumor's own signaling cascade include the inhibition of the protein kinase C (Carducci *et al.*, 2006) or the proteasome NF-kappa B by bortezomib (Dudek *et al.*, 2009; Hoffmann 2012).

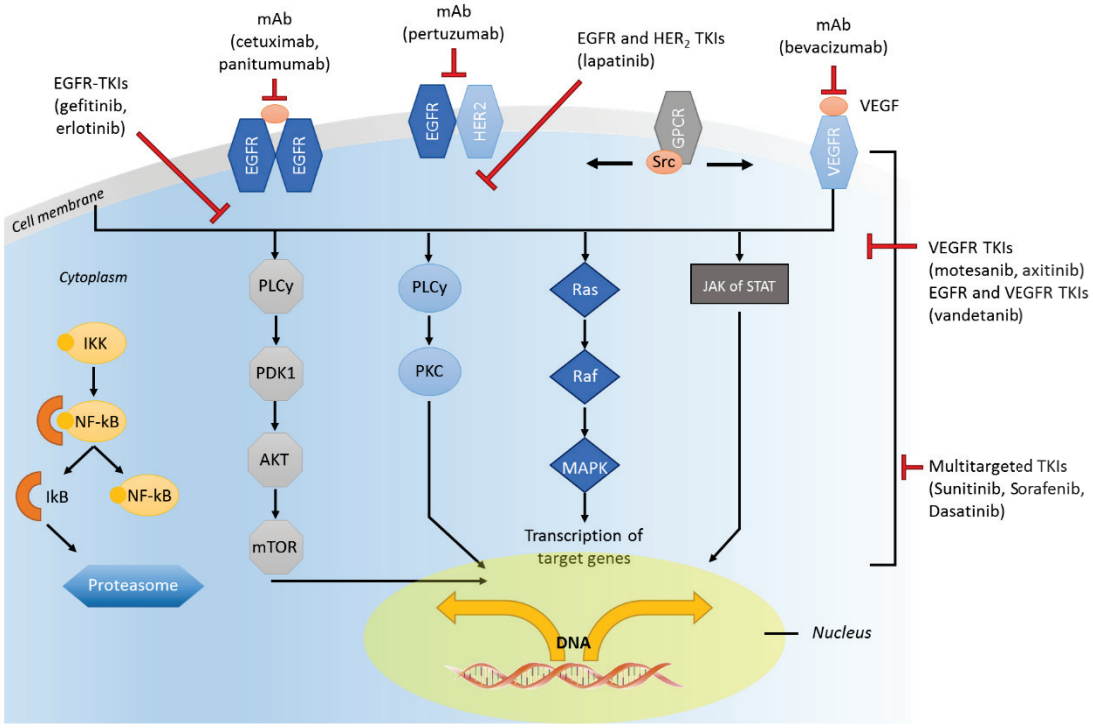


Figure 6: The complex signaling cascade at the cellular level in HNSCC with potential points of therapeutic targets. (Hoffmann, 2012).

### 3.4.2 **(Radio)-Immunotherapy**: a new arising type of targeted therapy

Several studies have suggested that the immune system has an important role in the therapeutic effects of radiation, promoting tumour cell death in the radiation field. In view of these interactions, combining radiation with checkpoint blockade immunotherapy could increase radiosensitization and improve local tumour control. Radiation-induced DNA and membrane damage, as well as cytoplasmic reactive oxygen species (ROS) activate many transcription factors and signalling pathways that modulate the immunophenotype and immunogenicity of tumour cells (Sharabi *et al.*, 2015) (Figure 7).

The changes in MHC class 1 expression that occur after radiation seemed to be mediated by radiation-induced activation of mTOR, and subsequent enhanced translation and antigen presentation (Reits *et al.*, 2006). Radiation also activates dendritic cells and enhances cross-presentation of tumour antigens resulting in activation and proliferation of tumour-specific CD8 T cells (Gupta *et al.*, 2012). The induction of antigen-specific immune responses is not sufficient for tumour eradication and cells of the adaptive immune system have to be able to infiltrate or invade into the tumour to eradicate it. In that sense, radiation has been demonstrated to increase tumour-infiltrating lymphocytes (Deng *et al.*, 2014; Sharabi *et al.*, 2015). Radiation has also been reported to modulate the expression of immune checkpoint

ligands, including PD-L1, on the surface of tumour cells and on immune cells in the tumour microenvironment (Parikh *et al.*, 2014). Many preclinical studies from several different groups have reported substantial increases in locoregional tumour control when radiation is combined with checkpoint blockade immunotherapy (Dovedi *et al.*, 2014; Deng *et al.*, 2014; Yoshimoto *et al.*, 2014) though it warrants further clinical investigation.

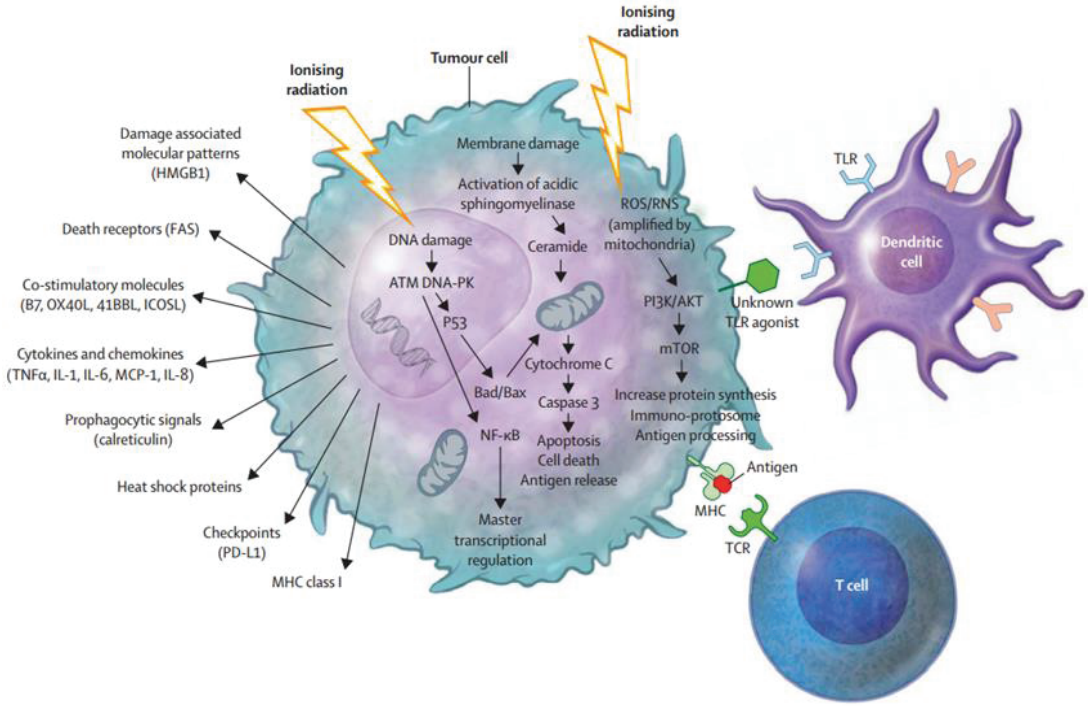


Figure 7*:* Radiation induces changes to the tumour cell immunophenotype (Sharabi *et al*., 2015).

In that sense, many murine studies have shown evidence for distant and persistent anti-tumour effects, which are probably immune-mediated, after radiosensitizing immunotherapy. The combination of radiation with anti-CTLA-4 antibodies was the first assay (Demaria *et al.*, 2005) that demonstrated a statistically significant improvement in local tumour control on a metastatic breast carcinoma cell line. Recently, similar results were obtained by Belcaid *et al.* (2014) using an orthotopic glioblastoma model to study the effects of stereotactic radiation combined with anti-CTLA-4 antibody (Belcaid *et al.*, 2014). Similar to anti-CTLA-4, several preclinical reports have noted the synergistic effects of radiation and anti-PD-1 immunotherapy on local control. Zeng *et al* (2013) used intracranial implantation of a mouse glioma cell line and presented evidence for a long-term survival of mice that received the combined treatment. In another study, Deng *et al* (2014) reported a significant improved local tumour control when radiation was combined with anti-PD-L1 in mouse models of breast and colorectal cancer (Zeng *et al.*, 2013; Deng *et al.*, 2014). All these results suggest immunotherapy as the fourth pillar in cancer treatment alongside surgery, chemotherapy, and radiation.

Immunotherapy is an arising treatment option that is being more and more studied for its potential as a cancer therapy option: it would be designed to boost the body's natural defenses in order to fight off cancer. This mode of therapy is of particular interest as the immune system plays a key role in the development of HNSCC, there is therefore a growing number of studies focusing on immunotherapy for HNSCC. Table 4 shows a selection of clinical immunotherapy trials in HNSCC patients.

FDA approved immunotherapeutic drugs

For recurrent or metastatic HNSCC patients (where the tumor does not respond to chemotherapy), there are two immunotherapeutic drugs that were approved in 2016 which are: pembrolizumab (Keytruda) which was approved by the FDA in August 2016, and Nivolumb (Obdivo), which was approved in November 2016. Both are immune checkpoint inhibitors. These two drugs were also approved for the treatment of certain patients that have advanced lung cancer or melanoma.

Pembrolizumab is a monoclonal antibody anti-PD-1 (programmed death-1) which potentiates the T-cells' responses, including anti-tumoral responses.

| Clinical trial title | Phase | Target | Population |
|---|---|---|---|
| Pembrolizumab (MK3475) Versus standard treatment for recurrent or metastatic Head and Neck Cancer (MK-3475-040/KEYNOTE-040) | III | PD-1 | R/M HNSCC after platinum failure |
| A study of pembrolizumab (MK-3475) for first line treatment of recurrent or metastatic squamous cell cancer of the Head and Neck (MK-3475 048/KEYNOTE-048) | III | PD-1 | R/M HNSCC first line |
| Tolerance and efficacy of pembrolizumab or cetuximab combined with RT in patients with locally advanced HNSCC (PembroRad) | II | PD-1 + Irradiation | Locally advanced HNSCC |
| Talimogene Laherparepvec with pembrolizumab for recurrent metastatic squamous cell carcinoma of the Head and Neck (MASTERKEY232) | I | PD-1 + oncolytic virus | R/M HNSCC after platinum failure |
| Trial of Nivolumab vs Therapy of investigator's choice in recurrent or Metastatic head and neck carcinoma (CheckMate 141) | III | PD-1 | R/M HNSCC after platinum failure |
| Study of Nivolumab in combination with Ipilimumab compared to the Standard of Care (Extreme Study Regimen) as First Line Treatment in Patients with recurrent or Metastatic Squamous Cell Carcinoma of the Head and Neck (CheckMate 651) | II | PD-1/CTLA-4 | R/M HNSCC first line |
| Safety study of Anti-LAG-3 with and without Anti-PD-1 in the treatment of solid tumors. | I | PD1/LAG-3 | R/M HNSCC immunotherapy naive |
| Study of MeDI4736 Monotherapy and in combination with tremelimumab versus standard of care therapy in patients with Head and Neck Cancer. | III | PD-1/CTLA-4 | R/M HNSCC after platinum failure |

Table 4: Selected clinical immunotherapy trials in HNSCC patients (Fuereder, 2016).

# Chapter II. Radiotherapy

As seen in the previous chapter, radiotherapy is very often used as a treatment option in HNSCC as an about 75% of patients with HNSCC will receive radiotherapy as their primary treatment or as adjuvant therapy. The concept of radiotherapy is the use of ionizing (high-energy) radiation in order to cause damages to cancer cells.

There are different types of radiations, of which not all are ionizing. Ionizing radiation is defined as a radiation, (energy emitted from a source), made-up of particles with sufficient energy to cause ionization when it encounters an atom in the medium through which it passes through, as it can remove tightly bonded electrons from it, and the atom therefore becomes charged.

The interaction of ionizing radiation with matter is characterized by the linear energy transfer (LET) which represents the density of energy absorbed by matter and is dependent on the distance travelled by the energy. LET is expressed in keV/µm and is represented by:

$$LET = dE/dl$$

Where: dE= the average energy transferred to matter,
dl: the distance travelled by the particle

The LET is dependent on two factors: the type of ionizing radiation and its energy. It is important to note that the energy deposited is different than the energy emitted by the source. The international unit used for ionizing radiation is Gray (Gy) which represents the number of Joules deposited for 1kg of matter.

## 1. *Interactions of ionizing radiations (photons) with matter*

The physical interactions between matter and particles are of three types:

- ✓ Atoms' ionization: if the energy of the incoming radiation is superior to the binding energy of electrons present in the matter, the electron is pulled off from its electronic cloud.
- ✓ Atoms' excitation: if the energy is not sufficient to pull-off the electron, it can still be sufficient to move the electron from its fundamental level to a level of higher energy, the atom is then excited.
- ✓ Thermal transfer: if the energy is not sufficient to excite the atom, it can be high enough to increase its kinetic energy of translation, rotation, and vibration, which is all known under the term of thermal transfers.

When ionizing radiation interacts with matter, a couple of physical interactions can occur including the photoelectric effect, the Compton effect, pair production, Thomson-Rayleigh diffusion, and/or nuclear reaction. The occurrence of these different phenomena depends on the kinetic energy of the incoming photons and the atomic number of the atoms encountered in their path.

### 1.1. The Photoelectric Effect

The **photoelectric effect** (Figure 8) is defined as the ejection of an electron from the surface of an atom following the interaction with an incoming photon, where the incoming photon has an energy equal or above the binding energy (W) of the electron. When the incident photon encounters an inner-shell of the atom and ejects an electron from this shell, the photon gives up all its energy to the electron which "flies-off" as a photoelectron carrying a kinetic energy equal to the photon energy minus W. At that time, the atom is in an excited state, to go back to its stable state, an electron from a higher orbital comes to fill out the space. The released energy that was needed, can then cause the emission of a fluorescent electron or be absorbed by another electron ejected from the atom, named the Auger electron (depicted in Figure 8).

The photoelectric effect is dependent on the atomic number of the matter crossed and when this last one is superior to 25, and occurs with incoming photons having a weak energy (inferior to 0.1 MeV).

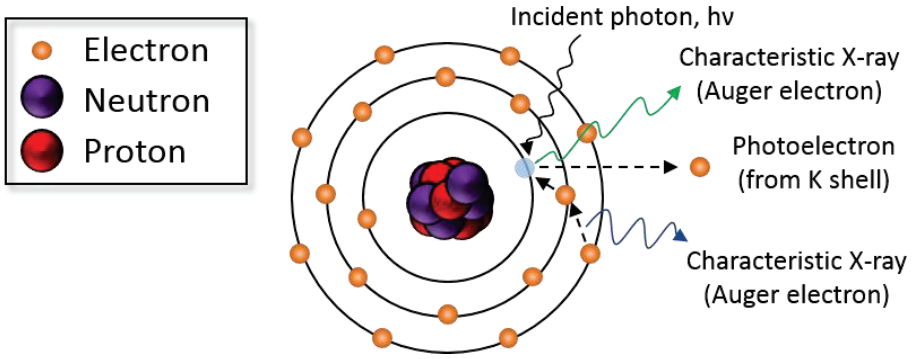


Figure 8: Representation of the photoelectric effect.

### 1.2. The Compton Effect

The **Compton effect** (Figure 9) occurs when the incident X-ray photon with relatively high energy (in average 1 MeV) ejects an electron from an atom and an X-ray photon of lower energy is scattered from the atom. The reaction produces an ion pair: a positive atom and a negative electron (recoil electron). The energy of the photon is distributed between the kinetic energy of recoil electron and the energy retained by the deflected photon. There are two

factors that determine the amount of energy the photon transmits. First, it depends on the initial energy (the higher the energy, the more difficult it is to deflect: high energy travel straight retaining most of the energy while low energy scatter back at an angle of 180°). The second factor is the angle of deflection, as the greater the angle, the less the energy is transmitted. With a direct hit, maximum energy is transferred to the recoil electron. The photon retains some energy and deflects back along its original path at an angle of 180°.

The probability of occurrence depends on the total number of electrons and the energy of radiation.

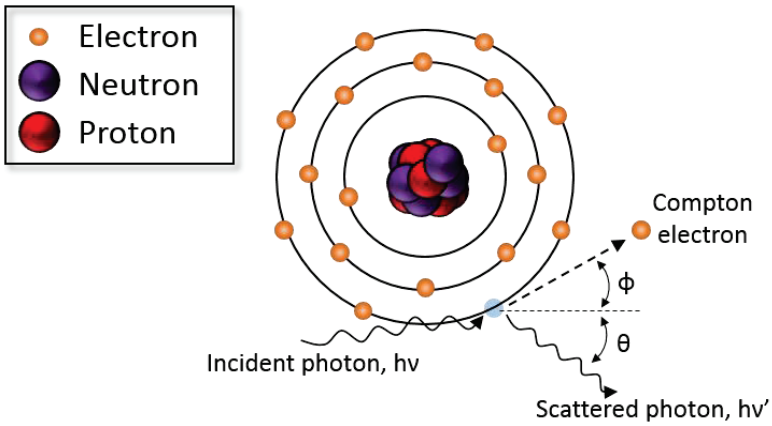


Figure 9: Representation of the Compton effect.

The similarities and differences between the photoelectric and Compton effects are summarized in the following table:

| **Photoelectric Effect** | **Compton Effect** |
|---|---|
| A low-energy phenomenon | A mid-energy phenomenon. |
| Photon delivers its total amount of energy to a single electron. | The photon transfers part of its energy to a single electron. |
| The photon disappears after the interaction. | The wavelength of the scattered photon is higher than that of the incident photon. |

Table 5: The photoelectric vs. Compton effect.

### 1.3. Pair production

An electron (●-) and a positron (●+) with the same mass and energy as the incident photon can be emitted from matter when the kinetic energy of the incoming photon is greater than 1.02 MeV (representing twice the mass of an electron at rest) and interacts with the atom's nucleus (see Figure 10). The emitted electron and positron lose their energy via ionization and excitation of the medium. The positron will undergo annihilation with a negative electron

of the environment, therefore emitting two γ-photons with individual energies of 0.511 MeV forming an angle of 180 degrees between them.

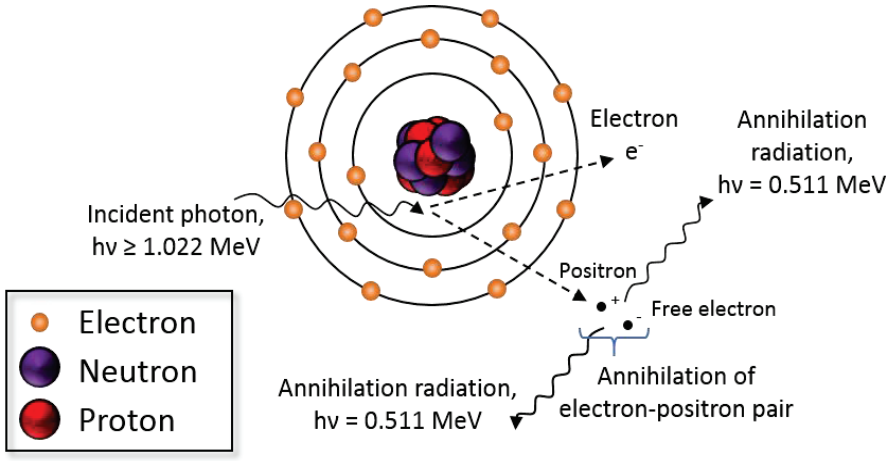


Figure 10: Representation of pair production.

The photoelectric effect, the Compton effect, and pair production are the three predominant types of interactions that occur during a radiotherapeutic treatment with the current photon energy used.

### 1.4. Thomson-Rayleigh diffusion

During the **Thomson-Rayleigh diffusion**, the incoming photon interacts with an electron which will absorb the energy and re-emits the electron with the same energy in another direction. However, it is important to note that this form of interaction does not occur often with ionizing radiation as this phenomenon occurs with very weak energy photons, such as those emitted in the specter of infrared, visible, and low-energy X-rays.

### 1.5. Nuclear reaction

A **nuclear reaction** will occur, as the name implies, when the incoming photon interacts directly with the atom's nucleus and there will be an emission of one or a few neutrons. Again, this interaction occurs very rarely in radiotherapy, as the photon energy required for this phenomenon to occur is quite high (greater than 10 MeV) which is very seldom used in medicine.

### 1.6. Predominance of each effect

The occurrence of each effect is dependent on the energy of the incoming photons as well as the atomic number of the elements present in the matter with which it will interact. These phenomena are well represented in the figure below.

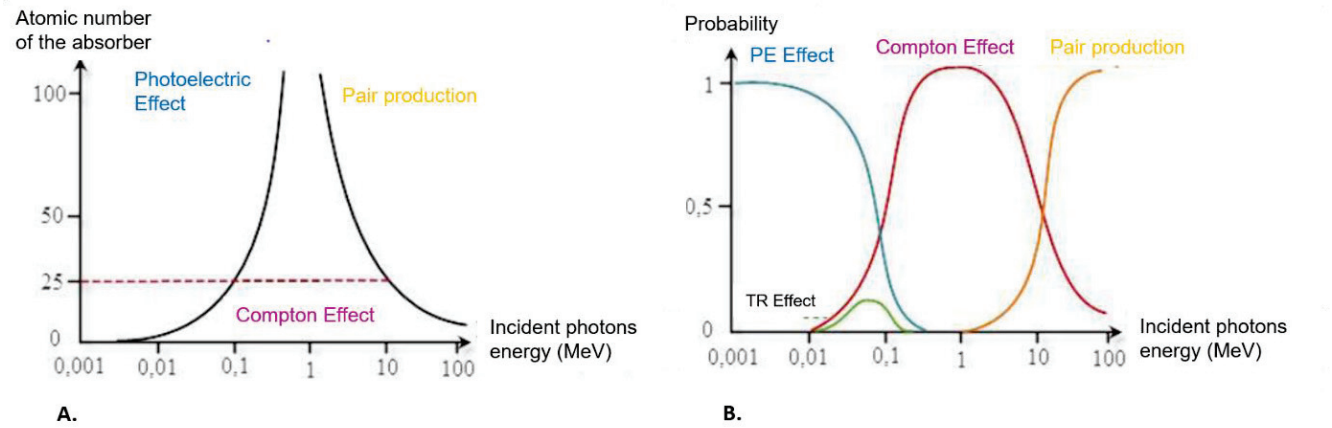


Figure 11: Relative importance of the three effects as a function of the incident photon's energy and the atomic number of the target: representation of the predominance of the photoelectric effect versus Compton effect versus pair production. **A**. Predominance of the different effects as a function of the absorbent type. **B**. Probability of having each physical effect as a function of the incident energy.

As previously mentioned, Thomson-Rayleigh diffusion is predominant in weak energy irradiation, while the nuclear reaction will occur solely if the photons' energy is very high. These effects occur in "extreme" cases, which make therefore make them rare in the medical field.

Therefore, the most predominant effects observed in the clinical field, are the photoelectric effect and pair production: these two effects are even so more dependent on the energy of the atomic number of the encountered matter. These interactions are therefore important when the atomic number of atoms encountered is superior to 25. The photoelectric effect is predominant in the case of low-energy photons (incident energy inferior to 0.1 MeV), while pair production is predominant when the incoming energy is superior to 10 MeV.

## *2. Biological effects of ionizing radiations: direct vs. indirect effect*

In order to simplify the understanding of the biological interactions of ionizing radiation with matter, we can distinguish two types of effects: direct and indirect. The subcellular target of direct effects is mainly DNA. The incoming electrons will directly cause damage to DNA, whereas the process goes through water radiolysis for indirect effects. These two types of effects are further discussed in the next paragraphs.

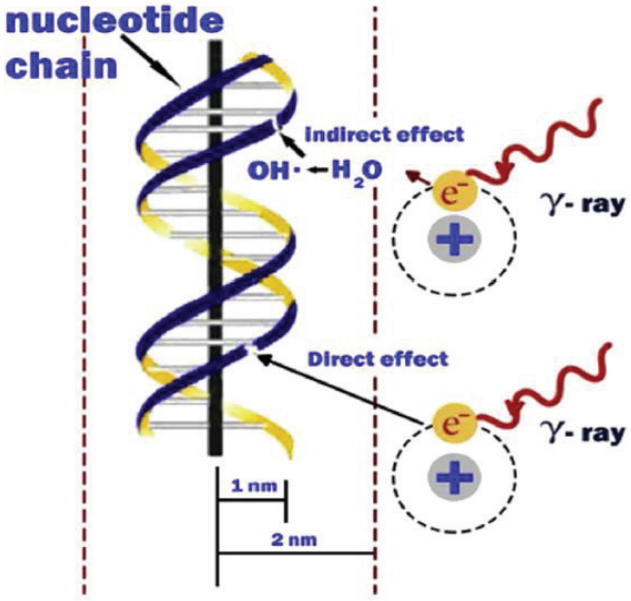


Figure 12: Direct vs. indirect effect following ionizing radiation. (Desouky *et al.*, 2015)

### 2.1. Direct effect

Ionizing radiation can have an effect with matter through the direct interaction of the electrons with cellular components: these molecules will therefore become excited or ionized. Radiation directly hits DNA, modifying its molecular structure. In order for the molecules to go back to their stable form, they will either release a photon of fluorescence or a rupture of a chemical covalent bond will occur and highly reactive species will appear. Electrons as well as these species will highly react with the cell's DNA. This interaction therefore leads to cell damage or even cell death if the cell is unable to repair the damage.

### 2.2. Indirect effect: water radiolysis

As cells are mainly composed of water (about 80%), an indirect effect can occur when the incoming radiation first interacts with the water molecules within cells (water radiolysis: see Figure 13). Following this interaction, free radicals will be produced, mainly hydroxyl (HO•) and alkoxy ($RO_2$•) (Jordan and Sonveaux, 2012). Free radicals are very highly reactive species that interact with DNA molecules and disrupt its structure. Hydrogen peroxide, $H_2O_2$, is also produced and is known to be toxic to cells, more so to DNA molecules.

These free radicals can also interact with other cellular organelles, such as mitochondria or other cellular constituents such as proteins, lipids, and will therefore cause damage to the cell.

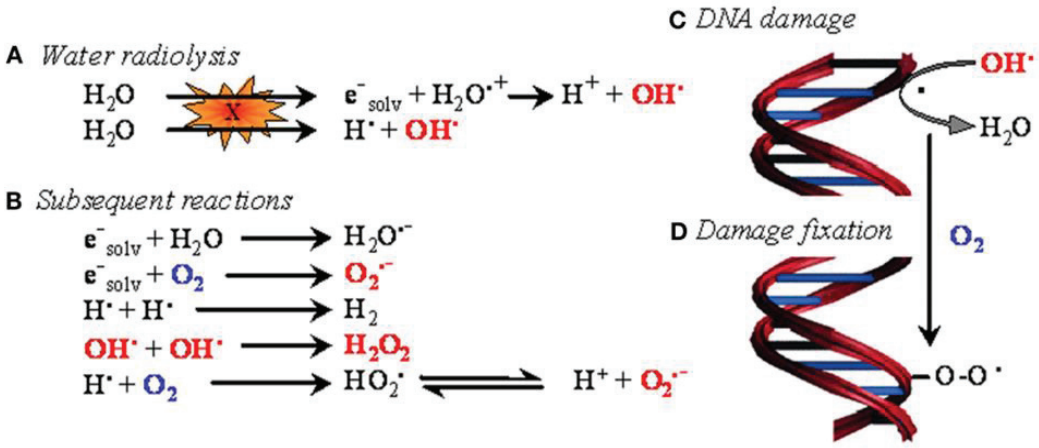


Figure 13: Schematic representation of the indirect effect of ionizing radiation. A. Water radiolysis. B. Subsequent reactions following water radiolysis. C. DNA damage. D. Damage fixation. (Jordan and Sonveaux, 2012).

## 3. DNA Damage induced by ionizing radiations and DNA damage repair

### 3.1. DNA damage

Following ionizing radiation, multiple DNA lesions can occur including base modifications, oxidative lesions, abasic sites, DNA-protein cross-link, single and double strand breaks. Figure 14 shows the different types of DNA damage that can occur while Table 6 shows the number of lesions caused by 1 Gray irradiation per nucleus.

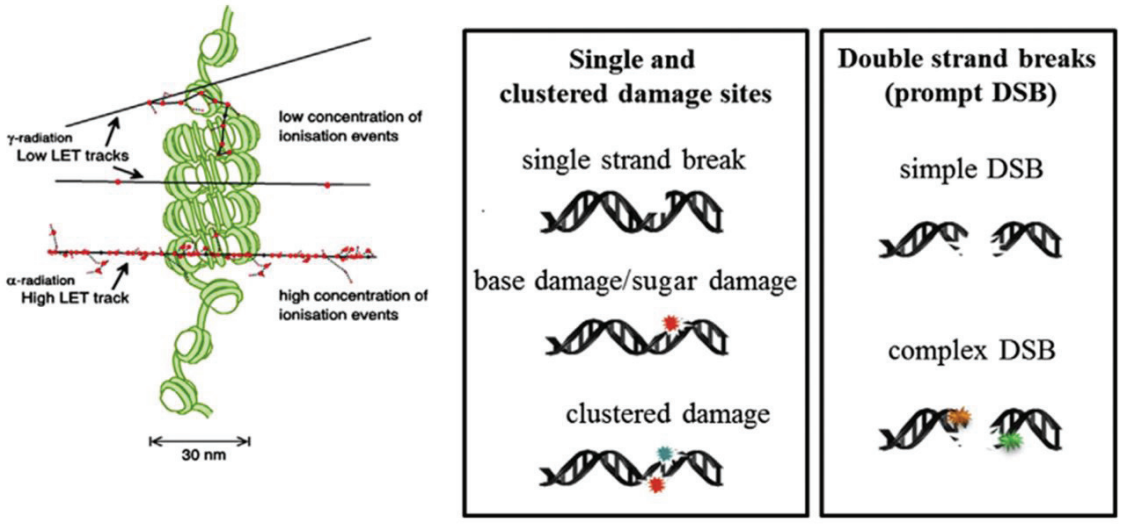


Figure 14: Types of DNA damage induced by ionizing radiation. (Lomax *et al.*, 2013)

| Type of DNA lesion | Number of lesions/Gray/Nucleus |
|---|---|
| Single-strand breaks | 750 |
| Double-strand breaks | 40 |
| Intra or inter-chain lesions | 30 |
| DNA-Protein bridging | 150 |
| Base Modifications | 1400 |
| Sugar Modifications | 1200 |

Table 6: Number of lesions per Gray per nucleus depending on the type of DNA damage.

Since not all DNA damages listed above were studied during this PhD work, I will only go further in details with three types of DNA lesions: base oxidation (8-oxo-guanine), single-strand breaks (SSBs), and double-strand breaks (DSBs).

### *3.1.1. Base modification*

Purine and pyrimidine bases, as well as the -ose constituents of DNA, can be oxidized by the hydroxyl radicals. One common type of base modification is the oxidation of the guanine base, the most frequent being 8-oxo-7,8-dihydrodeoxyguanine (8-oxoguanine).

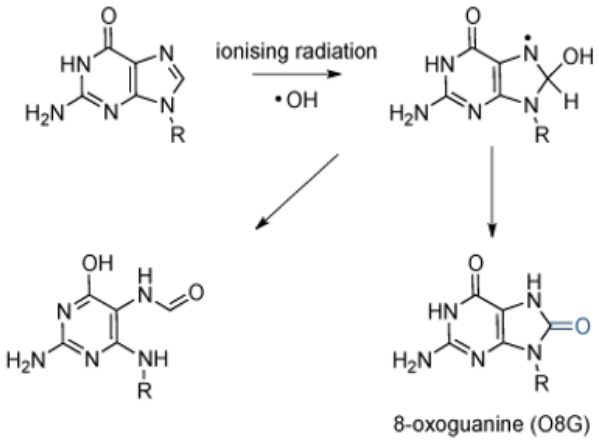


Figure 15: Oxidation of guanine following ionizing radiation. Molecular structure of guanine and 8-oxo-guanine. (Mutagenesis and DNA Repair, www.atdbio.com)

### *3.1.2. Single-strand breaks (SSB)*

Single-strand breaks are the result of the deoxyribose oxidation, which leads to the rupture of the phosphodiester bond between the phosphate and the deoxyribose (Evans *et al.*, 2004). This break leads to a spacing between the two DNA strands which allows water molecules to penetrate, which will in turn break the hydrogen bonds between the two DNA strands. The number of SSB increases with the radiation dose. However, these types of lesions are easily repaired by the cell and therefore has a low impact on the cell's viability.

### *3.1.3. Double-strand breaks (DSBs)*

Double-strand breaks are the result of, either a single hydroxyl radical on the deoxyribose with transfer of the formed radical on the opposite strand, or by two hydroxyl radicals going through the same regions in a lapse of time insufficient for the cell to repair the first break (Dikomey *et al.*, 1998). The number of these types of lesions is also dependent on the dose of irradiation, however these types of lesions are much harder for the cell to repair and therefore play an important role in the cell's fate: survival or death induced by irradiation.

DNA damage repair: Overview of the mechanisms involved

*Cell Cycle Checkpoint Regulation following IR-Induced DNA Damage*

The cells' fate is highly regulated by the cell cycle. In order to move through the cell cycle, the cell must pass checkpoints. Its successfulness in passing these checkpoints is highly dependent on the DNA's integrity. Two checkpoints exist during interphase, including the G1 checkpoint which will allow the cell to enter chromosomal replication, and the G2 checkpoint, which will allow the cell to enter mitosis. When the cell arrives at the checkpoint of the cell cycle, it will assess whether its genome is ready for division, or if repair needs to occur prior to division. Figure 16 shows the process a cell enters when it reaches a cell cycle checkpoint: a cell will have a few options depending on its DNA integrity. If the DNA has no errors it will progress to cell division. If the DNA needs repair, it will stop in the cycle and allow for the DNA to repair. If DNA repair is successful, the cell can progress to cell division. If the DNA is not repaired, one of two options can happen: the cell will die through apoptosis, or it will move on to cellular division however with mutations (which can lead to the development of cancer).

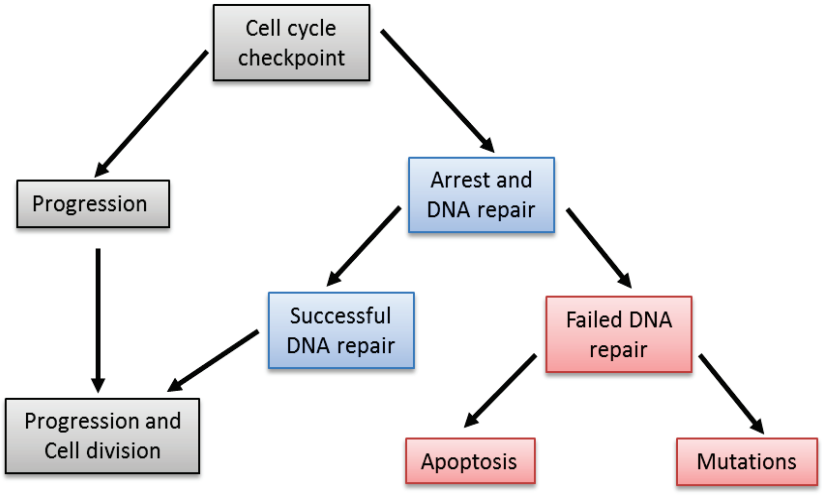


Figure 16: Potential fates of the cell at the cell cycle checkpoint. (Santivasi and Xia, 2014)

Ataxia Telangectasia mutated and Rad3 related (ATR) and Ataxia Telangectasia Mutated (ATM), two serine/threonine-specific protein kinases, are fundamental proteins involved in the repair of DNA-strand lesions. ATR is activated by the presence of single strand breaks,

generated from the uncoupling of helicase and DNA polymerase during replication fork stalling, while ATM is activated by double-stranded breaks. When SSB or DSBs are detected by ATR and ATM, these proteins are phosphorylated and activate downstream signaling for the repair of the lesions. Many different transducers and effectors are activated and play a role in these types of DNA repair (Santivasi and Xia, 2014; Brown and Baltimore, 2003; Jossen and Bermejo 2013; Lee and Paull, 2007).

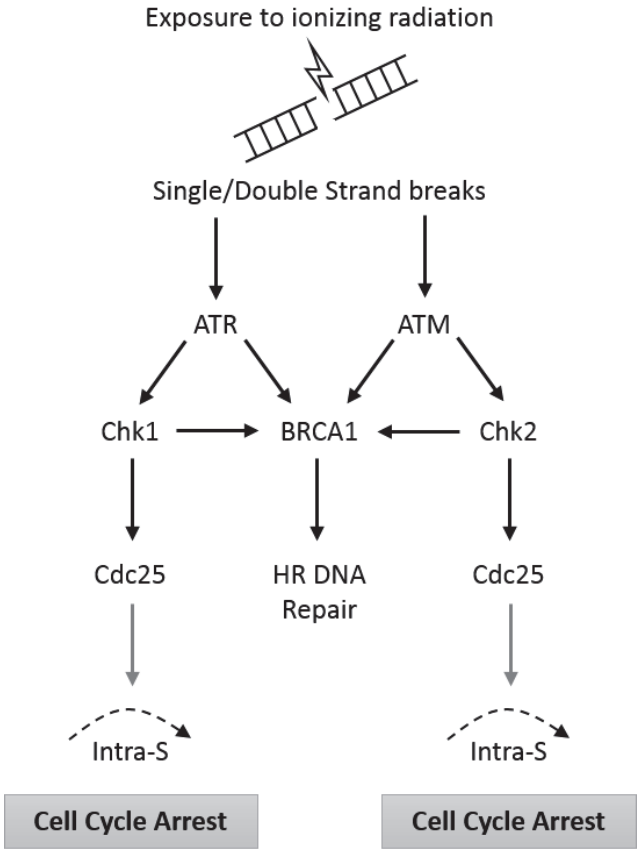


Figure 17: ATM and ATR regulate the S/G2 cellular response to DNA damage. (Santivasi and Xia, 2014)

Several DNA repair pathways exist depending on the type of DNA lesion. These include direct reversal, base excision repair (BER), nucleotide excision repair (NER), mismatch repair, homologous recombination (HR), and non-homologous end-joining (NHEJ). In the following paragraphs, we will focus on the three pathways studied in this work *i.e* for the repair of base oxidations, SSBs, and DSBs.

### *3.1.4. Base excision repair (BER)*

Base excision repair (BER) is by definition the repair system used for the repair of damaged bases resulting from small chemical modifications. BER can therefore be used for the repair of oxidized, methylated, alkylated or deaminated bases as well as abasic sites and single-strand breaks (Christmann *et al.*, 2003). The above-mentioned damages lead to a chemical structure modification of the DNA but does not deform its double-helix. This repair pathway is often

considered as the principal guardian of induced damages by the cellular metabolism, in particular from the oxidative stress (Hoeijmakers, 2001).

BER is composed of four main steps (see Figure 18) (Parsons and Dianov, 2013): 1. Recognition of the lesion by a DNA glycosylase specific to the damaged base, or by PARP1 in the case of a SSB; 2. Cleavage of the phosphodiester bond by an AP endonuclease (this step will not occur in SSB repair); 3. Repolymerization by specific proteins; 4. Ligation of the newly synthesized nucleotides.

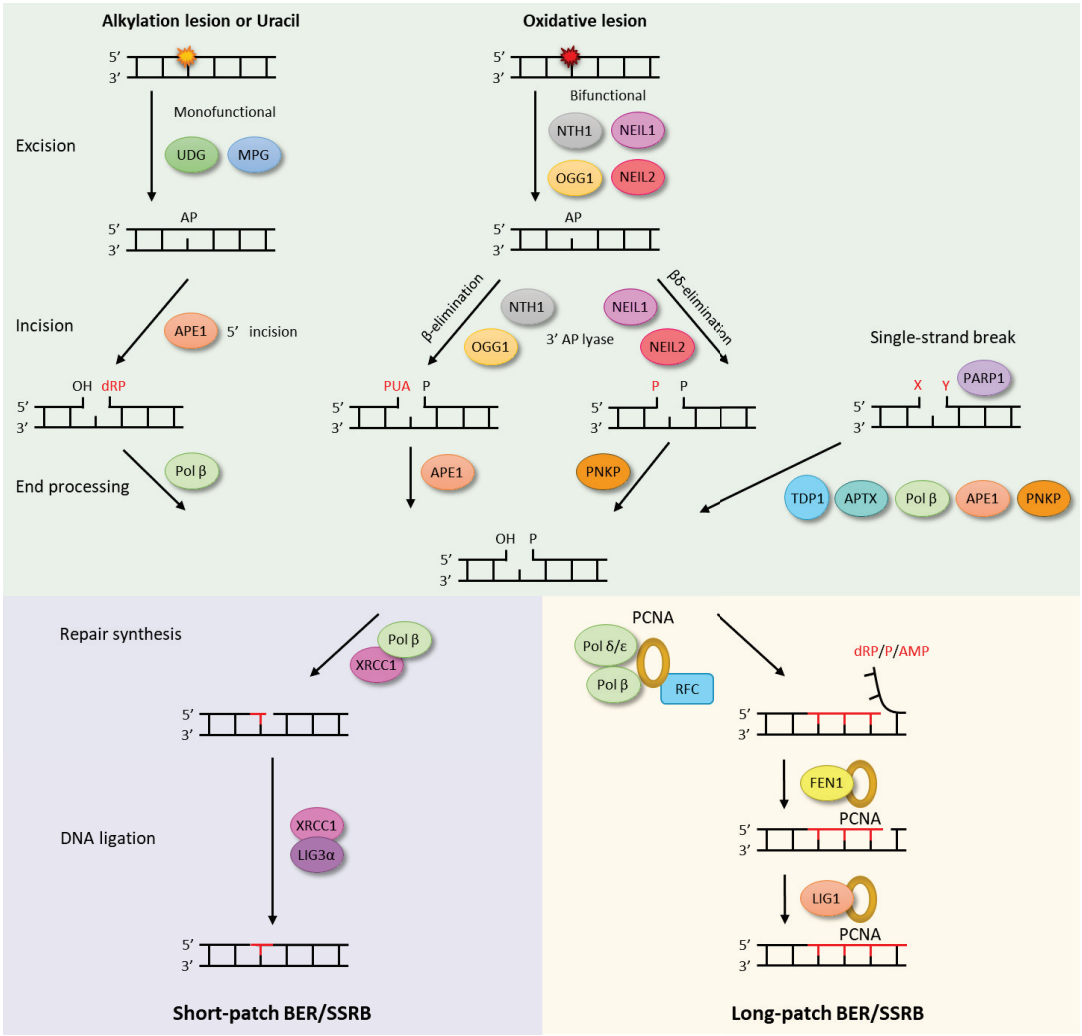


Figure 18: Schematic representation of the base excision repair pathway (BER) (Jeppesen *et al.*, 2011).

### *3.1.5. Homologous recombination (HR) and non-homologous end joining (NHEJ)*

Following double-strand breaks of DNA after ionizing radiation, the cell will respond using one of the two adequate repair mechanisms: homologous recombination (HR) or non-homologous end joining (NHEJ) (Figure 19). If the damages are not repaired or not properly repaired, DSBs can be sufficient to trigger apoptosis (Frosina, 2009).

In homologous recombination (HR), the cell uses a DNA template in order to re-synthesize the new DNA strand: it is characterized by deriving the correct sequence from a homologous strand of intact DNA, making it a "high-fidelity" repair (Santivasi and Xia, 2014). This mechanism uses nuclease-mediated resection of damaged DNA ends, polymerization of new DNA, and ligation to restore strand integrity (Santivasi and Xia, 2014). This repair pathway is mainly used during the S and G2 phases of the cell cycle.

Non-homologous end joining (NHEJ) functions occurs during the G1 phase of the cell cycle and will repair a wide variety of DSBs with distinct break structures and sequences (Lieber *et al.*, 2003). NHEJ is mainly regulated by DNA-PK and KU. Compared to HR, NHEJ shows little fidelity as it does not use or uses little homologous template to repair the break. This type of repair consists in digesting the damaged base, repolymerization/repair, and finally digestion (Weterings and Chen, 2008).

It was suggested that there is a connection between the malfunction of NHEJ and radioresistance: in several types of cancer, in particular in glioblastoma multiforme (GBM), the increased function of DNA-PK, primary enzyme used in NHEJ, was demonstrated to increase radiation resistance (Santivasi and Xia, 2014; Burma and Chen, 2004).

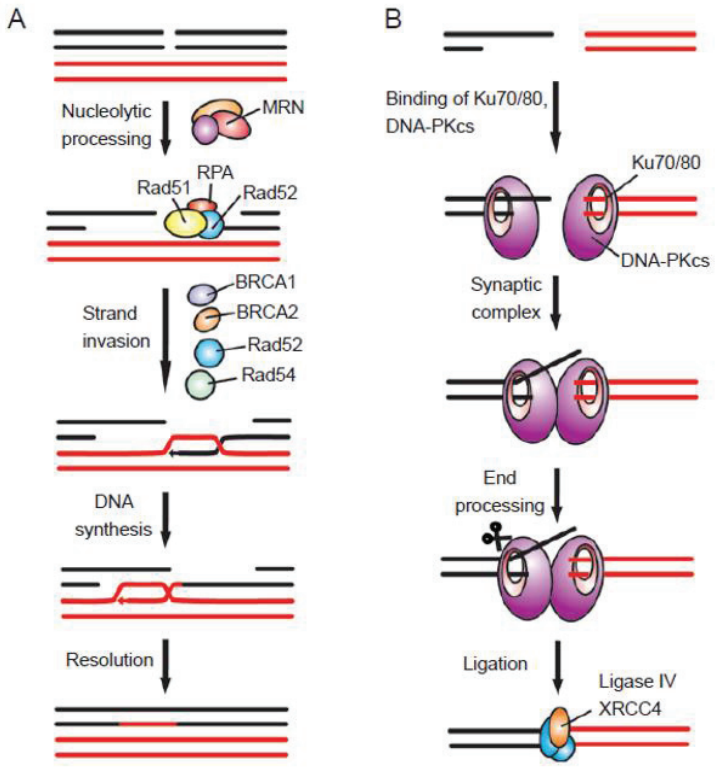


Figure 19: Overview of **A**. homologous recombination and **B**. non-homologous end-joining (Weterings and Chen, 2008).

## *4. Radiosensitizing strategies*

As mentioned above, radiation therapy plays an essential role in the treatment of numerous cancers including head and neck squamous cell carcinoma, yet therapeutic efficacy is hindered by treatment-associated toxicity and tumor recurrence. Moreover, a complementary approach is to explore mechanisms of reducing normal tissue injury that is induced by ionizing radiation, which is especially important in dose-escalation studies that aim to increase tumor control probability. Both approaches, increasing tumor cell kill and decreasing morbidity, can improve cure rates and the quality of life of cancer patients undergoing radiotherapy. Central to success is finding and exploiting genetic or microenvironmental differences between normal and malignant tissues.

Ionizing radiation as applied in the radiotherapy clinic induces a complex response in cells. Some processes aim to repair damage, whereas others counteract propagation of the damage or induce cell death. In addition, many aspects of the tumor microenvironment, such as hypoxia or vasculature development have been widely investigated with respect to improving radiotherapy. As the mechanisms that contribute to radioresistance are numerous, an extensive literature has been proposed for the understanding and the reversal of this phenomenon which cannot therefore be fully exposed in this manuscript. Among all the strategies explored, one can mention the modulation of the DNA damage response, the modulation of the cell cycle checkpoints, the modulation of the signal transduction pathways, receptor targeting strategies, the modulation of the microenvironment, the targeting of cancer stem cells (CSCs), and other directions, further described in the sections below.

### 4.1. Modulating the DNA damage response

Owing to genetic instability, tumors are often defective in one aspect of DNA repair but usually have backup pathways for accomplishing repair. Attacking these backup pathways can render the tumor radiosensitive while leaving the normal tissue relatively resistant. Inhibitors of important molecules in DNA damage repair, such as ATM (Zou *et al.*, 2008 ; Biddlestone-Thorpe *et al.*, 2013 ; Vecchio *et al.*, 2014 ; Dohmen *et al.*, 2017), ATR (Fokas *et al.*, 2012 ; Vávrová *et al.*, 2013 ; Šalovská *et al.*, 2014), DNA-dependent protein kinase (DNA-PK) (Du *et al.*, 2010 ; Niazi *et al.*, 2014 ; Dolman *et al.*, 2015 ; Mamo *et al.*, 2017) but also RAD 51 (Kobashigawa *et al.*, 2015 ; King *et al.*, 2017) or PARP (Hirai *et al.*, 2012 ; Wuster *et al.*, 2016 ; Lohse *et al.*, 2016) have been shown to sensitize cancer cells to radiotherapy. Besides DNA repair, other targets may be mentioned such as telomerase (Wang *et al.*, 2015 Wu *et al.*, 2017), histone deacetylase (Hehlgans *et al.*, 2013; Barrazuol *et al.*, 2015; Chun *et al.*, 2015). Transcription factors such as STAT3 (Bonner *et al.*, 2009; Zhang *et al.*, 2015; Ouédraogo *et al.*, 2016), TCF4 (Kendziorra *et al.*, 2011) or NFκB (Kim *et al.*, 2005; Watson *et al.*, 2009) have also been suggested as potential radiosensitizing targets.

Due to potential toxicity, only very few inhibitors of repair are on the market with an FDA approval. Ongoing clinical trials and targets are summarized in Annex 1.

Integrin cell adhesion molecules, as well as their associated adaptor proteins are also attractive targets which may play a crucial role in tumor cell resistance to cancer therapy (Cordes *et al*., 2006; Eke *et al*., 2013; Eke *et al*., 2012; Cordes *et al*., 2006; Nam *et al*., 2010; Weaver *et al*., 2002; Damiano *et al*., 2001; Cordes *et al*., 2003; Gao *et al*., 2014; Mantoni *et al*., 2011; Cabodi *et al*., 2010). Indeed, many essential pro-survival signals come from the tumor microenvironment including integrin-mediated cell adhesion to the ECM (Cordes et al., 2003; Hanahan and Weinberg, 2011). β1 integrin is an interesting radiosensitizing approach, as their targeting has shown a promising approach to overcome HNSCC radioresistance (Cordes, 2006; Eke *et al*., 2012; Cordes and Park, 2007; Eke *et al*., 2012). β1-integrin-mediated adhesion was shown to confer radioresistance due to their role in the regulation of DNA repair via the FAK/JNK1 signaling pathway (Dickreuter *et al*., 2015). In a recent study, Steglich *et al*. (2015) used a siRNA targeting the α3 integrin which resulted in a reduced clonogenic survival and enhanced radiosensitivity through the induction of apoptosis. It was demonstrated that these events were associated with the decrease of the phosphorylation of Akt, Cortactin and Paxillin. Moreover, the simultaneous inhibition of α3 and β1 integrin led to higher cytotoxicity and radiosensitization compared to α3 integrin alone (Steglich *et al*., 2015), a result which was however cell line-dependent.

Another dual targeting option, involving β1 integrin and EGFR, was tested in order to counteract inhibit radioresistance in HNSCC. The combined β1 integrin-EGFR targeting resulted in an enhanced cytotoxicity and radiosensitization in eight out of ten tested HNSCC cell lines, as a result of FAK dephosphorylation. *In vivo* experiments targeting integrins also showed a better tumor control. (Eke *et al*., 2015). Very recently, Koppenhagen *et al*. (2017) hypothesized that c-Abl tyrosine kinase could be an important mediator of β1 integrin signaling for radioresistance. They demonstrated a greater degree of radiosensitization in a subset of cancer cell lines with simultaneous β1-integrin/c-Abl targeting compared to monotherapies. This showed that c-Abl is an important determinant of radioresistance in cell lines originating from different solid tumors (Koppenhagen *et al*., 2017). And again, this showed the benefits of dual- or multi-targeting therapies.

### 4.2. Modulating cell cycle checkpoints

Interfering with the cell cycle control might result in a loss of G1 or G2/M block, failure of DNA repair and, thus, induction of cell death. Numerous *in vitro* studies have been published about the use of checkpoint kinases (CHKs) or cyclin-dependent kinases (CDKs) inhibitors as radiosensitizing agents. Among these, one can quote the specific inhibition of CHK-1 (Wang *et al.*, 2012; Collins *et al.*, 2013), CHK-2 (Jobson *et al.*, 2009; Riesterer *et al.*, 2011) or CDKs (Kodym *et al.*, 2009; Raqhavan *et al*., 2012). On the basis of these successful *in vitro* studies, second-generation pyridopyrimidine-derived inhibitors with high specificity towards CDK4/6 are for example being tested clinically (Michaud *et al.*, 2010). Palbociclib (PD0332991, PD) has received FDA approval for potential treatment of breast cancer, and Abemaciclib (LY2835219)

is undergoing a phase III trial for breast and lung cancer (Gelbert *et al.*, 2014; Barton *et al.*, 2013). However, only few pre-clinical studies have up to now addressed the combination of CDK-inhibitors with radiotherapy (Cen *et al.*, 2012; Barton *et al.*, 2013).

### 4.3. Modulating signal transduction pathways

As important intracellular factors, aberrant tumor transmembrane signal transduction pathways, which include the prosurvival cascades (PI3K／Akt, MAPK／ERK and JAK／STAT) and the pro-apoptosis pathways (Wnt), p53 and TNF-α／NF-κB), have been proved to be crucial determinants of the probability of cell sensitivity to radiation in various malignancies. Among the strategies inhibiting proliferative pathways, one can mention the PI3K/Akt pathway after combination of LY294002 and radiation (Liu *et al.*, 2011), BKM120 and radiation (Liu *et al.*, 2014) or PI3K/mTOR pathway after combination of NVP-BEZ 235 and radiation (Maity *et al.*, 2011 ; Potiron *et al.*, 2013 ; Kuger *et al.*, 2013).

Considering the MAPK/ERK pathway, AZD6244 has been reported to enhance radiosensitivity (Chung *et al.*, 2009). The co-targeting of PI3K and MAPK has also been successfully investigated (Williams *et al.*, 2012). With regard to the JAK/STAT pathway, several chemical compounds, including S3I-201, Stattic, STA-21 and a JAK kinase inhibitor AG490 have been reported to successfully inhibit JAK. STAT signaling and effectively improve the sensitization to radiation of tumors without obvious toxicity (Kim *et al.*, 2008). Among the strategies promoting pro-apoptotic pathways, the Wnt signaling pathway has been explored through the use of niclosamide (Yin et al, 2016), curcubitacin B (Duangmano *et al.*, 2012), LGK-974 (Tian *et al.*, 2017) or miRNAs (hsa-miR-138-2-3p); according to the predicted genes and pathways of differential miRNAs target, down-regulated expression of has-miR-138-2-3p under radiation was thought to play a key role in enhancing the radio-sensitivity in human laryngeal squamous cancer stem cells (Zhu *et al.*, 2017) as radiosensitizing agents.

Although understanding the cellular and molecular basis for innate and acquired resistance of cancer cells to radiotherapy is a prerequisite for overcoming this difficulty, there are potential concerns and challenges related to the clinical use of current targeted drugs owing to their low cancer selectivity and specificity. Therefore, the development of multi-targeting agents or direct conjugation of multifarious therapeutic molecular agents may accomplish promising efficacy.

### 4.4. Receptor targeting strategies

The recent shift to the development of anticancer therapies that target specific alterations in cancer cells, fueled by the clinical success of monoclonal antibodies (mAb) targeting growth factors or their receptors and inhibitors of receptor tyrosine kinases (TK) has also sparked an interest in combining molecular targeted therapies with radiation therapy. Bevacizumab, a monoclonal antibody against vascular endothelial growth factor A (VEGF-A), is a pioneering

targeted agent that has been studied in large clinical trials (Schmidt *et al.*, 2012). Although the toxicities of treatments were acceptable, similar survival to historical control were generally obtained, whatever the type of cancer studied (Small *et al.*, 2011; Chinot *et al.*, 2014). Concerning the Epidermal Growth Factor Receptor (EGFR), which is known to play an important role in tumor progression and treatment resistance for many types of malignancies including head and neck, colorectal and nonsmall lung cancer, many studies have shown the *in vitro* efficiency of anti-EGFR-targeted therapies in combination with radiotherapy (Raben *et al.*, 2005; Wang *et al.*, 2011; Lu et al, 2012). To date, the only FDA approved use of an anti-EGFR therapy (cetuximab) in combination with radiation therapy is for locally advanced head and neck cancer. In a large, multi-institutional, randomized trial, Bonner *et al.* (2010) reported an overall survival benefit when adding cetuximab to RT in locally advanced HNSCC. However, the follow-up study, RTOG 0522, which added cetuximab to cisplatin-based chemoradiation for locally advanced HNSCC, did not show a survival benefit with the addition of cetuximab (Ang *et al.*, 2014). Similarly, a recently reported randomized phase III trial for stage IIIA/B non–small-cell lung cancer (NSCLC), RTOG 0617, demonstrated no clinical benefit with the addition of cetuximab to standard or dose-escalated chemoradiation (Bradley *et al.*, 2015). A related EGFR antibody, panitumumab, has been examined in the randomized phase II trials for HNSCC, CONCERT-1 (Mesia *et al.*, 2015) and CONCERT-2 (Giralt *et al*, 2015): both treatments demonstrated no additional benefit with the addition of panitumumab.

Apart from anti-EGFR receptor antibodies, other small molecules such as EGFR-receptor tyrosine kinases inhibitors (erlotinib, afatinib…) have been reported to radiosensitize cancer cells *in vitro* (Tsai *et al.*, 2013; Huguet *et al.*, 2016). Although a phase II trial of erlotinib combined with temozolomide in addition to RT in glioblastoma multiforme reported better survival than historical controls (Prados *et al*, 2009). However, a randomized phase II trial comparing erlotinib plus cisplatin-based chemoradiation with chemoradiation alone in patients with locally advanced HNSCC demonstrated no difference in clinical complete response rates between the two groups (Martins *et al.*, 2013). So, there are many single institutional case series that have provided mixed data, with some suggesting safety and others suggesting unexpected toxicities. Despite this and given the important role EGFR plays in several types of cancer and the well-defined role of EGFR in the response to radiation therapy, this receptor remains an important target for radio- and chemoradiosensitization.

Another interesting target is the targeting of integrins as it was previously described in section 4.1.

### 4.5. Modulating the microenvironment

Two aspects of the tumor microenvironment have been widely investigated with respect to improving radiotherapy, namely hypoxia and vasculature development. Both can exert a considerable influence on the response to ionizing radiation and both are valid targets for improving the response to therapy. Considering the fact that hypoxia render cells more

resistant to killing by ionizing radiation, several groups suggested that inhibition of HIF-1α (a product of hypoxia-inducible genes) is a promising strategy for radiosensitization (Kessler *et al.*, 2010; Yang *et al.*, 2014; Jin *et al.*, 2015; Wozny *et al.*, 2015). Pre-treatment of tumors with elevated levels of oxygen prior to radiotherapy may represent a means for selectively targeting radiation-resistant hypoxic cancer cells, and could serve as a safe and effective adjuvant to radiation therapy (Clarke *et al.*, 2014). Recently, the use of oxygen mimetics was suggested as an innovative approach to the therapy management of resistant tumors (Kumar *et al.,* 2015). The second approach concerns the development of the vascular system, which is essential for progressive tumor growth. Treatments targeting angiogenesis, thus resulting in microvessel destabilization, was reported to potentiate irradiation in vitro and in vivo in cancer cells but not normal cells (Maggiorella *et al.*, 2009). More recently, Nox4 knockdown was demonstrated to suppress glioblastoma cells proliferation, invasion, and tumor associated angiogenesis, thus increasing their radiosensitivity *in vitro* (Li *et al.*, 2014).

### 4.6. Targeting cancer stem cells (CSCs)

The CSCs, also referred to as 'tumor-initiating cells,' possess inherent abilities such as self-renewal, differentiation, pluripotency and resistance to conventional chemo- and radiotherapies. These cells are also capable of invading and migrating to other tissues (metastasis). The end result is a highly recurrent, refractory and metastatic disease, following chemo- and radiotherapy. It has been suggested that the degree of radiosensitivity of the intact tumor may correlate with the number of CSCs at the time of treatment. Moreover, the ability of the remaining surviving cells at the end of radiation therapy to re-establish the CSC niche also influences the final outcome of radiation treatment. Targeting CSCs remains therefore an attracting challenge to overcome treatment failure and recurrence. In that sense, many attempts have been made to selectively kill these cells including selective targeting of cell cycle (Han *et a*l, 2013 ; Bertrand *et al.*, 2014), DNA damage response pathways (Lim *et al.,* 2014 ; King *et al.*, 2017), signal transduction pathways (Kahn *et al.*, 2014), anti-apoptotic pathways (Berghauser *et al.*, 2014; Gilormini *et al.,* 2016) or through the use of miRNA (Yang *et al.*, 2015 ; Zhu *et al.*, 2017). Carbon ion exposure has also been proposed as a promising and more effective tool to eradicate CSCs compared to photons (Bertrand *et al.*, 2014; Park *et al.*, 2017).

### 4.7. Other directions

Outside the targets mentioned above and apart from nanotechnologies, many reports have proposed other promising strategies to improve radiosensitization: modulation of oxidative stress (Boivin *et al.*, 2011; Xu *et al.*, 2013; Sun *et al.*, 2015), inhibition of heat shock proteins (Aloy *et al.*, 2008; Kabakov *et al*., 2010 ; Schilling *et al.*, 2017), ceramide metabolism (Alphonse *et al.*, 2004 ; Pchejetski *et al.*, 2010 ; Morad *et al.*, 2013), Bcl-2 family (Loriot *et al.* 2014; Zerp *et al.*, 2015; Gilormini *et al*., 2016), microtubule manipulation (Hoffstetter *et al.*, 2005 ; Forde

*et al.*, 2011). Various molecules such as curcumin (Verma, 2016), metformin (Koritzinski, 2015) or mitochondrial metabolism-interfering agents (Mitrakas *et al.*, 2014) have also been studied.

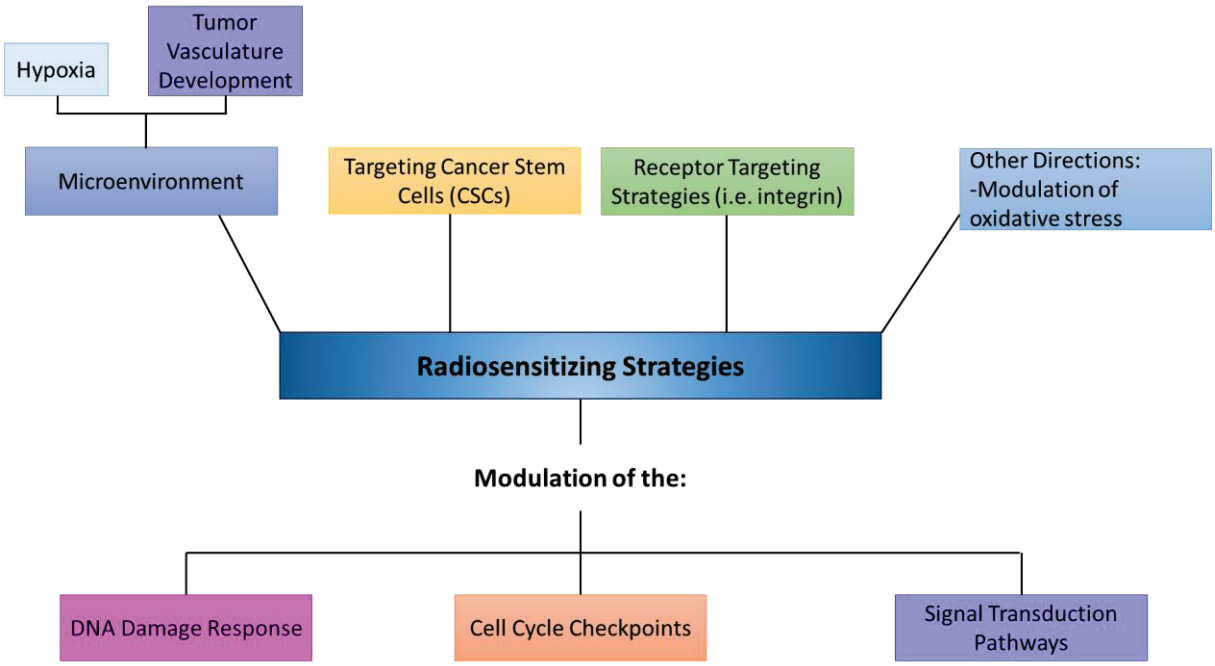


Figure 20: Schematic representation of existing and future radiosensitizing strategies for HNSCC.

# Chapter III. Nanotechnology: the rise of nanomedicine

As seen in the first chapter of this bibliography review, the 5-year survival for head and neck squamous cell carcinoma is quite low as it is less than 50%. In order to increase survival as well as the patient's quality of life, radio-sensitizing strategies are being more and more studied to increase radiotherapy efficacy. At the end of chapter 2, various radiosensitizing strategies were presented, however the focus of this PhD work is the use of nanoparticles to increase radiotherapy efficacy. As depicted in Figure 21, various approaches are available to do so. Our work will specifically focus on the use of gadolinium-based nanoparticles, a type of metal-based nanoparticles, as radiation sensitizers. However, prior to focusing our attention to Gd-based nanoparticles, we will first review the literature to discuss the background of nanotechnology and the rise of nanomedicine, the different definitions and notions that are important to know and understand, as well as discuss the different types of nanoparticles that exist as radiosensitizers.

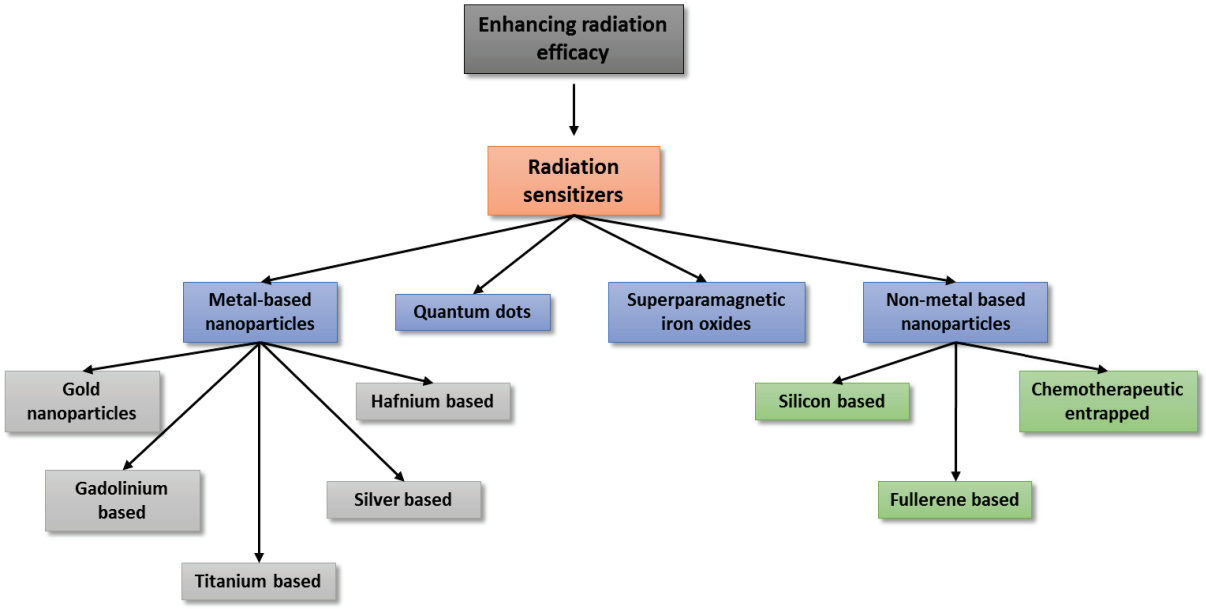


Figure 21: Different approaches for enhancing radiation efficacy with nanotechnology (Inspired from Kwatra *et al.*, 2013).

## 1. Generalities

Nanosciences can be defined as "the science and engineering implicated in the design, synthesis, characterization, and application of materials and devices whose smallest functional organization in at least one dimension is on the nanometer scale." (Silva, 2004)

Nanosciences can also be described as the understanding and control of matter that have a **dimension of roughly 1 to 100 nm, where unique phenomena enable novel applications**, and therefore can widely be used in biology and in medicine. Presently, 95% of all new potential therapeutics has poor pharmacokinetics and biopharmaceutical properties. There is

a huge need for novel drug fabrication in order to have specific interactions with the diseased tissue only. Therefore, one of the greatest values of nanosciences will be in the development of new and effective medical treatments as they open many opportunities for imaging, diagnostics, and specific drug delivery to diseased sites.

It is important to note the physico-chemical characterizations of nanomaterials which is of the outmost importance for nanomedicine applications.

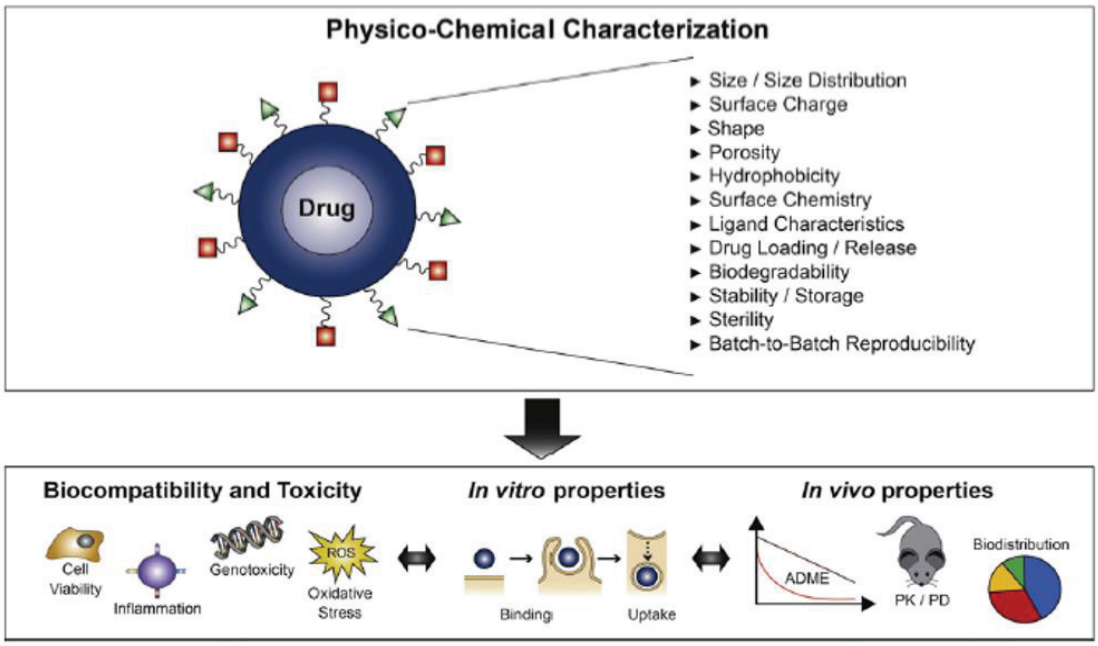


Figure 22: Cascade for nanomaterial characterization. The physico-chemical properties of nanocarriers affect their pharmacokinetic and pharmacodynamic profiles. Detailed characterization of nanomedicine products is necessary to predict their performance in the clinical setting. (Wicki *et al.*, 2015)

Nanotechnologies being a field with promises in a variety of applications is receiving increasing global investment from governments and industries (Paull *et al.*, 2003). Worldwide investment in nanotechnology-related research & development by government organizations has considerably increased as well as the number of publications and clinical trials (Figure 23).

In France, nanosciences and nanotechnology mobilize more than 5 300 researchers in 240 laboratories (Campus France, La recherche en nanosciences en France) and is ranked second after Germany for their investment in nanosciences' research, and 5$^{th}$ worldwide in terms of publications (Invest in France Agency, Les Nanotechnologies en France).

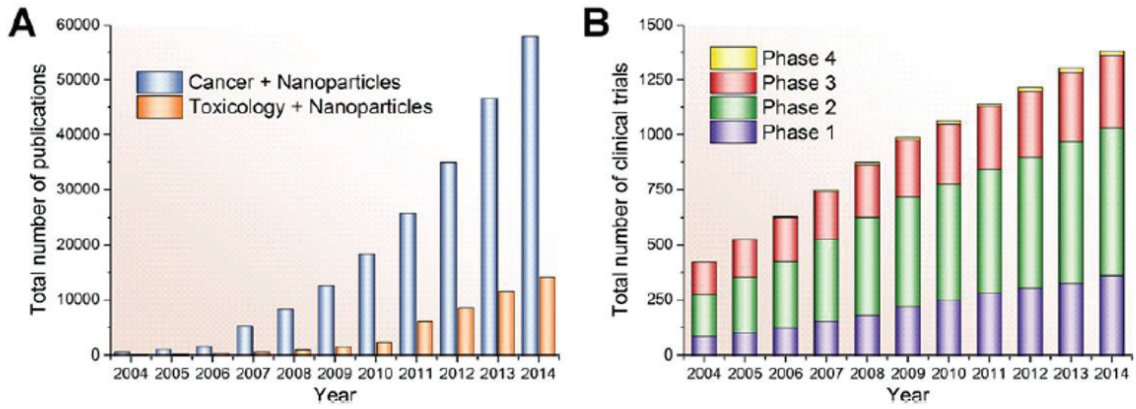


Figure 23: "Total number of publications (Web of Science®) and clinical trials (clinicaltrials.gov) during the last 10 years. (**A**) The number of publications in the field of nanoparticles for cancer therapy is increasing exponentially. The ratio between new publications in the field of cancer and new publications in the field of toxicology has remained stable over the last 4 years. (**B**) The number of launched clinical trials (phases 1, 2, 3, 4) investigating nanomedicine drugs for cancer therapy is increasing constantly over the last 10 years. However, the total number of clinical trials is only about 2% of the total number of publications in the field of cancer nanomedicine." (Wicki *et al.,* 2015).

### 1.1. Nanotechnologies for medical applications: Nanomedicine

An important growing field within nanotechnologies, is the development of nanomedicine in various domains including cancer diagnostics and therapy, neurology, cardiac diseases, lung diseases, vaccine delivery… (Thorley A. and Tetley T., 2013) Nanomedicine uses nanoscale materials, such as biocompatible nanoparticles and "nano-robots" for the diagnosis, delivery, sensing, or triggering purposes in a living organism.

### 1.2. Nanomedicine for cancer

One of the greatest hopes within medicine with nanotechnology is the potential for significant advances in the field of oncology. The transition from unspecific therapies to therapies which can target cancer growth with very considerable specificity can be realized with bio-nanotechnologies. Current popular cancer treatments such as chemotherapy and radiation therapy are non-specific. This leads to healthy tissue being damaged in the same way as cancerous tissue, limiting the dose that is safe for a patient to receive. In order to maximize the success of this nanoscale approach to cancer treatment, it remains necessary to learn more about the biological processes which drive cancer growth, the mechanisms which bind particles to cells, the course of uptake of particles within cancer cells as well as the biological functionalization of nanoparticles for cancer treatment.

There are many important reasons why there is such a drastic development of nanomedicine for cancer applications, including:

- Overcoming problems of solubility and chemical stability of anti-cancer drugs.
- Protection of anti-cancer compounds from biodegradation or excretion, therefore influencing the pharmacokinetic profile of a compound.

- Improving the distribution and the targeting of anti-tumor medication.
- The design so their payload is released upon a trigger resulting from a stimuli-sensitive nanomedicine therapeutics.
- The potential decrease of resistance of tumors against the cancer treatment (by increasing circulation time of compound and by mediating stimuli-responsive drug release as well as endocytic drug uptake).

### *1.2.1. Different types of nanoparticles used in cancer therapy*

Different types of nanoparticles can be used for cancer clinical care including viral nanoparticles, organic nanocarriers and inorganic nanoparticles. Each of these are represented in Figure 24 and each will be further discussed in the next paragraphs.

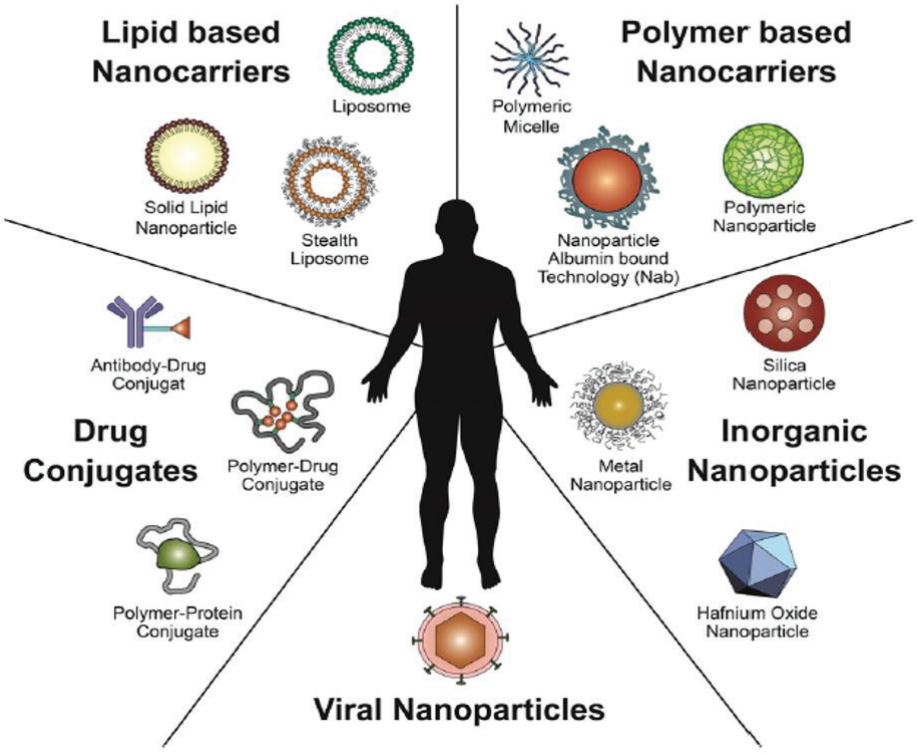


Figure 24: "Schematic illustration of established nanotherapeutic platforms. Different nanomedicine products such as drug conjugates, lipid-based nanocarriers, polymer-based nanocarriers, inorganic nanoparticles, and viral nanoparticles are used in clinical cancer care. (Wicki *et al.*, 2015)

**Viral nanoparticles** can be of interest in cancer therapy as the tumor-homing viruses engineered to express therapeutic proteins can be used. An example of such nanoparticle is JX-594 which is a poxvirus designated to replicate in tumor cells and induce their destruction via the activation of the EGFR-Ras-MAPK signaling pathway. The JX-594 viral nanoparticle also has the expression of granulocyte colony-stimulating factor (G-CSF) which potentially increases the immunological anti-tumor response. In a clinical study, 10 patients with primary or metastatic liver cancer were injected intratumorally with JX-594. Results showed 3 cases of partial remission and 6 cases of stable disease (Park B. *et al.*, 2008). In another phase 1 clinical trial, JX-594 was used to treat advanced solid tumors in 23 patients (Breitbach C. *et al.*,

2011). The virus was successful in that it specifically reached the tumor site while normal tissue showed no viral replication. Adjacent epithelium up took the particles however they were not active, therefore showing no toxicity. A dose-related anti-tumor activity of JX-594 was observed. This study was the first to show a dose-related viral replication and tumor response after intravenous injection of an oncolytic virus (Wicki *et al.*, 2015).

Other success using oncolytic nanoparticles included the OPTiM study in patients with advanced (stage IIIB-IV) melanoma (Andtbacka *et al.*, 2013). T-Vec, and other oncolytic viruses were tested in clinical trials however, none of which reached the market, mainly due to concerns arisen concerning their biosafety and cytocompatibility (Vile R. *et al.*, 2002).

**Organic nanocarriers** used for a wide range of applications whether for targeted or non-targeted drug delivery, included several subtypes: drug conjugates, lipid-based nanocarriers, natural polymers- protein and peptide or glycan nanocarriers, and last but not least synthetic polymer-based nanocarriers.

Drug conjugates are defined as "nanotherapeutics because of their size scale in the lower nanometer range and their conjugation to active pharmaceutical ingredients (Duncan, 2006; Hawe *et al.*, 2011). The active agents are covalently linked to targeted antibodies and peptides or to polymers. The conjugate is usually mono- or oligomeric, and is intended to improve targeted delivery of the drug without necessarily impacting on drug solubility, stability, or biodegradability. In contrast, nanocarriers based on lipids, proteins, glycans, or synthetic polymers usually encapsulate the drug, and they obviate the need to link the drug covalently to the carrier." Approved antibody conjugates include trastuzumab-emtansine which targets HER2-overexpression in breast cancer (Verma *et al.*, 2012) and brentuximab-vedotin against CD30-positive Hodgkin lymphoma and anaplastic large-cell lymphoma (Younes *et al.*, 2010). Polymer-drug conjugates are an interesting class as they change the pharmacokinetic profile of a drug (Duncan, 2006, Duncan *et al.*, 2005). As an example, the HPMA copolymer-doxorubicin conjugate PK1 is a novel anti-cancer agent with a significantly lower frequency of cardiotoxicity and alopecia compared to free doxorubicin. A phase 2 study showed promising signs of activity in breast cancer and non-small-cell lung cancer (Seymour *et al.*, 2009).

Lipid-based nanocarriers include two classes: liposomes (closed phospholipid bilayers) and micelles (normal phase, oil-in-water micelles). What makes them attractive is their capacity to carry 1 to 6 drug molecules per monoclonal antibody, which represents a load of three to four orders of magnitude compared to antibody-drug conjugates. The first nanocarrier approved by the U.S. FDA was pegylated liposomal doxorubicin (Doxil® or Caelyx®) in 1995 (Barenholz, 2012, Harrison *et al.*, 1995). Since then, five more lipid nanocarriers were approved for clinical use including: non-pegylated liposomal doxorubicin (Myocet) (Chan *et al.*, 2004), non-pegylated liposomal daunorubicin (DaunoXome®) (Gill *et al.*, 1996), non-pegylated liposomal cytarabine (DepoCyt®) (Gökbuget N. *et al.*, 2011), vincristine sulfate

liposomes (Marquibo®) (O'Brien *et al.*, 2013), and liposomal mifamurtide (Mepact®) (Frampton 2010, Meyers *et al.*, 2008). Although none of these are targeted, the nano-formulations of doxorubicin, daunorubicin, and vincristine prolong the half-life of the cytotoxic compounds and in turn improve their toxicity profiles. Liposomal formulations allow stable encapsulation of drugs but these formulations still reach the tumor via the enhanced permeability retention effect. In order to target them to the tumor tissue, liposomes will have to be modified on their surface to improve specificity. An example to target liposomes is the conjugation of antibodies, antibody fragments, or single-chain antibodies to its surface (Huwyler *et al.*, 1996, Koshkaryev *et al.*, 2013) By adding these compounds at its surface however, it was observed that the plasma half-life was reduced, probably due to the entrapment of Fc-containing ILs in the endoplasmic reticulum. Therefore, Fc-free antibodies were developed, such as anti-HER2, anti-EGFR (i.e. cetuximab) or anti-VEGFR2 (i.e. DC101) antibodies. (Huwyler *et al.*, 1996; Koshkaryev *et al.*, 2013; Mamot *et al.*, 2003 ; Mamot *et al.*, 2005 ; Park *et al.*, 2002 ; Wicki *et al.*, 2012). Further *in-vivo* studies on mice xenografted with human cancer cells showed that these antibody-grafted nanocarriers delivered their cytotoxic compounds specifically to the cells expressing the target antigen. In a clinical study, treatment of tumors (breast cancer in the MMTV-PyMT mouse model and HT-29 human colon cancer xenograft transplantation model) with anti-VEGR2-targeted and doxorubicin-loaded ILs resulted in a tumor shrinkage to $1/6^{th}$ of the size when compared to tumors treated with an identical dose of non-targeted liposomal doxorubicin (Wicki A. *et al.*, 2012). This study clearly demonstrated the benefits of using targeted lipid nanocarriers instead of their non-targeted counterparts. An additional advantage of these targeted lipid nanocarriers is their capacity to overcome multidrug resistance in cancer cells (Mamot *et al.*, 2012; Huwyler *et al.*, 2008). The first clinical trial with GAH-coated doxorubicin-loaded ILs (MCC-465) in patients with metastatic stomach cancer (Matsumura *et al.*, 2004) showed that out of 18 patients were treated, 10 of the 18 had stable disease but no remission was observed.

In addition, lipid nanocarriers have also been studied for systemic delivery of nucleic acids and other substances with short plasma half-life (Li and Rana 2014, Pecot *et al.*, 2011), as well as testing the feasibility and efficacy of siRNA delivery (Coelho *et al.*, 2013; Couvreur *et al.*, 2006).

There is only one type of protein-based nanoparticle that has reached the clinical setting: albumin-nanoparticle-bound paclitaxel (nab-paclitaxel; Abraxane®). This type of nanoparticle is being used in breast cancer, non-small-cell lung cancer, and pancreatic cancer. In this case, we cannot talk about an active targeted nanoparticle but it has been observed that albumin may mediate transcytosis of the compound via the gp60 receptor on the epithelium which enhances its deliver to the tumor site. (Predescu *et al.*, 2004). During the clinical trials, it was observed in breast cancer that nab-paclitaxel improved response rates compared to conventional paclitaxel (Gradishar *et al.*, 2005), and that nab-paclitaxel in combination with gemcitabine increased survival in pancreatic-cancer patients when compared to gemcitabine

monotherapy (Hoff *et al.*, 2013). Other albumin stabilized nanoparticles including ABI-008, ABI-009, and ABI-011. (Qu *et al.*, 2013) are under clinical trials.

No glycan nanocarriers for systemic cancer therapy has been approved yet but there are ongoing phase 1 and 2 trials for the proof-of-concept. It would seem that these types of nanoparticles show fewer side effects. For example, cyclodextrin nanoparticles were compared to free camptothecin in a phase 2 clinical trials and fewer side effects were observed as well as an overall response rate of 64% (Weiss *et al.*, 2013).

Synthetic polymer-based nanocarriers show much promise for nanomedicine therapeutics due to their chemical versatility (Kamaly *et al.*, 2012). Many types of synthetic polymer-based nanocarriers are under clinical trials and are summarized in Table 7 (see below).

Inorganic nanoparticles have also been of increased interest for cancer therapy. These types of nanoparticles have a variety of applications including imaging, radiosensitization, and drug delivery (Huang *et al.*, 2011). These types of nanoparticles will be further discussed, but just to mention a few, iron oxide nanoparticles are used for diagnostic purposes (Ross *et al.*, 2009) while others are being tested in clinical trials for the magnetic resonance imaging of tumors. An example of patented iron-oxide nanoparticle is NanoTherm®, an aqueous colloidal dispersion that is activated, after tumor internalization, through thermal ablation performed with an alternating magnetic field applicator (magnetic hyperthermia). This type of therapy was shown to be beneficial and robust data was already collected for glioblastoma (Rivera *et al.*, 2010). Although not approved worldwide, NanoTherm® gained marketing approval in several European countries (Wicki *et al.*, 2015).

Other inorganic nanoparticles are hafnium oxide nanoparticles which will be further discussed in details in the radiosensitization paragraph. As of 2015, no inorganic nanoparticle for drug delivery has received market approval but some of them are in the testing phase in clinical trials including pegylated colloidal gold-TNFα particles for cancer therapy (Libutti *et al.*, 2010) and silicon nanocarriers for parenteral peptide delivery (Kovalainen *et al.*, 2013).

| Product (Company) | Polymer | Drug | Indication | Status | Reference |
|---|---|---|---|---|---|
| ABI-008 (Abraxis/Celgene) | Albumin nanoparticle | Docetaxel | Metastatic breast cancer, prostate cancer | Phase 2 | Hawkins M.J. *et al.*, 2008) |
| ABI-009 (Abraxis/Celgene) | Albumin nanoparticle | Rapamycin | Solid tumors, lymphoma | Phase 1/2 | Gonzalez-Angulo A.M. *et al.*, 2013) |
| ABI-011 (Abraxis/Celgene) | Albumin nanoparticle | Thiocolchicine dimer | Solid tumors, lymphoma | Phase 1/2 | Celgene Corporation, 2014 |
| BIND-014 (Bind Therapeutics) | PEG-PLGA polymeric nanoparticle* | Docetaxel | Non-small-cell-lung cancer, prostate cancer | Phase 1/2 | Hrkach J. *et al.*, 2012) |
| CALAA-01 (Calando Pharmaceuticals) | Cyclodextrin polymeric nanoparticle** | siRNA targeting ribonucleotide | Solid tumors | Phase 1 | Davis M.E. *et al.*, 2010 |
| CRLX-101 (IT-101) (Cerulean Pharma) | Cyclodextrin nanoparticle | Camptothecin | Solid tumors, renal cell carcinoma, rectal cancer, non-small-cell lung cancer | Phase 1/2 | Gaur S. *et al.*,, 2014 |
| DHAD-PBCA-NP | Polymeric nanoparticle | Mitoxantrone | Heptacellular carcinoma | Phase 2 | Zhou Q. *et al.*, 2009 |
| Docetaxel-PNP (Samyang Biopharmaceuticals) | Polymeric nanoparticle | Docetaxel | Solid tumors | Phase 1 | Jung J. *et al.*, 2012 |
| Lipotecan (TLC388) (Taiwan Liposome) | Polymeric micelle | TLC388 (Camptothecin derivate) | Liver cancer, renal cancer | Phase 1/2 (orphan drug status) | Ghamande S. *et al.*, 2014 |
| Nanotax (CritiTech) | Polymeric nanoparticle | Paclitaxel | Peritoneal neoplasms | Phase 1 | Roby K.F. *et al.*, 2008 |
| Nanoxel (Fresenius Kabi Oncology) | Polymeric micelle | Paclitaxel | Advanced breast cancer | Phase 1 | Madaan A. *et al.*, 2013 |
| NC-4016 (NanoCarrier) | Polymeric micelle | Oxaliplatin | Solid tumors, lymphoma | Phase 1 | Ueno T. *et al.*, 2014 |
| NC-6004 (Nanoplatin) (NanoCarrier) | PEG-PGA polymeric micelle | Cisplatin | Pancreas cancer | Phase 2/3 | Plummer R. *et al.*, 2011 |
| NC-6300 (K-912) (Nanocarrier) | pH sensitive polymeric micelle | Epirubicin | Solid tumors | Phase 1 (Japan) | Harada M. *et al.*, 2011 |
| NK-012 (Nippon Kayaku) | PEG-PGA polymeric micelle | SN-38 (active metabolite of irinotecan) | Solid tumors, small cell lung cancer, breast cancer | Phase 2 | Hamaguchi T. *et al.*, 2010 |
| NK-105 (NanoCarrier Nippon Kayaku) | PEG-PAA polymeric micelle | Paclitaxel | Gastric cancer, breast cancer | Phase 2/3 | Kato K. *et al.*, 2012 |
| NK-911 (National Cancer Institute Japan/Nippon Kayaku) | PEG-PAA polymeric micelle | Doxorubicin | Solid tumors | Phase 1 | Matsumura Y. *et al.*, 2004 |
| Paclical (Oasmia Pharmaceutical) | Polymeric micelle | Paclitaxel | Ovarian cancer | Phase 3 (orphan drug status) | Oasmia Pharmaceutical AB, 2014 |
| SP1049C (Supratek Pharma) | Polymeric micelle*** | Doxorubicin | Advanced adenocarcinoma | Phase 2/3 | Valle J.W. *et al.*, 2011 |
| Transdrug BA-003 (Livatage) (BioAlliance Pharma) | Polymeric nanoparticle | Doxorubicin | Hepatocellular carcinoma | Phase 3 (2004 EU orphan drug status) | Barraud L. *et al.*, 2005 |

Table 7: Polymer-based nanocarriers in clinical trials. Polymer-based nanocarriers consist of a natural or synthetic polymer. Most commonly used natural polymers are proteins (e.g. albumin) or glycans (e.g. cyclodextrin). For active targeting strategies, the targeting ligand and cognate receptor are indicated. Products are listed alphabetically. Alternative names for the products are given in brackets. (Wicki *et al.*, 2015)

### 1.2.2. Passive versus active targeting

**Passive targeting** plays on the enhanced permeability and retention effect: it exploits the anatomical differences present between normal and diseased tissues. It occurs due to the extravasation of the nanoparticles at the diseased site where the microvasculature is leaky. In order for the nanoparticles to be able to reach the diseased site, they must be able to freely circulate in blood.

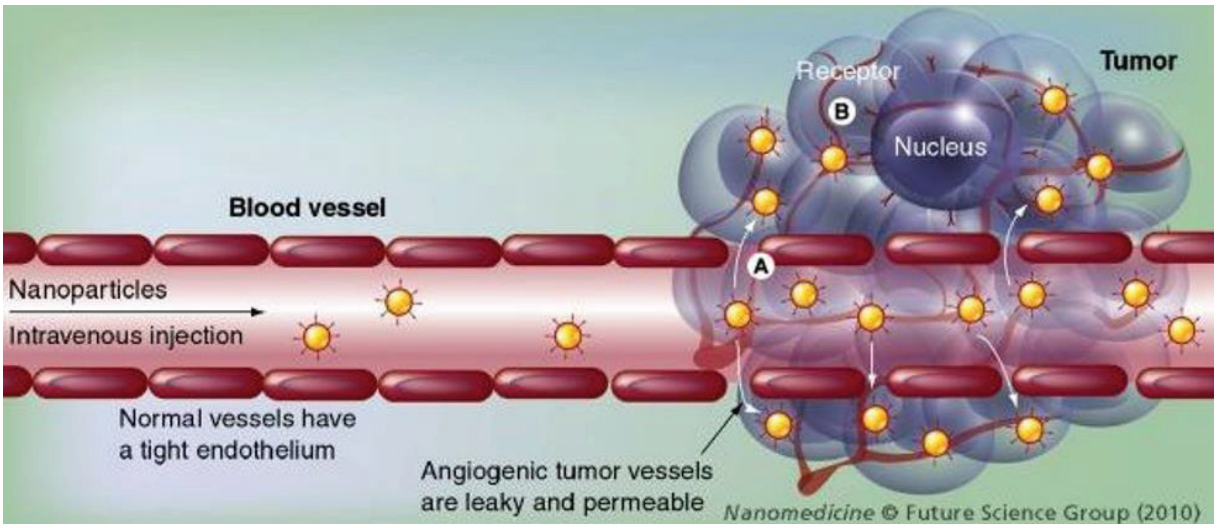


Figure 25: Representation of the enhanced permeability retention effect. The vasculature in tumors is leaky and permeable allowing small sized-objects (i.e. nanoparticles) to pass through.

**Active targeting** requires the conjugation of a receptor specific ligand that can promote site specific targeting. Success of drug targeting depends on the selection of the targeting moieties. The moiety should be abundant, have a high affinity and specificity, and must be well suited to chemical modification for conjugation. Ligands are coupled to nanoparticles in two ways: either by covalent or non-covalent bonding. Covalent bonding may be the formation of disulfide bonds, cross-linking between two primary amines, or the reaction between a carboxylic acid and a primary amine… Non-covalent bonding can imply the physical association of the targeting ligands to the nanocarrier surface. One of the advantages of non-covalent bonding is the elimination of rigorous, destructive reaction agents used. However, potential problems with non-covalent bonding include low and weak binding, poor control of the reactions as the ligand may not be in the desired orientation.

## 2. Nanoparticles coupled to Radiotherapy

As summarized in Figure 21, different types of nanoparticles can be used for radiosentization purposes. They can be divided in different subgroups, including polymeric nanoparticles (i.e. albumin nanoparticles, poly(lactic-co-glycolic acid) (PLGA) nanoparticles, high-Z nanoparticles (i.e. gold, gadolinium-based nanoparticles…), superparamagnetic nanoparticles (SPIONS), quantum dots and non-metal based nanoparticles.

## 2.1. Different types of radiosensitizing nanoparticles

In this paragraph, we will briefly describe different types of nanoparticles that can be used as radiation therapy sensitizers before focusing on AGuIX® which were used for this work.

### *2.1.1. Quantum dots*

Quantum dots (QDs) can be defined as small fluorescent nanocrystals (2 to 10 nm) that are composed of semiconductor materials displaying quantum mechanical properties due to their small size. QDs have the particularity that they can absorb a broad spectrum of electromagnetic waves and emit light usually in the near infrared range (Seeta Rama Raju *et al.*, 2015). QDs have a central core made of a metal or a metalloid that can be encapsulated by biocompatible molecules, such as ZnS and silica, to prevent them from being eliminated from the body before they reach cancer cells (Jin and Hildebrandt, 2012). Currently, due to their optical and electrical properties, their use is mainly as diagnostic agents (Wegner and Hildebrandt, 2015). A couple of quantum dots made of CaF, LaF, ZnS or ZnO have already been studied for their potential as radiosensitizers (Kwatra *et al.*, 2013; Juzenas *et al.*, 2008; Wang *et al.*, 2008). The mechanism of action relies on the generation of radical oxygen species upon the interaction of high-energy photons (X-rays and gamma rays) with the heavy metals since quantum dots have a high atom and electron density, which will in turn cause localized and targeted damage to cancer cells (Park *et al.*, 2006; Carter *et al.*, 2007; Kwatra *et al.*, 2013; Juzenas *et al.*, 2008).

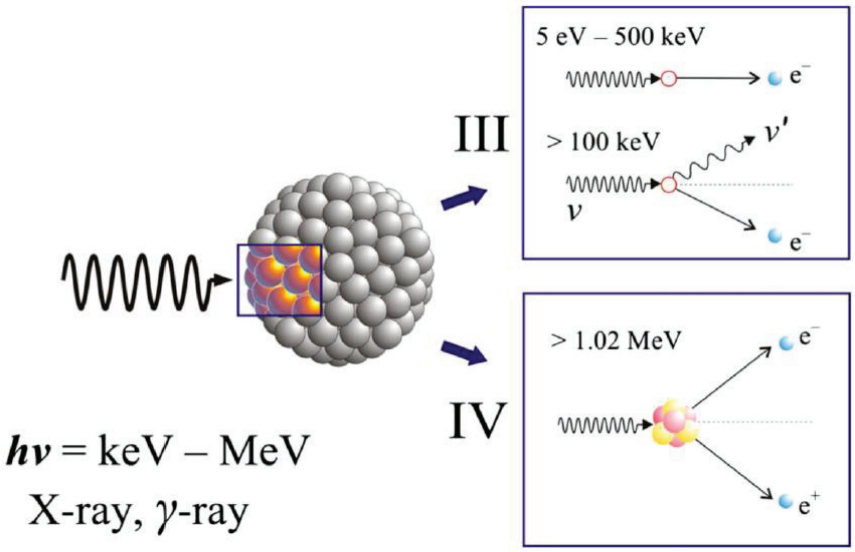


Figure 26: Mechanism of action following the interaction of high-energy photons with a quantum dot (Juzenas *et al.*, 2008).

It was observed that QDs are taken up by endocytosis and retained in lysosomes (Juzenas *et al.*, 2008; Silver and Ou 2005). QDs were also observed in the perinuclear region using an immunofluorescence staining of the lysosomal membrane protein LAMP-2 (Saftig, 2005). For a better internalization, QDs can be functionalized either by using a peptide containing a cell

entering signal (Zhou and Ghosh, 2007; Patel *et al.*, 2007), or targeting receptor-mediated endocytosis by binding specific peptidic receptors (Delehanty *et al.*, 2006). In cancer cells overexpressing the folate receptor, the functionalization of QDs with folate also showed an increased cellular internalization (Delehanty *et al.*, 2006; Bharali *et al.*, 2005; Schroeder *et al.*, 2007). (Juzenas *et al.*, 2008)

A recent study was published using tungsten sulfide QDs as multifunctional nanotheranostics for *in-vivo* dual-modal image-guided photothermal/radiotherapy synergistic therapy. (Yong *et al.*, 2015). The authors developed $WS_2$, QDs of a small size (3 nm) with good biocompatibility. As seen previously, this small size allows for the non-retention of the particles in the liver while allowing renal excretion. Due to its high Z number $WS_2$ was predicted to be a good radiosensitizer. Indeed, treatment of HeLa and HepG2 cells with these $WS_2$ QDs for 24h resulted in radiosensitization (inhibition of cell survival from 75% to 31%) without any toxicity when in absence of radiation. *In-vivo* studies indicated no obvious signs of abnormal mouse behavior in body weight, eating, drinking, nor activity. QDs accumulated in the kidney, liver, and spleen, without any further hepatic nor renal dysfunctions and promising results were obtained *in vivo*.

### *2.1.2. Superparamagnetic iron oxides*

Superparamagnetic iron oxide nanoparticles (SPIONS) are composed of an iron oxide core that gives them paramagnetic abilities when placed in a magnetic field (Seeta *et al.*, 2015). SPIONS are therefore used as contrast agents in magnetic resonance imaging (MRI) as well as for drug delivery to tumors. In addition, these types of nanoparticles have been studied for their potential radiosensitizing properties. SPIONS have shown negligible toxicity to healthy tissues which allows for their usage in therapy (Mikhaylov and Vasiljeva, 2011).

It was reported that these SPIONs can induce cytotoxic effects due to the production of ROS such as hydrogen peroxide, hydroxyl radical, hydroperoxyl radical and superoxide anion which in turn results in DNA (Huang *et al.*, 2013) and other cellular organelle damage (Kwatra *et al.*, 2013). In addition, an enhancement in radiation efficacy was observed on MCF-7 cells as the nanoparticles enhanced the impact of X-rays on ROS generation by about 240% (Klein *et al.*, 2012).

Another example studied is a superparamagnetic chitosan iron oxide nanoparticle carrying *human Adenovirus type 5 early region 1A* (E1A) gene. The E1A gene is known to reduce the expression of HER-2 and increase the expression of p53, two proteins that are known to play a role in the regulation of radioresistance in cancer (Kwatra *et al.*, 2013; Raybaud-Diogène *et al.*, 1997). The combination of genetic therapy with increased oxidative stress by iron oxide nanoparticles further enhanced the radiosensitivity of human cervical cancer in xenografted mice (Kwatra *et al.*, 2013; Shen *et al.*, 2010). A nanocomposite using $Fe_3O_4$/Ag conjugated to

the EGFR antibody could be used as a theranostic agent: this nanocomposite can be used as a diagnostic tool through MRI and was shown to be a radiosensitizer in nasopharyngeal carcinoma in a dose-dependent manner (Zhao *et al.*, 2012).

### *2.1.3. Non-metal based nanoparticles*

Non-metal based nanoparticles, although less largely used than metal-based nanoparticles, can also be used as radiosensitizing agents. For example, Klein *et al.* synthesized ultrasmall uncapped and aminosilanized oxidized silicon nanoparticles and tested them *in-vitro* on MCF-7 (breast cancer) and 3T3 cells (mouse fibroblast cells). Their results showed a radiosensitizing effect when the treated cells were exposed to X-rays of 3 Gy (Klein *et al.*, 2013). It was also reported that these nanoparticles induced a significant increase in ROS production that reached the mitochondria and caused oxidative stress damage within the organelle. The increased ROS production was observed in both the cancer cells and normal cells but the deleterious effects were more significant in cancer cells (Klein *et al.*, 2013; Kwatra *et al.*, 2013).

Another example of a non-metal-based nanoparticles is $C_{60}$, a fullerene that has potent anti-cancer activities and induces markers of autophagy in cancer cells (Zhang *et al.*, 2009) but significant toxicity in normal tissue was put in evidence which limits its use (Sayes *et al.*, 2005). In order to further explore its capacities, a team used nanocrystals of underivatized fullerene $C_{60}$ (Nano- $C_{60}$) at concentration that were non-toxic to normal cells and studied their radiosensitizing potential. B16 (mouse melanoma cell line) and SMMU-7721 (human hepato-carcinoma cell line) were treated with Nano- $C_{60}$ and exposed to γ-radiation and results showed enhanced membrane damage and induction of apoptotic cell death (Veeraraghavan *et al.*, 2011).

As previously mentioned, polymeric nanoparticles are also available and have been formulated using different chemotherapeutic agents either alone or in combination (Kwatra *et al.*, 2013). Genexol-PM, a clinically approved formulation of paclitaxel was studied on non-small cell lung cancer mouse xenograft models. This formulation was found to be both a better radiosensitizer than the normal drug and a safer therapeutic issue with much reduced exposure of the drug to the healthy lung tissue (Kwatra *et al.*, 2013; Werner *et al.*, 2013). Another example is a nanomiceller composite formulation of doxorubicin which showed a significant enhancement of radiation sensitivity in a multicellular spheroid of A549 lung cancer cell line (Xu *et al.*, 2012).

Biodegradable lipid polymer nanoparticles have also been designed using docetaxel as the entrapped drug and targeted to cancer tissue using folate. The studies indicated that the targeted nanoparticles showed better radiosensitizing properties as compared to drug alone or unmodified nanoparticles. The studies also showed that the radiosensitizing effects using nanoparticulate formulations significantly depends on the time gap between the dosing of the formulation and the radiation (Kwatra *et al.*, 2013; Werner *et al.*, 2011).

### *2.1.4. Metal-based nanoparticles*

Metal-based nanoparticles will be further discussed in the next chapter.

## 2.2. Focus on metal-based nanoparticles

### *2.2.1. Hafnium nanoparticles*

Hafnium oxide nanoparticles, NBTXR3, were designed so they concentrate in tumor cells to achieve intracellular high-energy dose deposit. Magglorella *et al.* (2012) studied hafnium oxide nanoparticles and observed a nine-fold radiation enhancement compared with water. In addition, the nanoparticles showed satisfactory dispersion and persistence within the tumor as they formed clusters in the cytoplasm of cancer cells. NBTXR3 nanoparticles have a hydrodynamic diameter of 50 nm, a polydispersity index of 0.100, and a zeta potential of -50 mV. The irradiation source was a cobalt-60 (average photon energy: 1.25 MeV) at a dose rate of 0.66 or 0.46 Gy/min, a 6-MV accelerator at a dose rate of 1Gy/min or an applicator coupled to a curietherapy device containing a high dose rate iridium-192 source (average photon energy: 0.38 MeV). The cell lines tested were HT1080 (human fibrosarcoma model), HCT116 (human colorectal tumor cell line), and A673 (human Ewing family type sarcoma model). Results showed the location of NBTXR3 nanoparticles in vesicles (endosomes) in the cell's cytoplasm. The energy release from the clusters of nanoparticles constitutes what the authors called a dose deposit 'hotspot', which could lead to high and localized destruction of biological subcellular structures and induce cell death (Maggiorella *et al.*, 2012).

A good dispersion of NBTXR3 was observed *in-vivo* following one IT injection with nanoparticles both in the central and peripheral areas of the tumor. After 14 days, the nanoparticles were still present in the tumor but the evaluation was no longer possible due to ethical mice sacrifice. A marked increase in the radiation response of HT1080 tumor xenografts was observed with an enhanced biological response (EBR) over 1.5 as well as an increase in the apoptotic response in the cells treated with NBTXR3 combined with irradiation. Six clinical trials using NBTXR3 are ongoing with one clinical trial completed. These clinical trials are summarized in Table 8 below.

| Study Title | Condition | Phase | Purpose |
|---|---|---|---|
| NBTXR3 Crystalline Nanoparticles and Radiation Therapy in Treating Patients With Soft Tissue Sarcoma of the Extremity | Adult Soft Tissue Sarcoma | 1 | To evaluate the feasibility of the NBTXR3 injection in the tumor, safety and the adequate dose of NBTXR3 when given with radiation therapy. |
| NBTXR3 Crystalline Nanoparticles and Stereotactic Body Radiation Therapy in the Treatment of Liver Cancers | Hepatocellular Carcinoma; Liver Cancer | 1/2 | To evaluate the safety and preliminary efficacy of NBTXR3 nanoparticles given by intralesional (IL) or intraarterial (IA) injection and activated by Stereotactic Body Radiation Therapy in the treatment of liver cancers. |
| NBTXR3 Nanoparticles and EBRT or EBRT With Brachytherapy in the Treatment of Prostate Adenocarcinoma | Prostate Cancer | 1/2 | Open-label involving 2 groups of patients newly diagnosed with either unfavorable intermediate risk or high-risk prostate adenocarcinoma. One group will receive only EBRT and the other group will receive a Brachytherapy boost and EBRT. Both groups will receive treatment with androgen deprivation. There will be consecutive steps, a dose escalation and a subsequent dose expansion part. |
| NBTXR3 Crystalline Nanoparticles and Radiation Therapy in Treating Patients With Locally Advanced Squamous Cell Carcinoma of the Oral Cavity or Oropharynx. | Head and Neck Cancer | 1 | Determination of the recommended doses and the early Dose Limiting Toxicities. Evaluation of the safety and tolerability of NBTXR3, evaluation of the objective response rate and the complete response rate as per response evaluation Criteria in Solid tumors and the tumor volume estimation; evaluation of the local progression free survival; evaluation of the progression free survival of NBTXR3; characterization of the body kinetics profile of NBTXR3; evaluation of the feasibility of local administration either intratumor or intra-arterial route. |
| NBTXR3 Crystalline Nanoparticles and Radiation Therapy in Treating and Randomized Patients in Two Arms With Soft Tissue Sarcoma of the Extremity and Trunk Wall | Adult Soft Tissue Sarcoma | 2/3 | To compare antitumor activity I terms of Pathological complete response rate of intratumor injection of NBTXR3 activated by external beam radiation therapy versus EBRT alone. Secondary outcome measures include the incidence of early and late TEAE, post-TEAE, SAE, and laboratory abnormalities; objective response rate by imaging (MRI) according to RECIST 1.1; tumor volume changes; resection margins, limb imputation rate. |
| A Study of PEP503 With Radiotherapy in Combination With Concurrent Chemotherapy for Patients With Head and Neck Cancer | Head and Neck Squamous Cell Carcinoma | 1/2 | Phase 1: Determination of the recommended doses and the dose limiting toxicities.<br>Phase 2: the rate of locoreginal control at one year.<br>Phase 1 and 2: Evaluation of the safety profile of PEP503 |
| A Study of PEP503(Radio-enahncer) With Radiotherapy and Chemotherapy for Patiens With Rectal Cancer | Rectal Cancer | 1/2 | Determining the safety profile: dose limiting toxicity, the recommended volume (dose, and the anti-tumor activity. |

*: PEP503= another name for NBTXR3.

Table 8: Ongoing clinical trials with NBTXR3 (hafnium oxide nanoparticles) as radiosensitizing agent in several different cancer types. (clinicaltrials.gov)

### *2.2.2. Silver nanoparticles*

Silver nanoparticles conjugated with BSA have shown a radiosensitizing effect on gastric cancer cells (Huang *et al.*, 2011) and hepatocellular carcinoma (Zheng *et al.*, 2013) probably resulting from the release of Ag+ cations from the silver microspheres inside the cells. These cations are oxidative agents and may capture electrons, which could further reduce the cellular ATP content and increase ROS production (Bergs *et al.*, 2015; Huang *et al.*, 2011).

Magnetic silver $Fe_3O_4$/Ag nanocomposites, conjugated to an EGFR-specific antibody (C225) were used as a theranostic agent for simultaneous molecular targeted cancer therapy and MRI diagnosis (Zhao *et al.*, 2012). The use of these nanoparticles in nasopharyngeal carcinoma cells (CNEs) showed a time- and concentration-dependent inhibition of proliferation and enhanced X-ray cytotoxicity by a factor of 2.26 (Zhao *et al.*, 2012).

### *2.2.3. Titanium nanoparticles*

Titanium is already used for photodynamic therapy, which is based on the generation of radical oxygen species (ROS) upon photoactivation. Historically, nanotitania has been used to induce cancer cell apoptosis and can be used as a photosensitizer in UV photodynamic therapy (PTD) for endobronchial and esophageal cancers (Townley *et al.*, 2012; Ozben, 2007). However, this technique is limited to superficial tumors due to its limitation of the penetration depth of UV light.

Very few studies have used titanium nanoparticles as radiosensitizing agents. In 2012, Townley *et al.* published a study with titania nanoparticles doped with rare earth elements. The nanoparticles were coated with silica to inhibit aggregation and to improve its biocompatibility. In this study, they used Hep-G2 cells, grown as 3D spheroids to best represent the tumor environment. The combined treatment led to an increase of apoptosis as assessed by the cells' morphology and the loss of contact between the cells within the spheroid. An *in-vivo* study was also undertaken used to test the efficacy of these nanoparticles: human non-small cell lung cancer xenografts were established by injecting A549 cells subcutaneously into the hind limb of SCID Beige mice. No toxicity due to nanoparticle treatment was observed, nanoparticle augmented radiation therapy as the tumor growth was reduced compared to radiation treatment alone: the tumors of mice who had received the nanoparticles were approximately half the size of the ones treated with irradiation alone. Once again, this study shows the potential use of titanium-based nanoparticles to enhance the efficacy of radiation therapy.

In 2013, Mirjolet *et al.* published their work on the radiosensitization of glioblastoma cell lines (SNB-19 and U87 MG) using titanate nanotubes (TiONts). TiONts have a diameter of about 10 nm with an inner cavity of about 4nm, and a length of about several hundred

nanometers. TiONts entered the cells via endocytosis with an invagination of the membrane or via a diffusion process and were free in cytosol or localized inside vesicles. Clonogenic assays showed a significant radiosensitization for cells incubated with the TiONts compared to control cells (SF2 = 0.36 vs. 0.18 for SNB-19 cells and 0.60 vs. 0.43 for U87MG cells). After 24h of treatment with or without TiONts, no differences in ROS production, early apoptosis and autophagy was observed. However, cell cycle analysis showed an increase, in both cell lines, of the number of cells in the G2 phase after treatment with TiONts. As cells in the G2 phase are more sensitive to radiation, treatment with TiONts led to a significant increase, in both cell lines, of γ-$H_2$AX foci as a result of DNA damage (residual DNA double-stranded-break).

More recently, Nakayama *et al.* (2016) used titanium peroxide nanoparticles combined to X-ray irradiation in a pancreatic cancer model. They observed an increase of hydroxyl radical and hydrogen peroxide levels in cells treated with PAA-TiOxNPs and X-ray irradiation but without any increase of the superoxide level. They also observed that X-ray + PAA-TiOxNPs induced a higher number of γ-H2AX foci and induction of apoptosis. *In-vivo* experiments showed a reduction of the tumor volume to 35.4% compared to X-ray alone without any toxicity throughout the 43 days of observation. Despite an intra-tumoral injection of PAA-TiOxNPs instead of intravenous injection, overall results from this study highlighted the potential of using PAA-TiOxNPs combined to radiotherapy in pancreatic cancer.

### *2.2.4. Gold nanoparticles*

Gold nanoparticles have been extensively studied in nanomedicine owing to its presumed biocompatibility and a potential better absorption of X-rays due to its high atomic number. Various studies show the efficient use of gold nanoparticles as radiosensitizers, with studies showing a Dose Enhancement Factor (DEF) of up to 50. Although their toxicity is yet to be further studied, detailed experiments were brought to light investigating the effects of different parameters of a nanoparticle including its size, shape, surface coating, concentration, and photon energy which each have an impact in the radiosensitizing capacities. However, we must keep in mind that different results were obtained according to the tumor cell lines studied. Moreover, as it was long believed that radiosensitization using gold nanoparticles would only be achievable in keV range, it was a big surprise to observe radiosensitization by gold nanoparticles using X-rays in the MeV range (as often used in the medical setting).

Gold nanoparticles represent a wide platform for a variety of different applications as it can be seen in Figure 27. The main *in-vitro* and *in-vivo* studies were summarized in a recent paper (Her *et al*, 2017) as shown in the following tables. From these tables, we can observe that gold nanoparticles have been widely studied with different sizes, types, and in different cellular models and different energies showing its wide application as a radiosensitizing agent.

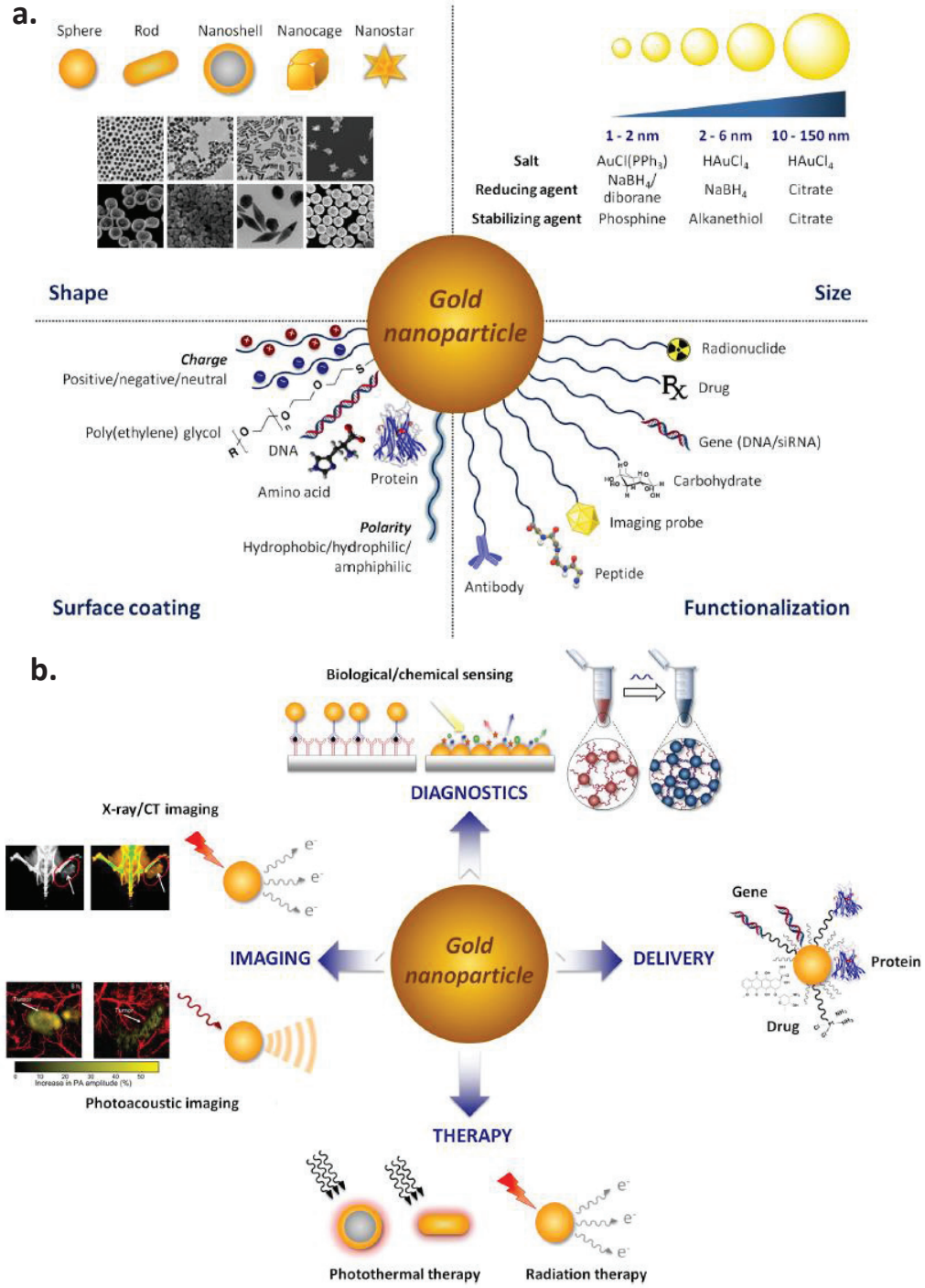


Figure 27: Different types of gold nanoparticles and their applications. **a**. The synthetic versatility of AuNPs. AuNPs offer a unique platform for straightforward manipulation of particle size, shape, surface coating and functionalization, enabling fine-tuning of particle properties. **b**. Biomedical applications of AuNPs. Owing to their unique physico-chemical, optical and electronic properties, AuNPs have been exploited for a wide range of applications in diagnostics, imaging, delivery, and therapy. (Her *et al.*, 2017)

| Author (Ref) | Size | Conc. | Surface | Cell line | Energy | DEF/Effect |
|---|---|---|---|---|---|---|
| Butterworth *et al.*, 2010 | 1.9 nm<br>0.24 µm | 2.4 µm | Proprietary thiol (AuroVist™) | AGO-1552B<br>Astro<br>DU-145<br>L132<br>MCF-7<br>MDA-MB-231<br>PC-3<br>T98G | 160 kVp | 1.97<br>0.96<br>0.81<br>0.87<br>1.09<br>1.11<br>1.02<br>1.91 |
| Chang *et al.*, 2008 | 13 nm | 10 nM | Citrate | B16F10 | 6 MeV $e^-$ | Significant decrease in SF at 8Gy with AuNPs vs. IR alone |
| Chattopadhyay *et al.*, 2013 | 30 nm | 2.4 mg/mL | PEG HER2 targeted (trastuzumab) | MDA-MB-361 | 100 kVp | 1.6 (targeted)<br>1.3 (non-targeted) |
| Chen *et al.*, 2015 | 28 nm (18 nm core) | 36 µg/mL | BSA | U87 | 160 kVp | 1.37 |
| Chithrani *et al.*, 2010 | 14 nm<br>50 nm<br>74 nm | 7 X $10^9$ NPs/mL | Citrate-AuNPs | HeLa | 105 kVp<br>220 kVp<br>660 keV (137-Cs)<br>6 MVp | 1.66<br>1.43<br>1.18<br>1.17 |
| Coulter *et al.*, 2012 | 1.9 nm | 12 µM (500 µg/mL) | Proprietary thiol (AuroVist™) | MDA-MB-231<br>DU145<br>L132 | 160 kVp | ~1.8 (MDA-MB-231) |
| Cui *et al.*, 2014 | 2.7 nm | 0.5 mg/mL | Tiopronin | MDA-MB-231 | 225 kVp | 1.04-1.44 |
| Geng *et al.*, 2011 | 14 nm | 1.25, 2.5, 5 nM | Glucose | SK-OV-3 | 90 kVp<br>6 MV | 1.44<br>1.3-1.37 |
| Jain *et al.*, 2014 | 1.9 nm | 12 µM (500 µg/mL) | Proprietary thiol (AuroVist™) | MDA-MB-231 | 160 kVp | 1.41 |
| Jain *et al.*, 2011 | 1.9 nm | 12 µM (500 µg/mL) | Proprietary thiol (AuroVist™) | MDA-MB-231<br>L132<br>DU145 | 160 kVp<br>6 MV<br>15 MV | 1.41<br>1.29<br>1.16 (MDA-MB-231) |

| | | | | | | |
|---|---|---|---|---|---|---|
| Joh *et al.*, 2013 | 12 nm | 1 mM | PEG | U251 | 150 kVp | ~1.3 |
| Kaur *et al.*, 2013 | 5-9 nm | 5.5 µmol/mL | Glucose | HeLa | Gamma (60-Co)<br>Carbon (62 MeV) | 1.52<br>1.39 |
| Khoshgard *et al.*, 2014 | 47-52 nm | 50 µM | PEG<br>Folate-conjugated | HeLa | Gamma (60-Co) | 1.64 (targeted)<br>1.35 (untargeted) |
| Kong *et al.*, 2008 | 10.8 nm | 15 µM | Cysteamine or glucose | MCF-7 | 200 kVp<br>662 keV (137-Cs)<br>60-Co | ~1.3 (cysteamine)<br>~1.6 (glucose) |
| Liu *et al.*, 2010 | 6.1 nm | 0.4-1 mM | PEG | EMT-6<br>CT26 | 6.5 keV<br>8.048 keV<br>160 kVp<br>6 MeV<br>3 MeV proton | ~2-45% decrease in survival rate |
| Liu *et al.*, 2008 | 4.7 nm | 500 µM | PEG | CT26 | 6 MV | 1.33-1.59 |
| Liu *et al.*, 2015 | 14.8 nm | 1.5-15 µg/mL | Citrate | HeLa | 50 kVp X-rays<br>70 keV/µm carbon | 1.14-2.88<br>1.27-1.44 |
| Rahman *et al.*, 2009 | 1.9 nm | 0.25, 0.5, 1 mM | Proprietary thiol (AuroVist™) | BAEC | 80 kVp<br>150 kVp<br>6 MeV<br>12 MeV | 20<br>1.4<br>2.9<br>3.7 |
| Roa *et al.*, 2009 | 10.8 nm | 15 nM | Glucose | Du-145 | 662 keV (137-Cs) | 1.24-1.38 |
| Taggart *et al.*, 2014 | 1.9 nm | 12 µM (500 µg/mL) | Proprietary thiol (AuroVist™) | MDA-MB-231<br>T98G<br>DU-145 | 225 kVp | 1.17-1.23 (MDA-MB-231)<br>1.35-1.90 (T98G)<br>1.01-1.1 (DU-145) |
| Wang *et al.*, 2013 | 13 nm | 20 nM | Glucose | A549 | 6 MV | 1.49 |
| Wang *et al.*, 2015 | 16 nm<br>49 nm | 20 nM | Glucose | MDA-MB-231 | 6 MV | 1.49 (16 nm)<br>1.86 (49 nm) |
| Wolfe *et al.*, 2015 | 31 X 9 nm | 0.3 optical density | PEG, goserelin-conjugated nanorods | PC3 | 6 MV | 1.19 (non-targeted)<br>1.36 (targeted) |

| | | | | | | |
|---|---|---|---|---|---|---|
| Zhang *et al.*, 2008 | 30 nm | 15 nM | Glucose | DU-145 | 200 kVp | > 1.3 |
| Zhang *et al.*, 2012 | 4.8, 12.1, 27.3, 46.6 nm | 0.05 mM | PEG | HeLa | 662 keV (137-Cs) | 20 nM<br>1.41 (4.8 nm)<br>1.65 (12.1 nm)<br>1.58 (27.3 nm)<br>1.45 (46.6 nm) |
| Zhang *et al.*, 2014 | <2 nm | 50 µg/mL | Glutathione (GSH) or BSO | HeLa | 662 keV (137-Cs) | ~1.3 (GSH)<br>~1.21 (BSA) |

Table 9: Summary of *in-vitro* studies using gold nanoparticles as radiosensitizers (Her S. *et al.*, 2015)
*Note: kVp: tube voltage/tube potential between the cathode and the anode, set by the operator. keV describes the energy of the particles. For information, for a regular tungsten anode, where the majority of the radiation is generated by bremsstrahlung interactions, and given typical exit window filtration, the average keV will be roughly 1/3$^{rd}$ of the kVp. kVp stands for kilovolts peak because it defines the top keV value the x-rays can have.

| Author | Size | Surface | Injection dose (i.v./i.t./i.p.) | Cell model | Energy | Outcome |
|---|---|---|---|---|---|---|
| Chang *et al.*, 2008 | 13 nm | Citrate | 200 µL, 200 nM AuNPs i.v. | B16F10 | 6 MeV $e^-$ | Significant tumor growth delay; increase in survival |
| Chattopadhyay *et al.*, 2013 | 30 nm | PEG HER2 targeted (trastuzumab) | ~0.8 mg Au (4.8 mg/g tumor) i.t. | MDA-MB-361 | 100 kVP, 11 Gy | Tumor growth inhibition (46% vs. 16%) |
| Chen *et al.*, 2015 | 28 nm (18 nm core) | BSA | 1.3 mg/mL (250 µL) i.v. | U87 | 160 kVp, 3Gy at 2h post-inj + 2 Gy at 24h post-injection | Tumor regression |
| Hainfeld *et al.*, 2004 | 1.9 nm | Proprietary thiol (AuroVist™) | 1.35 g Au/kg<br>2.7 g Au/kg i.v. | EMT-6 | 250 kVp, 26 Gy | 50% long-term survival (> 1 year at 1.35 g Au/kg)<br>86% long-term survival (> 1 year at 2.7 g Au/kg) |
| Hainfeld *et al.*, 2010 | 1.9 nm | Proprietary thiol (AuroVist™) | 1.9 g/kg i.v. | SCCVII | 68 keV<br>42 Gy<br>157 keV<br>50.6 Gy | Increase in median survival (53 vs. 76 days at 68 keV; 31 vs. 49 days at 157 keV) |
| Hainfeld *et al.*, 2013 | 1.9 nm | Proprietary thiol (AuroVist™) | 4 g Au/kg i.v. | Tu-2449 | 100 kVp, 30Gy | 50% long-term tumor-free survival (>1 year) |
| Joh *et al.*, 2013 | 12 nm | PEG | 1.25 g Au/kg i.v. | U251 | 175 kVp<br>20 Gy | Median survival (28 vs 14 days) |
| Wolfe *et al.*, 2015 | 31 X 9 nm | PEG, goserilin-conjugated nanorods | 100 µL, 40 µM AuNPs i.v. | PC3 | 6 MV | Tumor growth delays 17 days (targeted) and 3 days (untargeted) |
| Zhang *et al.*, 2012 | 4.8, 12.1, 27.3, 46.6 nm | PEG | 4 mg/kg i.v. | HeLa | 662 keV (137-Cs) | Tumor growth inhibition |
| Zhang *et al.*, 2014 | <2 nm | Glutathione (GSH) or BSA | 10 mg/kg i.p. | U14 | 662 keV (137-Cs) | ~55 (GSH-AuNPs) and ~38% (BSA-AuNPs) decrease in tumor volume. |

Table 10: Summary of *in-vivo* studies using gold nanoparticles as radiosensitizers (Her *et al.*, 2015).

### *2.2.5. Gadolinium nanoparticles*

Gadolinium-based nanoparticles have been receiving increased interest as these nanoparticles can be used as theranostic agents: for both imaging (in MRI) and therapy (combined with radiotherapy for example). This is the case with the 2 nm gadolinium nanoparticles developed by Le Duc *et al.* (2014) which were shown to accumulate preferentially in tumors via the EPR effect (discussed previously). As an example, Figure 28 shows the enhanced contrast properties given by Gd-nanoparticles which have accumulated in the tumor (brain of a 9L gliosarcoma-bearing rat) by the EPR effect, 20 min following injection, whereas they are not found in the healthy tissue. Since these types of nanoparticles can be followed by MRI, image-guided microbeam radiation therapy can be applied: the healthy tissue will be spared while the tumor will receive a greater dose of irradiation. Better survival rates were reported using this technique in 9 L gliosarcoma-bearing rats.

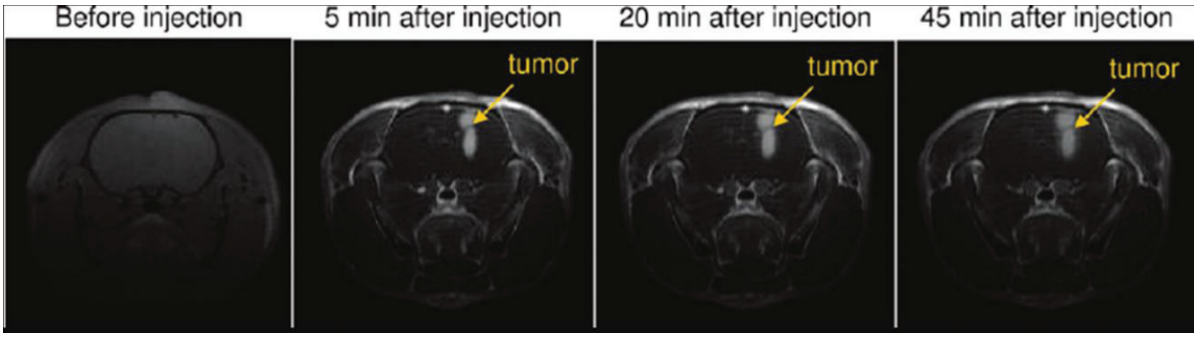


Figure 28: T1-weighted MRI images of the brain of a 9LGS-bearing rat before and 5, 20, and 45 minutes after intravenous injection of GBNs. (Le Duc *et al.*, 2011)

Another example where gadolinium was used is in gadolinium-chemotherapeutic conjugates. One of these is motexafin gadolinium which is greatly studied and was licensed by the FDA for the treatment of non-small cell lung cancer with secondary brain metastases (Richards and Mehta, 2007). By creating an imbalance in the radical scavenging capability of the target cells (oxidation of various intracellular metabolites such as ascorbate, NADPH, and glutathione) which in turn promotes the generation of ROS, this drug leads to a potential lethal radiation-induced damage to DNA (*i.e*. double-stranded breaks). In addition, it was observed that motexafin-gadolinium suppresses the activity of **ribonucleotide reductase** which in turn inhibits the processes of DNA synthesis and repair.

## 2.3. Physicochemical mode of action of high-Z metal NPs

The nanoparticles effectively provide dose enhancement through an enhanced interaction cross-section with the X-ray photons (Townley *et al.*, 2012) which therefore increase therapeutic efficiency and cause localized damage to DNA and organelles within the cancer cells.

The interaction of the ionizing radiations with high-Z metal nanoparticles will undergo via the photoelectric effect inner-shell ionization: one of the deeply bound electrons will be

expelled. The resulting atom is unstable and a re-arrangement of the electronic orbitals either by emission of low energy photons (fluorescence) and electrons (Auger emissions) will occur. From a single inner-shell ionization, several Auger emissions can occur: the process is referred to as the Auger cascade. Electrons issued from the Auger cascade of energies of a few keV or less with penetrations of 10-100 nm, and will therefore deposit their energy very locally.

The phases of radiosensitization can be divided into three phases: the physical phase, the chemical phase, and the biological phase. During the physical phase of radiosensitization, there are three main types of physical interactions that will occur between photons and the high-Z metal of the nanoparticles: the photoelectric effect, usually followed by Auger cascades, the Compton effect, and pair production. These three types of interactions were previously described in Chapter II. The chemical phase corresponds to competitive reactions between radical scavenging agents (such as GSH) and ROS production. At last, the biological phase corresponds to the responses of the biological targets to the ionizing radiation at the molecular, cellular, and tissue levels. In radiobiology, these responses are described as the 5Rs: **r**epair, **r**eoxygenation, **r**edistribution, **r**epopulation, and intrinsic **r**adiosensitivity. (Cui *et al*., 2017) These 5Rs are considered to be the key factors which will in turn the outcome of the treatment (Steel *et al*., 1989; Harrington *et al*., 2007; Pajonk *et al*., 2010). See Figure 29 for a schematic representation of these 3 phases of radiosensitization.

This property of high localized dose of deposited energy is highly attractive for the use of nanoparticles in combination with radiotherapy: the tumor will receive a high deposition of energy following irradiation in the presence of the nanoparticles inside of the tumors, while sparing healthy tissues (since the nanoparticles will accumulate preferentially in the tumor site either via the EPR effect or by active targeting of the nanoparticles to the tumor site). This high deposition of energy would therefore 1) spare healthy tissues and therefore reduce toxic effects of radiotherapy and 2) allow for a decreased dose delivery to the tumor and therefore better the quality of life for the patient.

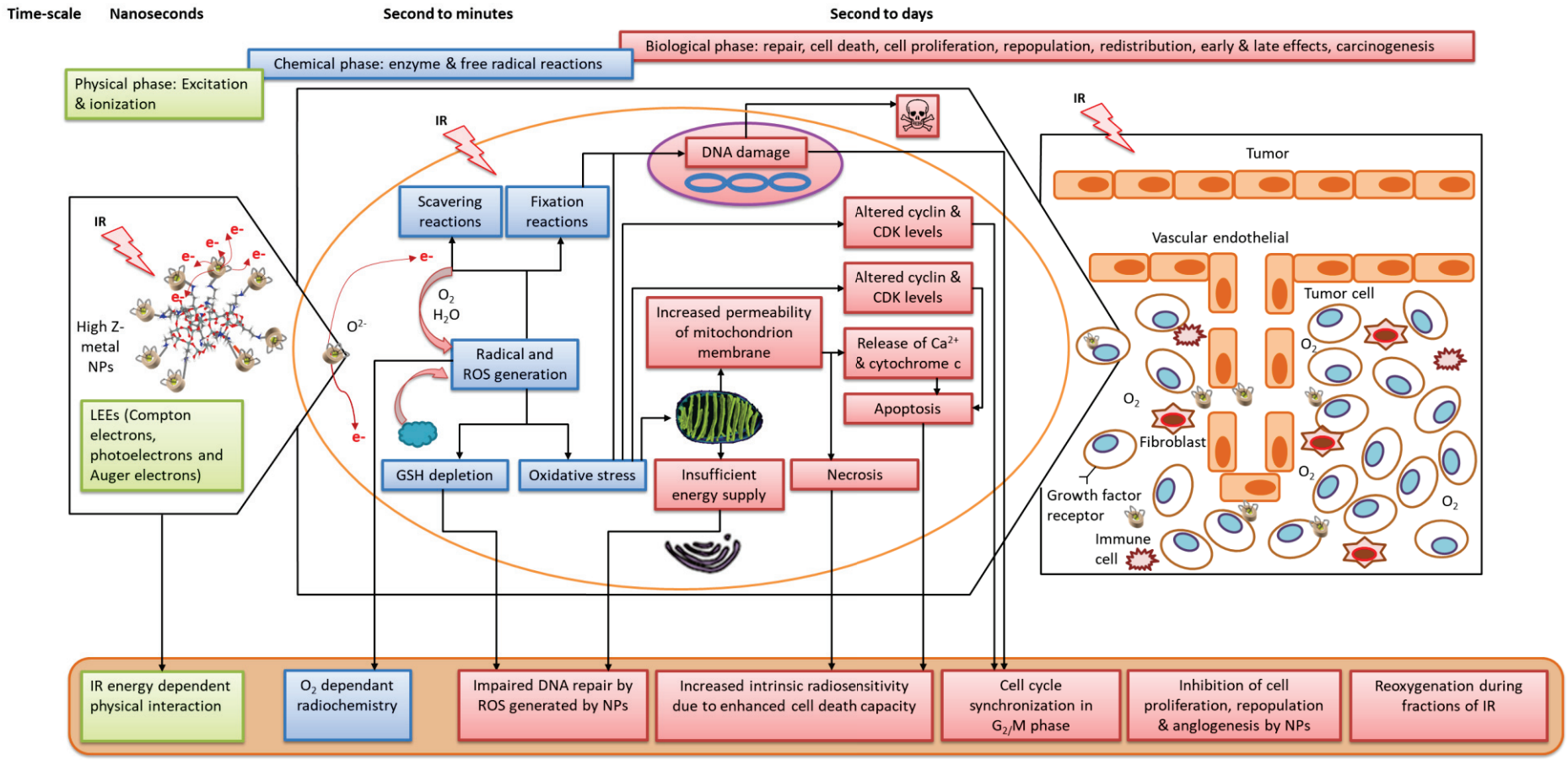


Figure 29: Schematic representation of the physical, chemical, and biological phases following the interactions of X-rays with heavy metal nanoparticles. (Inspired from Cui *et al.*, 2017; Joiner and van der Kogel, 2009)

## *3. AGuIX® (Activation and Guidance of Irradiation by X-ray) nanoparticles*

In order to minimize the dose of ionizing radiations delivered to the patient while enhancing the radio sensitivity of tumors, a new approach on the rise is the development of hybrid nanoparticles made of gadolinium oxides. Gadolinium, a rare earth metal, is a high-Z element currently used as a contrast agent for MRI. Free gadolinium ions cannot be used as it is highly toxic in humans, but can be used by chelating the gadolinium with DOTAREM (gadoterate muglumine), which is a gadolinium-based contrast agent indicated for intravenous for magnetic resonance imaging (MRI) and which allows $Gd^{3+}$ to form a stable non-toxic complex.

AGuIX® present multiple characteristics that make them an attractive radiosensitizer including their small size (hydrodynamic diameter < 5 nm), high colloidal stability and good gadolinium chelation, absence of *in-vivo* toxicity, high EPR effect, biocompatibility and possibility of IV injection, facilitated renal excretion, and their use as a contrast agent for MRI which makes it a **theranostic agent** (Sancey *et al.*, 2014).

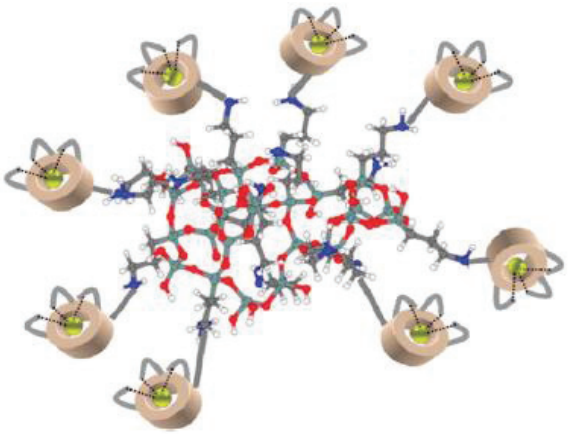

Figure 30: Schematic representation of AGuIX® nanoparticles. Gadolinium atoms are represented in yellow and are chelated by DOTA derivatives (brownish color), and the polysiloxane matrix which is mainly composed of silicon (grey), oxygen (red), and nitrogen (blue).

### 3.1. AGuIX® as radiosensitizers: state-of the-art

As previously mentioned, adding a high-Z element such as gadolinium will allow for an increased interaction with the incoming radiation (see details above, general mechanisms of action for heavy metal nanoparticles), which will in-turn causes increased damages to cancer cells. Since water is the major constituents of cells (~80%), the coefficient of photon mass energy absorption is quite low compared to that of gadolinium (Figure 31 below (a)). In addition, in Figure 31 b, we can observe the energy deposited as a function of the distance from the nanoparticles (total energy decomposed in auger-and photo-electrons).

Many *in-vitro* and *in-vivo* studies were done in a variety of models in order to validate the use of AGuIX® for clinical applications. We will first discuss the studies performed *in-vitro* to then discuss what was found *in vivo*.

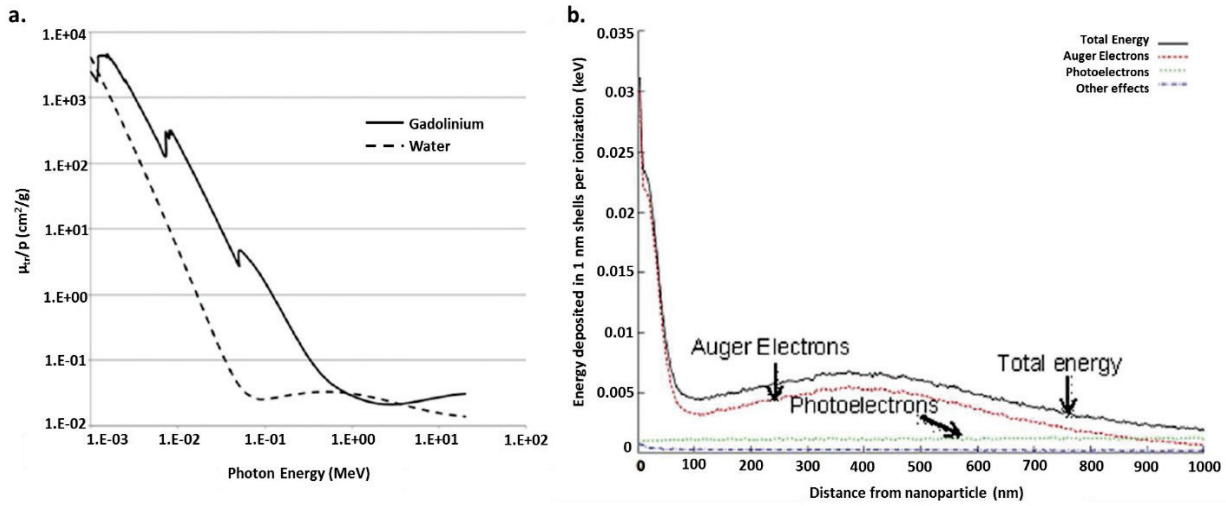


Figure 31: **a.** Comparison of photon mass energy absorption coefficients for gadolinium and soft tissues. **b.** Illustration of nanoscale effects around irradiated AGuIX® gadolinium nanoparticles. (Sancey *et al.,* 2014)

### *3.1.1. In vitro* studies

Many studies were performed on different cellular models as well as using different energies were already performed which validated the use of AGuIX® as a radiosensitizing agent. A few will be detailed in this section.

In 2014, Luchette *et al.* (Luchette *et al.*, 2014) demonstrated a radiosensitizing effect of AGuIX® on HeLa cells when treating the cells with 0.5mM AGuIX® for one hour in culture media with an average dose enhancement of 1.54 and 1.15 for 220 kVp and 6 MV energies respectively. They also calculated the sensitivity enhancement ratio (SER) at 4 Gy of 1.54 and 1.28 for 220 kVp and 6 MV energies respectively (SER calculated by dividing the $SF_{4Gy}$ + AGuIX® over $SF_{4Gy}$). Internalization of AGuIX® inside the cells was measured by ICP-MS and the intracellular concentration of gadolinium was of 0.059 mM. An observation was made by the author that was often observed by others, that radiosensitization depended on the radiation dose as variation was observed between the different irradiation doses. Additionally, by taking into account the energy used for radiotherapy, the authors observed that radiosensitization also varied with the energy of the incoming beam: kVp versus MV. The authors hypothesized that the radiosensitization was primarily caused by photoelectrons. Since the probability of photoelectric interaction is inversely proportional to the cube of the photon energy, these are more present in kVp-range energies (lower energy and therefore

high photoelectric interaction probability) (Butterworth *et al.*, 2010; Rahman *et al.*, 2009; Chithrani *et al.*, 2010; Jain *et al.*, 2011).

Another study was published in 2015 (Detappe *et al.*, 2015) showing a radiosensitizing effect on Panc-1 cells (pancreatic cancer cell model). Again, two photon energies were used: 220 kVp and 6 MV (same as the energies previously used on HeLa cells), but in addition they also test a flattening filter free 6 MV beam (FFF). The cells were treated with 0.5 mM AGuIX®, and different incubation times were tested: 30 min, 1, 3, 6, 24, and 48 hours. They observed a saturation of the internalization of AGuIX® after 30 minutes of treatment with a quantification of 1.25 pg of gadolinium internalized per cell. Transmission Electron Microscopy (TEM) images were taken in order to observe the localization of AGuIX® in Panc-1 cells after 1 hour of internalization: the nanoparticles were predominantly localized in the cytoplasm in vacuoles. A clonogenic survival assay (in the presence of AGuIX® during irradiation) was done to observe the radiosensitizing effect of AGuIX®, and the following were found:

- For the 220 kVp irradiation: SER (4Gy): 1.41; DEF 20%: 1.31
- For the 6 MV STD: SER (4Gy): 1.12; DEF 20%: 1.23
- For the 6 MV FFF: SER (4 Gy) 1.20; DEF 20%: 1.3

In 2015, another gadolinium-based nanoparticle (AGuIX® of first generation, chelated by DTPA) were validated for the radiosensitizing potential in a head and neck squamous cell carcinoma (HNSCC) model. SQ20B J.L. cells were treated with 0.4 mM or 0.6 mM AGuIX® and the irradiation was done using a 250kV photon irradiator. A radiosensitizing potential was observed with corresponding SER (2 Gy) of 1.2 (0.4 mM GBNs) and 2.06 (0.6 mM GBNs). Localization was studied using confocal microscopy using GBNs-Cya5.5 nanoparticles and a strictly cytosolic localization was observed. ICP-OES was performed to quantify gadolinium content and 1.24 pg/cell of gadolinium was found. Cytotoxicity tests showed not toxicity issues 72h after nanoparticle treatment. In order to see if the nanoparticles had an influence on DNA double-stranded breaks (DSBs) even though the nanoparticles are not localized in the nucleus, foci γH2Ax were quantified. Thirty minutes after a 2 Gy irradiation, 0.4 mM GBNs induced an increase of γH2Ax by 41% while 0.6 mM GBNs increased γH2Ax by 53%. Twenty-four hours after the 2 Gy irradiation, the non-treated cells returned to their basal level of γH2Ax while in cells treated, 30% of the initial number of γH2Ax remained. Following cell cycle analysis and caspase-2 tests, it was concluded that the combination of GBNs with photonic irradiation inhibited cell proliferation, modified the distribution of cells in the cell cycle and induced mitotic catastrophe leading to apoptotic cell death (Miladi *et al.*, 2015).

Kobt *et al.* studied a melanoma model (B16F10) and published in 2016 showing a radiosensitizing effect of AGuIX® *in-vitro* as well as *in-vivo* (later discussed). B16F10 cells were treated with 0.6 mM of AGuIX® for one hour in serum free DMEM. In order to study the localization of the AGuIX® in B16F10 cells, confocal microscopy was used with FITC-labeled

AGuIX® nanoparticles. The nanoparticles were located in the cytoplasm inside vesicles: these results were confirmed with TEM. The SER at 2 Gy was calculated and found to be 2.08 with a DEF of 1.3. They also observed an increase in the directly lethal damage as the α-factor increased (the α-factor is obtained from the linear quadratic equation using the clonogenic survival curve assay). Foci γH2Ax were counted at thirty minutes and 24 hours. While no changes were observed with the addition of AGuIX® at 30 minutes after 2 Gy irradiation, 24 hours after irradiation, the number of residual γH2Ax increased by an average of 9 (19.3 foci/nucleus after irradiation alone versus 28 foci/nucleus after irradiation + 0.6 mM AGuIX®). (Kobt *et al.*, 2016)

Novel nanoparticles are being developed with the addition of the bismuth ion on AGuIX® in order to further increase their radiosensitizing potential. This silica-based nanoparticle (SiBiGdNP) therefore contains both gadolinium and bismuth which makes it a nanoparticle suitable for use as an imaging agent in both MRI and CT. A549 Non-Small Cell Lung Cancer (NSCLC) cells were treated with 0.5 mM of SiBiGdNP for 30 minutes prior to irradiation. Irradiation with the addition of SiBiGdNP resulted in a dose enhancement factor of 1.99. An increase in γH2Ax and 53BP1 foci was observed along with a significant increase in apoptosis. (Detappe *et al.*, 2017)

These studies as well as other studies using AGuIX® are summarized below in Table 11.

| Investigator (team, town) | Radiation/energy | Cell line | NP/incubation time | Biological effect |
|---|---|---|---|---|
| K. Butterworth (Queen's University, Belfast, UK) | 225 keV | Prostate: DU145 | From 0.1 to 5.0 mM AGuIX-DTPA/1h | 1.17< SF < 2.50 |
| | | Glioblastoma : T98G | | SF= 1.25 |
| | | Prostate : PC-3 | | 1.25< SF < 1.33 |
| R. Berbeco (Harvard, Boston, MA) | 220 kVp X-ray | Cervical carcinoma- HeLa | 0.5mM AGuIX-DOTA/1h | $SER_{4Gy}$= 1.50<br>DEF= 1.5 |
| C. Rodriguez-Lafrasse (University Lyon, Lyon, France | 250 kV | Head and neck squamous cell carcinoma- SQ20B | 0.4mM AGuIX-DTPA /1h | SF2 = 0.60 vs 0.72 (SER = 1.2_ |
| | | | 0.6 mM AGuIX-DTPA /1h | SF2= 0.35 vs 0.72 (SER = 2.00) |
| | | SQ20B cancer stem cells | 0.6 mM AGuIX-DTPA /1h | SF2= 0.6 vs 0.82 (SER= 1.60) |
| M. Dutreix (Institut Curie, Paris, France) | 660 keV | Glioblastoma- U-87MG | 0.1 mM/1h | γH2Ax + 80% vs irradiation only |
| | | | 0.5mM/1h | |
| R. Berbeco (Harvard, Boston, MA) | 6MV | Cervical carcinoma- HeLa | 0.5 mM AGuIX-DOTA/1h | SER4Gy = 1.30<br>DEF = 1.2 |
| M. Barberi-Heyob (CRAN, Nancy, France) | 6 MV | Glioblastoma- U-87MG | From 0.01 to 0.50 mM AGuIX-DOTA/24h | SER frp, 1.10 to 1.50 |
| G. Blondiaux (CERI, Orleans, France) | Neutron cyclotron (Orleans, France) | Mouse lymphoma- EL4 | From 0.05 to 0.30 mM | Estimated SER3Gy >2.00 |
| S. Lacombe (University of Paris-Sud, Orsay, France) | Ions He2+ beam (Chiba, Japan) | Chinese hamster ovary carcinoma- CHO | 1.0mM /6h | SER = 1.14 |
| S. Lacombe (University of Paris-Sud, Orsay, France) | C6+ beam (200 MeV/ma) (Chiba, Japan) | Chinese hamster ovary carcinoma- CHO | 1.0mM /6h | SER4Gy = 1.50 |
| C. Rodriguez-Lafrasse (University Lyon, Lyon, France | C6+ (33.6 keV µm-1) (Caen, France) | Head and neck squamous cell carcinoma- SQ20B | 0.3mM/1h | SER= 1.33 |
| | | | 0.6mM/1h | SER= 1.59 |

Table 11: Studies of radiosensitizing effect of AGuIX® in various cellular models. (DEF: Dose Enhancement Fraction; NP, nanoparticle; SER, sensitizing enhancement ratio; SF, survival fraction. Non-human lines are indicated.
[a] AGuIX®-DTPA; [b] AGuIX®-DOTA)

### *3.1.2. In-vivo* studies

*In-vivo* studies were realized to validate the radiosensitizing effect observed *in vitro* with the aim of being able to move on to clinical trials with AGuIX®. *In vivo*, AGuIX® nanoparticles accumulated via the EPR effect after intravenous injection (Lux *et al.*, 2011; Sancey *et al.*, 2014; LeDuc *et al.*, 2014; LeDuc *et al.*, 2011; Dufort *et al.*, 2016). They were tested in several models including glioma, head and neck, lungs, pancreas, melanoma, and multiple brain metastases, and showed a high efficiency for both use as a contrast agent in MRI and a radiosensitizing agent using external X-rays which makes it a strong theranostic agent.

In 2014, 9L-gliosarcoma (9LGS) cells were implanted in the brain of male fisher F344 rats. After an intravenous injection of an aqueous solution containing 40 mM of AGuIX®, a rapid highlight of the kidney and later of the bladder was observed by MRI. In addition, angiography images showed a clear highlight of the blood brain vessels with a better contrast for the nanoparticles bearing tumors due to the higher relaxivity and longer residence time in the blood circulation. The authors observed an accumulation of AGuIX® in the tumor via the EPR effect. Irradiation of the animals 20 minutes after the intravenous injection of AGuIX® leads to an important increase of the median survival time to 102.5 days which corresponds to an increased life span of 439%. (Le Duc *et al.*, 2014)

In 2015, gadolinium-based nanoparticles (chelated by DTPA) showed a radiosensitizing effect in SQ20B xenografted tumors. *In vivo* optical images were acquired and showed an intra-tumoral localization of nanoparticles immediately after injection and for 15 minutes. The combination of the nanoparticles with a 10 Gy irradiation strongly limited tumor growth: the mean tumor growth was 5-fold smaller in tumors that received the combined treatment compared to the tumors that had received irradiation only. Increased apoptotic cell death as well as an altered tumor proliferation was observed after the addition of nanoparticle treatment alongside radiation. (Miladi *et al.*, 2015)

In 2016, after showing a radiosensitizing effect of AGuIX® on B16F10 melanoma cells, these cells were othotopically grafted into mouse brains to mimic melanoma brain metastases. A kinetic study was performed in order to determine the amount of nanoparticles as well as their distribution within the tumor cells *versus* the surrounding healthy tissues. It was concluded that radiation exposure could be performed from 1 to 24 hours after injection of the AGuIX® solution (substantial uptake of AGuIX and absence in healthy tissue). Irradiation was done five days after tumor implantation and 3.5 hours post AGuIX-injection for a highest tumor to healthy tissue ratio. When compared to the control group, the addition of AGuIX® prior to irradiation improved treatment efficacy by 3-fold: the increase in life span for the irradiated-only tumor was 8.3 % while it increased to 25% with the addition of AGuIX®. (Kotb *et al.*, 2016)

In 2017, SiBiGdNP also showed their radiosensitizing potential *in vivo* in a fast-growing subcutaneous xenograft solid tumor model (A549 lung adenocarcinoma). The group treated with SiBiGdNP followed by radiation showed a statistically significant improvement in tumor growth delay and survival. A significant increase in DNA damage was also observed in the tumor when the irradiation was performed after SiBiGdNP treatment (89%) compared to radiation alone (67%), and compared to non-irradiated treated and non-treated cells control groups (8 and 5% respectively). (Detappe *et al.*, 2017)

In 2016, a safety evaluation and imaging properties of AGuIX® was done in nonhuman primates (NHP). This study was performed in the context of MRI studies in atherosclerosis bearing animals and healthy controls. In healthy NHP, the pharmacokinetics and toxicity profiles demonstrated the absence of dose, time, and sex-effects, as well as a suitable tolerance of intravenous administration of the nanoparticles. This preliminary investigation reports the efficient and safe imaging of atherosclerotic plaques. Although this study does not show the radiosensitizing properties of AGuIX®, we can show with this study the multiple facets and opportunities that these nanoparticles offer as a strong imaging agent. (Kotb *et al.*, 2016)

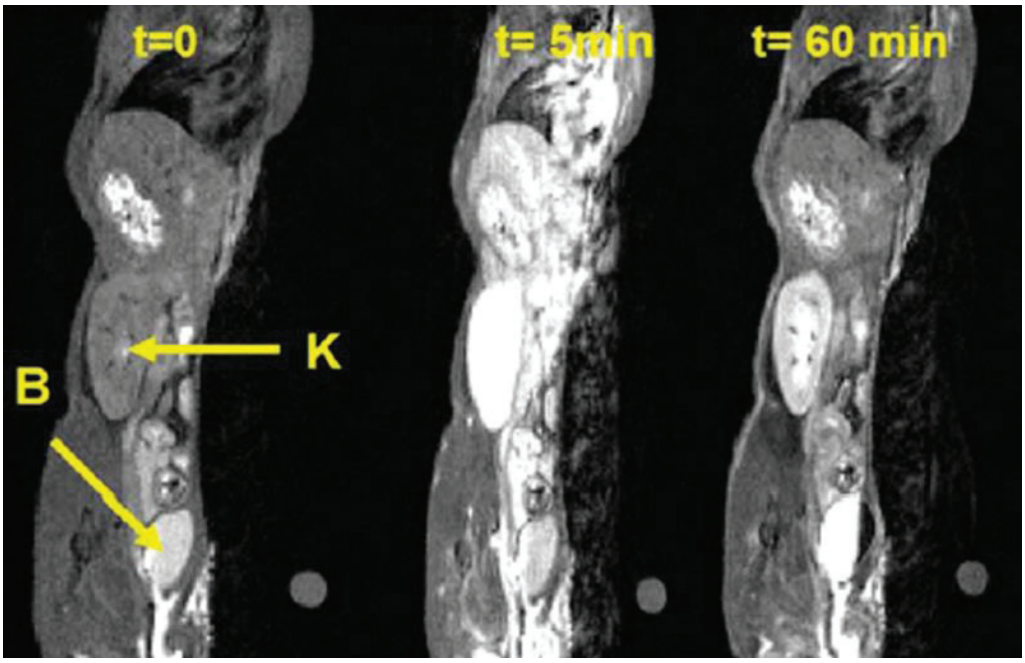


Figure 32: T1-weighted image of a slice, including a kidney (K) and bladder (B) of a mouse before (t=0), 5 min after and 60 min after intravenous injection of AGuIX® nanoparticles. (Sancey *et al.*, 2014)

*AGuIX® renal kinetics and mechanism of elimination (Sancey et al., 2015)*

*In vivo* studies showed a rapid kidney accumulation and renal clearance of AGuIX® nanoparticles. This is mainly due to its small size (hydrodynamic diameter <6nm) (Deen, 2004). Twenty-four hours after intravenous injection, less than 0.2% of the injected dose of the radiolabeled particles was observed in any other organ (Sancey *et al.*, 2015; Lux *et al.*,

2011; Mignot *et al.*, 2013; Kryza *et al.*, 2011; Bianchi A *et al.*, 2013). After injection, AGuIX® nanoparticles rapidly reached the kidneys, as early as 5 minutes after IV injection. One week after injection, most of the signal had been cleared, indicating effective particle elimination from the body via urine (Figure 32).

*AGuIX® nanoparticle biodegradation and toxicity studies*

Concerning the elimination of AGuIX®, it was shown that small degraded particles were eliminated from the body in the first minutes post-injection, whereas full native AGuIX® NPs were entrapped in the proximal convoluted tubules from a few hours to several days before elimination from the organism as native AGuIX® NPs. (Sancey *et al.*, 2015).

Prior to a clinical application, a safety evaluation of AGuIX® was essential. The renal function, assessed through the serum creatinine levels and histological analysis as well as the Maximum Dose Tolerated (MDT), see Table 12). Serum creatinine results showed a transient small increase 30 minutes after AGuIX® administration whereas histological studies showed neither atrophic tubules nor necrotic cells in the tubules, the absence of lesions in the glomeruli and the absence of fibrosis or edema the interstitial tissue. The authors therefore concluded that the observed modifications were **slight** and **transient** after three consecutive injections of AGuIX® NPs. (Sancey *et al.*, 2015)

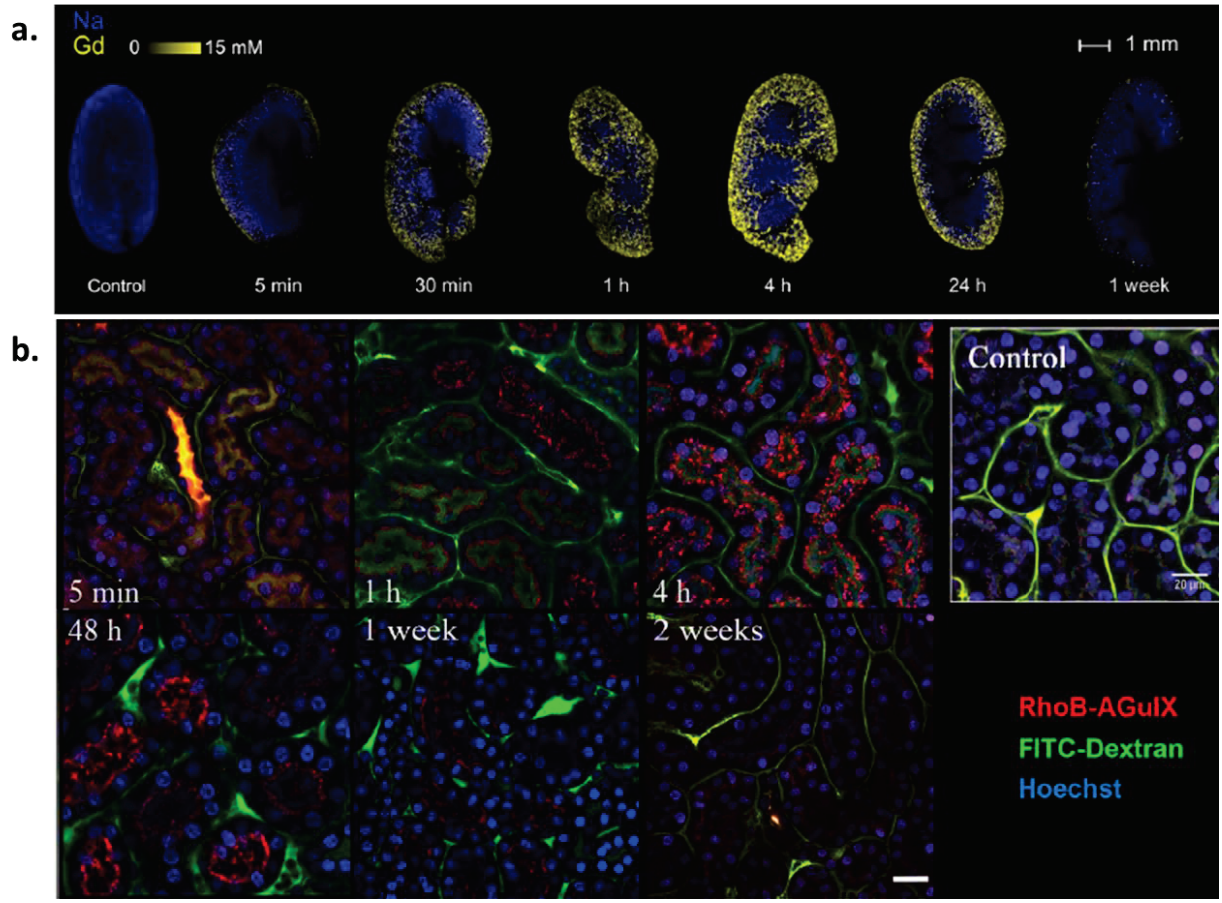


Figure 33: a. Quantitative imaging of Gd and sodium (Na) by LIBS, related to the distribution of AGuIX NPs in the kidney as a function of elapsed time after administration. b. Two-photon microscopy of mice kidneys, from 5 minutes to 2 weeks after a single injection of 200 µL of Rhodamine B-AGuIX (red) at 40 mM Gd. The nucleus and vessels were stained by injecting 50 µL of a mixture of Hoechst 33342 (blue) and FITC-Dextran 70 kDa (green) 5 min before acquisition. (Sancey *et al.*, 2015)

| dose/inj | AGuIX NPs concn | experimental state score (ESS) | | | | | wt variation | |
|---|---|---|---|---|---|---|---|---|
| µmol/mouse | g/L | diarrhea | lethargy | closed eyes | difficulty waking after anesthesia | total | % | no. of deaths |
| 30 | 150 | 0 | 0 | 0 | 0 | 0 | +3.2 | 0 |
| 40 | 200 | 0 | 0 | 0 | 1 | 1 | +5.4 | 0 |
| 50 | 250 | 0 | 0 | 0 | 2 | 2 | +0.8 | 0 |
| 75 | 500[c] | 0 | 0 | 0 | 3 | 3 | +0.5 | 1[b] |

Table 12: Determination of the Maximum Dose Tolerated (MDT) of AGuIX® in non-tumor bearing Mice after a Single IV Injection. (Sancey *et al.*, 2015)

### *3.1.3. Ongoing and upcoming clinical trials*

After ten years of academic research for the preclinical proof of concept, clinical trials have started in 2016. The first clinical trial is on brain metastases and is sponsored by the University Hospital of Grenoble-Alpes (NANO-RAD, Dr. C. Verry). The study is a dose-escalation study with 5 dose levels (3 patients/dose level): 15, 30, 50, 75, and 100 mg/kg. Patients with multiple brain metastases have a high mortality with a life expectancy of less than 4 months: this is

mostly due to a poor distribution of cytotoxic and targeted therapies. The study protocol is schematized in Figure 34 (obtained from S. Dufort, nhTherAGuIX).

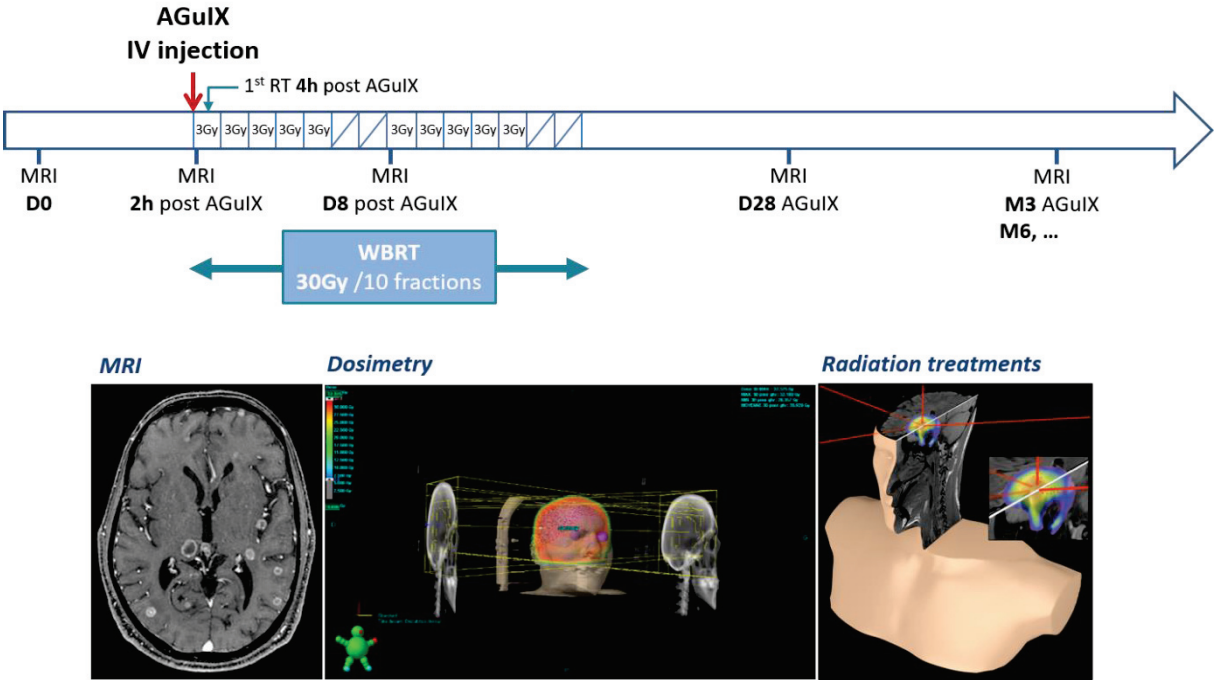


Figure 34: Timeline of the study protocol for the first in Man NANORAD-Phase I.

The primary objective of the study was to determine the maximal tolerated dose (MTD). Four additional secondary objectives were also defined:

- Secondary objective 1: Pharmacokinetic characteristics of AGuIX®- samples of blood will be taken at T= 0, 15, 30 minutes, and 1, 2, 4, 6, 10 (or 12), 24 hours, and 8 days after AGuIX® injection; as well as urine samples over 24 hours (3 fractions at 4h and 1 fraction at 12h) and at 8 days.
- Secondary objective 2: MRI & AGuIX® tumor targeting by evaluating the distribution and elimination of AGuIX® in brain metastases and surrounding healthy tissues.
- Secondary objective 3 and 4: Therapeutic response consisting in the evaluation of the intracranial progression free survival and the evaluation of the overall survival.

Inclusion criteria were the following: patients had cerebral metastases non-eligible to a local treatment by surgery or excision surgery nor stereotactic radiotherapy aged 18 years or older with no upper limit. The Eastern Cooperative Oncology Group (EcOG) performance status must be equal or greater than 3, have no prior brain irradiation. Moreover, an absence of renal insufficiency and normal hepatic function is needed. All the details can be found on: https://clinicaltrials.gov/ct2/show/NCT02820454?term=AGuIX&recrs=a&rank=1

More clinical trials on other types of cancers are underway. A clinical trial is currently going through ANSM (Agence National de Sécurité du Médicament et des produits de santé) to hopefully start the trial in 2018. A clinical trial will hopefully start in 2019 on Head and Neck

Cancer, as well as on glioblastoma and lung cancer. Many institutes are involved in this project.

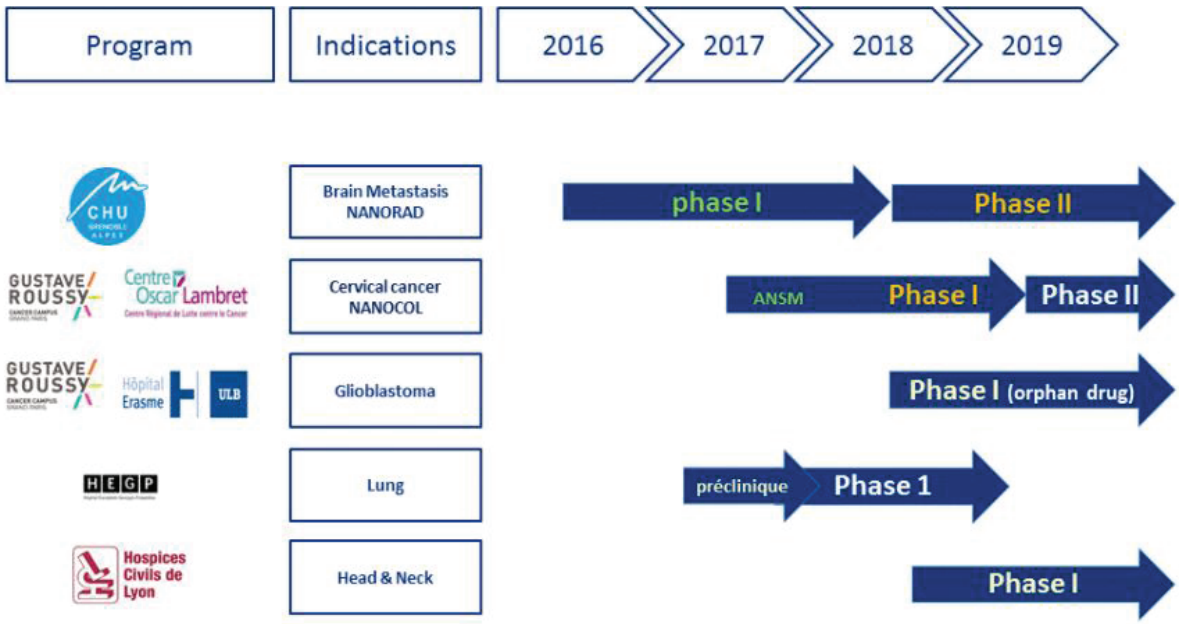


Figure 35: Pipeline of clinical trials with AGuIX®.

# Chapter IV. Radical Oxygen Species (ROS) in Cancer, the role of mitochondria and other organelles

Cellular exposure to ionizing radiation leads to oxidizing events that alter the atomic structure through the direct interactions of radiation with target macromolecules or via products of water radiolysis that results in the generation of reactive chemical species by the stimulation of oxidases and nitric oxide synthases (see Figure 36 below).

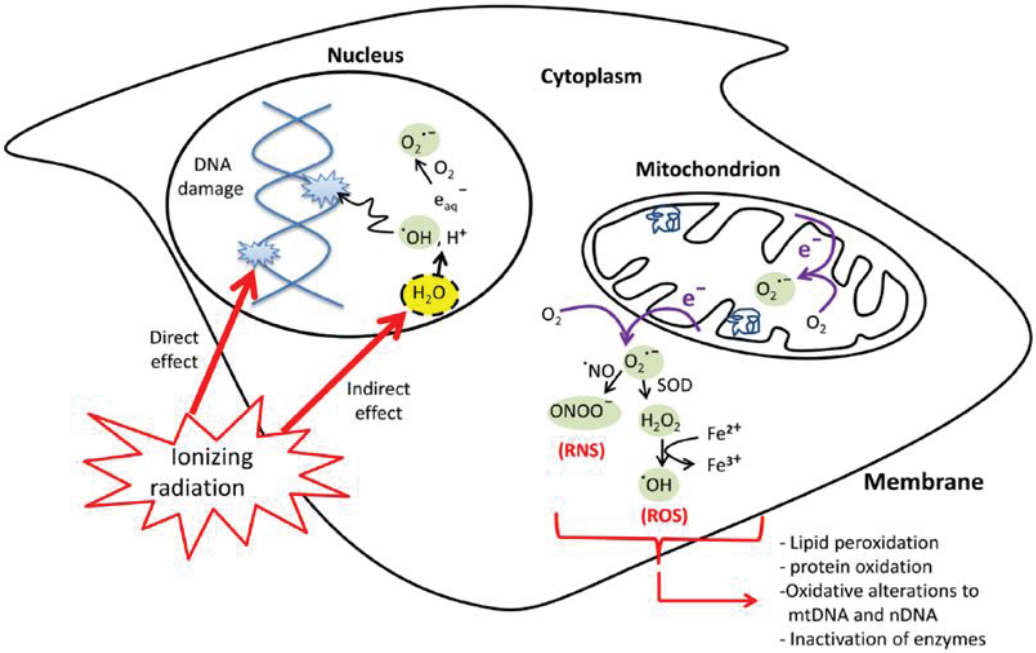


Figure 36: Effects of ionizing radiation on different subcellular compartments. (Taken from Azzam *et al*, 2014)

Ionizing radiation may also disrupt mitochondrial functions significantly contributing to persistent alterations in lipids, proteins, nuclear DNA (nDNA) and mitochondrial DNA (mtDNA).

## 1. *Water radiolysis and generation of reactive oxygen species*

As previously seen in Chapter II, water is the major (~80%) constituent of cells. The absorption of energetic radiations by water results in both excitations and ionizations leading to the production of free radicals that in turn can attack other critical molecules (indirect effect). The complex events linked to the absorption of high-energy photons can be divided into four consecutive temporal stages: during the first or "physical" stage, the energy deposition is caused by the incident radiation and secondary electrons are generated. The resulting species are extremely unstable and undergo fast reorganization in the second or "physicochemical" stage. During the third stage, the various chemically reactive species diffuse and react with one another or with the environment. In the final, biological stage, the

cells respond to the damage resulting from the products formed in the preceding stages. The species produced in the radiolysis of pure deaerated water are $e^-aq$, $^\bullet OH$, $H^\bullet$, $H_2$, and $H_2O_2$, respectively (Ferrradini and Jay-Gerin, 1999). In the presence of oxygen, $e^-aq$ and $H^\bullet$ atoms are rapidly converted to superoxide/perhydroxyl ($O_2^{\bullet-}/HO_2^\bullet$) radicals. In biological systems, organic radicals ($R^\bullet$) are also formed, initiated by $^\bullet OH$ radicals for example which usually react rapidly with $O_2$ to give peroxyl radicals ($RO_2^\bullet$). The $RO_2^\bullet$ radicals can abstract $H^\bullet$ from other molecules to form hydroperoxides (ROOH), a reaction known to be involved in lipid peroxidation.

## 2. Generation of reactive nitrogen species

Ionizing radiation can also stimulate inducible nitric oxide synthase (NOS) activity in hit cells (Mikkelsen *et al*, 2003), thereby generating large amounts of nitric oxide ($^\bullet NO$). $^\bullet NO$ reacts with $O_2^{\bullet-}$ to form the peroxynitrite anion ($ONOO^-$) which is highly reactive and capable of attacking a wide range of cellular targets, including lipids, thiols, proteins and DNA bases but in their immediate vicinity. By contrast, the much lower reactivity of $H_2O_2$ and $O_2^{\bullet-}$ allows them to diffuse a longer distance away from the originating site. In the presence of catalytic redox metal ions (principally $Fe^{2+}$ and $Cu^+$), these species lead to the production of $^\bullet OH$ radicals via Fenton and Haber-Weiss chemistry which can enhance damage (Halliwell and Gutteridge, 2007).

## 3. Other sources of reactive species

An additional major source of intracellular ROS is the NADPH oxidases which are enzyme complexes that catalyzes the production of superoxide from $O_2$ and NADPH (for the four isoforms NOX1, NOX2, NOX3 and NOX5) and the production of $H_2O_2$ by NOX4 (Meitzler *et al.*, 2014). Whereas tissue distribution varies greatly, cellular localization is somewhat less diverse. All NOX proteins exist as transmembrane species and have been found, to varying degrees, at the plasma membrane surface. Intracellular localization has been characterized for NOX1, NOX4, and NOX5 in such structures as trafficking vesicles, the ER, mitochondria, or nuclear membranes (Fulton, 2009; Graham *et al.*, 2010). Mitochondrial ROS are the largest contributor to cellular ROS and it was estimated that 1% of the total mitochondrial $O_2$ consumption is used to produce superoxide (Quinlan *et al.*, 2012; Handy and Loscalzo, 2012). Mitochondria have seven known sites capable of producing superoxide (Murphy, 2009; Brand, 2010) but the sites with the greatest maximum capacities to produce superoxide ($O_2^{\cdot-}$) are at complex I and complex III of the electron transport chain. $O_2^{\cdot-}$ is then converted to hydrogen peroxide ($H_2O_2$) by superoxide dismutase in the matrix (SOD2; also known as MnSOD), or in the intermembrane space (SOD1; also known as CuZn–SOD). The $H_2O_2$ is degraded in the matrix by glutathione peroxidase 1 (GPX1) or peroxiredoxins (PRDX3 or PRDX5) using reducing equivalents obtained from the oxidation of reduced glutathione (GSH). Oxidized glutathione (GSSG) is reduced by glutathione reductase, which obtains its equivalents from NADPH oxidation. $H_2O_2$ generated in the matrix can oxidize proteins, lipids or mitochondrial DNA (mtDNA). Oxidized proteins are repaired by the enzymatic systems thioredoxin/thioredoxin

reductase and glutaredoxin (GRX)/glutathione/glutathione reductase, as well as the methionine sulfoxide reductase depending on the oxidized damage. TRX2 and GRX are subsequently reduced by thioredoxin reductase 2 or by glutathione. Lipid hydroperoxides are reduced by GPX4. Ultimately, all ROS removal depends on the availability of GSH, which is maintained by the availability of NADPH in the respective compartments. Different subcellular compartments can be affected by ETC-derived ROS, depending on where the superoxide is generated: ROS can be driven toward the intermembrane space or released in the matrix. When high levels of ROS overwhelm the antioxidant capacities in both compartments, ROS can reach cytosol since they have some ability to cross membranes, $H_2O_2$ through aquaporins and superoxide through anion channels (Han *et al.*, 2003; Bienert *et al.*, 2007). They can then participate in redox signaling or cause oxidative damage.

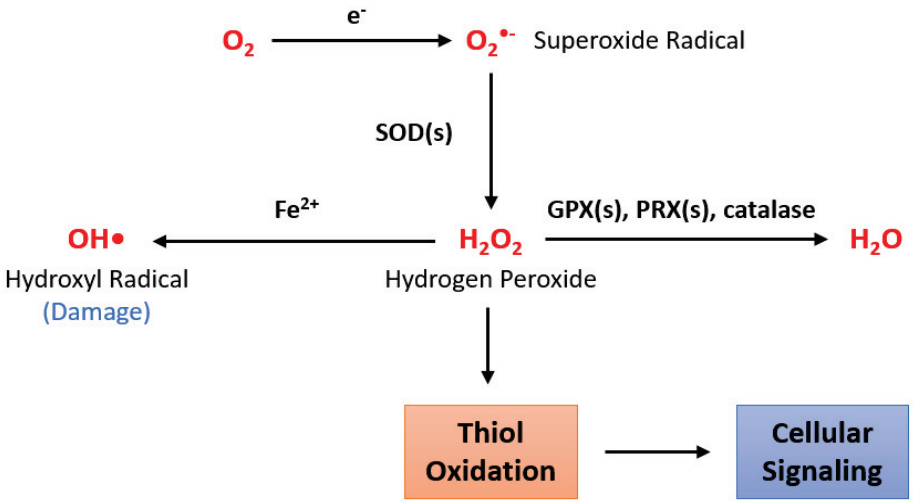


Figure 37: Production of ROS and their evolution: either they degrade to water after the action of antioxidants or in the presence of $Fe^{2+}$, they are converted to OH• which can cause damages to cells. (Sullivan *et al.*, 2014)

## 4. Reactive oxygen species (ROS) signaling pathways regulation

Cytosolic ROS (cROS) and mitochondrial ROS (mROS) act as signaling molecules regulating various signaling pathways. For example, it was observed that they:

- enhance phosphoinositide 3-kinase signaling (PI3K). This pathway is hyper-activated in many cancers and it has been shown to increase proliferation, promote survival, and increase cellular mobility (Cantley, 2002).
- activate hypoxia-inducible factors (HIFs) in order to initiate a transcriptional network which allows tumor cells to adapt to their lower oxygen microenvironment. It was observed that transcriptional targets of HIFs include genes that promote survival under hypoxia, shifting to a metabolism with increased glycolysis, and the activation of angiogenesis (Semenza, 2003)
- modify the cell's metabolism.
- The overproduction of ROS in cancer cells increases tumorigenic mutations which in turn increases the production of ROS.

Surprisingly, in cancerous cells, a vicious circle is put in place as ROS will stimulate the production of even more ROS which will in turn increase mitochondrial mutations which will increase mROS production. Moreover, high mitochondrial ROS levels can result in long mitochondrial permeability transition pore (mPTP) openings which may release a ROS burst leading to the destruction of mitochondria, and if propagated from mitochondrion to mitochondrion, a phenomenon called ROS-induced ROS release (Zorov *et al.*, 2014).

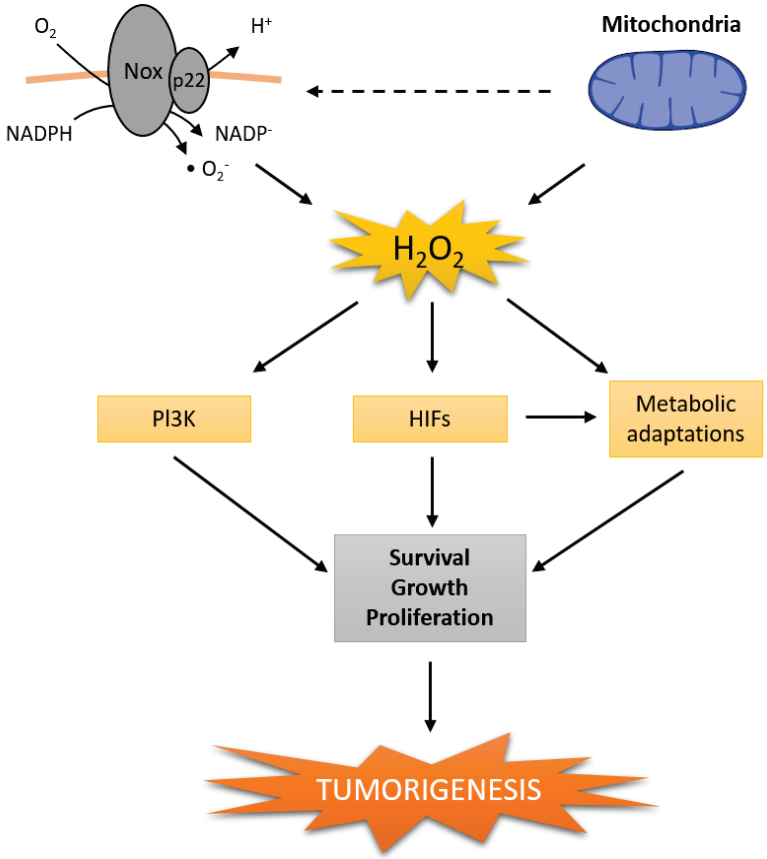


Figure 38: Increased ROS in cells will modify cellular signaling pathways which in turn will promote cell survival, growth, and proliferation which leads to tumorigenesis. (Sullivan *et al.*, 2014)

## 5. *Mitochondria and delayed effects of ionizing radiation*

### 5.1. Generalities

Mitochondria is a double membrane-bound organelle found in all eukaryotic cells and are mostly known as the "power house" of the cell as it provides energy (ATP) to the cell. Although energy production is one of the most known and important function of mitochondria, it is not its only role: mitochondria are also involved in many other tasks such as signaling, cellular differentiation and cell death, which makes it a central organelle in the control of the cell's fate.

Mitochondria are complex organelles which cooperate with their host cells by contributing to bioenergetics, metabolism, biosynthesis, and cell death or survival functions. One of the

particularities of mitochondria is that it has its own circular DNA composed of 16 569 bp encoding for 37 genes of which codes for 13 polypeptides of the mitochondrial electron transport chain (ETC), 2 rRNA, and 22 tRNA. As we will see later, mitochondrial DNA can also be affected by IR, and more specifically, a common deletion of 4977 bp was put in evidence (Peng *et al.*, 2006; Prithivirajsingh *et al.*, 2004). The study of this common deletion can be a functional test since it most likely results from the increased production of mROS. A schematic representation of the mtDNA is represented in Figure 39 showing the full length and what it codes for, as well as where the common deletion occurs.

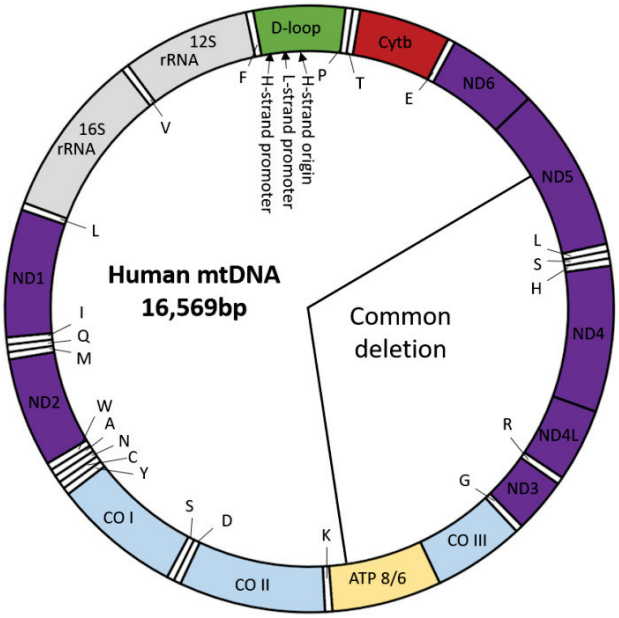


Figure 39: Schematic representation of the mtDNA and the delimitation of the common deletion (Shen *et al.*, 2010).

### 5.2. mROS production after ionizing radiations

Upon cellular exposure to ionizing radiation, ROS generating-oxidases may be activated, antioxidants modulated, and metabolic activity altered in response to the oxidative insult. Among the multitude of induced effects, IR may disrupt mitochondrial functions because they occupy a substantial fraction of cell volume, they consume about 90% of the body's oxygen and are the richest source of ROS (Cadenas and Davies, 2000) as they divert about 1-5% of electrons from the ETC to the formation of superoxide radicals by ubiquinone-dependent reduction (Boveris *et al.*, 1976). The leakage of electrons (mainly from complexes I and III of the ETC) results in the reduction of $O_2$ to create superoxide ($O_2^{\bullet}$). Radiation causes further leakage of electrons from the ETC and therefore results in excess $O_2^{\bullet -}$ generation (Droge, 2002), in addition to the ROS produced during water radiolysis. ROS production by mitochondria plays multiple roles in signalling cascades (Sabharwal and Schumacker, 2014 as a review) and mediates apoptosis (Wu and Bratton, 2015) whereas excess ROS may cause

mutations in mitochondrial DNA, and damage or alter the expression of proteins required for critical mitochondrial and cellular functions.

### 5.3. mROS damage to mitochondrial DNA

Considering mitochondrial DNA (mtDNA), short- and long-term radiation-induced ROS/RNS could result in damage to mtDNA and/or nuclear DNA (nuDNA) coding for mitochondrial ETC subunits as well as the biochemical machinery necessary for their proper expression and assembly. Unlike nuclear DNA, mtDNA is not protected by histones; therefore, the proofreading capacity is limited and ROS that is generated in the matrix can attack it (Alexeyev *et al.,* 2013). Accordingly, the rate of mitochondrial mutation is much greater than for nuclear DNA (Larssen *et al*., 2005). Among the potential mutations, which include insertions, point mutations and changes in mtDNA copy number, the 'common deletion' in the mitochondrial genome is one of the major events following ROS attack. This deletion involves the loss of 4977 base pairs coding for genes that include subunits of the mitochondrial ATPase, NADH dehydrogenase complex I and cytochrome c oxidase (Prithivirajsingh *et al*, 2004). It has been proposed that the 'common deletion' leads to inefficient mitochondrial metabolism and thus increased ROS production (Biskup and Moore, 2006).

Figure 40 schematizes the damages that can result to mitochondrial DNA mutations throughout different stages of the tumorigenic growth. When ROS production is low, the mitochondrial biosynthetic capacity is intact and therefore there are no or very few mtDNA mutations. With a high ROS production, but when the mitochondrial biosynthetic capacity remains intact even with mtDNA mutations, tumorigenicity is increased. Only once the mitochondrial biosynthetic capacities are impaired due to the high ROS production (too much) will the tumorigenicity decrease as cells will die.

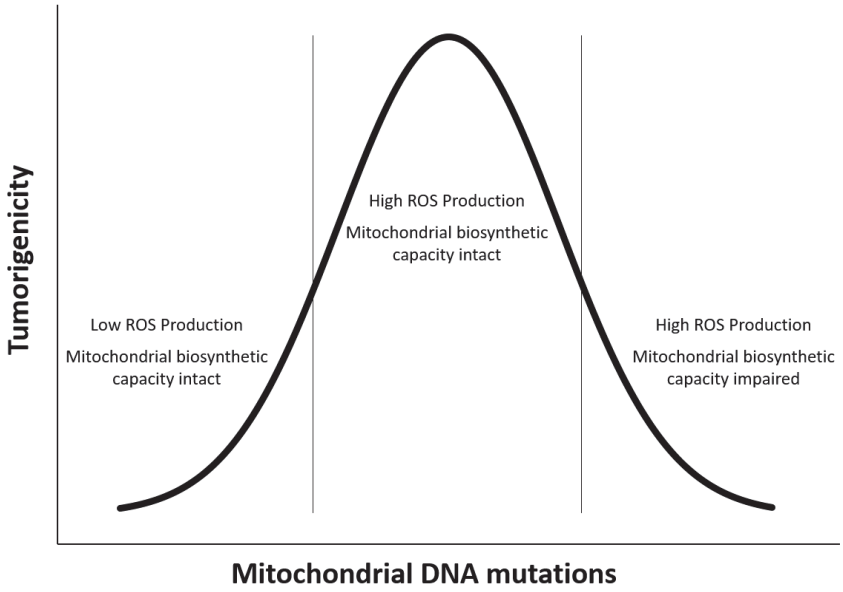


Figure 40: Evolution of tumorigenicity as a function of mitochondrial DNA mutations (Sullivan *et al.*, 2014).

### 5.4. Other damages induced by mROS

Considering other mitochondrial functions, the inner mitochondrial membrane is located near the site of ROS production and is therefore prone to lipid peroxidation. Peroxidation of mitochondrial phospholipids can increase proton permeability of the inner mitochondrial membrane (Stewart and Heales, 2003), alter the fluidity and other biophysical properties of mitochondrial membranes and impair biochemical functions of various transporters and respiratory enzymes in the inner and outer membranes. In that sense, cardiolipin (CL), a phospholipid located at the level of the inner mitochondrial membrane, is known to be intimately involved in several mitochondrial bioenergetics processes as well as mitochondrial-dependent steps in apoptosis and mitochondrial membrane stability and dynamics (Paradies *et al.*, 2010). Oxidation of CL promotes the detachment of cytochrome c from mitochondria (Petrosillo *et al.*, 2001) leading to the permeabilization of the outer mitochondrial membrane and the triggering of apoptosis (Ott *et al.*, 2007). Moreover ROS may promote mitochondrial permeability transition by causing oxidation of thiol groups on the adenine nucleotide translocator, which is believed to form part of the mitochondrial permeability transition pore (Valko *et al.*, 2007).

## *6. Radical oxygen species and their implication in tumorigenesis*

It is a well-known fact that mitochondria, even in a normal cell, produce reactive oxygen species (mROS) as a natural byproduct of the ETC. These mROS will act as signaling molecules and can stimulate a cell towards a “pro-growth” response. It is all a question of balance: mROS produced by the ETC will be counteracted by anti-oxidant enzymes. However, if the cell is unable to maintain its redox homeostasis, it can lead to a tumor-like signaling and metabolic reprogramming. Increased ROS production has long been observed to be a hallmark of many

tumors and cancer cell lines (Szatrowski and Nathan, 1991). As previously mentioned, ROS can cause damage to proteins, lipids, and DNA, therefore it is believed that ROS, if not counteracted, can promote genomic instability in turn leading to tumors (Ames *et al.*, 1993). As we can observe in Figure 40, tumor cells generate increased ROS capable of increasing tumorigenesis by activating signaling pathways regulating cellular proliferation, metabolic alterations, and angiogenesis: the cell is in a state of increased ROS which promotes tumorigenesis but the level of ROS is not high enough to be toxic to the cells. Only once the ROS levels have surpassed a certain level will they become toxic to the cell and the cell will die. However, it is hard to know where that threshold is and it is often cell type-dependent. Since ROS seems to play a crucial role in carcinogenesis, researchers have used this knowledge to develop therapeutic approaches to kill cancer cells, and these approaches will be described in the next paragraph.

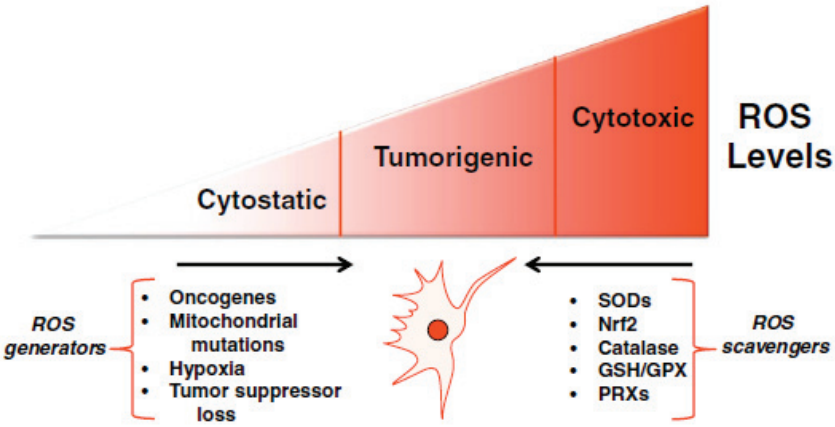


Figure 41: Representation of the ROS levels in three different cell states alongside with the main ROS generators and ROS scavengers (Sullivan *et al.*, 2014)

### 6.1. Targeting Radical Oxygen Species for therapy: a clinical approach

Even though all the different mechanisms on how ROS promotes tumorigenesis are not fully understood, it was clearly demonstrated that ROS play an important role in the spread of cancer as mentioned previously. Therefore, two therapeutic approaches were studied in which case both target ROS. One involves the suppression of ROS production in order to inhibit cellular proliferation, and the second does the opposite by increasing ROS to overcome the "threshold" and selectively kill cancer cells. On Figure 42, one of the approaches tries to bring back the cell to its cytostatic state, while the other aims at overcoming the threshold so that the ROS levels are cytotoxic. Figure 42 schematizes these two approaches.

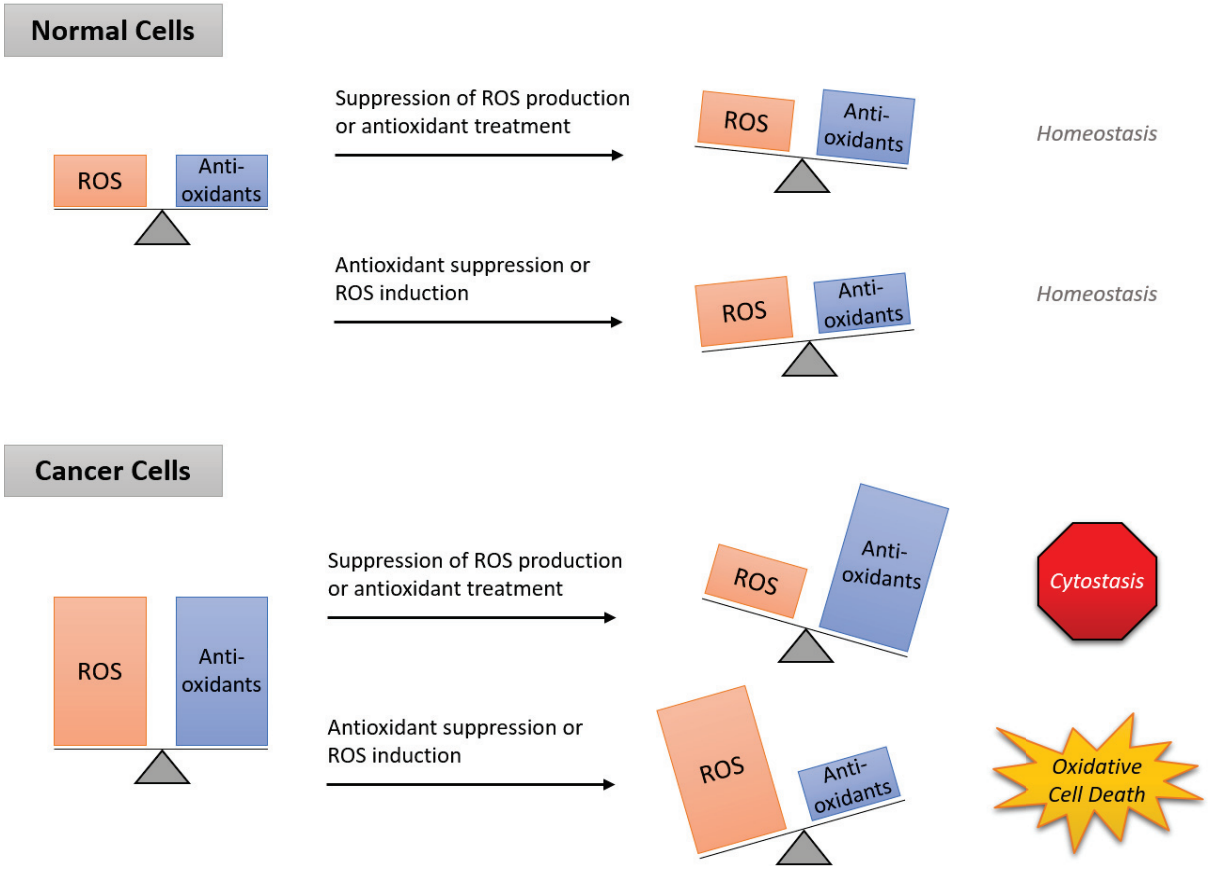


Figure 42: Balance of ROS and anti-oxidants in normal and cancer cells. In normal cells, this balance is modified depending on the stresses that the cell undergoes but will always remain in homeostasis. In cancer cells, ROS levels are elevated but so are antioxidants. Two therapeutic approaches are studied: one to restore cytostasis while the other induces oxidative cell death. (Sullivan *et al.*, 2014)

### *6.1.1. Suppressing ROS to inhibit proliferation*

Since it was observed that ROS stimulates proliferation, one approach was to inhibit ROS production. The first case studies involved treatments of antioxidants such as antioxidant vitamins, including β-carotene and vitamin A or E, however results were contrary to what was expected: this supplementary treatment of antioxidants increased the risk of cancer (Omenn *et al.*, 1996; Klein *et al.*, 2011). In addition, an *in-vivo* study on genetic mouse models of K-Raf- or B-Raf-induced lung cancer, treatment with NAC or vitamin E enhanced tumor growth and accelerated mortality in a significant way (Sullivan and Chandel, 2014). It is therefore important to further study the therapeutic option of inhibiting ROS as some mechanisms are not yet well understood. Explanations were formulated stating that such treatments lack specificity, however it is still vague. It is also important to note that the immune system is an important modulator of cancer growth and has been shown to be sensitive to ROS levels (Sena *et al.*, 2013).

Another approach studied was the direct inhibition of ROS production. However, decreasing mROS will automatically inhibit the ETC which is not a good option as it will lead to

toxicity through inhibition of mitochondrial respiration. Again, surprising results were obtained, as patients taking the drug metformin, an inhibitor of complex I of the ETC, have a reduced risk of cancer incidence and mortality (Noto *et al.*, 2012; El-Mir *et al.*, 2000; Owen *et al.*, 2000). Another approach is to inhibit NADPH oxidases: loss of NOX 4 showed an activation of apoptosis in pancreatic cancer cells (Mochizuki *et al.*, 2006). Additional positive results were obtained using inhibitors of NADPH oxidase activity on mouse models of cancer *in-vivo* (Bhandarkar *et al.*, 2009; Munson *et al.*, 2012).

#### *6.1.2. Increasing ROS to selectively kill cancer cells*

Increasing ROS production in order to overcome the threshold and have a cytotoxic level of ROS has been proposed in different therapeutic approaches. Indeed, as seen in Chapter 3, the use of nanoparticles to radiosensitize cancer cells is expected to increase the ROS levels to a toxic level to provoke cell death. This mechanism is also how many current chemotherapeutics function (Conklin; 2004).

Another interesting approach used is the inhibition of antioxidants since cancer cells increase their expression in order to maintain homeostasis. By inhibiting antioxidants, the cells will be exposed to their endogenously produced ROS which, without defense, can be toxic (Gorrini *et al.*, 2013). Another approach involves the use of chemical drugs such as dimethylfumarate (a glutathione depleting agent) and L-buthionine sulfoximine (a GSH biosynthesis inhibitor) so the cell is unable to "counter-act" with the submerging quantity of ROS produced. It was observed that the transient alteration of the cellular redox buffering before irradiation triggered apoptosis in a head and neck squamous cell carcinoma model (Boivin *et al.*, 2011).

## *7. Effects of ionizing radiation on lysosomes and other cell organelles*

Most studies studying the effects of ionizing radiation focus on the damages done on the nucleus, and more specifically on DNA. As these effects were already thoroughly discussed in Chapter 2, we will therefore focus on a quick overview of the other organelles that can also be damaged by ionizing radiation such as lysosomes, plasma membrane or the endoplasmic reticulum.

### 7.1. Effects of ionizing radiation on lysosomes

In attempts to explain the cytotoxic effects of radiation damage, $HO^{\cdot}$ has been repeatedly invoked as an important intermediate, because $HO^{\cdot}$ forms by radiolysis of water. However, it should be noted that even small amounts of $H_2O_2$ formed intra-lysosomally should induce substantial Fenton-type chemistry leading to lysosomal rupture with release of hydrolytic enzymes and redox-active iron (Persson *et al.*, 2005). Released lysosomal redox-active iron may partly relocate to nuclear and mitochondrial DNA, causing site-specific $HO^{\cdot}$ production in

the presence of oxidative stress (Tenopoulou *et al.,* 2005). Such site-specific $HO^{\cdot}$ induction would be much more powerful with respect to DNA damage than random formation of $HO^{\cdot}$ due to radiolysis of water.

### 7.2. Effects of ionizing radiation on other cell organelles

IR has also recently been shown to induce endoplasmic reticulum (ER) stress thereby activating the unfolded protein response (UPR) signaling pathway in intestinal epithelial cells, an activation that precedes caspase activation in irradiated IEC-6 cells. (Lee *et al.*, 2014). ER stress has also been shown to trigger both apoptosis and autophagy, and act as an important mediator linking the two programmed cell death pathways (Moretti *et al.,* 2007).

Apart from the radiation-induced plasma membrane signaling involving the acid SMase/ceramide pathway (see Chapter V), the effects of IR on biological membranes include alterations in membrane proteins, peroxidation of unsaturated lipids accompanied by perturbations of the lipid bilayer polarity and fluidity (Berroud *et al.*, 1996). Moreover, membrane lipid peroxidation results in increased membrane permeability to small molecules and ions (Stanimirovic *et al.*, 1995). The inability of plasma membrane to maintain ionic homeostasis could therefore result in cell death.

# Chapter V. Ionizing Radiation (IR)-induced cell death

Several modes of cell killings, such as apoptosis, necrosis, autophagy, mitotic catastrophe, and senescence, occur after exposure to IR (see below). Among these, apoptosis and mitotic catastrophe are major forms of cell death induced by IR.

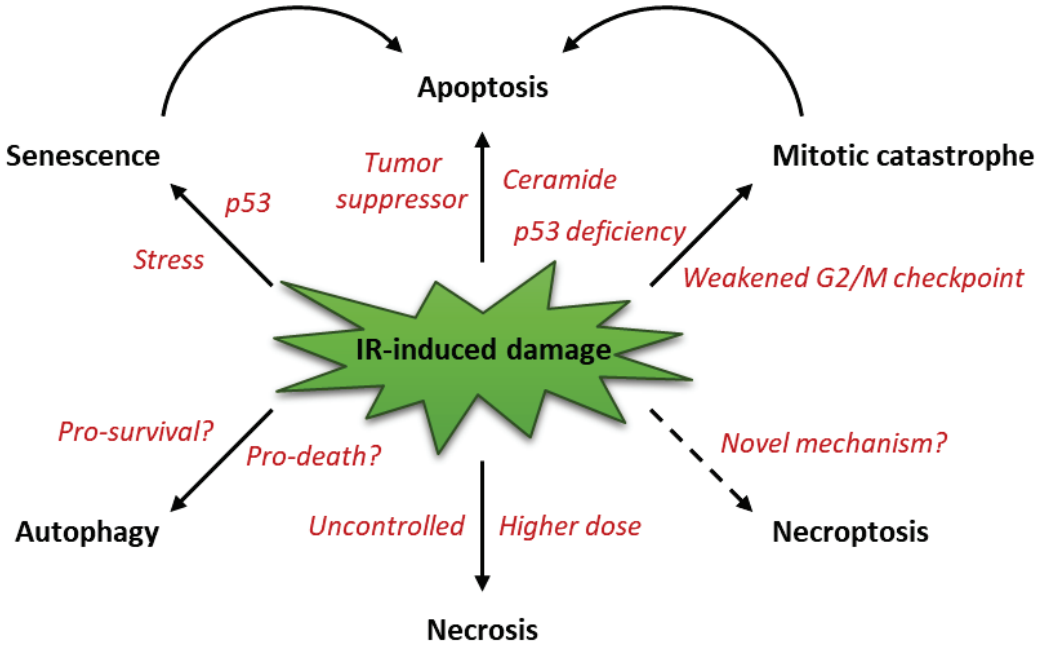


Figure 43: Ionizing radiation (I.R.)-induced cell deaths (Kim B. *et al.*, 2015)

## 1. Apoptosis

Apoptosis is a prevalent form of cell death underlying radiation therapy. Among a spectrum of cellular components, DNA is the main target of IR. Damaged DNA triggers signaling transduction pathways involved in cell cycle arrest and apoptosis. Radiation induces mostly the intrinsic apoptotic pathway (mitochondrial release of cytochrome c and subsequent apoptosome formation), but depending on the dose and cell type, the extrinsic apoptotic pathway (death receptor-mediated caspase activation) or the membrane stress pathway (ceramide production and subsequent second messenger signaling) might be the consequence of irradiation (Takasawa *et al.*, 2005).

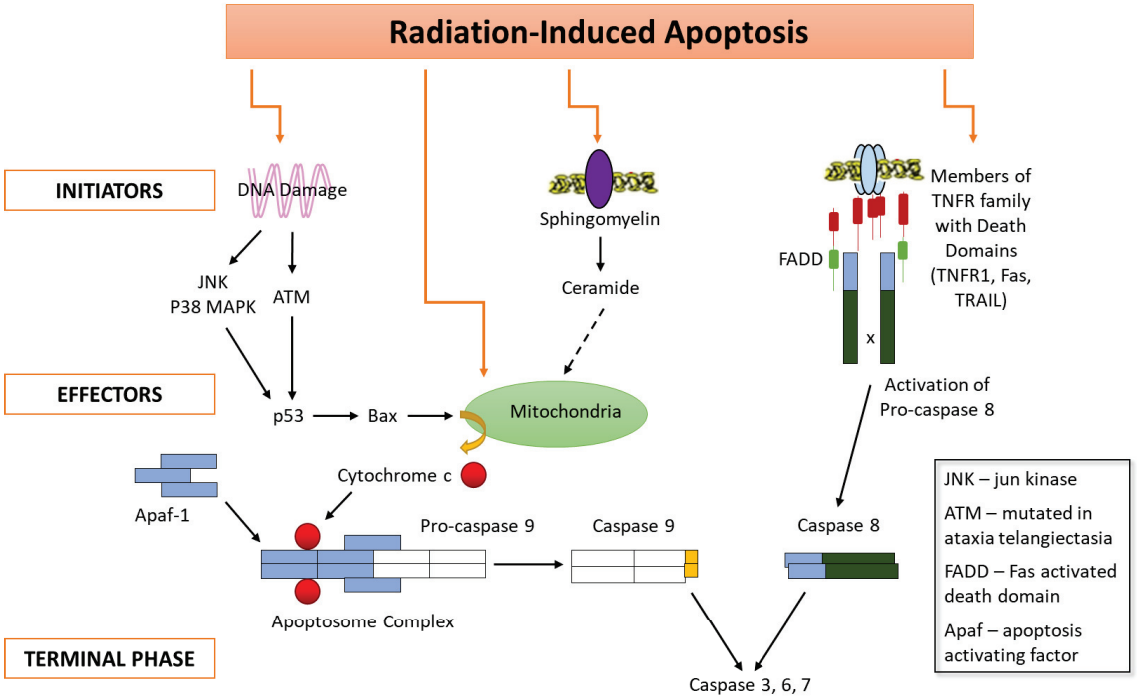


Figure 44: Different signaling pathways activated following radiation-induced apoptosis (Bill McBride, Dept Radiation Oncology, David Geffen School Medicine, UCLA).

### 1.1. The intrinsic apoptotic pathway

The intrinsic apoptotic pathway is initiated by signaling following SSBs and DSBs if DNA repair is not successful (Gudkov and Komarova, 2003). The control and regulation of apoptotic mitochondrial events occur through members of the Bcl-2 protein family (Cory and Adams, 2002), which govern the mitochondrial membrane permeability and can be either pro-apoptotic or anti-apoptotic. Following p53 activation in response to IR, an overexpression of PUMA, Bax and NOXA occurs (Kuribayashi *et al.*, 2011). After its translocation to the mitochondria, PUMA disrupts a complex by p53 and the anti-apoptotic protein Bcl-Xl. Liberated p53 dissolves the complex of the anti-apoptotic Bcl-2 and the pro-apoptotic Bax. Released Bax then triggers cell death by the permeabilization of the outer mitochondrial membrane and the subsequent release of cytochrome c (Dejean *et al.*, 2006). In addition, IR enhances the production of mitochondrial ROS which in turn also triggers cytochrome c release (Ogura *et al.*, 2009). The release of cytochrome c into the cytosol leads to the formation of the cytochrome c/APAF1/caspase-9 containing apoptosome complex (Cain *et al.*, 2000). The initiator caspase-9 then activates the effector caspases-3 and -7, thus inducing the post-mitochondrial-mediated caspase cascade (Cain *et al.*, 1999) which results in the activation of cytoplasmic endonuclease and further degradation of nuclear material.

### 1.2. The extrinsic apoptotic pathway

Radiation-induced apoptosis is also executed through the extrinsic apoptotic pathway : the activation of p53 by radiation causes downstream transactivation of the receptor CD95, DR5 and the CD95 ligand (Sheard, 2001). The complex formation between death receptors and

their cognate death ligands results in receptor trimerization and clustering of death domain receptors. Furthermore, recruitment of an adaptor protein like as Fas-associated death domain (FADD) mediated by Death Domain (DD) leads to the formation of the death inducing signaling complex (DISC) by the interaction between pro-caspase 8 and FADD. The resulting complex activates caspase-8 as a caspase initiator which in turn triggers executioner caspases 3 and 7 which results in cell death (Fulda and Debatin, 2006).

### 1.3. The membrane stress apoptotic pathway

DNA damage-independent apoptotic processes do not require p53. Radiation-induced plasma membrane damage results in the activation of sphingomyelinase (Kolesnick, 2002), followed by the release of ceramide, which acts as the second messenger. Once released, ceramide exhibits diverse effects on signalling complexes including the:
- activation of stress-activated protein kinases (SAPKs) such as JNK and p38 (Ruvolo, 2003),
- activation of the kinase suppressor of Ras (KSR-1) pathway resulting in the up-regulation of the downstream MAPK pathway (Zhang *et al.*, 1997),
- binding to cathepsin D
- recruitment and activation of protein phosphatases (Pettus *et al.*, 2002)
- …

## *2. Mitotic catastrophe*

Along with apoptosis, mitotic catastrophe accounts for the majority of IR-induced cancer cell death. Mitotic catastrophe or mitotic cell death results from the premature induction of mitosis before completion of the S and G2 phases (Castedo *et al.*, 2004). Aberrant mitosis produces an atypical chromosome segregation and cell division causing the formation of giant cells with aberrant nuclear morphology, multiple nuclei, or several micronuclei (Eriksson *et al.*, 2007). Interestingly, mitotic catastrophe can be enhanced by a p53 deficiency and a weakened G2/M checkpoint (Ianzini *et al., 2006).* The induction of mitotic catastrophe induced by IR is associated with the increased expression of cyclin B1 and the kinase activity of Cdc2 (Ianzini *et al.*, 1997).

As a conclusion, it has been suggested that IR-induced cellular damage may induce the premature entry of cells into mitosis and that mitotic cell death may be a key contributor to the loss of clonogenic potential in tumor cells and solid tumors exposed to IR, especially those with a p53 deficiency.

## *3. Necrosis and necroptosis*

Necrosis has historically been regarded as an uncontrolled, *i.e.*, not genetically regulated, form of cell death. Necrosis is much less common after IR treatment but does occur. The decision as to whether they will undergo apoptosis or necrosis after IR exposure seems to be dose-dependent in some cancer cell types, as shown by Rainaldi and co-workers (2003). More

recently, a programmed/genetically regulated type of necrosis, necroptosis, was identified : this program is caspase-independent and controlled by the receptor-interacting protein 1 and 3 (RIP1/3) kinases (Cho *et al.*, 2009). Although little is known about this type of death, recent studies indicate necroptosis to be a novel mechanism of IR-induced death of some endocrine cancer cell types, such as thyroid and adrenocortical carcinoma cells (Neh *et al.*, 2011).

### 4. Senescence

Senescent cells are viable but non-dividing and undergo irreversible cell cycle arrest and stop DNA synthesis. Cellular senescence is a process that results from multiple mechanisms, including telomere shortening, tumor suppressor signals such as p53 and p16INK4A/pRb, and DNA damage. Although p53-independent mechanisms have also been described in IR-induced senescence (Chen *et al.*, 2010), a genetically regulated response to IR-induced DNA damage is usually seen in solid tumor-derived cell lines, especially those with wild-type p53 (Mirzayans *et al.*, 2005). Indeed, the IR-induced retardation of tumor growth is largely attributable to the induction of senescence, not apoptosis, in some lung cancer cell types (Luo *et al.*, 2013).

### 5. Autophagy

Autophagy induced by radiation is critical to the cell fate's decision, particularly in solid tumors (Jaboin *et al.*, 2007). Autophagy induced by radiation play bi-directional effects in the cell fate's decision whether cells survive or die depending on the severity and duration of this phenomenon (Dalby *et al.*, 2010). Besides, dual activity of autophagy on tumor cell fate *in-vitro* (Mo *et al.,* 2014 ; Wu *et al.*, 2014), as well as recently *in-vivo* studies, also demonstrated that irradiation-induced autophagy exerts a crucial activity on tumor clearance by the immune system (Huang *et al.*, 2014).

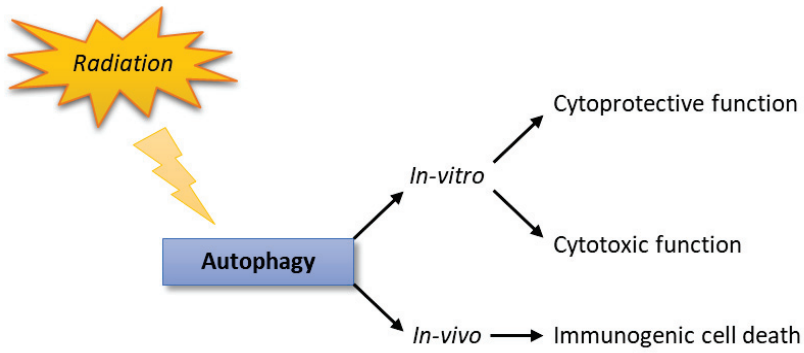


Figure 45: *In-vitro* and *in-vivo* observations following autophagy induced by radiation.

As radiation can directly or indirectly damage DNA which can activate the repair signaling pathway, a large number of proteins participating in the DNA damage repair signaling pathway such as p53 (Fei *et al.*, 2003), ATM, PARP1 (Rodriguez-Vargas *et al.*, 2012) , FOXO3a, mTOR (Kim *et al.*, 2011) and SIRT1 (Lapierre *et al.*, 2015) are involved in the regulation of autophagy.

However, emerging recent evidence suggests that ionizing radiation can also cause injury to extranuclear targets such as the plasma membrane, mitochondria and endoplasmic reticulum (ER) and induce the accumulation of ceramide, ROS, and $Ca^{2+}$ concentration which can in turn activate many signaling pathways modulating autophagy. Ceramide can induce ER stress (Jiang *et al.*, 2014) and mitochondrial dysfunction (Sentelle *et al.*, 2012) , which are two important autophagic triggers. ROS is an essential activator of cytoplasmic signaling cascades such as p38, JNK, HIF-1α which activate autophagy-related signaling pathways (Liu *et al.*, 2014). ROS can also cause injury to mitochondria and ER which elevate the levels of ROS and $Ca^{2+}$ concentration and decrease ATP (Zhang *et al.*, 2013). Changes to these molecules are important to induce autophagy. Moreover, ROS production activates ER membrane sensors of ER stress which in turn triggers autophagy. All these radiation-induced autophagic triggers are illustrated below.

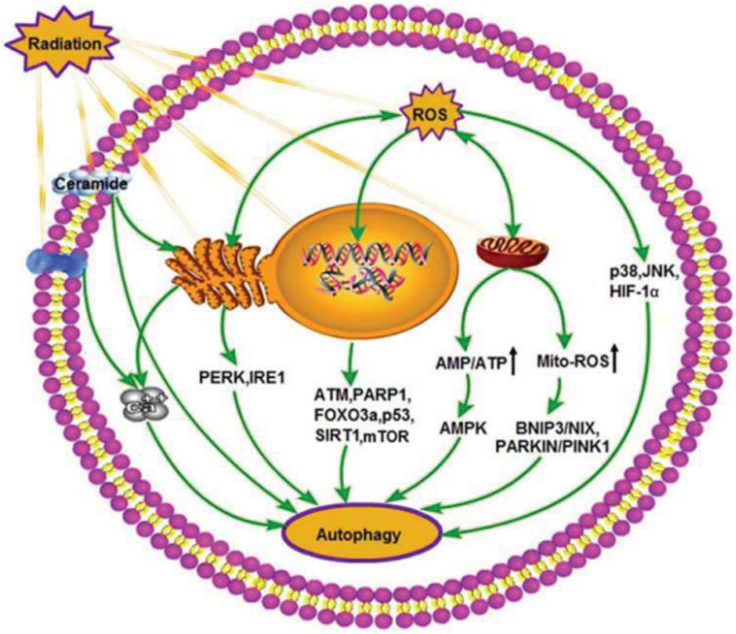


Figure 46: Radiation-induced autophagic triggers (Hu *et al.*, 2016).

# Materials and Methods

# 1. Cell culture and treatments

## 1.1. Cell Culture

SQ20B J.L. cell line was used as the *in vitro* model in this study. This cell line was derived from a human larynx radioresistant carcinoma obtained from the John Little Laboratory (Harvard School of Public Health, Boston, USA). SQ20B J.L. cells were previously characterized with a 2Gy survival fraction of 72%.

The cells were cultured in Dulbecco's Modified Eagle's Medium-Glutamax (DMEM-Glutamax) containing 4.5 g/L of glucose (ThermoFisher ref 10566016), supplemented by 10% of fetal calf serum (FCS) (PAA ref A15-151), 0.04 mg/l of hydrocortisone (Sigma ref H0396), 100 U/ml of penicillin and 0.1 g/L of streptomycin (PAA ref P11-010). The cells were kept in an incubator at a constant temperature of 37°C and 5% $CO_2$.

## 1.2. AGuIX® (Activation and Guidance of Irradiation by X-ray) nanoparticles

AGuIX® nanoparticles were provided by a collaborative research group, the laboratory of O. Tillement (FENNEC Team director, part of the Institut Lumière Matière laboratory, University Claude Bernard Lyon 1).

These nanoparticles are made of a polysiloxane core grafted to 7-10 Gd-DOTA species via amide functions in the periphery. Their molecular mass is about 8.5 +/- 1 kDa with a hydrodynamic diameter of 3.0+/- 0.1nm. A detailed description of these nanoparticles was previously reported by Sancey *et al* (2014). Figure 47 shows a schematic representation of AGuIX® nanoparticles along with their main characteristics.

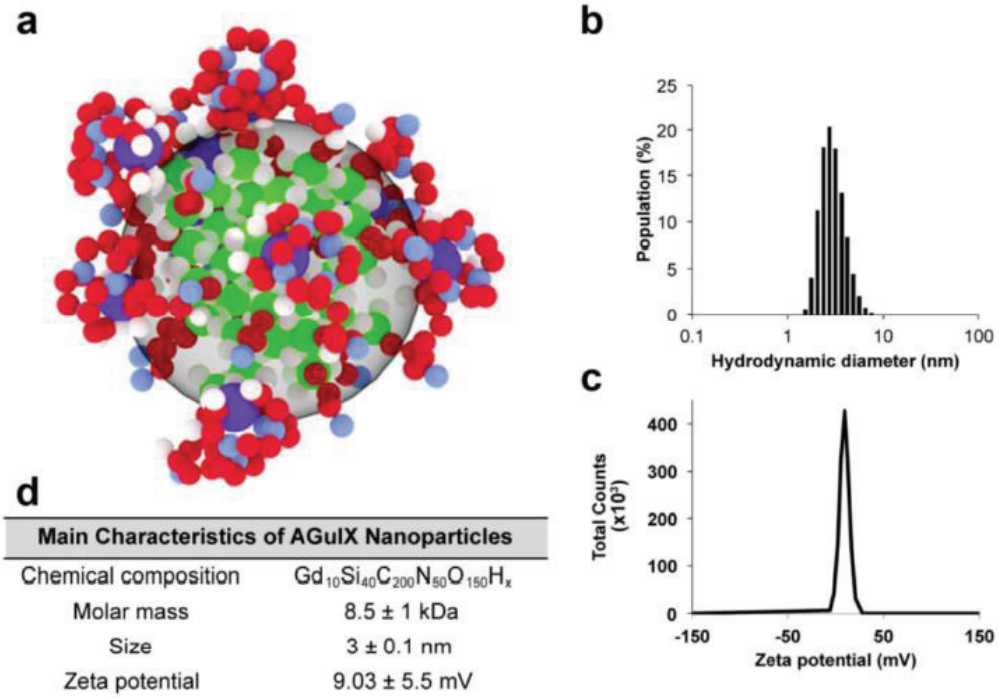


d

| Main Characteristics of AGuIX Nanoparticles | |
|---|---|
| Chemical composition | $Gd_{10}Si_{40}C_{200}N_{80}O_{150}H_x$ |
| Molar mass | 8.5 ± 1 kDa |
| Size | 3 ± 0.1 nm |
| Zeta potential | 9.03 ± 5.5 mV |

Figure 47: Characterization of AGuIX® nanoparticles. **a**. Schematic representation of AGuIX®. **b**. Hydrodynamic diameter and **c**. Zeta potential, measured by DLS **d**. Physical properties of AGuIX®. (Kotb *et al., 2016*)

### 1.3. AGuIX® treatment of SQ20B cells

*Preparation of the AGuIX® solution*

AGuIX® were received lyophilized for a better conservation. The day of the treatment, AGuIX® are resuspended in sterile $dH_2O$ for a minimum of one hour. AGuIX® were then diluted to the appropriate concentration in DMEM alone. Once resuspended, the nanoparticles are kept for a maximum of 24 hours for stability purposes.

*SQ20B treatment*

SQ20B J.L. cells were seeded at a density of 40 000 cells/$cm^2$ 16 hours prior to AGuIX® treatment. Before treatment, cells were washed with Phosphate-Buffered Saline (PBS), and then incubated with 0.8mM Gd for 24 hours in DMEM-Glutamax alone (without FCS). After the 24 hours of incubation with AGuIX®, the nanoparticles were removed, the cells were washed twice with PBS and full SQ20B J.L. culture media was added to the flasks before irradiation.

### 1.4. DMF/BSO treatment

After the 24h AGuIX® treatment, the cells were rinsed twice with PBS. The cells were then incubated for four hours prior to irradiation with dimethylfumarate (DMF 250 mM solubilized in DMSO), a GSH-depleting agent, and L-buthionine sulfoximine (BSO 100 mM solubilized in

PBS) an inhibitor of GSH biosynthesis, at working concentrations of 100µM each. Controls without DMF/BSO were done in parallel to directly compare both conditions.

### 1.5. Photon Irradiation

Monolayers of cultured cells were irradiated using an X-Rad 320 irradiator (Precision X-ray Inc., North Branford, CT) located at the Lyon-Sud Medical School, with an energy of 250 kV and an intensity of 15 mA delivered at a dose rate of 2Gy/min. The distance between the beam and the cells was kept constant at 50 cm. Figure 48 is a photo taken of the interior of the X-Rad 320 irradiator and the screen for the control panel.

**Note: the cells were never irradiated in the presence of AGuIX®. After the 24 hours treatment, the "non-internalized" nanoparticles were washed off, and the cells were irradiated solely with the nanoparticles inside the cells or the ones that had adhered to the cells' membrane.*

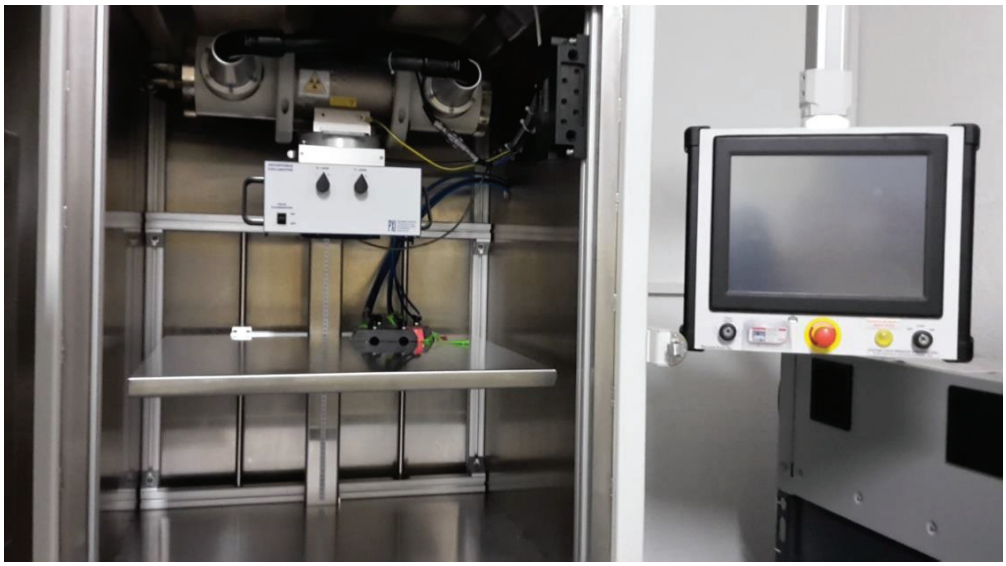

Figure 48: Photo of the interior of the X-ray irradiator (Laboratory of Cellular and Molecular Radiobiology, Lyon-Sud Medical School, Lyon, France).

## 2. *Characterization of the radiosensitization effect of SQ20B J.L. cells by AGuIX®*

### 2.1. Determining the AGuIX® concentration and ideal medium for a radiosensitizing effect

This next section will describe the protocol used for determining the radiosensitizing conditions of SQ20B JL cells with AGuIX® nanoparticles. The radiosensitizing effect of AGuIX® was determined and validated by the **clonogenic survival curve assay**.

SQ20B J.L. cells were plated in 25 $cm^2$ flasks at a density of one million 16 hours prior to AGuIX® treatment. The cells were then treated as previously detailed in paragraph 1.3. After AGuIX® treatment (0 or 0,8mM Gd), cells were washed twice with PBS, placed in fresh SQ20B

J.L. medium, and irradiated at varying doses from 0 to 10 Gy. The cells were then trypsinized and reseeded in 25 $cm^2$ flasks at different cell densities (see table below) depending on the treatment received. For each treatment conditions, two cell concentrations were seeded in triplicates for a total of 6 X 25$cm^2$ flasks per condition (see Table 13 for seeding concentrations). Cell survival was assessed by the standard colony formation assay as described by *Beuve et al*., 2008.

| Dose (Gy) | 0mM Gd | 0,8mM Gd |
|---|---|---|
| 0 | 150/300 | 150/300 |
| 1 | 150/300 | 150/300 |
| 2 | 200/400 | 200/400 |
| 3 | 300/600 | 300/600 |
| 4 | 400/800 | 400/800 |
| 5 | 500/1000 | 500/1000 |
| 6 | 800/1600 | 800/1600 |
| 8 | 1000/2000 | 1000/2000 |
| 10 | 2500/5000 | 2500/5000 |

Table 13: Seeding concentrations of SQ20B J.L. cells for the clonogenic cell survival assay depending on the treatment conditions.

Once the cells were re-seeded in fresh SQ20B J.L. cell medium, they were placed in the 37°C-5% $CO_2$ incubator until the control (0mM Gd-0Gy) had undergone six cellular divisions (which corresponds to a clone of 64 cells). A cell that was able to divide six times is considered a viable cell. The cells were fixed for thirty minutes using a 96% ethanol solution and then colored using Giemsa for another thirty minutes. The Giemsa was diluted in distilled water at a fraction of $1/20^{th}$. The clones of 64 cells or bigger were then counted using the colony counter COLCOUNT™ (Oxford Optronix), and the survival was calculated using the following formula:

Survival = number of colonies/ (PE * number of seeded cells)
where PE is the plating efficiency measured at 0 Gy (number of colonies/number of seeded cells)

The survival curves are then established using the linear quadratic equation $S= \exp(-\alpha D-\beta D^2)$, where:

- S = survival,
- D = the dose,
- α= tangent at the origin of the curve describing the immediate lethal lesions
- β = tangent of the curve after the “shoulder” describing sub-lethal lesions

The ratio α/β therefore measures the repair capacities of the cell and therefore characterizes a cell or tissue type.

### *2.1.1. Survival Fraction at 4Gy ($SF_{4Gy}$)*

In order to isolate the radiosensitizing concentration of AGuIX®, concentrations varying from 0 to 3 mM Gd along with three different culture media were tested: HBSS, PBS $Ca^{2+}/Mg^{2+}$, and serum-free DMEM-Glutamax. In order to screen these different conditions, the survival fraction at 4Gy ($SF_{4Gy}$) was evaluated. Each time the following technique was used:

Cells were plated at a density of 1 million in 25 $cm^2$ flasks. Once plated, the cells were treated with AGuIX® concentration varying from 0-3 mM Gd for one hour. The AGuIX® solution was then removed and the cells were washed twice with PBS and placed back in their culture medium. The cells were irradiated at 4Gy, then trypsinized and re-seeded in 25$cm^2$ flasks at the following clonal densities: 150 and 300 cells for the control (0Gy) and 400 and 800 cells for the cells that had received a 4Gy irradiation. The cells were then put back in the incubator and left between 8-12 days, until the untreated and non-irradiated cells had clones of at least 64 cells (6 divisions). Once clones had reached the 64 cells, cells were washed twice with PBS, fixed, stained, and counted as previously described.

Once the radiosensitizing AGuIX® concentration was determined, different incubation times were tested: 1h, 4h, 12h, and 24h in order to optimize the radiosensitizing effect. The same $SF_{4Gy}$ protocol was used.

### *2.1.2. Determining the quantity of gadolinium internalized by Inductively Coupled Plasma-Atomic Emission Spectrometry (ICP-AES)*

Cells were plated at a density of 7 million in 175 $cm^2$ flasks and incubated with different AGuIX® concentrations. After treatment, the cells were rinsed twice with PBS and trypsinized, centrifuged at 300 x g for 5 minutes at room temperature (RT), and rinsed twice with PBS. The samples were then kept as dry pellets at 4°C until further treatment.
The samples were transferred in 50 mL falcon tubes and 2 mL of ultrapure water was added. For the next step (the mineralization step), the samples were transferred to a new 50 mL falcon tube followed by the addition of 4-5 mL of aqua regia (composed of a mix of nitric acid and hydrochloric acid, optimally at a molar ratio of 1:3). The samples were kept at 80°C for three hours. Ten mL was then filtered through a 0.2 µm filter and analyzed with a Varian 710-ES (ILM- Fennec Team).

### *2.1.3. Toxicity studies*

#### 2.1.3.1. Trypan blue toxicity assay

In order to verify cellular toxicity of AGuIX® treatment in SQ20B JL cells, trypan blue toxicity assay was performed. Trypan blue is used as a viability test as cells that uptake trypan blue are considered non-viable.

SQ20B J.L. cells were plated in six-well plates at a density of 400 000 cells per well and treated with AGuIX® for either one or twenty-four hours in serum-free DMEM-Glutamax. After treatment, cells were rinsed twice with PBS and put back in their culture medium. For the times over 24h, the cells were trypsinized and re-plated as to not exceed an 80% confluency.

At t = 24h, 48h, 72h, 120h and up to 7 days, the cells were trypsinized; 10 µL of trypan blue solution was added to 10 µL of the cell suspension and the cell viability was measured using the Countess automated cell counter (Invitrogen) that allow to quantify the number of total cells, live cells, dead cells, and percent viability.

#### 2.1.3.2. 3-(4,5-dimethylthiazol-2-yl)-2,5-diphenyltetrazolium bromide (MTT) toxicity assay

The 3-(4,5-dimethylthiazol-2-yl)-2,5-diphenyltetrazolium bromide (MTT) assay is a colorometric assay used to measure the cellular metabolic activity. NAD(P)H-dependent cellular oxidoreductase enzyme activities reflect the number of viable cells: the enzymes are capable of reducing the tetrazolium dye MTT to its insoluble formazon: we will then observe a purple color which is more or less dark depending on the number of viable cells.

SQ20B JL cells were plated in six-well plates at a density of 400 000 cells per well and treated with AGuIX® for either one or twenty-four hours in serum-free DMEM-Glutamax. After treatment, cells were rinsed twice with PBS, trypsinized and re-plated in 96-well plates.

At t = 24h, 48h, 72h, 120h and up to 7 days, 200 µL of a solution at 0.5 g/ml of MTT (Sigma, M-5655) was added to each well. The plate was incubated for two hours at 37°C and 5% $CO_2$. The wells were then rinsed twice with PBS and 100 µL of DMSO were added to each well and left for thirty minutes under agitation (during which the DMSO will dilute the crystallized MTT). At the end, the plate was read at an absorbance of 560 nm using the SpectraMax M2 spectrophotometer (Molecular Devices).

### *2.1.4. Proliferation assay: confluency percentage measurements by Incucyte*

SQ20B J.L. cells were plated in 25 $cm^2$ flasks and received corresponding treatments. After either a 0 or 10 Gy irradiation, cells were trypsinized and re-seeded in a 96-well plate at a density of 5 000 cells per well. Pictures were taken in phase contrast by the Incucyte (Essen Biosciences) every two hours for 7 days. Photographs of the IncuCyte where the plates are put is shown in Figure 49.

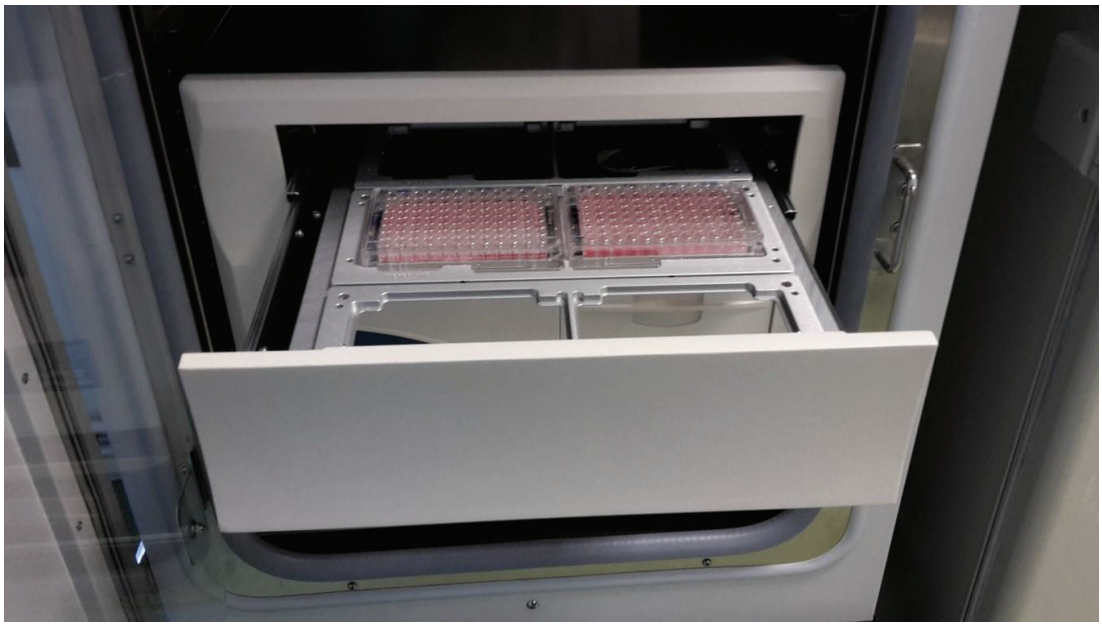

Figure 49: Interior of the IncuCyte apparatus.

## 2.2. Cellular localization of AGuIX® in SQ20B JL cells

### *2.2.1. Confocal microscopy*

Cells were plated in two-chambers LabTek®II Chambered #1.5 German Coverglass System (Dutscher) and AGuIX® covalently linked to Cya5.5 (as a fluorescent marker) were used.

For co-localization studies with the nucleus, the cells were fixed in 4% PFA for 20 minutes, rinsed three times with PBS for 5 minutes and then exposed to DAPI (1µM) (4',6'-diamidino-2-phenylindole) for 15 minutes. After staining the nucleus, the cells were rinsed three times with PBS for 5 minutes and then kept in 1 mL of PBS for observation under the confocal spinning disk microscope of the µLife Platform (see Figure 50) (CEA-Grenoble).

For the co-localization studies with the mitochondria or lysosomes, live-cell imaging was performed. SQ20B J.L. cells were incubated with either 200 nM Mitotracker-Green (Invitrogen) for 45 min or 75 nM Lysotracker-green (Invitrogen) for 45 minutes in culture medium prior to AGuIX®-Cya5.5 treatment. The probes were then washed out and the cells

rinsed twice with PBS before treatment with AGuIX®-Cya5.5. After 24 hours of incubation, the AGuIX®-Cya5.5 were washed out of the cells, and the cells were observed using the confocal spinning disk of the µLife Platform (CEA-Grenoble).

AGuIX®-Cya5.5 were excited with a laser at 642 nm, while Lysotracker and Mitotracker-Green were excited at 491 nm. Images were taken in 60X oil objective on a z-width of 15 µm with step-sizes of 0,5 µm.

Figure 50: Confocal spinning-disk microscope (µLife Platform, CEA-Grenoble, Grenoble, France).

A kinetic study was also done in order to observe the internalization of AGuIX® in time: 1h – 2h – 4h – 6h.

## *3. Study of cell death after AGuIX® treatment + irradiation*

### 3.1. Study of apoptosis and necrosis

The CaspACE™ FITC-VAD-FMK in situ Marker (Promega) was used to quantify total caspase activity by flow cytometry. The cells were trypsinized and incubated with 5 µM CaspACE™ FITC-VAD-FMK for 20 minutes at room temperature. The cells are then washed twice with PBS and resuspended in PBS for flow cytometry analysis with an excitation at 488 nm and emission at 530 nm (LSRII, BD, Biosciences- Lyon Sud Medical School, see Figure 51 showing a photo of the LSRII used throughout the thesis). Figure 52 represents the graphs obtained using the DIVA software. After a 10Gy irradiation, the peak expands and slightly shifts to the right representing an increase in the number of cells positively stained by the marker.

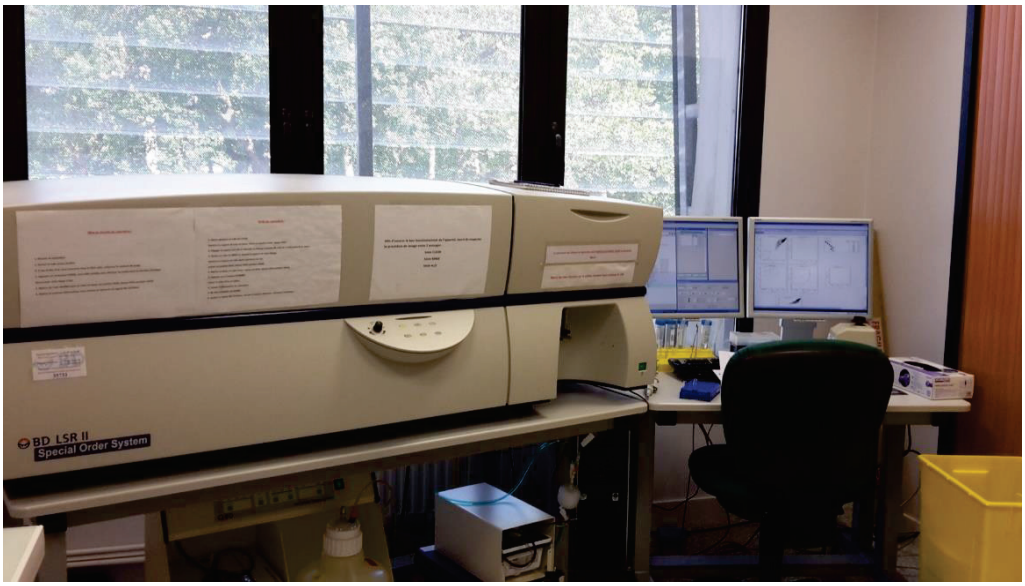


Figure 51: LSR II BD Biosciences and the computer for acquisition. (Lyon-Sud Medical School, Lyon, France).

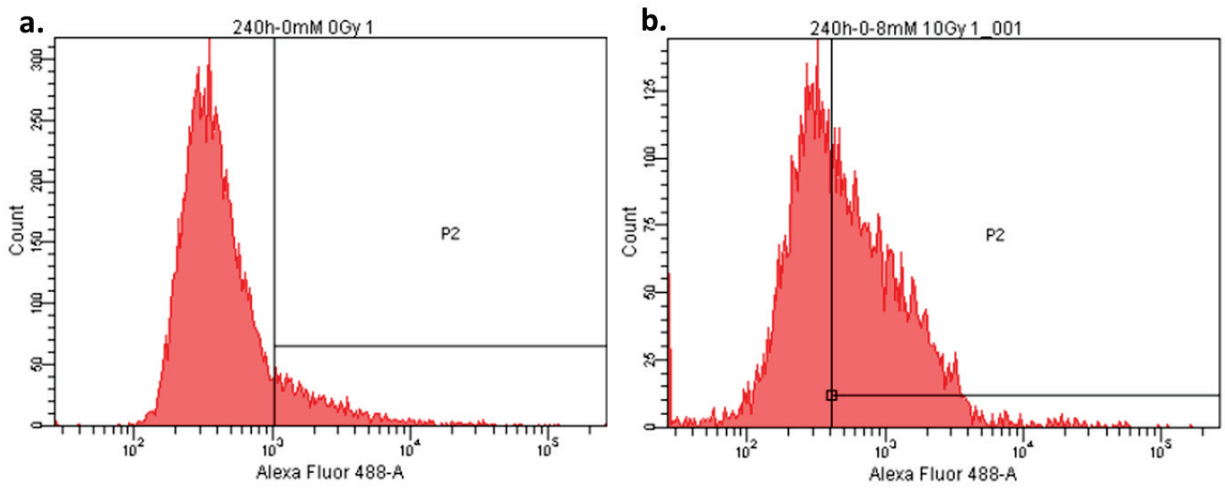


Figure 52: Representative graphs of total caspase analysis in flow cytometry (LSRII). **a**. 0mM Gd 0Gy; **b**. 0,8mM Gd 10Gy.

Apoptosis and necrosis were studied using the Annexin V/P.I. assay (Alexa Fluor 488 Annexin V/Dead, Ref V13241, Life Technologies SAS). The cells were trypsinized and marked for 15 minutes with 1 µL of annexin and 1 µL of P.I. per tube in 200 µL of 1X buffer provided in the kit, as instructed by the manufacturer. The cells were then centrifuged and washed once with PBS. The cells were re-suspended in 500 µL of PBS and analyzed using the FACSCalibur (Becton Dickinson). The excitation/emission wavelength was 488/530 for Annexin FITC and 585/45 for propidium iodide (CEA-Grenoble).

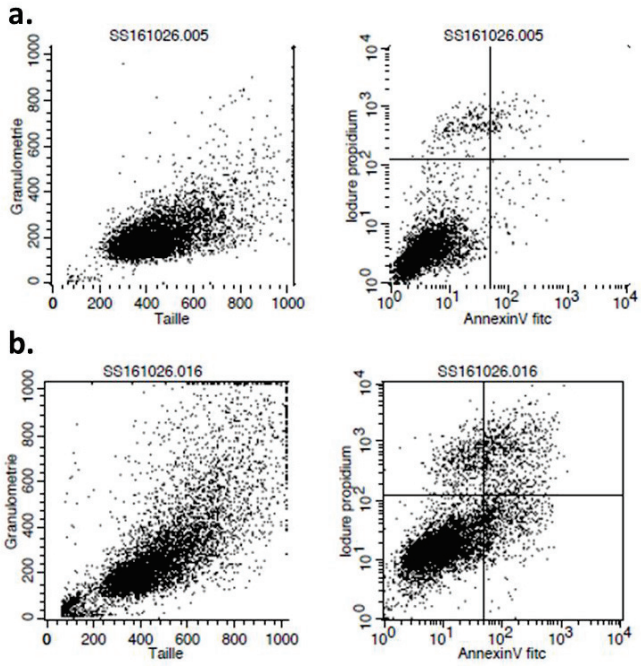


Figure 53: Representative graphs of Annexin/P.I. in flow cytometry (FACSCalibur). **a**. 0mM Gd 0Gy; **b**. 0,8mM Gd 10Gy. (CEA-Grenoble, Grenoble, France)

### 3.2. Study of the cell cycle kinetics

Samples were collected at 24, 48, 72, 192, and 240 hours after a 10Gy irradiation. **Note*: Two things are important to note. First, the supernatant must be kept (the trypsin will be stopped using this supernatant) and after trypsination, the cells must be kept on ice at all times. After trypsination, the cells were centrifuged for 10 minutes at 300 x g at 4°C and rinsed twice with cold PBS. The cells were then re-suspended in 250 µL of PBS and 2 mL of 70% ethanol per tube was added in order to fix the cells. The cells must remain in the 70% ethanol for at least 24h prior to the proceeding of the protocol.

For cell cycle analysis by flow cytometry by flow cytometry, the cells were centrifuged for five minutes at 300 x g and 4°C, rinsed twice with cold PBS and then marked with 500 µL of a DAPI (4',6'-diamidino-2-phenylindole) solution with a final concentration of 1 µg/mL in PBS. The samples were then analyzed by flow cytometry at an excitation wavelength of 355 nm and an emission of 450 nm (FACScan, BD LSRII flow cytometer, BD Biosciences). The different phases of the cell cycle (sub-G1, G0/G1, S, G2/M, and 4n) can be studied and quantified as is shown in Figure 54.

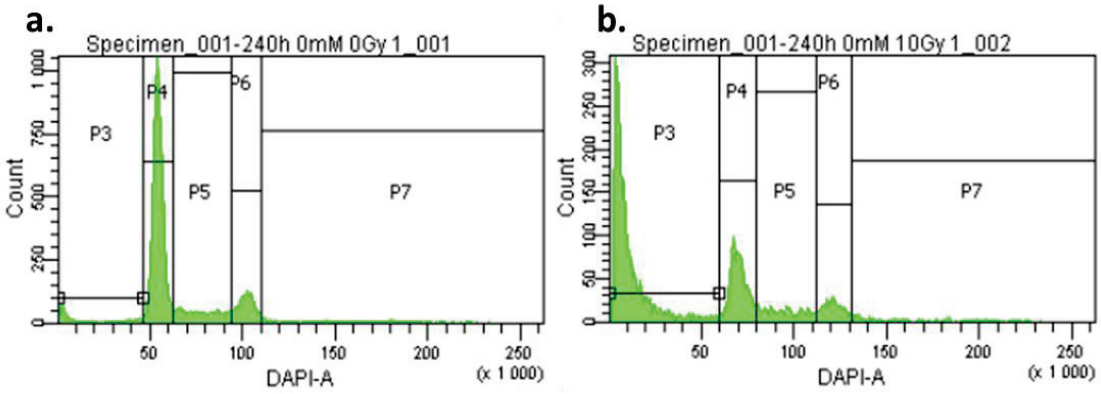


Figure 54: Schematic representation of a cell cycle in flow cytometry (LSRII BD Biosciences- Lyon-Sud Medical School Lyon, France). The different cell cycle phases are represented by P3: sub-G1, P4: GO-G1, P5: S, P6: G2/M, and P7: 4n. **a**. 0mM Gd 0Gy, **b**. 0mM Gd 10Gy.

## 3.3. Study of other cellular death pathways via Western Blot

Senescence and autophagy were explored via Western Blot using the p16 and p21 antibodies for senescence and LC3B for autophagy.

### *3.3.1. Sample preparation for Western Blot*

At t = 24, 48, 72, 120, 192, and 240 hours after a 10Gy irradiation, the cells were trypsinized, centrifuged for 5 minutes at 300 x g at 4°C and rinsed twice with PBS. The samples were then stored at -80°C as dry pellets. Once all samples were collected, we proceeded with protein extraction: the cells were lysed with 100-500 µL of lysis buffer (150 mM NaCl, 50 mM Tris-HCl pH 8.0, 1% Triton X-100) containing anti-proteases and anti-phosphatases (Roche) for 30 minutes at 4°C. The lysates were then centrifuged at 15 000 x g for 20 minutes at 4°C. The supernatants were then transferred to a new labelled Eppendorf tube while the pellet was thrown away (the pellet contains the cells' debris).

The protein concentration of each sample was measured using the Bicinchonic Acid (BCA) assay. A standard curve was done with bovine serum albumin, with concentrations varying from 0-80 mg/L. The standard and the samples were incubated with SDS 0.05% and BCA-$CuSO_4$ 0.01% for 30 minutes at 37°C and the absorbance was measured at a wavelength of 562 nm.

### *3.3.2. Polyacrylamide Gel Electrophoresis (SDS-PAGE) and transfer on a nitrocellulose membrane*

Depending on the studied protein, 20 µg or 40 µg was diluted to the $4^{th}$ in a denaturing buffer (Laemmli buffer: 125 mM Tris-HCl pH 6.8, 20% glycerol, 2% SDS, 5% β-mercaptoethanol, 0.05% bromophenol blue) and denatured for 5 minutes at 95°C. The samples were then deposited on the polyacrylamide gel.

## Gel preparation

12% polyacrylamide gels were casted using the Bio-Rad's TGX Stain-Free™ Fast Cast™ Acrylamide kit 12% (BioRad Catalog number 161-0185). These gels include unique trihalo compounds that allow rapid fluorescent detection of proteins without staining (known as Stain-Free™ Technology). The protocol for the gel preparation is shown in Figure 55. Fully prepared casted gels were also used.

1) Resolver solution preparation

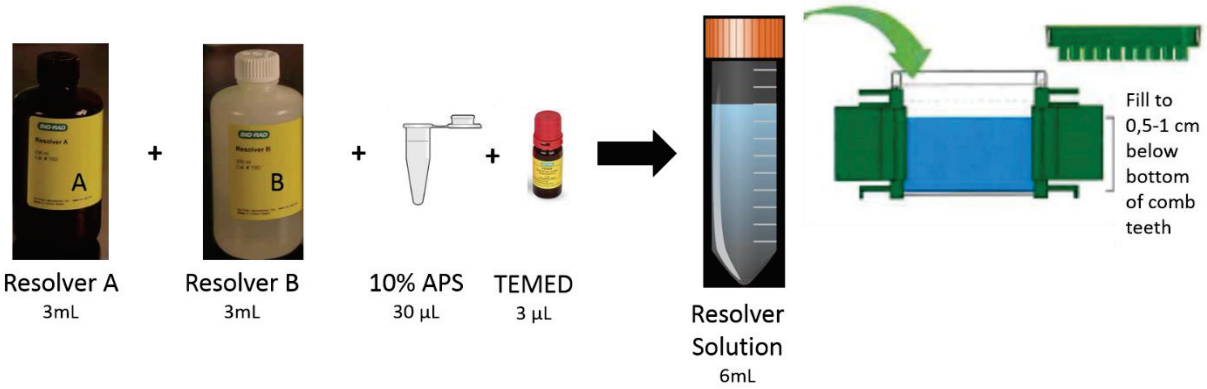


2) Stacker solution preparation

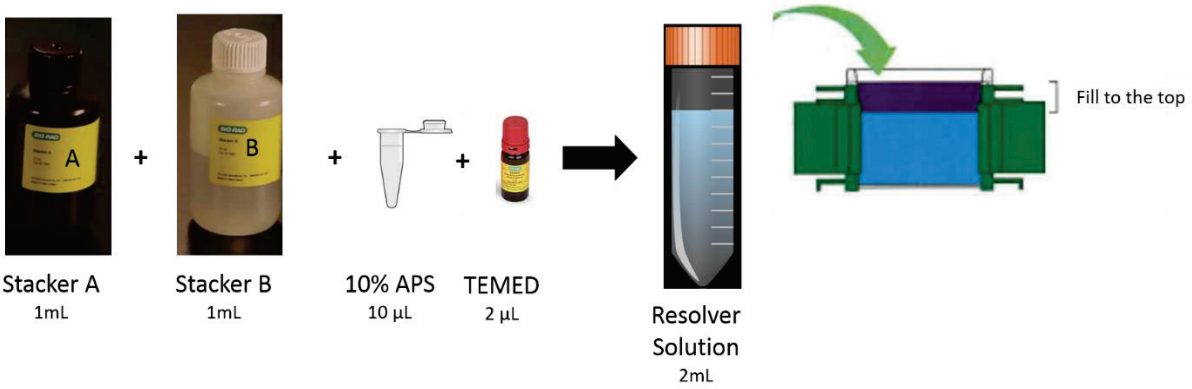


3) Insertion of comb and polymerization


Figure 55: Schematic representation of the three different steps for the preparation of the gel for Western-Blot.

Gel migration

The protein samples previously prepared were deposited onto the polyacrylamide gel. A protein molecular weight standard (Amersham™ ECL™ Rainbow™ Marker-Full Range, GE Lifesciences Ref RPN800E) was deposited in the first lane. The migration was performed at 100 V for 15 minutes and then increased to 120 V for about 90 minutes in a Mini-PROTEAN® Tetra Cell (Bio-Rad) tank. The migration buffer used was Tris-Glycine Buffer 10X (Sigma T4904) diluted to 1X and 1% SDS (TGS-Glycine Buffer 1X-1% SDS).

After migration, the gel was removed from its cast and placed in the BioRad system in order to activate total proteins (by activating all tryptophans) for later normalization during analysis. The trihalo compounds (mentioned earlier) react with tryptophan residues in a UV-Induced reaction to produce a fluorescence, which can be detected by the imager within gels.

Next, a semi-dry transfer was performed with the Trans-Blot Turbo Transfer System (Bio-Rad) and consumables that are ready-to-use: paper filters and a nitrocellulose membrane already incubated in transfer buffer. The transfer program with the following parameters was used:

- For MiniGel: 1,3A- 25V-7 minutes
- For 2 MiniGels or 1 MidiGel: 2.5A-25V-7 minutes

The protocol then slightly varied depending on the protein of interest and will therefore be described separately.

Protein of interest: **p16**

After transfer, the nitrocellulose membrane was rinsed for 5 minutes in PBS (Phosphate Buffer Saline) and incubated for one-hour with the blocking solution (PBS-Tween 0.5%-5% milk). The membrane was then rinsed three times with the solution PBS-Tween 0.5% for 5 minutes. Next, the primary antibody was incubated (1/2 000 dilution) in PBS-Tween 0.5%-Milk 1% for one hour at room temperature (RT) under gentle agitation. Then, the membrane was rinsed three times with PBS-Tween 0.5% for 5 minutes and the secondary antibody, goat antibody anti-mouse HRP (1/10 000) was incubated for one hour under gentle agitation at RT. The secondary antibody was removed and the membrane rinsed three times with PBS-Tween 0.5% for 5 minutes followed by 2 washes with PBS alone. Finally, the membrane was exposed for about 30 seconds to the revelator solution Clarity™ Western ECL Substrate (Sigma, Cat#170-5061). The protein was revealed using the BioRad ChemiDoc XRS system (Molecular Imager) and normalized with GAPDH.

Protein of interest: **p21**

After transfer, the nitrocellulose membrane was rinsed for 5 minutes in TBS (Tris-Buffered saline, Sigma T5912) and incubated for one-hour with the blocking solution (TBS-Tween 0.5%-5% milk). The membrane was then rinsed with the solution TBS-Tween 0.5% for 5 minutes three times and incubated with the primary antibody (1/500 dilution) in TBS-Tween 0.5%-Milk 5% overnight at 4°C. The following morning, the membrane was rinsed three times with TBS-Tween 0.5% for 5 minutes and incubated with the secondary antibody, the goat antibody anti-mouse HRP (1/10 000) for one hour under gentle agitation at RT. The secondary antibody was removed and the membrane was rinsed three times with TBS-Tween 0.5% for 5 minutes followed by 2 washes with TBS alone. The membrane was then exposed for 5 minutes to the revelator solution Clarity™ Western ECL Substrate (Sigma, Cat#170-5061) and the protein was revealed using the BioRad ChemiDoc XRS system (Molecular Imager).

Protein of interest: **LC3B**

After transfer, the nitrocellulose membrane was rinsed for 5 minutes in TBS and then incubated for one-hour with the blocking solution (TBS-5% milk-1% BSA). The membrane was then rinsed with the solution TBS-Tween 0.1% for 10 minutes three times. Next, the primary antibody is incubated (1/2 000 dilution) in the blocking buffer overnight at 4°C. The membrane was then rinsed in water once and then three times with TBS-Tween 0.1% for 10 minutes followed by the incubation with the secondary antibody, rabbit IgG HRP-conjugated (1/20 000) in blocking buffer for one hour under gentle agitation at RT. The secondary antibody was removed and the membrane is washed three times with PBS-Tween 0.1% for 10 minutes followed by 2 washes with TBS alone. The membrane was then exposed for 5 minutes and the protein revealed as described above.

| Protein of interest | Supplier/Reference | Production host | Protein Quantity | SDS-Page Gel | Blocking solution | Dilution |
|---|---|---|---|---|---|---|
| p16 (16 kDa) | BD Biosciences/550834 | Mouse | 40 µg | 16% | PBS-0,5%Tween20-5% Milk | 1/2000 |
| p21 (21 kDa) | Sigma/P1484 | Mouse | 40 µg | 12% | TBS-0,5%Tween20-5% Milk | 1/500 |
| LC3B (17 kDa) | BioTechne/NB100-2220 | Rabbit | 20 µg | Gradient | TBS-0,5%Tween20-1% BSA- 5% Milk | 1/2000 |

Table 14: List of proteins of interest studied by Western Blot analysis with references and protocol details.

### *3.3.3. Revelation and analysis*

Following an exposition of 5 minutes to the revelator solution Clarity™ Western ECL Substrate, the BioRad Imager system was used for the imaging of the gels. Depending on the antibody tested, images were taken every minute for approximately one hour. The images were then analyzed using the ImageLab Software. Figure 56 shows the Amersham™ ECL™ Rainbow™ Marker full range ladder which is used to determine the molecular weights of the bands that appear on the membrane. On the left is the apparatus used for revelation.

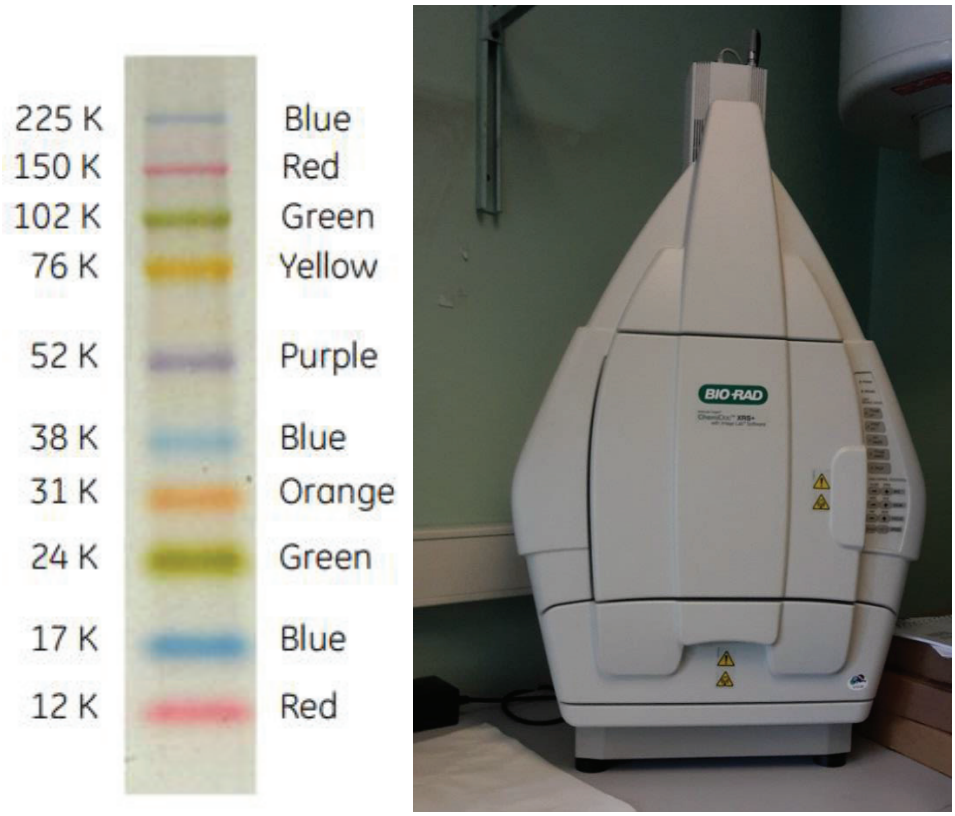


Figure 56: Amersham™ ECL™ Rainbow™ Marker-Full Range, GE Lifesciences Ref RPN800E (left); BIO-RAD ChemiDOc™ XRS (right) (INAC/SyMMES/CIBEST, CEA-Grenoble, Grenoble, France).

## *4. Kinetic study of cellular and mitochondrial radical oxygen species (ROS) production induced by AGuIX® + IR*

### 4.1. Cytoplasmic reactive oxygen species assay

CM-$H_2$DCFDA (Thermo Fischer, C6827), a general oxidative stress indicator, was used to detect cellular ROS production in SQ20B JL cells 0h-120h after a 10 Gy irradiation. After AGuIX® treatment, cells were rinsed twice with HBSS after which, for the times t = 0 min, 15 min, 30 min, 1h, 4h, and 24h, the cells were incubated for 10 minutes with a 2.5µM CM-$H_2$DCFDA solution prior to the 10Gy irradiation. For the T= 48h, 72h, and 120h, the cells were trypsinized, reseeded, and incubated with the same conditions before the collection of cells. At the

corresponding times, the cells were rinsed twice with PBS, trypsinized, and the trypsin was inhibited using the recovered culture medium. The cells were centrifuged twice and then re-suspended in PBS for flow cytometry analysis using the blue laser with an excitation at 488nm and a maximum emission at 525 nm (LSRII, BD Biosciences, Lyon-Sud Medical School).

### 4.2. Mitochondrial reactive oxygen species assay

MitoSOX™ red assay (Thermo Fischer, M36008), a specific mitochondrial superoxide indicator, was used to detect mitochondrial ROS more specifically. MitoSOX™ was used at a concentration of 5 µM in HBSS for 10 minutes. The same protocol was used as described for the CM-$H_2$DCDA assay. Fluorescence intensity was measured by flow cytometry at an excitation wavelength of 488 nm and emission wavelength of 575 nm (LSRII, BD Biosciences, Lyon-Sud Medical School).

## 5. Study of nuclear damages induced by AGuIX® + IR

### 5.1. Detection of single-stranded breaks: Comet assay +/- FPG

Cells were plated in six-well plates at a density of 400 000 cells per well in triplicate and irradiated at either 4 or 10Gy. Four times were analyzed after irradiation: immediately after (0 min), 30 min, 2 h, and 24 h post-irradiation. For each treatment conditions, 3 slides without FormamidoPyrimidine [fapy]-DNA Glycosylase (FPG) and 3 slides with FPG were prepared and an internal positive control (+$H_2O_2$) was included.

#### *5.1.1. Slide preparations*

The slides should be prepared at least one day in advance. 100 mL of normal agarose at 1% (1 g of agarose in 100 mL of PBS without $Ca^{2+}$ nor $Mg^{2+}$) was prepared by melting the agarose on a heat block under gentle agitation. Each slide was dipped in the agarose and then left to dry overnight.

#### *5.1.2. Collection of the cells*

The cells were trypsinized as typical protocol. The cells were then centrifuged at 300 x g for 5 minutes at 4°C and then re-suspended in freezing buffer at a concentration of 200 000 cells in 100 µL (for 50 mL of freezing buffer: final concentrations of 85.5 g/L sucrose, 11.76 g/L sodium citrate, 50 mL/L DMSO, and the pH was adjusted to 7.6 with a few drops of citric acid 0.1 M. The volume was then adjusted to 50 mL with milli-Q d$H_2O$ and the solution filtered through a 0.2 µm filter and kept at 4°C). The cells were then stocked at -80°C until further treatment.

*5.1.3. Depositing the cells on the slides*

A 0.6 % solution of low-melt agarose was prepared in PBS. The solution should be well diluted but should not be brought to a boil. The solution was added in Eppendorf tubes before the addition of the 900 µL of low-melt agarose solution. The tubes were placed in the pre-heated 37°C water bath. The previously collected cells were taken out from the -80°C and dipped in the water bath to unfreeze them. After centrifugation for 5 minutes at 300 x g at 4°C, the supernatant was removed and the pellet re-suspended in 100 µL of PBS to the 900 µL of low-melt agarose. The solution was homogenized and 100 µL of the solution was added to each slide (deposition of about 20 000 cells per slide). A coverslide was immediately put and the slides were put on ice for a minimum of 10 minutes.

*5.1.4. $H_2O_2$ positive control*

The coverslide was removed and 100 µL per slide of a 50 µM $H_2O_2$ solution was deposited. A coverslide was immediately put over and the slide put back on ice for 10 minutes. After removing the coverslide, the slide was rinsed with 1 mL of PBS. *Note*: a maximum of the PBS should be removed from the slide.

*5.1.5. Cell lysis*

After removing the coverslide, the slides were placed at the bottom of a container where they will be covered with lysis buffer for one hour (a 1 L solution is prepared with the following final concentrations: 2.5 M NaCl, 10 mM Tris, 0.1 M EDTA; the pH was then adjusted to 10 with concentrated NaOH). Immediately prior to use, to 133,5 mL of the previously prepared solution, 15 mL of DMSO and 1.5 mL of Triton are mixed. After cell lysis, the slides were rinsed three times for 5 minutes with Tris-HCl 0.4 M, pH 7.4 (dilution by 1/3 of the previously prepared 1L of Tris-HCl 1.2 M (145,5 g of Tris was weighed and the pH was then adjusted to 7.4 with concentrated HCl).

*5.1.6. Incubation with Fpg (formamidopyrimidine [fapy]-DNA glycosylase)*

The slides were left to dry for about 5 minutes on the lab-bench while the FPG solutions were prepared as follows:

- With FPG: FPG 0.05 u/µL (1.25 µL/slide) + FPG buffer diluted 10 times in milli-Q $H_2O$.
- Without FPG: FPG buffer diluted 10 times in milli-Q $H_2O$.

For each condition, 100 µL of the with FPG solution or without FPG solution was deposited on the slides and a coverslip was put down. The slides were set on a humidified bed and put

in a 37°C incubator for one hour. After the one-hour incubation, the slides were put on an ice-bed in order to stop the enzymatic reaction.

#### *5.1.7. Migration*

After removing the coverslips, the slides were placed in an electrophoresis tank. The slides were covered with the electrophoresis buffer (0.3 M NaOH and 1mM EDTA diluted in MilliQ $dH_2O$) that was previously prepared and stored at 4°C. An "equilibration" time of 30 minutes was observed before starting the electrophoresis which was performed at a voltage of 25 V, 300 mA, for 30 minutes. After migration, the electrophoresis buffer was thrown out, and the slides were rinsed three times for 5 minutes in Tris-HCl 0,4 M buffer.

#### *5.1.8. Analysis*

The counting of the comet assay by microscopy was usually done the following day. For a reading within the next 15 days, 50 µL of Gel Red was added per slide and a coverslip was put right away. For each slide, comets were counted under the microscope using the 10X objective: a minimum of 50 comets were counted per slide. For storage, the slides were kept at 4°C in the dark.

### 5.2. Detection of double-stranded breaks: Foci YH2AX

Cells were plated in six-well plates at a density of 400 000 cells per well in duplicate for each condition: 30 minutes and 24 hours after a 2Gy irradiation. Cells were rinsed twice with cold PBS and then fixed in a 4% PFA (paraformaldehyde) solution for 20 minutes. The cells were rinsed 3 times with PBS in order to remove any traces of PFA.

After collection, the cells were permeabilized for 5 minutes with a permeabilization buffer made of PBS-0,2% Triton X100 solution. The cells were then washed 3 times for 5 minutes with a wash solution (PBS-0,1% Tween 20- 0,05% Triton X100) and then aspecific sites were blocked with a PBS- 0.2% milk-5% FCS- 0,05% Triton X100 for 10 minutes. This blocking step was followed by a one-hour incubation of the monoclonal primary antibody produced in mouse: the anti-phospho-histone H2AX (Ser 139) clone JBW301 (Invitrogen Ref 05-636) 100 µl of the antibody solution (1/1000 dilution in blocking buffer) was deposited on each coverslide. Following the hour incubation with the primary antibody, the cells were rinsed 3 times for 5 minutes with the wash buffer and then incubated for one hour with the secondary antibody Alexa-Fluor 488-antiIgG against mouse produced in goat (Invitrogen Ref A11001) (1/500 dilution in blocking buffer). The cells were then rinsed twice for five minutes in a PBS-0,1% Tween 20 solution. The nucleus of cells was stained with DAPI at a concentration of 1 µg/ml for 15 minutes and washed three times in PBS for 5 minutes each. Each coverslide was then mounted using the mounting medium Fluoromount (Sigma).

Slides were left to dry for about 24 hours and are then polished for an optimal conservation. Each slide was then counted for a minimum of 300 nuclei per slide using the Metafer analysis system which uses both the intensity and size as parameters to distinguish a foci under a 63X objective.


Figure 57: The Metafer platform used for γH2AX analysis along with the microscope (Lyon-Sud Medical School).

A kinetic study 0 min- 30 min - 1h – 2h – 4h – 6h – 24h was once realized in triplicate in order to study the repair kinetics of DNA double-stranded breaks. The study with T= 30 minutes and 24 hours was done in triplicate with duplicate slides for each condition.

## 5.3. Quantification of 8-oxo-G by HPLC-MS/MS

### *5.3.1. DNA Extraction*

Each dry pellet was re-suspended in 750 µL of the lysis buffer A and transferred in 2 mL Eppendorf tubes. The buffer lysis A solution is composed of 10.97 g of sucrose, 101 mg of $MgCl_2$, 121 mg of Tris, 100 µL of deferoxamine, and 1 mL of Triton X100. The pH was adjusted to 7.5 before the addition of Triton X100 and the volume was adjusted to 100 mL. This buffer allows the lysis of the cells' plasma membrane. The tubes were then centrifuged for 5 minutes at 1500 x g at RT. The supernatant was removed and 750 µL of Lysis buffer solution A was again added to the tubes and centrifuged at 1500 x g for 5 minutes at room temperature. After removing the supernatant, the pellet was re-suspended in 300 µL of lysis buffer B (for a volume of 100 mL: 186 mg of EDTA-$Na_2$, 121 mg Tris, 150 µL deferoxamine. The pH was verified and adjusted to 8.0). Eighteen µL of 10% SDS (Sodium Dodecyl Sulfate) was added to the mixture and the solution vortexed. 1.5 µL of RNAse A (Sigma, ref R5125-250mg) (100 mg/ml) and 3.5 µL of RNAse T1 (1U/µL) were added and the suspension was incubated at 50 °C for 15 minutes. Fifteen µL of protease (Qiagen ref 19157) per sample was then added and the mixture vortexed and incubated at 37° C for one hour. Following the hour incubation, 600 µL of a NaI

solution was added (20 mM EDTA-$Na_2$, 7.6 M NaI, 40 mM Tris/HCl, 0.30 mM deferoxamine) followed by 1 mL of 100 % isopropanol per sample. Each sample was gently agitated and then centrifuged for five minutes at 5000 x g at RT. The supernatant was then removed and 500 µL of 40% isopropanol was added. The samples were once again centrifuged for 5 minutes at 5000 x g at RT. The supernatant was removed and 500 µL of 70% ethanol was added followed by a centrifugation at 5000 x g for 5 minutes at RT. Following this centrifugation, a maximum of the supernatant was carefully removed and the pellet was re-suspended with 50 µL of deferoxamine 0.1 mM.

*5.3.2. Enzymatic Digestion*

A mix was prepared so that each sample received:

- 0.25 µL of phosphodiesterase II at 0.1 U/µL (Sigma, ref P9041-25U)
- 0.5 µL of DNase II at 10U/µL (Sigma, ref D4138-20KU)
- 2.5 µL of Nuclease P1 at 0.2U/µL (Sigma ref N8630-1VL)
  (P1 buffer solution: 300 mM ammonium acetate (Sigma ref A1542-250g), 1 mM ZnSO4 (Sigma), adjusted pH to 5.3. For the nuclease P1, a concentration of 0.2U/µL was used. The nuclease P1 was diluted in the P1 buffer)
- 2.5 µL of MNSPDE buffer
  (For a 10X solution: 200 mM succinic acid (Sigma ref S3674-100g) and 100 mM CaCl2 (Sigma ref C1016-100G) adjusted to pH6)

5.5 µL of the mix was added to each sample and the samples were vortexed and incubated for 2 hours at 37°C. The samples were vortexed after the first 30 minutes of incubation.

After the two hours of incubation, 6.55 µL of the following mix was added to each sample:

- 6µL of phosphatase alkaline buffer (500 mM Tris (Sigma ref 34549), 1mM EDTA (Sigma ref T6066), pH8)
- 0.5 µL of phosphodiesterase I (Sigma, ref P3243-1VL)
- 2 units of alkaline phosphatase (Sigma ref P6774-2KU)

After a 2-hour incubation of the samples at 37°C, 3.5 µL of 0.1N HCl was added to each sample before centrifugation at 5000 x g for 5 minutes. If ethanol remained in the tubes, it was evaporated by speed vacuum for 10 minutes. The samples were then transferred to HPLC vials and kept at 4°C or -20°C until HPCL MS/MS analysis. (*Note*: while transferring samples to HPLC vials, one must be careful with air bubbles at the bottom of the vials.)

*5.3.4. Analysis by HPLC MS/MS*

The measurements were made with a TSQ Quantum Ultra electrospray ionization tandem mass spectrometer (Thermo Fisher Scientific Inc.).


Figure 58: Photograph of the HPLC coupled to a MS/MS for detection of 8-oxo-guanine (INAC/SyMMES/CIBEST, CEA-Grenoble, Grenoble, France).

## 6. Functional consequences on the mitochondria of AGuIX® + I.R.

### 6.1. Common deletion of mitochondrial DNA

The cells were trypsinized and rinsed twice with PBS and kept at -80°C as a dry cellular pellet until further treatment.

#### *6.1.1. Cell lysis*

The cells were lysed with a buffer containing Tween 20, NP40, Tris HCl pH 8.3 completed with $dH_2O$ to which proteinase K was added to a final concentration of 0,1 mg/mL. The cellular pellets were then grinded to explode the mitochondrial membranes using the Tissue Lyser II at a 30Hz frequency for 2 minutes. The samples were then incubated in a heat block set at 56°C for 30 minutes followed by 15 min incubation at 98°C to inactivate the Proteinase K.

#### *6.1.2. Sample preparation*

In order to prepare the sample solutions for PCR analysis, the samples underwent a series of dilution. First, the lysis buffer previously used was diluted by a factor of 7 and sonicated for 10min. The samples were diluted as follows: 20 µL of lysat + 40 µL non-sonicated lysis buffer + 60 µL of milliQ $H_2O$. Twenty µL of this first dilution were then added to 80 µL of the sonicated diluted lysis buffer to have a final dilution of 1/9.

### *6.1.3. Mix preparation*

The Fast Start DNA Master Syber Green I kit (Roche) was used for the PCR assay. First, the Mastermix was prepared by adding 10 µL of tube 1a to 1b. Then the PCR mix was prepared as follows (volumes per sample):

- 0.4 µL of forward Primer 20 µM
- 0.4 µL of reverse Primer 20 µM
- 7.4 µL of nuclease free $H_2O$
- 4.8 µL of $MgCl_2$

The mix was vortexed and 2 µL of the Mastermix was added.

15 µL of this mix was added to each well of the PCR plaque and 5 µL of each sample was deposited. The plaque was then centrifuged at 700 rpm for 5 minutes at room temperature.

The thermal profile for the PCR (Stratagene) was as follows: 1 cycle for 10 minutes at 95°C (denaturation), 45 cycles at 5 seconds at 54°C, 8 seconds at 72°C (amplification), 20 seconds at 95°C, 30 seconds at 68°C, 30 seconds at 98°C (fusion).

Three couple of primers were used: total mitochondrial DNA (tot mtDNA), deleted mitochondrial (del mtDNA), and GAPDH.

The total and deleted mitochondrial DNA were both normalized with GAPDH before calculation of the ratio: deleted mtDNA/total mtDNA.

| Primer | **F**orward/**R**everse | Sequence |
|---|---|---|
| Tot mtDNA | F | 5'- GGACTAACCCCTATACCTTCTGCAT -3' |
| | R | 5'- CGGGTGTGCTCTTTTAGCTGTT -3' |
| Del mtDNA | F | 5'- CCTTACACTATTCCTCATCACCCAA -3' |
| | R | 5'- TGTGGTCTTTGGAGTAGAAACCTGT -3' |
| GAPDH | F | 5'- CTGACCTTTACTCCTGCCCTTTG -3' |
| | R | 5'- CATGGTATTCACCACCCCACTATG -3' |

Table 15: Corresponding chosen primers.

## 6.2. The mitochondrial membrane potential

The JC-1 (5',5', 6, 6'-tetrachloro-1, 1', 3, 3'-tetraethylbenzimidazolycarbocyanine iodide) dye (Sigma-Aldrich, Ref T4069) was used to measure the mitochondrial membrane potential drop. After trypsination, the cells were incubated with JC-1 for 20 minutes at 37°C at a concentration of 5 µM. Cells were then analyzed using flow cytometry with an excitation wavelength of 488 nm and an emission wavelength of 525 nm (LSRII, BD Biosciences).

Measuring glutathione content in SQ20B J.L. cells

*Sample preparation*

Cells were plated at a density of 150 000 cells in six-well plates and were treated with 0mM or 0,8mM of AGuIX®, and depleted or not of glutathione (see section DMF/BSO treatment). At t =0 minutes and 24 hours after irradiation, glutathione measurements were performed. At a given time, the supernatant was removed and the cells were washed twice in PBS. 150 µL of R1 (composed of NEM/EDTA/γGLU-GLU) was added to each well and the wells were shaken for 10 seconds. N-ethymaleimide (NEM) is used to block glutathione in its reduced form therefore avoiding the generation of artefactual high levels of glutathione disulfide. Next, 50 µL of R2 (6% ASS) was added and the wells were again shaken for 10 seconds. The plates were then left to rest for 30 minutes at room temperature. After the scraping step, the solution from the well was removed from each well and centrifuged for 10 minutes at 4500 tr/minutes at 4°C. The supernatant was then transferred to a clean 1,5 mL Eppendorf tube.

*HPLC MS/MS*

Glutathione concentration (from a cell pellet) was measured by HPLC MS/MS (Agilent Technologies, Venissieux, France), in a positive electrospray ionization mode after a separation by chromatography on a 150mm×2mm stability 100 BS-C17 column (CIL Cluzeau, Sainte Foy La Grande, France). Briefly, after removal of proteins by sulfosalycic acid 6%, the stabilization of glutathione by 20 mM of NEM and adding gamma glutamyl-glutamic acid as an internal standard, the cell pellet was degraded by a freeze/thaw cycle followed by a centrifugation at 10.000g during 10 minutes. The supernatant was then diluted in a mobile phase and injected into the chromatographic system.

The elution was performed using a mobile phase containing MeOH/acetate ammonium buffer (8mM) adjusted to pH 2.7 (63/37, V/V) in an isocratic mode. Chromatograms were recorded in single ion monitoring $(M+H)^+$ at m/z 277 for gamma glutamyl-glutamic acid, at 308 for GSH, at 433 for GSH-NEM and 613 for GSSG for 10 minutes. The results were integrated with Chemstation software (Agilent Technologies (version B.01.01)).

# 7. Proteomic Analysis

## 7.1. Sample preparation

### *7.1.1. AGuIX® treatment and Irradiation (Lyon-Sud Medical School)*

Cells were plated at a density of 40 000 cells/cm$^2$ 16 hours prior to AGuIX® treatment in T7 flasks. The next day, the cells were treated with 0mM Gd or 0.8mM Gd for 24 hours. Prior to irradiation, AGuIX® were removed from the medium, the cells were rinsed twice with PBS and then irradiated at 10 Gy and put back in the incubator at 37°C 5% $CO_2$ for 24 hours.

Twenty-four hours after irradiation, the cells were trypsinized and each flask was separated into two:

- One half would be used for protein extraction in order to dose the quantity of proteins using the BCA assay (previously detailed)
- Cells will be re-suspended in Laemmli 2X buffer for a final concentration of 3 µg/µl for proteomics analysis.

For quality check, the samples used for protein extraction were ran through a polyacrylamide gel electrophoresis. The gel was stained using a Coomassie blue solution, and de-stained with an acetic acid solution.

The samples were then brought to the EDyP Platform (CEA - Grenoble) in dry ice for further preparation of the samples for proteomic analysis.

## 7.2. Shut-gun Proteomics (EDyP Platform)

### *7.2.1. Protein extraction and digestion*

Once the samples were received by the platform, a staking gel (so proteins are concentrated in one single band) was done and each band (4 total for the 4 separate samples), was cut out of the gel for further treatment: each sample was treated and digested by trypsin in order to separate proteins into peptides (smaller fragments for nanoLC MS/MS).

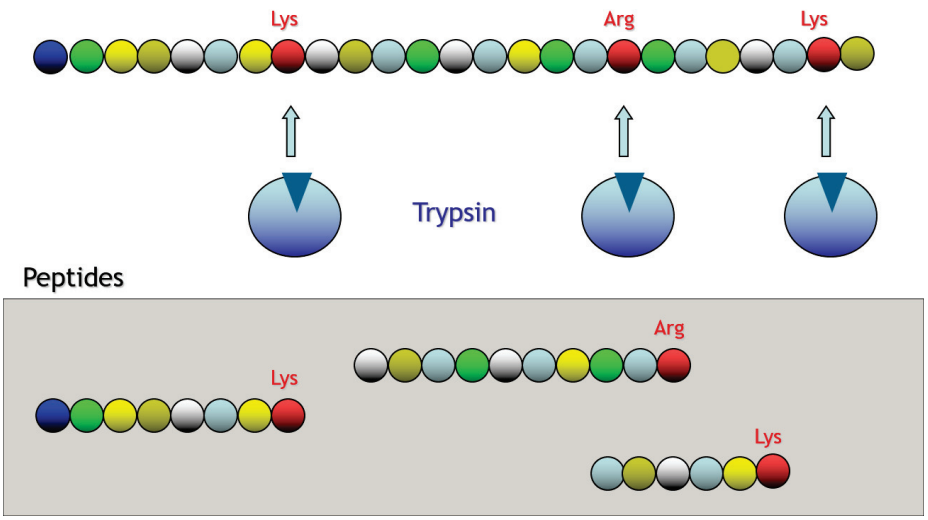


Figure 59: Schematic representation of trypsin digestion of proteins. Trypsin will cut proteins after lysine or arginine. After trypsin digestion, different lengths of peptides were obtained.

### *7.2.2. Nano Liquid-chromatography*

After digestion of proteins by trypsin, the peptides are injected into the liquid chromatography (nanoLC because a volume between 5-10 µl (which is equivalent to 500 ng) at a rate of 300 nl/min). The peptides are then fragmented in the mass spectrometer (Orbitrap Velos from Thermo) and fragmentation spectra are obtained.

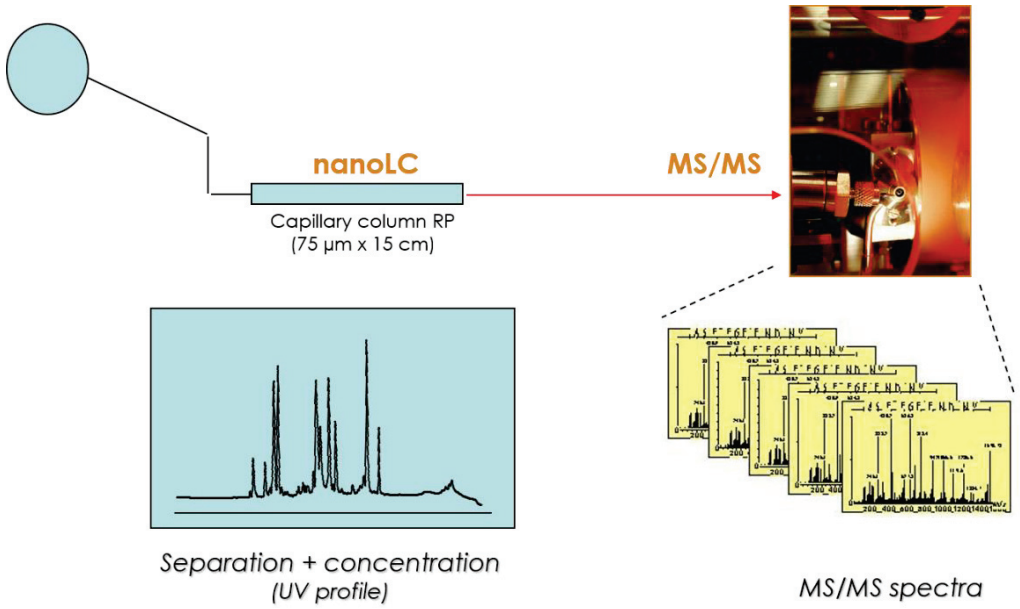


Figure 60: Schematic representation of nano-Liquid Chromatography followed by Mass Spectroscopy MS/MS. Representation of spectra obtained from the MS/MS.

### *7.2.3. Sequence information*

Once the spectra are obtained, the sequence of amino acids of peptides is determined and ran through bioinformatics tools to identify the full-length proteins. In parallel, in order to validate the experimental results, an available protein database underwent *in silico* tryptic digestion followed by *in silico* fragmentation to then obtain masses which were compared to the experimental masses. Using bioinformatics tools, the proteins were identified and protein identifications were validated using a software named Proline.

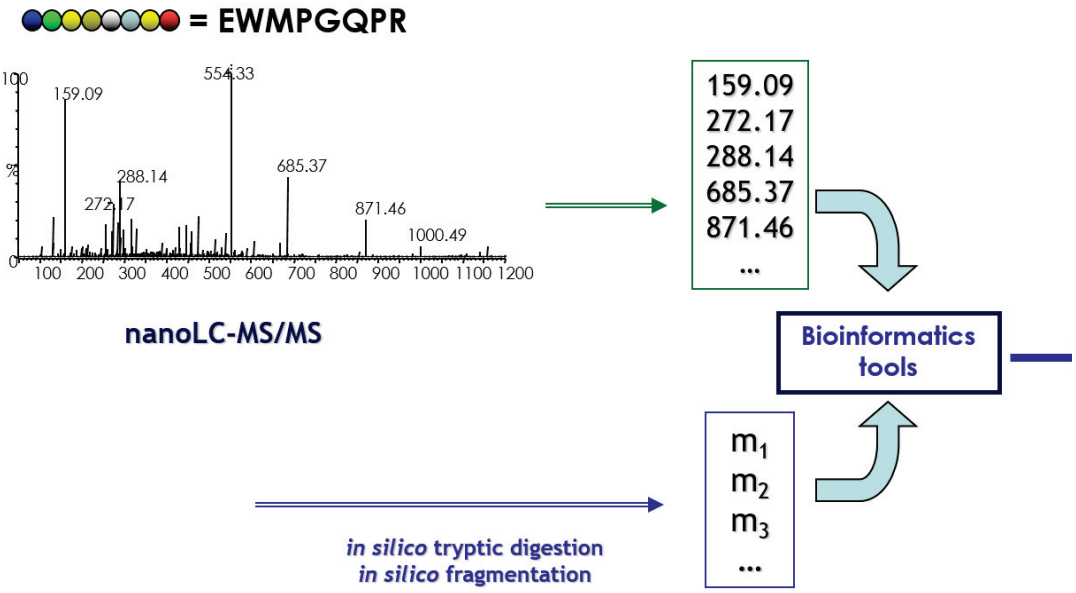


Figure 61: Following nanoLC MS/MS, amino acids are determined from the spectra, and using bioinformatics tools, proteins are identified.

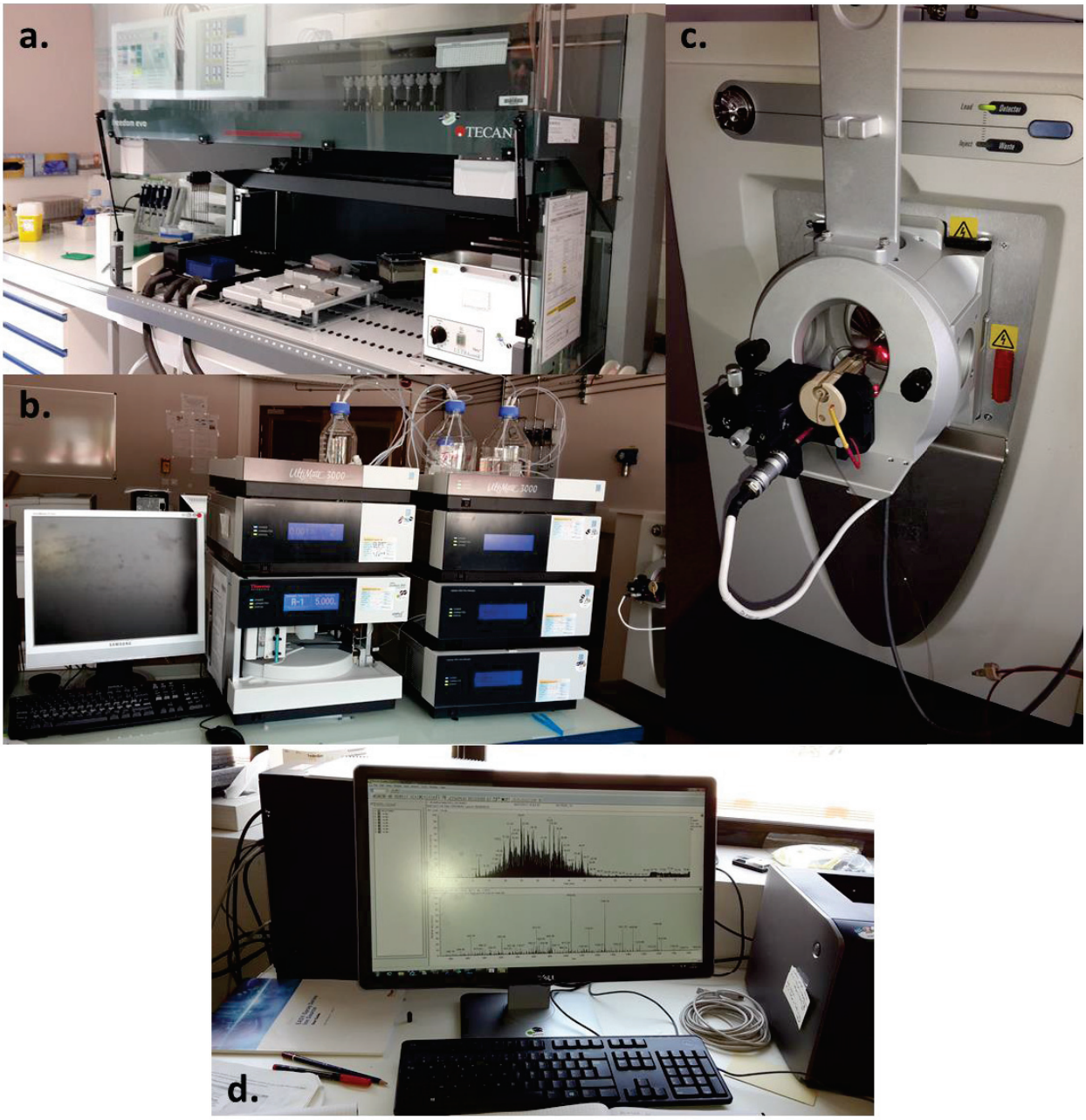


Figure 62: Photos representing the equipment used for the Proteomics study (EdYP Platform, CEA-Grenoble, Grenoble, France). a. Protein extraction and digestion by a robotized system; b. Nano-Liquid Chromatography; c. MS/MS; d. Sequence information, peak integration.

### *7.2.4. Data analysis*

Once all data was extracted and protein identification was finished, an Excel worksheet was given with the name of identified proteins, fold-change, and spectral counts.

In the Excel sheet, the following was detailed:

- Pep: the number of peptides corresponding to the protein
- SC (**S**pectral **C**ount): number of peptides observed for one protein, but these peptides can be shared peptides between different proteins

- SCC (**S**pecific **S**pectral **C**ount): number of peptides specific to a unique protein
- WSC (**W**eighted **S**pectral **C**ount): logarithmic calculation which takes into account SC and SCC

Two different techniques were used in order to further analyze the results obtained and the analysis was focused on the comparison of 10Gy versus 0,8mM Gd + 10 Gy.
The fold-change was calculated as the ratio:

**0,8mM Gd + 10 Gy / 10 Gy**

First, proteins with a fold change of ≤ 0,8 (under-expression) or ≥ 1,2 (over-expression) were identified (which corresponded to 800+ proteins) and then ran through proteomics bioinformatics analysis tools to identify modulated signaling pathways. One such tool used for the analysis of the results was DAVID (**D**atabase for **A**nnotation, **V**isualization and **I**ntegrated **D**iscovery https://david.ncifcrf.gov/).

Another analysis technique which is used by the EDyP platform is more drastic and will consider a significant fold-change only when a protein was over-expressed or under-expressed by a minimum factor of 5. 16 proteins were modulated using these more drastic cut-offs, and individual bibliography research using PubMed was done.

# Results & Discussion

# Chapter I. Characterization of the radiosensitizing effects of AGuIX®

*Radiosensitization using high-Z metal nanoparticles has shown great promises to improve radiotherapy treatment in radio-resistant tumors, such as in Head and Neck Squamous Cell Carcinoma (HNSCC). In this study, we have used a new formulation of gadolinium-based nanoparticles named AGuIX® (Activated Guidance Irradiation by X-rays) in order to determine their potential as a radiosensitizer in vitro, using SQ20B J.L. cells, a radio-resistant HNSCC cell line.*

*Therefore, this first chapter of the Results & Discussion section is devoted to the characterization of the effects of AGuIX® nanoparticles which includes the optimization of the radiosensitizing conditions of AGuIX® on this cellular model. Firstly, different concentrations, media, and incubation times have been tested. Next, the potential toxicity has been checked, and the cellular localization of AGuIX® with respect to the nucleus, mitochondria, and lysosomes has been studied using confocal microscopy.*

Although we will not develop the imaging potential of these nanoparticles since this work is only focused on an *in vitro* model to explain the mechanisms of radiosensitization, it is important to **underline** their **theranostic potential** for their use in the clinical field. Indeed, Gadolinium (Z= 64, M= 157.25), with its seven unpaired electrons, **is one of** the most interesting element as a contrast agent **since** the paramagnetic effect of one ion and its influence on the relaxation time directly depend upon the number of unpaired electrons generating the electronic spin that interferes with the nuclear spin of hydrogen (Lorusso *et al.,* 2005, Rohrer *et al.*, 2005).

Prior experiments in our laboratory used nanoparticles with Diethylenetriaminepentaacetic acid (DTPA) as the gadolinium chelating agent and presented evidence for a radiosensitizing effect (Miladi *et al*., 2015). However, toxicity issues were raised as DTPA was not a strong enough chelating agent and could therefore potentially release gadolinium. Free gadolinium is highly toxic to humans with increasing evidence showing that the chemical instability of the chelate can lead to exchanges with other metal ions (zinc $Zn^{2+}$, copper $Cu^{2+}$, or calcium $Ca^{2+}$), which can in turn have biological consequences. The ionic radius of $Gd^{3+}$ (107.8 pm) is close to that of $Ca^{2+}$ (114 pm) and this element is an inorganic blocker of many types of voltage-gated calcium channels at the nano- to micro-molar concentrations. It consequently inhibits these physiological processes which depend upon $Ca^{2+}$ influx (contraction of smooth, skeletal, and cardiac muscle, transmission of nervous influx, blood coagulation, etc.) (Lansman, 1990; Biagi and Enjyeart, 1990; Evans, 1990). Gadolinium can also inhibit the activity of some enzymes ($Ca^{2+}$-activated-ATPase in the sarcoplasmic reticulum of skeletal muscle fibers, some dehydrogenases and kinases, glutathione S-transferases, *etc*.) (Evans, 1990; Itoh and Kawakita, 1984), and has a remarkable capacity to depress the reticuloendothelial system (Evans, 1990). The chelator DTPA was therefore dropped and was replaced by 1,4,7,10-tetraazacyclododecane-1,4,7,10-tetraacetic acid (DOTA), a stronger gadolinium chelating agent.

Two parameters are important when discussing the stability of a gadolinium contrast agent to insure the non-release of gadolinium: the **thermodynamic stability** and the **kinetic stability**. By definition, as gadolinium is chelated, a thermodynamic equilibrium exists between the metal [M], the ligand [L], and the complex [ML]:

$$[M] + [L] \rightleftharpoons [ML]$$

The toxicity of gadolinium complexes depends on their ability to release $Gd^{3+}$ ions. The stability of gadolinium complexes is expressed in terms of log $K_{therm}$, where $\mathbf{K_{therm}}$ is the **thermodynamic stability** constant, defined as:

$$K_{therm} = [ML]/[M][L]$$

The better stability of Gd-chelated agent by DOTA can also be explained by the chemical structures of DOTA, which has a cyclic structure, versus DTPA, which has a linear chemical structure (Figure 63).

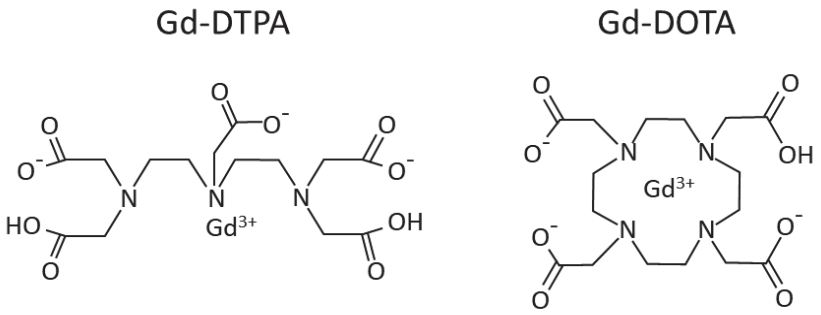


Figure 63: Chemical structures of Gd-DTPA (linear) versus Gd-DOTA (cyclic) chelating agents. (Idée *et al.*, 2006)

| Ligand L | Log K' | Log $K_{therm}$ (GdL) | Log $K_{therm}$ (CaL) | Log $K_{therm}$ (CuL) | Log $K_{therm}$ (ZnL) |
|---|---|---|---|---|---|
| ***DTPA*** | 17.7 | 22.1 | 10.7 | 21.4 | 18.3 |
| ***DOTA*** | 18.8 | 25.8 | 17.2 | 22.6 | 21.0 |

Table 16: The log K' value and the $K_{therm}$ constants for the ligand and different elements found in the body depending on the ligand type: DTPA versus DOTA. (Idée *et al.*, 2006)

Another parameter that is important to take note of is the **kinetic rate** at which equilibrium is reached, estimated through the half-life ($T_{1/2}$) of dissociation of the complex. In a very acidic medium, the complex dissociation is a pseudo-first-order reaction, with:

$$\text{Dissociation rate} = k_{diss}[H^+]\,[GdL].$$

As $[H^+]$ is considerably higher than [GdL] throughout the whole dissociation process, it was considered that $[H^+]$ is constant and equal to $[H^+]_0$. Therefore:

$$\text{Dissociation rate} = k_{obs}[GdL]$$

where

$$k_{obs} = k_{diss}[H^+]_0.$$

| Gadolinium chelates | $K_{obs}$ ($s^{-1}$) | $T_{1/2}$ |
|---|---|---|
| Gd-DTPA | 1.2 X 10-3 | 10 min |
| Gd-DOTA | 2.1 X 10-5 | >1 month |

Table 17: $K_{obs}$ values and $T_{1/2}$ for DTPA and DOTA chelating agents. (Idée *et al.*, 2006)

The main physicochemical criterion to minimize any transmetallation *in vivo* is the **kinetic stability**. It is now well-established that the **macro-cyclic ligand (*i.e.* DOTA) has a much slower**

**decomplexation and transmetallation reaction kinetics** and is consequently characterized by an inertia to decomplexation or transmetallation. (Idée *et al.*, 2006)

An additional factor probably in-part responsible for having to re-determine the radiosensitizing conditions is that the DTPA-gadolinium-based nanoparticles were designed differently as they had a gadolinium oxide core surrounded by polysiloxane shell while AGuIX® nanoparticles have a polysiloxane core surrounded by gadolinium chelates covalently grafted on the inorganic matrix. Very often, as it was mentioned in the bibliography review, the conditions used for one type of nanoparticle on a specific cell line is not completely transferable to another couple nanoparticle/cell line. It was therefore very important to determine the conditions for use before moving on.

## 1. Determining the optimal radiosensitizing conditions of AGuIX® nanoparticles on SQ20B J.L. cells

In order to determine the optimal radiosensitizing conditions of AGuIX® nanoparticles in SQ20B J.L. cells, several parameters and experimental conditions were tested including: various culture media, increasing NPs concentrations from 0 to 3 mM Gd, and the time of incubation. The survival fraction at 4Gy ($SF_{4Gy}$) assay was used as a first preliminary test to screen a greater number of conditions to establish the best radiosensitizing effect. Thereafter, a full clonogenic survival curve was performed in order to validate the radiosensitizing concentration isolated by the $SF_{4Gy}$ assay.

### 1.1. Assessing of the concentration and media parameters

In order to test one parameter after another, the first treatment time used was one hour as previously validated with DTPA NPs on SQ20B J.L. cells (Miladi *et al.*, 2015). Three culture media were successively tested (HBSS, PBS $Ca^{2+}/Mg^{2+}$, and serum-free DMEM-Glutamax), with increasing AGuIX® concentrations from 0mM Gd (control) to 3mM Gd. Two independent experiments were done for each tested media, including six 25$cm^2$ flasks with two varying cell concentrations.

#### *1.1.1. AGuIX® treatment in HBSS media*

Hanks' Balanced Salt Solution (HBSS) was the first media tested according to the previous study with DTPA NPs (Miladi *et al.*, 2015).

✓ **$SF_{4Gy}$ assay**

Figure 64 shows the $SF_{4Gy}$ obtained for the different concentrations of AGuIX®.

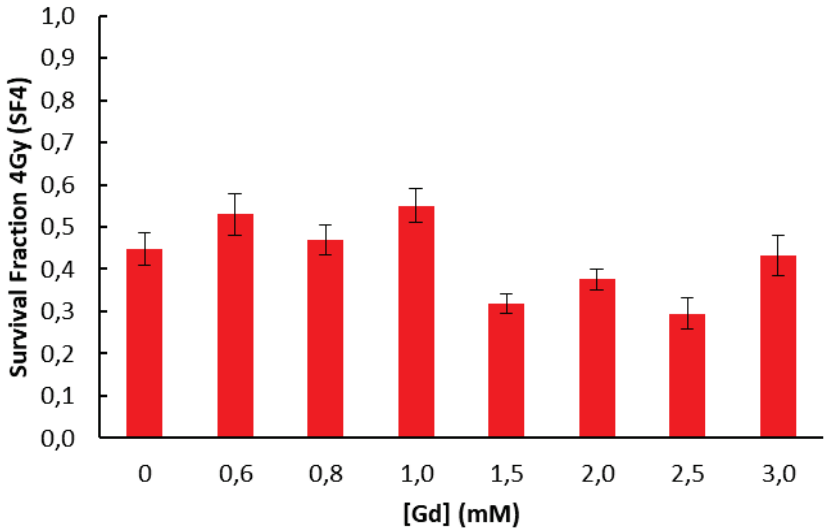


Figure 64: Survival fraction at 4Gy varying concentration from 0-3 mM Gd in HBSS media (n=2).

In this culture medium, **1.5 mM Gd** was the smallest radiosensitizing concentration obtained with a $SF_{4Gy}$ of 0.32 compared to 0.45 for untreated cells.

✓ **Full clonogenic survival curve assay**

Next, the complete clonogenic survival curve was performed using the AGuIX® concentration isolated by the $SF_{4Gy}$ assay, *i.e.* **1.5 mM Gd**. As depicted in Figure 65, no significant radiosensitizing effect was obtained under these experimental conditions. This result is the mean of two independent experiments.

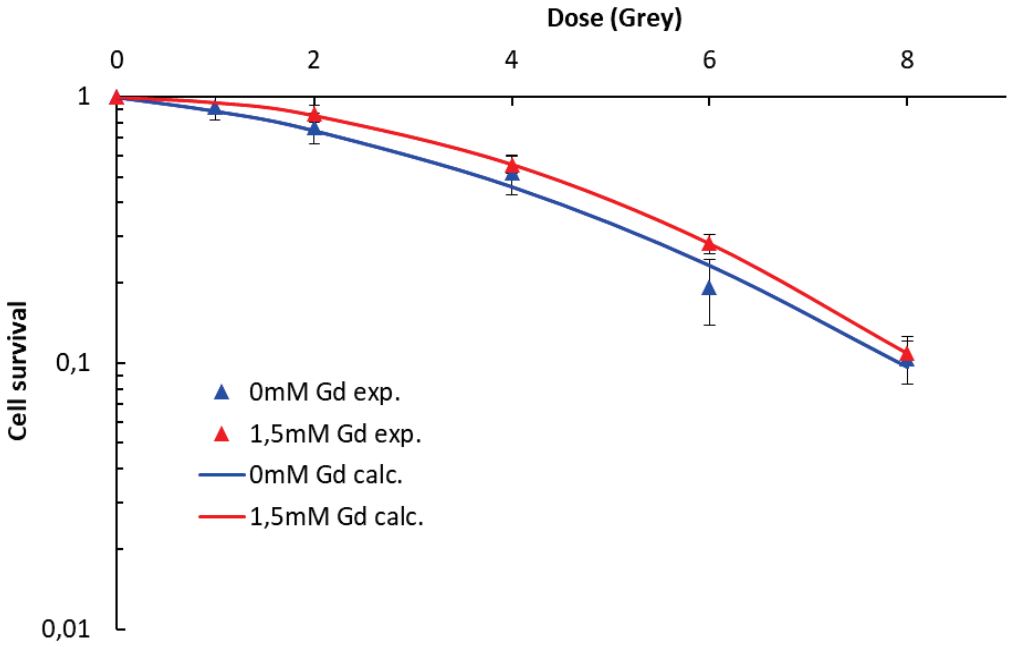


Figure 65: Clonogenic survival assay 0-8 Gy following a 1h AGuIX® treatment in HBSS media at 1.5mM Gd. Blue: 0mM Gd, red: 1,5mM Gd. (n = 2). Each experimental point represents the counting of 6 independent T25cm$^2$ flasks, and the curve represents the combination of two independent experiments.

| [Gd] (mM) | α | β | 10% Survival | 50% Survival | EBR-10% | EBR-50% |
|---|---|---|---|---|---|---|
| **0** | 0.095 | 0.0247 | 7.92 | 3.72 | 0.972 | 0.847 |
| **1.5** | 0.0127 | 0.0331 | 8.15 | 4.39 | | |

Table 18: Summary of the parameters evaluating the radiosensitizing effect of AGuIX® at 1.5mM Gd in HBSS. (The α and β parameter are calculated using the linear quadratic equation $S=\exp(-\alpha D-\beta D^2)$, described page 126 of the Materials and Methods section).

As can be seen in Table 18, whether we look at the 10% Enhanced Biological Response (EBR) or the 50% EBR, it is lower than 1, which means that treating the cells with AGuIX® prior to radiation does not increase cellular death. In addition, one might notice in Figure 65, that the red curve (cells treated with 1.5mM Gd) is over that of the untreated cells, however, most error bars overlap and therefore we can conclude that there are no significant differences in the survival fraction between untreated and treated cells.

Collectively, after analyzing the clonogenic survival curve assay, **we did not validate 1.5 mM Gd for 1 hour in HBSS as a working radiosensitizing condition**.

### *1.1.2. AGuIX® treatment in Phosphate Buffer Saline (PBS) $Ca^{2+}/Mg^{2+}$*

Phosphate Buffer Saline (PBS) with $Ca^{2+}$ and $Mg^{2+}$ was the second medium tested. (*Note: $Ca^{2+}/Mg^{2+}$ was necessary, otherwise the cells would unattach from the flask).

✓ **$SF_{4Gy}$ assay**

Figure 66 shows the $SF_{4Gy}$ obtained for the different concentrations of AGuIX® tested.

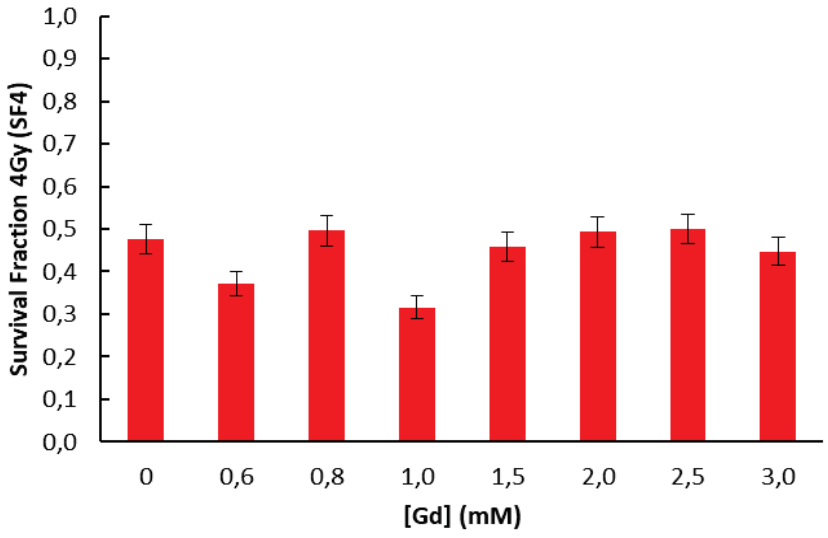


Figure 66: Survival fraction at 4Gy varying concentration from 0-3 mM Gd in PBS $Ca^{2+}/Mg^{2+}$ media (n=2).

In this medium, **1.0mM Gd** was the smallest radiosensitizing concentration obtained with a $SF_{4Gy}$ of 0.32 compared to 0.48 for untreated cells.

✓ **Full clonogenic survival curve assay**

Again, the complete clonogenic survival curve was then performed using the gadolinium concentration isolated by the $SF_{4Gy}$ assay, *i.e.* **1mM Gd**. As it can be observed in Figure 67, no significant radiosensitizing effect was obtained in this medium with 1mM Gd.

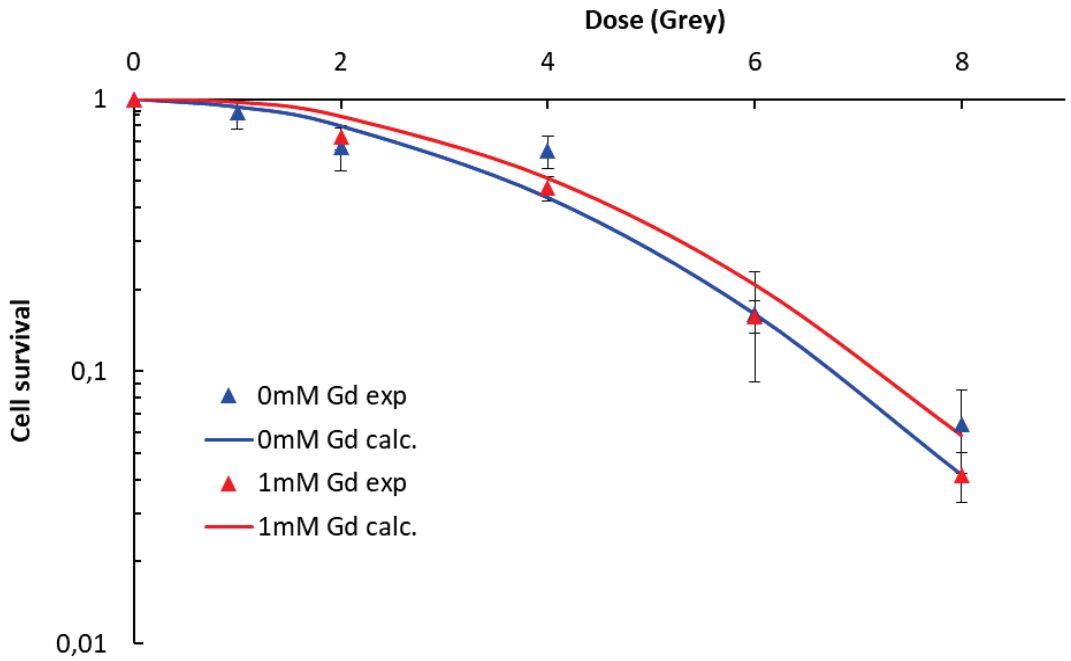


Figure 67: Clonogenic survival assay 0-8 Gy following a 1h AGuIX® treatment in PBS $Ca^{2+}/Mg^{2+}$ media at 1mM Gd. Blue: 0mM Gd, red: 1mM Gd (n= 2).

| [Gd] (mM) | α | β | 10% | 50% | EBR-10% | EBR-50% |
|---|---|---|---|---|---|---|
| **0** | 0.0189 | 0.0473 | 6.75 | 3.62 | 0.935 | 0.889 |
| **1.0** | -0.0217 | 0.0471 | 7.22 | 4.07 | | |

Table 19: Summary of the parameters evaluating the radiosensitizing effect of AGuIX® at 1mM Gd in PBS $Ca^{2+}/Mg^{2+}$.

As can be seen in Table 19, both the 10% and the 50% EBR were lower than 1, which means that treating the cells with 1 mM AGuIX® prior to radiation does not improve survival. Again, one might notice in Figure 67 that the red curve (cells treated with 1mM Gd) is over that of the untreated cells with error bars overlapping which means that there are no differences in the survival fraction between untreated and treated cells. At last, a negative α value was obtained whereas no difference concerning the β parameter occurred between untreated and treated cells.

In this culture medium, the clonogenic survival curve assay did not allow us to choose **1mM Gd for 1 hour in PBS $Ca^{2+}$/$Mg^{2+}$ as a working radiosensitizing condition.**

### *1.1.3. AGuIX® treatment in serum-free DMEM-Glutamax*

Dulbecco's Modified Eagle's Medium was the third and last media tested.

✓ **$SF_{4Gy}$ assay**

Figure 68 shows the $SF_{4Gy}$ obtained for the different concentrations of AGuIX® tested.

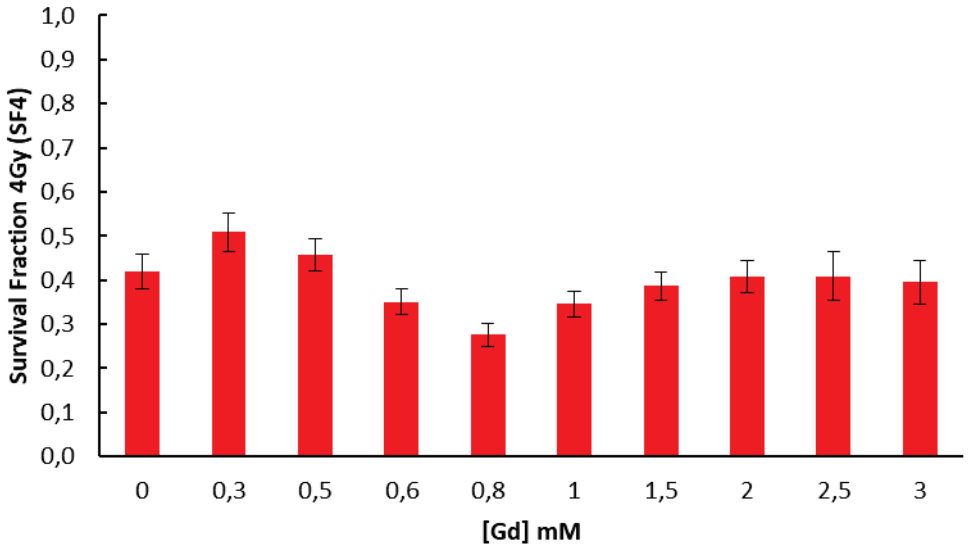


Figure 68: Survival fraction at 4Gy varying concentration from 0-3 mM Gd in serum-free DMEM-Glutamax media (n=2).

The concentration **0.8 mM Gd** was noted as the best radiosensitizing concentration when the treatment was done in serum-free DMEM-Glutamax with a $SF_{4Gy}$ of 0.28 compared to 0.42 for untreated cells.

✓ **Full clonogenic survival curve assay**

When performing the full clonogenic assay using 0.8 mM Gd in serum-free DMEM-Glutamax, no radiosensitizing effect was observed, as can be seen in Figure 69. We were therefore unable to validate the concentration of 0.8mM Gd in DMEM-Glutamax.

As can be seen in Table 20, both the 10% and 50% EBR were close to 1 thus confirming the absence of a radiosensitizing effect. As shown in Figure 69, the survival curves obtained for untreated and treated cells were very close to each other. However, we can note a difference in the α parameter, as it is doubled in the presence of nanoparticles, which suggest that more immediate lethal lesions should occur, whereas no significant difference was obtained concerning the β parameter.

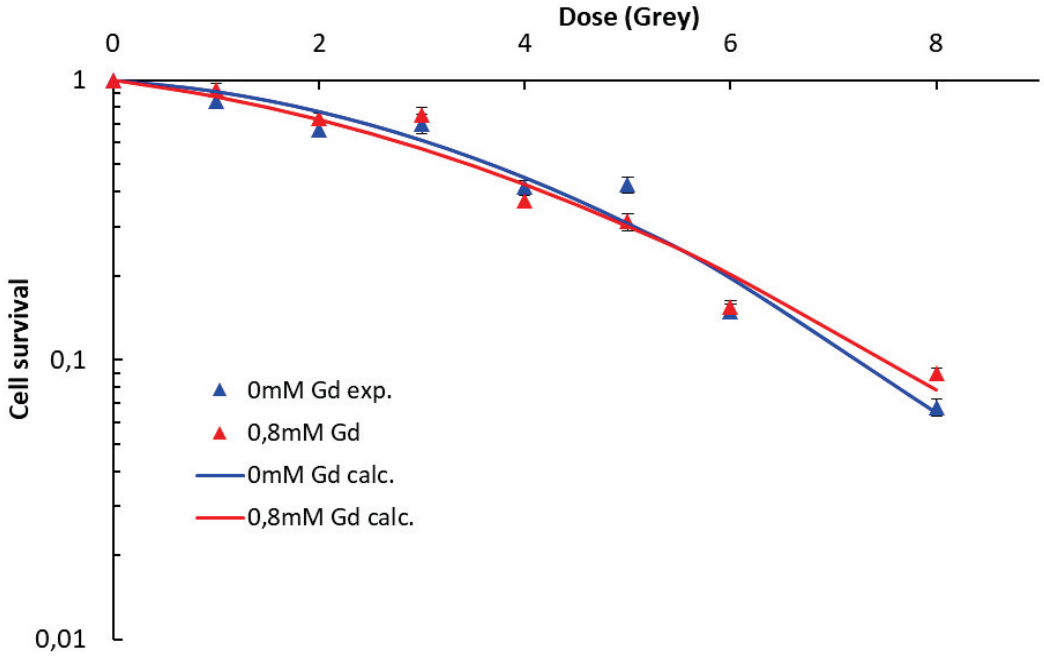


Figure 69: Clonogenic survival assay 0-8 Gy following a 1h AGuIX® treatment in serum-free DMEM-Glutamax media. Blue: 0mM Gd, red: 0.8mM Gd (n= 9).

| [Gd] (mM) | α | β | 10% | 50% | EBR-10% | EBR-50% |
|---|---|---|---|---|---|---|
| **0** | 0.0589 | 0.0354 | 7.25 | 3.65 | 0.964 | 1.058 |
| **0.8** | 0.1103 | 0.026 | 7.52 | 3.45 | | |

Table 20: Summary of the parameters evaluating the radiosensitizing effect of AGuIX® at 0.8mM Gd in serum-free DMEM-Glutamax.

When treating the cells for 1 hour with **0.8mM Gd in serum-free DMEM-Glutamax for one hour, we do not observe any radiosensitizing effect**.

The three mediums tested are quite different in their composition: some are isotonic solutions (PBS and HBSS) whereas DMEM-Glutamax is a much more complex solution containing inorganic salts, amino acids, vitamins, and phenol red. The complete ingredient lists for HBSS, PBS $Ca^{2+}$/$Mg^{2+}$, and DMEM-Glutamax with corresponding concentrations can be found in Annex 3.

When analyzing the results obtained for the $SF_{4Gy}$ assay in all three media, an interesting observation can be made, and that it that there is no linear relationship between the Gd concentration used and the $SF_{4Gy}$: the radiosensitizing effect of AGuIX® does not represent a linear relationship. Indeed, one could think that as the AGuIX® concentration is increased, the radiosensitizing effect would increase. Surprisingly, a U-shaped curve occurred. Considering the results obtained with the full clonogenic survival curve assays, *i.e.* since there was no

significant radiosensitizing effect whatever the culture medium or the Gd concentration used, we decided to increase the incubation time with the AGuIX® nanoparticles before irradiation.

## 1.2. Increasing the incubation time

As the lowest concentration of AGuIX® isolated from the $SF_{4Gy}$ assays was obtained in serum-free DMEM Glutamax, we further used these experimental conditions with increasing the incubation time: 1 hour (reference treatment time), 4, 12, and 24 hours. Moreover, we quantified the amount of AGuIX® taken up by the cells by inductively coupled plasma atomic emission spectroscopy (ICP-AES) in order to investigate if more AGuIX® internalized would improve radiosensitization.

### *1.2.1. Internalization of AGuIX in SQ20B J.L. cells: ICP-AES experiments*

In order to quantify gadolinium internalization by SQ20B J.L. cells, a kinetic study ranging from 1h up to 24h was performed with ICP-AES.

As mentioned above, a concentration of 0.8mM Gd in serum-free DMEM-Glutamax was used throughout these experiments. The results are summarized in Figure 70.

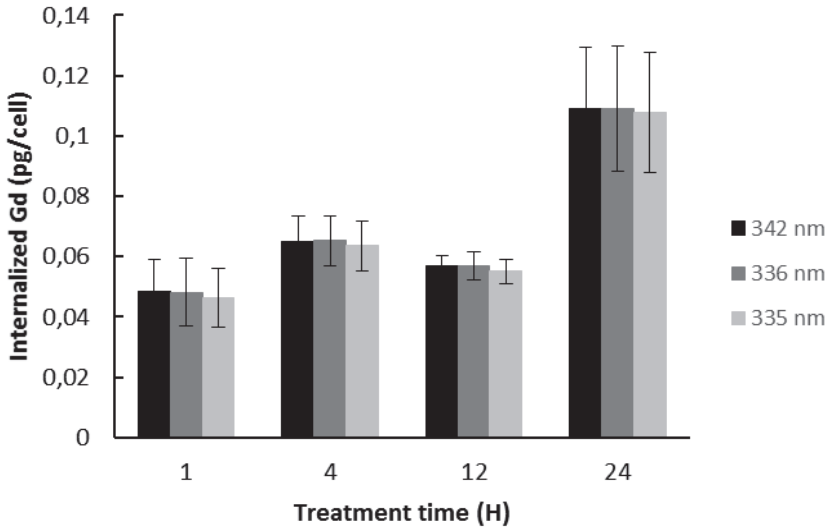


Figure 70: Quantity of gadolinium internalized by SQ20B J.L. cells as a function of the incubation time (1-4-12-24 hours of exposure to 0.8 mM Gd) in serum-free DMEM-Glutamax quantified by ICP-AES. The three wavelengths of gadolinium are represented (342, 336, and 332 nm). This is a mean of 2 independent experiments with three flasks for each, and three separate readings from the ICP.

After one-hour of incubation with the AGuIX®, SQ20B J.L. cells internalized about 0.05 pg Gd/cell. This value was not significantly modified even after 4 and 12 hours of treatment (ICP values are 1h: 0.0484; 4h: 0.0651; 12h: 0.0571 pg/cell, respectively). However, under the same experimental conditions, about **0.11 pg of gadolinium** per cell was internalized after 24 hours of AGuIX® treatment, whatever the wavelengths of gadolinium (335, 336, and 342 nm)

used. This is more than 10 times lower than the quantity that was internalized by these cells when treated with the DTPA-gadolinium-based nanoparticles (1.24 pg/cell: Miladi *et al.*, 2015). When compared to other studies, the quantity of nanoparticles internalized by SQ20B J.L. cells is quite low. Indeed, 0.4 pg Gd/cell was found in B16F10 melanoma cells after 1 hour of treatment with 0.6 mM Gd (Kobt *et al.*, 2016), while 1.25 pg Gd/cell were found in Panc-1 cells after only 30 minutes of incubation (Detappe *et al.*, 2015), whereas 0.059 mM of gadolinium was taken up by HeLa cells, one hour after treatment with 0.5 mM Gd (Luchette *et al.*, 2014).

### *1.2.2. Survival Fraction at 4Gy ($SF_{4Gy}$) response when increasing AGuIX® treatment time:*

Following these experiments, the impact of this longer incubation time with AGuIX® was checked with the $SF_{4Gy}$ assay and a full clonogenic survival curve was performed.

✓ **$SF_{4Gy}$ assay**

Figure 71 shows the $SF_{4Gy}$ obtained for the different concentrations of AGuIX® tested while Table 21 shows the enhanced biological response (EBR).

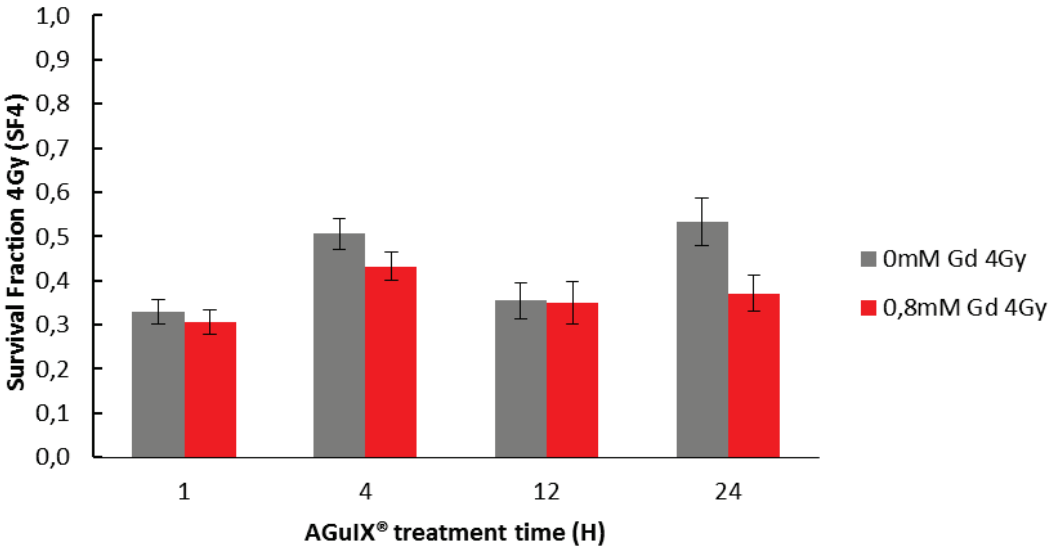


Figure 71: Survival fraction at 4Gy at 0.8mM Gd following different AGuIX® treatment times (1h-4h-12h-24h). The values are the mean ± SD of three independent experiments.

As depicted in Figure 71, a significant decrease of the $SF_{4Gy}$ was obtained only after a 24h incubation time with AGuIX®. This result was perfectly correlated with the ICP-AES experiments and underline the fact that a minimum amount of internalized Gd can result in a significant biological effect.

The EBR values were calculated and are enumerated in Table 21.

| Treatment time (H) | EBR (4Gy) |
|---|---|
| 1 | 1.076 |
| 4 | 1.173 |
| 12 | 1.018 |
| 24 | 1.436 |

Table 21: Calculated Enhanced Biological Response (EBR) at 4Gy for the four different incubation times at 0.8mM Gd in serum-free DMEM-Glutamax.

The treatment time of **24 hours** was retained as the optimal treatment time at a concentration of 0.8 mM Gd in serum-free DMEM-Glutamax with a $SF_{4Gy}$ of 0.37 compared to 0.53 for untreated cells. This represented an EBR of **1.436**.

✓ **Full clonogenic survival curve assay**

The experimental conditions reported above were then validated with the clonogenic survival curve assay. Figure 72 shows a significant radiosensitizing effect of 0.8 mM AGuIX® when incubated for 24h before irradiation in serum-free DMEM-Glutamax. A summary of the parameters evaluating the radiosensitizing effect of AGuIX® under these treatment conditions is reported in Table 22.

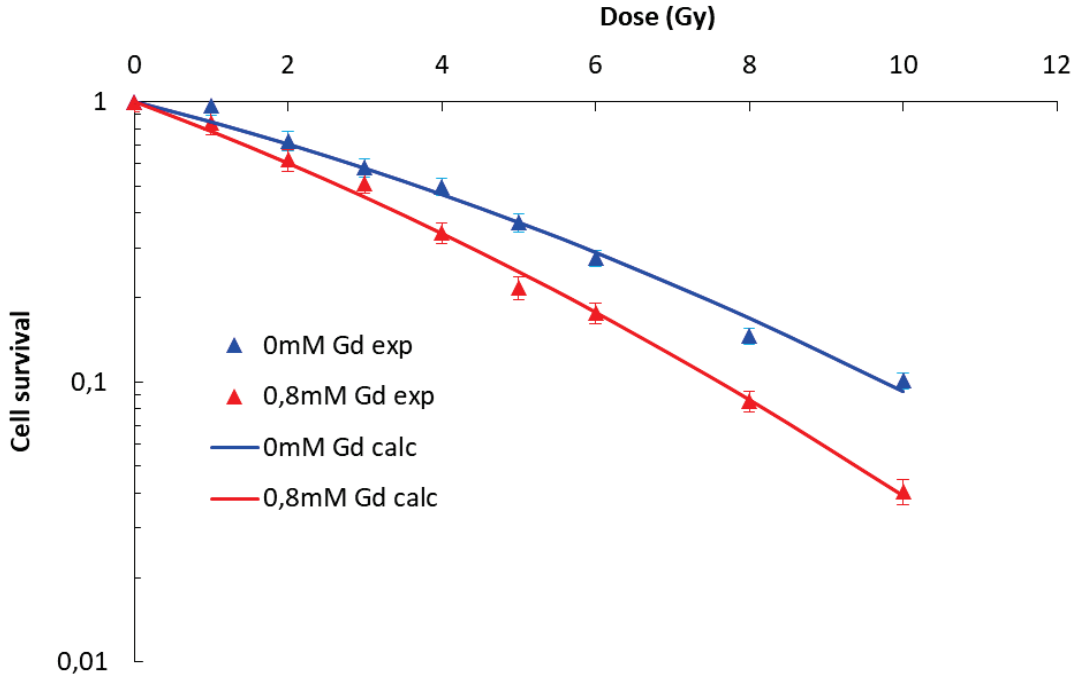


Figure 72: Clonogenic survival assay 0-10 Gy following a 24h AGuIX® treatment in serum-free DMEM-Glutamax at a concentration of 0.8mM Gd. Blue: 0mM Gd, red: 0,8mM Gd. This result is the mean ± SD of three independent experiments. (***, $p<0.005$ vs. irradiated SQ20B cells).

| [Gd] (mM) | α | β | 10% | 50% | EBR-10% | EBR-50% |
|---|---|---|---|---|---|---|
| **0** | 0.1593 | 0.0079 | 9.75 | 3.65 | 1.281 | 1.377 |
| **0.8** | 0.2357 | 0.0088 | 7.61 | 2.65 | | |

Table 22: Summary of parameters evaluating the radiosensitizing effect of the addition of AGuIX® for 24 hours at 0.8mM Gd in serum-free DMEM-Glutamax.

Radiosensitization with NPs can occur after various conditions of treatment (concentration, incubation time …) depending on the cell line and the type of nanoparticles used. For example, Townley *et al.* studied X-ray-activable titania nanoparticles on two rhabdomyosarcoma and MCF-7 cells, and incubated them at 225 nmoles per well overnight (Townley et al., 2012), while gold nanoparticles have been used in varying concentration going from 1 nM (14 nm gold nanoparticles coated with citrate used on HeLa cells in combination with a photon energy of 220 kVp Chithrani *et al.*, 2010) to 1 mM on BAEC cells using a 150 kVp irradiator with an observed DEF of 4 (Rahman *et al.*, 2009). There are many different kinds of gold nanoparticles developed as radiosensitizers, different sized nanoparticles, with different coatings, used in a variety of cell lines and with different types of irradiation, all of which are summarized in Coulter *et al.*, 2013. Even in the studies of AGuIX® as radiosensitizers, different concentrations varying from 0.05 mM to 1.0 mM, and various incubation times have been used to observe a radiosensitizing effect in different cell lines as can be seen in Table 11 of the bibliography review. (Sancey *et al.*, 2014)

**Our radiosensitizing conditions with AGuIX® and SQ20B J.L. cells were finally determined to be 0.8 mM Gd for 24 hours in serum-free DMEM-Glutamax**. With these conditions, the **$SF_{4Gy}$** is **1.382** and we have a 50% Enhanced Biological Factor (EBR) of **1.377**. This 50% EBR was calculated following the clonogenic survival curve assay (and therefore the nine irradiation doses were taken into account when calculating the value), whereas in Table 21, we have an EBR (4Gy) at 1.436, value which was calculated with only two points. This EBR is in the same range compared to what is currently published in studies using AGuIX® nanoparticles as a radiation sensitizer, whether in HeLa (cervical cancer), Panc-1 (pancreatic cancer), U87 (glioblastoma), and B16F10 (melanoma), with DEFs varying from 1.17 (Panc-1) to 1.54 (HeLa).

In 2014, Štefančíková *et al.* reported an enhancement factor close to 23% in U87 cells treated with 0.5 mM Gd for 6 hours which corresponds to a decrease of the $SF_{2Gy}$ to 0.24 compared to 0.31 in untreated cells. Moreover, they showed an increase in the α-parameter (with an α of 0.4 in untreated cells *vs* 0.71 in treated cells respectively), a result slightly higher than our (0.16 in untreated cells *vs* 0.24 in treated cells). Two years later, they published another study where U87 cells were treated with 1 mM Gd for one hour, which resulted in an EBR of 1.47. In HeLa cells, Berbeco *et al.* (2014) tested two irradiation sources: 220 kV and 6 MV (to see their potential in a clinical setting). When treating HeLa cells with 0.5 mM Gd for one hour, they observed a $SER_{4Gy}$ of 1.54 when irradiating at 220 kVp and 1.28 after exposure

to 6 MV. The average DEF was calculated to be 1.54 at 220 kVp while it was a little lower for the 6 MV irradiation source: 1.15.

Collectively, these results and our current study, suggest that the extent of radiosensitization with AGuIX® nanoparticles essentially depends on the cellular model used. Indeed, whatever the time of incubation or the concentration of AGuIX® used in these different cellular models, radiosensitization occurs with a fairly comparable EBR.

Prior to definitively using the experimental conditions defined above for the rest of this PhD work, we wanted to verify the impact of using a full medium (containing 10% FBS) on the radiosensitizing effect of AGuIX®. Indeed, previous work in the lab demonstrated that an agglomeration of DTPA-based nanoparticles occurred in the presence of FCS.

Figure 73 and Table 23 show the results obtained with the clonogenic survival assay when treating SQ20B J.L. cells with the conditions previously determined for AGuIX®, but in full media (in the presence of 10% FCS).

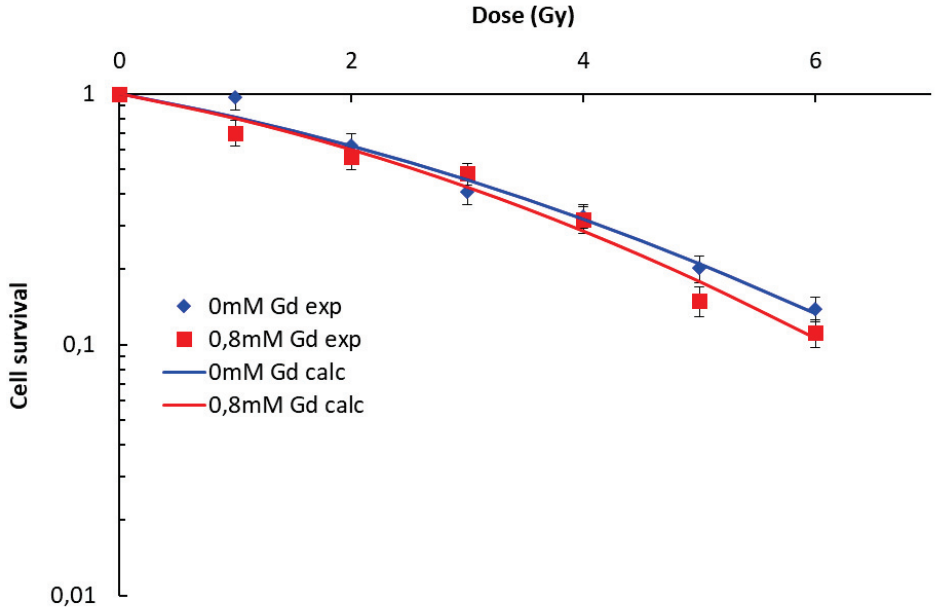


Figure 73: Clonogenic survival assay 0-6 Gy following a 24h AGuIX® treatment in full media at a concentration of 0.8mM Gd. Blue: 0mM Gd, red: 0,8mM Gd.

| [Gd] (mM) | α | β | 10% | 50% | EBR-10% | EBR-50% |
|---|---|---|---|---|---|---|
| **0** | 0.1906 | 0.0241 | 6.58 | 2.7 | 1.079 | 1.059 |
| **0.8** | 0.1979 | 0.0293 | 6.1 | 2.55 | | |

Table 23: Summary of the parameters evaluating the radiosensitizing effect of the addition of AGuIX® in full media.

In the presence of 10% FCS (full SQ20B J.L. medium), using the radiosensitizing conditions determined in serum-free DMEM-Glutamax, **no radiosensitizing effect was observed** as assessed by the survival curve assay (**Figure 73**) and the various radiobiological parameters reported in Table 23**.** In addition, the α and β values are also the same, as can be seen in Table 23.

**After testing different AGuIX® concentrations in different media using the $SF_{4Gy}$ and the clonogenic survival curve assays, as well as quantifying the gadolinium intake of SQ20B J.L. cells, the following radiosensitizing conditions were determined for AGuIX® nanoparticles in the SQ20B J.L. cellular model: a concentration of 0.8 mM Gd for 24 hours in serum-free DMEM-Glutamax. These are the set conditions for the rest of the work presented throughout this PhD work.**

## 2. *Toxicity study*

Once the radiosensitizing conditions treatment were determined, we verified the treatment toxicity of **AGuIX®** in the absence of irradiation. In this study, three tests were used: a proliferation assay, the trypan blue assay, and the MTT assay, respectively.

### 2.1. Proliferation assay: % confluency measurements by IncuCyte

The IncuCyte live imaging allows an optimized *in vitro* microscope based on the proliferation of SQ20B J.L. cells, taking a picture in phase contrast every two hours for up to seven days. This assay was realized up to 168h after treatment with AGuIX®. As depicted in Figure 74, SQ20B J.L. cells continued to proliferate, whether the cells had been treated with 0mM Gd or 0.8mM Gd in free-serum DMEM-Glutamax.

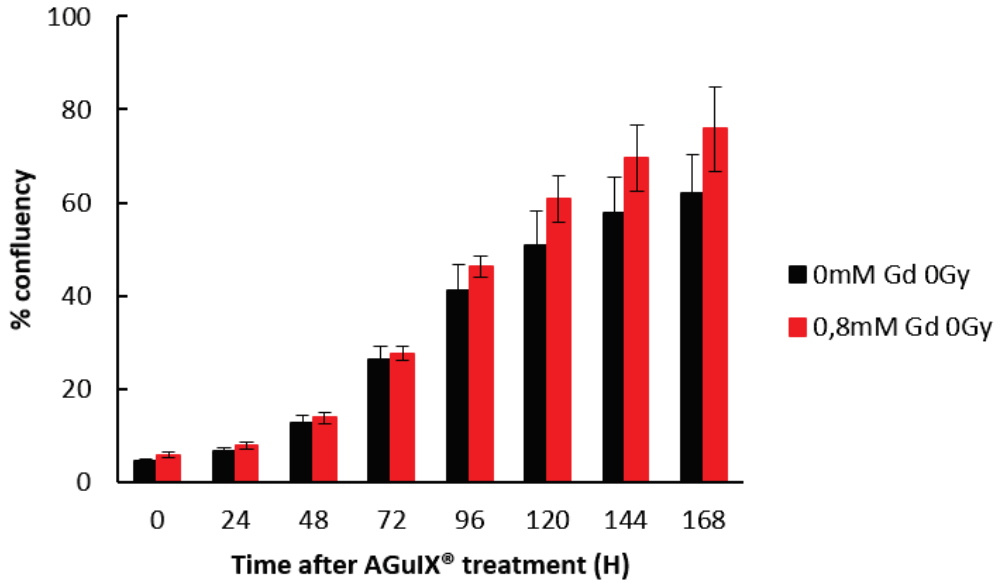


Figure 74: Proliferation assay measuring the percentage confluency using the IncuCyte Live Cell Analysis (n=2).

### 2.2. Cell viability: Trypan Blue assay

The trypan blue assay is a dye exclusion test widely used to monitor cellular toxicity: viable cells have intact cell membranes which do not allow trypan blue to enter, whereas nonviable cells will have a blue cytoplasm. The percent viability was calculated by dividing the number of viable cells by the number of total cells (live + dead cells).

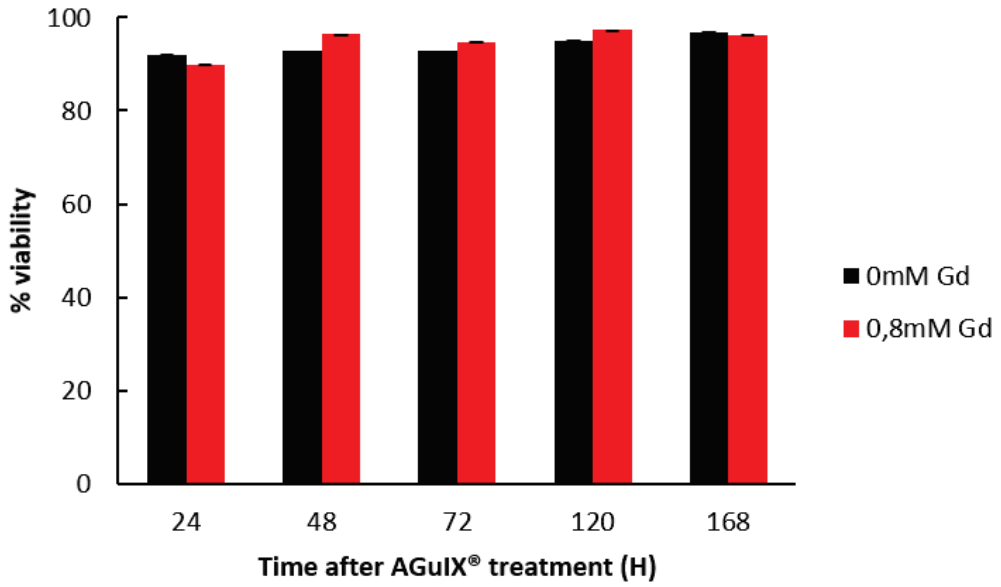


Figure 75: Percentage of viability using the blue trypan assay (n=3).

As can be observed in Figure 75, the percent viability of SQ20B J.L. cells with or without AGuIX® treatment remains unchanged, thus demonstrating the absence of AGuIX® toxicity.

### 2.3. Mitochondrial activity: MTT assay

A third assay was performed in order to validate the absence of toxicity following AGuIX® treatment: the MTT assay. This assay is a colorimetric assay for assessing the cell's metabolic activity. NAD(P)H-dependent cellular oxidoreductase enzymes may, under defined conditions, reflect the number of viable cells present. These enzymes are capable of reducing the tetrazolium dye MTT 3-(4,5-dimethylthiazol-2-yl)-2,5-diphenyltetrazolium bromide to its insoluble formazan, which has a purple color. Mitochondrial activity was measured starting 48 hours after treatment, (the time 24 hours was used as a reference), until 7 days after AGuIX® treatment. As seen in Figure 76, AGuIX® treatment does not significantly affect mitochondrial activity.

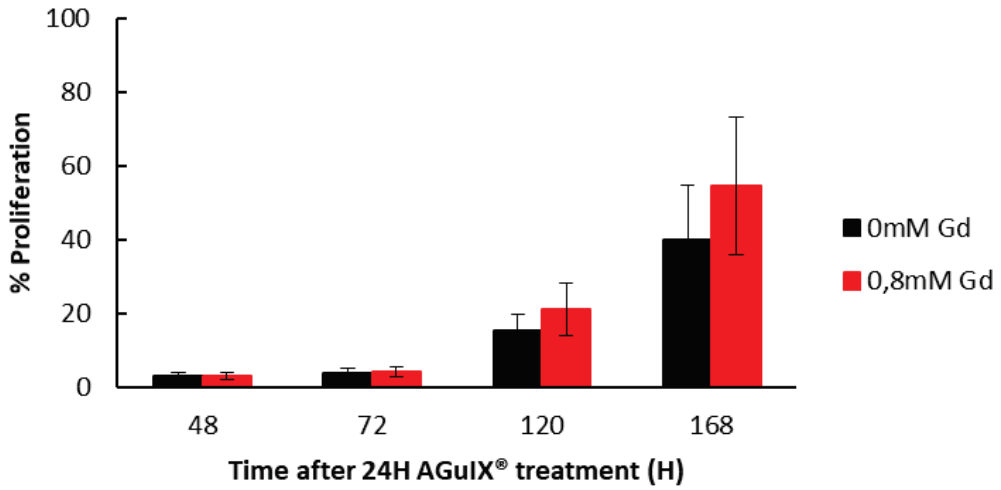


Figure 76: Percent (%) of proliferation measured by the MTT assay (n=3).

Using these three different assays, we have clearly demonstrated that the previously determined **AGuIX® treatment conditions** were **not toxic** to cells, nor at the cellular level (blue trypan assay) nor at the mitochondrial level (MTT assay).

These same tests were also performed with an additional control, *i.e.* SQ20B J.L. cells in their full medium (in the presence of 10% FCS). No significant differences were noted between cells that were always in full media compared to cells that had been in serum-free DMEM-Glutamax for 24 hours.

## 3. *Subcellular localization of AGuIX® in SQ20B J.L. cells*

The nanoparticles' localization inside cells once internalized is of great interest as it can help in the understanding of the cellular mechanisms by which radiosensitization could occur. We therefore focused on their localization with respect to the nucleus, mitochondria, and lysosomes, using AGuIX® bound to Cya5.5 for an application in confocal microscopy.

### 3.1. With respect to the nucleus

After twenty-four hours of incubation with AGuIX®-Cya5.5, cells were fixed in 4% PFA and the nuclei were stained with DAPI. Thirty-one slices were taken (Z-positions). The pictures taken shown in Figure 77 are representative of more than 100 cells that were imaged.

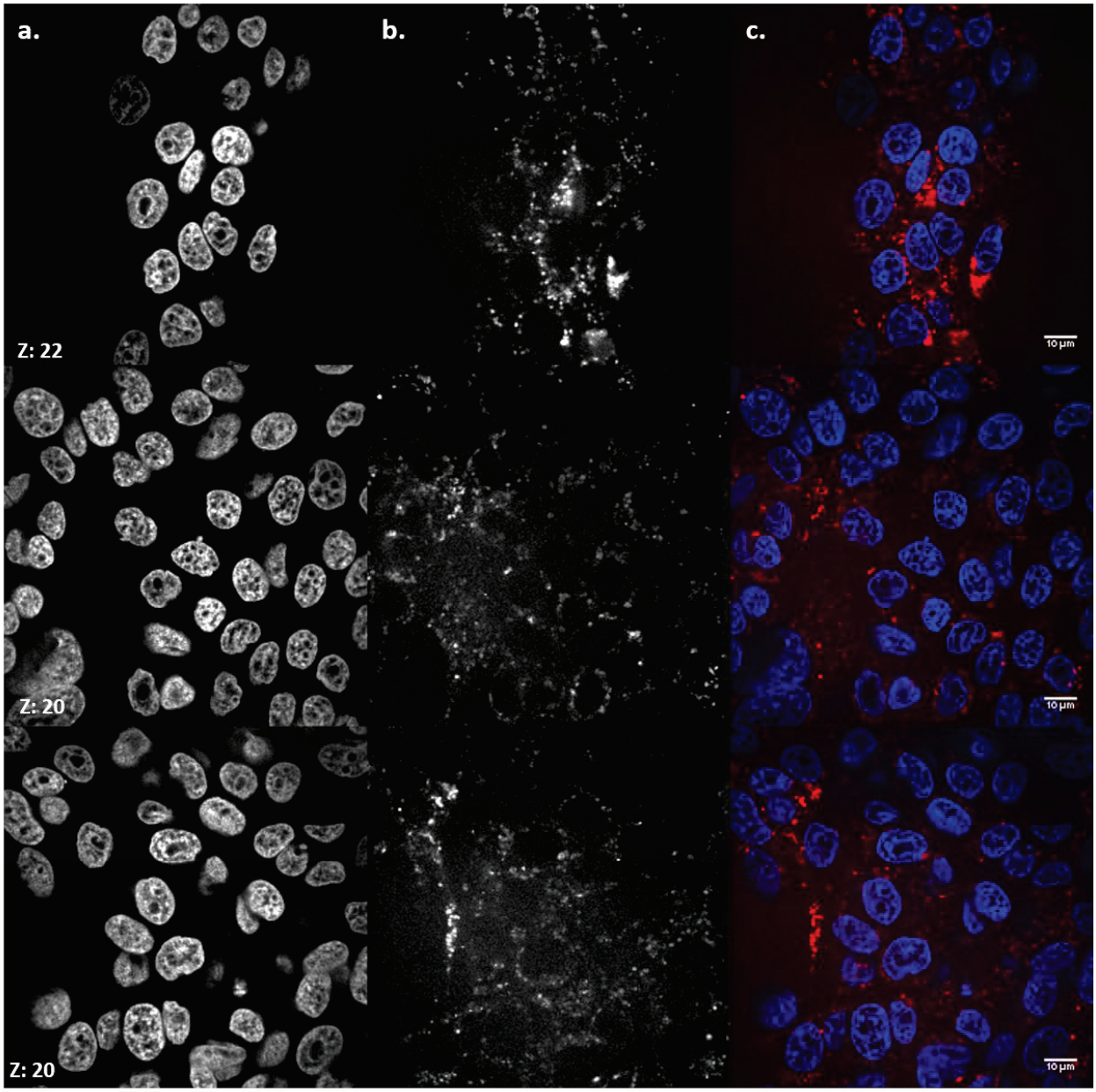


Figure 77: Three separate planes of the localization of AGuIX®-Cya5.5 nanoparticles in SQ20B J.L. cell line with respect to the nucleus with a confocal spinning-disk microscope (µLife Platform, CEA-Grenoble). a. DAPI (nucleus); b. AGuIX®-Cya5,5; c. Merge. Experiments realized on fixed cells (4% PFA); 60X, with S. Gerbaud- team Biomics.

As shown in Figure 77, no co-localization of AGuIX® nanoparticles with the nucleus occurred, a result which is in accordance with previous published worked, whether with AGuIX® (Štefančíková *et al.*, 2014; Kobt *et al.*, 2016), or other types of nanoparticles.

### 3.2. With respect to mitochondria

After twenty-four hours of incubation with AGuIX®-Cya5.5, cells were put in a humidified chamber kept at 37°C and 5% $CO_2$ to visualize live cells, without fixing them. The cells were stained with Mitotracker-Green prior to the incubation with AGuIX®-Cya5.5. Thirty-one slices

were taken (Z-positions). The pictures taken shown in Figure 78 are representative of more than 100 cells that were imaged.

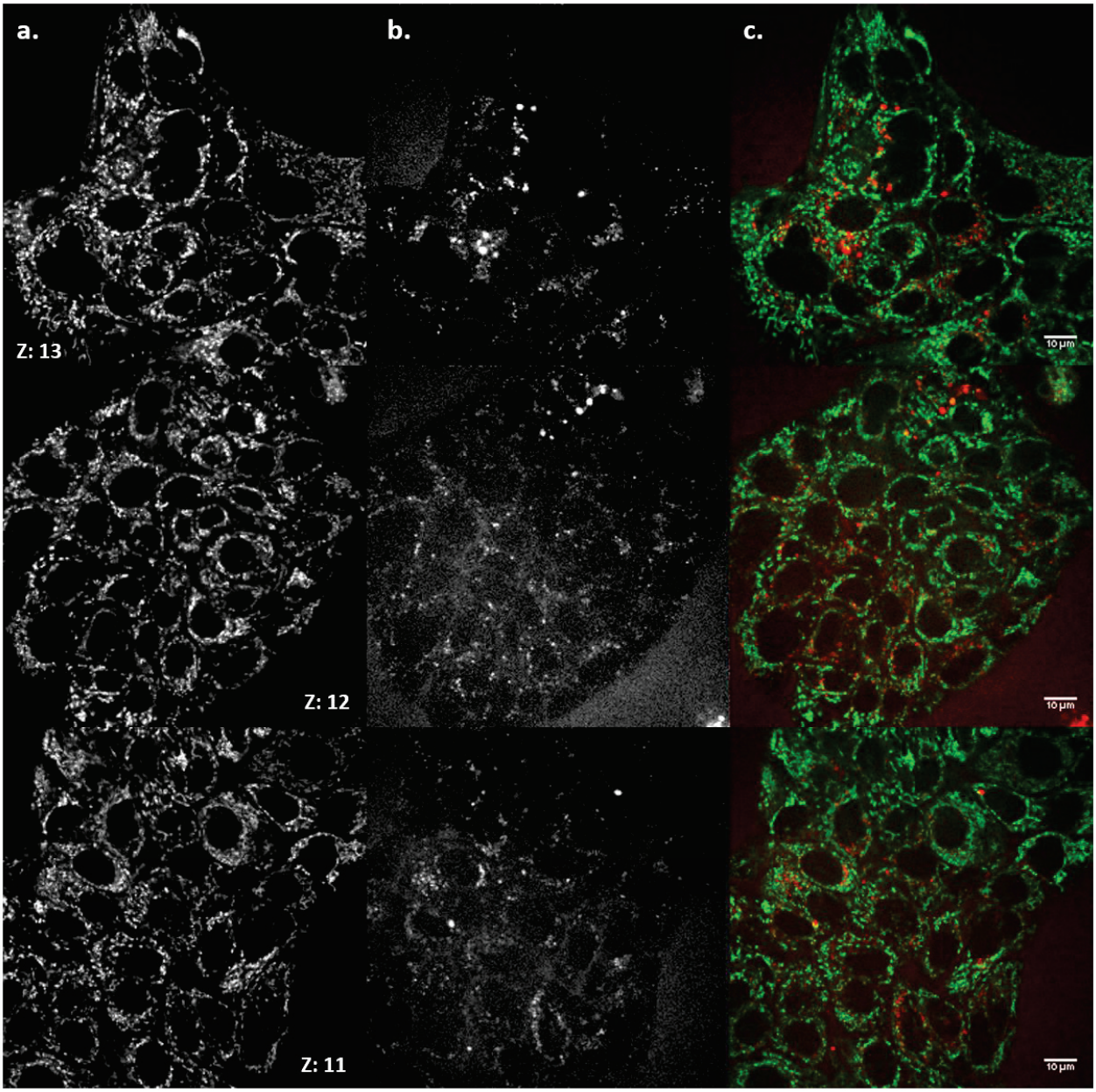


Figure 78: Three separate planes of the localization of AGuIX® nanoparticles in SQ20B J.L. cell line with respect to mitochondria with a confocal spinning-disk microscope (µLife Platform, CEA-Grenoble). a. Mitotracker-green; b. AGuIX® -Cya5,5; c. Merge. Experiments realized on live cells; 60X, with S. Gerbaud- team Biomics.

As can be observed in Figure 78, no co-localization of AGuIX®Cya5.5 nanoparticles with mitochondria was obtained. This is in accordance with Štefančíková *et al.* (2014), who had also done co-localization studies between mitochondria and AGuIX®-Cya5.5.

### 3.3. With respect to lysosomes

After twenty-four hours of incubation with AGuIX®-Cya5.5, cells were put in a humidified chamber kept at 37°C and 5% $CO_2$ to visualize live cells, without fixing them. The cells were stained with Lysotracker-Green prior to the incubation with AGuIX®-Cya5.5. Thirty-one slices were taken (Z-positions).

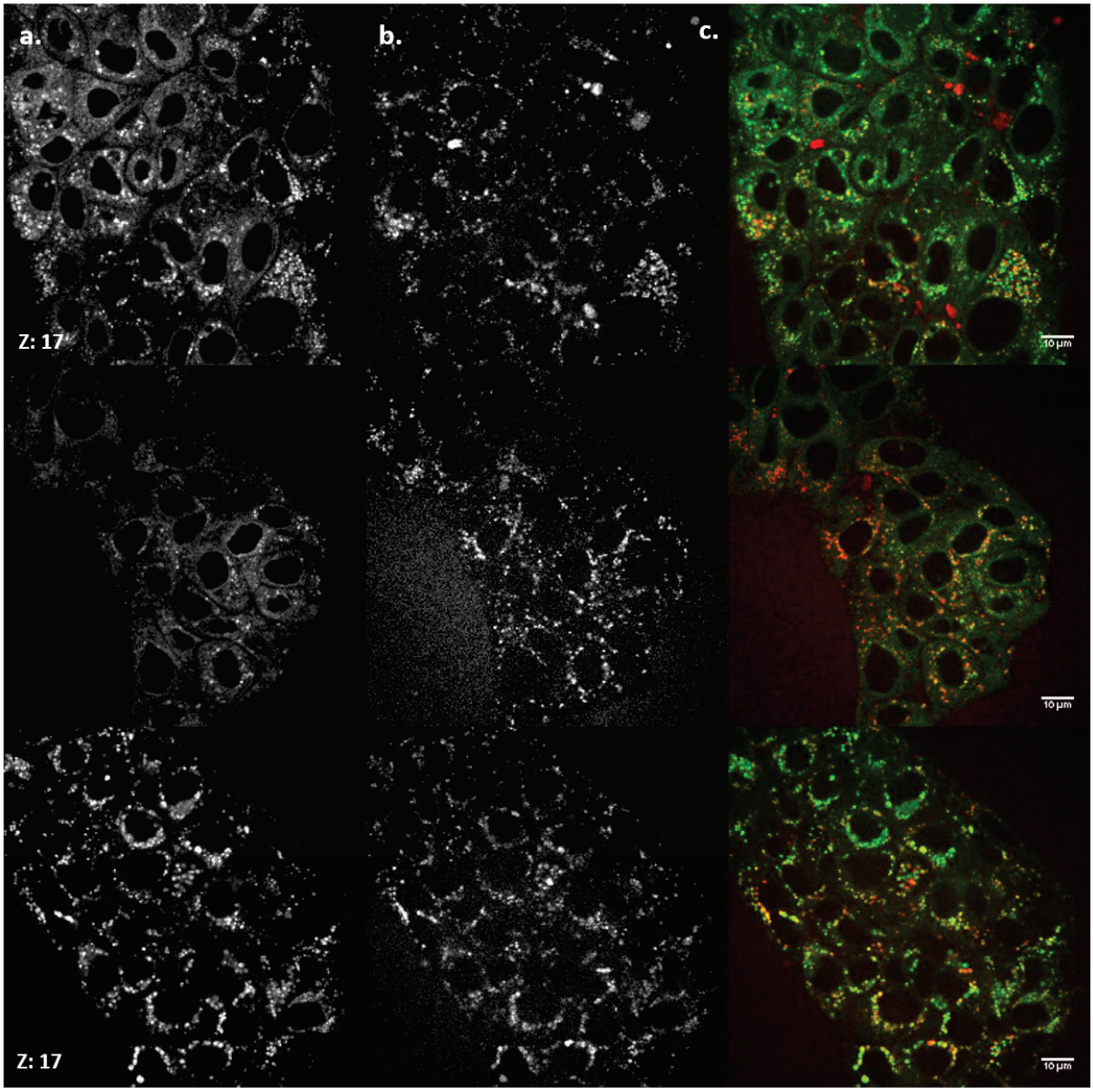


Figure 79: Three separate planes of the localization of AGuIX® nanoparticles in SQ20B J.L. cell line in respect to lysosomes with a confocal spinning-disk microscope (µLife Platform, CEA-Grenoble). a. Lysotracker-green; b. AGuIX® -Cya5,5; c. Merge. Experiment realized on live cells; 60X, with S. Gerbaud-team Biomics.

The pictures taken shown in Figure 79 is representative of more than 100 cells that were imaged. As depicted in Figure 79, we can observe a major co-localization of AGuIX®-Cya5.5 with lysosomes whereas some free AGuIX®-Cya5.5 remain in the cytosol.

### 3.4. Kinetic study of the internalization of AGuIX® by confocal microscopy: 1h-2h-4h-6h, with respect to the lysosomes

This next section illustrates the kinetics of the internalization of AGuIX® nanoparticles inside SQ20B J.L. cells.

Indeed, in Figure 80, we can observe that very few nanoparticles are internalized after one hour of treatment, and that as time goes by, more nanoparticles appear in the cells. In addition, we observe that after 1 and 2 hours of incubation, the internalized nanoparticles are free in the cytoplasm as there is no co-localization between AGuIX®-Cya5.5 and lysosomes. However, starting at the time point of 4 hours, we start observing some co-localization. We can therefore speculate that the internalization of nanoparticles by the lysosomes is a slow process. Figure 80 shows one set x-and y-locations, however more than ten photos were taken for each time points with more than ten cells per microscopic field and the same pattern was observed.

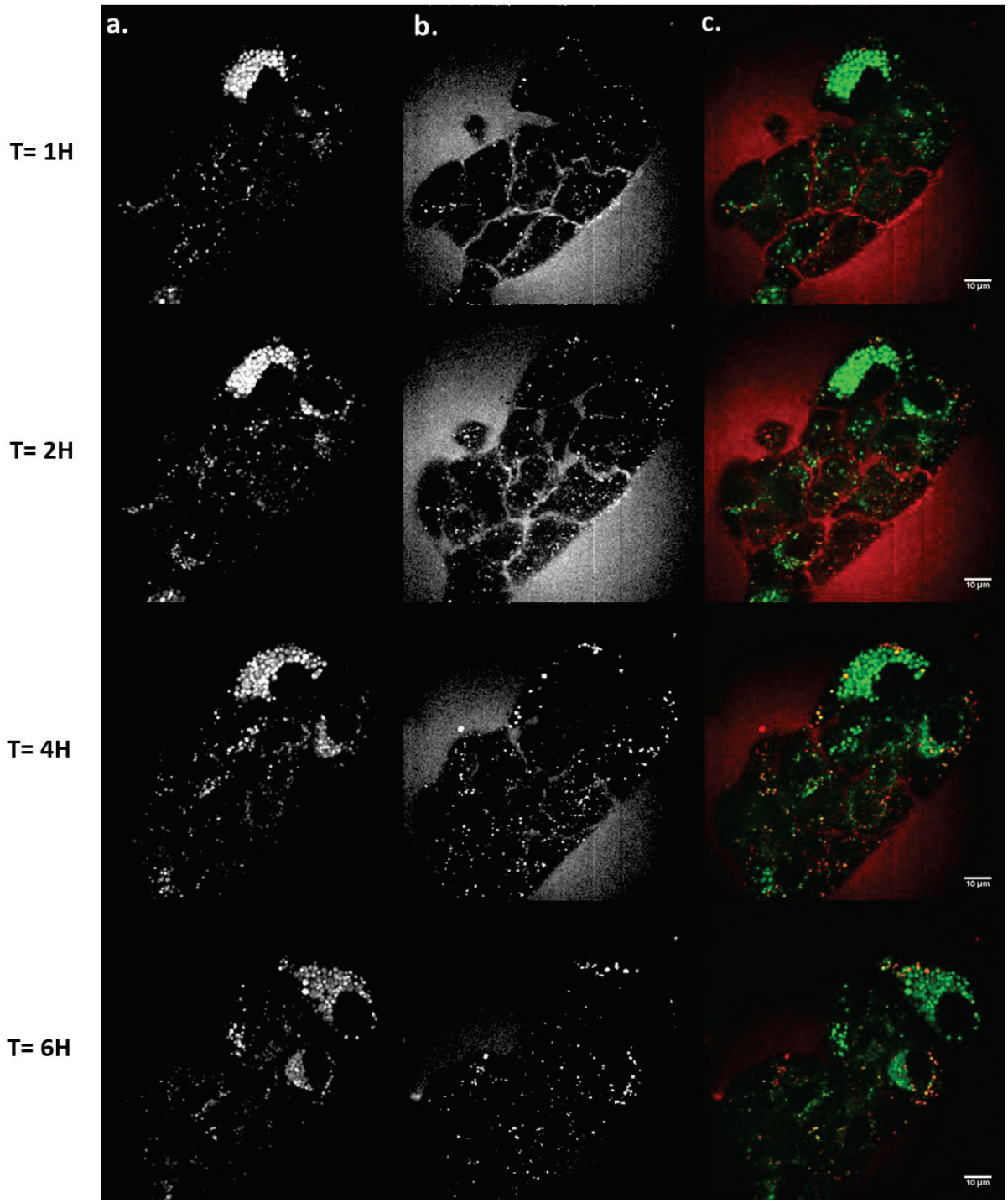


Figure 80: Kinetic study (1-2-4-6 hours) of the localization of AGuIX® nanoparticles in SQ20B J.L. cell line in respect to lysosomes with a confocal spinning-disk microscope (µLife Platform, CEA-Grenoble). a. Lysotracker-green; b. AGuIX® -Cya5,5; c. Merge. Experiment realized on live cells, on the same x and y location, and Z= 16; 60X, with S. Gerbaud- team Biomics.

Collectively, our results clearly indicate that under our experimental conditions, AGuIX® are not targeted to the nucleus nor to the mitochondria. **AGuIX® mostly co-localize with lysosomes** although some AGuIX® stay free in the cytosol. Our results are in accordance with those published by Štefančíková *et al.* (2014) which used confocal microscopy and transmission electron microscopy (TEM) to observe the localization of AGuIX® in U87 cells

(human glioblastoma cells). In a first experiment, using label-free AGuIX® and SR-DUV microscopy, they showed that AGuIX® nanoparticles (free of dye) enter the cells and remain located exclusively in the cytoplasm. TEM experiments confirmed these results, namely that no electron dense regions were found in the cell nucleus but NPs clusters appeared vesicles with average diameters between 400-800 nm which corresponds to endosomes and lysosomes (Huotari and Helenius; 2011). Moreover, membrane invagination was observed which would suggest that AGuIX® enter U87 cells via endocytosis. Using confocal microscopy, the intra-lysosomal localization of AGuIX® was definitely proven. This observation was also obtained with AGuIX® in Chinese Hamster Ovary (CHO) cells (Porcel *et al.*, 2014). AGuIX® clusters of sizes between 400-900 nm were observed regardless of the concentration used, 0.6 or 1 mM Gd or the incubation time (1 hour, 6 hours, and 12 hours). The authors observed AGuIX® in U87 cells for up to 37 hours (end time of their observation). Furthermore, after 1 hour of incubation, TEM images revealed an AGuIX® localization in vacuoles in the cytoplasm in Panc-1 cells (Detappe *et al.*, 2015).

Using FITC-labeled AGuIX® particles and confocal microscopy, Kobt *et al.* (2016) recently reported that nanoparticles were inside vesicles, a result confirmed by TEM images. (Kobt *et al.*, 2016).

All these studies demonstrated that AGuIX® enter the cells mainly via the endocytic pathway and remain in vesicular structures such as lysosomes. As some AGuIX® seem to stay freely in the cytosol, they might enter the cells independently of the endocytic pathway or might have been released after lysosome leakage. However, they are never found within the nucleus nor the mitochondria.

**CHAPTER I TAKE-HOME MESSAGE:**

**The conditions for the radiosensitization of SQ20B J.L. cells with AGuIX® were determined as follows: 0.8mM Gd for 24 hours in serum-free DMEM-Glutamax; this corresponds to 0.11 pg of gadolinium internalized per cell. These conditions are not toxic to cells whether at the cellular or the mitochondrial level. In addition, it was demonstrated that AGuIX® are exclusively localized in the cytoplasm: there is no co-localization between AGuIX® nanoparticles and the nucleus, nor do they co-localize with the mitochondria. AGuIX® nanoparticles were found to be either free in the cytosol or internalized by lysosomes. This internalization by the lysosomes seemed to be a slow process as assessed by the microscopy kinetic study.**

# Chapter II. Study of the Oxidative Stress Induced by the combined treatment of AGuIX® + I.R. and its functional consequences on mitochondria

*Owing to the physical properties of high-Z metal nanoparticles, the over-production of radical oxygen species (ROS) is the most widespread hypothesis for the molecular mechanisms underlying the expected radiosensitizing effect when used in combination with ionizing radiation. This hypothesis has therefore been translated for AGuIX® in cellular models, although this has not always been proven in vitro.*

*In addition to damages to the nucleus which will be studied in Chapter IV, ionizing radiations can induce damages to the plasma membrane, as well as cellular organelles such as the mitochondria. Mitochondria are the power-houses of a eukaryotic cell, and damages to the mitochondria can be an indicator of cells undergoing stress which could in turn lead to cellular death.*

*The following chapter of the Results & Discussion section is therefore devoted to the kinetic study of both cytosolic (cROS) and mitochondrial (mROS) ROS in order to check if ROS and oxidative stress are indeed the initiating mechanisms leading to radiosensitization. Two subcellular oxidative stress markers, i.e. the mitochondrial membrane potential and the common deletion of the mitochondrial DNA, were investigated.*

## *1. Study of the oxidative stress (cytosolic and mitochondrial reactive oxygen species) induced by the the combined treatment of AGuIX® + I.R.*

Besides theoretical data concerning nanoparticles irradiated in water, such information in cellular models is lacking. The generation of both cytosolic and mitochondrial ROS was therefore investigated by flow cytometry using the fluorescent probes CM-$H_2$DCFDA and Mitosox for cROS (cytosolic ROS) and mROS (mitochondrial ROS), respectively.

### 1.1. Cytosolic Radical Oxygen Species (cROS)

In order to quantify the production of cROS after the combined treatment, a kinetic study starting right after irradiation until five days post-irradiation was performed. A representative graph obtained by flow cytometry using CM-$H_2$DCFDA is shown in Figure 81. CM-$H_2$CDFDA is a fluorescent probe allowing for the measurement of cytosolic reactive oxygen species. This probe is better retained in cells and diffused passively into the cells, where its acetate groups are cleaved by the intracellular esterases and its thiols-reactive chloromethyl group reacts with intracellular glutathione and other thiols. The resulting oxidation produces a fluorescent adduct.

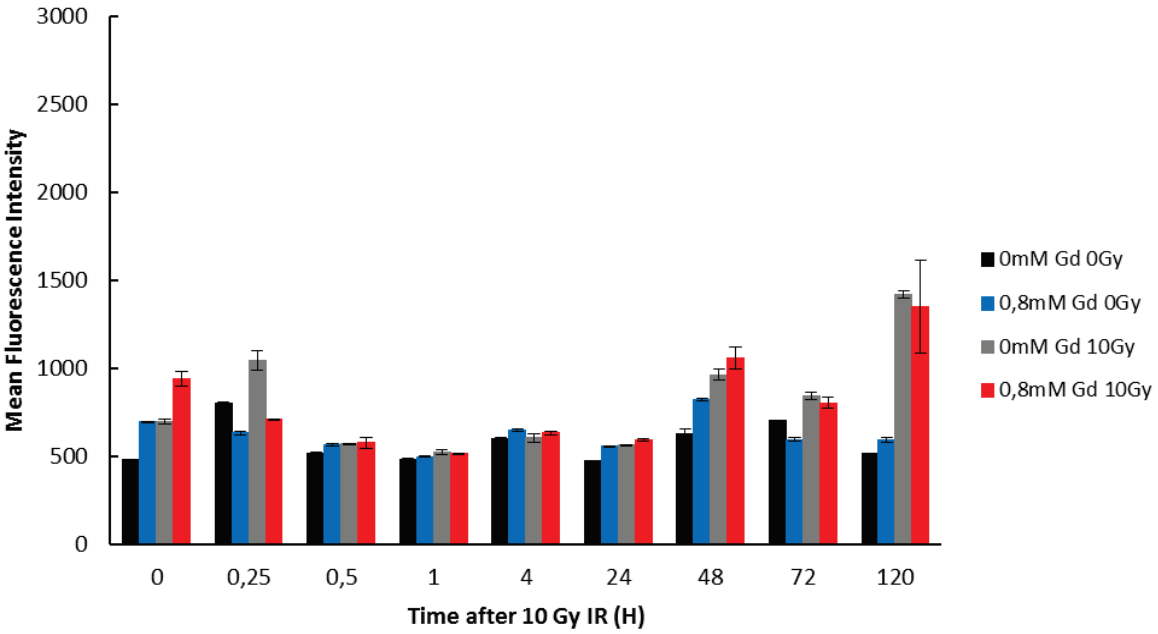


Figure 81: Kinetic study of cytosolic ROS (cROS) production, 0 to 120 hours after a 10 Gy irradiation measured by flow cytometry as a function of the mean fluorescence intensity. This figure is representative of one of three independent experiments, with triplicate samples for each condition.

Under our experimental conditions, Figure 81 shows that the addition of AGuIX® did not induce a significant increase of cROS production compared to irradiation alone, regardless of the time after irradiation, except immediately after irradiation where we had a 35% increase of cROS with AGuIX®treatment combined with irradiation. As previously reported in SQ20B J.L. cells (Alphonse *et al.*, 2002; Bionda *et al.*, 2008), the increase of cROS is late following the

exposure to radiation but the incubation with AGuIX® did not induce any additional effect for the times tested starting at 15 min post-irradiation.

### 1.2. Mitochondrial ROS (mROS)

As mitochondria are an important source of ROS within most mammalian cells (Turrens, 2003), the same kinetic experiment was performed for mROS production. A representative graph obtained by flow cytometry using the MitoSox as a specific probe is shown in Figure 82.

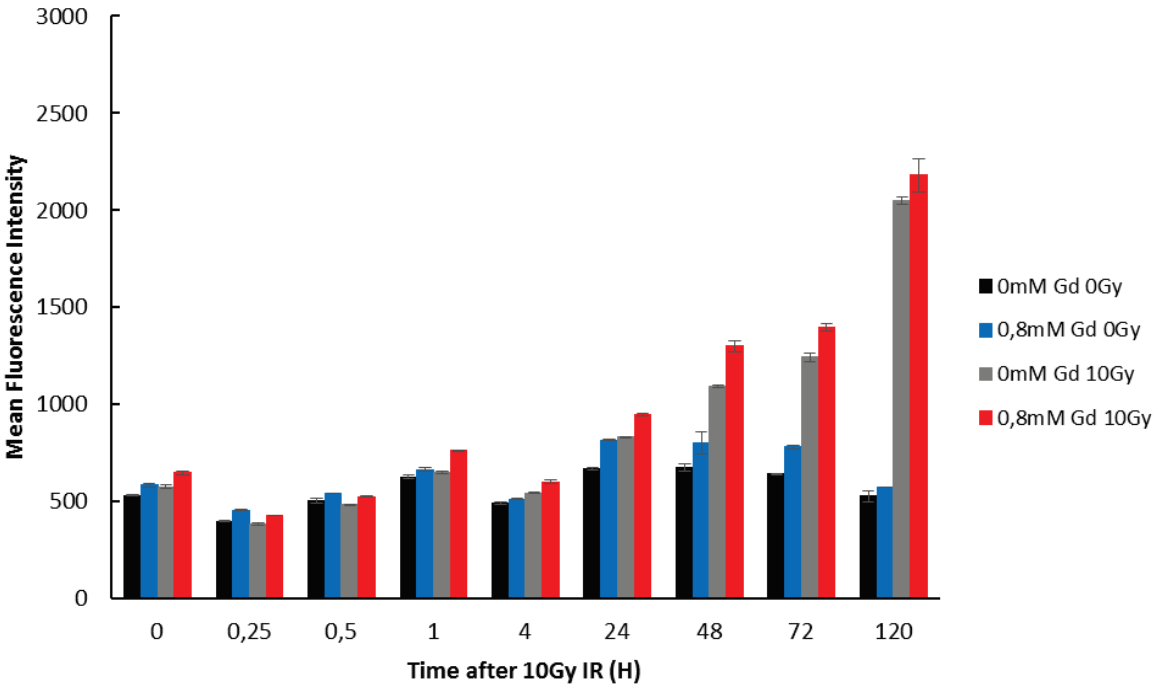


Figure 82: Kinetic study of mitochondrial ROS (mROS) production, 0 to 120 hours after a 10 Gy irradiation measured by flow cytometry as a function of the mean fluorescence intensity. This figure is representative of three independent experiments, with triplicate samples for each condition.

As observed with cROS, the addition of AGuIX® does not induce any significant additional mROS compared to radiation alone (Figure 82), regardless the time after irradiation. As mentioned previously, the increase of mROS after radiation alone is delayed in time, starting at 24 hours after irradiation (+14% AGuIX® + irradiation *versus* irradiation alone) and a peak at 48 hours (+19%) which then decreases 72 and 120 hours after irradiation (the increase between the two treatments is less important). Collectively, these results are surprising because the incubation with AGuIX® prior to radiation was expected to enhance massively ROS production in SQ20B J.L. cells.

However, it is well known that some cancer cells with upregulated redox and antioxidant ability can escape from the damaging effects of radiation by scavenging ROS, leading to radioresistance (Lee *et al*, 2004; Diehn *et al.*, 2009). This is particularly true for the SQ20B J.L. cell line (Boivin *et al*, 2011) which exhibits a very high endogenous level of reduced

glutathione, the major non-enzymatic cellular anti-oxidant. By transiently inhibiting this anti-oxidant system (4-hour treatment with DMF and BSO prior to irradiation), we were able to trigger apoptosis in this radio-resistant cancer cell line. Indeed, GSH is a major ROS-scavenging system in cells and important redox modulating enzymes such as the peroxidases, peroxiredoxins and thiol reductases rely on the pool of reduced GSH as their source of reducing equivalents (Forman *et al.*, 2009; Boivin *et al.*, 2011).

## 2. *Kinetic study of the mitochondrial membrane potential ($\Psi_m$) after AGuIX® + I.R.*

The mitochondrial membrane potential is a biological marker of mitochondrial dysfunction which occurs before the cells enter apoptosis. The different treatment conditions were studied, to see whether the combination treatment of AGuIX® + I.R. induced a bigger percentage drop of the mitochondrial membrane potential which would reflect a mitochondrial stress.

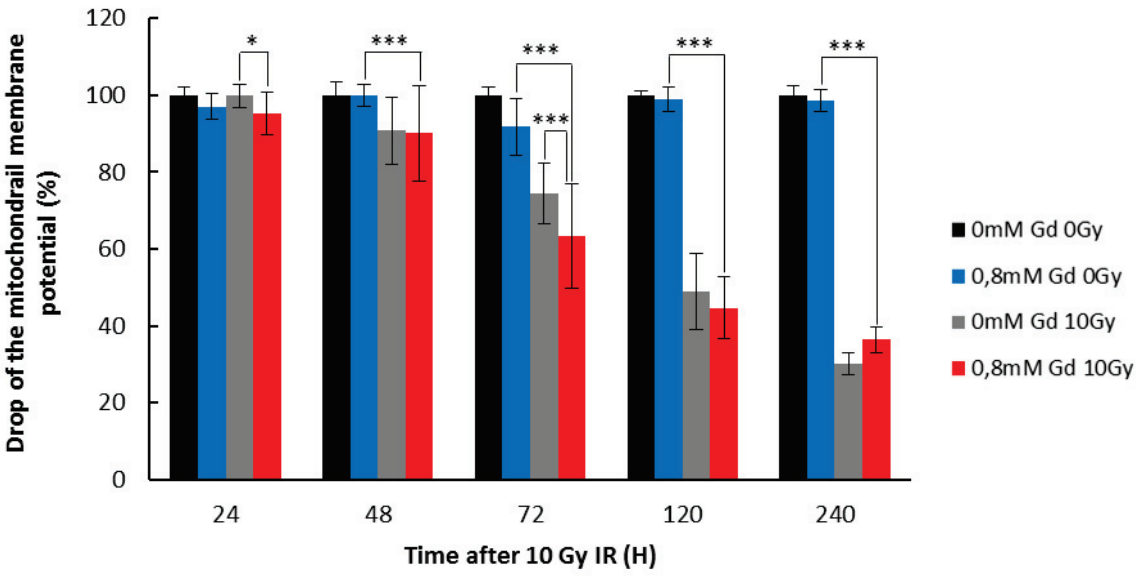


Figure 83: Kinetic study 24-240 hours post-irradiation of the percentage drop in the mitochondrial membrane potential (Ψm) depending on the treatment conditions. This figure is representative of three independent experiments. All samples were normalized to the control (0mM Gd 0Gy), and the statistics was done on 0.8mM Gd 0Gy *versus* 0.8mM Gd 10Gy, and 0mM Gd 10Gy *vs*. 0.8mM Gd 10Gy. Statistical analysis was realized with the Student's t test. Significant results have a p value <0.05 (*), <0.01 (**), or <0.005 (***).

As can be observed in Figure 83, we can first conclude that the addition of AGuIX® alone does not induce a drop in the mitochondrial membrane potential, while 72 hours post-irradiation, we start observing a drop of the mitochondrial membrane potential which is persistent through 10 days post-irradiation. Indeed, 72 hours post-irradiation, the cells have a 74% drop in their mitochondrial membrane potential compared to 63.4% with the addition of AGuIX® (representing a greater drop by 15%), which was not significant. However, this small difference is even less at T= 120 and 240 hours post-irradiation which leads to the

conclusion that we cannot report any significant differences between irradiated only cells and those treated with AGuIX® prior to irradiation. Although the drop of Ψm has already been reported in SQ20B J.L cells following irradiation (Alphonse *et al*, 2002), the combined treatment did not have any additional effect on the alteration of the mitochondrial transmembrane potential (except at 72h post IR).

### 3. *Study of the mitochondrial DNA (mtDNA) common deletion after AGuIX® + I.R.*

The mitochondrial DNA (mtDNA) is also known as a target of oxidative stress and thus a cellular marker indicating that the cell is undergoing an oxidative attack. In this next section, the common deletion of mtDNA was quantified at two different irradiation time points: 24 and 72 hours. 24 hours was chosen in order to observe the "initial" level of damages, and 72 hours allowed for the cells to in part recover from the irradiation and allow for replication. It is important to note that mtDNA deletions induced by radiation are not immediately present after treatment because their formation requires mtDNA replication (Prithivirajsingh *et al.*, 2004; Kubota *et al.*, 1997). In addition, in many other assays throughout this PhD work, we started observing an effect of irradiation 72 hours post-irradiation, which can be explained by the high resistance to irradiation of these cells. Two different irradiation doses were studied: 4 and 10 Gy. The results are expressed as the ratio of deleted mtDNA over the total mtDNA.

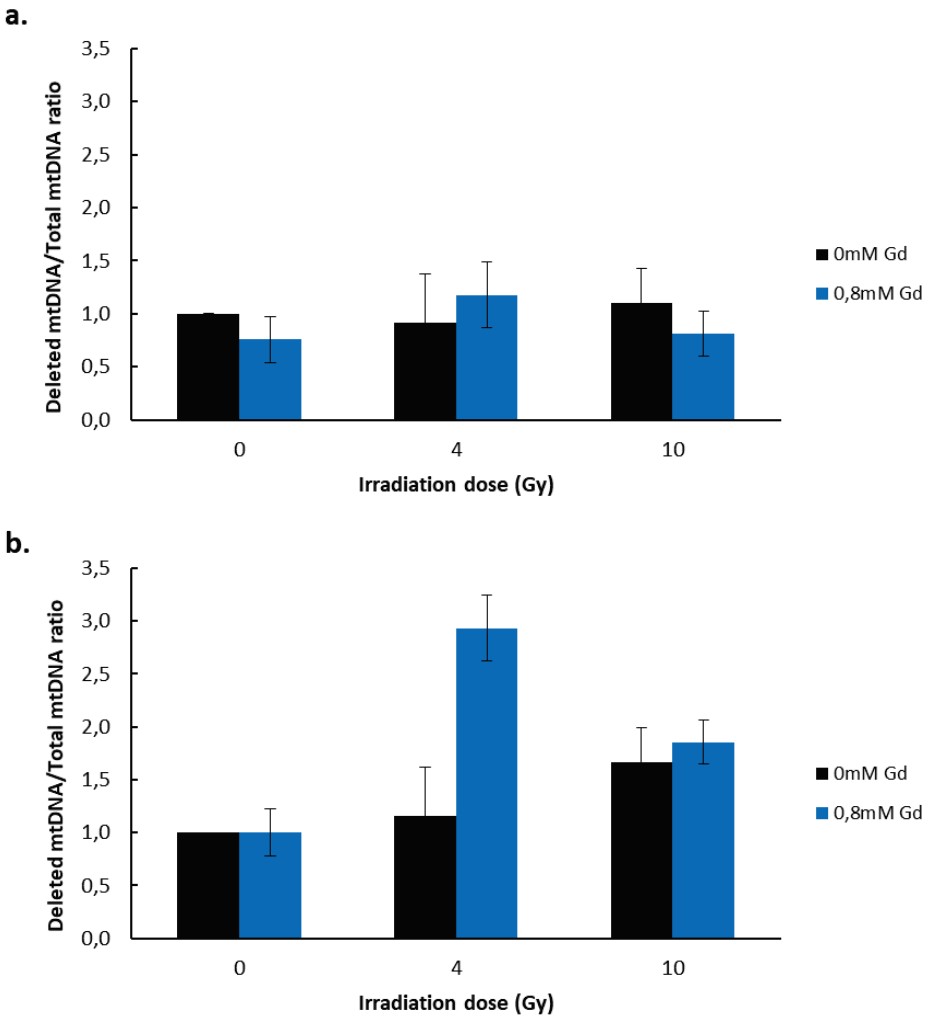


Figure 84: Deleted mtDNA/total mtDNA ratio for SQ20B J.L. cells following different treatment conditions. **a.** 24 hours post-irradiation. **b.** 72 hours post-irradiation. Representative data of two independent experiments with biological triplicates.

As can be seen in Figure 84, we did not observe any differences 24 hours post-irradiation in accordance with what is found in the literature. Seventy-two hours after irradiation alone, there is no effect after a 4 Gy irradiation (deleted mtDNA/total mtDNA ratio = 1.16) while this ratio increased after a 10 Gy exposure (ratio deleted mtDNA/total mtDNA = 1.67. Irradiation alone does not induce the common deletion of the mitochondrial DNA. The treatment with AGuIX® had no influence on the deleted mtDNA/total mtDNA ratio, 24h after radiation, whatever the dose applied. However, 72h after a 4 Gy irradiation, we observed an increase in the amount of deleted mitochondrial DNA with a ratio of deleted mtDNA/total mtDNA of 2.93 which is statistically significant, using the Student test, compared to irradiated only cells. It is interesting to note that there are no differences detected after the combined treatment of nanoparticles with the 10 Gy irradiation. One of the hypothesis emitted was that there is a higher death rate of the cells that received 10 Gy and in turn had a damaged mtDNA, which therefore led to the measurements of cells that were able to resist the treatment.

## *4. Radiosensitization after the addition of DMF/BSO treatment*

In order to bypass the antioxidant ability of SQ20B J.L. cells, we lowered their GSH content after the incubation with AGuIX® but prior to the irradiation. Under these conditions, we hypothesized that a significant increase of ROS caused by the addition of AGuIX® prior to radiation should be highlighted.

### 4.1. Quantification of the endogenous GSH content in SQ20B J.L. cells

According to Boivin *et al.* (2011), we first incubated SQ20B J.L. cells for 4h with a mixture of 100 µM dimethylfumarate (DMF, solubilized in DMSO), a GSH-depleting agent, and 100 µM L-buthionine sulfoximine (BSO, solubilized in PBS), a GSH biosynthesis inhibitor before measuring their endogenous GSH content.

As shown in Figure 85a, control experiments showed that no major differences in the GSH content occurred between non-treated and AGuIX® treated cells. As shown in Figure 85b, the endogenous GSH content was measured immediately after a 10Gy irradiation. Exposure to radiation alone led to a decrease of the GSH content (276 µmol/l *vs.* 312 µmol/l in control cells), a decrease even more marked for cells treated with AGuIX® before irradiation (203 µmol/l vs 312 µmol/l in control cells) was noted. Although these values indicate that a significant amount of GSH was consumed after irradiation, with all the more after AGuIX® treatment, there remains a sufficient quantity to scavenge ROS.

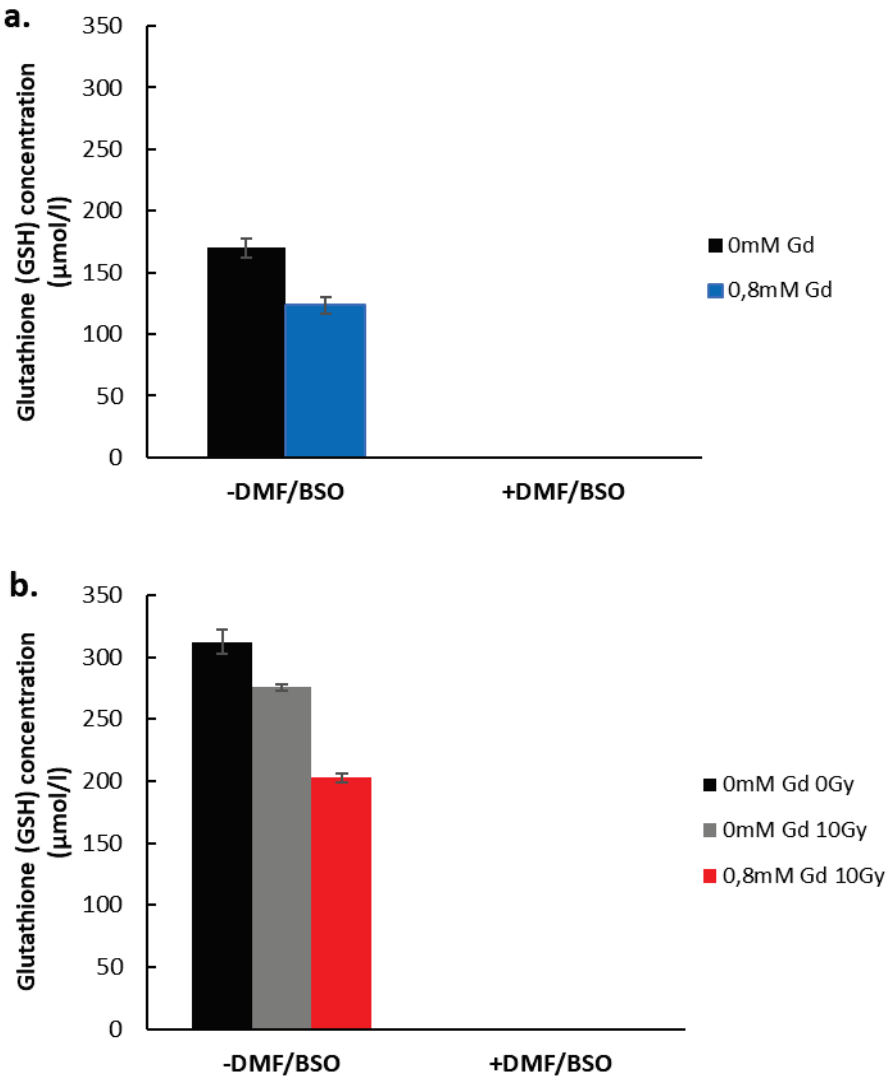


Figure 85: Glutathione (GSH) concentration (µmol/l) measured in SQ20B J.L. cells with or without DMF/BSO treatment. a. Samples collected right after DMF/BSO treatment, cells were not irradiated. b. 24 hours after a 10Gy irradiation (n=2).

Figure 85b shows that after incubation of SQ20B cells with DMF/BSO before radiation and/or treatment with AGuIX®, the levels of endogenous GSH were undetectable.

### 4.2. Comparative study of cytosolic ROS produced with or without the addition of DMF/BSO

In view of the results reported above, the kinetic study of both cROS and mROS production was evaluated up to four hours following a 10 Gy irradiation ± AGuIX®, with and without DMF/BSO. (*Note*: *Since we had to trypsinize and re-seed the cells starting with samples 24 hours post-irradiation, the cells would therefore be in the absence of DMF/BSO, we decided to look at the prior kinetic points, up to 4 hours after irradiation, to see if there was an early boost of cROS post-irradiation with AGuIX® in the presence of DMF/BSO. The same was done for the mROS experiment*).

When compared to Figure 87a, (without DMF/BSO treatment), the results presented in Figure 87b show a huge increase of cROS immediately after irradiation which is reinforced by the prior treatment with AGuIX®. This increase dropped at fifteen and thirty minutes until a second increase in cROS started after one hour and peaked four hours after irradiation. In both cases, treatment with AGuIX® led to a boost of cROS compared to radiation alone. This will be further explained in the discussion section.

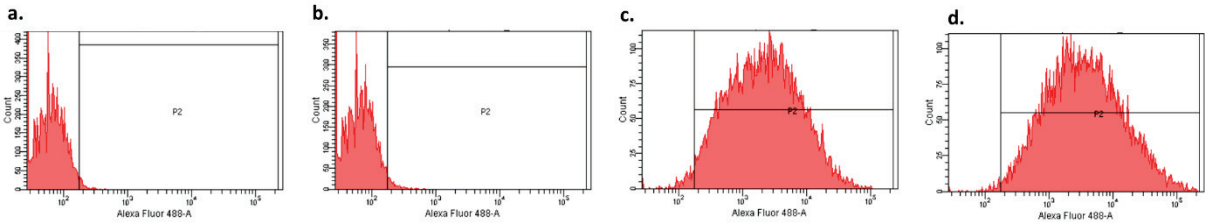


Figure 86: Example of a flow cytometry CM-$H_2$DCFDA analysis. a. 0mM Gd 0Gy; b. 0.8mM Gd 0Gy; c. 0mM Gd 10Gy; d. 0.8mM Gd 10Gy; with DMF/BSO treatment prior to a 10 Gy irradiation.

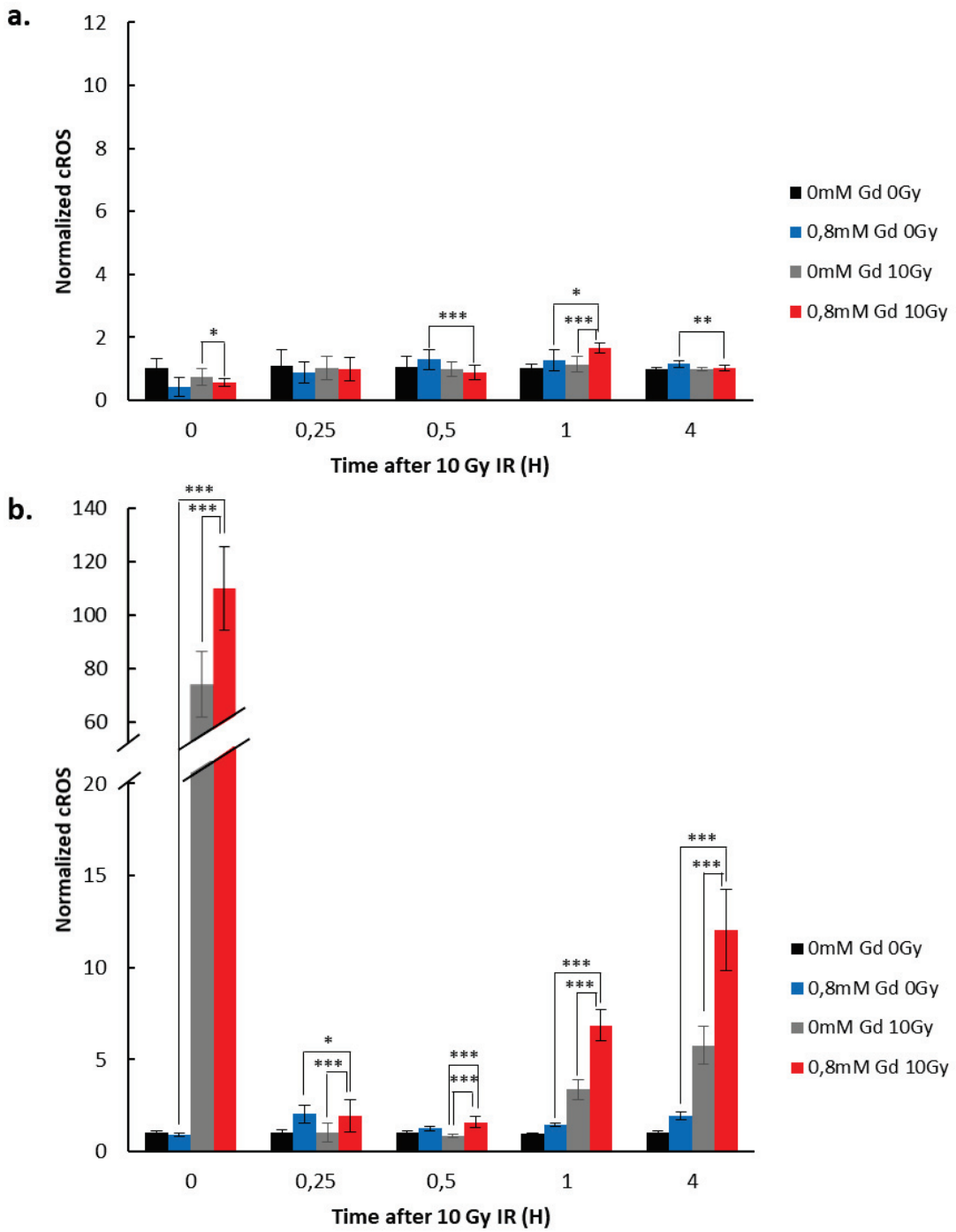


Figure 87: Kinetic study (0-4hours) of cytosolic ROS (cROS) measured by the LSRII flow cytometer (BD Biosciences) using the CM-$H_2$DCFDA assay, normalized to the non-treated non-irradiated cells. **a.** Without DMF/BSO treatment. **b.** With DMF/BSO treatment 4 hours prior to the 10 Gy irradiation. These results are representative of two independent experiments with triplicate samples for each. (p-value *: <0.05; **<0.01; ***: <0.005).

### 4.3. Comparative study of mitochondrial ROS produced with or without the addition of DMF/BSO

Compared to Figure 88a in which no differences were observed between 10Gy versus AGuIX® + 10Gy, depletion of cells from its GSH content resulted in a burst in mROS immediately after irradiation without any significant difference between irradiated cells and irradiated cells treated with AGuIX®. However, this increase is not maintained over time. It should also be noted that this initial burst of mROS is much lower quantitatively than that obtained for cROS. This can be in part explained by the fact that the initial ROS produced after water radiolysis within mitochondria should escape the organelle rapidly. As AGuIX® did not enter mitochondria (see Chapter I), this could explain the absence of difference between mROS obtained after radiation alone *versus* AGuIX® + radiation.

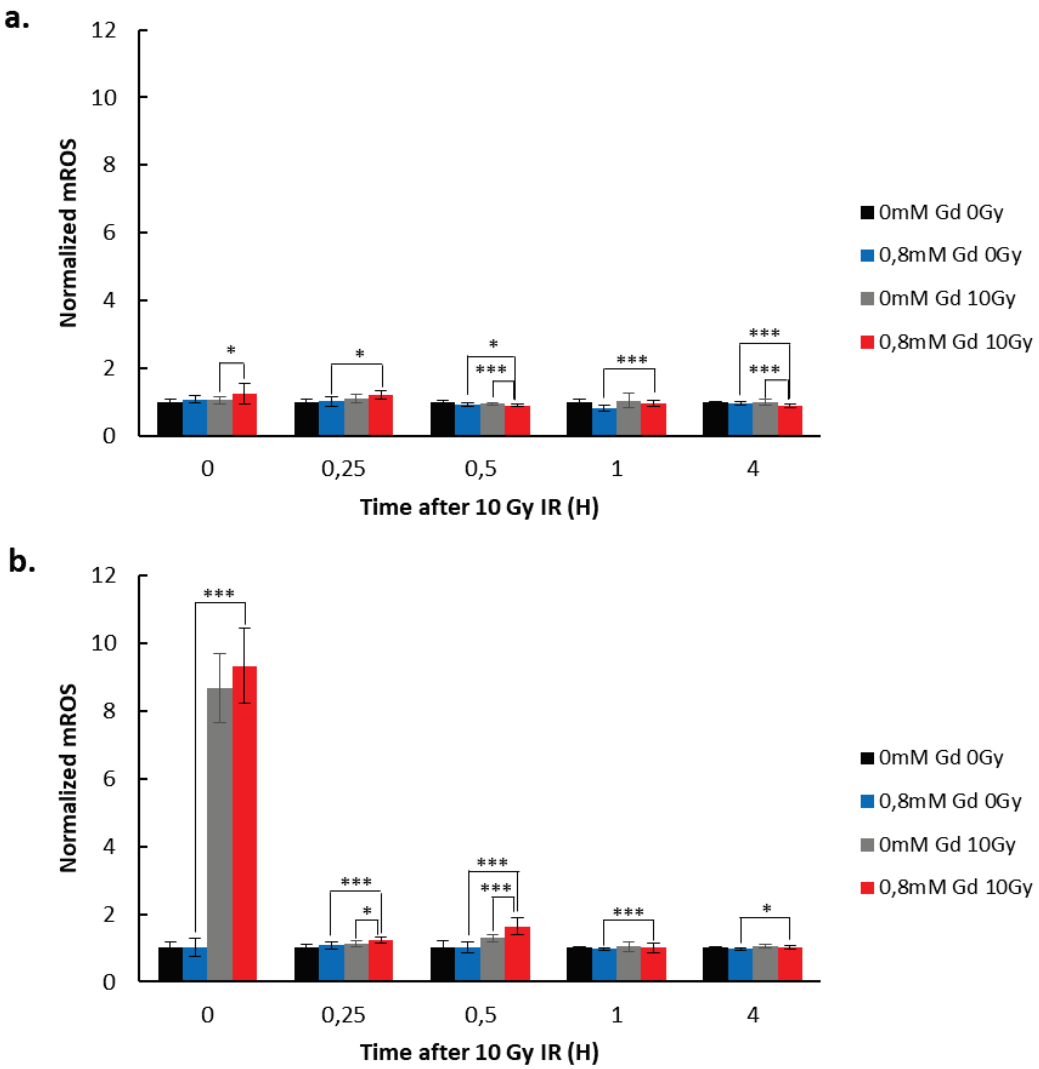


Figure 88: Kinetic study (0- 4hours) of mitochondrial ROS (mROS) measured by the LSRII flow cytometer (BD Biosciences) using the Mitosox assay, normalized to the non-treated non-irradiated cells. **a.** Without DMF/BSO treatment. **b.** With DMF/BSO treatment 4 hours prior to the 10 Gy irradiation. Representative results of two independent experiments with triplicate samples for each. (p-value *: <0.05; **<0.01; ***: <0.005).

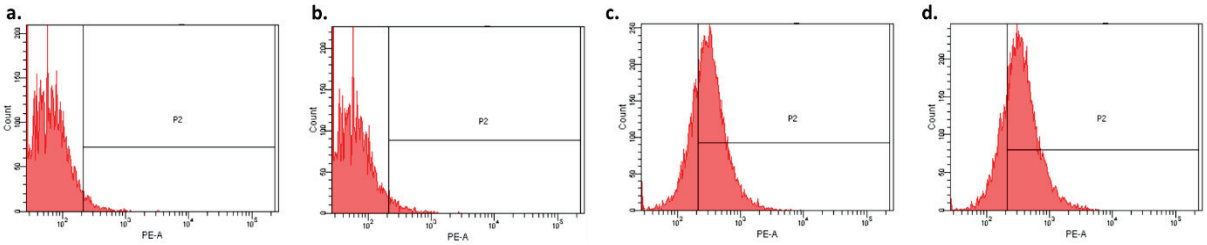


Figure 89: Example of a flow cytometry Mitosox analysis. a. 0mM Gd 0Gy; b. 0.8mM Gd 0Gy; c. 0mM Gd 10Gy; d. 0.8mM Gd 10Gy; with DMF/BSO treatment prior to a 10 Gy irradiation.

## 5. *Studying the effect of DMF/BSO treatment on the clonogenic survival assay*

As the amount of cROS is increased after the irradiation of SQ20B cells treated with DMF/BSO, this should have consequences on the clonogenic curve assay.

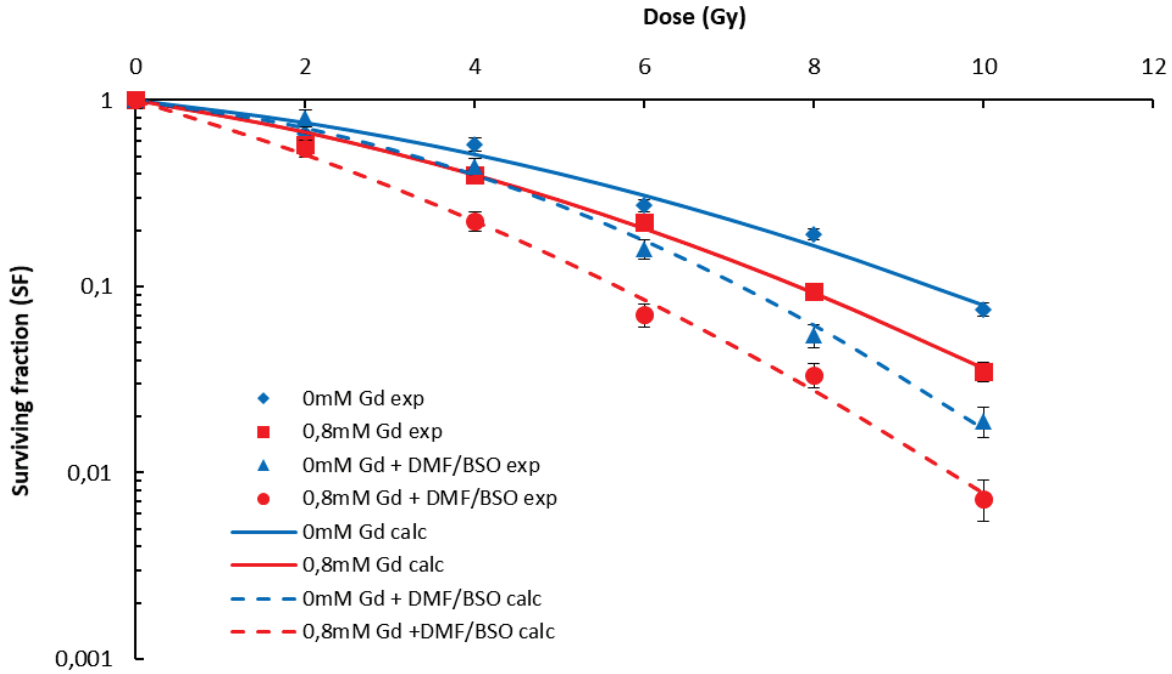


Figure 90: Clonogenic survival assay 0-10 Gy for SQ20B J.L. cells, with various treatment protocols; +/- AGuIX® and +/- DMF/BSO. (exp.= experimental values; calc.= calculated values using the quadratic linear formula). (***, p<0.005 vs. irradiated SQ20B cells)

As shown in Figure 90, an additional radiosensitizing effect occurred after depletion of the GSH cellular content: the 50% survival EBR increased up to 1.6, which is better than any currently published data. Again, this effect is dose dependent, with an EBR (10Gy) up to 2.5 after the addition of AGuIX® in GSH-depleted cells (see Table 24).

| DMF/BSO | WITHOUT | | | WITH | | |
|---|---|---|---|---|---|---|
| [Gd] (mM) | 0 | 0,8 | EBR | 0 | 0,8 | EBR |
| 0 Gy | 1 | 1 | - | 1 | 1 | - |
| 2Gy | 0.76 | 0.67 | 1.134 | 0.71 | 0.51 | 1.392 |
| 4Gy | 0.51 | 0.40 | 1.275 | 0.40 | 0.22 | 1.818 |
| 6 Gy | 0.31 | 0.20 | 1.550 | 0.18 | 0.08 | 2.250 |
| 8 Gy | 0.17 | 0.09 | 1.889 | 0.06 | 0.03 | 2.000 |
| 10 Gy | 0.08 | 0.04 | 2.000 | 0.02 | 0.008 | 2.500 |

Table 24: Calculated survival fractions at different irradiation doses (0-10 Gy) depending on the different treatments (+/- AGuIX® and +/- DMF/BSO).

| DMF/BSO | WITHOUT | | WITH | |
|---|---|---|---|---|
| [Gd] (mM) | 0 | 0,8 | 0 | 0,8 |
| α | 0.11 | 0.164 | 0.1134 | 0.2995 |
| β | 0.0143 | 0.168 | 0.0293 | 0.0187 |
| 10% | 9.3 | 7.8 | 7.1 | 5.7 |
| 50% | 4.1 | 3.2 | 3.3 | 2.1 |
| EBR-10% | 1.192 | | 1.246 | |
| EBR-50% | 1.281 | | 1.571 | |

Table 25: Summary of the parameters evaluating the radiosensitizing effect of the addition of AGuIX® and/or DMF + BSO.

Collectively, our results strongly suggest that the addition of the AGuIX® treatment in combination with irradiation is not sufficient to overflow the total anti-oxidant defenses of SQ20B J.L. cells, despite a significant radiosensitizing effect. However, when cells are depleted from their glutathione content, the combined treatment results in an excess of oxidative stress when compared to radiation alone, thereby resulting in an improvement of radiosensitization.

**CHAPTER II TAKE-HOME MESSAGE:**

**In this second chapter of Results & Discussion, we have demonstrated that no statistical differences in terms of cROS and mROS were produced between irradiated only and AGuIX® + irradiated samples. However, when depleting SQ20B J.L. cells from their glutathione content prior to irradiation, a huge increase of cROS and a moderate increase of mROS can occur right after irradiation, increase that is reinforced with AGuIX®. Under these experimental conditions, a significant improvement of the 50% EBR (close to 1.6) could be obtained.**

# Chapter III. Study of the different types of cellular deaths induced by the combination of AGuIX® + I.R.

*The clonogenic survival assay demonstrated an EBR of 1.3 when treating cells for 24 hours with 0.8mM Gd implying that the combined treatment, AGuIX®/ionizing irradiation, leads to an increase in cell death, or a decrease in cell proliferation. However, one question remains: which type of cell death or cellular death pathway(s) is (are) activated with the addition of AGuIX®?*

*In this next chapter, we will therefore study the five main types of radiation-induced cell death: apoptosis (via the total caspases activation and the Annexin V/P.I. assays), necrosis (via the Annexin V/P.I. assay), mitotic catastrophe (via the cell cycle distribution), senescence and autophagy (via the Western Blot analysis of p16 and p21 for senescence, and LC3B for autophagy).*

## 1. Apoptosis, Necrosis, and Mitotic Catastrophe

As described in the bibliography section, different types of cellular deaths can result following ionizing radiation. Most commonly known and observed types of deaths are apoptosis, necrosis, and mitotic catastrophe. Therefore, three different types of tests were done to answer the question whether the radiosensitizing effect observed with the addition of the AGuIX® treatment is a result of an increase in these cell death pathways. The first set of results shown will be the results obtained using the total caspases kit for apoptosis and the annexin V/P.I. assay where apoptotic cells can be isolated from necrotic cells. Mitotic catastrophe was checked through the cells' distribution in the different phases of the cell cycle.

### 1.1. Total Caspases activation

The activity of total caspases was measured by flow cytometry with a starting point at 24 hours after irradiation until 10 days after. A representative graph obtained showing the shift of fluorescence intensity following a 10Gy irradiation measured by flow cytometry 10 days post-irradiation is represented in Figure 91.

As summarized in Figure 92, the activation of caspases started at 48 hours after irradiation alone and increased with time up to 81.5% of positive cells at 240h compared to the control. However, we did not notice any significant differences between AGuIX® treated cells and those that were only irradiated, whatever the time course after irradiation. These results demonstrated that the treatment with AGuIX® does not increase the number of apoptotic cells under our experimental conditions.

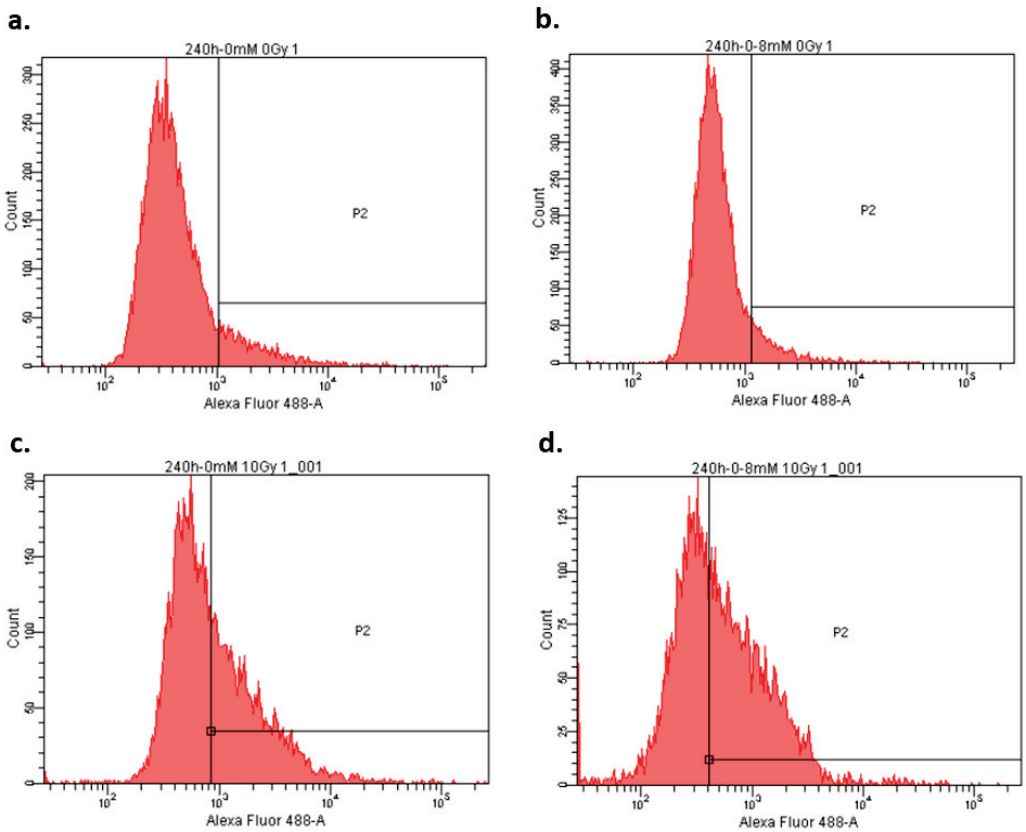


Figure 91: Representative graphs at 10 days after irradiation of flow cytometry analysis measuring the fluorescence intensity of Alexa Fluor 488. a. 0mM Gd 0Gy; b. 0.8mM Gd 0Gy; c. 0mM Gd 10Gy; d. 0.8mM Gd 10Gy.

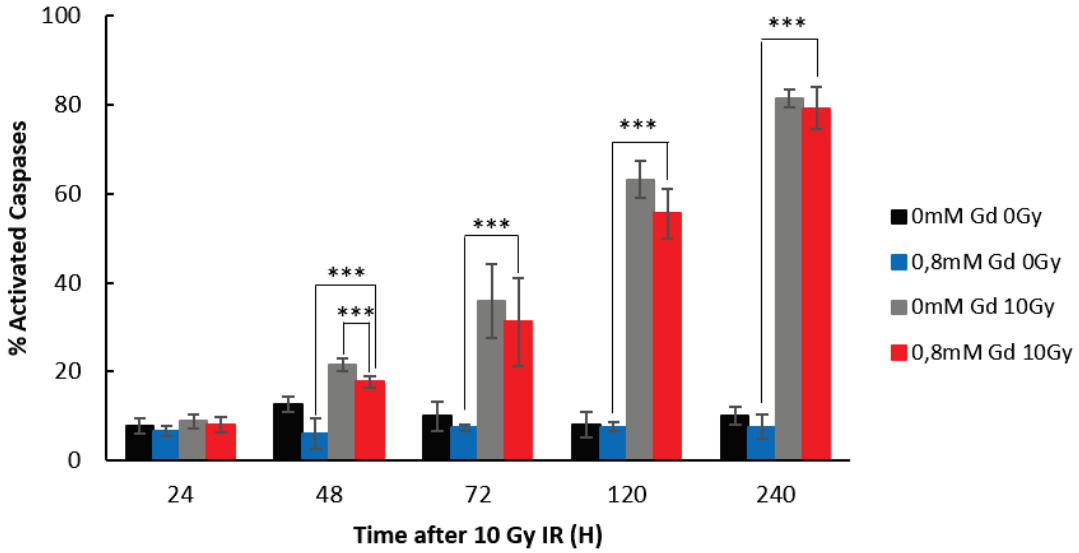


Figure 92: Kinetic study of apoptosis from 24 hours to 10 days following a 10 Gy irradiation in SQ20B J.L. cells using the CaspACE™ FITC-VAD-FMK kit to observe the activation of total caspases following the different treatment conditions. An increase in the activation of caspases appears starting at 48 hours post-irradiation (between 0.8mM Gd and 0.8mM Gd 10Gy). However, we do not observe any statistical differences between irradiated only and the cells that received prior AGuIX® treatment. Representative results of three independent experiments with triplicate samples for each. (p-value *: <0.05; **<0.01; ***: <0.005).

### 1.2. Annexin V/P.I.

The Annexin V/P.I. assay was used to measure necrosis, which is another irradiation-induced cellular death pathway. In addition, this assay allowed us to confirm the results regarding apoptosis. Figure 93 shows the representative graphs of Annexin V *versus* Propidium Iodide obtained by flow cytometry 10 days post-irradiation.

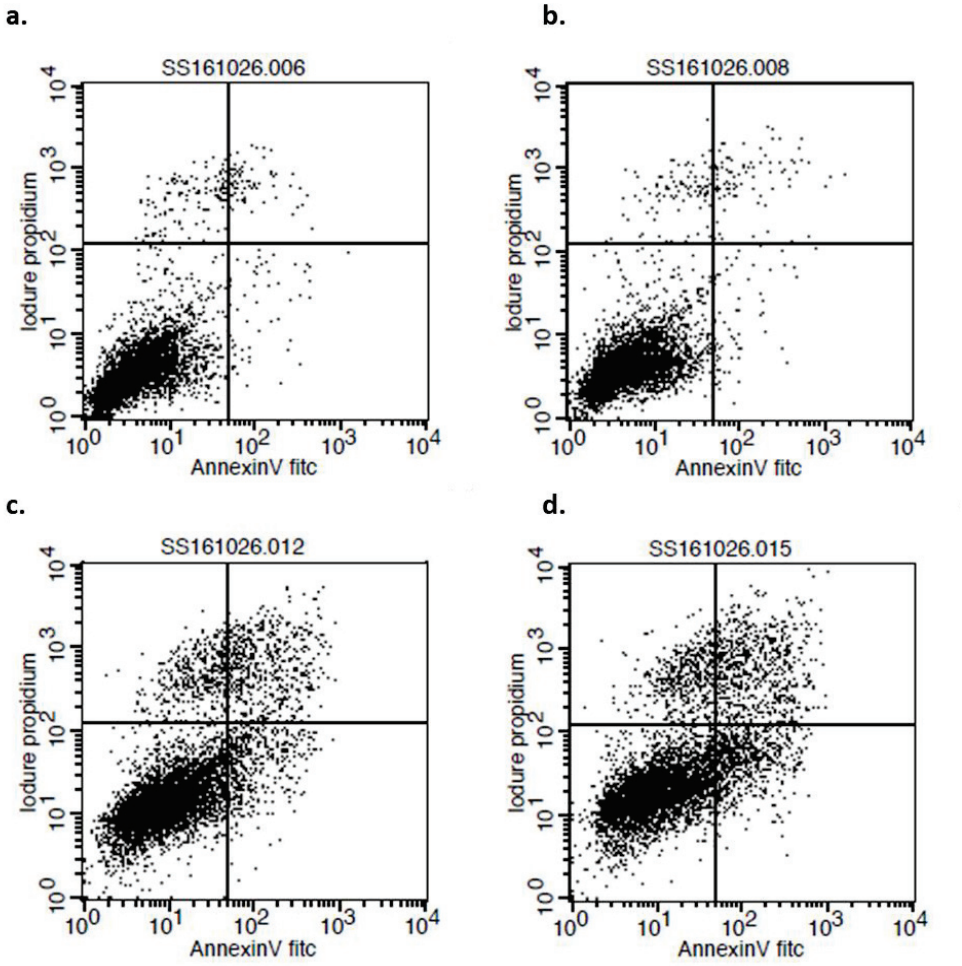


Figure 93: Representative graphs of Annexin/P.I. in flow cytometry (FACSCalibur); the x-axis represents the cells marked by Annexin V-FITC; while the y-axis represents Propidium Iodide marked cells. If cells are on the bottom left corner, they are considered negative for both markers which are live cells (Annexin-V – and P.I. -); top left corner are cells that are positive for P.I. (Annexin-V – and P.I. +) …; top right are cells that are positive for both markers (Annexin-V + and P.I. +) which are the necrotic cells; and bottom right corner are positive only for Annexin-V (Annexin-V + and P.I. -) which are the early apoptotic cells. a. 0mM Gd 0Gy; b. 0,8mM Gd 0Gy; c. 0mM Gd 10Gy; d. 0.8mM Gd 10Gy.

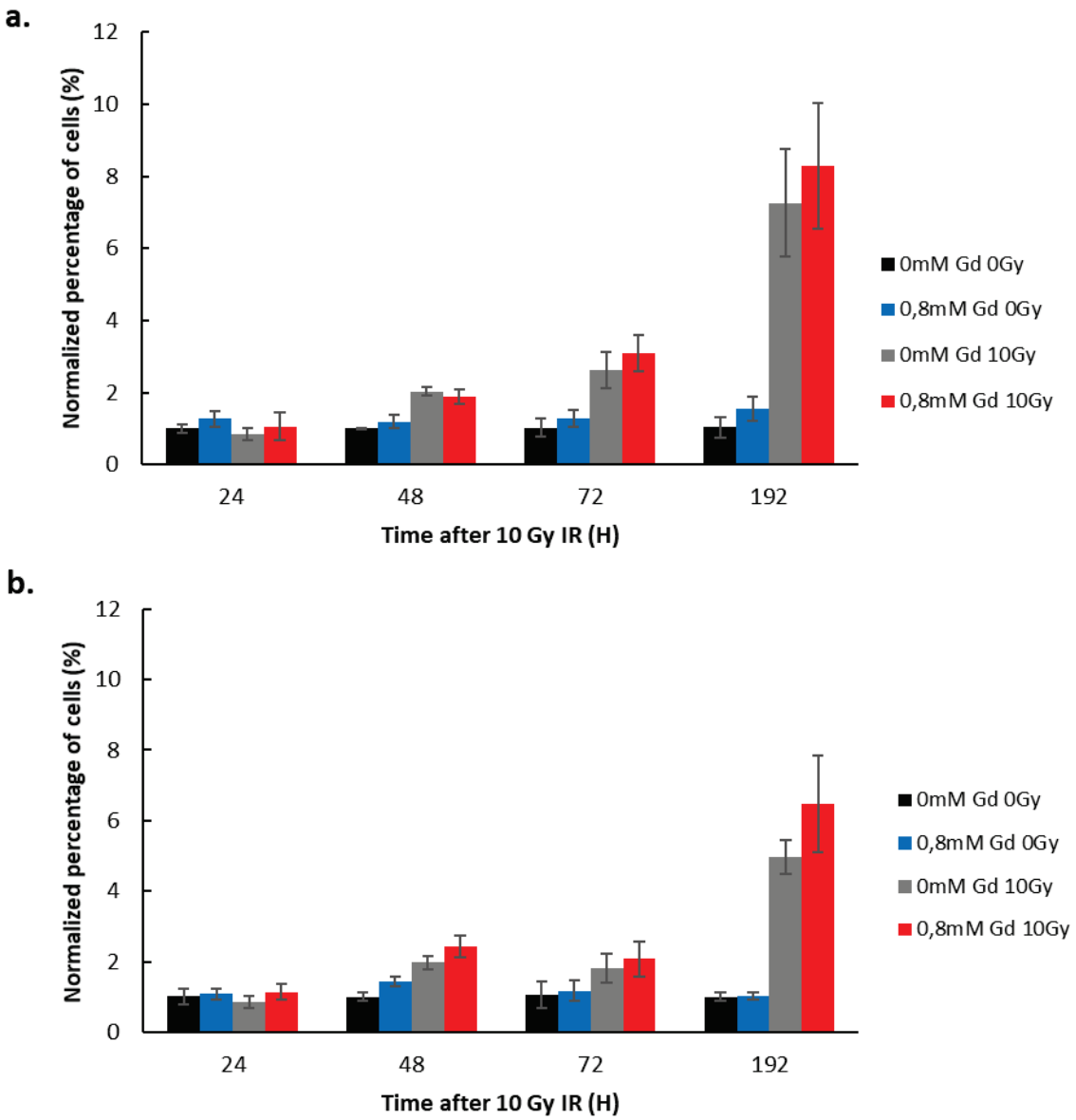


Figure 94: Kinetic study of apoptosis *versus* necrosis in SQ20B J.L. cells using the Annexin/P.I. kit to evaluate the cellular death pathways after the different treatment conditions. **a.** Early apoptosis. **b.** Late apoptosis/necrosis (n=1).

As shown in Figure 94, the addition of AGuIX® to irradiation did not induce any significant increase of neither apoptotic nor necrotic cells and this, regardless of the time after irradiation. Concerning apoptosis, this result confirmed those obtained with the total caspase assay reported above.

### 1.3. Study of the cell cycle

By studying the cell cycle, we are able to observe whether cells are undergoing apoptosis (sub-G1) or mitotic catastrophe (polyploid cells) as well as the number of cells in the G2/M phase (phase where DNA damage is repaired). Indeed, radioresistant cells have often been

shown to have an increased number of cells in the G2/M phase. Figure 95 shows the raw results obtained from the Diva Software analysis.

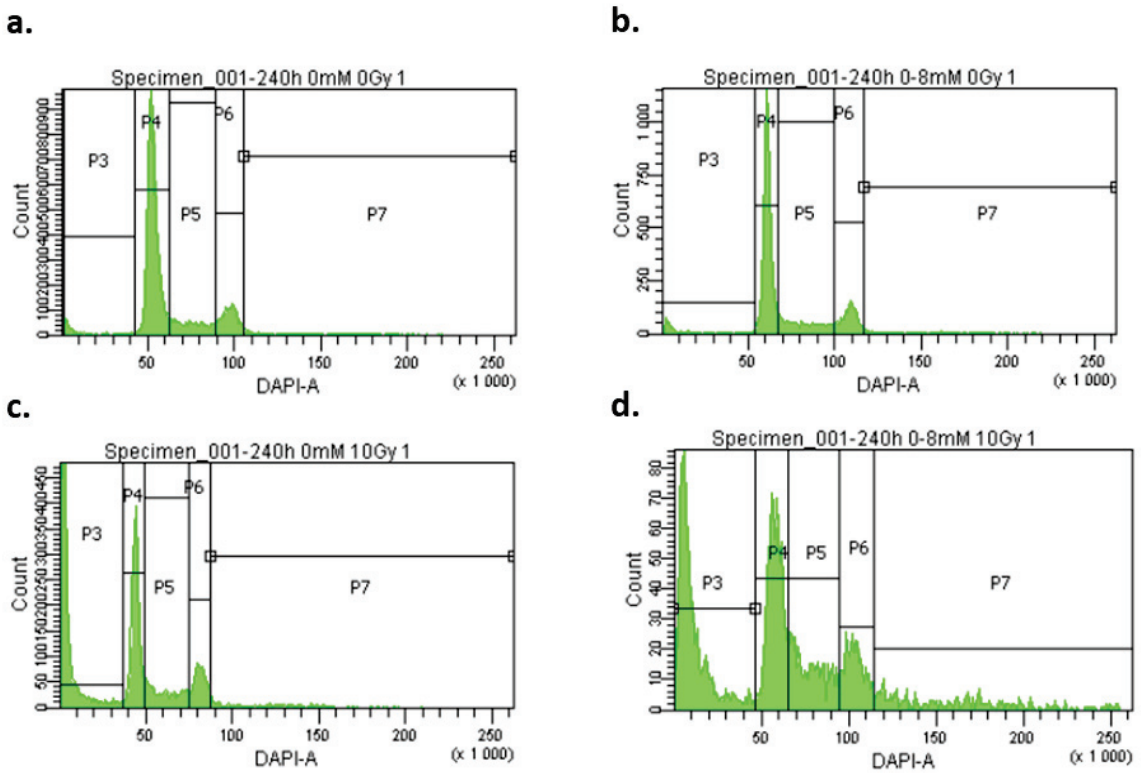


Figure 95: Representative graphs of the cell cycle analysis 240 hours post-irradiation, using the Diva Software analysis after flow cytometry. a. 0mM Gd 0Gy; b. 0.8mM Gd 0Gy; c. 0mM Gd 10Gy; d. 0.8mM Gd 10Gy. Phases of the cell cycle: sub-G1 (P3); G1 (P4); S (P5); G2/M (P6); Polyploid (P7).

As it can be observed in Figure 96, we did not observe any significant differences between AGuIX®-treated/irradiated cells compared to irradiated cells, whatever the cell cycle phase. Concerning the sub-G1 phase (apoptosis), the results confirm those obtained with the caspases assay as well as the P.I./Annexin reported above. Concerning the G2/M phase, besides a transient increase obtained at 24h after irradiation alone, no significant differences between the different treatment conditions were obtained. Finally, the percentage of polyploid cells remained low (around 10% for AGuIX® treated and irradiated cells), even 10 days after irradiation.

Collectively, our results allow us to conclude that the treatment with AGuIX® before irradiation does not induce any additional increase in apoptosis compared to irradiation only (confirmed with 3 different assays), nor mitotic catastrophe, nor necrosis.

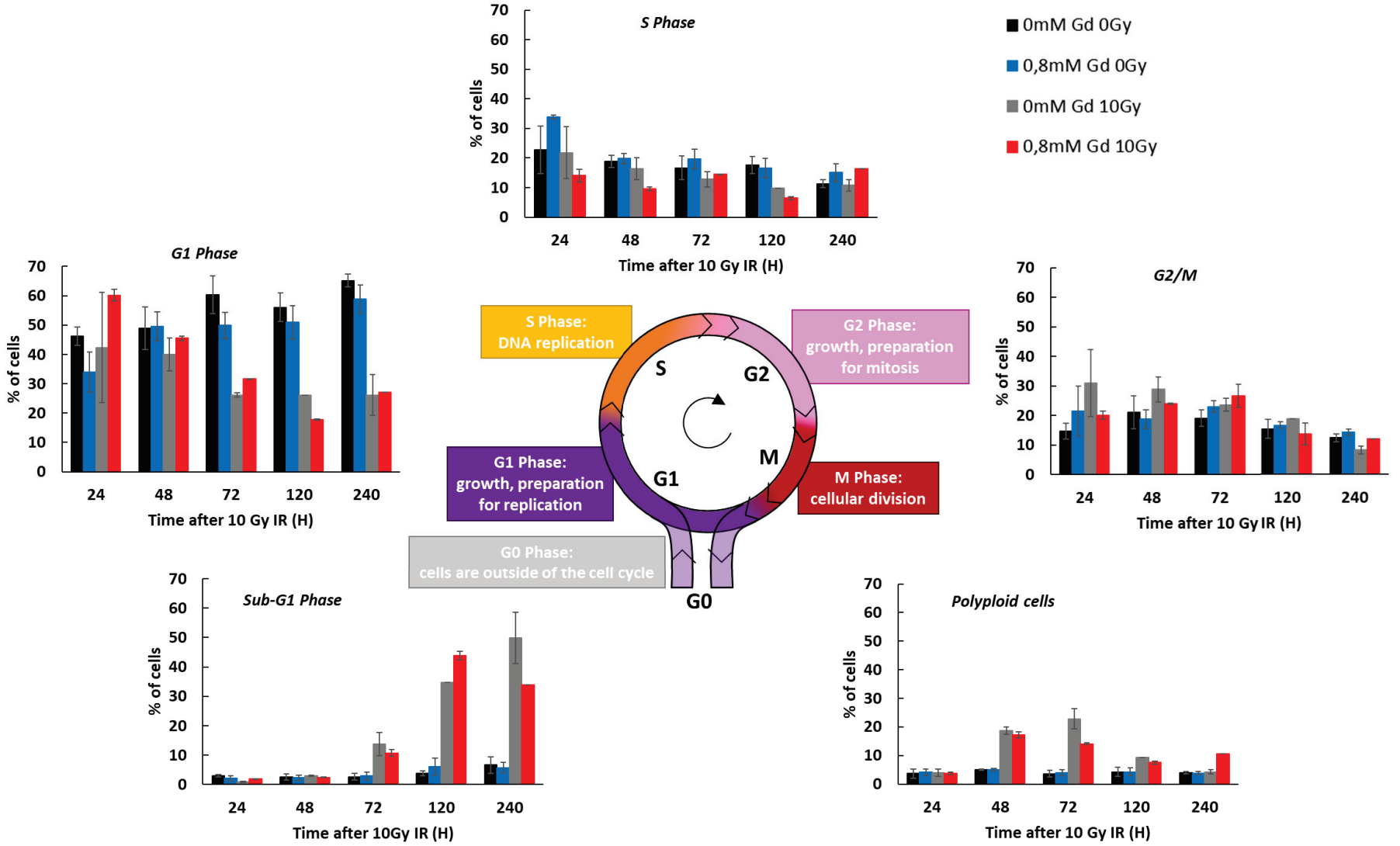


Figure 96: Kinetic study of the different cell cycle stages after a 10 Gy irradiation (n= 3).

Therefore, two other cellular deaths pathways potentially induced by ionizing radiation, namely senescence and autophagy, were investigated by Western Blot analysis, using p16, p21, and LC3B specific antibodies. For p16, results were normalized using GAPDH, which is an ubiquitous protein often used for normalization purposes, whereas total proteins were used for the normalization of p21 and LC3B.

## 2. *Kinetic study of senescence*

The analysis of the expression of two proteins, namely p16 and p21, are conventionally used to monitor cells undergoing senescence (Stein *et al*, 1999).

### 2.1. p16

p16, also known as cyclin-dependent kinase inhibitor 2A, is a tumor suppressor protein as it slows down the cell cycle by prohibiting the progression of the cell from the G1 phase to the S phase. As previously mentioned, the homozygous deletion of p16 is frequently found in HNSCC. p16 is extensively used as a biomarker which is associated with a more favorable prognosis as measured by cancer-specific survival, recurrence-free survival, as well as locoregional control…

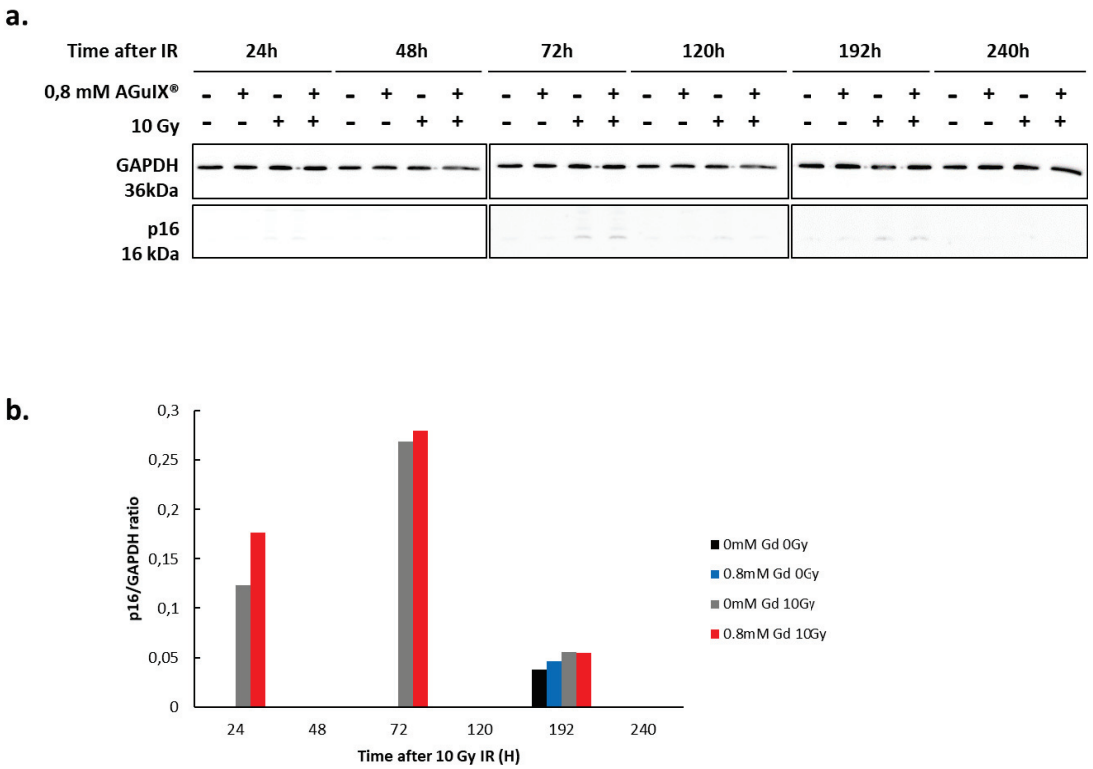


Figure 97: p16 protein expression analysis by Western Blot. a. W/B membrane for p16 normalized by GAPDH. b. Calculated ratio p16/GAPDH (arbitrary units) (n=2).

As shown in Figure 97, p16 expression is very low or even absent in SQ20B J.L. cells, independent of the time after irradiation. The pre-treatment with AGuIX® did not increase the expression of p16, whatever the time course studied.

### 2.2. p21

p21$^{Cip1}$ (also known as p21$^{Waf1}$), known as cyclin dependent kinase inhibitor 1, represents a major target of p53 activity, thus linking DNA damage to cell cycle arrest.

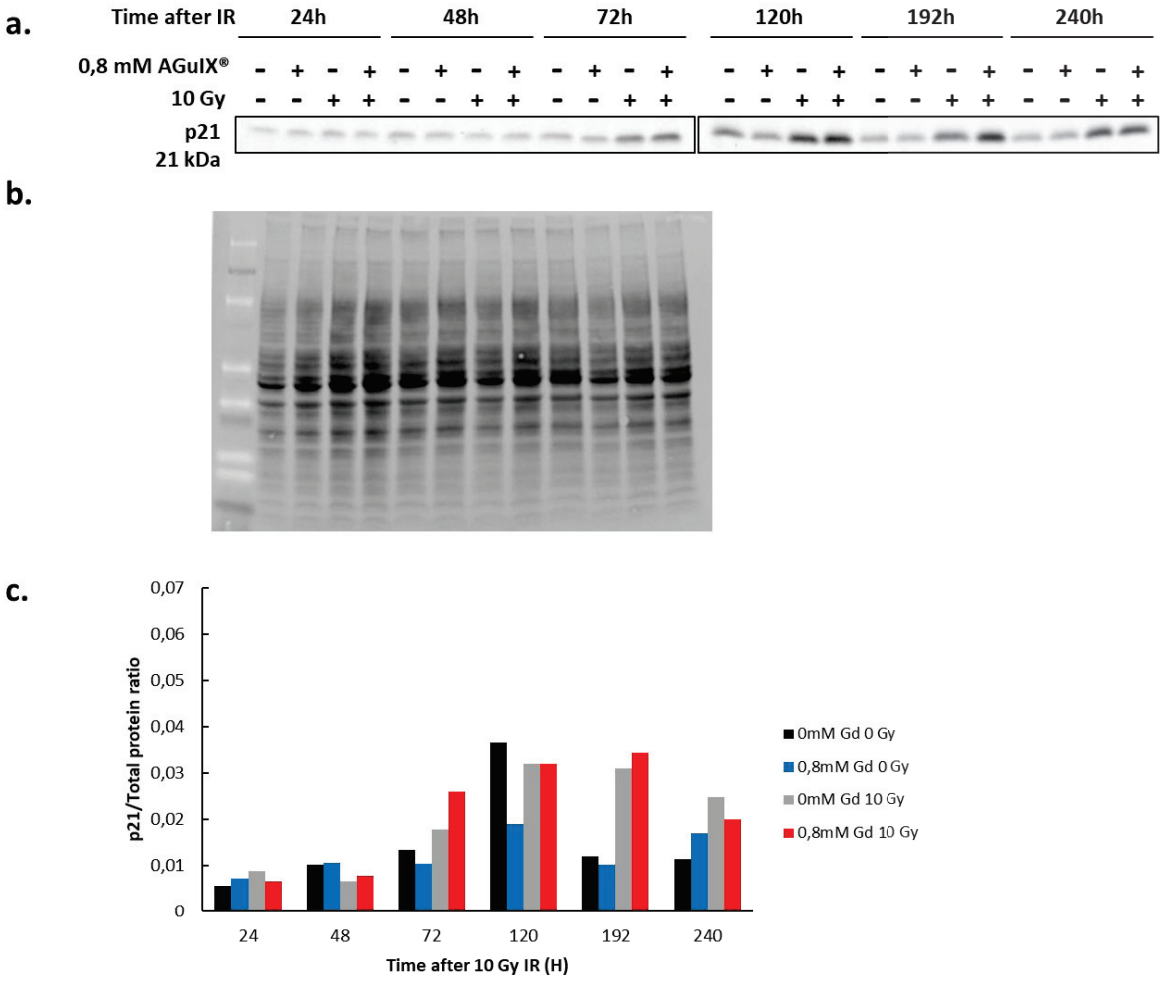


Figure 98: p21 protein expression analysis by Western Blot. a. W/B membrane for p21. b. Membrane of total proteins used for normalization purposes. c. Calculated ratio p21/total proteins (arbitrary units) (n=2).

As can be seen in Figure 98, there is a small increase of p21 expression in SQ20B J.L. which started 72h after irradiation and peaked after 120h before decreasing. Nevertheless, no differences were observed after treatment with AGuIX® compared to irradiated cells alone. We

can conclude that the enhanced biological effect obtained by the addition of AGuIX® does not involve senescence.

### *3. Kinetic study of autophagy*

Autophagy was studied by Western Blot using the LC3-B antibody. The microtubule-associated protein 1A/1B-light chain 3 (LC3) is a soluble protein with a molecular mass of approximately 17 kDa that is ubiquitously distributed in mammalian tissues and cultured cells (Tanida *et al,* 2008). LC3 is the most widely used marker of autophagosomes, with the identification of the two isoforms: LC3B-I and LC3B-II.

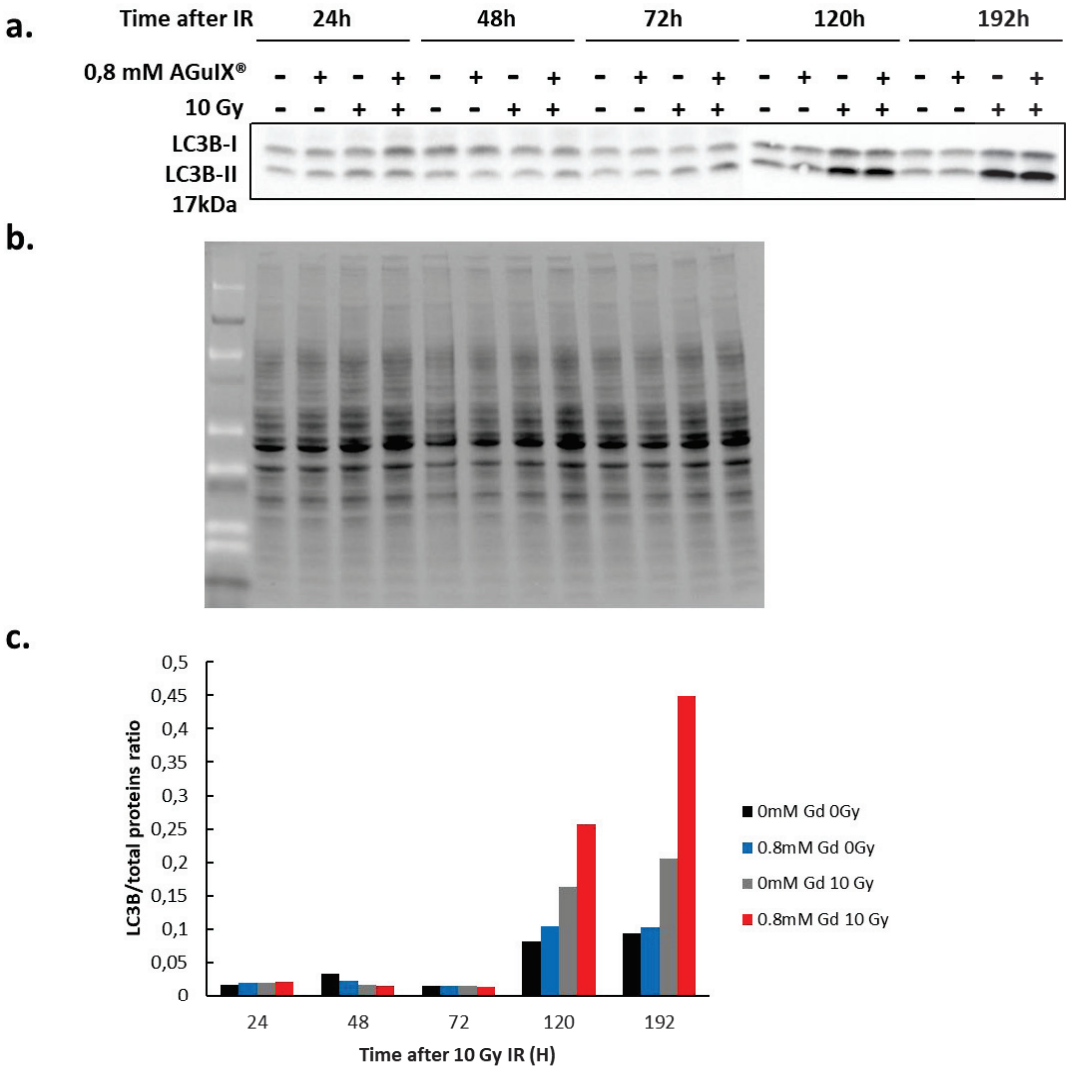


Figure 99: LC3B protein expression analysis via Western Blot. a. W/B membrane for LC3B (I+II). b. Membrane of total proteins used for normalization purposes. c. Calculated ratio LC3B/total proteins (arbitrary units). This figure is representative of two independent experiments (n=2).

As shown in Figure 99, although no differences in LC3B protein expression occurred up to 72 hours after irradiation, a significant increase was obtained starting at 120h after irradiation with a significant difference after the addition of AGuIX® compared to irradiation alone (+62.5 %). 192h after irradiation, the increase of LC3B expression reached **+ 114%** compared to radiation alone and **+ 350%** compared to AGuIX® alone. In addition, we can also note, that there is no difference in LC3B expression between non-treated and treated cells in the absence of irradiation, which indicates that AGuIX® alone did not induce autophagy.

From these results, we can conclude that AGuIX® combined to radiation induced autophagy in SQ20B J.L. cells, a result which could explain the increase of the EBR obtained in Chapter 1 of the Results section.

The objective of this chapter was to determine by which mechanism AGuIX® sensitize SQ20B J.L. cells to radiation therapy. Although radiation alone has been previously reported to trigger late apoptosis and mitotic catastrophe (Alphonse *et al*, 2013), our results demonstrate that neither apoptosis, necrosis, mitotic catastrophe, nor senescence were involved in the radio-enhancing effect of AGuIX®. Autophagy was the only cell death pathway that was specifically found to be triggered after AGuIX® treatment combined with radiation.

Although the radiosensitizing effect of AGuIX® was previously reported to occur in different cellular models (Kotb *et al*., 2016; Štefančíková et al., 2014; Štefančíková *et al.*, 2016; Porcel *et al.*, 2014; Detappe *et al.*, 2015;…), none of these have presented evidence for the involvement of one particular type of cellular death pathway in the radiosensitizing effect obtained. Only one study using DTPA-based gadolinium nanoparticles showed that the combined treatment led to mitotic catastrophe followed by late apoptosis. These results were confirmed either with TEM microscopy as well as caspase-2 activation. Besides radiosensitization, the use of gadolinium oxide ($Gd_2O_3$) NPs has been very recently reported to regulate apoptosis through the upregulation of Bax/Bcl-2 gene expression (Alarifi *et al.*, 2017), while the induction of apoptosis in MCF-7 cells was demonstrated to occur after ER stress (Wang *et al.*, 2014) induced by gadolinium endohedral metallofullerenol ([Gd@C82(OH)22]n) NPs.

Apart from gadolinium NPs, many reports have been published concerning the effect of other type of NPs in the triggering of apoptosis whether in association with radiotherapy or not. In association with radiotherapy, one can cite the effect of gold nanorods on melanoma cells (Xu *et al.*, 2012), the effect of thio-glucose-bound gold nanoparticles (Glu-GNPs) on lung cancer cells (Wang *et al.*, 2013), or the effect of silver NPs on glioma cells (Liu *et al.*, 2013; Liu *et al.*, 2016).

Concerning autophagy, it was demonstrated that some NPs are able to trigger autophagy independently of radiation exposure: this is the case for oleic acid-coated iron oxide NPs, $TiO_2$

NPs (Kenzaoui *et al.*, 2012), silica NPs (Wei *et al*., 2017) or glycan-coated silver NPs (Panzarini *et al.*, 2015). Combined with radiation, recent reports also presented evidence for a radiosensitizing effect involving autophagy: with AgNPS in glioma cells at clinically relevant megavoltage energies (Liu *et al.*, 2016), copper cysteamine NPs in colorectal carcinoma (Liu *et al.*, 2017), or selenium NPs in breast cancer cells (Cheng *et al*, 2017). By contrast, no triggering of autophagy was obtained in glioblastoma following the treatment with titanate nanotubes combined, or not, with radiation (Mirjolet *et al.*, 2013).

All these results presented clearly suggest that the cell death pathways involved either in the radiosensitization or in anti-cancer toxicity is dependent on the type of nanoparticle, its physico-chemical characteristics, as well as the cellular model studied.

**CHAPTER III TAKE-HOME MESSAGE:**

**In this third chapter of Results & Discussion, we overviewed the various types of cellular deaths pathways induced by ionizing radiation. We have concluded that the enhanced biological response observed with the clonogenic survival assay with AGuIX® treatment was due to autophagy. No significant differences were noted after AGuIX® treatment combined with irradiation compared to irradiation alone in terms of apoptosis, necrosis, mitotic catastrophe, and senescence.**

# Chapter IV. Study of the DNA-damage induced by AGuIX® combined with radiation

*As reviewed in the second chapter of the bibliography section, the main cellular target of ionizing radiation is DNA. The track of a charged particle (an electron or an ion) may pass through and ionize the DNA directly (direct action), or ionize water molecules in the vicinity, thereby producing highly reactive oxygen species (ROS), which can diffuse to DNA and react with the target molecule (indirect action). Chemical reactions in DNA induced either by the direct or indirect action may result in DNA damage such as base oxidation, single strand breaks (SSBs) or double strand breaks (DSBs). Although base damage and SSB are of minor relevance for cell survival, since these lesions are essentially all repaired, a fraction of DSBs (which increases with radioresistance) cannot be repaired because of their higher complexity, and constitute the most severe DNA damage after irradiation leading to cell death, senescence, mutations, or genomic instability.*

*Even though AGuIX® nanoparticles did not enter the nucleus, as previously seen in Chapter 1, it was possible that AGuIX® combined to radiation might have an effect on the cellular DNA repair capacities.*

*In this next chapter, we have therefore studied three types of DNA-damage potentially induced by AGuIX® combined with radiation. Single-strand breaks (SSBs) and oxidative DNA damage have been assessed by the comet assay, and double-strand breaks (DSBs) by the γH2Ax foci assay. Additionally, an experiment focusing on the quantification of base oxidation (namely guanine) was assessed via HPLC coupled to MS/MS.*

## 1. Detection of DNA single-strand-breaks (SSBs) and DNA oxidative damage

Single-strand breaks were studied via the comet assay at four different time points (t= 0, t= 30, t=120 min and t= 24h), and after a 4Gy irradiation (black bars). As shown in Figure 100 panel a, right after irradiation (0'), the initial peak (maximum) of SSBs induced by radiation alone or with the combined treatment is very low as these breaks are usually repaired very rapidly. No further increase of SSBs was obtained, whatever the time point (panels b, c and d), after radiation alone or with the combined treatment.

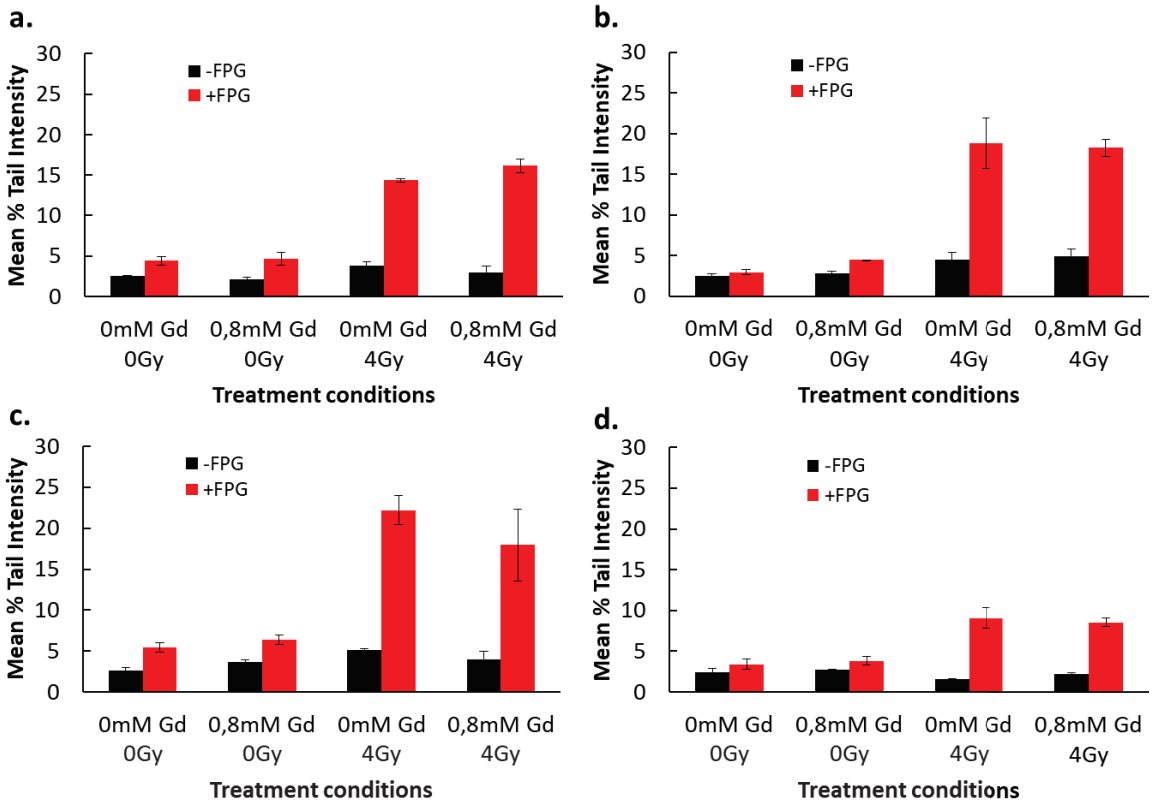


Figure 100: Kinetic study of single-strand breaks (-FPG) and oxidative damage (+FPG) following a 4 Gy irradiation +/- AGuIX® expressed in terms of the mean % tail intensity. a. 0 min post-irradiation ; b. 30min post-irradiation ; c. 2 hours post-irradiation ; d. 24h post-irradiation. This figure represents biological triplicates of an independent experiment, but is representative of three independent experiments (n=3).

After treatment with formamidopyrimidine DNA glycosylase (FPG enzyme, red bars), which led us to quantify the oxidation of the guanine base, an increase of base oxidation was observed immediately after irradiation (panel a), which remained sustained until 120 min (panel c) and then decreased under the control values after 24h. AGuIX® treatment combined to radiation led to a slight increase of 8-oxo-guanine (+ 13%) at t=0, compared to radiation alone, whereas no differences are observed at t= 30 minutes, two hours, and twenty-four hours post-irradiation.

## *2. Quantitative measurement of 8-oxo-guanine by HPLC-MS/MS*

In view of the results that were obtained by the comet assay (+FPG), it seemed that the oxidative damage occurred after the combined treatment, this immediately after irradiation. As the comet assay is only a semi-quantitative method, we have sought to further quantify the 8-oxo-guanine damages by HPLC coupled to MS/MS.

Samples were therefore prepared using two irradiation doses, 4 and 10 Gy, at the same time points. As can be observed in Table 26, no differences were noted between the different treatments as for each sample we remained in the background noise of the apparatus and we were therefore unable to conclude about the 8-oxo-guanine damages.

However, this experiment was only done once. Most likely, the irradiation doses are too low and increasing the irradiation dose to 40, or even 100 Gy, would have probably allowed the observation of some differences.

| Treatment conditions | Time after irradiation (H) 0 | 0.5 | 2 | 24 |
|---|---|---|---|---|
| 0mM Gd 0Gy | 0.38 | 0.35 | 0.38 | 0.28 |
| 0.8mM Gd 0Gy | 1.00 | 0.93 | 0.49 | 0.17 |
| 0mM Gd 4Gy | 0.74 | 0.38 | 0.33 | 0.35 |
| 0.8mM Gd 4Gy | 0.78 | 0.32 | 0.55 | 0.38 |
| 0mM Gd 10Gy | 0.17 | 0.35 | 0.20 | 0.48 |
| 0.8mM Gd 10Gy | 0.69 | 0.54 | 0.27 | 0.88 |

Table 26: Quantitative measurement by HPLC-MS/MS of 8-oxo-guanine DNA damage expressed in terms of 8-oxodGuo/$10^6$ normal bases for different time points post-irradiation dependent on the treatment conditions.(Biological triplicates).

## *3.* Detection of DNA double-stranded breaks (DSBs)

The γH2AX assay exploits the phosphorylation of the histone variant H2AX (resulting in γH2AX) in response to the induction of DNA DSBs. This event can be visualized microscopically within a cell using a specific fluorescent antibody. This presents an important advantage of measuring the number of foci *in situ*, thus allowing the quantitation of the radiation response in individual cells, and building the distribution of cells with respect to this response.

### 3.1. Initial (30 min) and residual (24h) γH2Ax after 2 Gy irradiation

Previous studies on SQ20B J.L. cells have identified an initial peak of γH2Ax foci 30 minutes post-irradiation which corresponds to the maximum of DSBs obtained, and the residual number of foci after DNA repair, 24 hours post-irradiation (Hanot *et al.*, 2012). We therefore selected

these two-time points in order to evaluate the impact of AGuIX® combined with a 2 Gy irradiation on this biomarker of DSBs. For this assay, we used an irradiation dose of 2Gy, as at greater doses, the quantification of γH2Ax foci are impossible to count (too many). The results are summarized in Figures 101-103. The software used for the acquisition and analysis of γH2AX is Metafer (Metasystems, Heidelberg, Germany). The foci's size and intensity were independently determined for each independent experiment.

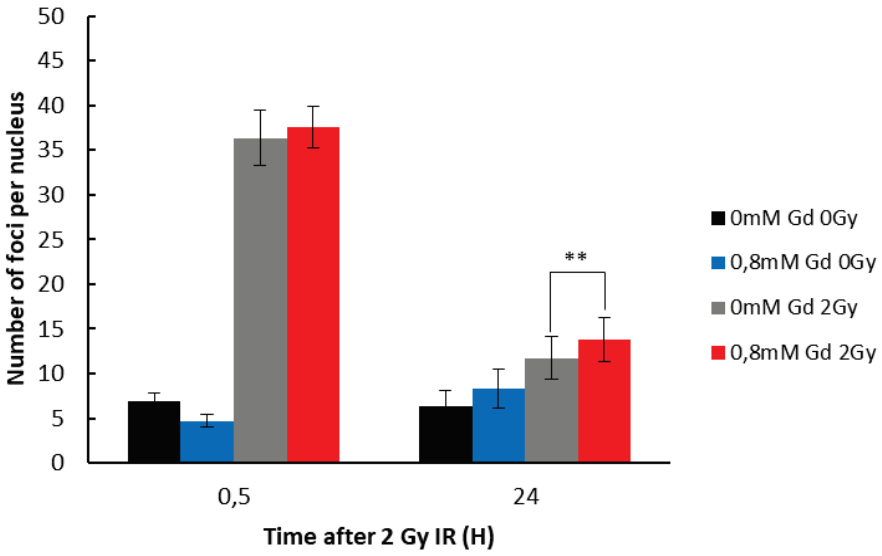


Figure 101: Initial (30 minutes) and residual (24 hours) γH2Ax per nucleus after a 2Gy irradiation +/- AGuIX®. Duplicate slides and three independent experiment, 600+ nuclei were counted (p-value *: <0.05; **<0.01; ***: <0.005).

As can be seen in Figure 101, there are no significant differences between untreated and treated cells, 30 minutes after irradiation. However, the number of residual foci (at t=24 hours) was slightly but significantly increased after the addition of AGuIX® (+17%; 0.8mM Gd + 2Gy *versus* 2Gy). The quantification of DSBs was performed using microscopy images as represented in Figure 102 (nucleus in blue and γH2Ax foci in green). For each independent experiment, more than 600 nuclei were counted.

Besides the global analysis of the number of γH2Ax foci, one can also follow cell to cell variability of radiation-induced foci by looking at the distribution of the nuclei plotted as a function of the number of foci per nucleus (Figure 103).

Thirty minutes after irradiation (Figure 103a), no significant differences were obtained in the distribution of γH2Ax foci after the combined treatment (AGuIX® + irradiation), compared to radiation alone. The same can be stated for Figure 103b. Indeed, in Figure 103b, which represents the distribution of γH2Ax foci 6h after irradiation, no significant differences were obtained in the

distribution of nuclei displaying γH2Ax foci after treatment with AGuIX® compared to radiation alone. However, for the residual γH2Ax foci (24 hours after irradiation), we can observe that the number of cells displaying less than 5 foci per nucleus and between 25-36 foci is greater for untreated, irradiated cells compared to AGuIX®-treated cells (Figure 103c). The main result of this analysis was obtained with cells displaying more than 50 foci per nucleus that were significantly increased after treatment with AGuIX® prior to radiation compared to radiation alone.

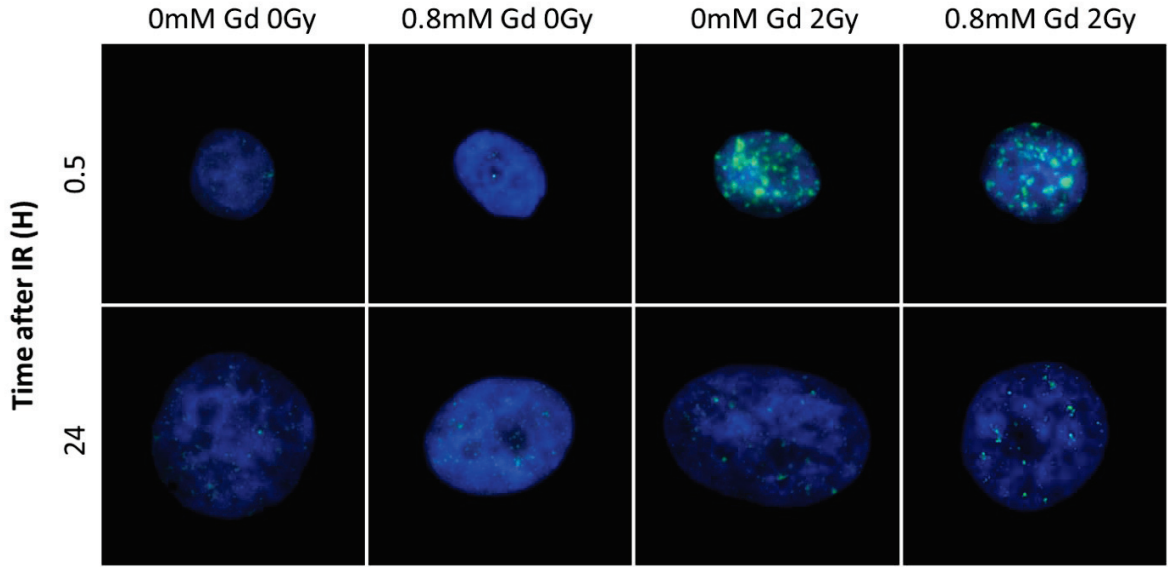


Figure 102: Representative nuclei depending on the treatment conditions and the time post-irradiation. Blue: nucleus (DAPI); green: γH2Ax (Alexa-Fluor 488).

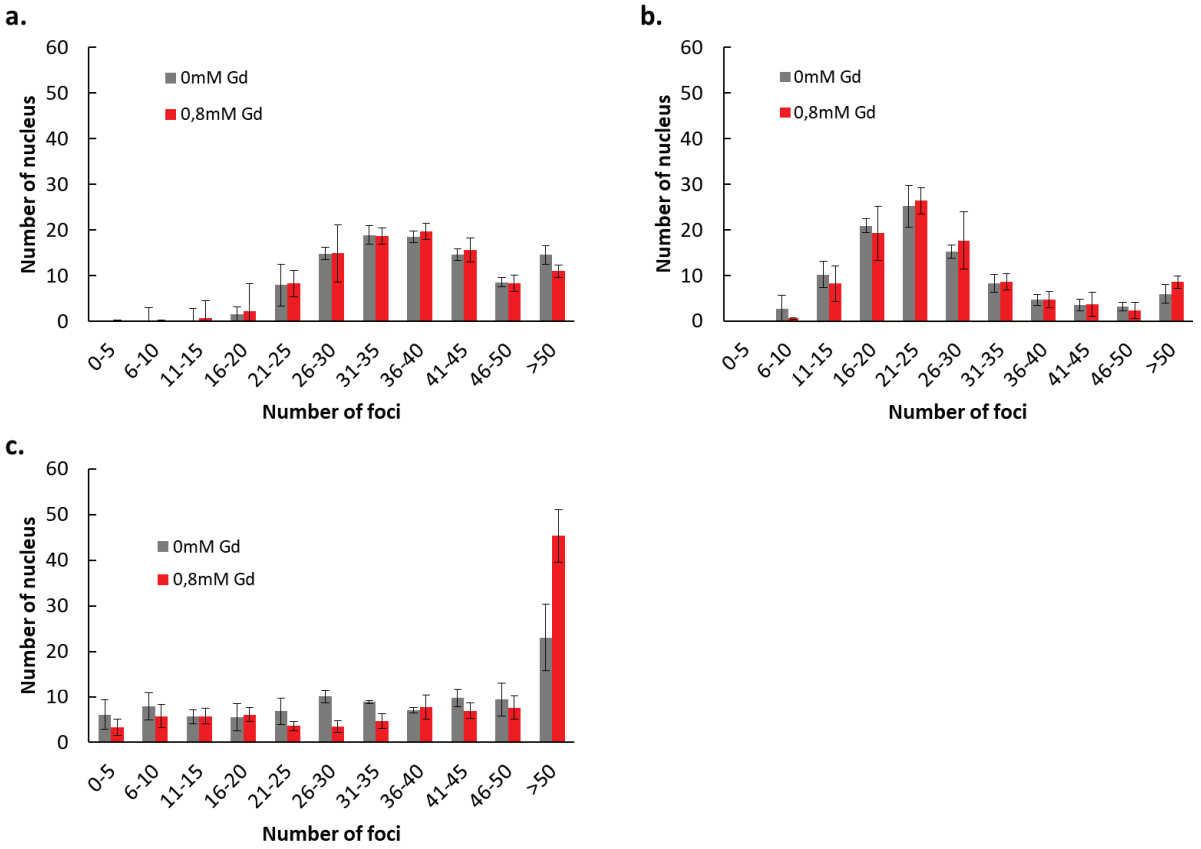


Figure 103: Distribution classes of the number of foci/nucleus as a function of the number of nucleus included in the class: irradiated only cells (2Gy) versus AGuIX® + irradiated cells (0.8mM Gd 2Gy). a. 30 minutes post-irradiation (initial number of γH2Ax); b. 6 hours post-irradiation c. 24 hours post-irradiation (residual γH2Ax). 300+ nuclei were counted for each condition.

Collectively, these results indicate that the global analysis of the residual γH2Ax foci reported in Figure 101 did not reflect some interesting results such as the presence of nuclei displaying a very high number of residual foci which have been thus highlighted, and which probably represent very complex and clustered DSBs induced specifically after treatment with AGuIX®. Moreover, one must keep in mind that SQ20B J.L. cells do not necessarily internalize the same number of AGuIX® which can result in a variability of residual DSBs after irradiation.

### 3.2. Kinetic study of the formation and repair of DSBs

To study whether the combination treatment of AGuIX® + irradiation had an influence on the dynamics of DNA repair in SQ20B J.L. cells, we decided to perform a kinetic study with intermediate time points including one, two, four, and six hours post-irradiation.

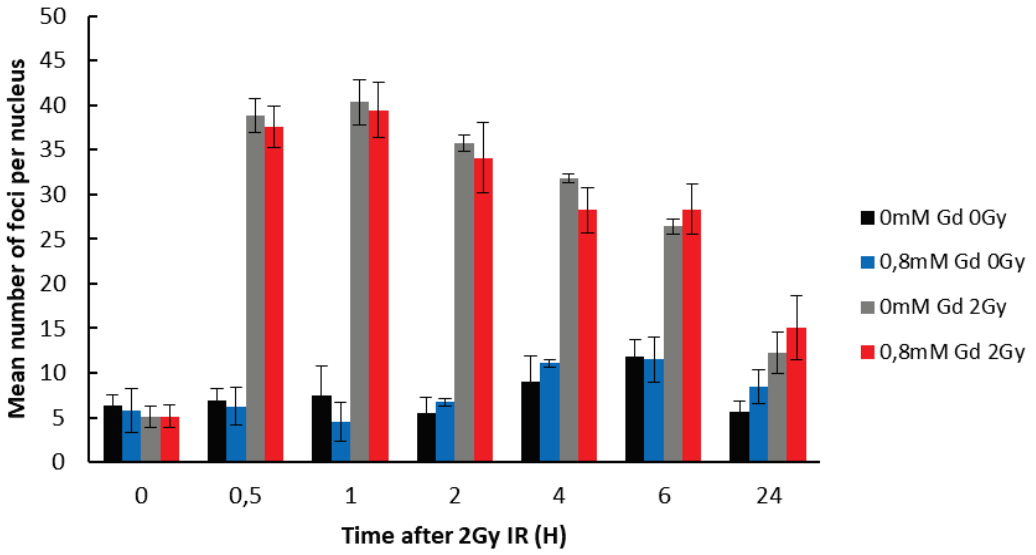


Figure 104: Kinetic study (0-0.5-1-2-4-6-24 hours) of foci γH2Ax after a 2 Gy irradiation depending on the different treatment conditions. Each condition was done in biological triplicate with a minimum of 300 nuclei quantified per biological sample.

As can be observed in Figure 104, there were no significant differences between the two experimental conditions*, i.e* treatment with AGuIX® before irradiation *versus* irradiation alone. From these results, we can conclude that treatment of cells with AGuIX® before radiation had no influence on the kinetics of DNA repair in SQ20B J.L. cells.

In order to explain the slight differences concerning the residual γH2Ax foci obtained after treatment with AGuIX® (see Figure 103), we should keep in mind that a maximum dose of 2Gy has to be used to be able to count γH2Ax foci. When referring to the clonogenic survival curve in Figure 72, the difference between untreated and AGuIX®-treated cells exposed to a 2Gy irradiation is not very important (ratio of 1.1). This might be one limitation of the γH2Ax foci assay to estimate unrepaired DNA damage.

Despite the absence of NPs within nuclei, the question as to whether the radiosensitizing effect induced by the combination treatment of AGuIX® + irradiation is dependent or not on DNA-damage has been studied by teams working with AGuIX® as well as other metal-based nanoparticles as radiosensitizing agents. Although similar results were found for initial DSBs, results varied for the number of residual foci, 24 hours after photons irradiation. Indeed, an increase of 45% of residual DSBs compared to non-treated cells was reported in a melanoma model (Kobt *et al.*, 2016), an increase of 40 % in a head and neck cell line (Wozny *et al.*, 2017) whereas no increase of DSBs were obtained in glioblastoma cells after the addition of AGuIX® combined to radiation (Štefančíková *et al.*, 2016). These results strongly underline the large

variations in the results obtained, depending on the treatment conditions as well as the cellular type studied.

For other metal-based NPs, such as gold nanoparticles, similar contradictory results have been reported. As an example, the use of 1.9 nm gold nanoparticles did not enhance radiation-induced DSBs formation nor inhibit DNA repair in MDA-MB-231 breast cancer cells irradiated with MV electrons (Jain *et al.*, 2011). In contrast, the combination of 50 nm citrate-coated gold NPs with 6 MV photons resulted in an increase of DSBs in HeLa cells (Chitrani *et al.*, 2010; Berbeco *et al.*, 2012). For gold NPs, It would seem that bigger diameter NPs tend to induce DNA damages, whereas smaller ones do not.

**CHAPTER IV TAKE-HOME MESSAGE:**

**In this chapter focusing on the DNA-damage induced by the combination of AGuIX® with irradiation, it appears that despite the absence of AGuIX® within nuclei, the radiosensitization obtained by AGuIX® nanoparticles also involves DNA-damage. Although only slight differences in the average number of residual DSBs were obtained after treatment with AGuIX® prior to irradiation, some significant differences were noticed in some cells that displayed a high number of foci per nucleus (>50) as a reflection of unrepairable complex DNA damages.**

# Chapter V. Shotgun/Bottom-up Proteomics study: preliminary experiments

Although the *cellular experiments that were undertaken in this work (ROS production measurement, study of the different types of I.R-induced cell deaths, DNA-damage …) are commonly used for the studies on the radiosensitizing effects of nanoparticles, the complexity of the molecular mechanisms implemented requires more efficient and informative experimental approaches. Among these, proteomics was chosen because the proteome reflects more accurately the dynamic state of a cell and can help identify a molecular signature on the cell's behavior based on protein pathways as well as signaling cascades*.

*The goal of this preliminary analysis was therefore to observe the change of the proteomic profile of SQ20B J.L. cells after AGuIX® + photon irradiation using the shotgun proteomics technique. This type of analysis was initiated to provide more in-depth analysis of potential protein targets and signaling pathways that would be modulated following this combined treatment.*

*It is important to keep in mind, that this project could be in itself a thesis topic, but here, it was undertaken during the last months of our work to open into a new perspective that should lead to future work. In addition, this study should create new opportunities and challenges for those seeking to gain greater understanding of the mode of action of NPs at the subcellular level.*

Proteomics is the study of all the proteins of a proteome: the term proteomics arise from merging the term "protein" and "genomics" (Wilkins *et al.*, 1996; James, 1997). Why did we choose to study proteomics instead of the genome (genomics) or transcriptome (transcriptomics)? Because the proteins are the end result and the direct bio-functional molecules in the living organisms. It is considered as a post-genomic discipline that identifies and quantifies all the proteins of a proteome, including expression, cellular localization, interactions, post-translational modification, and turnover as a function of time, space, and cell type (Zhang *et al.*, 2013). There are possibly 100 000 protein forms encoded by the approximate 20 235 genes of the human genome (Gstaiger and Aebersold, 2009).

The technique used was shotgun proteomics, also referred as "bottom-up" protein analysis, which refers to the characterization of proteins by the analysis of peptides released from the protein through proteolysis (Wolters *et al*., 2001; Yates, 2004; Link AJ *et al.*, 1999; Yates, 1998). Shotgun proteomics provides an indirect measurement of proteins through peptides derived from proteolytic digestion of intact proteins. In a typical shotgun proteomics experiment, the peptide mixture is fractionated and subjected to LC-MS/MS analysis. Peptide identification is then achieved by comparing the tandem mass spectra derived from the peptide fragmentation with theoretical tandem mass spectra generated from *in silico* digestion of a protein database. Protein inference is accomplished by assigning peptide sequences to proteins. Because peptides can be either uniquely assigned to a single protein or shared by more than one protein, the identified proteins may be further scored and grouped based on their peptides (Zhang *et al.*, 2013). This technique was further explained previously, in the Material and Methods section, however it is important to keep in mind this process when analyzing and discussing the results.

As introduced above, a proteomic study was performed to observe the proteins' dynamics 24 hours post-irradiation. This time point, which is close to the irradiation time, is important for a preliminary study, in order to see what strategies/mechanisms of defense the cell activates or disactivates following the treatment applied. We should therefore pinpoint the disrupted proteins and/or signaling pathways that can lead to cell death (radiosensitization) or cell survival (radioresistance).

The results obtained from this preliminary study are described in the next section and have been analyzed in two separate ways: (1) first, by using a set cut-off often discussed in scientific papers and chosen by both hosting labs: greater than or equal to **1.2** (for the over-expressed proteins), and less than or equal to **0.8** (for under-expressed proteins). (2) Secondly, modulated proteins will be considered only if their expression varied by a factor of a minimum of five: an over-or under-expression of a factor 5. Figure 105 summarizes the results obtained with shut-gun proteomics with more than two-thousand proteins identified.

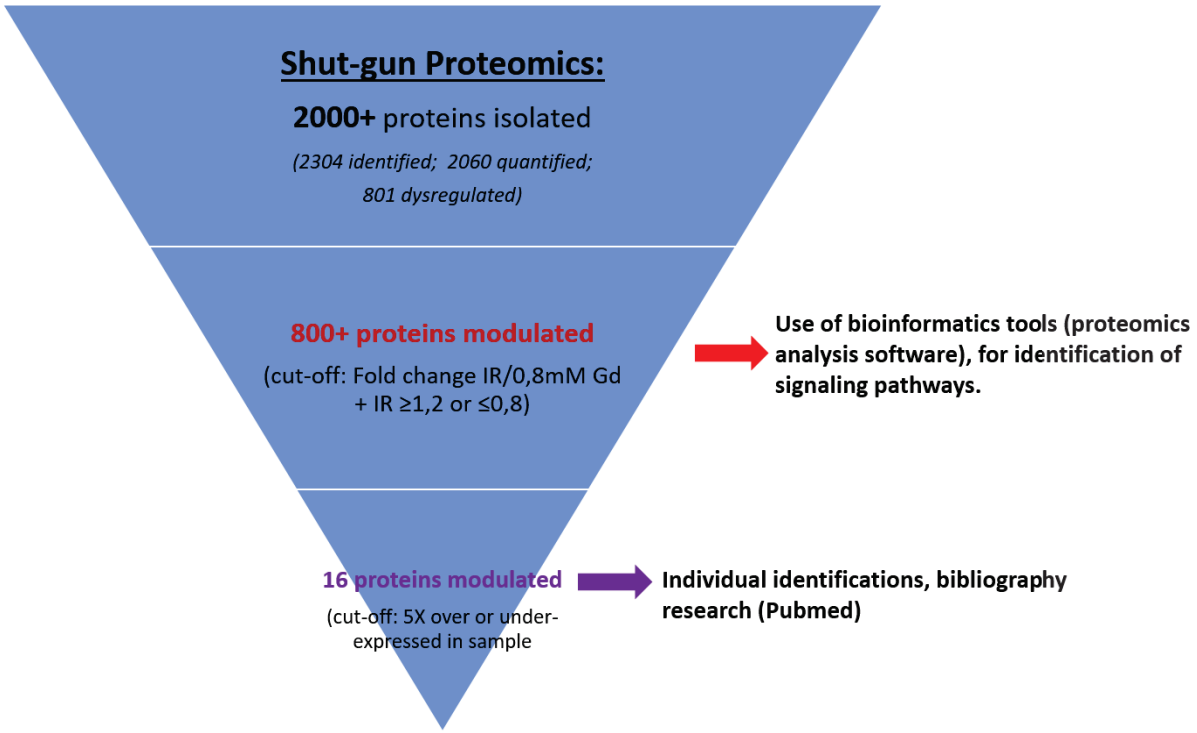


Figure 105: Summary of the raw data obtained following shot-gun proteomics for SQ20B J.L. cells and how the analysis can be done.

We will first mention the different signaling pathways that were put in evidence when using two different bioinformatics tools (**D**atabase for **A**nnotation, **V**izualization, and **I**ntegrated **D**iscovery (DAVID) software and **I**ngenuity **P**athway **A**nalysis (IPA)) with the proteins that were modulated by a minimum of 20%, which represented, as can be seen in Figure 105, more than 30% of the total number of identified proteins.

## *1. Analysis of proteins with a fold-change ≥ 1.2 (over-expression) or ≤0.8 (under-expression) using the DAVID software*

### 1.1. DAVID Software Analysis

When applying the cut-off ≤0.8 or ≥1.2, more than 800 proteins were identified as modulated. In order to analyze such a list of proteins, the software DAVIDS Bioinformatics Genomics was used, as described in the Materials and Methods section. By using this software, the following pathways were identified (see list below, with the number of genes identified in the corresponding pathway):

- ✓ Metabolic pathways (15 genes)
- ✓ Valine, leucine, and isoleucine degradation (5 genes)

- ✓ Carbon metabolism (6 genes)
- ✓ Butanoate metabolism (3 genes)
- ✓ Propanoate metabolism (3 genes)
- ✓ Beta-Alanine metabolism (3 genes)
- ✓ Fatty acid degradation (3 genes)
- ✓ Oxidative phosphorylation (4 genes)
- ✓ Fatty acid metabolism (3 genes)
- ✓ Glycolysis/Gluconeogenesis (3 genes)
- ✓ Fatty acid elongation (2 genes)

The metabolic pathway seems to be implicated in the cells' reaction to the combined treatment, as 15 genes are modulated within the pathway. It is also interesting to note that some of the identified pathways have a direct implication with the energy metabolism of a eukaryotic cell, such as oxidative phosphorylation, glycolysis/gluconeogenesis. Since a cell needs energy in order to survive, and the main organelle where ATP production is produced in the mitochondria, these results seem to correlate with previous results obtained during the course of the PhD.

These pathways are summarized in Figure 106 with the most affected metabolic pathway (with the most modulated proteins) being the glycan biosynthesis and metabolism as well as the lipid metabolism, as can be observed in Figure 106. The names of the corresponding modulated genes are listed in Table 27. Genes implicated in the other identified pathways by the DAVIDS software are listed in Table 28-31.

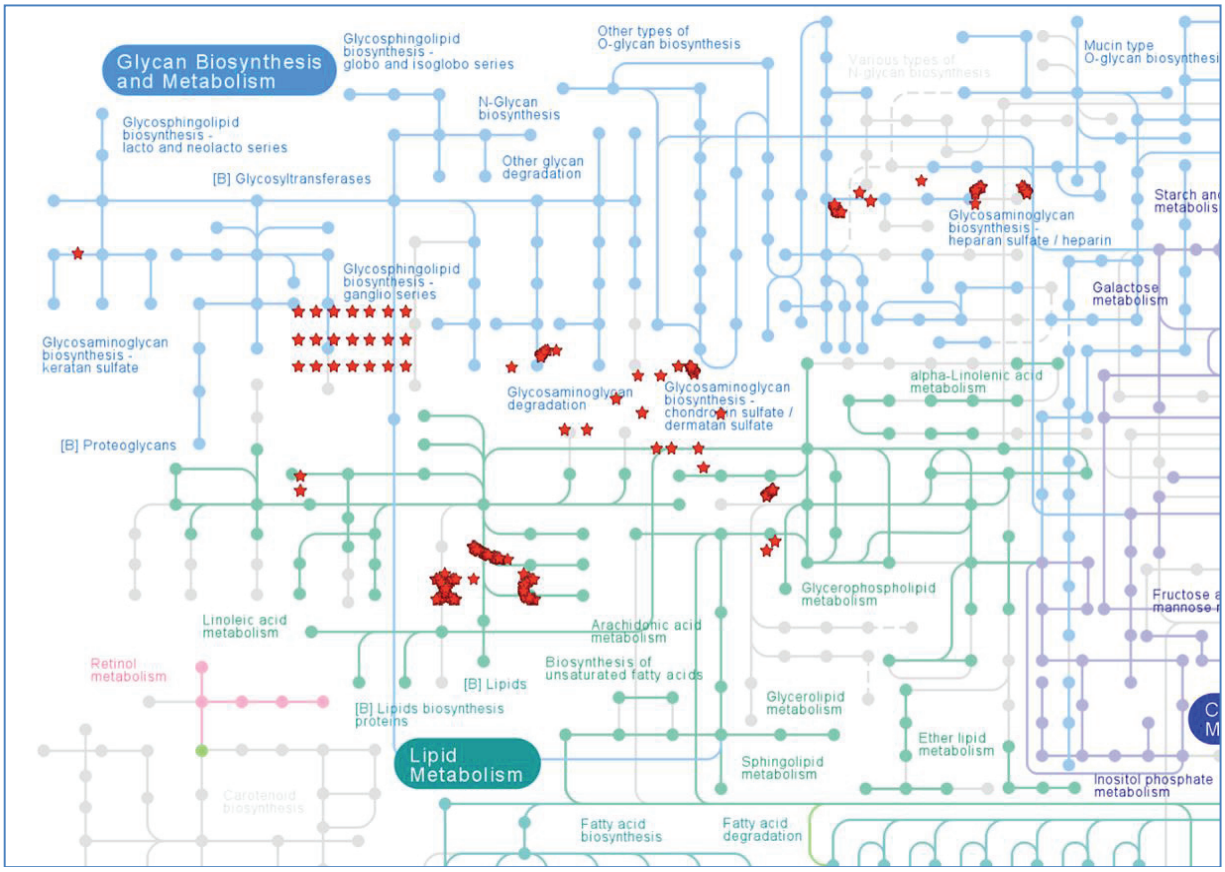


Figure 106: Modulated proteins in the metabolic pathways, with 15 genes being affected. Analysis performed with the DAVID Software. (*Note: the red stars represent the modulated proteins).

| **Modulated genes** | **OVER**- or **UNDER**-expressed in 0.8mM Gd 10Gy |
|---|---|
| 3-hydroxyisobutyrate dehydrogenase (HIBADH) | UNDER |
| 3-hydroxymethyl-3-methylglutaryl-CoA lyase (HMGCL) | UNDER |
| ATP synthase, H+ transporting, mitochondrial Fo complex subunit G(ATP5L) | OVER |
| NADH: ubiquinone oxidoreductase core subunit S3 (NDUFS3) | OVER |
| NADH: ubiquinone oxidoreductase subunit A12 (NDUFA12) | OVER |
| Acyl-CoA dehydrogenase, C-4 to C-12 straight chain (ACADM) | OVER |
| Aldehyde dehydrogenase 1 family member A1 (ALDH1A1) | OVER |
| Aldehyde dehydrogenase 3 family member A1 (ALDH3A1) | OVER |
| Aldehyde dehydrogenase 4 family member A1 (ALDH4A1) | OVER |
| Dihydrolipoamide S-acetyltransferase (DLAT) | OVER |
| Enoyl-CoA hydratase, short chain 1 (ECHS1) | OVER |
| Hydroxyacyl-CoA dehydrogenase (HADH) | UNDER |
| Pyruvate dehydrogenase (lipoamide) alpha 1 (PDHA1) | UNDER |
| Serine hydroxymethyltransferase 2 (SHMT2) | OVER |
| Succinate-CoA ligase ADP-forming beta subunit (SUCLA2) | UNDER |

Table 27: Modulated genes within the metabolic pathways.

Table 28 summarizes the genes modulated in the carbon metabolism, while Table 29 lists modulated genes from the citrate cycle.

| **Modulated genes** | **OVER**- or **UNDER**-expressed in 0.8mM Gd 10Gy |
|---|---|
| Acyl-CoA dehydrogenase, C-4 to C-12 straight chain (ACADM) | OVER |
| Dihydrolipoamide S-acetyltransferase (DLAT) | OVER |
| Enoyl-CoA hydratase, short chain 1 (ECHS1) | OVER |
| Pyruvate dehydrogenase (lipoamide) alpha 1 (PDHA1) | OVER |
| Serine hydroxymethyltransferase 2 (SHMT2) | OVER |
| Succinate-CoA ligase ADP forming beta subunit (SUCLA2) | UNDER |

Table 28: Modulated genes in the carbon metabolism.

| Modulated genes | **OVER**- or **UNDER**-expressed in 0.8mM Gd 10Gy |
|---|---|
| Dihydrolipoamide S-acetyltransferase (DLAT) | OVER |
| Pyruvate dehydrogenase (lipoamide) alpha 1 (PDHA1) | OVER |
| Succinate-CoA ligase ADP-forming beta subunit (SUCLA2) | UNDER |

Table 29: Modulated genes in the citrate cycle (TCA Cycle).

Figure 107 schematizes the mitochondrial transport chain and the modulated proteins with Table 30 enumerating them.

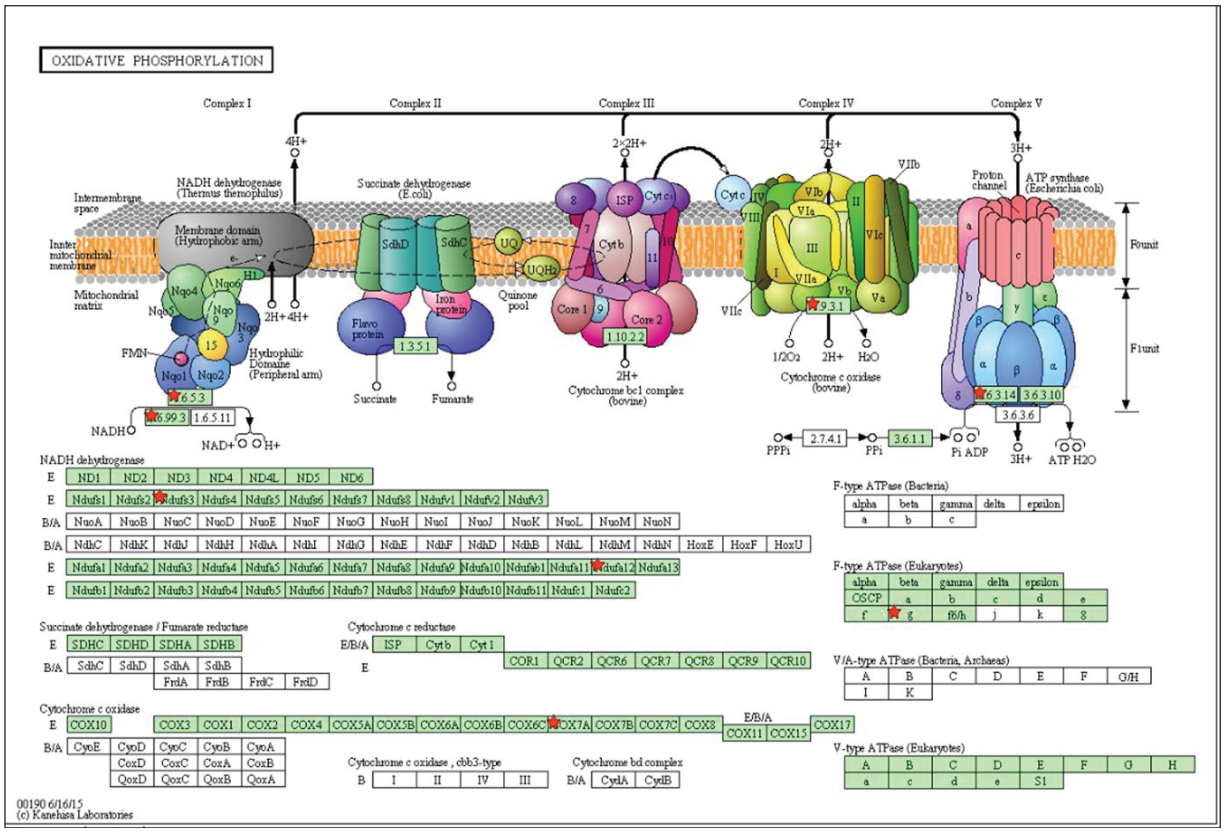


Figure 107: Illustration of the mitochondrial Electron Transport Chain (ETC) where oxidative phosphorylation occurs. (*Note: the red stars represent the modulated proteins).

| **Modulated genes** | **OVER**- or **UNDER**-expressed in 0.8mM Gd 10Gy |
|---|---|
| ATP synthase, H+ transporting, mitochondrial Fo complex subunit G (ATP5L) | OVER |
| NADH: ubiquinone oxidoreductase core subunit S3 (NDUFS3) | OVER |
| NADH: ubiquinone oxidoreductase subunit A12 (NDUFA12) | OVER |
| Cytochrome c oxidase subunit 7A2 (COX7A2) | OVER |

Table 30: Modulated genes in the oxidative phosphorylation.

| **Modulated genes** | **OVER**- or **UNDER**-expressed in 0.8mM Gd 10Gy |
|---|---|
| Aldehyde dehydrogenase 3 family member A1 (ALDH3A1) | OVER |
| Dihydrolipoamide S-acetyltransferase (DLAT) | OVER |
| Pyruvate dehydrogenase (lipoamide) alpha 1 (PDHA1) | OVER |

Table 31: Modulated genes in the glycolysis/gluconeogenesis pathway.

Observing the modulated genes within a signaling pathway is one way to analyze the results. With the DAVIDS software, we can also classify the proteins by their location and/or their biological functions. Since throughout this PhD work, we, in part, wanted to observe the mitochondrial consequences of the combined treatment, as well as the oxido-reduction state of the cells, Table 32 lists the **modulated mitochondrial proteins** (72 proteins were identified as mitochondrial proteins), while Table 33 lists the **modulated oxidoreductase proteins** (37 proteins).

| Gene Name | **Fold change (IR/IR + AGuIX®)** | **OVER**- or **UNDER**-expressed in 0.8mM Gd 10Gy |
|---|---|---|
| 2,4-dienoyl-CoA reductase 1, mitochondrial(DECR1) | - | UNDER |
| 3-hydroxyisobutyrate dehydrogenase(HIBADH) | 2.000 | UNDER |
| 3-hydroxymethyl-3-methylglutaryl-CoA lyase(HMGCL) | 2.000 | UNDER |
| 5-phosphohydroxy-L-lysine phospho-lyase(PHYKPL) | - | UNDER |
| ATP synthase, H+ transporting, mitochondrial Fo complex subunit D(ATP5H) | - | OVER |
| ATP synthase, H+ transporting, mitochondrial Fo complex subunit G(ATP5L) | 0.500 | OVER |
| ATPase family, AAA domain containing 3B(ATAD3B) | - | OVER |
| BCL2 like 1(BCL2L1) | - | OVER |
| BRI3 binding protein(BRI3BP) | - | OVER |
| G elongation factor mitochondrial 1(GFM1) | 2.000 | UNDER |
| NADH:ubiquinone oxidoreductase core subunit S3(NDUFS3) | 0.333 | OVER |
| NADH:ubiquinone oxidoreductase subunit A12(NDUFA12) | 0.500 | OVER |
| NADH:ubiquinone oxidoreductase subunit A6(NDUFA6) | - | OVER |
| NADH:ubiquinone oxidoreductase subunit S5(NDUFS5) | - | UNDER |
| NDUFA4, mitochondrial complex associated(NDUFA4) | - | UNDER |
| OPA1, mitochondrial dynamin like GTPase(OPA1) | - | UNDER |
| SAMM50 sorting and assembly machinery component(SAMM50) | - | UNDER |
| TP53 induced glycolysis regulatory phosphatase(TIGAR) | 0.500 | OVER |
| Acyl-CoA dehydrogenase family member 9(ACAD9) | 2.000 | UNDER |
| Acyl-CoA dehydrogenase, C-4 to C-12 straight chain(ACADM) | 0.500 | OVER |
| Acyl-CoA thioesterase 9(ACOT9) | 0.500 | OVER |
| Adenylate kinase 4(AK4) | - | UNDER |
| Aldehyde dehydrogenase 4 family member A1(ALDH4A1) | 0.500 | OVER |
| Apolipoprotein O(APOO) | - | OVER |
| Biphenyl hydrolase like(BPHL) | - | OVER |
| caseinolytic mitochondrial matrix peptidase proteolytic subunit(CLPP) | 2.000 | UNDER |
| Clusterin(CLU) | - | UNDER |
| Coproporphyrinogen oxidase(CPOX) | - | OVER |

| | | |
|---|---|---|
| Cytochrome b5 reductase 3(CYB5R3) | 0.500 | OVER |
| Cytochrome c oxidase subunit 7A2(COX7A2) | 0.500 | OVER |
| Cytochrome c1(CYC1) | - | UNDER |
| Dihydrolipoamide S-acetyltransferase(DLAT) | 0.500 | OVER |
| Dynamin 1 like(DNM1L) | - | UNDER |
| Enoyl-CoA delta isomerase 1(ECI1) | - | UNDER |
| Enoyl-CoA hydratase, short chain 1(ECHS1) | 0.200 | OVER |
| Ferredoxin reductase(FDXR) | - | UNDER |
| Glycerol-3-phosphate dehydrogenase 2(GPD2) | - | UNDER |
| Holocytochrome c synthase(HCCS) | - | OVER |
| Hydroxyacyl-CoA dehydrogenase(HADH) | 2.000 | UNDER |
| Leucine zipper and EF-hand containing transmembrane protein 1(LETM1) | 1.500 | UNDER |
| Mitochondrial antiviral signaling protein(MAVS) | 0.500 | OVER |
| Mitochondrial carrier 2(MTCH2) | - | OVER |
| Mitochondrial ribosomal protein L24(MRPL24) | - | UNDER |
| Mitochondrial ribosomal protein L37(MRPL37) | 0.500 | OVER |
| Mitochondrial ribosomal protein L39(MRPL39) | - | OVER |
| Mitochondrial ribosomal protein L4(MRPL4) | - | OVER |
| Mitochondrial ribosomal protein L46(MRPL46) | - | UNDER |
| Mitochondrial ribosomal protein S15(MRPS15) | - | UNDER |
| Mitochondrial ribosomal protein S22(MRPS22) | 2.000 | UNDER |
| Mitochondrial ribosomal protein S23(MRPS23) | 0.500 | OVER |
| Mitochondrial ribosomal protein S25(MRPS25) | - | UNDER |
| Mitochondrial ribosomal protein S28(MRPS28) | 1.500 | OVER |
| Mitochondrial ribosomal protein S9(MRPS9) | 2.000 | UNDER |
| Monoamine oxidase A(MAOA) | - | UNDER |
| Peptidyl-tRNA hydrolase 2(PTRH2) | - | UNDER |
| Peptidylprolyl cis/trans isomerase, NIMA-interacting 4(PIN4) | - | OVER |
| Polyribonucleotide nucleotidyltransferase 1(PNPT1) | - | OVER |
| Protein kinase cAMP-activated catalytic subunit alpha(PRKACA) | - | OVER |
| Pseudouridylate synthase 1(PUS1) | - | OVER |
| Pyruvate carboxylase(PC) | - | OVER |

| | | |
|---|---|---|
| Pyruvate dehydrogenase (lipoamide) alpha 1(PDHA1) | 0.500 | UNDER |
| Queuine tRNA-ribosyltransferase catalytic subunit 1(QTRT1) | - | UNDER |
| Ras homolog family member T2(RHOT2) | - | OVER |
| Serine hydroxymethyltransferase 2(SHMT2) | 0.445 | OVER |
| Solute carrier family 25 member 13(SLC25A13) | 0.200 | OVER |
| Solute carrier family 25 member 4(SLC25A4) | - | OVER |
| Succinate-CoA ligase ADP-forming beta subunit(SUCLA2) | 2.000 | OVER |
| Synaptojanin 2 binding protein(SYNJ2BP) | - | OVER |
| Thioredoxin reductase 2(TXNRD2) | 0.667 | UNDER |
| Translocase of outer mitochondrial membrane 40(TOMM40) | 0.250 | OVER |
| Transmembrane protein 126A(TMEM126A) | - | OVER |
| Tyrosyl-tRNA synthetase 2(YARS2) | - | OVER |

Table 32: Modulated mitochondrial genes.

| Gene Name | **Fold change (IR/IR + AGuIX®)** | **OVER**- or **UNDER**-expressed in 0.8mM Gd 10Gy |
|---|---|---|
| 2,4-dienoyl-CoA reductase 1, mitochondrial(DECR1) | - | UNDER |
| 3-hydroxyisobutyrate dehydrogenase(HIBADH) | 2.000 | UNDER |
| C-terminal binding protein 1(CTBP1) | - | UNDER |
| C-terminal binding protein 2(CTBP2) | - | UNDER |
| NAD(P)H quinone dehydrogenase 1(NQO1) | 2.000 | UNDER |
| NADH:ubiquinone oxidoreductase core subunit S3(NDUFS3) | 0.333 | OVER |
| Acyl-CoA dehydrogenase family member 9(ACAD9) | 2.000 | UNDER |
| Acyl-CoA dehydrogenase, C-4 to C-12 straight chain(ACADM) | 0.500 | OVER |
| Aldehyde dehydrogenase 1 family member A1(ALDH1A1) | 0.500 | OVER |
| Aldehyde dehydrogenase 3 family member A1(ALDH3A1) | 0.500 | OVER |
| Aldehyde dehydrogenase 4 family member A1(ALDH4A1) | 0.500 | OVER |
| Aldo-keto reductase family 7 member A2(AKR7A2) | 0.500 | OVER |
| AlkB homolog 5, RNA demethylase(ALKBH5) | - | OVER |
| Biliverdin reductase B(BLVRB) | 2.000 | UNDER |
| Carbonyl reductase 3(CBR3) | - | OVER |
| Coproporphyrinogen oxidase(CPOX) | - | OVER |
| Cytochrome P450 family 51 subfamily A member 1(CYP51A1) | - | UNDER |
| Cytochrome b5 reductase 1(CYB5R1) | - | UNDER |
| Cytochrome b5 reductase 3(CYB5R3) | 0.500 | OVER |
| Dehydrogenase/reductase 7(DHRS7) | - | OVER |
| Dihydrofolate reductase(DHFR) | - | UNDER |
| Ferredoxin reductase(FDXR) | - | UNDER |
| Glycerol-3-phosphate dehydrogenase 2(GPD2) | - | UNDER |
| Hydroxyacyl-CoA dehydrogenase(HADH) | 2.000 | UNDER |
| Hydroxysteroid dehydrogenase like 2(HSDL2) | - | OVER |
| Inosine monophosphate dehydrogenase 1(IMPDH1) | - | OVER |
| Monoamine oxidase A(MAOA) | - | OVER |
| Procollagen-lysine,2-oxoglutarate 5-dioxygenase 3(PLOD3) | - | UNDER |
| Prolyl 3-hydroxylase 1(P3H1) | - | UNDER |
| Pyruvate dehydrogenase (lipoamide) alpha 1(PDHA1) | 0.500 | OVER |
| Retinol dehydrogenase 10 (all-trans)(RDH10) | - | OVER |

| | | |
|---|---|---|
| Saccharopine dehydrogenase (putative)(SCCPDH) | 2.000 | UNDER |
| Sepiapterin reductase (7,8-dihydrobiopterin:NADP+ oxidoreductase)(SPR) | - | UNDER |
| Thioredoxin domain containing 12(TXNDC12) | - | UNDER |
| Thioredoxin reductase 1(TXNRD1) | - | OVER |
| Thioredoxin reductase 2(TXNRD2) | 0.667 | OVER |
| Tumor protein p53 inducible protein 3(TP53I3) | - | UNDER |

Table 33: Modulated proteins with an oxidoreduction function.

### 1.2. IPA Analysis

When analyzing proteomics results, it is important to use multiple analysis software to compare and complete the analysis, one being complementary of the other.

Since the results obtained were analyzed using a free trial, it is important to note that the number of runs was limited and not all functions of the IPA software were "activated". However, several interesting facts came out during these analysis. First, the clathrin-mediated endocytosis pathway was clearly present due to the internalization of the nanoparticles. Next, the NRF2, NFκB, and Myc signaling pathways seem to play a critical role in the radiosensitization by AGuIX® nanoparticles. Again, the mitochondria seem to be affected with the addition of AGuIX® treatment.

Twenty-three molecules were associated with clathrin-mediated endocytosis signaling and are summarized in Table 34, while the 22 modulated proteins associated with the NRF2-mediated oxidative stress response are listed in Table 35.

| **Gene Name** | **OVER** or **UNDER-**expressed in 0.8mM Gd 10Gy | **Localization** | **Type(s)** |
|---|---|---|---|
| Actin gamma 1 | OVER | Cytoplasm | Other |
| ARP3 actin related protein 3 homolog | UNDER | Plasma membrane | Other |
| Adaptor related protein complex 1 beta | OVER | Cytoplasm | Transporter |
| Adaptor related protein complex 2 | UNDER | Cytoplasm | Transporter |
| Adaptor related protein complex 2 beta | UNDER | Plasma membrane | Transporter |
| Apolipoprotein A1 | UNDER | Extracellular Space | Transporter |
| ADP ribosvlation factor 6 | OVER | Plasma Membrane | Transporter |
| Actin related protein 2/3 complex | OVER | Cytoplasm | Other |
| Cell division cycle 42 | UNDER | Cytoplasm | Enzyme |
| Clathrin light chain B | OVER | Plasma membrane | Other |
| Clusterin | UNDER | Cytoplasm | Other |
| Casein kinase 2 alpha 2 | OVER | Cytoplasm | Kinase |
| Casein kinase 2 beta | UNDER | Cytoplasm | Kinase |
| Cortactin | UNDER | Plasma Membrane | Other |
| Dynamin 1 like | UNDER | Cytoplasm | Enzyme |
| Hepatocyte growth factor-regulated | OVER | Cytoplasm | Other |
| Heat shock protein family A (Hsp70) | UNDER | Cytoplasm | Enzyme |
| Integrin subunit beta 1 | UNDER | Plasma Membrane | Transmembrane Receptor |
| Myosin VI | OVER | Cytoplasm | Other |
| Myosin IE | OVER | Cytoplasm | Enzyme |
| Prenylcysteine Oxidase 1 | OVER | Cytoplasm | Enzyme |
| Phosphatidylinositol binding clathrin | UNDER | Cytoplasm | Other |
| Ras-related C3 botulinum toxin | OVER | Plasma Membrane | Enzyme |

Table 34: List of the 23 modulated proteins associated with clathrin-mediated endocytosis signaling. Gene name, over-or under-expressed, cell localization, and corresponding type.

| **Gene Name** | **OVER** or **UNDER-**expressed in 0.8mM Gd 10Gy | **Localization** | **Type(s)** |
|---|---|---|---|
| Actin gamma 1 | OVER | Cytoplasm | Other |
| Aldo-keto reductase family 7 member A2 | UNDER | Cytoplasm | Enzyme |
| Caseinolytic mitochondrial matrix | OVER | Cytoplasm | Peptidase |
| CREB binding protein | UNDER | Nucleus | Transcription regulator |
| Cullin 3 | OVER | Nucleus | Enzyme |
| DnaJ heat shock protein family (Hsp40) Member A2 | UNDER | Nucleus | Enzyme |
| DnaJ heat shock protein family (Hsp40) Member A3 | OVER | Cytoplasm | Other |
| DnaJ heat shock protein family (Hsp40) Member JB11 | OVER | Cytoplasm | Other |
| DnaJ heat shock protein family (Hsp40) Member C8 | UNDER | Nucleus | Other |
| DnaJ heat shock protein family (Hsp40) Member C9 | OVER | Nucleus | Other |
| DnaJ heat shock protein family (Hsp40) Member C10 | UNDER | Cytoplasm | Enzyme |
| Epoxide hydrolase 1 | OVER | Cytoplasm | Peptidase |
| FK506 binding protein 5 | UNDER | Nucleus | Enzyme |
| Glutathione S-transferase theta 1 | OVER | Cytoplasm | Enzyme |
| 3-hydroxyacyl-CoA dehydratase 3 | UNDER | Cytoplasm | Enzyme |
| Mitogen-activated protein kinase kinase 1 | UNDER | Cytoplasm | Kinase |
| Microsomal glutathione S-transferase 2 | UNDER | Cytoplasm | Enzyme |
| NAD(P)H quinone dehydrogenase 1 | OVER | Cytoplasm | Enzyme |
| NRAS proto-oncogene GTPase | OVER | Plasma Membrane | Enzyme |
| Protein kinase C iota | OVER | Cytoplasm | Kinase |
| Thioredoxin | UNDER | Cytoplasm | Enzyme |
| Thioredoxin reductase 1 | OVER | Cytoplasm | Enzyme |

Table 35: List of the 22 modulated proteins associated with NRF2-mediated oxidative stress response. Gene name, over-or under-expressed, cell localization, and corresponding type.

Although one might argue that an over- or under- expression of 20% is small, in biology, a small variation can have an important biological impact. This is why we thought it was interesting to analyze the proteomic results obtained using these low cut-off values.

## 2. *Analysis of proteins with a fold change of 5X over or under-expressed: the identification of 16 modulated proteins*

The analysis was then focused by restricting even more the cut-off of what was considered significant: the cut-off was therefore set by taking into account a change in protein expression starting at 5 times over or under-expressed: in this case, sixteen proteins were identified and are summarized in the table below (Table 36).

| **Protein** | **OVER** or **UNDER-** expressed in 0.8mM Gd 10Gy | **Localization** |
|---|---|---|
| Heterogeneous nuclear ribonucleoprotein L | UNDER | Nucleus/Cytoplasm |
| S-formylglutathione hydrolase | OVER | Cytoplasm |
| Crk-like protein | OVER | Cytoplasm |
| Calcium-binding mitochondrial carrier protein Aralar2 | OVER | Mitochondria |
| Proteasome subunit beta type | OVER | Nucleus/Cytoplasm |
| cDNA FLI78268, *highly similar to homo sapiens fusion* | OVER | Nucleus |
| cDNA FLI78655, *highly similar to Homo sapiens exportin 5 (XPO5)* | OVER | Nucleus |
| Urindine phosphorylase 1 | OVER | Cytoplasm, association with cytoskeleton |
| FACT complex subunit SPT16 | UNDER | Nucleus |
| Nuclear cap binding protein subunit 1 | UNDER | Cytosol, mitochondrion nuclear cap binding complex, nucleoplasm |
| AP-2 complex subunit beta | UNDER | Plasma membrane |
| Polyadenylate-binding protein | UNDER | Cytosol/nucleus |
| Low-molecular weight phosphotyrosine protein phosphatase | UNDER | Cytosol |
| H.Sapiens ras-related Hrab1A protein | UNDER | Endoplasmic reticulum |
| Nuclear pore complex protein Nup205 | UNDER | Nuclear membrane |
| Ribonucleoside-diphospate reductase | UNDER | Cytoplasm |

Table 36: List of proteins with an over- or under- expression of at least 5 times with its cellular localization.

After reviewing the literature on the above-cited proteins, we focused on the **ribonucleoside-diphosphate reductase** (RNR) as a potential promising target, which was found to be under-

expressed after treatment with AGuIX® nanoparticles in addition to the irradiation. Indeed, RNR has already been identified, and serves as a prognostic and predictive biomarker in many different types of cancers (i.e. in hepatocellular carcinoma, thyroid carcinoma, colorectal cancers, pancreatic cancers, nasopharyngal carcinoma, …) Moreover, an elevated RNR activity and/or the over-expression of this protein has been related to an increase of drug resistance as well as an increase of both the angiogenic and invasive potential of the cancer cells.

**R**ibo**n**ucleotide-**r**eductase (RNR) is a unique enzyme, because it is responsible for reducing ribonucleotides to their corresponding deoxyribonucleotides, which are the building blocks required for DNA replication and repair. Dysregulated RR activity is therefore associated with genomic instability, malignant transformation, and cancer development. RNR is composed of two sub-units: RRM1 and RRM2, containing two homodimers. RRM1 contains allosteric regulatory sites and catalytic domain, while RRM2 contains two irons for catalytic activity. RRM2 is inducible by p53 and is necessary for DNA repair, as well as mitochondrial DNA maintenance for example.

This protein has already been the topic of several studies for its potential as a therapeutic target in some cancers via the use, in particular, of siRNA directed against RNR. Studies include its inhibition via an siRNA to reverse tamoxifen resistance in breast cancer (Shah *et al.*, 2014), the suppression of oral squamous cell carcinoma (OSCC) cell growth (Iwamoto *et al.*, 2015), the induction of autophagy in hepatocellular carcinoma (Chen *et al.*, 2014), as well as the reduction of cell proliferation and invasion via apoptosis induction in gastric adenocarcinoma (Kang *et al.*, 2014). Moreover, two studies by Rahman *et al.*, using siRNA nanoparticles targeting RRM2, demonstrated an induction of apoptosis, the suppression of cell proliferation, and an inhibition of the tumors' growth (Rahman *et al.*, 2012), regulated via an increase of Bcl-2 degradation (Rahman *et al.*, 2013). The use of gemcitabine, an RNR inhibitor, allowed the restoration of docetaxel sensitivity in OSCC. The targeting of RNR with a microRNA inhibited glioma proliferation (Jiang *et al.*, 2017), and the combination of clofarabine and the inhibition of RNR with a siRNA caused the reduction of xenografts in multiple myeloma (Sagawa *et al.*, 2017).

The study of RNR as a potential target in HNSCC has also been extensively studied, *in vitro*, *in vivo*, and in clinical trials. Indeed, an *in vitro* and *in vivo* efficacy of the combined treatment of hydroxyurea, an RNR inhibitor, with a histone deacetylase inhibitor (valproic acid, VPA) on HNSCC cell lines freshly established from human tumors, was demonstrated. This effect was shown to be induced by BIM induction and EGFR down-regulation (Stauber *et al.*, 2012). We can also cite two clinical trials using RNR inhibitors. First, there is an ongoing Phase II assay on 27 grade III and grade IV patients studying the radiosensitizing effect of gemcitabine, an RNR inhibitor, however important side effects remain a hold-back (Agular-Ponce *et al.*, 2004). Secondly, a phase II assay

on 32 patients with recurrent and metastatic HNSCC was undertaken with 3-AP Triapine, a RNR inhibitor, but showed only a modest effect (Nutting *et al.*, 2009).

Western Blot analysis was needed to be performed in order to validate this under-expression of RNR when SQ20B J.L. cells are treated with AGuIX®. RRM1 and RRM2 specific antibodies were therefore used. Our first experiments with anti-RRM1 antibody did not give any results, in terms of expression following the combined treatment. Actually, the modulation of RRM2 expression, via the validation by Western Blot experiments, is still in progress. One must keep in mind that the analysis of the proteome under our experimental conditions constitute preliminary experiments that need to be strengthened in the near future.

At the time point-chosen, twenty-four hours post-irradiation, we are able to observe, not only proteins that would in the long-term lead to cell death, but also proteins that could help the cells to resist cell death (those radioresistant mechanisms activated by the cells). It would have been interesting to do a kinetic study in time, perhaps up to 240 hours post-irradiation (end-point of the clonogenic survival curve assay), to observe what proteins were still over- or under-expressed. We would expect that after the combined treatment of AGuIX® and I.R., proteins leading to cell survival (resistance) would be under-expressed, while those leading to cell death would be over-expressed. It is clear from this preliminary proteomic study that the resulting cell death by the radiosensitization of AGuIX® is the result of multiple signaling pathways.

In this chapter, we have shown that proteomics is certainly a very powerful and useful approach in our problematic. This technique could also allow us to understand the link between lysosome, autophagy, and complex DNA damage highlighted in this work after the combined treatment of AGuIX® and radiation.

**CHAPTER V TAKE-HOME MESSAGE:**

**Shot-Gun Proteomics is a powerful approach which allowed us to isolate 2000 + proteins with more that 800 proteins modulated when the fold-change IR/0.8mM Gd + IR cut-off was set at ≥1.2 or ≤0.8. When using bioinformatics tools, it was observed that the energetic metabolism of the cell was probably affected.**

**When the cut-off was set at 5X OVER- or UNDER- expressed, 16 proteins were modulated, among which the ribonucleoside-disphosphate reductase caught our attention as it impacts cancer susceptibility, and can serve as a target for anti-cancer therapies.**

# General Discussion

Head and neck cancer represents a major worldwide health concern, with 90% classified as squamous cell carcinoma. These cancers arise from the epithelial lining of the oral cavity, oropharynx, larynx and hypopharynx (Jemal *et al.*, 2007; Boyle and Levin, 2008), and is strongly associated with certain lifestyle risk factors including tobacco, alcohol consumption. More recently, the infection by HPV 16 or 18 was also identified as a risk factor (Kreimer *et al*., 2005). The five-year overall survival rate of HNSCC patients is quite low, as it remains between 40 and 50%. This low 5-year survival rate can be, in part, attributed to the fact that 2/3$^{rd}$ of patients present Stage III, IVa/b at diagnosis, which is advanced and therefore requires a much harsher treatment, yet less effective. Indeed, the remaining one-third of the patients diagnosed at an early stage of the disease (Stage I or II) has a rather optimal survival rate, and the treatment usually involves a single treatment modality with either surgery or radiation, as chemotherapy or a combination of chemotherapy and radiation is not indicated in these cases. For Stage III/IV patients, postoperative concomitant chemo-radiation, which is a much heavier treatment plan, has huge impacts on the patients' quality of life associated with a low survival rate. For all these reasons, HNSCC remains an important worldwide health concern, ranked amongst the top cancer in terms of diagnostics as well as for cancer-related deaths, due to its high recurrence and radioresistance.

While radiation therapy plays an essential role in HNSCC treatment, its therapeutic efficacy is hindered by treatment-associated toxicity and tumor recurrence. The use of radiotherapy in HNSCC has one main limitation which is the close proximity of numerous radiation-sensitive organs in the head and neck area. Careful radiation planning is needed in order to preserve the organs' function and the patients' quality of life, while keeping in mind that the radiotherapeutic dose delivered must be maximized in order to achieve loco-regional tumor control and patient survival. Indeed, toxicity to surrounding healthy tissues limits the dose deliverable to the patient. In order to reduce this toxicity, conventional RT is based on a fractionated regime, (Joiner, 2009) (for HNSCC, doses of 2Gy 5 times a week for 7 weeks, totaling a dose of 70Gy). This fractionation allows for the recovery of healthy tissues to sub-lethal irradiation doses (known as the optimal therapeutic window) (Baskar *et al*., 2012; Kim and Tannock, 2005). In addition, HNSCC tumors include a high degree of heterogeneity in genotype, phenotype, and microenvironment, leading to a variability in their radiation sensitivity and responses in different populations of tumor cells (Meacham and Morrison, 2013; Burrell *et al*., 2013, Junttila and de Sauvage, 2013).

In order to counteract radioresistance and overcome its limitations, it is necessary to combine radiotherapy with an agent that will increase the dose delivered to the tumor while sparing the healthy tissue, which defines a performing radiosensitizing agent. Up to now, the only recent radiosensitizing agent approved by the FDA, is cetuximab, an EGFR antibody but its success remains disappointing. In order to develop efficient radiosensitizing agents for HNSCC, it is

important to improve our understanding on the different mechanisms underlying HNSCC radioresistance.

One thoroughly studied pathway is the DNA damage response (DDR). Alterations of the DDR in cancer cells strongly contribute to radioresistance by preventing mutations and/or cell death. A strong link has been identified between Ku80 and radioresistance, as its overexpression has been linked with markedly worsened locoregional recurrence and overall survival (Moeller *et al*., 2011; Chang *et al*., 2006; Nimura *et al*., 2007; Chang *et al*., 2008). Two additional proteins were identified for their implication in radioresistance due to their involvement in NHEJ DDR are PARP (poly-(ADP-ribose) polymerase) (Nowsheen *et al*., 2011) and the enzyme TRIP 13 (Scheckenbach *et al*., 2014). The overexpression and mutation of Rad-51, a homologous recombination (HR) factor was associated with worse clinical outcomes for chemoradiation. Therefore, both NHEJ and HR were identified as pathways that play an important role in radioresistance. ATM and ATR are two proteins particularly vital in the initiation of DDR, and their subsequent promotion of DNA repair through HR and NHEJ. These proteins play a role in the regulation of the cell cycle progression using checkpoint kinases 1/2 (CHEK1/2) to control cyclin dependent kinase (CDK) activity in order to delay the cell cycle and allow time to repair the cells. The understanding of these mechanisms led to effectively elicit radiosensitization of HNSCC if the ATM-CHEK2 and ATR-CHEK1 pathways were disrupted (Sankunny *et al*., 2014; Mansour *et al*., 2013). However, the knockdown of CDK2 sensitized HNSCC cell to radiation in monolayer culture, but failed to significantly do so in a physiologically representation cell culture model which used a 3D extracellular matrix (ECM) (Soffar *et al*., 2013).

A well-known protein, with a role as a central regulator of many cellular processes and which has a very important role and influence in the radioresistance of HNSCC by contributions to the DDR and cell death, is p53. Indeed, mutant p53 is thought to contribute to radiation failure in HNSCC (Alsner *et al*., 2001; Koch *et al*., 1996; Alsner *et al*., 2001). The use of metformin potentialized radiotherapy both *in vitro* and *in vivo* on TP53 mutational status, while no influence was observed on wild-type TP53. In an effort to understand this phenomenon, the authors hypothesized that cells with mutated TP53 favor the glycolytic metabolic pathway for energy production, which would explain their sensitivity to metformin (Sandulache *et al*., 2012). Patients receiving post-operative radiation therapy and are concurrently treated with metformin had less locoregional recurrence and improved survival compared with matched controls (85% vs. 41%) (Skinner *et al*., 2012). A Phase I dose-finding study in HNSCC to examine the addition of metformin to chemoradiation is underway (NCT02325401).

Cell cycle modulators such as SAR-020106, a CHEK1 inhibitor, promoted mitotic entry of cells after radiation-induced G2/M arrest, which in turn led to an increased apoptosis in p53-deficient

HNSCC cells. In this study, reduced tumor growth with no evidence of metastasis nor toxicity were observed in a mouse xenograft model that had received the combined treatment of SAR-020106 with irradiation (Borst *et al*., 2013). No clinical trials are ongoing for SAR-020106, but a phase I trial for CCT245737, another isolated CHEK1 inhibitor is underway. Another compound of interest is P276-00 which inhibits the cyclin-d/CD4/P16/pRB/E2F axis and can induce apoptosis by triggering G1/S arrest (Mishra *et al*., 2013). Other agents include Olaparib, a PARP inhibitor, which showed an additive effect when treated in combination with PF-0477736, a CHEK1 inhibitor on HPV-positive HNSCC cell lines. A phase I trial combining Olaparib and cetuximab, with RT in advanced HNSCC is currently ongoing (NCT01758731).

Other radioresistant features of HNSCC include for example the tumor's microenvironment, the interplay of immune response to radiation therapy, the cancer stem cell paradigm and the dysfunction of pathways leading to apoptotic cell death. Indeed, the epidermal growth factor receptor is responsible for an aberrant signaling which can mediate resistance to radiation by modifying the induction of apoptosis. Pathways downstream of EGFR, such as PI3K/Akt/mTOR or MAPK/ERK, may also contribute to the radioresistance by mitigating apoptosis (Ettl *et al*., 2015; Nakagawa *et al*., 2012). We already mentioned that Cetuximab, an anti-EGFR drug approved by the FDA was disappointing in terms of efficacy. Focus therefore turned to fully-humanized monoclonal EGFR antibodies such as Panitumumab. However, Panitumumab plus RT had similar outcomes to chemoradiotherapy in locoregional control at two-year follow-up (51% versus 61%, respectively) with the regimens showing a similar toxicity profile (Giralt *et al.*, 2015). Nevertheless, it was demonstrated that the inhibition of EGFR in HNSCC can actually trigger a tumor promoting inflammatory response via NOX4, which could partly explain the disappointing results obtained with Cetuximab and Panitumumab. In addition, therapeutic failure of EGFR inhibition may occur due to the superfluous effects of EGFR's downstream pathways MAPK/ERK and PI3K/Akt/mTOR, which promote NHEJ DNA repair via DNA-PKs (Saki *et al*., 2013; Toulany *et al*., 2005; Minjgee *et al*., 2011; Gupta *et al*., 2002). Therefore, another approach was the development of tyrosine kinase inhibitors (TKIs) such as gefitinib and erlotinib, which can act on the intracellular portion of the receptor to inhibit phosphorylation of downstream effectors. Up to now, an ongoing Phase II trial did not show any improvements in term of outcomes and an increased toxicity was observed (Rodriguez *et al*., 2012).

As both cetuximab and TKIs have encountered low response rates in clinical practice, EGFR antisense DNA has also been investigated as another way to target EGFR signaling (Lai *et al*., 2009). Phase I trials using EGFR antisense DNA with Cetuximab and radiation therapy are ongoing (NCT0090346, NCT01592721). Besides these trials, other small molecules such as panobinostat (an histone deacetylase inhibitor), or dasatinib, a Bcr-Abl and Src family tyrosine kinase inhibitor, are under clinical evaluation. Figure 8 summarizes these different targeted pathways.

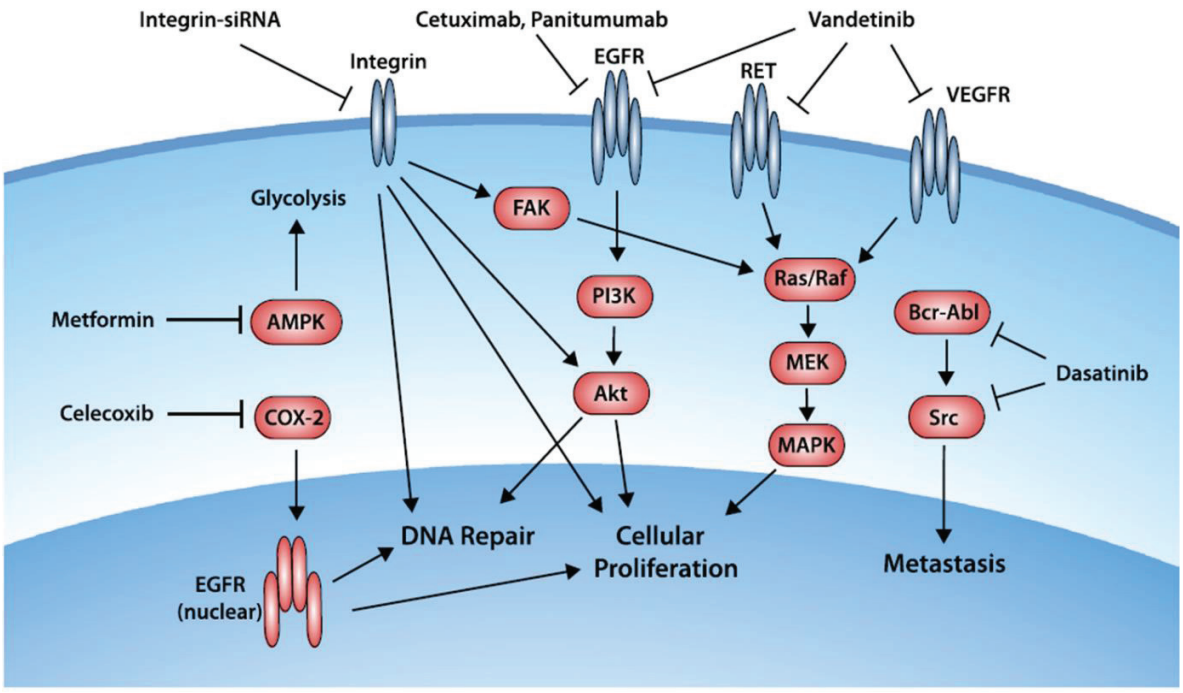


Figure 108: Molecular-targeted therapies in development for the treatment of head and neck squamous cell carcinoma. Arrows indicate signal modulation and bars denote inhibition. (Yamamoto *et al*., 2016)

Research in the development of radiosensitizing strategies has also focused on the improvement of radiotherapy efficacy in terms of increase of the dose delivered to the tumor while sparing the surrounding healthy tissues. These radiosensitizing strategies will play on one or more, of the 5 Rs of Radiobiology (namely **R**epair, **R**edistribution, **R**eoxygenation, **R**epopulation, and intrinsic **R**adiosensitivity) which are considered as the biological factors that determine the "success or failure" of RT (Steel *et al*., 1989; Pajonk *et al*., 2010; Brown *et al*., 2014). One option, among others, the use of nanoparticles. As overviewed in the bibliography section (see Chapter 3), different types of nanoparticles can be used as radiation sensitizers (metal-based, quantum dots, superparamagnetic iron oxides and non-metal-based nanoparticles). Among these, high-Z metal nanoparticles and in particular gold nanoparticles have received much attention for their radiosensitizing potential. As stated in the review published by Cui *et al*. (2017), a radiosensitizer enhances radiation therapy at different levels:

- at the molecular and cellular levels, by modifying pathways involved in DNA repair, cell cycle checkpoint and progression, as well as cellular death and proliferation (to achieve higher levels of cell death by irradiation).
- at the tissue level, by preventing the tumor regrowth by killing subpopulations of cancer cells that would normally be radioresistant (*i.e.* those under hypoxia or in the S phase), by

inhibiting tumor angiogenesis or reducing tumor hypoxia prior to irradiation, by regulating the function of tumor blood vessels as well as diminishing oxygen and nutrient supply and by damaging tumor blood vessels post irradiation (Seiwert *et al*., 2007: Ma *et al.*, 2003).

Moreover, during the developmental stage of any kind of drug, one must keep in mind the requirements for its clinical translation. As stated by Coleman and Mitchell (1999) and Wardman (Wardmann, 2007), there are a number of key items that must be examined including (1) the **identification of targets of the radiosensitizer**; (2) the **accessibility of radiosensitizer targets for radiosensitization**; (3) the **stability of the targets** and finally, the (4) **toxicity of the radiosensitizer enhanced RT to tumor relative to normal tissues**. These identified steps for gold nanoparticles can be translated to all types of NPs, such as the gadolinium-based nanoparticles used in this study.

Although the use of nanoparticles, as radiosensitizers has been extensively studied, the translation into clinics is still insufficient. As reviewed by Brun and Sicard-Roselli (2016), many unanswered questions remain among which the lack of consensus between the different studies. As an example, the cell line, radiation energy, physicochemical properties of the NPs (size, shape, and surfactant used), concentrations, incubation times have varied significantly in the different studies which makes it near to impossible to make comparisons which in turn would lead to meaningful conclusions (since we are not comparing the exact same things) (Jain *et al.*, 2011; Coulter *et al*., 2012). However, consistent findings concerning AuNPs radiosensitization between these studies led to interesting points:

(1) AuNPs enhance the effects of high energy photon RT where the Compton effect dominates (Kong *et al*., 2008; Rahman *et al*., 2009; Chithrani *et al*., 2010), providing evidence that they can be used at clinically relevant energies;

(2) their cellular localization in close proximity to biological components has a great impact on their radiosensitization capabilities;

(3) they are found to be sequestered as clusters in endosomal and lysosomal vacuoles following cell entry. The impact of the nanoparticle's size is influenced at the level of the cellular uptake, rather than an influence on the biological impact once internalized, and the manner of energy deposition of electrons generated following NPs + IR (Chithrani *et al*., 2010; Chithrani *et al*., 2010); and lastly

(4) hypoxia has been reported to diminish radiosensitization by AuNPs, due to the important roles of oxygen in RT (Cui *et al*., 2014; Jain *et al*., 2014).

These different observations on AuNPs should be translated to other types of nanoparticles, although this remains to be demonstrated. (Cui *et al*., 2017). For a successful translation to

clinics, the understanding of the different mechanisms that underpin its effectiveness should involve multidisciplinary collaborations between chemists, radiation oncologists, radiation physicists, and molecular biologists.

In this work, AGuIX® nanoparticles were used to evaluate their potential as a radiosensitizing agent while trying to understand their potential mechanism of action at the cellular level. AGuIX® are gadolinium-based nanoparticles that have been developed mainly for imaging due to their magnetic resonance contrast properties but they also have a potential role in radiation therapy as a radiosensitizer (Le Duc et al., 2011; Porcel et al., 2010; Le Duc *et al*., 2014; Sancey *et al*., 2014; Mignot *et al*., 2013; Kotb *et al*., 2016; Mowat *et al*., 2011; Štefančíková *et al*., 2014; Miladi *et al*., 2015). In order to improve the effectiveness of gadolinium chelators as MRI contrast agents (Frullano and Caravan, 2011), the formulation of AGuIX® has moved towards a macrocyclic chelator (DOTA) instead of a linear gadolinium chelator (DTPA). In the present study, the radiosensitizing potential of this new formulation of AGuIX® in the HNSCC cell model SQ20B J.L. was demonstrated, resulting in a $SF_{4Gy}$ of 1.382 with an Enhanced Biological Factor (EBR) of 1.3 which is similar to what is currently published for other studies using AGuIX®, namely in HeLa (cervical cancer) (Luchette *et al*., 2014), Panc-1 (pancreatic cancer) (Detappe *et al*., 2015), U87 (glioblastoma) (Štefančíková *et al*., 2014; Štefančíková *et al*., 2016), and B16F10 (melanoma) cells (Kotb *et al*., 2016), with DEFs varying from 1.17 to 1.54.

Regarding AGuIX®, and more generally high-Z NPs, one question that is often raised concerns whether there is a preferential localization of AGuIX® for radiosensitization. In accordance with Štefančíková *et al.* (2014) in glioblastoma, we showed that AGuIX® are not targeted to the nucleus nor the mitochondria but are mostly located in lysosomes, while a few AGuIX® remain free in the cytosol. Similar results were also obtained in CHO cells for example, where NP clusters of sizes between 400-900 nm were observed in the cytoplasm regardless of the concentration used or incubation time (Porcel *et al*., 2014).

One other main question addressed during this PhD was to further understand which connections may exist between the physical and biological effects of AGuIX®. The hypothetical mechanism behind the use of metal-based nanoparticles is based on the over-production of secondary electrons leading to an increase of cellular ROS which in turn would lead to cell death. Evidence obtained to date suggests that the generation of ROS as well as oxidative stress strongly contribute to the biological impact of gold nanoparticles (Taggart et al., 2014; Butterworth et al., 2012; Nel *et al*., 2006; Xia *et al*., 2006; Cui *et al*., 2013; Pan *et al*., 2009; Mroz *et al*., 2008; Rim *et al*., 2013; Berbeco *et al*., 2012). However, only a few data are up to now available *in vitro*. As pointed out in this work, and despite of radiosensitization, the increase of ROS production following the combined treatment was lower than expected. One possible explanation was that SQ20B cells, as many other radioresistant cancer cells, exhibit upregulated antioxidant systems

(see Zhou *et al*., as a review). Previous work from our lab effectively reported that SQ20B cells display a high endogenous glutathione (GSH) content which largely contributes to their radioresistant properties. Although GSH is a major ROS-scavenging system in cells, the important redox modulating enzymes including the peroxidases, peroxiredoxins, and thiol reductases also rely on the pool of reduced GSH as their source of reducing equivalents (Boivin *et al*., 2011; Forman *et al*., 2009). In view of these elements, a transient GSH-depleting strategy was previously investigated which resulted in the radiosensitization of the SQ20B cell line used in this study (Boivin *et al*., 2011). Using the same experimental approach, *i.e* after GSH depletion, we clearly demonstrated that the pretreatment of cells with AGuIX® resulted in a net increase of cellular ROS after radiation thereby strongly suggesting a ROS-mediated radiosensitizing effect of AGuIX®. No increase of ROS was obtained in mitochondria under the same experimental conditions, probably because AGuIX® did not enter mitochondria. The increase of cellular ROS was further evidenced through the clonogenic survival curve by an increase of the EBR from 1.3 to 1.6. Nevertheless, one must keep in mind that it still remains very difficult, if not impossible, to discriminate for sure a direct production of ROS by AGuIX® as a consequence of irradiation, from an overproduction of ROS as a cellular response and therefore to conclude about an additive or a synergetic effect of irradiation and AGuIX®. Anyway, our results suggest that lowering endogenous antioxidant defenses could be an interesting strategy to optimize the radiosensitizing effect of AGuIX®.

However, radical oxygen species also play a central role in carcinogenesis and a strong link exists between mitochondria and ROS. Indeed, ROS, in the form of superoxide, hydroxyl free radicals and hydrogen peroxide are produced from physiological metabolic reactions. Mitochondria are major contributors to cellular ROS and multiple antioxidant pathways are present to neutralize excess of ROS including superoxide dismutase (SOD2), glutathione, thioredoxin, and peroxiredoxins. The early observation that cancer cells have a high ROS levels compared to normal cells let to an overly simple hypothesis that inhibiting ROS could be a successful therapeutic strategy. However, a more complex picture was emerging, where ROS can stimulate signaling and proliferation whereas the concomitant upregulation of antioxidant pathways can prevent ROS-mediated cytotoxicity and thus may even enhance tumor survival (Vyas *et al*., 2016; Shadel and Horvath, 2015; Sullivan and Chandel, 2014). This paradigm is illustrated in the figure below schematically representing this “threshold” concept.

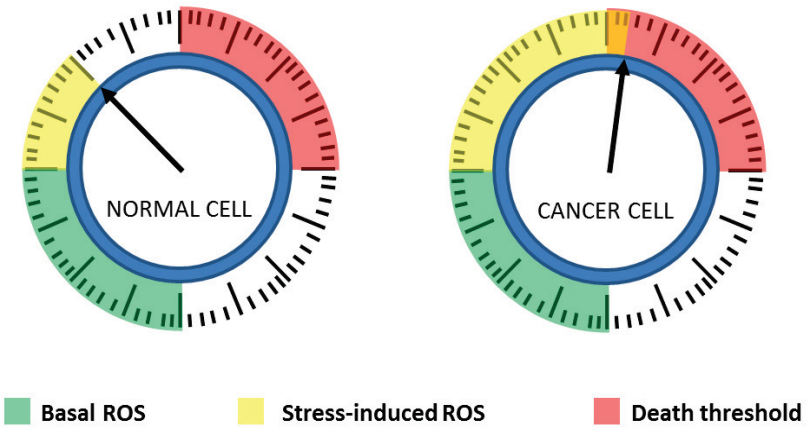


Figure 109: ROS levels in normal versus cancer cells. Cancer cells have elevated basic ROS level compared to normal cells. It can be therapeutically utilized by various anticancer agents, which further increases ROS generation to such as toxic level and may induce death specifically in cancer cells, but not in normal cells (Galadari *et al*., 2017).

Thus, manipulating the endogenous antioxidant content is a double-edged sword that needs a careful evaluation before use.

Next, the different types of cellular deaths known to be induced by radiation therapy (apoptosis, necrosis, mitotic catastrophe, senescence, and autophagy) were studied after the combined treatment. To our knowledge, only one study using DTPA-based gadolinium nanoparticles reported that the combined treatment led to an increase of mitotic catastrophe followed by late apoptosis (Miladi *et al.*, 2015). Otherwise, many reports were published concerning the effect of other type of NPs in the triggering of apoptosis. In combination with radiotherapy, examples include the effect of gold nanorods on melanoma cells (Xu *et al*, 2012), the effect of thio-glucose-bound gold nanoparticles (Glu-GNPs) on lung cancer cells (Wang *et al*, 2013), or the effect of silver NPs on glioma cells (Liu *et al*, 2013; Liu *et al*, 2016). With this new formulation of AGuIX®, no enhancement of apoptosis nor mitotic catastrophe were obtained after radiation. Among the other alternative cell death modalities, autophagy and/or autophagic cell death was the only cellular event that was significantly enhanced after AGuIX® compared to radiation alone. Thus, it is not particularly surprising that excessive autophagy (as obtained after our combined treatment) can promote cell death rather than cell survival. Although the specific mechanism that links between radiation and autophagy has not been well established, some studies have connected the mTOR pathway to radiation-induced cell death, as radiation could cause decreased phosphorylation of the autophosphorylation site of p-mTOR (decreased p-mTOR/mTOR ratio) (Paglin *et al*, 2005). Up to now, many trials have been conducted to modulate autophagy for improving the outcome of cancer treatment in combination with currently used treatment modalities such as radiotherapy in different cancer types (Tam *et al*, 2017). Among

these, some studies using different types of nanoparticles combined with radiation presented evidence for a radiosensitizing effect involving autophagy: AgNPS in glioma cells at clinically relevant megavoltage energies (Liu *et al*, 2016), copper cysteamine NPs in colorectal carcinoma (Liu *et al*, 2017) or selenium NPs in breast cancer cells (Cheng *et al*, 2017).

Apoptosis only accounts for 20% or less of radiation-induced cell death, strongly supporting the involvement of other types of I.R. induced cell-death (Schleicher *et al.*, 2010). In our case, the only type of death that resulted in an enhancement between irradiation alone and the combined treatment was autophagy. Autophagy, derived from "auto" (self) and "phagos" (to eat), is a catabolic process in which the cells digest and recycle their own cytoplasmic contents, to ensure healthy cellular homeostasis by eliminating waste and long-lived or damaged cellular constituents. Indeed, autophagy is an augmented cellular protein recycling pathway in some cancer cell death (PCD) type II under certain circumstances. Autophagy has a dual role in cancer, as autophagy help cancer cells survive under nutrient-limiting conditions by recycling protein and protecting cancer cells from cellular damage caused by anti-cancer drugs or ionizing radiation, possibly by removing damaged macromolecules or organelles. Additionally, some anti-cancer therapy typically induces autophagy in proportion to noxious stimuli, and defective or excessive autophagy leads to autophagic cell death (Shintani *et al.*, 2004; Lambert *et al.*, 2008). It would seem that autophagy occurs more under apoptosis-defective conditions (Yousefi *et al*., 2006; Luo *et al*., 2007), and therefore, autophagy after irradiation plays different roles according to the dose of radiation and propensity of cells to undergo apoptosis after lethal damage (Jo *et al.*, 2015). The authors concluded that radiation-induced apoptosis occurs later than autophagy and is caspase-independent, which could explain the results that were obtained during this PhD work as no significant differences were observed between irradiation alone versus irradiation + AGuIX® treatment. Autophagy plays an important role in cancer because of its tumor suppressing and tumor protecting functions (Tam *et al.*, 2017). The phosphatidylinositol-3-kinase (PI3K)-protein kinase B (Akt)-mTOR pathway is one of the most important autophagy signaling pathways in cancer growth and progression (Nagelkerke *et al*., 2015), and as it was discussed in the bibliography review, the PI3Ks, AKT, and mTOR signaling networks are aberrant in HNSCC (Molinolo *et al*., 2009).

Increased autophagic cell-death induced by the combined treatment was an interesting result, as the role of autophagy in radiation therapy is an ongoing debate, as to whether it has a cytoprotective role or a cytotoxic one (Jaboin *et al*., 2007). Autophagy induced by radiation plays a bi-directional effect in the cell's fate decision since survival or death may depend on the severity and duration of the stress (Li *et al*., 2016; Hu *et al*., 2016). When the stress is mild, autophagy can degrade and recycle damaged or unwanted cellular constituents in autophagolysosomal vesicles to provide additional energy supply during stress, which has an essential effect in the quality of control of organelles and cellular adaptation to stress (Ito *et al.*, 2005; Hu *et al.*, 2016). Indeed,

the cytoprotective function of autophagy induced by radiation is considered to reflect the cell's capacity to eliminate toxic species such as free radicals and damaged and unwanted proteins or organelles to generate energy and metabolic precursors (Yang *et al.*, 2015). Although some studies have shown that autophagy enhanced the anticancer effects of radiotherapy on patients affected by oral squamous cell carcinoma and glioblastoma (Wu *et al*., 2014; Saglar *et al*., 2014), other studies have shown that tumor resistance to radiation therapy is linked to the upregulation of autophagy (colon cancer, prostate cancer, glioma, nasopharyngeal, breast cancer) (Sun *et al*., 2015; Yang *et al.*, 2015). These contradictory results therefore call for an ongoing debate on the real role of autophagy in cancer therapy. Cytotoxic autophagy is named autophagic cell death and can be also called type II apoptosis (Gewirtz *et al.*, 2009). Studies have shown that several proteins involved in the DNA damage repair signaling pathways or in the oxidative stress signaling pathways participate in the modulation of autophagy. Reactive oxygen/nitrogen species generated in the context of radiation exposure are essential activators of cytoplasmic signaling cascades such as p38 MAPK, JNK, HIF-1α, which play essential roles in the regulation of autophagy (Liu *et al.*, 2014).

Autophagy is therefore a double-edged sword that can either promote the destruction or the protection of tumor cells, based on the different tumor types and stage, and may interact with current treatment modalities. Figure 110 demonstrates the different outcomes of autophagy on cancer cells.

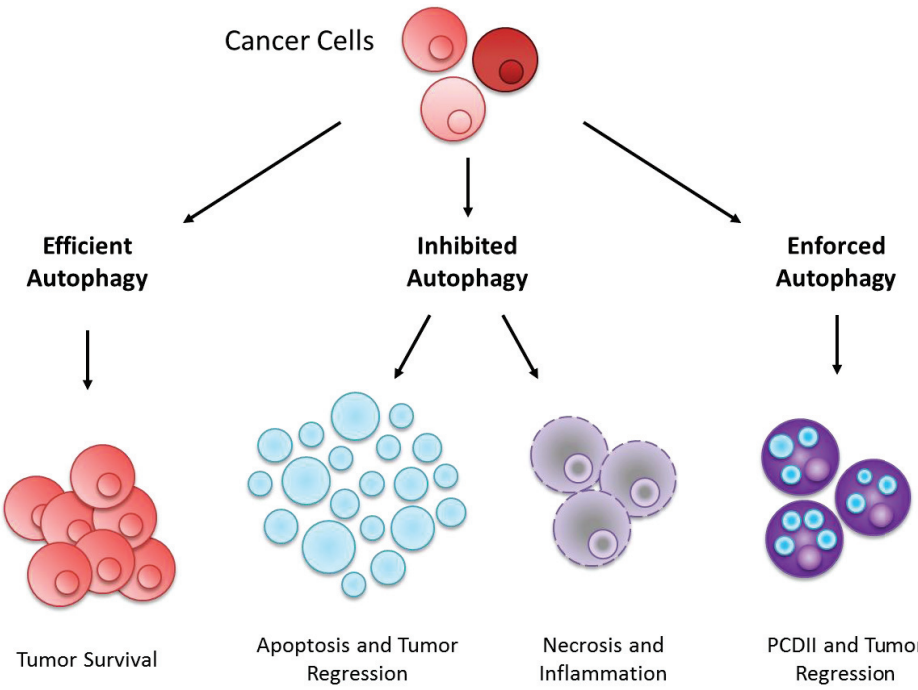


Figure 110: Effects of efficient or deregulated autophagy in cancer development (Inspired from Aredia et al., 2012).

In this work, evidence is presented for an enhancement of autophagy with AGuIX® after radiation. As visualized with fluorescence microscopy, AGuIX® could trigger autophagic cell death or autosis an autophagy-dependent non-apoptotic form of cell death, characterized by unique morphological changes such as focal swelling of the perinuclear space or ER disappearance (Liu and Levine, 2015). However, at this stage of our work, our results do not really allow us to distinguish for sure between cell death accompanied by signs of autophagy (i.e cell death with autophagy) from cell death as a consequence of autophagy (autophagic cell death, such as autosis) (Liu and Levine, 2015). Further exploration of the crosstalk between increased autophagy due to AGuIX® treatment with irradiation should be further studied.

Another interesting fact to note is the potential link that exists between lysosomes and autophagy, as the lysosome has an important role in this process, as shown in Figure 111. Lysosomes are actors of autophagy as these organelles are part of the autophagosome composition, without which, autophagy would not occur. In addition, it has been very recently suggested that one unique and defining aspect of regulated autophagic cell death is the absolute requirement for lysosome membrane permeabilization (LMP) (Karch *et al*., 2017). Although the authors demonstrated the requirement of the Bax/Bak proteins to increase LMP, LMP is known to occur in response to a large variety of stimuli (Johansson *et al*., 2010), among which ROS is one of them (Denamur *et al*., 2011; Oku *et al*., 2017). As AGuIX® were found to be mainly localized in lysosomes, the exposure of cells to radiation led to an increase of ROS, most certainly in lysosomes. Because lysosomes are organelles extremely active in redox reaction and contain significant amounts of transition metals, like iron (Yu *et al*., 2003), ROS produced after exposure of AGuIX® to radiation may form other reactive species such as $HO^{\cdot}$ through the Fenton reaction (Baird *et al*., 2006) which are highly deleterious to lysosomal membranes. Future studies should be designed to address this hypothesis.

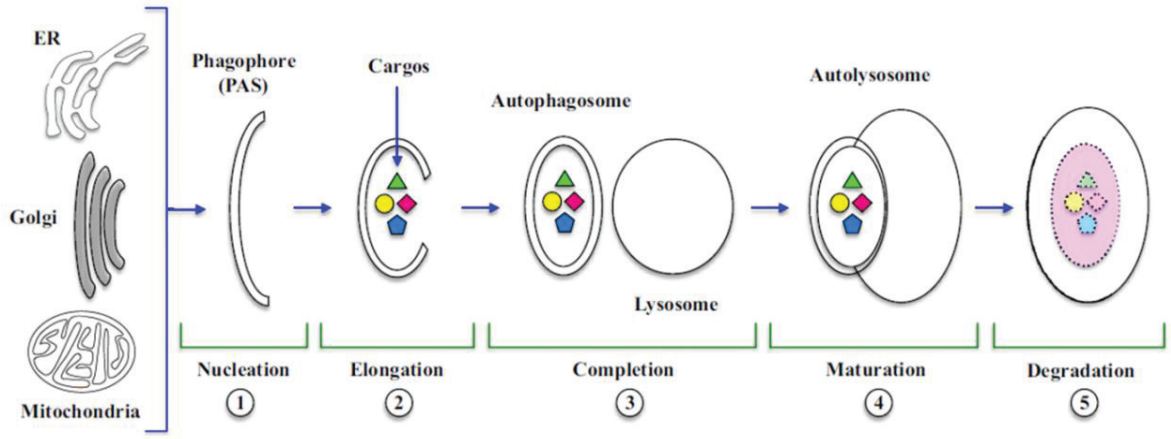


Figure 111: Autophagosome and autolysosome formation (Aredia *et al.*, 2012).

In an effort to understand the effect of AGuIX® at the subcellular level, another question can be asked: is it mandatory to target the nucleus to have a radiosensitizing effect? The ongoing debate as to whether the radiosensitizing effect induced by the combined treatment is DNA-damage dependent or not was studied by several teams working with AGuIX®, as well as other metal-based NPs. Although similar results were found for initial DSBs, results varied for the number of residual foci, 24 hours after irradiation and AGuIX® treatment. Indeed, an increase of residual DSBs, was reported in a melanoma model (Kotb *et al*., 2016) or in in a head and neck cell line (Wozny *et al*., 2017) whereas no increase of DSBs were obtained in glioblastoma cells (Štefančíková *et al*., 2016) under the same experimental conditions. Although the residual DSBs, expressed as the number of cells that still have $\gamma H_2Ax$ foci 24h after the combined treatment was moderately increased in this study, the number of cells displaying more than 50 foci per nucleus, was significantly increased after treatment with AGuIX® when compared to radiation alone. This observation suggests that the treatment with AGuIX® caused a net increase of more complex and lethal DSBs compared to radiation alone, a result which is in perfect accordance with the increase of the α parameter obtained from the clonogenic survival curve assay. All these data strongly underline the large variations in the results obtained, depending on the conditions of treatment used, as well as the cellular type studied. For other metal-based NPs, such as gold NPs, similar contradictory results have been reported. As an example, the use of 1.9 nm gold nanoparticles did not enhance radiation-induced DSBs formation nor inhibit DNA repair in MDA-MB-231 breast cancer cells irradiated with MV electrons (Jain *et al*., 2011), while the combination of 50 nm citrate-coated gold NPs with 6 MV photons resulted in an increase of DSBs in HeLa cells (Chithrani *et al*., 2010; Berbeco *et al*., 2012).

In this study, we demonstrated that AGuIX® were able to radiosensitize SQ20B, an HNSCC cell line, via the induction of intracellular ROS which strengthened the radiation effect. Once taken up by cells, AGuIX® largely accumulated in lysosomes and resulted in the generation of further complex DNA damage. Moreover, autophagy and/or autophagic cell death appeared to mediate the effectiveness of this treatment combination. However, future studies are required to understand the mechanisms linking lysosomes-entrapped AGuIX® with the upregulation of autophagy/autophagic cell death after radiation. There seems to be a strong link between the regulation of ROS, autophagy, and the lysosomal metabolism, with a very fine regulation of these three factors which will make the balance lean to either the side of cell death or cell survival. The end result of radiosensitization using AGuIX® is the result of a combination of pathways, and does not rely on only one mechanism. As discussed, the notion of balance and threshold is very important in the radiosensitizing effect of AGuIX® nanoparticles in HNSCC.

# Conclusion & Perspectives

Head and Neck cancer remains a huge health burden, ranked 6$^{th}$ most common cancer worldwide. This is in particular due to its high radioresistance against which the development of new performing therapeutic sensitizing strategies is needed. By definition, a radiosensitizing agent should increase the radiation dose received by the tumor and increase lethal damages while sparing the healthy tissue in order to avoid recurrence and improve the patients' quality of life. Among the different options of radiosensitizing strategies, high-Z metal nanoparticles have recently been the subject of growing interest. Nanotechnology has been proposed as a novel experimental field since the early 2000s, and gave rise to nanomedicine, with much promise being shown with regards to a potential transition into clinical practice.

In this study, we have used a novel formulation of gadolinium-based nanoparticles, named AGuIX®, as a potential radiosensitizing agent on an *in vitro* HNSCC radioresistant cell line model, SQ20B J.L. The first aim of this study was to determine the best radiosensitizing conditions of AGuIX® in this model, and to characterize them in terms of potential toxicity, and to look for their cellular localization once internalized. We successfully demonstrated that radiosensitization occurred in SQ20B J.L. cells when treated with 0.8 mM Gd for 24 hours in serum-free DMEM-Glutamax. This concentration and time of incubation resulted in a $SF_{4Gy}$ of 1.382 and a 50% Enhanced Biological Factor (EBR) of 1.4. Internalized AGuIX® nanoparticles amounted to about 0.11 pg of Gd per cell, as measured by ICP-AES, and were demonstrated by confocal microscopy to mostly co-localize with lysosomes but not with the nucleus nor the mitochondria. Toxicity assays showed that the treatment did not induce any toxicity to SQ20B J.L. cells in the absence of ionizing irradiation, whether at the cellular or the mitochondrial level.

The second aim of this work was to understand the mechanisms through which the radiosensitizing effects of SQ20B J.L. cells with AGuIX® could occur. Indeed, one main question remains in the field of radiosensitization by nanoparticles: what links exist between the physical, chemical, and biological phases? To answer these questions, we firstly investigated the involvement of the oxidative stress potentially resulting from the combination of AGuIX® to radiation therapy. Secondly, the different types of radiation-induced cell death pathways were investigated to bring an explanation of what was obtained with the clonogenic survival assay. Thirdly, DNA-damage and repair were measured after the combined treatment, as DNA is known to be the primary target of radiotherapy.

The increase in cytosolic and mitochondrial ROS was minimal when cells were treated with AGuIX® prior to irradiation. As radioresistant cells are most of the time overprotected against oxidative stress (as previously demonstrated in our lab for SQ20B J.L. cells), which in part explains their radioresistance capacities, we used a pharmacological approach (DMF + BSO) to deplete the cells from their high endogenous reduced glutathione content, four hours prior to irradiation and after AGuIX® treatment. Under these experimental conditions, a clear increase in cROS right after

irradiation occurred, reinforced by the prior treatment with AGuIX® before irradiation. This phenomenon is observed again, one and four-hours post-irradiation. In terms of mROS, a significant increase was observed immediately after irradiation which was not maintained over time. This should be explained by the fact that AGuIX® do not co-localize with mitochondria, the initial burst probably resulting from water radiolysis products. After glutathione depletion, the amount of ROS was significantly increased which had an impact on the clonogenic survival curve, with the 50% EBR increasing from 1.281 to 1.571. Altogether, these results strongly suggested that the initial effect of AGuIX® was in part subdued by the endogenous high level of antioxidant defenses of SQ20B J.L. cells. In view of the results obtained and with regards to the involvement of oxidative stress in the radiosensitization process, a simultaneous antioxidant treatment with AGuIX® and radiation should perhaps be evaluated *in vivo* to improve this radiosensitizing strategy. However, this should be done with extreme caution since we may keep in mind that antioxidant activity can have divergent effects on cancer cells depending on the cellular context.

Concerning mitochondria, no significant differences were observed after the combined treatment *versus* radiation alone, either through the loss of the mitochondrial membrane potential or the amount of mROS generated. Another functional test was the measurement of the common deletion of mtDNA, an early oxidative stress marker for which an increase was obtained, 72 hours after a 4 Gy irradiation.

Apoptosis, necrosis, mitotic catastrophe, senescence, and autophagy are classically the five types of cell deaths involved after radiation exposure. Our results showed that apoptosis, necrosis, mitotic catastrophe, and senescence remained unchanged after the combined treatment compared to radiation alone. Autophagy/autophagic cell death was the only cell death pathway that was specifically triggered after the treatment with AGuIX® before radiation. This result is intriguing, as autophagy is a double-edged sword in radiotherapy and cancer in general, with cytotoxic as well as cytoprotective roles. Further investigations should be undertaken for a better understanding of this finding.

Considering DNA damage, although no differences were noted for the amount of initial double strand breaks (DSBs), *i.e* 30 minutes after a 2Gy irradiation, a significant increase of residual complex DSBs was obtained after the combined treatment as evidenced by the number of cells displaying more than 50 foci/nucleus which was significantly increased after AGuIX® treatment compared to radiation alone (45 nuclei with 50 or more foci/nucleus versus 23 nuclei with 50 or more foci/nucleus). These results confirm those obtained through the clonogenic survival curve (see the increase of the α parameter) namely that AGuIX® treatment results in the persistence of more complex and lethal DSBs compared to radiation alone.

In order to investigate more deeply how radiosensitization via AGuIX® could occur, a preliminary proteomic approach was initiated in order to highlight some subcellular targets

potentially involved. After setting a selective cut-off, this approach allowed us to highlight 16 proteins that were at least 5 times over- or under-expressed when SQ20B J.L. cells were treated with AGuIX®. Among these, the ribonucleoside-diphosphate reductase (RNR) also known as **ribonucleoside diphosphate reductase** (rNDP) caught our attention because it is an enzyme that catalyzes the formation of deoxyribonucleotides from ribonucleotides and that play a fundamental role in the maintenance of a constant deoxyribonucleotides cellular content for cell division and DNA repair. Moreover, this protein has already been suggested as a promising prognostic and predictive biomarker in many different types of cancer: generally, its over-expression is attributed to a bad prognosis (increase of drug resistance, increase in angiogenic and invasive potential of cancer cells). Therefore, its under-expression after AGuIX® + radiation, could be a hypothesis to explain how AGuIX® combined to radiation can radiosensitize SQ20B J.L. cells. Confirmation of these results by Western blotting experiments is currently under investigation.

To summarize the results obtained during the course of this study, we can state the following: we have demonstrated that the new formulation of AGuIX® designed with DOTA as a chelating agent are able to radiosensitize SQ20B J.L., an HNSCC cell line, via the induction of intracellular ROS which strengthens the radiation effect. Once taken up by cells, AGuIX® largely accumulated in lysosomes and resulted in the generation of complex DNA damage. Moreover, autophagy and/or autophagic cell death appears to mediate the effectiveness of this treatment combination. The proteomic analysis allowed the isolation of a potential target with great promise, the ribonucleoside-diphosphate reductase. It clearly seems that the radiosensitizing effect observed results from a combination of events.

The results obtained during this PhD thesis are summarized in the figure below. However, future studies are required to understand the mechanisms linking lysosomes-entrapped AGuIX® with the upregulation of autophagy/autophagic cell death after radiation. It clearly seems that the effect observed results from a combination of events leading to the radiosensitization of HNSCC and certainly not only via one mechanism. These results should also be confirmed in other radioresistant HNSCC cell lines before *in vivo* studies. The proteomic study should also be strengthened by taking into account the other over- and under-expressed proteins in this radiosensitizing protocol.

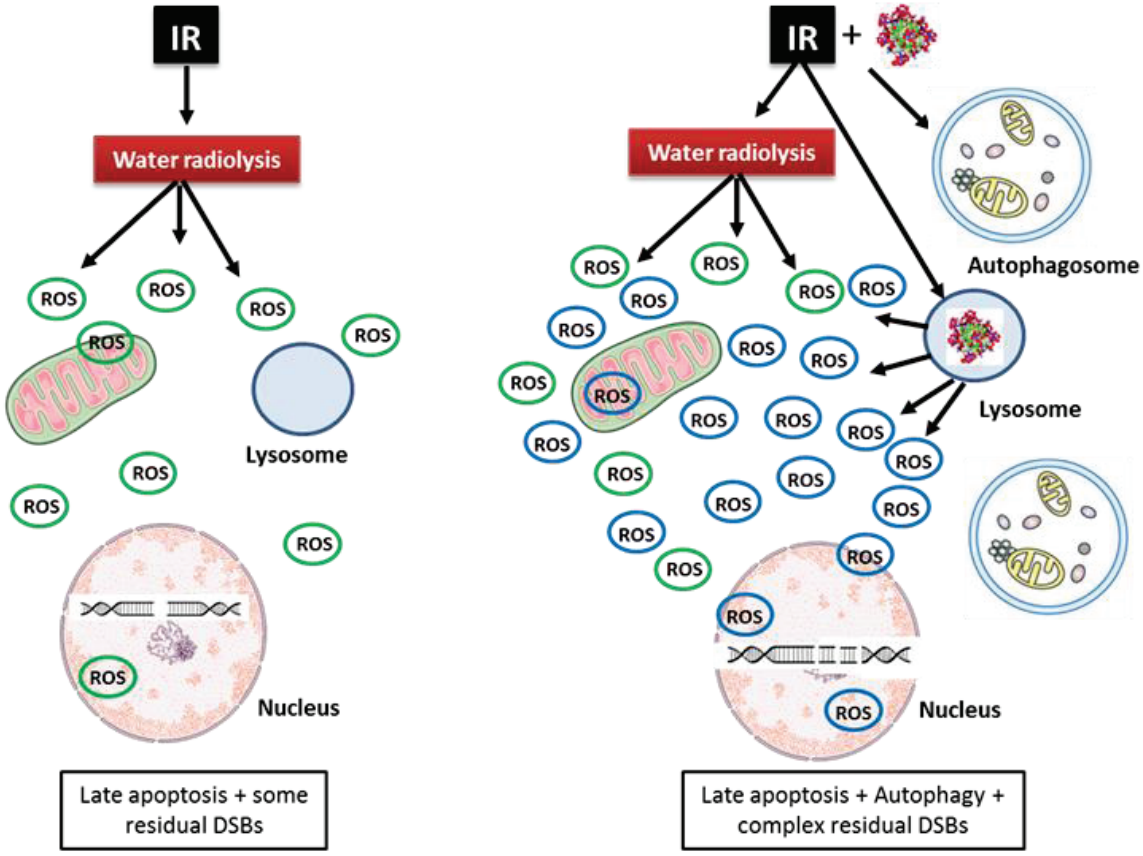


Figure 112: Schematic representations of results obtained following irradiation versus irradiation + AGuIX® treatment.

Although there are still many questions remaining unclear and needing further investigation, this PhD shed, at least some light, into the potential mechanisms involved in the radiosensitization of SQ20B J.L. by AGuIX® nanoparticles, an essential step to move towards more clinical trials.

# Résumé Français

## Introduction

Les cancers des Voies Aérodigestives Supérieures (VADS) représentent un souci majeur de santé, classés au 6$^{eme}$ rang par ordre de fréquence. Près de 600 000 nouveaux cas sont diagnostiqués par an, et ceux-ci sont responsables de 350 000 morts au niveau mondial. Leurs taux de survie à 5 ans est inférieur à 50% : ce faible taux est dû à leur radioresistance intrinsèque et leur forte probabilité de récurrence. La majorité des cas de ces cancers représente des carcinomes de cellules squameuses et regroupe l'ensemble des cancers de la cavité buccale, l'oropharynx, hypopharynx ainsi que les sinus de la face. Les principaux facteurs de risques de ces cancers incluent notamment le tabac, l'alcool, et plus récemment, l'infection par le virus HPV (Human Papilloma Virus) a été identifié comme cause. Les traitements en vigueur incluent la chimiothérapie, la radiothérapie, ou la chirurgie, ou une combinaison entre ces différents traitements. Le choix du traitement dépendra de la phase à laquelle le patient est diagnostiqué (Stade I/II *versus* stades plus avancés du cancer). Les avancées récentes visent donc le développement de stratégies radiosensibilisantes, les nanotechnologies représentant actuellement un axe de recherche prometteur.

Parmi ces nanotechnologies, l'utilisation de nanoparticules comme agent radiosensibilisant est très étudié, du fait de leurs très intéressantes propriétés physico-chimiques. Tout d'abord, leur petite taille et leur rapport surface/volume permettent d'augmenter la dose d'irradiation reçue par les cellules tumorales tout en épargnant les tissus sains avoisinants. Au cours de ce travail, nous avons utilisé des nanoparticules à base de gadolinium, les AGuIX®, qui sont composées d'un squelette de silice, avec des fonctions amine ($NH_2$) sur lesquelles sont greffées des ions de gadolinium avec une molécule hautement chélatrice, le DOTAGA. Elles possèdent de multiples propriétés, essentielles pour être utilisées comme agent radiosensibilisant : une petite taille (entre 2-5 nm de diamètre hydrodynamique), une stabilité colloïdale élevée, une bonne chélation du gadolinium, une absence de toxicité *in vivo* ainsi qu'une excellente excrétion rénale. De plus, ces nanoparticules sont biocompatibles et peuvent être injectées par voie intra-veineuse. Leur petite taille devrait optimiser leur pouvoir radiosensibilisant par un effet EPR élevé, ce qui permet d'augmenter la dose locale dans la tumeur tout en épargnant le tissu sain. De plus, les AGuIX® peuvent être utilisées en tant qu'agent de contraste pour l'IRM, ce qui en fait un excellent agent théranostique (utilisation pour le diagnostic et la thérapie). L'hypothèse mécanistique sur laquelle se base l'effet radiosensibilisant des nanoparticules à base de Z élevé est la suivante : les AGuIX® étant composées de nombreux atomes de gadolinium, entre 7 et 10 par nanoparticules, l'irradiation devrait entraîner une surproduction d'électrons secondaires ainsi que des cascades d'électrons Auger, et donc un dépôt dose locale très élevé (de l'ordre de centaines de Gray) à proximité des AGuIX®. Ceci se traduit ensuite par une forte augmentation des radicaux libres oxygénés (RLO), qui exerceront leur effet délétère sur de multiples cibles subcellulaires (protéines, lipides, ADN …) avec pour conséquence l'activation de diverses voies

de mort cellulaires. Cette hypothèse se base pour l'instant essentiellement sur des résultats obtenus à l'aide de modèles théoriques et il est donc important de les valider tout d'abord sur des modèles cellulaires tumoraux. Le but de cette thèse a donc été est donc de démontrer l'efficacité des AGuIX® en tant qu'agent radiosensibilisant dans les cancers des VADS tout en essayant de comprendre les mécanismes de réponse de la cellule à ce traitement.

Ce travail a été réalisé sur une lignée cellulaire des cancers des VADS radiorésistante ($SF_{2Gy}$= 0.72), les SQ20B J.L. Les nanoparticules utilisées sont donc les AGuIX®, et un irradiateur X-Rad 320 (Energie : 250 kV, 2Gy/min, intensité : 15 mA) pour l'irradiation photonique a été utilisé. Ce travail a été divisé en quatre parties. La première a consisté à déterminer et valider sur notre modèle les conditions expérimentales optimales de radiosensibilisation par les AGuIX® et de préciser leur localisation subcellulaire après internalisation. Dans la suivante, nous avons voulu vérifier sur ce modèle cellulaire si le traitement combiné génère effectivement une surproduction de RLO, ceci à l'échelle de la mitochondrie mais également de la cellule entière. Une optimisation du traitement combiné AGuIX®/irradiation a également été testée, la lignée résistante SQ20B étant particulièrement bien protégée contre le stress oxydant. Ensuite, nous avons recherché si un type de mort cellulaire radio-induite apoptose, nécrose, catastrophe mitotique, senescence, ou autophagie) était augmenté ou bien spécifiquement déclenché par le traitement combiné. Comme conséquences de l'irradiation, différents dommages de l'ADN ont été étudiés et quantifiés : les cassures simples brins, les dommages oxydatifs (mesure de la 8-oxo-guanine) ainsi que les cassures doubles brins qui sont les cassures les plus létales. Enfin, une approche préliminaire de protéomique a été initiée afin d'identifier des cibles moléculaires potentielles impliquées dans cette radiosensibilisation.

Les résultats obtenus sont divisés en cinq chapitres, avec des explications condensées qui sont accompagnés, pour certains chapitres, par une figure récapitulative des résultats majeurs obtenus.

**<u>Chapitre I</u> : Caractérisation de l'effet radiosensibilisant des AGuIX®**

Après avoir testé différents temps d'incubation et différentes concentrations d'AGuIX®, un traitement des cellules SQ20B avec à une concentration de 0.8 mM de Gd pendant 24 heures s'est révélé être celui donnant l'effet radiosensibilisant le plus satisfaisant. De plus, en absence d'irradiation, les AGuIX® ne sont pas toxiques, ni à l'échelle cellulaire, ni à l'échelle mitochondriale. Une fois internalisées, les AGuIX® sont presque exclusivement localisées dans les lysosomes ; aucune colocalisation avec le noyau ou bien les mitochondries n'ayant été observée par microscopie confocale. Ces résultats sont représentés dans la Figure 114 ci-dessous.

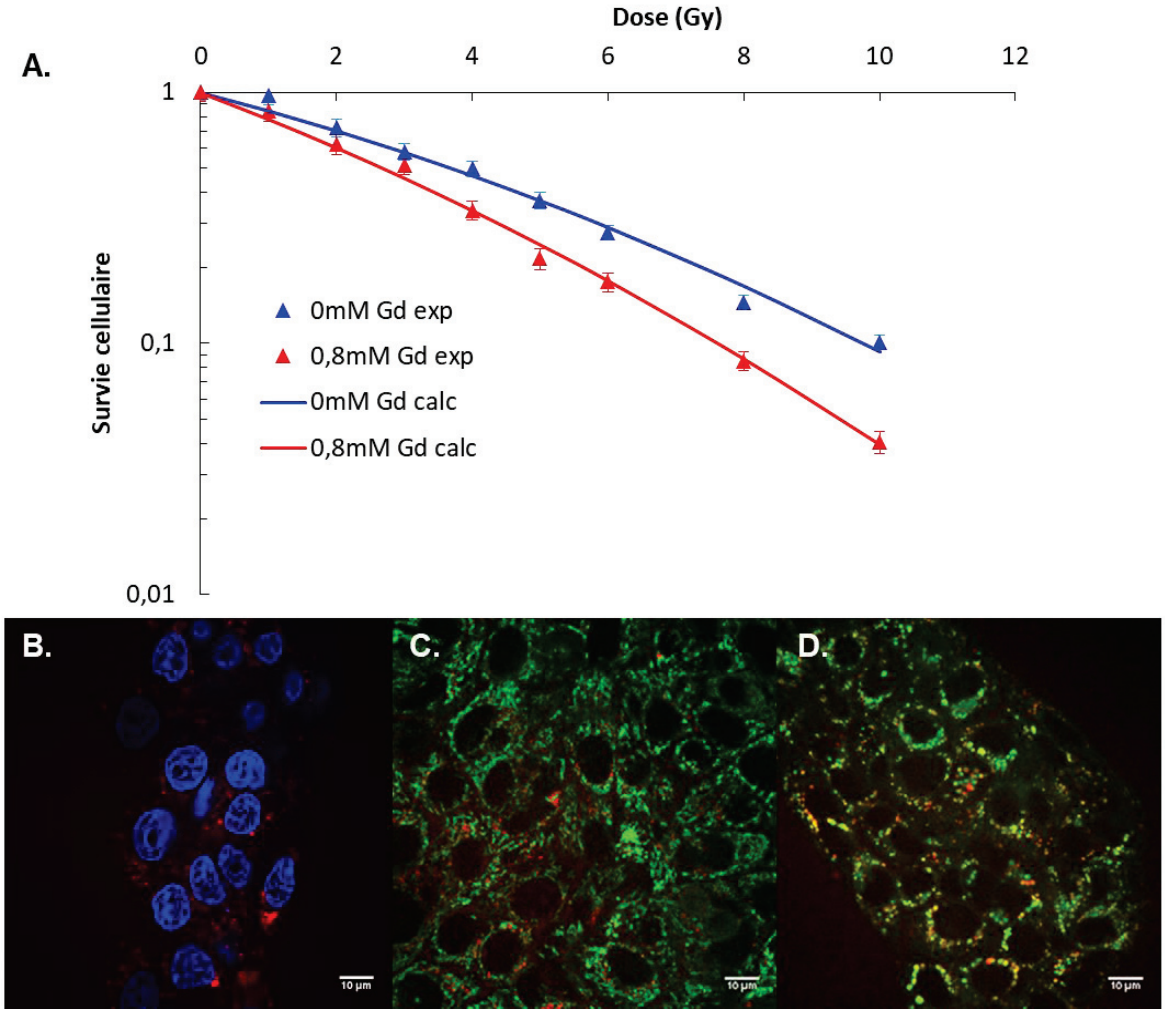


Figure 113: Effet radiosensibilisant des AGuIX® et leurs localisations subcellulaires. **A.** Courbe de survie clonogénique des SQ20B J.L. 0-10 Gy suite à un traitement de 0.8mM Gd pendant 24h dans du DMEM-Glutamax sans sérum de veau fœtal. (Bleu : 0mM Gd ; rouge : 0.8 mM Gd) ; **B-D** : Internalisation des AGuIX®-Cya5.5 (rouge) en microscopie confocal de fluorescence, 60X par rapport aux **B.** noyaux (DAPI : bleue) ; **C.** mitochondries (Mitotracker-Vert) ; et **D.** lysosomes (Lysotracker-Vert). Ces images sont représentatives de plus de 200 cellules.

**Chapitre II : Etude du stress oxydant induit par le traitement combiné AGuIX® + I.R. et ses conséquences fonctionnelles sur l'activité mitochondriale.**

Une étude cinétique des radicaux libres oxygénées (RLO) cytosoliques (RLOc) et mitochondriaux (RLO)m a ensuite été réalisée après une irradiation à 10Gy pour vérifier si l'hypothèse mécanistique évoquée précédemment au cours des études théoriques permettait d'expliquer l'effet radiosensibilisant, ou son déclenchement, obtenu après traitement par les AGuIX®. Nous avons montré que la différence entre l'irradiation seul et le traitement combiné (AGuIX® + irradiation) était minime à la fois pour les RLOc et RLOm. Ces résultats nous ont surpris,

compte-tenu de l'effet radiosensibilisant obtenu. Cependant, il est bien connu que les cellules cancéreuses radiorésistantes sont le plus souvent très bien protégées par un équipement anti-oxydant très performant qui leur permet de détoxifier tout ou partie des RLO radio-induits. En ce sens, une étude, faite préalablement au sein du laboratoire, avait démontré que les cellules SQ20B possède un taux endogène de glutathion très élevé. A l'aide d'un traitement pharmacologique (association DMF + BSO) permettant de dépléter la cellule de son contenu en glutathion après traitement avec les nanoparticules, 4 heures avant irradiation. Une étude cinétique de la production de RLO à des temps courts, de 0 minute à 4 heures, puis plus longs jusqu'à 72 heures, a ensuite été réalisée. Dans ces conditions, nous avons mettre en évidence une nette augmentation des RLOc a été observée juste après irradiation, augmentation encore plus nette avec le après pré-traitement par les AGuIX®. Après diminution une deuxième vague de RLOc apparait une heure et quatre heures après irradiation. Concernant les RLOm, l'augmentation est nette, tout de suite après irradiation mais aucune différence n'a été obtenue entre l'irradiation seule et le traitement combiné. Cela vient probablement du fait que les nanoparticules ne sont pas internalisées par les mitochondries, les RLO mesurés provenant uniquement de la radiolyse de l'eau. Grâce à ses expériences de déplétion, nous pouvons donc conclure, que les RLO jouent bien un rôle dans la radiosensibilisation observée, celle-ci étant minimisée dans la cellule en conditions basales, du fait de ses défenses antioxydantes élevées. Une courbe de survie cellulaire clonogénique a été faite après déplétion en glutathion : les résultats montrent que, le 50% EBR passe de 1.281 à 1.571. Les résultats obtenus pour les RLOc sont représentés dans la Figure 115.

Les tests fonctionnels mitochondriales n'ont montré aucun changement significatif entre irradiation seule et AGuIX® + irradiation, comme en témoigne la chute du potentiel membranaire mitochondrial obtenue après irradiation Par contre, en ce qui concerne la délétion commune de l'ADN mitochondrial, 72 heures après une irradiation de 4Gy, le ratio ADNmt délété/ADNmt total a augmenté de 2.93, ce qui est une différence significative entre l'irradiation seule et le traitement combiné. Ce résultat est donc un élément supplémentaire confirmant l'implication des RLO dans l'effet radiosensibilisant des AGuIX®.

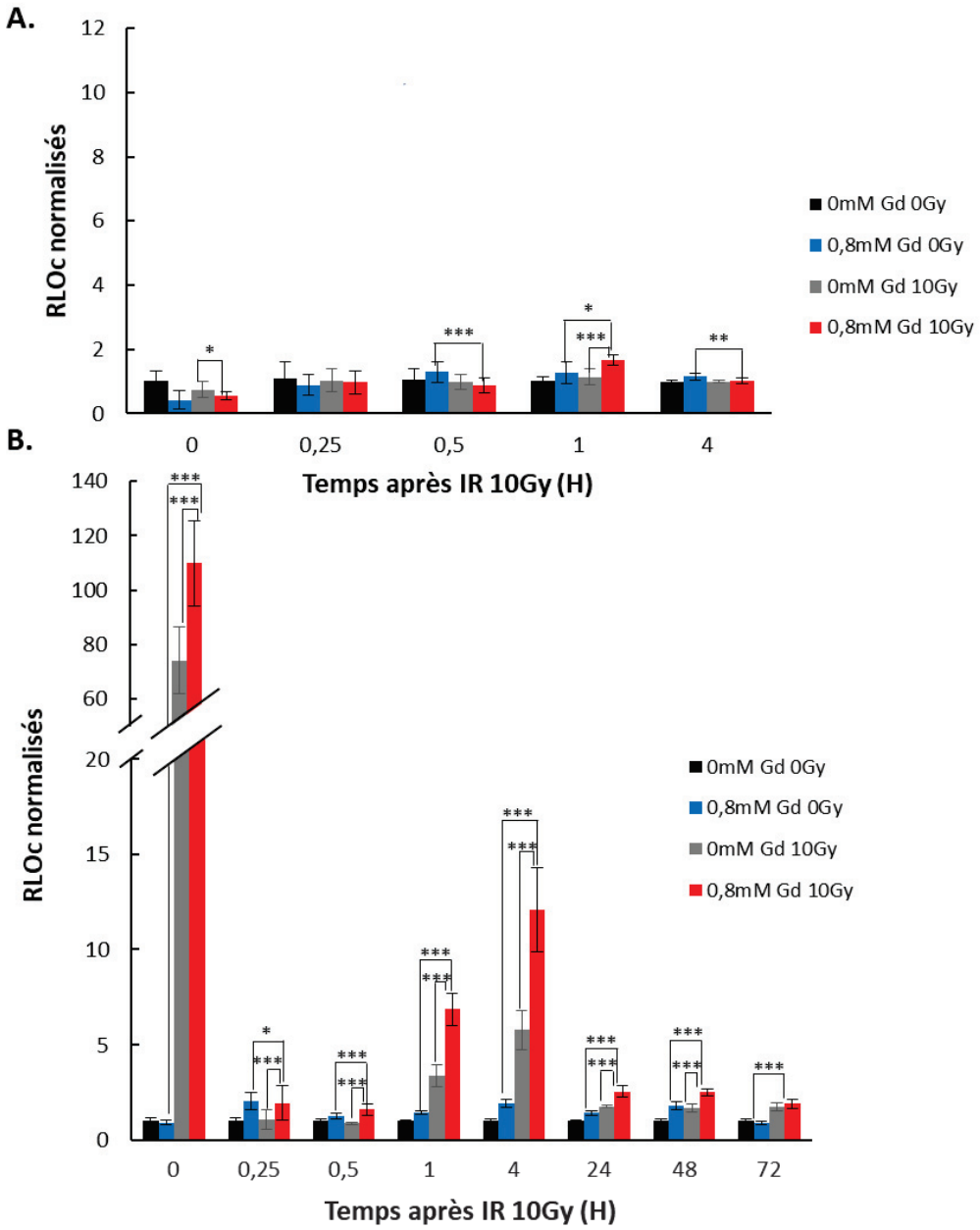


Figure 114: Etude cinétique (0-72h) des RLO cytosolique (RLOc) mesurée en cyrtométrie de flux (LSRII flow cytometer, BD Biosciences) en utilisant la sonde CM-$H_2$DCFA, normalisée par rapport aux cellules non-traitées et non-irradiées. **A.** Sans déplétion de glutathion. **B.** Avec déplétion de glutathion.

**Chapitre III : Etude des différents types de mort cellulaires radio-induites par le traitement combiné AGuIX® + I.R.**

Comme il a été démontré avec la courbe de survie clonogénique, le traitement des SQ20B J.L. avec les nanoparticules AGuIX® combiné à l'irradiation photonique augmente la mort des cellules SQ20B, dont le type était à préciser. Cinq types de morts radio-induites ont été étudiés au cours

de cette thèse : l'apoptose, la nécrose, la catastrophe mitotique, la senescence, et enfin l'autophagie. Aucune différence significative n'a été trouvée entre l'irradiation seule et le traitement combiné pour ces différents types de mort à **l'exception de l'autophagie**. Nous avons donc démontré que le traitement par les AGuIX® avant irradiation augmente de façon spécifique l'autophagie et/ou la mort cellulaire autophagique. La Figure 116 illustre ce résultat (quantification du Western Blot du LC3B et confirmation par microscopie confocale).

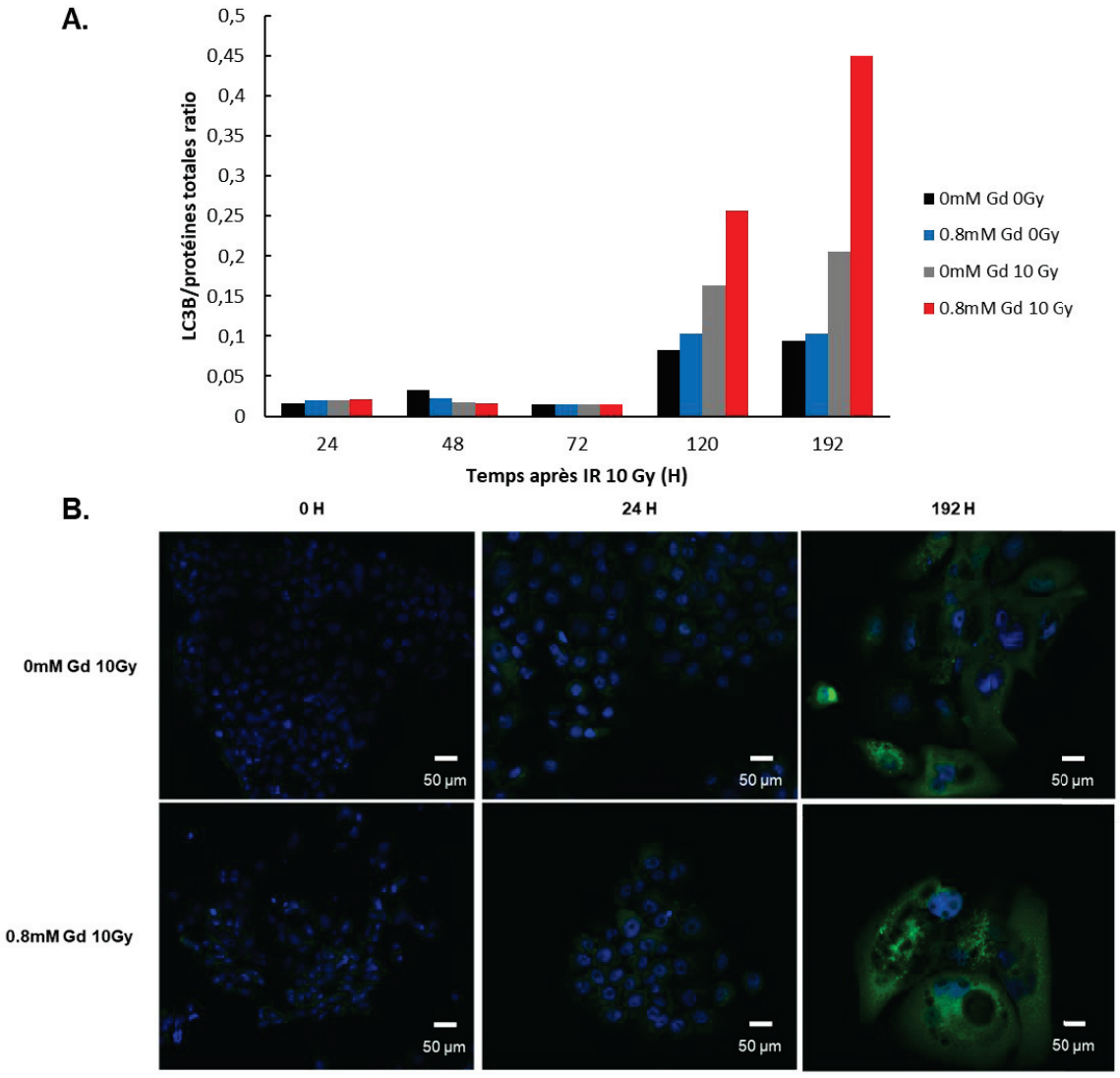


Figure 115: Augmentation de la mort cellulaire par autophagie suite au traitement combiné (AGuIX® + irradiation). **A.** Quantification par Western Blot de l'expression de LC3B en fonction des protéines totales de 24 à 192 heures après une irradiation de 10Gy. **B.** Photo de microscopie, a 10X, 10 Gy *versus* 10 Gy + 0.8mM Gd 0, 24, et 192 après irradiation. (Bleu : DAPI ; Vert : LC3B-Alexa Fluor 488).

**<u>Chapitre IV</u> : Etude des dommages induit à l'ADN par les AGuIX® combinées à l'irradiation.**

Au cours de cette thèse, plusieurs dommages radio-induits ont été étudiés : les cassures simples brins, les dommages oxydatifs (8-oxo-guanine, de façon qualitative avec le test des comets + FPG et de façon quantitative en HPLC MS/MS) ainsi que les cassures double-brins. En ce qui concerne les cassures simple-brin, aucune différence entre l'irradiation seul et le traitement combiné n'a été relevée. Pour la mesure des 8-oxo-guanines, alors qu'une augmentation de ces dernières avaient été mise en évidence avec l'enzyme FPG, nous n'avons valider quantitativement ces résultats par HPLC-MS. Enfin, en ce qui concerne les cassures double-brins, aucune différence n'a été obtenue pour les cassures initiales (T=30 min). Pour les cassures résiduelles à 24h, une augmentation importante des CDBs résiduelles complexes (présentant plus de 50 foci par noyau) a été observée après pré-traitement par les AGuIX®, un résultat parfaitement corrélé avec l'augmentation du paramètre α obtenu par la courbe de survie clonogénique. Ces résultats sont représentés dans la Figure 117B.

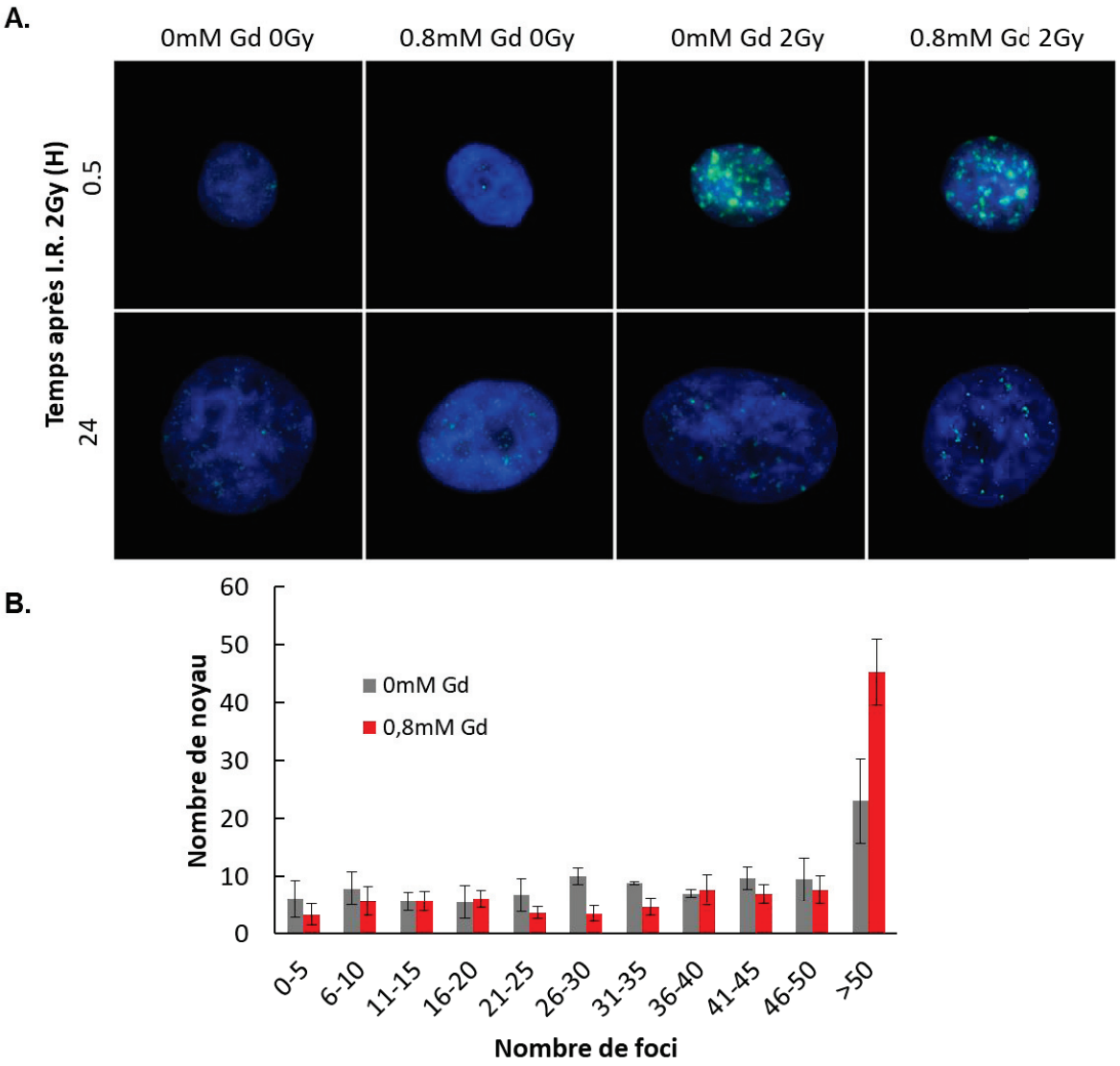


Figure 116: Mesure des cassures doubles brins de l'ADN (γH2Ax). **A.** Image représentative des CDBs suite aux différents traitements, bleu : noyau (DAPI), vert : γH2Ax. **B.** Quantification du nombre de CDBs complexes résiduelles (24h après irradiation), suite à 2Gy, 0 (gris) vs. 0.8 mM Gd, exprimée en fonction du nombre de noyau contenant x nombre de foci.

**Chapitre V : Etude Protéomique- expériences préliminaires**

L'étude protéomique, quoique préliminaire, s'est révélée montrée très informative. Selon le cut-off choisi, et avec les outils de bio-informatiques, plusieurs voies de signalisation se sont révélées comme étant potentiellement modulées après traitement par les AGuIX® et l'irradiation. Une des voies avec plusieurs protéines impliquées (sur- ou sous-expression de 20%) concerne le métabolisme cellulaire. En outre, 72 protéines mitochondriales et 39 protéines impliquées dans les défenses antioxydantes ont été modulées. Avec un cut-off beaucoup plus sélectif (facteur

minimum de 5), l'étude a permis de mettre en évidence 16 protéines différentiellement exprimées après traitement combiné. Parmi elles, une a retenu notre attention : la ribonucléotide réductase qui est significativement sous-exprimée dans nos conditions expérimentales. En effet, la surexpression de cette protéine est connue comme étant la plupart du temps liée à un mauvais pronostic, ceci dans de nombreux cancers. Du fait de sa fonction biologique, à savoir la fourniture de désoxyribonucléotides pour la synthèse et/ou la réparation de l'ADN, sa sous-expression suite au traitement combiné serait une piste permettant de mieux comprendre la radiosensibilisation par les AGuIX®.

**Conclusion**

L'utilisation de nanoparticules AGuIX® en tant qu'agent radiosensibilisant a été démontrée et validée sur une lignée radiorésistance des cancers VADS, les SQ20B. Cette effet radiosensibilisant est le résultat d'une induction de RLO qui a renforcé l'effet de l'irradiation. Les AGuIX® internalisées sont localisées majoritairement dans les lysosomes et l'effet combiné du traitement des AGuIX® avec l'irradiation a induit des cassures double brins de l'ADN résiduelles et plus complexes. L'autophagie et/ou la mort autophagique expliquerait l'augmentation de l'effet délétère de l'irradiation induit par les AGuIX®. Le lien entre l'internalisation des AGuIX® dans les lysosomes et le déclenchement de la mort par autophagie sera la prochaine étape dans la compréhension des résultats déjà obtenus. De plus, l'étude protéomique initiée au cours cette étude, a permis d'isoler une protéine en particulier, la ribonucléotide réductase, qui semblerait jouer un rôle important dans la radiosensibilisation des AGuIX® dans les cancers des VADS. La confirmation des résultats obtenus par d'autres méthodes (WB) constitue également un axe majeur dans la poursuite de ce travail.

# Bibliography References

# A

Alarifi S, Ali H, Alkahtani S, Alessia MS. Regulation of apoptosis through bcl-2/bax proteins expression and DNA damage by nano-sized gadolinium oxide. *Int J Nanomedicine* 2017;**12**:4541–51.

Alevizos I, Mahadevappa M, Zhang X, Ohyama H, Kohno Y, Posner M, *et al*. Oral cancer in vivo gene expression profiling assisted by laser capture microdissection and microarray analysis. *Oncogene* 2001;**20**:6196-204.

Alexeyev M, Shokolenko I, Wilson G, Ledoux S. The maintenance of mitochondrial DNA integrity—critical analysis and update. *Cold Spring Harb Perspect Biol* 2013;**5**:a012641.

Alphonse G, Aloy MT, Broquet P, Gerard JP, Louisot P, Rousson R, et al. Ceramide induces activation of the mitochondrial/caspases pathway in Jurkat and SCC61 cells sensitive to gamma-radiation but activation of this sequence is defective in radioresistant SQ20B cells. *Int J Radiat Biol* 2002;**78**:821-35.

Alphonse G, Bionda C, Aloy MT, Ardail D, Rousson R, Rodriguez-Lafrasse C. Overcoming resistance to gamma-rays in squamous carcinoma cells by poly-drug elevation of ceramide levels. *Oncogene* 2004;**23**:2703-15.

Alphonse G, Maalouf M, Battiston-Montagne P, Ardail D, Beuve M, Rousson R, *et al*. p53-independent early and late apoptosis mediated by ceramde after exposure of tumor cells to photon or carbon ion irradiation. *BMC Cancer* 2013;**13**:151.

Al-Sarraf M. Chemotherapeutic management of head and neck cancer. *Cancer Metast Rev* 1987;**6**:191-8.

Ames BN, Shigenaga MK, Gold LS. DNA lesions, inducible DNA repair, and cell division: three key factors in mutagenesis and carcinogenesis. *Environ Health Perspect* 1993;**101** Suppl 5:35-44.

Andtbacka RHI, Collichio FA, Amatruda T, Senzer NN, Chesney J, Delman KA, et al. OPTiM : a randomized phase III trial of talimogene laherparepvec (T-VEC) versus subcutaneous (SC) granulocyte-macrophage colony-stimulating factor (GM-CSF) for the treatment (tx) of unresected stage IIIB/C and IV melanoma. *J Clin Oncol* 2013;**31**.

Ang KK, Berkey BA, Tu X, Zhang HZ, Katz R, Hammond EH, *et al*. Impact of epidermal growth factor receptor expression on survival and pattern of relapse in patients with advanced head and neck carcinoma. *Cancer Res* 2002;**62**:7350-6.

Ang KK, Zhang Q, Rosenthal DI, Nguyen-Tan PF, Sherman EJ, Weber RS, *et al*. Randomized phase III trial of concurrent accelerated radiation plus cisplatin with or without cetuximab for stage III to IV head and neck carcinoma: RTOG 0522. *J Clin Oncol* 2014;**32**:2940-2950.

Aredia F, Guaman Ortiz LM, Giansanti V, Scovassi AI. Autophagy and Cancer. *Cells* 2012;**1**:520-34.

Armand JP, Couteau C. Chemotherapy in head and neck cancer. *Eur J Cancer* 1995 ;**31**:819-22.

Azzam EI, Jay-Gerin JP, Pain D. Ionizing radiation-induced metabolic oxidative stress and prolonged cell injury. *Cancer Lett* 2012;**327**:48–60.

## B

Baird SK, Kurz T, Brunk UT. Metallothionein protects against oxidative stress induced lysosomal destabilization. *Biochem J* 2006;**394**:275–83.

Barazzuol L, Jeynes JC, Merchant MJ, Wéra AC, Barry MA, Kirkby KJ, *et al*. Radiosensitization of glioblastoma cells using a histone deacetylase inhibitor (SAHA) comparing carbon ions with X-rays. *Int J Radiat Biol* 2015;**91**:90-8.

Barenholz Y. Doxil®—the first FDA-approved nano-drug: lessons learned. *J Control Release* 2012;**160**:117–34.

Barton KL, Misuraca K, Cordero F, Dobrikova E, Min HD, Gromeier M, Kirsch DG, *et al*. PD-0332991, a CDK4/6 inhibitor, significantly prolongs survival in a genetically engineered mouse model of brainstem glioma. *PLoS ONE* 2013;**8**:e77639.

Baskar R *et al*. Cancer and radiation therapy: current advances and future directions. *Int J Med Sci* 2012;**9**:193-9.

Belcaid Z, Phallen JA, Zeng J, See AP, Mathios D, Gottschalk C, *et al*. Focal radiation therapy combined with 4-1BB activation and CTLA-4 blockade yields long-term survival and a protective antigen-specific memory response in a murine glioma model. *PLoS One* 2014;**9**:e101764.

Berbeco RI, Korideck H, Ngwa W, Kumar R, Patel J, Sridhar S, *et al*. DNA damage enhancement from gold nanoparticles for clinical MV photon beams. *Radiat Res* 2012;**178**:604-8.

Berghauser Pont LM, Spoor JK, Venkatesan S, Swagemakers S, Kloezeman JJ, Dirven CM, *et al*. The Bcl-2 inhibitor Obatoclax overcomes resistance to histone deacetylase inhibitors SAHA and LBH589 as radiosensitizers in patient-derived glioblastoma stem-like cells. *Genes Cancer* 2014;**5**:445-59.

Bergs JW, Wacker MG, Hehlgans S, Piiper A, Multhoff G, Rödel G, et al. The role of recent nanotechnology in enhancing the efficacy of radiation therapy. *Biochim Biophys Acta* 2015;**1856**:130-43.

Bernier J, Domenge C, Ozsahin M, Matuszewska K, Lefèbvre JL, Greiner RH, *et al*. Postoperative irradiation with or without concomitant chemotherapy for locally advanced head and neck cancer. *N Engl J Med* 2004;**350**:1945-52.

Berroud A, Le Roy A, Voisin P. Membrane oxidative damage induced by ionizing radiation detected by fluorescence polarization. *Radiat Environ Biophys* 1996;**35**:289-95.

Bertrand G, Maalouf M, Boivin A, Battiston-Montagne P, Beuve M, Levy A, *et al*. Targeting head and neck cancer stem cells to overcome resistance to photon and carbon ion radiation. *Stem Cell Rev* 2014;**10**:114-26.

Beuve M, Alphonse G, Maalouf M, Colliaux A, Battiston-Montagne P, Jalade P, et al. Radiobiologic parameters and local effect model predictions for head-and-neck squamous cell carcinomas exposed to high linear energy transfer ions. *Int J Radiat Oncol Biol Phys* 2008;**71**:635-42.

Bhandarkar SS, Jaconi M, Fried LE, Bonner MY, Lefkove B, Govindarajan B, *et al*. Fulvene-5 potently inhibits NADPH oxidase 4 and blocks the growth of endothelial tumors in mice. *J Clin Invest* 2009;**119**:2359-65.

Bharali DJ, Lucey DW, Jayakumar H, Pudavar HE, Prasad PN. Folate-receptor-mediated delivery of InP quantum dots for bioimaging using confocal and two-photon microscopy. *J Am Chem Soc* 2005;**127**:11364–71.

Biagi BA, Enyeart JJ. Gadolinium blocks low-and high-threshold calcium currents in pituitary cells. *Am J Physiol* 1990;**259**:C515-20.

Bianchi A, Dufort S, Lux F, Courtois A, Tillement O, Coll JL, et al. Quantitative biodistribution and pharmacokinetics of multimodal gadolinium-based nanoparticles for lungs using ultrashort TE MRI. *MAGMA* 2014;**27**:303-16.

Biddlestone-Thorpe L, Sajjad M, Rosenberg E, Beckta JM, Valerie NC, Tokarz M, *et al*. ATM kinase inhibition preferentially sensitizes p53-mutant glioma to ionizing radiation. *Clin Cancer Res* 2013;**19**:3189-200.

Bienert GP, Møller AL, Kristiansen KA, Schulz A, Møller IM, Schjoerring JK *et al*. Specific aquaporins facilitate the diffusion of hydrogen peroxide across membranes. *J Biol Chem* 2007;**282**:1183-92.

Bier H, Hoffmann T, Hauser U, Wink M, Ochler M, Kovar A, *et al*. Clinical trial with escalating doses of the antiepidermal growth factor receptor humanized monoclonal antibody EMD 72 000 in

patients with advanced squamous cell carcinoma of the larynx and hypopharynx. *Cancer Chemother Pharmacol* 2001;**47**:519-24.

Bindhu OS, Ramadas K, Sebastian P, Pillai MR. High expression levels of nuclear factor kappa B and gelatinases in the tumorigenesis of oral squamous cell carcinoma. *Head Neck* 2006;**28**:916-25.

Bionda C, Athias A, Poncet D, Alphonse G, Guezquez A, Gambert P, et al. Differential regulation of cell death in head and neck cell carcinoma through alteration of cholesterol levels in lipid rafts microdomains. *Biochem Pharmacol* 2008;**75**:761-72.

Biskup S and Moore DJ. Detrimental deletions: mitochondria, aging and Parkinson's disease. *Bioessays* 2006;**28**:963–7.

Blasco MA, Svider PF, Raza SN, Jacobs JR, Folbe AJ, Saraf P, *et al*. Systemic therapy for head and neck squamous cell carcinoma: Historical perspectives and recent breakthroughs. *Laryngoscope* 2017;**127**:2565-69.

Boeckx C, Baay M, Wouters A, Specenier P, Vermorken JB, Peeters M, *et al*. Anti-epidermal growth factor receptor therapy in Head and Neck Squamous Cell Carcinoma: Focus on potential molecular mechanisms of drug resistance. *Oncologist* 2013;**18**:850-64.

Boivin A, Hanot M, Malesys C, Maalouf M, Rousson R, Rodriguez-Lafrasse C, *et al*. Transient alteration of cellular redox buffering before irradiation triggers apoptosis in head and neck carcinoma stem and non-stem cells. *PLoS One* 2011;**6**:e14558.

Bonner JA, Harari PM, Giralt J, Azarnia N, Shin DM, Cohen RB, *et al*. Radiotherapy plus cetuximab for squamous-cell carcinoma of the head and neck. *N Engl J Med* 2006;**354**:567-78.
Bonner JA, Harari PM, Giralt J, Cohen RB, Jones CU, Sur RK, *et al*. Radiotherapy plus cetuximab for locoregionally advanced head and neck cancer: 5-year survival data from a phase 3 randomized trial, and relation between cetuximab-induced rash and survival. *Lancet Oncol* 2010;**11**:21-8.

Bonner JA, Trummell HQ, Willey CD, Plants BA, Raisch KP. Inhibition of STAT-3 results in radiosensitization of human squamous cell carcinoma. *Radiother Oncol* 2009;**92**:339-44.

Borst GR, McLaughlin M, Kyula JN, Neijenhuis S, Khan A, Good J, *et al*. Targeted radiosensitization by the Chk1 inhibitor SAR-020106. *Int J Radiat Oncol Biol Phys* 2013;**85**:1110-8.
Bourhis J, Overgaard J, Audry H, Ang KK, Saunders M, Bernier J, *et al*. Hyperfractionated or accelerated radiotherapy in head and neck cancer: a meta-analysis. *Lancet* 2006;**368**:843-54.

Boveris A, Cadenas E, Stoppani AO. Role of ubiquinone in the mitochondrial generation of hydrogen peroxide. *Biochem J* 1976;**156**:435–44.

Boyle JO, Hakim J, Koch W, van der Riet P, Hruban RH, Roa RA, et *al.* The incidence of p53 mutations increases with progression of head and neck cancer. *Cancer Res* 1993;**53**:4477-80.

Bradley JD, Paulus R, Komaki R, Masters G, Blumenschein G, Schild S, *et al*. Standard-dose versus high-dose conformal radiotherapy with concurrent and consolidation carboplatin plus paclitaxel with or without cetuximab for patients with stage iiia or iiib non-small-cell lung cancer (RTOG 0617): a randomised, two-by-two factorial phase 3 study. *Lancet Oncol* 2015;**16**:187-199.

Brand MP. The sites and topology of mitochondrial superoxide production. *Exp Gerontol* 2010;**45**:466-72.

Breitbach CJ, Burke J, Jonker D, Stephenson J, Haas AR, Chow LQM *et al.* Intra-venous delivery of a multi-mechanistic cancer-targeted oncolytic poxyvirus in humans. *Nature* 2011;**477**:99-102.

Brown EJ, Baltimore D. Essential and dispensable roles of ATR in cell cycle arrest and genome maintenance. *Genes Dev* 2003;**17**:615-28.

Brown JM, Carlson DJ, Brenner DJ. The tumor radiobiology of SRS and SBRT: are more than the 5 Rs involved? *Int J Radiat Oncol Biol Phys* 2014;**88**:254-62.

Budach V, Stuschke M, Budach W, Baumann M, Geismar D, Grabenbauer G, *et al*. Hyperfractionated accelerated chemoradiation with concurrent fluorouracil-mitomycin is more effective than dose-escalated hyperfractionated accelerated radiation therapy alone in locally advanced head and neck cancer: final results of the radiotherapy cooperative clinical trials group of the German Cancer Society 95-06 Prospective Randomized Trial. *J Clin Oncol* 2005;**23**:1125-35.

Burma S, Chen DJ. Role of DNA-PK in the cellular response to DNA double-strand breaks. *DNA Repair (Amst)* 2004;**3**:909-18.

Butterworth KT, Coulter JA, Jain S, Forker J, McMahon SJ, Schettino G, *et al*. Evaluation of cytotoxicity and radiation enhancement using 1.9 nm gold particles: potential application for cancer therapy. *Nanotechnology* 2010;**21**:295101.

Butterworth KT, McMahon SJ, Currell FJ, Prise KM. Physical basis and biological mechanisms of gold nanoparticle radiosensitization. *Nanoscale* 2012;**4**:4830-8.

# C

Cabodi S, del Pilar Camacho-Leal M, Di Stefano P, Defilippi P. Integrin signaling adaptors: not only figurants in the cancer story. *Nat Rev Cancer* 2010;**10**:858–70.

Cadenas E, Davies KJ. Mitochondrial free radical generation, oxidative stress, and aging. *Free Radic Biol Med* 2000;**29**:222–30.

Cain K, Bratton SB, Langlais C, Walker G, Brown DG, Sun XM, *et al*. APAF-1 oligomerizes into biologically active approximately 700-kDa and inactive approximately 1.4-MDa apoptosome complexes. *J Biol Chem* 2000;**275**:6067–70.

Cain K, Brown DG, Langlais C, Cohen GM. Caspase activation involves the formation of the aposome, a large (approximately 700 kDa) caspase-activating complex. *J Biol Chem* 1999;**274**:22686–92.

Califano J, van der Riet P, Westra W, Nawroz H, Clayman G, Piantadosi S, *et al.* Genetic progression model for head and neck cancer: implications for field cancerization. *Cancer Res* 1996;**56**:2488-92.

Campus France (campusfrance.org) La recherche en nanosciences en France. 2013.

Canetta R, Rozencweig M, Carter SK. Carboplatin: the clinical spectrum to date. *Cancer Treat Rev* 1985:**12**:125-36.

Cantley LC. The phosphoinositide 3-kinase pathway. *Science* 2002;**296**:1655-7.

Carducci MA, Musib L, Kies MS, Pili R, Truong M, Brahmer JR, et al. Phase I dose escalation and pharmacokinetic study of enzastaurin, an oral protein kinase C beta inhibitor, in patients with advanced cancer. *J Clin Oncol* 2006;**24**:4092-9.

Carter JD, Cheng NN, Qu Y, Suarez GD, Guo T. Nanoscale energy deposition by X-ray absorbing nanostructures. *J Phys Chem, B* 2007;**111**:11622–11625.

Castedo M, Perfettini JL, Roumier T, Andreau K, Medema R, Kroemer G. Cell death by mitotic catastrophe: A molecular definition. *Oncogene* 2004;**23**:2825–37.

Cen L, Carlson BL, Schroeder MA, Ostrem JL, Kitange GJ, Mladek AC, *et al*. p16-CDK4-RB axis controls sensitivity to a cyclin-dependent kinase inhibitor. PD0332991 in glioblastoma xenograft cells. *Neuro Oncol* 2012;**14**:870–881.

Chan S, Davidson N, Juozaityte E, Erdkamp F, Pluzanska A, Azarnia N, *et al*. Phase III trial of liposomal doxorubicin and cyclophosphamide compared with epirubicin and cyclophosphamide as first-line therapy formetastatic breast cancer. *Ann Oncol* 2004;**15**:1527–1534.

Chang HW, Kim SY, Yi SL, Son SH, Song DY, Moon SY, *et al*. Expression of Ku80 correlates with sensitivities to radiation in cancer cell lines of the head and neck. *Oral Oncol* 2006;**42**:979-86.

Chang MY, Shiau AL, Chen YH, Chang CJ, Chen HH, Wu CL. Increased apoptotic potential and dose-enhancing effect of gold nanoparticles in combination with single-dose clinical electron beams on tumor-bearing mice. *Cancer Sci* 2008;**99**:1479–84.

Chang HW, Roh JL, Jeong EJ, Lee SQ, Kim SW, Choi SH, et al. Wnt signaling controls radiosensitivity via cyclooxygenase-2-mediated Ku expression in head and neck cancer. *Int J Cancer* 2008;**122**:100-7.

Chattopadhyay N, Cai Z, Kwon YL, Lechtman E, Pignol JP, Reilly RM. Molecularly targeted gold nanoparticles enhance the radiation response of breast cancer cells and tumor xenografts to X-radiation. *Breast Cancer Res Treat* 2013;**137**:81–91.

Chen F, Zhang XH, Hu XD, Liu PD, Zhang HQ. The effects of combined selenium nanoparticles and radiation therapy on breast cancer cells in vitro. *Artif Cells Nanomed Biotechnol* 2017;**7**:1-12.
Chen N, Yang WT, Bao Y, Xu HL, Qin SB, Tu Y. Bsa capped Au nanoparticle as an efficient sensitizer for glioblastoma tumor radiation therapy. *RSC Adv.* 2015;**5**:40514–20.

Chen WS, Yu YC, Lee YJ, Chen JH, Hsu HY, Chiu SJ. Depletion of securin induces senescence after irradiation and enhances radiosensitivity in human cancer cells regardless of functional p53 expression. *Int J Radiat Oncol Biol Phys* 2010;**77**:566–74.

Chinot OL, Wick W, Mason W, Henriksson R, Sara F, Nishikawa R, *et al*. Bevacizumab plus radiotherapy-temozolomide for newly diagnosed glioblastoma. *N Engl J Med* 2014;**370**:709-722.

Chithrani DB, Jelveh S, Jalali F, van Prooijen M, Allen C, Bristow RG, *et al*. Gold nanoparticles as radiation sensitizers in cancer therapy. *Radiat Res* 2010;**173**:719–28.

Cho YS, Challa S, Moquin D, Genga R, Ray TD, Guildford M, *et al*. Phosphorylation-driven assembly of the RIP1–RIP3 complex regulates programmed necrosis and virus-induced inflammation. *Cell* 2009;**137**:1112–23.

Chithrani BD, Jelveh S, Jalai F, van Prooijen M, Allen C, Bristow RG, *et al*. Gold nanoparticles as radiation sensitizers in cancer therapy. *Radiat Res* 2010;**173**:719-28.

Chithrani DB, Dunne M, Stewart J, Allen C, Jaffray DA. Cellular uptake and transport of gold nanoparticles incorporated in a liposomal carrier. *Nanomedicine* 2010;**6**:161-9.

Christmann M, Tomicic MT, Roos WP, Kaina B. Mechanisms of human DNA repair: an update. *Toxicology* 2003;**193**:3-34.

Chun SG, Park H, Pandita RK, Horikoshi N, Pandita TK, Schwartz DL, *et al*. Targeted inhibition of histone deacetylases and hedgehog signaling suppress tumor growth and homologous recombination in aerodigestive cancers. *Am J Cancer Res* 2015;**5**:1337-52.

Chung EJ, Brown AP, Asano H, Mandler M, Burgan WE, Carter D, *et al*. In vitro and in vivo radiosensitization with AZD6244 (ARRY-142886), an inhibitor of mitogen-activated protein kinase/extracellular signal-regulated kinase 1/2 kinase. *Clin Cancer Res* 2009;**15**:3050-7.

Clarke RH, Moosa S, Anzivino M, Wang Y, Floyd DH, Purow BW, *et al*. Sustained radiosensitization of hypoxic glioma cells after oxygen pretreatment in an animal model of glioblastoma and in vitro models of tumor hypoxia. *PLoS One* 2014;**9**:e111199.

Coelho T, Adams D, Silva A, Lozeron P, Hawkins PN, Mant T, *et al*. Safety and efficacy of RNAi therapy for transthyretin amyloidosis, *N Engl J Med* 2013;**369**:819–29.

Cohen EE, Sharma MR, Janisch L, Llobrera M, House L, Wu K, *et al*. A phase I study of sirolimus and bevacizumab in patients with advanced malignancies. *Eur J Cancer* 2011;**47**:1484-9.

Collado M, Blasco MA, Serrano M. Cellular senescence in cancer and aging. *Cell* 2007;**130**:223-33.

Coleman CN, Mitchell JB. Clinical radiosensitization: why it does and does not work. *J Clin Oncol* 1999;**17**:1-3.

Conklin KA. Chemotherapy-associated oxidative stress: impact on chemotherapeutic effectiveness. *Integr Cancer Ther* 2004;**3**:294-300.

Cooper JS, Pajak TF, Forastiere AA, Jacobs J, Campbell BH, Saxman SB, *et al*. Postoperative concurrent radiotherapy and chemotherapy for high-risk squamous-cell carcinoma of the head and neck. *N Engl J Med* 2004;**350**:1937-44.

Cordes N, Meineke V. Cell adhesion-mediated radioresistance (CAM-RR): extracellular matrix-dependent improvement of cell survival in human tumor and normal cells in vitro. *Strahlenther Onkol* 2003;**179**:337–344.

Cordes N, Park CC. beta1 integrin as a molecular therapeutic target, *Int J Radiat Biol* 2007;**83**:753–60.

Cordes N, Seidler J, Durzok R, Geinitz H., Brakebusch C. beta1-integrinmediated signaling essentially contributes to cell survival after radiation-induced genotoxic injury. *Oncogene* 2006;**25**:1378–90.

Cordes N. Integrin-mediated cell-matrix interactions for prosurvival and antiapoptotic signaling after genotoxic injury. *Cancer Lett* 2006;**242**:11–19.

Cory S, Adams JM. The BCL2 family: Regulators of the cellular life-or-death switch. *Nat Rev Cancer* 2002;**2**:647–56.

Coulter JA, Jain S, Butterworth KT, Taggart LE, Dickson GR, McMahon SJ, *et al*. Cell type-dependent uptake, localization, and cytotoxicity of 1.9 nm gold nanoparticles. *Int J Nanomedicine* 2012;**7**:2673–85.

Couvreur P, Stella B, Reddy LH, Hillaireau H, Dubernet C, Desmaële D, *et al*. Squalenoyl nanomedicines as potential therapeutics. *Nano Lett* 2006;**6**:2544–48.

Cui L, Zahedi P, Saraceno J, Bristow R, Jaffray D, Allen C. Neoplastic cell response to tiopronin-coated gold nanoparticles. *Nanomedicine* 2013;**9**:264-73.

Cui L, Tse K, Zahedi P, Harding SM, Zafarana G, Jaffray DA, *et al*. Hypoxia and cellular localization influence the radiosensitizing effect of gold nanoparticles (aunps) in breast cancer cells. *Radiat Res* 2014;**182**:475–88.

Cui L, Her S, Borst GR, Bristow RG, Jaffray DA, Allen C. Radiosensitization by gold nanoparticles: Will they ever make it to the clinic? *Radiother Oncol* 2017;**124**:344-56.

## D

Dalby KN, Tekedereli I, Lopez-Berestein G, Ozpolat B. Targeting the prodeath and prosurvival functions of autophagy as novel therapeutic strategies in cancer. *Autophagy* 2010;**6**:322-29.

Damiano JS, Hazlehurst LA, Dalton WS. Cell adhesion-mediated drug resistance (CAM-DR) protects the K562 chronicmyelogenous leukemia cell line from apoptosis induced by BCR/ABL inhibition, cytotoxic drugs, and gamma irradiation. *Leukemia* 2001;**15**:1232–9.

Deen WM. What determines glomerular capillary permeability? *J Clin Invest* 2004;**114**:1412-14.

Dejean LM, Martinez-Caballero S, Manon S, Kinnally KW. Regulation of the mitochondrial apoptosis-induced channel, MAC, by BCL-2 family proteins. *Biochim Biophys Acta* 2006;**1762**:191–201.

Delehanty JB, Medintz IL, Pons T, Brunel FM, Dawson PE, Mattoussi H. Self-assembled quantum dot-peptide bioconjugates for selective intracellular delivery. *Bioconjug Chem* 2006;**17**:920–27.

Demaria S, Kawashima N, Yang AM, Devitt ML, Babb JS, Allison JP, *et al*. Immune-mediated inhibition of metastases after treatment with local radiation and CTLA-4 blockade in a mouse model of breast cancer. *Clin Cancer Res* 2005;**11**:728–34.

Denamur S, Tyteca D, Marchand-Brynaert J, Van Bambeke F, Tulkens PM, Courtoy PJ, et al. Role of oxidative stress in lysosomal membrane permeabilization and apoptosis induced by gentamicin, an aminoglycoside antibiotic. *Free Radic Biol Med* 2011;**51**:1656–65.

Deng L, Liang H, Burnette B, Beckett M, Darga T, Weichselbaum RR, *et al*. Irradiation and anti-PD-L1 treatment synergistically promote antitumor immunity in mice. *J Clin Invest* 2014;**124**:687–95.

Desouky O, Ding N, Zhou G. Targeted and non-targeted effects of ionizing radiation. *Journal of Radiation Research and Applied Sciences* 2015;**8**:247-54.

Detappe A, Kunjachan S, Rottmann J, Robar J, Tsiamas P, Korideck H, *et al*. AGuIX nanoparticles as a promising platform for image-guided radiation therapy. *Cancer Nanotechnol* 2015;**6**:4.

Detappe A, Thomas E, Tibbitt MW, Kinjachan S, Zavidij O, Parnandi N, *et al*. Ultrasmall Silica-Based Bismuth Gadolinium Nanoparticles for Dual Magnetic Resonance-Computed Tomography Image Guided Radiation Therapy. *Nano Lett* 2017;**17**:1733-40.

Dickreuter E, Eke I, Krause M, Borgmann K, van Vugt MA, Cordes N. Targeting of b1 integrins impairs DNA repair for radiosensitization of head and neck cancer cells. *Oncogene* 2015;**35**:1353-62.

Diehn M, Cho RW, Lobo NA, Kalisky T, Dorie MJ, Kulp AN, *et al*. Association of reactive oxygen species levels and radioresistance in cancer stem cells. *Nature* 2009;**458**:780–3.

Dikomey E, Dahm-Daphi J, Brammer I, Martensen R, Kaina B. Correlation between cellular radiosensitivity and non-repaired double-strand breaks studied in nine mammalian cell lines. *Int J Radiat Biol* 1998;**73**:269-78.

Dohmen AJC, Qiao X, Duursma A, Wijdeven RH, Lieftink C, Hageman F, *et al*. Identification of a novel ATM inhibitor with cancer cell specific radiosensitization activity. *Oncotarget* 2017;**8**:73925-73937.

Dolman ME, van der Ploeg I, Koster J, Bate-Eya LT, Versteeg R, Caron HN, *et al*. DNA-Dependent Protein Kinase As Molecular Target for Radiosensitization of Neuroblastoma Cells. *PLoS One* 2015;**10**:e0145744.

Dovedi SJ, Adlard AL, Lipowska-Bhalla G, McKenna C, Jones S, Cheadle EJ, *et al*. Acquired resistance to fractionated radiotherapy can be overcome by concurrent PD-L1 blockade. *Cancer Res* 2014;**74**:5458–68.

Dreyfuss AI, Clark JR, Norris CM, Rossi RM, Lucarini JW, Busse PM, et al. Docetaxel: an active drug for squamous cell carcinoma of the head and neck. *J Clin Oncol* 1996:**14**:1672-8.

Droge W. Free radicals in the physiological control of cell function. *Physiol Rev* 2002;**82**:47–95.

Du L, Zhou LJ, Pan XJ, Wang YX, Xu QZ, Yang ZH, *et al*. Radiosensitization and growth inhibition of cancer cells mediated by an scFv antibody gene against DNA-PKcs in vitro and in vivo. *Radiat Oncol* 2010;**5**:70.

Duangmano S, Sae-Lim P, Suksamrarn A, Patmasiriwat P, Domann FE. Cucurbitacin B Causes Increased Radiation Sensitivity of Human Breast Cancer Cells via G2/M Cell Cycle Arrest. *J Oncol* 2012;2012:601682.

Dudek AZ, Lesniewski-Kmak K, Shehadeh NJ, Pandey ON, Franklin M, Kratzke RA, et al. Phase I study of bortezomib and cetuximab in patients with solid tumours expressing epidermal growth factor receptor. *Br J Cancer* 2009;**100**:1379-84.

Dufort S, Le Duc G, Salomé M, Bentivegna V, Sancey L, Bräuer-Krisch E, *et al*. The High Radiosensitizing Efficiency of a Trace Gadolinium-Based Nanoparticles in Tumors. *Sci Rep* 2016;**6**:29678.

Duncan R, Vicent MJ, Greco F, Nicholson RI/ Polymer-drug conjugates: towards a novel approach for the treatment of endocrine-related cancer. *Endocr Relat Cancer* 2005;**12**(Suppl. 1):S189–S199.

Duncan R. Polymer conjugates as anticancer nanomedicines. *Nat Rev Cancer* 2006;**6**:688–701.

# E

Eke I, Cordes N. Focal adhesion signaling and therapy resistance in cancer. *Semin Cancer Biol* 2015;**31**:65-75.

Eke I, Deuse Y, Hehlgans S, Gurtner K, Krause M, Baumann M, *et al*. beta(1)Integrin/FAK/cortactin signaling is essential for human head and neck cancer resistance to radiotherapy. *J Clin Invest* 2012;**122**:1529–40.

Eke I, Dickreuter E, Cordes N. Enhanced radiosensitivity of head and neck squamous cell carcinoma cells by beta1 integrin inhibition. *Radiother Oncol* 2012;**104**:235–42.

Eke I, Schneider L, Förster C, Zips D, Kunz-Schughart LA, Cordes N. EGFR/JIP-4/JNK2 signaling attenuates cetuximab-mediated radiosensitization of squamous cell carcinoma cells. *Cancer Res* 2013;**73**:297–306.

Eke I, Zscheppang K, Dickreuter E, Hickmann L, Mazzeo E, Unger K, et al. Simultaneous β1 integrin-EGFR targeting and radiosensitization of human head and neck cancer. *J Natl Cancer Inst* 2015;**107**:dju419.

Eke I, Zscheppang K, Dickreuter E, Hickmann L, Mazzeo E, Unger K. Simultaneous b1 integrin-EGFR targeting and radiosensitization of human head and neck cancer. *J Natl Cancer Inst* 2015;**107**.pii:dju419.

El-Mir MY, Nogueira V, Fontaine E, Averet N, Rigoulet M, Leverve X. Dimethylbiguanide inhibits cell respiration via an indirect effect targeted on the respiratory chain complex I. J Biol Chem 2000;275:223-28.

Eriksson D, Lofroth PO, Johansson L, Riklund KA, Stigbrand T. Cell cycle disturbances and mitotic catastrophes in HeLa Hep2 cells following 2.5 to 10 Gy of ionizing radiation. *Clin Cancer Res* 2007;**13**:5501s–08s.

Ettl T, Viale-Bouroncle S, Hautmann MG, Gosau M, Kolbl O, Reichert TE, *et al*. AKT and MET signalling mediates antiapoptotic radioresistance in head and neck cancer cell lines. *Oral Oncol* 2015;**51**:158-63.

Evans CH. Biochemistry of the lanthanides, Plenum Press, New York, 1990.

Evans MD, Dizdaroglu M, Cooke MS. Oxidative DNA damage and disease: induction, repair and significance. *Mutat Res*, 2004;**567**:1-61.

# F

Fei P and El-Deiry WS. P53 and radiation responses. *Oncogene* 2003;**22**:5774-83.

Ferradini C and Jay-Gerin JP. Radiolysis of water and aqueous solutions: history and present state of the science. *Can J Chem* 1999;**77**:1542–75.

Fokas E, Prevo R, Pollard JR, Reaper PM, Charlton PA, Cornelissen B, *et al*. Targeting ATR in vivo using the novel inhibitor VE-822 results in selective sensitization of pancreatic tumors to radiation. *Cell Death Dis.* 2012;**3**:e441.

Forastiere A, Koch W, Trotti A, Sidransky D. Head and neck cancer. *N Engl J Med* 2001;**345**:1890-900.

Forastiere AA, Goepfert H, Maor M, Pajak TF, Weber R, Morrison W, *et al*. Concurrent chemotherapy and radiotherapy for organ preservation in advanced laryngeal cancer. *N Engl J Med* 2003;**349**:2091-8.

Forde JC, Maginn EN, McNamara G, Martin LM, Campiani G, Williams DC, *et al*. Microtubule-targeting-compound. PBOX-15 radiosensitizes cancer cells in vitro. *Cancer Biol Ther* 2011;**11**:421-8.

Forman HJ, Zhang H, Rinna A. Glutathione: overview of its protective roles, measurement, and biosynthesis. *Mol Aspects Med* 2009;**30**:1-12.

Frampton JE. Mifamurtide: a review of its use in the treatment of osteosarcoma. *Paediatr Drugs* 2010;**12**:141–53.

Frosina G. DNA repair and resistance of gliomas to chemotherapy and radiotherapy. *Mol Cancer Res* 2009;**7**:989-99.

Fuereder T. Immunotherapy for head and neck squamous cell carcinoma. *memo* 2016;**9**:66-69.

Fulda S and Debatin KM. Extrinsic versus intrinsic apoptosis pathways in anticancer chemotherapy. *Oncogene* 2006;**25**:4798–811.

Fulton DJ. Nox 5 and the regulation of cellular function. *Antioxid Redox Signal* 2009;**11**:2243-523.

## G

Galadari S, Rahman A, Pallichankandy S, Thayyullathil F. Reactive oxygen species and cancer paradox: To promote or to suppress? *Free Rad Biol Med* 2017;**104**:144-64.

Gao H, Peng C, Liang B, Shahbaz M, Liu S, Wang B, *et al*. β6 integrin induces the expression of metalloproteinase-3 and metalloproteinase-9 in colon cancer cells via ERK-ETS1 pathway. *Cancer Lett* 2014;**354**:427–37.

Gelbert LM, Cai S, Lin X, Sanchez-Martinez C, del Prado M, Lallena MJ, *et al*. Preclinical characterization of the CDK4/6 inhibitor LY2835219: In vivo cell cycle-dependent/independent anti-tumor activities alone/in combination with gemcitabine. *Investig New Drugs* 2014;**32**:825–837.

Geng F, Song K, Xing JZ, Yuan C, Yan S, Yang Q, *et al.* Thio-glucose bound gold nanoparticles enhance radio-cytotoxic targeting of ovarian cancer. *Nanotechnology* 2011;**22**:285101.

Gewirtz DA, Hilliker ML, Wilson EN. Promotion of autophagy as a mechanism for radiation sensitization of breast tumor cells. *Radiother Oncol* 2009;**92**:323-8.

Gill PS, Wernz J, Scadden DT, Cohen P, Mukwaya GM, von Roenn JH, *et al*. Randomized phase III trial of liposomal daunorubicin versus doxorubicin, bleomycin, and vincristine in AIDS-related Kaposi's sarcoma. *J Clin Oncol* 1996;**14**:2353–64.
Gilormini M, Malesys C, Armandy E, Manas P, Guy JB, Magné N, *et al*. Preferential targeting of cancer stem cells in the radiosensitizing effect of ABT-737 on HNSCC. *Oncotarget* 2016;**7**:16731-44.

Giralt J, Trigo J, Nuyts S, Ozsahin M, Skladowski K, Hatoum G, *et al*. Panitumumab plus radiotherapy versus chemoradiotherapy in patients with unresected, locally advanced squamous-cell carcinoma of the head and neck (CONCERT-2): a randomised, controlled, open-label phase 2 trial. *Lancet Oncol* 2015;**16**:221-32.

Gökbuget N, Hartog CM, Bassan R, Derigs HG, Dombret H, Greil R, *et al*. Liposomal cytarabine is effective and tolerable in the treatment of central nervous system relapse of acute lymphoblastic leukemia and very aggressive lymphoma. *Haematologica* 2011;**96**:238–44.

Gorrini C, Harris IS, Mak TW. Modulation of oxidative stress as an anticancer strategy. Nature revies Drug discovery 2013;12:931-47.

Gradishar WJ, Tjulandin S, Davidson N, Shaw H, Desai N, Bhar P, *et al*. Phase III trial of nanoparticle albumin-bound paclitaxel compared with polyethylated castoroil-based paclitaxel in women with breast cancer. *J Clin Oncol* 2005;**23**:7794–7803.

Graham J, Muhsin M, Kirkpatrick P. *Nat Rev Drug Discov* 2004;**3**:549-50.

Graham KA, Kulawiec M, Owens KM, Li X, Desouki MM, Chandra D, *et al*. NADPH oxidase 4 is an onco-protein localized to mitochondria. *Cancer Biol Ther* 2010;**10**:223-31.

Grandis JR, Tweardy DJ. Elevated levels of transforming growth factor alpha and epidermal growth factor receptor messenger RNA are early markers of carcinogenesis in head and neck cancer. *Cancer Res* 1993;**53**:3579-84.

Gstaiger M, Aebersold R. Applying mass spectrometry-based proteomics to genetics, genomics and network biology. *Nat Rev Genet* 2009;**10**:617-27.

Gudkov AV, Komarova EA. The role of p53 in determining sensitivity to radiotherapy. *Nat Rev Cancer* 2003;**3**:117–29.

Gupta A, Probst HC, Vuong V, Landshammer A, Muth S, Yagita H, *et al*. Radiotherapy promotes tumor-specific effector CD8+ T cells via dendritic cell activation. *J Immunol* 2012;**189**:558–66.

Gupta AK, McKenna WG, Weber CN, Feldman MD, Goldsmith JD, Mick R, *et al*. Local recurrence in head and neck cancer: relationship to radiation resistance and signal transduction. *Clin Cancer Res* 2002;**8**:885-92.

## H

Hainfeld JF, Dilmanian FA, Slatkin DN, Smilowitz HM. Radiotherapy enhancement with gold nanoparticles. *J Pharm Pharmacol* 2008;**60**: 977-85.

Hainfeld JF, Dilmanian FA, Zhong Z, Slatkin DN, Kalef-Ezra JA, Smilowitz HM. Gold nanoparticles enhance the radiation therapy of a murine squamous cell carcinoma. *Phys Med Biol* 2010;**55**:3045–59.

Hainfeld JF, Smilowitz HM, O'Connor MJ, Dilmanian FA, Slatkin DN. Gold nanoparticle imaging and radiotherapy of brain tumors in mice. *Nanomedicine* 2013;**8**:1601–09.

Halliwell B and Gutteridge JMC. Free Radicals in Biology and Medicine. 4th. Oxford University Press; Oxford: 2007.

Han YK, Lee JH, Park GY, Chun SH, Han JY, Kim SD, *et al*. A possible usage of a CDK4 inhibitor for breast cancer stem cell-targeted therapy. *Biochem Biophys Res Commun* 2013;**430**:1329-33.

Hanahan D, Weinberg RA. Hallmarks of cancer: the next generation. *Cell* 2011;**144**:646-74.

Handy DE and Loscalzo J. Redox regulation of mitochondrial function. *Antioxid Redox Signal* 2012;**16**:1323-67.

Harrington K, Jankowska P, Hingorani M. Molecular biology for the radiation oncologist: the 5Rs of radiobiology meet the hallmarks of cancer. *Clin Oncol (R Coll Radiol)* 2007;**19**:561–71.

Harrison M, Tomlinson D, Stewart S. Liposomal-entrapped doxorubicin: an active agent in AIDS-related Kaposi's sarcoma. *J Clin Oncol* 1995;**13**:914–20.

Hawe A, Hulse WL, Jiskoot W, Forbes RT. Taylor dispersion analysis compared to dynamic light scattering for the size analysis of therapeutic peptides and proteins and their aggregates *Pharm Res* 2011;**28**:2302–2310.

He QY, Chen J, Kung HF, Yuen AP, Chiu JF. Identification of tumor-associated proteins in oral tongue squamous cell carcinoma by proteomics. *Proteomics* 2004;**4**:271-8.

Hehlgans S, Haase M, Cordes N. Signalling via integrins: implications for cell survival and anticancer strategies. *Biochim Biophys Acta - Rev Cancer* 2007;**1775**:163–80.

Hehlgans S, Storch K, Lange I, Cordes N. The novel HDAC inhibitor NDACI054 sensitizes human cancer cells to radiotherapy. *Radiother Oncol* 2013;**109**:126-32.

Her S, Jaffray DA, Allen C. Gold nanoparticles for applications in cancer radiotherapy: Mechanisms and recent advancements. *Adv Drug Deliv Rev* 2017;**109**:84-101.

Hirai T, Shirai H, Fujimori H, Okayasu R, Sasai K, Masutani M. Radiosensitization effect of poly(ADP-ribose) polymerase inhibition in cells exposed to low and high liner energy transfer radiation. *Cancer Sci* 2012;**103**:1045-50.

Hoeijmakers JH. Genome maintenance mechanisms for preventing cancer. *Nature* 2001;**411**:366-74.

Hoff DDV, Ervin TJ, Arena FP, Chiorean EG, Infante JR, Moore MJ, *et al*. Results of a randomized phase III trial (MPACT) of weekly nab-paclitaxel plus gemcitabine versus gemcitabine alone for patients withmetastatic adenocarcinoma of the pancreas with PET and CA19-9 correlates. *J Clin Oncol* 2013;**31**

Hoffmann TK. Systemic Therapy strategies for head-neck carcinumos: Current status. *GMS Curr Top Otorhinollaryngol Head Neck Surg* 2012;**11**:Doc03.

Hofstetter B, Vuong V, Broggini-Tenzer A, Bodis S, Ciernik IF, Fabbro D, *et al*. Patupilone acts as radiosensitizing agent in multidrug-resistant cancer cells in vitro and in vivo. *Clin Cancer Res* 2005;**11**:1588-1596.

https://clinicaltrials.gov/ct2/show/NCT02820454?term=AGuIX&recrs=a&rank=1

Hu L, Wang H, Huang L, Zhao Y, Wang J. Crosstalk between autophagy and intracellular radiation response (Review). *Int J Oncol* 2016;**49**:2217-26.

Huang HC, Barua S, Sharma G, Dey SK, Rege K. Inorganic nanoparticles for cancer imaging and therapy. *J Control Release* 2011;**155**:344–57.

Huang HC, Barua S, Sharma G, Dey SK, Rege K. Inorganic nanoparticles for cancer imaging and therapy. *J Control Release* 2011;**155**:344–57.

Huang YH, Yang PM, Chuah QY, Lee YJ, Hsieh YF, Peng CW *et al*. Autophagy promotes radiation-induced senescence but inhibits bystander effects in human breast cancer cells. *Autophagy* 2014;**10**:1212-28.

Huguet F, Fernet M, Giocanti N, Favaudon V, Larsen AK. Afatinib, an Irreversible EGFR Family Inhibitor, Shows Activity Toward Pancreatic Cancer Cells, Alone and in Combination with Radiotherapy, Independent of KRAS Status. *Target Oncol* 2016;**11**:371-81.

Huotari J, Helenius A. Endosome maturation. *EMBA J* 2011 ;**30** :3481-500.
Huwyler J, Drewe J, Krähenbuhl S. Tumor targeting using liposomal antineoplastic drugs. *Int J Nanomedicine* 2008;**3**:21–29.

Huwyler J, Wu D, Pardridge WM. Brain drug delivery of small molecules using immunoliposomes. *Proc Natl Acad Sci U. S. A.* 1996;**93**:14164–69.

## I

Ianzini F, Bertoldo A, Kosmacek EA, Phillips SL, Mackey MA. Lack of p53 function promotes radiation-induced mitotic catastrophe in mouse embryonic fibroblast cells. *Cancer Cell Int* 2006;**6**,11.

Ianzini F, Mackey MA. Spontaneous premature chromosome condensation and mitotic catastrophe following irradiation of HeLa S3 cells. *Int J Radiat Biol* 1997;**72**:409–21.

Idée JM, Port M, Raynal I, Schaefer M, Le Greneur S, Corot C. Clinical and biological consequences of transmetallation induced by contrast agents for magnetic resonance imaging: a review. *Fundam Clin Pharmacol* 2006;**20**:563-76.

Invest in France Agency. Les Nanotechnologies en France. http://www.thenewfrance.com

Ito H, Daido S, Kanzawa T, Kondo S, Kondo Y. Radiation-induced autophagy is associated with LC3 and its inhibition sensitizes malignant glioma cells. *Int J Oncol* 2005;**26**:1401-10.

Itoh N, Kawakita M. Characterization of Gd3+ and Tb3+ binding sites on Ca2+, Mg2+-adenosine triphosphatase of sarcoplasmic reticulum. *J Biochem* 1984;**95**:661-9.

# J

Jaboin JJ, Shinohara ET, Moretti L, Yang ES, Kaminski JM, Lu B. The role of mTOR inhibition in augmenting radiation induced autophagy. *Technol Cancer Res Treat* 2007;**6**:443-7.

Jain S, Coulter JA, Butterworth KT, Hounsell AR, McMahon SJ, Hyland WB, *et al*. Gold nanoparticle cellular uptake, toxicity and radiosensitisation in hypoxic conditions. *Radiother Oncol* 2014;**110**:342–47.

Jain S, Coulter JA, Hounsell AR, Butterworth KT, McMahon SJ, Hyland WB, *et al*. Cell-specific radiosensitization by gold nanoparticles at megavoltage radiation energies. *Int J Radiat Oncol Biol Phys* 2011;**79:**531–39.

James P. Protein identification in the post-genome era: the rapid rise of proteomics. *Q Rev Biophys* 1997;**30**:279-331

Jeppesen DK, Bohr VA, Stevnsner T. DNA repair deficiency in neurodegeneration. *Prog Neurobiol* 2011;**94**:166-200.

Jiang W and Ogretmen B. Autophagy paradox and ceramide. *Biochim Biophys Acta* 2014;**1841**:783-92.

Jin Z and Hilderbrandt N. Semiconductor quantum dots for in vitro diagnostics and cellular imaging. *Trends Biotechnol* 2012;**30**:394-403.

Jin Z, Aixi Y, Baiwen Q, Zonghuan L, Xiang H. Inhibition of hypoxia-inducible factor-1 alpha radiosensitized MG-63 human osteosarcoma cells in vitro. *Tumori* 2015;**101**:578-84.

Joh DY, Sun L, Stangl M, Al Zaki A, Murty S, Santoiemma PP, *et al*. Selective targeting of brain tumors with gold nanoparticle-induced radiosensitization. *PLoS One* 2013;**8**:e62425.

Joiner M, editor. Basic clinical radiobiology. London: Hodder Arnold; 2009. p. 1-10.

Jordan BF, Sonveaux P. Targeting tumor perfusion and oxygenation to improve the outcome of anticancer therapy. *Front Pharmacol* 2012;**3**:94.

Jordan RC, Catzavelos GC, Barrett AW, Speight PM. Differential expression of bcl-2 and bax in squamous cell carcinomas of the oral cavity. *Eur J Cancer B Oral Oncol* 1996;**32B**:394-400.

Jossen R, Bermejo R. The DNA damage checkpoint response to replication stress: A Game of Forks. *Front Genet* 2013;**4**:26.

Junttila MR, de Sauvage FJ. Influence of tumour micro-environment heterogeneity on therapeutic response. *Nature* 2013;**501**:346-54.

Juzenas P, Chen W, Sun YP, Choelho M, Generalov R, Generalova N, *et al*. Quantum dots and nanoparticles for photodynamic and radiation therapies of cancer. *Adv Drug Deliv Rev* 2008;**60**:1600-14.

# K

Kabakov AE, Kudryavtsev VA, Gabai VL. Hsp90 inhibitors as promising agents for radiotherapy. *J Mol Med (Berl)* 2010;**88**:241-7.

Kahn J, Hayman TJ, Jamal M, Rath BH, Kramp T, Camphausen K, *et al*. The mTORC1/mTORC2 inhibitor AZD2014 enhances the radiosensitivity of glioblastoma stem-like cells. *Neuro Oncol* 2014;**16**:29-37.

Kamaly N, Xiao Z, Valencia PM, Radovic-Moreno AF, Farokhzad OC. Targeted polymeric therapeutic nanoparticles: design, development and clinical translation. *Chem Soc Rev* 2012;**41**:2971–3010.

Karin M, Greten FR. NF-kappaB: linking inflammation and immunity to cancer development and progression. *Nat Rev Immunol* 2005;**5**:749-59.

Karch J, Schips TG, Maliken BD, Brody MJ, Sargent MA, Kanisicak O, et al. Autophagic cell death is dependent on lysosomal membrane permeability through Bax and Bak. *eLife* 2017; **6**. Pii: e30543.

Kaur H, Pujari G, Semwal MK, Sarma A, Avasthi DK. In vitro studies on radiosensitization effect of glucose capped gold nanoparticles in photon and ion irradiation of Hela cells. *Nucl Instrum Methods Phys Res, Sect B* 2013;**301**:7–11.

Kendziorra E, Ahlborn K, Spitzner M, Rave-Fränk M, Emons G, Gaedcke J, *et al*. Silencing of the Wnt transcription factor TCF4 sensitizes colorectal cancer cells to (chemo-) radiotherapy. *Carcinogenesis* 2011;**32**:1824-31.

Kenzaoui BH, Bernasconi CC, Guney-Ayra S, Juillerat-Jeannere L. Induction of oxidative stress, lysosome activation and autophagy by nanoparticles in human brain-derived endothelial cells. *Biochem J* 2012;**441**:813-21.

Kessler J, Hahnel A, Wichmann H, Rot S, Kappler M, Bache M, *et al*. HIF-1α inhibition by siRNA or chetomin in human malignant glioma cells: effects on hypoxic radioresistance and monitoring via CA9 expression. *BMC Cancer* 2010;**10**:605.

Khoshgard K, Hashemi B, Arbabi A, Rasaee MJ, Soleimani M. Radiosensitization effect of folate-conjugated gold nanoparticles on HeLa cancer cells under orthovoltage superficial radiotherapy techniques. *Phys Med Biol* 2014;**59**:2249–63.

Kim BH, Yin CH, Guo Q, Bach EA, Lee H, Sandoval C, *et al*. A small-molecule compound identified through a cell-based screening inhibits JAK ⁄ STAT pathway signaling in human cancer cells. *Mol Cancer Ther* 2008;**7**:2672–80.

Kim BM, Hong Y, Lee S, Liu P, Lim JH, Lee YH, *et al*. Therapeutic Implications for Overcoming Radiation Resistance in Cancer Therapy. *Int J Mol Sci* 2015;**16**:26880-913.

Kim BY, Kim KA, Kwon O, Kim SO, Kim MS, Kim BS, et al. NF-kappaB inhibition radiosensitizes Ki-Ras-transformed cells to ionizing radiation. *Carcinogenesis* 2005;**26**:1395-403.

Kim J, Kundu M, Viollet B, Guan KL. AMPK and mTOR regulate autophagy through direct phosphorylation of Ulk1. *Nat Cell Biol* 2011;**13**:132-41.

Kim JJ, Tannock IF. Repopulation of cancer cells during therapy: an important cause of treatment failure. *Nat Rev Cancer* 2005;**5**:516-25.

King HO, Brend T, Payne HL, Wright A, Ward TA, Patel K, *et al*. RAD51 Is a Selective DNA Repair Target to Radiosensitize Glioma Stem Cells. *Stem Cell Reports* 2017;**8**:125-139.

King HO, Brend T, Payne HL, Wright A, Ward TA, Patel K, *et al*. RAD51 Is a Selective DNA Repair Target to Radiosensitize Glioma Stem Cells. *Stem Cell Reports* 2017;**8**:125-139.

Klein EA, Thompson IM Jr, Tangen CM, Crowley JJ, Luda MS, Goodman PJ, *et al*. Vitamin E and the risk of prostate cancer: the selenium and vitamin E cancer prevetion trial (SELECT). *JAMA* 2011;**306**:1549-56.

Klein S, Dell'Arciprete ML, Wegmann M, Distel LV, Neuhuber W, Gonzalez MC, *et al*. Oxidized silicon nanoparticles for radiosensitization of cancer and tissue cells. *Biochem Biophys Res Commun* 2013;**434**:217-22.

Klein S, Sommer A, Distel LVR, Neuhuber W, Kryschi C. Superparamagnetic iron oxide nanoparticles as radiosensitizer via enhanced reactive oxygen species formation. *Biochem Biophys Res Commun* 2012;**425**:393-7.

Kobashigawa S, Morikawa K, Mori H, Kashino G. Gemcitabine Induces Radiosensitization Through Inhibition of RAD51-dependent Repair for DNA Double-strand Breaks. *Anticancer Res* 2015;**35**:2731-7.

Kolesnick R. The therapeutic potential of modulating the ceramide/sphingomyelin pathway. *J Clin Investig* 2002;**110**:3–8.

Kong T, Zeng J, Wang XP, Yang XY, Yang J, McQuarrie S, *et al*. Enhancement of radiation cytotoxicity in breast-cancer cells by localized attachment of gold nanoparticles. *Small* 2008;**4**:1537–43.

Koppenhagen P, Dickreuter E, Cordes N. Head and neck cancer cell radiosensitization upon dual targeting of c-Abl and beta1-integrin. *Radiother Oncol* 2017;**124**:370-8.

Koritzinsky M. Metformin: A Novel Biological Modifier of Tumor Response to Radiation Therapy. Int J Radiat Oncol Biol Phys. 2015 Oct 1;93(2):454-64.

Koshkaryev A, Sawant R, Deshpande M, Torchilin V. Immunoconjugates and long circulating systems: origins, current state of the art and future directions. *Adv Drug Deliv Rev* 2013;**65**:24–35.

Kotb S, Detappe A, Lux F, Appaix F, Barbier EL, Tran VL, et al. Gadolinium-Based Nanoparticles and Radiation Therapy for Multiple Brain Melanoma Metastases: Proof of Concept before Phase I Trial. *Theranostics* 2016;**6**:418-27.

Kovalainen M, Mönkäre J, Kaasalainen M, Riikonen J, Lehto VP, Salonen J, *et al*. Development of porous silicon nanocarriers for parenteral peptide delivery. *Mol Pharm* 2013;**10**:353–59.

Kryza D, Taleb J, Janier M, Marmuse L, Miladi I, Bonazza P, *et al*. Study of nanometric hybrid gadolinium oxide particles as a multimodel SPECT/MR/Optical Imaging and theragnostic agent. *Bioconjugate Chem* 2011;**22**:1145-52.

Kubota N, Hayashi J, Inada T, Iwamura Y. Induction of a particular deletion in mitochondrial DNA by X rays depends on the inherent radiosensitivity of the cells. *Radiat Res* 1997;**148**:395-8.

Kuger S, Graus D, Brendtke R, Günther N, Katzer A, Lutyj P, *et al*. Radiosensitization of Glioblastoma Cell Lines by the Dual PI3K and mTOR Inhibitor NVP-BEZ235 Depends on Drug-Irradiation Schedule. *Transl Oncol* 2013;**6**:169-79.

Kumar P, Bacchu V, Wiebe LI. The chemistry and radiochemistry of hypoxia-specific, radiohalogenated nitroaromatic imaging probes. *Semin Nucl Med* 2015;**45**:122-35.

Kuribayashi K, Finnberg N, Jeffers JR, Zambetti GP, El-Deiry WS. The relative contribution of pro-apoptotic p53-target genes in the triggering of apoptosis following DNA damage in vitro and in vivo. *Cell Cycle* 2011;**10**:2380–9.

Kwatra D, Veugopal A, Anant S. Nanoparticles in radiation therapy : a summary of various approaches to enhance radiosensitization in cancer. *Transl Cancer Res* 2013;**2**:330-42.

## L

Lai SY, Koppikar P, Thomas SM, Childs EE, Egloff AM, Seethala RR, et al. Intratumoral epidermal growth factor receptor antisense DNA therapy in head and neck cancer: first human application and potential antitumor mechanisms. *J Clin Oncol* 2009;**27**:1235-42.

Lambert LA, Qiao N, Hunt KK, Lambert DH, Mills GB, Meijer L, et al. Autophagy : a novel mechanism of synergistic cytotoxicity between doxorubicin and roscovitine in a sarcoma model. *Cancer Res* 2008;**68**:7966-74.

Lansman JB. Blockade of current through single calcium channels by trivalent lanthanide cations. Effect if ionic radius on the rates of ion entry and exit. *J Gen Physiol* 1990;**95**:679-96.

Lapierre LR, Kumsta C, Sandri M, Ballabio A, Hansen M. Transcriptional and epigenetic regulation of autophagy in aging. *Autophagy* 2015;**11**:867-80.

Larsen NB, Rasmussen M, Rasmussen LJ. Nuclear and mitochondrial DNA repair: similar pathways? *Mitochondrion* 2005;**5**:89–108.

Le Duc G, Miladi I, Alric C, Mowat P, Bräuer-Krisch E, Bouchet A, et al. Toward an image-guided microbeam radiation therapy using gadolinium-based nanoparticles. *ACS Nano* 2011;**5**:9566-74.

Le Duc G, Roux S, Paruta-Tuarez A, Dufort S, Brauer E, Marais A, et al. Advantages of gadolinium based ultrasmall nanoparticles vs molecular gadolinium chelates for radiotherapy guided by MRI for glioma treatment. *Cancer Nanotechnol.* 2014;**5**:4.

Lee ES, Lee HJ, Lee YJ, Jeong JH, Kang S, Lim YB. Chemical chaperones reduce ionizing radiation-indcued endoplasmic reticulum stress and cell death in IEC-6 cells. *Biochem Biophys Res Commun* 2014;**450**:1005-9.

Lee HC, Kim DW, Jung KY, Park IC, Park MJ, Kim MS, *et al*. Increased expression of antioxidant enzymes in radioresistant variant from U251 human glioblastoma cell line. *Int J Mol Med* 2004;**13**:883–7.

Lee JH, Paull TT. Activation and regulation of ATM kinase activity in response to DNA double-strand breaks. *Oncogene* 2007;**26**:7741-8.

Leemans CR, Braakhuis BJ, Brakenhoff RH. The molecular biology of head and neck cancer. *Nat Rev Cancer* 2011;**11**:9-22.

Leethanakul C, Patel V, Gillespie J, Pallente M, Ensley JF, Koontongkaew S, *et al*. Distinct pattern of expression of differentiation and growth-related genes in squamous cell carcinomas of the head and neck revealed by the use of laser capture microdissection and cDNA arrays. *Oncogene* 2000;**19**:3220-4.

Li Y, Han N, Yin T, Huang L, Liu S, Liu D, *et al*. Lentivirus-mediated Nox4 shRNA invasion and angiogenesis and enhances radiosensitivity in human glioblastoma. *Oxid Med Cell Longev* 2014;2014:581732.

Li Z, Rana TM. Therapeutic targeting of microRNAs: current status and future challenges. *Nat Rev Drug Discov* 2014;**13**:622-38.

Libutti SK, Paciotti GF, Byrnes AA, Alexander HR, Gannon WE, Walker M, *et al*. Phase I and pharmacokinetic studies of CYT-6091, a novel PEGylated colloidal gold-rhTNF nanomedicine. *Clin Cancer Res* 2010;**16**:6139–49.

Lim YC, Roberts TL, Day BW, Stringer BW, Kozlov S, Fazry S, *et al*. Increased sensitivity to ionizing radiation by targeting the homologous recombination pathway in glioma initiating cells. *Mol Oncol* 2014;**8**:1603-15.

Link AJ, Eng J, Schieltz DM, Carmack E, Mize GJ, Morris DR, *et al*. Direct analysis of protein complexes using mass spectrometry. *Nat Biotechnol* 1999;**17**:676-82.

Liu CJ, Wang CH, Chen ST, Chen HH, Leng WH, Chien CC, *et al*. Margaritondo, Enhancement of cell radiation sensitivity by PEGylated gold nanoparticles, *Phys Med Biol* 2010;**55**:931–45.

Liu CJ, Wang CH, Chien CC, Yang TY, Chen ST, Leng WH, *et al*. Enhanced Xray irradiation-induced cancer cell damage by gold nanoparticles treated by a new synthesis method of polyethylene glycol modification. *Nanotechnology* 2008;**19**:295104.

Liu P, Huang Z, Chen Z, Xu R, Wu H, Zang F, *et al*. Silver nanoparticles: a novel radiation sensitizer for glioma? *Nanoscale* 2013;**5**:11829-36.

Liu Y, Cui Y, Shi M, Zhang Q, Wang Q, Chen X. Deferoxamine promotes MDA-MB-231 cell migration and invasion through increased ROS-dependent HIF-1α accumulation. *Cell Physiol Biochem* 2014;**33**:1036-46.

Liu Y, Levine B. Autosis and autophagic cell death: the dark side of autophagy. *Cell Death Differ* 2015;**22**:367–376.

Liu P, Jin H, Guo Z, Ma J, Zhao J, Li D, *et al*. Silver nanoparticles outperform gold nanoparticles in radiosensitizing U251 cells in vitro and in an intracranial mouse model of glioma. *Int J Nanomedicine* 2016;**11**:5003-14.

Liu Y, Cui B, Qiao Y, Zhang Y, Tian Y, Jiang J, *et al*. Phosphoinositide-3-kinase inhibition enhances radiosensitization of cervical cancer in vivo. *Int J Gynecol Cancer* 2011;**21**:100-5.

Liu Y, Cui Y, Shi M, Zhang Q, Wang Q, Chen X. Deferoxamine promotes MDA-MB-231 cell migration and invasion through increased ROS-dependent HIF-1α accumulation. *Cell Physiol Biochem* 2014;**33**:1036-46.

Liu Y, Liu X, Jin X, He P, Zheng X, Dai Z, *et al.* The dependence of radiation enhancement effect on the concentration of gold nanoparticles exposed to low- and high-LET radiations. *Phys Med* 2015;**31**:210–18.

Liu Z, Xiong L, Ouyang G, Ma L, Sahi S, Wang K, *et al*. Investigation of Copper Cysteamine Nanoparticles as a New Type of Radiosensitiers for Colorectal Carcinoma Treatment. *Scientific Reports* 2017;**7**:9290.

Lohse I, Kumareswaran R, Cao P, Pitcher B, Gallinger S, Bristow RG, *et al*. Effects of Combined Treatment with Ionizing Radiation and the PARP Inhibitor Olaparib in BRCA Mutant and Wild Type Patient-Derived Pancreatic Cancer Xenografts. *PLoS One* 2016;**11**:e0167272.

Lomax ME, Folkes LK, O'Neill P. Biological consequences of radiation-induced DNA damage: relevance to radiotherapy. *Clin Oncol (R Coll Radiol)* 2013;**25**:578-85.

Loriot Y, Mordant P, Dugue D, Geneste O, Gombos A, Opolon P, *et al*. Radiosensitization by a novel Bcl-2 and Bcl-XL inhibitor S44563 in small-cell lung cancer. *Cell Death Dis* 2014;**5**:e1423.

Lorusso V, Pascolo L, Fernetti C, Anelli PL, Uggeri F, Tiribelli C. Magnetic resonance contrast agents: from the bench to the patient. *Curr Pharm Des* 2005;**11**:4079-98.

Lu H, Liang K, Lu Y, Fan Z. The anti-EGFR antibody cetuximab sensitizes human head and neck squamous cell carcinoma cells to radiation in part through inhibiting radiation-induced upregulation of HIF-1α. *Cancer Lett* 2012;**322**:78-85.

Luchette M, Korideck H, Makrigiorgos M, Tillement O, Berbeco R. Radiation dose enhancement of gadolinium-based AGuIX nanoparticles on HeLa cells. *Nanomedicine* 2014;**10**:1751-5.

Luo S, Rubinsztein DC. Atg5 and Bcl-2 provide novel insights into the interplay between apoptosis and autophagy. Cell Death Differ 2007;14:1247-50.

Luo H, Yount C, Lang H, Yang A, Riemer EC, Lyons K, *et al*. Activation of p53 with Nutlin-3a radiosensitizes lung cancer cells via enhancing radiation-induced premature senescence. *Lung Cancer* 2013;**81**:167–73.

Lux F, Mignot A, Mowat P, Louis C, Dufort S, Bemhard C, et al. Ultrasmall rigid particles as multimodal probes for medical applications. *Angew Chem Int Ed Engl* 2011;**50**:12299-303.

# M

Madoc-Jones H, Mauro F. Interphase action of vinblastine and vincristine: differences in their lethal action through the mitotic cycle of cultured mammalian cells. *J Cell Physiol* 1968;**72**:185-96.

Maggioreela L, Barouch G, Devaux C, Pottier A, Deutsch E, Bourhis J, et al. Nanoscale radiotherapy with hafnium oxide nanoparticles. *Future Oncol* 2012;**8**:1167-81.

Maggiorella L, Aubel C, Haton C, Milliat F, Connault E, Opolon P, *et al*. Cooperative effect of roscovitine and irradiation targets angiogenesis and induces vascular destabilization in human breast carcinoma. *Cell Prolif* 2009;**42**:38-48.

Maity A, Cerniglia GJ, Karar J.Radiosensitization by the Dual PI3K/mTOR Inhibitor NVP-BEZ235. *Int J Rad Oncol* 2011;**81**:S84-S85.

Mamo T, Mladek AC, Shogren KL, Gustafson C, Gupta SK, Riester SM, *et al*. Inhibiting DNA-PKCS radiosensitizes human osteosarcoma cells. *Biochem Biophys Res Commun* 2017;**486**:307-313.

Mamot C, Drummond DC, Greiser U, Hong K, Kirpotin DB, Marks JD, *et al*. Epidermal growth factor receptor (EGFR)-targeted immunoliposomesmediate specific and efficient drug delivery to EGFR- and EGFRvIII-overexpressing tumor cells. *Cancer Res* 2003;**63**:3154–61.

Mamot C, Drummond DC, Noble CO, Kallab V, Guo Z, Hong K, *et al*. Epidermal growth factor receptor-targeted immunoliposomes significantly enhance the efficacy of multiple anticancer drugs in vivo. *Cancer Res* 2005;**65**:11631–38.

Mamot C, Ritschard R, Wicki A, Küng W, Schuller J, Herrmann R, *et al*. Immunoliposomal delivery of doxorubicin can overcome multidrug resistance mechanisms in EGFR-overexpressing tumor cells. *J Drug Target* 2012;**20**:422–32.

Mansour WY, Bogdanova NV, Kasten-Pisula U, Rieckmann T, Kocher S, Borgmann K, et al. Aberrant overexpression of miR-421 downregulates ATM and leads to a pronounced DSB repair defect and clinical hypersensitivity in SKX squamous cell carcinoma. *Radiother Oncol* 2013;**106**:147-54.

Mantoni TS, Lunardi S, Al-Assar O, Masamune A, Brunner TB. Pancreatic stellate cells radioprotect pancreatic cancer cells through β1-integrin signaling. *Cancer Res* 2011;71:3453–8.

Martins RG, Parvathaneni U, Bauman JE, Sjar,a AL. Raez LE, Papagikos MA, *et al*. Cisplatin and radiotherapy with or without erlotinib in locally advanced squamous cell carcinoma of the head and neck: a randomized phase II trial. *J Clin Oncol* 2013;**31**:1415-21.

Matsumura Y, Gotoh M, Muro K, Yamada Y, Shirao K, Shimada Y, *et al.* Phase I and pharmacokinetic study of MCC-465, a doxorubicin (DXR) encapsulated in PEG immunoliposome, in patients with metastatic stomach cancer, *Ann Oncol* 2004;**15**:517–25.

Meacham CE, Morrison SJ. Tumour heterogeneity and cancer cell plasticity. *Nature* 2013;**501**:328-37.

Meitzler JL, Antony S, Wu Y, Juhasz A, Liu H, Jiang G, et al. NADPH Oxidases: A Perspective on Reactive Oxygen Species Production in Tumor Biology. *Antioxid Redox Signal* 2014;**20**:2837-89.

Mesia R, Henke M, Fortin A, Minn H, Yunes Ancona AC, Cmelak A, *et al*. Chemoradiotherapy with or without panitumumab in patients with unresected, locally advanced squamous-cell carcinoma of the head and neck (CONCERT- 1): a randomised, controlled, open-label phase 2 trial. *Lancet Oncol* 2015;**16**:208-20.

Meyers PA, Schwartz CL, Krailo MD, Healey JH, Bernstein ML, Betcher D, *et al*. Osteosarcoma: the addition of muramyl tripeptide to chemotherapy improves overall survival—a report from the Children's Oncology Group, *J Clin Oncol* 2008;**26**:633–38.

Michaud K, Solomon DA, Oermann E, Kim JS, Zhong WZ, Prados MD, *et al*. Pharmacologic inhibition of cyclin-dependent kinases 4 and 6 arrests the growth of glioblastoma multiforme intracranial xenografts. *Cancer Res* 2010;**70**:3228–3238.

Mignot A, Truillet C, Lux F, Sancey L, Louis C, Denat F, et al. A top-down synthesis route to ultrasmall multifunctional Gd-based silica nanoparticles for theranostic applications. *Chemistry* 2013;**19:**6122-36.

Mikhaylov G, Vasiljeva O. Promising approaches I using magnetic nanoparticles in oncology. *Biol Chem* 2011;**392**:955-60.

Mikkelsen RB, Wardman P. Biological chemistry of reactive oxygen and nitrogen and radiation-induced signal transduction mechanisms. *Oncogene* 2003;**22**:5734–54.

Miladi I, Aloy MT, Armandy E, Mowat P, Kryza D, Magne N, et al. Combining ultrasmall gadolinium-based nanoparticles with photon irradiation overcomes radioresistance of head neck squamous cell carcinoma. *Nanomedicine* 2015;**11**:247-57.

Minjgee M, Toulany M, Kehlbach R, Giel K, Rodemann HP. K-RAS(V12) induces autocrine production of EGFR ligands and mediates radioresistance through EGFR-dependent Akt signaling and activation of DNA-PKcs. *Int J Radiat Oncol Biol Phys* 2011;**81**:1506-14.

Mirjolet C, Papa AL, Créhange G, Raguin O, Seignez C, Paul C, et al. The radiosensitization effect of titanate nanotubes as a new tool in radiation therapy for glioblastoma: A proof-of-concept. *Radiother Oncol* 2013;**108**:136-42.

Mirzayans R, Scott A, Cameron M, Murray D. Induction of accelerated senescence by gamma radiation in human solid tumor-derived cell lines expressing wild-type TP53. *Radiat Res* 2005;**163**:53–62.

Mishra A, Bharti AC, Varghese P, Saluja D, Das BC. Differential expression and activation of NF-kappB family proteins during oral carcinogenesis: Role of high risk human papillomavirus infection. *Int J Cancer* 2006;**119**:2840-50.

Mishra BP, Lobo AS, Joshi KS, Rathos MJ, Kumar GA, Padigaru M. Molecular mechanisms of anti-tumor properties of P276-00 in head and neck squamous cell carcinoma. *J Transl Med* 2013;**11**:42.

Mitrakas AG, Kalamida D, Koukourakis MI. Effect of mitochondrial metabolism-interfering agents on cancer cell mitochondrial function and radio/chemosensitivity. *Anticancer Drugs* 2014;**25**:1182-91.

Mo N, Lu YK, Xie WM, Liu Y, Zhou WX, Wang HX, *et al*. Inhibition of autophagy enhances the radiosensitivity of nasopharyngeal carcinoma by reducing Rad51 expression. *Oncol Rep* 2014;**32**:1905-12.

Mochizuki T, Furuta S, Mitsushita J, Shang WH, Ito M, Yokoo Y, *et al*. Inhibition of NADPH oxidase 4 activates apoptosis via the AKT/apoptosis signal-regulating kinase 1 pathway in pancreatic cancer PANC-1 cells. *Oncogene* 2006;**25**:3699-3707.

Moeller BJ, Yordy JS, Williams MD, Giri U, Raju U, Mokentine DP, *et al*. DNA repair biomarker profiling of head and neck cancer: Ku80 expression predicts locoregional failure and death following radiotherapy. *Clin Cancer Res* 2011;**17**:2035-43.

Molinolo AA, Amornphimoltham P, Squarize CH, Castilho RM, Patel V, Gutkind JS. Dysregulated Molecular Networks in Head and Neck Carcinogenesis. *Oral Oncol* 2009;**45**:324-34.

Morad SA, Levin JC, Tan SF, Fox TE, Feith DJ, Cabot MC. Novel off-target effect of tamoxifen—inhibitio
n of acid ceramidase activity in cancer cells. *Biochim Biophys Acta* 2013;**1831**:1657-64.

Moretti L, Cha YI, Niermann KJ, Lu B. Switch between apoptosis and autophagy: radiation-induced endoplasmic reticulum stress? *Cell Cycle* 2007;**6**:793-8.

Mowat P, Mignot A, Rima W, Lux F, Tillement O, Roulin C, et al. In Vitro radiosensitizing effects of ultrasmall gadolinium based particles on tumour cells. *J Nanosci Nanotechnol* 2011;**11**:7833-9.

Mroz RM, Schins RP, Li H, Jimenez LA, Drost EM, Holownia A, et al. Nanoparticle-driven DNA damage mimics irradiation-related carcinogenesis pathways. *Eur Respir J* 2008;**31**:241-51.

Munson JM, Fried L, Rowson SA, Bonner MY, Karumbaja L, Diaz B, *et al*. Anti-invasive adjuvant therapy with imipramine blue enhances chemotherapeutic efficacy against glioma. *Sci Transl Med* 2012;**4**:127ra36.

Murphy PM. How mitochondria produce reactive oxygen species. *Biochem J* 2009;**417**:1-13.
Nakanishi C, Toi M. Nuclear factor-kappaB inhibitors as sensitizers to anticancer drugs. *Nat Rev Cancer* 2005;**5**:297-309.

# N

Nagelkerke A, Bussink J, Geurts-Moespot A, Sweep FC, Span PN. Therapeutic targeting of autophagy in cancer. Part II: pharmacological modulation of treatment-induced autophagy. *Semin Cancer Biol* 2015;**31**:99-105.

Nakayama M, Sasaki R, Ogino C, Tanaka T, Morita K, Umetsu M, et al. Titanium peroxide nanoparticles enhanced cytotoxic effects of X-ray irradiation against pancreatic cancer model through reactive oxygen species generation in vitro and in vivo. *Radiat Oncol* 2016;**11**:91.
*Nanotechnol* 2008;**8**:1312–15.
Nakagawa Y, Takahashi A, Kajihara A, Yamakawa N, Imai Y, Ota I, et al. Depression of p53-independent Akt survival signals in human oral cancer cells bearing mutated p53 gene after exposure to high-LET radiation. *Biochem Biophys Res Commun* 2012;**423**:654-60.

Nam JM, Onodera Y, Bissell MJ, Park CC. Breast cancer cells in three dimensional culture display an enhanced radio response after coordinate targeting of integrin alpha5beta1 and fibronectin. *Cancer Res* 2010;**70**:5238–48.

Neh MA, Lin CI, Kozono DE, Whang EE, Cho NL, Zhu K, *et al*. Necroptosis is a novel mechanism of radiation-induced cell death in anaplastic thyroid and adrenocortical cancers. *Surgery* 2011;**150**:1032–39.

Nel A, Xia T, Madler L, Li N. Toxic potential of materials at the nanolevel. *Science* 2006;**311**:622-7.

Niazi MT, Mok G, Heravi M, Lee L, Vuong T, Aloyz R, *et al*. Effects of dna-dependent protein kinase inhibition by NU7026 on dna repair and cell survival in irradiated gastric cancer cell line N87. *Curr Oncol* 2014;**21**:91-6.

Nimura Y, Kawata T, Uzawa K, Okamura J, Liu C, Saito M *et al*. Silencing Ku80 using small interfering RNA enhanced radiation sensitivity in vitro and in vivo. *Int J Oncol* 2007;**30**:1477-84.

Noto H, Goto A, Tsujimoto T, Noda M. Cancer risk in diabetic patients treated with metformin: a systemic review and meta-analysis. *PloS One* 2012;**7**:e33411.

Nowsheen S, Bonner JA, Yang ES. The poly(ADP-Ribose) polymerase inhibitor ABT-888 reduces radiation-induced nuclear EGFR and augments head and neck tumor response to radiotherapy. *Radiother Oncol* 2011;**99**:331-8.

## O

O'Brien S, Schiller G, Lister J, Damon L, Goldberg S, Aulitzky W, *et al*. High-dose vincristine sulfate liposome injection for advanced, relapsed, and refractory adult Philadelphia chromosome-negative acute lymphoblastic leukemia. *J Clin Oncol* 2013;**31**:676–83.

Ogura A, Oowada S, Kon Y, Hirayama A, Yasui H, Meike S, *et al*. Redox regulation in radiation-induced cytochrome c release from mitochondria of human lung carcinoma A549 cells. *Cancer Lett* 2009;**277**:64–71.

Oku Y, Murakami K, Irie K, Hoseki J, Sakai Y. Synthesized Aβ42 Caused Intracellular Oxidative Damage, Leading to Cell Death, via Lysosome Rupture. *Cell Struct Funct* 2017;**42**:71-79.

Omenn GS, Goodman GE, Thomquist MD, Balmes J, Cullen MR, Glass A, et al. Effects of a combination of beta carotene and vitamin A on lung cancer and cardiovascular disease. *N Engl J Med* 1996;**334**:1150-55.

Ondrey FG, Dong G, Sunwoo J, Chen Z, Wolf JS, Crowl-Bancroft CV, *et al*. Constitutive activation of transcription factors NF-(kappa)B, AP-1, and NF-IL6 in human head and neck squamous cell carcinoma cell lines that express pro-inflammatory and proangiogenic cytokines. *Mol Carcinog* 1999;**26**:119-29.

Ongoing clinical trials with NBTXR3 (hafnium oxide nanoparticles) as radiosensitizing agent in several different cancer types (clinicaltrials.gov)

Ott M, Gogvadze V. Orrenius S, Zhivotovsky B. Mitochondria, oxidative stress and cell death. *Apoptosis* 2007;**12**:913–22.

Ouédraogo ZG, Müller-Barthélémy M, Kemeny JL, Dedieu V, Biau J, Khalil T, et al. STAT3 Serine 727 Phosphorylation: A Relevant Target to Radiosensitize Human Glioblastoma. *Brain Pathol* 2016;**26**:18-30.

Owen MR, Doran E, Halestrap AP. Evidence that metformin exerts its anti-diabetic effects through inhibition of complex 1 of the mitochondrial respiratory chain. *Biochem J* 2000;**348**:607-14.

Ozben T. Oxidative stress and apoptosis: impact on cancer therapy. *J Pharm Sci* 2007;**96**:2181-96.

## P

Paglin S, Lee NY, Nakar C, Fitzgeral M, Plotkin J, Deuel B, et al. Rapamycin-sensitive pathway regulates mitochondrial membrane potential, autophagy, and survival in irradiated MCF-7 cells. *Cancer Res* 2005;**65**:11061-70.

Pajonk F, Vlashi E, McBride WH. Radiation resistance of cancer stem cells: the 4R's of radiobiology revisited. *Stem Cells* 2010;**28**:639-48.

Pan Y, Leifert A, Ruau D, Neuss S, Bornemann J, Schmid G, et al. Gold nanoparticles of diameter 1.4nm trigger necrosis by oxidative stress and mitochondrial damage. *Small* 2009;**5**:2067-76.

Panzarini E, Mariano S, DiniVie L. Glycans coated silver nanoparticles induces autophagy and necrosis in HeLa cells. *AIP Conference Proceedings* 2015;**1667**:020017.

Paradies G, Petrosillo G, Paradies V, Ruggiero FM. Oxidative stress, mitochondrial bioenergetics, and cardiolipin in aging. *Free Radic Biol Med* 2010;**48**:1286-95.

Parikh F, Duluc D, Imai N, Clark A, Misiukiewicz K, Bonomi M, *et al*. Chemoradiotherapy-induced upregulation of PD-1 antagonizes immunity to HPV-related oropharyngeal cancer. *Cancer Res* 2014;**74**:7205–16.

Park BH, Hwang TC, Liu DY, Sze HS, Kim JS, Kwon HC, *et al*. Use of a targeted oncolytic poxyvirus, JX-594, in patients with refractory primary or metastatic liver cancer: a phase I trial. *Lancet Oncol* 2008;**9**:533-42.

Park JW, Hong K, Kirpotin DB, Colbern G, Shalaby R, Baselga J, *et al*. Anti-HER2 immunoliposomes: enhanced efficacy attributable to targeted delivery. *Clin Cancer Res* 2002;**8**:1172–81.

Park SJ, Heo K, Choi C, Yang K, Adachi A, Okada H, *et al*. Carbon ion irradiation abrogates Lin28B-induced X-ray resistance in melanoma cells. *J Radiat Res* 2017;**8**:1-7.

Park YS, Liz-Marzan LM, Kasuya A, Kobayashi Y, Nagao D, Konno M, Mamykin S, Dmytruk A, Parsons JL, Dianov GL. Co-ordination of base excision repair and genome stability. *DNA Repair (Amst)* 2013;**12**:326-33.

Patel LN, Zaro JL, Shen WC. Cell penetrating peptides: intracellular pathways and pharmaceutical perspectives. *Pharm Res* 2007;**24**:1977–92.

Paull R, Wolfe J, Hébert P, Sinkula M. Investing in nanotechnology. *Nat Biotechnol* 2003;**21**:1144-7.

Pchejetski D, Bohler T, Brizuela L, Sauer L, Doumerc N, Golzio M, *et al*. FTY720 (fingolimod) sensitizes prostate cancer cells to radiotherapy by inhibition of sphingosine kinase-1. *Cancer Res* 2010;**70**:8651-61.

Pecot CV, Calin GA, Coleman RL, Lopez-Berestein G, Sood AK. RNA interference in the clinic: challenges and future directions. *Nat Rev Cancer* 2011;**11**:59–67.

Peinnequin A, Poyot T, Dib A, Aubourg A, Mouret C, Demeilliers C. Direct quantification of mitochondrial DNA and its 4.9-kb common deletion without DNA purification. *Anal Biochem* 2011;**409**:298-300.

Peng TI, Yu PR, Chen JY, Wang HL, Wu HY, Wei YH, et al. Visualizing common deletion of mitochondrial DNA-augmented mitochondrial reactive oxygen species generation and apoptosis upon oxidative stress. *Biochim Biophys Acta* 2006;**1762**:241-55.

Persson HL, Kurz T, Eaton JW, Brunk UT. Radiation-induced cell death : importance of lysosomal destabilization. *Biochem J* 2005;**389**:877-84.

Petrosillo G, Ruggiero FM, Pistolese M, Paradies G. Reactive oxygen species generated from the mitochondrial electron transport chain induce cytochrome c dissociation from beef-heart submitochondrial particles via cardiolipin peroxidation: possible role in the apoptosis. *FEBS Lett* 2001;**509**:435–8.

Pettus BJ, Chalfant CE, Hannun YA. (2002) Ceramide in apoptosis: an overview and current perspectives. *Biochim Biophys Acta* 2002;**1585**:114–25.

Pignon JP, le Maître A, Maillard E, Bourhis J. Metaanalysis of chemotherapy in head and neck cancer (MACH-NC): an update on 93 randomized trials and 17,346 patients. *Radiother Oncol* 2009;**92**:4-14.

Poeta ML, Manola J, Goldwasser MA, Forastiere A, Benoit N, Califano JA, *et al*. TP53 mutations and survival in squamous-cell carcinoma of the head and neck. *N Engl J Med* 2007;**357**:2552-61.
Porcel E, Liehn S, Remita H, Usami N, Kobayashi K, Furusawa Y, et al. Platinum nanoparticles: a promising material for future cancer therapy? *Nanotechnology* 2010;**21**:85103.

Porcel E, Tillement O, Lux F, Mowat P, Usami N, Kobayashi K, et al. Gadolinium-based nanoparticles to improve the hadrontherapy performances. *Nanomedicine* 2014;**10**:1601-8.

Posner MR, Hershock DM, Blajman CR, Mickiewicz E, Winquist E, Gorbounova V, *et al*. Cisplatin and fluorouracil alone or with docetaxel in head and neck cancer. *N Engl J Med* 2007;**357**:1705-15.

Potiron VA, Abderrahmani R, Giang E, Chiavassa S, Di Tomaso E, Maira SM, *et al*. Radiosensitization of prostate cancer cells by the dual PI3K/mTOR inhibitor BEZ235 under normoxic and hypoxic conditions. *Radiother Oncol* 2013;**106**:138-46.

Prados MD, Chang SM, Butowski N, DeBoer R, Parvataneni R, Carliner H, *et al*. Phase II study of erlotinib plus temozolomide during and after radiation therapy in patients with newly diagnosed glioblastoma multiforme or gliosarcoma. *J Clin Oncol* 2009;**27**:579-584.

Predescu D, Vogel SM, Malik AB. Functional andmorphological studies of protein transcytosis in continuous endothelia. *Am J Physiol Lung Cell Mol Physiol* 2004;**287**:L895–L901.

Prime SS, Davies M, Pring M, Paterson IC. The role of TGF-beta in epithelial malignancy and its relevance to the pathogenesis of oral cancer (part II). *Crit Rev Oral Biol Med* 2004;**15**:337-47.

Prithivirajsingh S, Story MD, Bergh SA, Geara FB, Ang KK, Ismail SM, et al. Accumulation of the common mitochondrial DNA deletion induced by ionizing radiation. *FEBS Lett* 2004;**571**:227-32.

# Q

Qu W, Chen WH, Kuang Y, Zeng X, Cheng SX, Zhou X, *et al*. Avidin–biotin interaction mediated peptide assemblies as efficient gene delivery vectors for cancer therapy. *Mol Pharm* 2013;**10**:261–69.

Qin H, Luo J, Zhu YP, Xi HL, Yang WQ, Lei WB. Combination of taxanes, cisplatin and fluorouracil as induction chemotherapy for locally advanced head and neck cancer: a meta-analysis. *PLoS One* 2012;**7**:e51526.

Quinlan CL, Treberg JR, Perevoshchikova IV, Orr AL, Brand MD. Native rates of superoxide production from multiple sites in isolated mitochondria measured using endogenous reporters. *Free Radic Biol Med* 2012;**53**:1807-17.

# R

Raben D, Helfrich B, Chan DC, Ciardiello F, Zhao L, Franklin W, *et al*. The effects of cetuximab alone and in combination with radiation and/or chemotherapy in lung cancer. *Jr Clin Cancer Res* 2005;**11**:795-805.

Raghavan P, Tumati V, Yu L, Chan N, Tomimatsu N, Burma S, et al. AZD5438, an inhibitor of Cdk1, 2, and 9, enhances the radiosensitivity of non-small cell lung carcinoma cells. *Int J Radiat Oncol Biol Phys* 2012;84(4):e507-14.

Rahman WN, Bishara N, Ackerly T, He CF, Jackson P, Wong C, *et al*. Enhancement of radiation effects by gold nanoparticles for superficial radiation therapy. *Nanomed Nanotechnol Biol Med* 2009;**5**:136–42.

Rainaldi G, Ferrante A, Indovina PL, Santini MT. Induction of apoptosis or necrosis by ionizing radiation is dose-dependent in MG-63 osteosarcoma multicellular spheroids. *Anticancer Res* 2003;**23**:2505–18.

Raybaud-Diogène H, Fortin A, Morency R, Roy J, Monteil RA, Têtu B. Markers of radioresistance in squamous cell carcinomas of the head and neck: a clinocopathologic and immunohistochemical study. *J Clin Oncol* 1997;**15**:1030-8.

Reits EA, Hodge JW, Herberts CA, Groothuis TA, Chakraborty M, Wansley EK, *et al*. Radiation modulates the peptide repertoire, enhances MHC class I expression, and induces successful antitumor immunotherapy. *J Exp Med* 2006;**203**:1259–71.

Retif P, Pinel S, Toussaint M, Frochot, Chouikrat R, Bastogne T et al. Nanoparticles for Radiation Therapy Enhancement : the Key Parameters. *Theranostics* 2015;**5**:1030-45.

Richards GM, Mehta MP. Motexafin gadolinium in the treatment of brain metastases. *Expert Opin Pharmacother* 2007;**8**:351-9.

Riesterer O, Matsumoto F, Wang L, Pickett J, Molkentine D. Giri U, *et al*. A novel Chk inhibitor, XL-844, increases human cancer cell radiosensitivity through promotion of mitotic catastrophe. *Investig New Drugs* 2011;**29**:514–522.

Rim KT, Song SW, Kim HY. Oxidative DNA damage from nanoparticle exposure and its application to workers' health: a literature review. *Saf Health Work* 2013;**4**:177-86.

Rima W, Sancey L, Aloy MT, Armandy E, Alcantara GB, Epicier T, et al. Internalization pathways into cancer cells of gadolinium-based radiosensitizing nanoparticles. *Biomaterials* 2013;**34**:181-95

Rivera Gil P, Hühn D, del Mercato LL, Sasse D, Parak WJ. Nanopharmacy: inorganic nanoscale devices as vectors and active compounds. *Pharmacol Res* 2010;**62**:115–25.

Roa W, Zhang X, Guo L, Shaw A, Hu X, Xiong Y, *et al.* Gold nanoparticle sensitize radiotherapy of prostate cancer cells by regulation of the cell cycle. *Nanotechnology* 2009;**20**:375101.

Rodriguez CP, Adelstein DJ, Rybicki LA, Saxton JP, Lorenz RR, Wood BG, et al. Single-arm phase II study of multiagent concurrent chemoradiotherapy and gefitinib in locoregionally advanced squamous cell carcinoma of the head and neck. *Head Neck* 2012;**34**:1517-23.

Rodríguez-Vargas JM, Ruiz-Magaña MJ, Ruiz-Ruiz C, Majuelos, Melguizo J, Peralta-Leal A, *et al*. ROS-induced DNA damage and PARP-1 are required for optimal induction of starvation-induced autophagy. *Cell Res* 2012;**22**:1181-98.

Rogosnitzky M, Branch S. Gadolinium-based contrast agent toxicity: a review of known and proposed mechanisms. *Biometals* 2016;**29**:365-76.

Rohrer M, Bauer H, Mintorovitch J, Requardt M, Weinmann HG. Comparison of magnetic properties of MRI contrast media solutions at different magnetic field strengths. *Invest Radiol* 2005;**40**:715-24.

Ross RW, Zietman AL, Xie W, Coen JJ, Dahl DM, Shipley WU, *et al*. Lymphotropic nanoparticle-enhancedmagnetic resonance imaging (LNMRI) identifies occult lymph node metastases in prostate cancer patients prior to salvage radiation therapy. *Clin Imaging* 2009;**33**:301–05.

Ruvolo PP. Intracellular signal transduction pathways activates by ceramide and its metabolites. *Pharm Res* 2003;**47**:383 – 92.

# S

Sabharwal SS and Schumacker PT. Mitochondrial ROS in cancer: initiators, amplifiers or an Achilles' heel? *Nat Rev Cancer* 2014;**14**:709-21.

Sacco AG, Cohen EE. Current treatment options for recurrent or metastatic head and neck squamous cell carcinoma. *J Clin Oncol* 2015;**33**:3305–13.

Saftig, P. Lysosomal membrane proteins. In: Saftig, P., editor. Lysosomes, Eurekah, Landes Bioscience. Springer Science and Business Media; New York: 2005. p. 37-49. Georgetown.

Saglar E, Unlu S, Babalioglu I, Gokce SC, Mergen H. Assessment of ER stress and autophagy induced by ionizing radiation in both radiotherapy patients and ex vivo irradiated samples. J *Biochem Mol Toxicol* 2014;**28**:413-17.

Saki M, Toulany M, Rodemann HP. Acquired resistance to cetuximab is associated with the overexpression of Ras family members and the loss of radiosensitization in head and neck cancer cells. *Radiother Oncol* 2013;**108**:473-8.

Šalovská B, Fabrik I, Ďurišová K, Link M, Vávrová J, Řezáčová M, *et al*. Radiosensitization of human leukemic HL-60 cells by ATR kinase inhibitor (VE-821): phosphoproteomic analysis. *Int J Mol Sci.* 2014;**15**:12007-26.
Sancey L, Kotb S, Truillet C, Appaix F, Marais A, Thomas E, et al. Long-term in vivo clearance of gadolinium-based AGuIX nanoparticles and their biocompatibility after systemic injection. *ACS Nano* 2015;**9**:2477-88.

Sancey L, Lux F, Kotb S, Roux S, Dufort S, Bianchi A, et al. The use of theranostic gadolinium-based nanoprobes to improve radiotherapy efficacy. *Br J Radiol* 2014;**87**:20140134.

Sandulache VC, Skinner HD, Ow TJ, Zhang A, Xia X, Luchak JM, et al. Individualizing antimetabolic treatment strategies for head and neck squamous cell carcinoma based on TP53 mutational status. *Cancer* 2012;**118**:711-21.

Sankunny M, Rarikh RA, Lewis DW, Gooding WE, Saunders WS, Gollin SM. Targeted inhibition of ATR or CHEK1 reverses radioresistance in oral squamous cell carcinoma cells with distal chromosome arm 11q loss. Genes Chromosomes *Cancer* 2014;**53**:129-43.

Santivasi WL, Xia F. Ionizing radiation-induced DNA damage, response, and repair. *Antioxid Redox Signal* 2014;**21**:251-9.

Sawhney M, Rohatgi N, Kaur J, Shishodia S, Sethi G, Gupta SD, *et al*. Expression of NF-kappaB parallels COX-2 expression in oral precancer and cancer: association with smokeless tobacco. *Int J cancer* 2007;**120**:2545-56.

Sayes CM, Gobin AM, Ausman KD, Mendez J, West JL, Colvin VL. Nano-C60 cytotoxicity is due to lipid peroxidation. *Biomaterials* 2005;**26**:7587-95.

Schilling D, Garrido C, Combs SE, Multhoff G. The Hsp70 inhibiting peptide aptamer A17 potentiates radiosensitization of tumor cells by Hsp90 inhibition. *Cancer Lett* 2017;**390**:146-152.

Schleicher SM, Moretti L. Varki V, Lu B. Progress in the unraveling of the endoplasmic reticulum stress/autophagy pathway and cancer: implications for future therapeutic approaches. *Drug Resist Updat* 2010;**13**:79-86.

Schmidt B, Lee HJ, Ryeom S, Yoon SS. Combining bevacizumab with radiation or chemoradiation for solid tumors: a review of the scientific rationale, and clinical trials. *Curr Angiogenes* 2012;**1**:169-179.

Schroeder JE, Shweky I, Shmeeda H, Banin U, Gabizon A. Folate-mediated tumor cell uptake of quantum dots entrapped in lipid nanoparticles. *J Control Release* 2007;**124**:28–34.

Seeta Rama Raju G, Benton L, Pavitra E, Su Yu J. Multifunctional nanoparticles : recent progress in cancer therapeutics. *Chem Commun* 2015;**51**:13248.
Semenza GL. Targeting HIF-1 for cancer therapy. *Nat Rev Cancer* 2003;**3**:721-32.

Sena LA, Li S, Jairaman A, Prakriya M, Ezponda T, Hildeman DA, *et al*. Mitochondria are required for antigen-specific T cell activation through reactive oxygen species signaling. *Immunity* 2013;**38**:225-36.

Sentelle RD, Senkal CE, Jiang W, Ponnusamy S, Gencer S, Selvam SP, *et al*. Ceramide targets autophagosomes to mitochondria and induces lethal mitophagy. *Nat Chem Biol* 2012;**8**:831-8.

Seymour LW, Ferry DR, Kerr DJ, Rea D, Whitlock M, Poyner R, *et al.* Phase II studies of polymer-doxorubicin (PK1, FCE28068) in the treatment of breast, lung and colorectal cancer. *Int J Oncol* 2009;**34**:1629–1636.

Shadel GS, Horvath TL. Mitochondrial ROS signaling in organismal homeostasis. *Cell* 2015;**163**:560-9.

Sharabi AB, Nirschl CJ, Kochel CM, Nirschl TR, Francica BJ, Velarde E, *et al*. Stereotactic radiation therapy augments antigen-specific PD-1 mediated anti-tumor immune responses via cross-presentation of tumor antigen. *Cancer Immunol Res* 2015;**3**:345–55.

Sheard MA. Ionizing radiation as a response-enhancing agent for CD95-mediated apoptosis. *Int J Cancer* 2001;**96**:213-20.

Shen L, Fang H, Chen T, He J, Zhang M, Wei X, et al. Evaluating mitochondrial DNA in cancer occurrence and development. *Ann N Y Acad Sci* 2010;**1201**:26-33.

Shen LF, Chen J, Zeng S, Zhou RR, Zhu H, Zhong MZ, *et al*. The superparamagnetic nanoparticles carrying the E1A gene enhance the radiosensitivity of human cervical carcinoma in nude mice. *Mol Cancer Ther* 2010;**9**:2123-30.

Shintani T, Klionsky DJ. Autophagy in health and disease: a double-edged sword. *Science* 2004;**306**:990-5.

Siegel RL, Miller KD, Jemal A. Cancer statistics, 2016. *CA Cancer J Clin* 2016;**66**:7–30.

Silver J, Ou W. Photoactivation of quantum dot fluorescence following endocytosis. *Nano Lett* 2005;**5**:1445–49.

Skinner HD, Sandulache VC, Ow TJ, Meyn RE, Yordy JS, Beadle BM, et al. TP53 disruptive mutations lead to head and neck cancer treatment failure through inhibition of radiation-induced senescence. *Clin Cancer Res* 2012;**18**:290-300.

Small W, Jr., Mulcahy MF, Rademaker A, Bentrem DJ, Benson AB, Weitner BB, *et al*. Phase II trial of full-dose gemcitabine and bevacizumab in combination with attenuated three-dimensional conformal radiotherapy in patients with localized pancreatic cancer. *Int J Radiat Oncol Biol Phys* 2011;**80**:476-482.

Soffar A, Storch K, Aleem E, Cordes N. CDK2 knowckdown enhances head and neck cancer cell radiosensitivity. *Int J Radiat Biol* 2013;**89**:523-31.

Sommer A, Santi DV. Purification and amino acid analysis of an active site peptide from thymidylate synthetase containing covalently bound 5'-fluoro-2'-deoxyuridylate and methylene tetrachloride. *Biochem Biophys Res Commun* 1974;**57**:689-96.

Stanimirovic DB, Wong J, Ball R, Durkin JP. Free radical-induced endothelial membrane dysfunction at the site of blood-brain barrier: relationship between lipid peroxidation, Na, K-ATPase activity, and 51Cr release. *Neurochem Res* 1996;**20**:1417-27.

Stauber RH, Knauer SK, Habtemichael N, Bier C, Unruhe B, Weisheit S, *et al*. A combination of a ribonucleotide reductase inhibitor and histone deacetylase inhibitors downregulates EFGR and triggers BIM-dependent apoptosis in head and neck cancer. *Oncotarget* 2012;**3**:31-43.

Steel GG, McMillan TJ, Peacock JH. The 5Rs of radiobiology. *Int J Radiat Biol* 1989;**56**:1045-8.

Štefančíková L, Lacombe S, Salado D, Porcel E, Pagáčová E, Tillement O, et al. Effect of gadolinium-based nanoparticles on nuclear DNA damage and repair in glioblastoma tumor cells. *J Nanobiotechnology* 2016;**14**:63.

Štefančíková L, Porcel E, Eustache P, Li S, Salado D, Marco S, et al. Cell localization of gadolinium-based nanoparticles and related radiosensitizing efficacy in glioblastoma cells. *Cancer Nanotechnol* 2014;**5**:6.

Steglich A, Vehlow A, Eke I, Cordes N. α integrin targeting for radiosensitization of three-dimensionally grown human head and neck squamous cell carcinoma cells. *Cancer Lett* 2015;**357**:542-8.

Stein GH, Drullinger LF, Soulard A, Dulić V. Differential roles for cyclin-dependent kinase inhibitors p21 and p16 in the mechanisms of senescence and differentiation in human fibroblasts. *Mol Cell Biol* 1999;**19**:2109-17.

Stewart VC and Heales SJ. Nitric oxide-induced mitochondrial dysfunction implications for neurodegeneration. *Free Radic Biol Med* 2003;**34**:287–303.

Sullivan LB and Chandel NS. Mitochondrial reactive oxygen species and cancer. *Cancer Metab* 2014;**2**:17.

Sun C, Wang ZH, Liu XX, Yang LN, Wang Y, Liu Y, *et al*. Disturbance of redox status enhances radiosensitivity of hepatocellular carcinoma. *Am J Cancer Res* 2015;**5**:1368-81.

Sun Q, Liu T, Yuan Y, Guo Z, Xie G, Du S, *et al*. MiR-200c inhibits autophagy and enhances radiosensitivity in breast cancer cells by targeting UBQLN1. *Int J Cancer* 2015;**136**:1003-12.

Szatrowski TP, Nathan CF. Production of large amounts of hydrogen peroxide by human tumor cells. *Cancer Res* 1991;**51**:794-8.

# T

Taggart LE, McMahon SJ, Currell FJ, Prise KM, Butterworth KT. The role of mitochondrial function in gold nanoparticle mediated radiosensitization. *Cancer Nanotechnol* 2014;**5**:5.

Takasawa R, Nakamura H, Mori T, Tanuma S. Differential apoptotic pathways in human keratinocyte HaCaT cells exposed to UVB and UVC. *Apoptosis* 2005;**10**:1121–30.

Takeda M, Ohuchi N. X-ray absorption of gold nanoparticles with thin silica shell. *J Nanosci Nanotechnol* 2006;**6**:3503–06.

Tam SY, Wu VW, Law HK. Influence of autophagy on the efficacy of radiotherapy. *Radiat Oncol* 2017;**12**:57.

Tanida I, Ueno T, Kominami E. LC3 and Autophagy. *Methods Mol Biol* 2008;**445**:77-88.
Temam S, Kawaguchi H, El-Naggar AK, Jelinek J, Tang H, Liu DD, *et al*. Epidermal growth factor receptor copy number alterations correlate with poor clinical outcome in patients with head and neck squamous cancer. *J Clin Oncol* 2007;**25**:2164-70.

Tenopoulou M, Doulias PT, Barbouti A, Brunk U, Galaris D. Role of compartmentalized redox-active iron in hydrogen peroxide-induced DNA damage and apoptosis. *Biochem J* 2005;**387**:703-10.

Thorley AJ, Tetley TD. New perspectives in nanomedicine. *Pharmacol Ther* 2013;**140**:176-85.

Tian D, Shi Y, Chen D, Liu Q, Fan F. The Wnt inhibitor LGK-974 enhances radiosensitivity of HepG2 cells by modulating Nrf2 signaling. *Int J Oncol* 2017;**51**:545-54.

Todd R, Hinds PW, Munger K, Rustgi AK, Opitz OG, Suliman Y, *et al*. Cell cycle dysregulation in oral cancer. *Crit Rev Oral Biol Med* 2002;**13**:51-61.

Toulany M, Dittmann K, Kruger M, Baumann M, Rodemann HP. Radioresistance of K-Ras mutated human tumor cells is mediated through EGFR-dependent activation of PI3K-AKT pathway. *Radiother Oncol* 2005;**76**:143-50.

Townley HE, Kim J, Dobson P. In vivo demonstration of enhanced radiotherapy using rare earth doped titania nanoparticles. *Nanoscale* 2012:**4**:5043-50.

Tsai YC, Yeh CH, Tzen KY, Ho PY, Tuan TF, Pu YS, *et al*. Targeting epidermal growth factor receptor/human epidermal growth factor receptor 2 signalling pathway by a dual receptor tyrosine kinase inhibitor afatinib for radiosensitisation in murine bladder carcinoma. *Eur J Cancer* 2013;**49**:1458-66.

Turrens JF. Mitochondrial formation of reactive oxygen species. *J Physiol* 2003;**552**:335-44.

# V

Valko M, Leibfritz D, Moncol J, Cronin MT, Mazur M, Telser J. Free radicals and antioxidants in normal physiological functions and human disease. *Int J Biochem Cell Biol* 2007;**39**:44-84.

Vávrová J, Zárybnická L, Lukášová E, Řezáčová M, Novotná E, Sinkorová Z, *et al*. Inhibition of ATR kinase with the selective inhibitor VE-821 results in radiosensitization of cells of promyelocytic leukaemia (HL-60). *Radiat Environ Biophys* 2013;**52**:471-9.

Vecchio D, Daga A, Carra E, Marubbi D, Baio G, Neumaier CE, *et al*. Predictability, efficacy and safety of radiosensitization of glioblastoma-initiating cells by the ATM inhibitor KU-60019. *Int J Cancer* 2014;**135**:479-91.

Veeraraghavan J, Natarajan M, Lagisetty P, Awasthi V, Herman TS, Aravindan N. Impact of curcumin, raspberry extract, and neem leaf extract on rel protein-regulated cell death/radiosensitization in pancreatic cancer cells. *Pancreas* 2011;**40**:1107-19.

Velic D, Couturier AM, Ferreira MR, Rodrigue A, Poirier GG, Fleury F, *et al*. DNA damage signaling and repair inhibitors: the long-sought-after Achilles' heel of cancer. *Biomol* 2015;**5**:3204-59.

Verma S, Miles D, Gianni L, Krop IE, Welslau M, Baselga J, *et al*. Trastuzumab emtansine for HER2 positive advanced breast cancer. *N Engl J Med* 2012;**367**:1783–1791.
Verma V. Relationship and interactions of curcumin with radiation therapy. *World J Clin Oncol* 2016;**7**:275-83.

Vermoken JB, Trigo J, Hitt R, Koralewski P, Diaz-Rubio E, Rolland F, *et al*. Open-label uncontrolled, multicenter phase II study to evaluate the efficacy and toxicity of cetuximab as a single agent in patients with recurrent and/or metastatic squamous cell carcinoma of the head and neck who failed to respond to platinum-based therapy. *J Clin Oncol* 2007;**25**:2171-7.

Vermorken JB, Remenar E, van Herpen C, Gorlia T, Mesia R, Degardin M, *et al*. Cisplatin, fluorouracil, and docetaxel in unresectable head and neck cancer. *N Engl J Med* 2007;**357**:1695-704.

Vile R, Ando D, Kirn D. The oncolytic virotherapy treatment platform for cancer: Unique biological and biosafety points to consider. *Cancer Gene Ther* 2002;**9**:1062–1067.

Vousden KH, Lane DP. P53 in health and disease. *Nat Rev Mol Cell Biol* 2007;**8**:275-83.

Vyas S, Zaganjor E, Haigis MC. Mitochondria and cancer. *Cell* 2016;**166**:555-66.

# W

Wang C, Li X, Wang Y, Liu Z, Fu L, Hu L. Enhancement of radiation effect and increase of apoptosis in lung cancer cells by thio-glucose-bound gold nanoparticles at megavoltage radiation energies. *J Nanopart Res* 2013;**15**:1642.

Wang CH, Jiang YH, Li XH, Hu LK. Thioglucose-bound gold nanoparticles increase the radiosensitivity of a triple-negative breast cancer cell line (MDA-MB-231). *Breast Cancer* 2015;**22**:413–20.

Wang CH, Li XH, Wang Y, Liu Z, Fu L, Hu LK. Enhancement of radiation effect and increase of apoptosis in lung cancer cells by thio-glucose-bound gold nanoparticles at megavoltage radiation energies. *J Nanoparticle Res* 2013;**15**:1642.

Wang L, Meng J, Cao W, Li Q, Qiu Y, Sun B, *et al*. Induction of apoptosis through ER stress and TP53 in MCF-7 cells by the nanoparticle [Gd@C82(OH)22]n: A systems biology study. *Methods* 2014;**67**:394-406.

Wang M, Morsbach F, Sander D, Gheorghiu L, Nanda A, Benes C, *et al*. EGF receptor inhibition radiosensitizes NSCLC cells by inducing senescence in cells sustaining DNA double-strand breaks. *Cancer Res* 2011;**71**:6261-9.

Wang X, Ma Z, Xiao Z, Liu H, Dou Z, Feng X, *et al*. Chk1 knockdown confers radiosensitization in prostate cancer stem cells. *Oncol Rep* 2012;**28**:2247-54.

Wang Y, Sun C, Mao A, Zhang X, Zhou X, Wang Z, et al. Radiosensitization to X-ray radiation by telomerase inhibitor MST-312 in human hepatoma HepG2 cells. *Life Sci* 2015;**123**:43-50.

Wang YH, Chen Z, Zhou XQ. Synthesis and photoluminescence of ZnS quantum dots. *J Nanosci Nanotechnol* 2008;**8**:1312-5.

Wardman P. Chemical radiosensitizers for use in radiotherapy. *Clin Oncol* (R Coll Radiol) 2007;**19**:397-417.

Watson C, Miller DA, Chin-Sinex H, Losch A, Hughes W, Sweeney C, et al. Suppression of NF-kappaB activity by parthenolide induces X-ray sensitivity through inhibition of split-dose repair in TP53 null prostate cancer cells. *Radiat Res* 2009;**171**:389-96.

Weaver VM, Lelièvre S, Lakins JN, Chrenek MA, Jones JCR, Giancotti F, *et al*. beta4 integrin-dependent formation of polarized three-dimensional architecture confers resistance to apoptosis in normal and malignant mammary epithelium. *Cancer Cell* 2002;**2**:205–16.

Wegner KD and Hildebrandt N. Quantum dots: bright and versatile in vitro and in vivo fluorescence imaging biosensors. *Chem Soc Rev* 2015;**44**:4792-834.

Wei F, Wang Y, Luo Z, Li Y, Duan Y. New findings of silica nanoparticles induced ER autophagy in human colon cancer cell. *Sci Rep* 2017;**7**:42591.

Wei-Lin L, Ming G, Kai-Yuan T, Chiao-Ling T, Feng-Ming H, Ann-Lii C, et al. Targeting Phosphatidylinositide3-Kinase/Akt pathway by BKM120 for radiosensitization in hepatocellular carcinoma. *Oncotarget* 2014;**5**:3662–3672.

Weiss GJ, Chao J, Neidhart JD, Ramanathan RK, Bassett D, Neidhart JA, *et al*. First-in-human phase 1/2a trial of CRLX101, a cyclodextrin-containing polymercamptothecin nanopharmaceutical in patients with advanced solid tumor malignancies. *Invest New Drugs* 2013;**31**:986–1000.

Wener ME, Copp JA, Karve S, Cummings ND, Sukumar R, Li C, et al. Folate-targeted polymeric nanoparticle formulation of docetaxel is an effective molecularly targeted radiosensitizer with efficacy dependent on the timing of radiotherapy. *ACS Nano* 2011;**5**:8990-8.
Werner ME, Cummings ND, Sethi M, Wang EC, Sukumar R, Moore DT, et al. Preclinical evaluation of Genexo-PM, a nanoparticle formulation of paclitaxel, as a novel radiosensitizer for the treatment of non-small cell lung cancer. *Int J Radiat Oncol Biol Phys* 2013;**86**:463-68.

Weterings E, Chen DJ. The endless tale of non-homologous end-joining. *Cell Res* 2008;**18**:114-24.

Wicki A, Rochlitz C, Orleth A, Ritschard R, Albrecht I, Herrmann R, *et al*. Targeting tumor-associated endothelial cells: anti-VEGFR2 immunoliposomes mediate tumor vessel disruption and inhibit tumor growth. *Clin Cancer Res* 2012;**18**:454–64.

Wicki A, Witzigmann D, Balasubramanian V, Huwyler J. Nanomedicine in cancer therapy: Challenges, opportunities, and clinical applications. *J Control Release* 2015;**200**:138-57.

Wilkins MR, Pasquali C, Appel RD, Ou K, Golaz O, Sanchez JC, *et al*. From proteins to proteomes : large scale protein identification by two-dimentional electrophoresis and amino acid analysis. *Biotechnology (NY)* 1996;**14**:61-5.

Williams TM, Flecha AR, Keller P, Ram A, Karnak D, Galbán S, *et al*. Cotargeting MAPK and PI3K signaling with concurrent radiotherapy as a strategy for the treatment of pancreatic cancer. *J Mol Cancer Ther* 2012;**11**:1193-202.

Wolfe T, Chatterjee D, Lee J, Grant JD, Bhattarai S, Tailor R, *et al.* Targeted gold nanoparticles enhance sensitization of prostate tumors to megavoltage radiation therapy in vivo. *Nanomedicine* 2015;**11**:1277–83.

Wolters DA, Washburn MP, Yates JR 3rd. An automated multidimensional protein identification technology for shotgun proteomics. *Anal Chem* 2001;**73**:5683-90.

Wozny AS, Lauret A, Battiston-Montagne P, Guy JB, Beuve M, Cunha M, *et al*. Differential pattern of HIF-1α expression in HNSCC cancer stem cells after carbon ion or photon irradiation: one molecular explanation of the oxygen effect. *Br J Cancer* 2017;**116**:1340-1349.

Wu CC and Bratton SB.Regulation of the Intrinsic Apoptosis Pathway by Reactive Oxygen Species. ANTIOXIDANTS & REDOX SIGNALING 2013, Volume 19, Number 6, 546-558.

Wu SY, Liu YW, Wang YK, Lin TH, Li YZ, Chen SH *et al*. Ionizing radiation induces autophagy in human oral squamous cell carcinoma. *J BUON* 2014;**19**:137-44.

Wu X, Zhang J, Yang S, Kuang Z, Tan G, Yang G, *et al*. Telomerase antagonist imetelstat increases radiation sensitivity in esophageal squamous cell carcinoma. *Oncotarget* 2017;**8**:13600-13619.
Wurster S, Hennes F, Parplys AC, Seelbach JI, Mansour WY, Zielinski A, *et al*. PARP1 inhibition radiosensitizes HNSCC cells deficient in homologous recombination by disabling the DNA replication fork elongation response. Oncotarget. 2016;**7**:9732-41.

# X

Xia T, Kovochich M, Brant J, Hotze M, Sempf J, Oberley T, et al. Comparison of the abilities of ambient and manufactured nanoparticles to induce cellular toxicity according to an oxidative stress paradigm. *Nano Lett* 2006;**6**:1794-807.

Xu W, Teng L, Pang B, Li P, Zhou C, Huang P, et al. The Radiosensitization Of Melanoma Cells By Gold Nanorods Irradiated With MV X-Ray. *Nano Biomed Eng* 2012;**4**:6-11.

Xu WH, Han M, Dong Q, Fu ZX, Dia YY, Liu H, et al. Doxorubicin-mediated radiosensitivity in multicellular spheroids from a lung cancer cell line is enhanced by composite micelle encapsulation. *Int J Nanomedicine* 2012;**7**:2661-71.

Xu Y, Fang F, Miriyala S, Crooks PA, Oberley TD, Chaiswing L, *et al*. KEAP1 is a redox sensitive target that arbitrates the opposing radiosensitive effects of parthenolide in normal and cancer cells. *Cancer Res* 2013;**73**:4406-17.

Xu Y, Fang F, Miriyala S, Crooks PA, Oberley TD, Chaiswing L, *et al*. KEAP1 is a redox sensitive target that arbitrates the opposing radiosensitive effects of parthenolide in normal and cancer cells. *Cancer Res* 2013;**73**:4406-17.

# Y

Yamamoto VN, Thylur DS, Bauschard M, Schmale I, Sinha UK. Overcoming radioresistance in head and neck squamous cell carcinoma. *Oral Oncol* 2016;**63**:44-51.

Yang W, Shen Y, Wei J, Liu F. MicroRNA-153/Nrf-2/GPx1 pathway regulates radiosensitivity and stemness of glioma stem cells via reactive oxygen species. *Oncotarget* 2015;**6**:22006-27.

Yang Y, Yang Y, Yang X, Whu H, Guo W , Chen X, et al. Autophagy and its function in radiosensitivity. *Tumour Biol* 2015;**36**:4079-87.

Yang X, Zhu H, Ge Y, Liu J, Cai J, Qin Q, *et al*. Melittin enhances radiosensitivity of hypoxic head and neck squamous cell carcinoma by suppressing HIF-1α. *Tumour Biol* 2014;**35**:10443-8.

Yates JR 3rd. Mass spectral analysis in proteomics. *Annu Rev Biophys Biomol Struct* 2004;**33**:297-316.

Yates JR 3rd. Mass spectrometry and the age of the proteome. *J Mass Spectrom* 1998;**33**:1-19.

Ye H, Yu T, Teman S, Ziober BL, Wang J, Schwarz JL, *et al*. Transcriptomic dissection of tongue squamous cell carcinoma. *BMC Genomics* 2008;9-69.

Yin L, Gao Y, Zhang X, Wang J, Ding D, Zhang Y, *et al*. Niclosamide sensitizes triple-negative breast cancer cells to ionizing radiation in association with the inhibition of Wnt/β-catenin signaling. *Oncotarget* 2016;**7**:42126-42138.

Yong Y, Cheng X, Bao T, Zu M, Yan L, Yin W, et al. Tungsten Sulfide Quantum Dots as Multifunctional Nanotheranostics for In Vivo Dual-Modal Image-Guided Photothermal/Radiotherapy Synergistic Therapy. *ACS Nano* 2015;**9**:12451-63.

Yoshimoto Y, Suzuki Y, Mimura K, Ando K, Oike T, Sato H, *et al*. Radiotherapy-induced anti-tumor immunity contributes to the therapeutic efficacy of irradiation and can be augmented by CTLA-4 blockade in a mouse model. *PLoS One* 2014;**9**:e92572.

Younes A, Bartlett NL, Leonard JP, Kennedy DA, Lynch CM, Sievers EL, *et al*. Brentuximab vedotin (SGN-35) for relapsed CD30-positive lymphomas, *N Engl J Med* 2010;**363**:1812–1821.

Yousefi S, Perozzo R, Schmid I, Ziemiecki A, Schaffner T, Scapozza L, et al. Calpain-mediated cleavage of Atg5 switches autophagy to apoptosis. *Nat Cell Biol* 2006;**8**:1124-32.

Yu Z., Persson HL, Eaton JW, Brunk UT. Intralysosomal iron: a major determinant of oxidant-induced cell death. *Free Radic Biol Med* 2003;**34**:1243–52.

# Z

Zeng J, See AP, Phallen J, Jackson CM, Belcaid Z, Ruzevick J, *et al*. Anti-PD-1 blockade and stereotactic radiation produce long-term survival in mice with intracranial gliomas. *Int J Radiat Oncol Biol Phys* 2013;**86**:343–49.

Zerp SF, Stoter TR, Hoebers FJ, van den Brekel MW, Dubbelman R, Kuipers GK, *et al*. Targeting anti-apoptotic Bcl-2 by AT-101 to increase radiation efficacy: data from in vitro and clinical pharmacokinetic studies in head and neck cancer. *Radiat Oncol* 2015;**10**:158.

Zhang J, Chiu J, Zhang H, Qi T, Tang Q, Ma K, *et al*. Autophagic cell death induced by resveratrol depends on the Ca(2+)/AMPK/mTOR pathway in A549 cells. *Biochem Pharmacol* 2013;**86**:317-28.

Zhang Q, Yang W, Man N, Zheng F, Shen Y, Sun K, *et al*. Autophagy-mediated chemosensitization in cancer cells by fullerene C60 nanocrystal. *Autophagy* 2009;**5**:1107-17.

Zhang Q, Zhang C, He J, Guo Q, Hu D, Yang X, *et al*. STAT3 inhibitor stattic enhances radiosensitivity in esophageal squamous cell carcinoma. *Tumour Biol* 2015;**36**:2135-42.

Zhang X, Xing JZ, Chen J, Ko L, Amanie J, Gulavita S, *et al*. Enhanced radiation sensitivity in prostate cancer by gold-nanoparticles. *Clin Invest Med* 2008;**31**:E160–E167.

Zhang XD, Chen J, Luo Z, Wu D, Shen X, Song SS, *et al.* Enhanced tumor accumulation of Sub-2 nm gold nanoclusters for cancer radiation therapy. *Adv Healthcare Mater* 2014;**3**:133–41.

Zhang XD, Wu D, Shen X, Chen J, Sun YM, Liu PX, *et al*. Size-dependent radiosensitization of PEG-coated gold nanoparticles for cancer radiation therapy. *Biomaterials* 2012;**33**:6408–19.
Zhang Y, Fonslow BR, Shan B, Baek MC, Yates JR 3rd. Protein analysis by Shotgun/Bottom-Up Proteomics. *Chem Rev* 2013;**113**:2343-94.

Zhang Y, Yao B, Delikat S, Bayoumy S, Lin XH, Basu S, *et al*. Kinase suppressor of Ras is ceramide-activated protein kinase. *Cell* 1997;**89**:63–72.

Zhao D, Sun X, Tong J, Ma J, Bu X, Xu R, *et al*. A novel multifunctional nanocomposite C225-conjugated Fe3O4/Ag enhances the sensitivity of nasopharyngeal carcinoma cells to radiotherapy. *Acta Biochim Biophys Sin (Shangai)* 2012;**44**:678-84.

Zheng Q, Yang H, Wei J, Tong JL, Shu YQ. The role and mechanisms of nanoparticles to enhance radiosensitivity in hepatocellular cell. *Biomed Pharmacother* 2013;**67**:569-75.

Zhou M, Ghosh I. Quantum dots and peptides: a bright future together. *Biopolymers* 2007;**88**:325– 39.

Zhou S, Ye W, Shao Q, Zhang M, Liang J. Nrf2 is a potential therapeutic target radioresistance in human cancer. *Crit Rev Oncol Hematol* 2013;**88**:706-15.

Zhu Y, Shi LY, Lei YM, Bao YH, Li ZY, Ding F, *et al*. Radiosensitization effect of hsa-miR-138-2-3p on human laryngeal cancer stem cells. *PeerJ* 2017;**5**:e3233.

Zhu Y1, Shi LY2, Lei YM3, Bao YH3, Li ZY4, Ding F4, *et al*. Radiosensitization effect of hsa-miR-138-2-3p on human laryngeal cancer stem cells. *PeerJ* 2017;5:e3233.

Ziober AF, Patel KR, Alawi F, Gimotty P, Weber RS, Feldman MM, *et al*. Identification of a gene signature for rapid screening of oral squamous cell carcinoma. *Clin Cancer Res* 2006;**23**:5960.

Zorov DB, Juhaszova M, Sollott SJ. Mitochondrial reactive oxygen species (ROS) and ROS-induced ROS release. *Physiol Rev* 2014;**94**:909-50.

Zou J, Qiao X, Ye H, Yang Y, Zheng X, Zhao H, *et al*. Antisense inhibition of ATM gene enhances the radiosensitivity of head and neck squamous cell carcinoma in mice. *J Exp Clin Cancer Res* 2008;**27**:56.

# Annexes

Annex 1: The DNA damage response pathways and its inhibitors. Ongoing clinical trials and targets. (Velic *et al*., 2015)

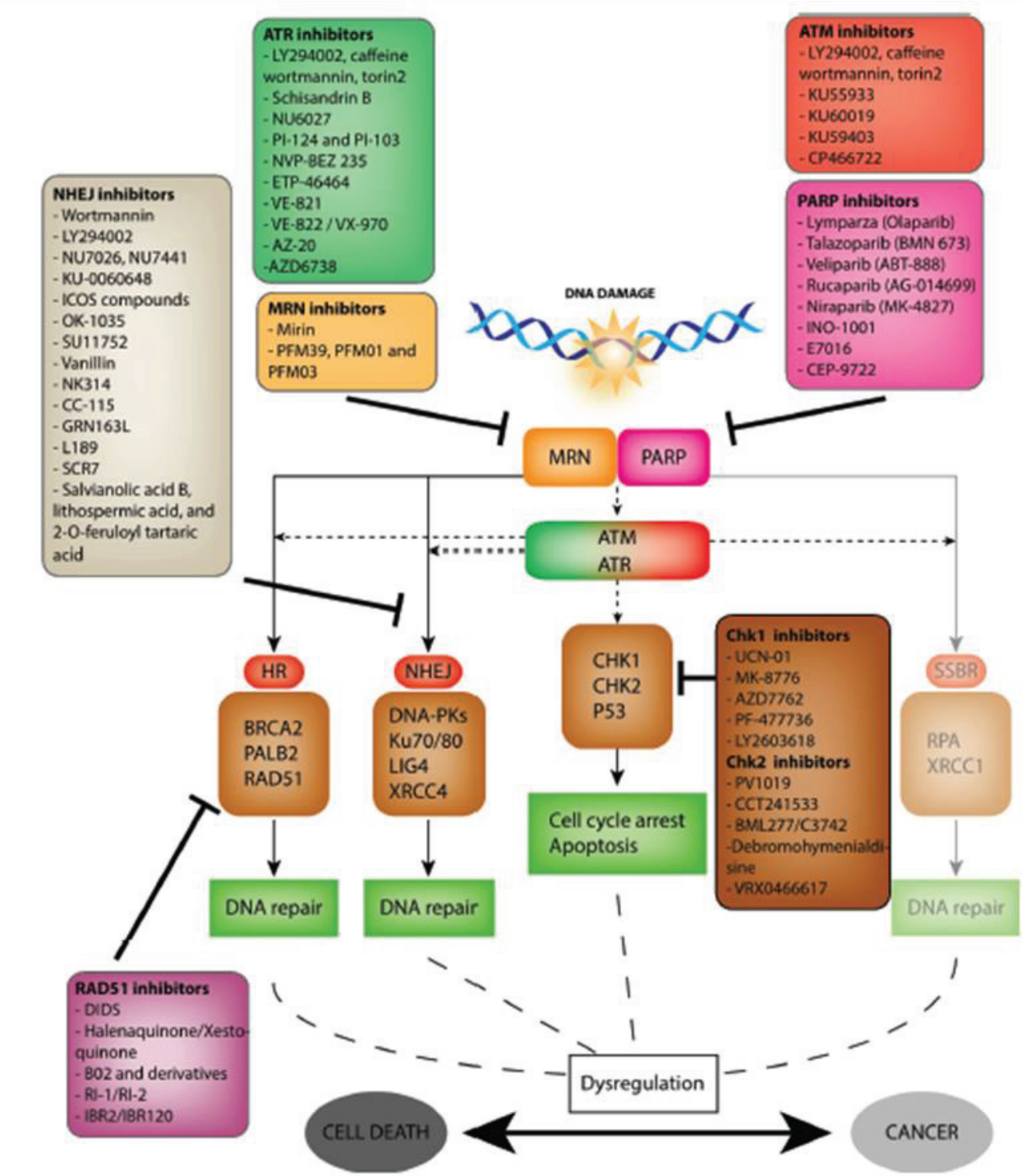

# Annex 2: AGuIX® synthesis and characterization during the synthesis

Gadolinium-based nanoparticles are synthesized in five main steps:

- The first step consists in the synthesis of the oxide core $Gd_2O_3$: $GdCl_3$ is dissolved in diethylene glycol (DEG) and reacts with concentrated sodium hydroxide (10 M) to form the $Gd_2O_3$ core.
- In the second one, the $Gd_2O_3$ core is englobed by a polysiloxane layer by adding TEOS (tetraethyl orthosilicate) and APTES (3-aminopropyl)triethoxysilane). A mix of DEG, ultra-pure $dH_2O$ and the catalyzer TEA (triethylamine) is added in parallel. The "coating" is followed by measuring the nanoparticles' size by DLS (Dynamic Light Scattering) every 24 hours. At the end of the reaction, the temperature as well as the agitation are decreased and the solution must stay at room temperature for at least 72 hours.
- The third step, performed at room temperature for 48 to 72 hours, is grafting the DOTAGA which consists in the reaction between the anhydride present on the DOTAGA anhydride and the amines present at the surface of the nanoparticle to create amide bonds.
- In the fourth step, the nanoparticles are precipitated in acetone, filtrated under vacuum and then re-dispersed in ultra-pure $dH_2O$. The solution is left to mature for one hour prior to evaporating the acetone under a ventilated hood. The solution is then purified by tangential filtration at 5 kDa and left to rest for a minimum of 12 hours: this purification/rest step is repeated three times. The particles' purity is then verified by HPLC: if the ratio area of the principal peak/total area of all peaks is superior or equal to 90%, the solution is filtered through a 1.2 µm followed by a 0.2 µm filter.
- Finally, in order to store the nanoparticles' solution, the last step consists in the lyophilization and conditioning of the nanoparticles. For it, the solution is first divided in pilulier and frozen at -80°C for more than 2h prior to being lyophilized (in the next 7 days after freezing, the pressure is of 0.041 mbar, for a time of 48 hours or more). The samples are then conditioned and labeled. Figure 29 represents all the synthesis steps described for the formulation of AGuIX® (Mignot *et al.,* 2013)

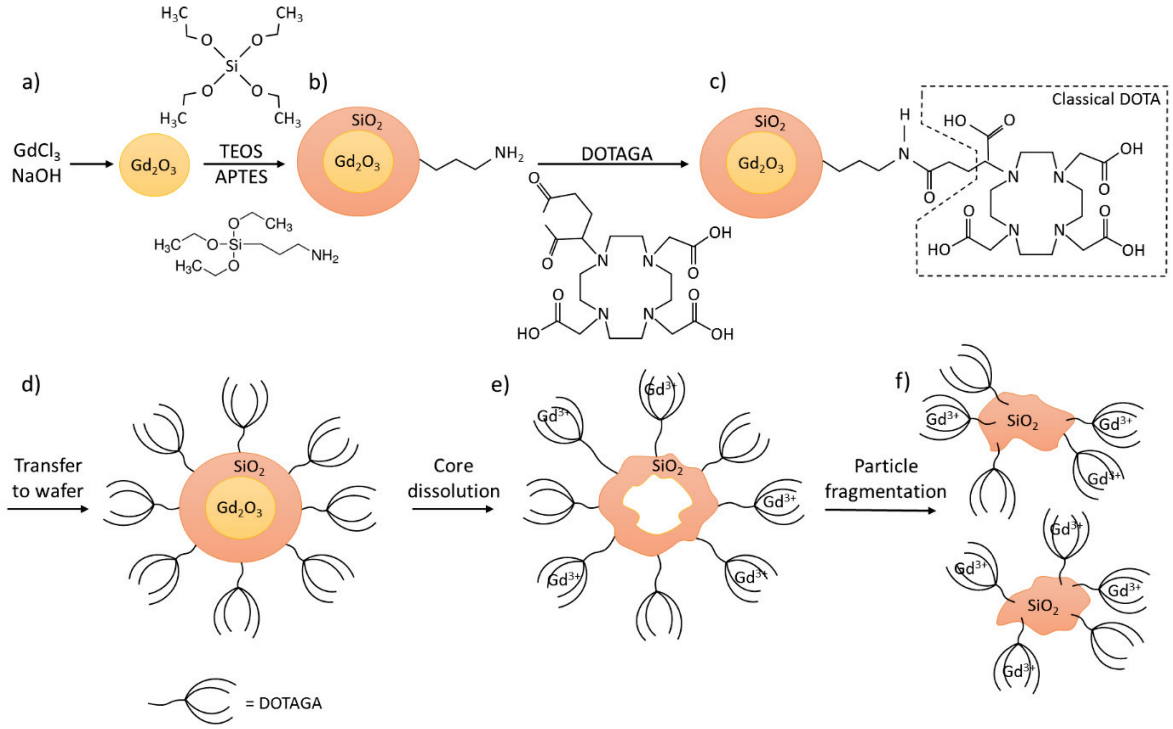


Figure 29: Scheme of SRP synthesis a) core synthesis; b) polysiloxane shell synthesis; c) DOTAGA grafting; d) transfer to water; e) core dissolution, f) polysiloxane fragmentation (Mignot *et al.*, 2013)

Throughout the synthesis steps, the nanoparticles are characterized with different techniques: their size is controlled using DLS followed by HPLC. At the end of the fourth step, a measure by relaxometry is done to determine the T1- relaxation time value. The concentrations in gadolinium (bound and free) are measured, as well as the synthesis yield.

# Annex 3: Media composition of HBSS, PBS $Ca^{2+}/Mg^{2+}$, and DMEM-Glutamax™

| Components | Molecular Weight | Concentration (mg/L) | mM |
|---|---|---|---|
| *Inorganic Salts* | | | |
| Calcium chloride (CaCl2) (anhyd.) | 111.0 | 140.0 | 1.2612612 |
| Magnesium chloride (MgCl2-6H2O) | 203.0 | 100.0 | 0.49261084 |
| Magnesium Sulfate (MgSO4-7H2O) | 246.0 | 100.0 | 0.40650406 |
| Potassium Chloride (KCl) | 75.0 | 400.0 | 5.3333335 |
| Potassium Phosphate monobasic (KH2PO4) | 136.0 | 60.0 | 0.44117647 |
| Sodium Bicarbonate (NaHCO3) | 84.0 | 350.0 | 4.1666665 |
| Sodium Chloride (NaCl) | 58.0 | 8000.0 | 137.93103 |
| Sodium Phospate dibasic (Na2HPO4) anhydrous | 142.0 | 48.0 | 0.33802816 |
| *Other components* | | | |
| D-Glucose | 180.0 | 1000.0 | 5.5555553 |

HBSS composition with the corresponding molecular weight, concentration (mg/L), and molarity (mM).

## PBS $Ca^{2+}/Mg^{2+}$

| Components | Molecular Weight | Concentration (mg/L) | mM |
|---|---|---|---|
| *Inorganic Salts* | | | |
| Calcium chloride (CaCl2) (anhyd.) | 111.0 | 100.0 | 0.9009009 |
| Magnesium chloride (MgCl2-6H2O) | 203.0 | 100.0 | 0.49261084 |
| Potassium Chloride (KCl) | 75.0 | 200.0 | 2.6666667 |
| Potassium Phosphate monobasic (KH2PO4) | 136.0 | 200.0 | 1.4705882 |
| Sodium Chloride (NaCl) | 58.0 | 8000.0 | 137.93103 |
| Sodium Phospate dibasic (Na2HPO4-7H2O) | 268.0 | 2160.0 | 8.059702 |

PBS $Ca^{2+}/Mg^{2+}$ composition with the corresponding molecular weight, concentration (mg/L), and molarity (mM).

DMEM-Glutamax™ composition with the corresponding molecular weight, concentration (mg/L), and molarity (mM).

| Components | Molecular Weight | Concentration (mg/L) | mM |
|---|---|---|---|
| *Amino Acids* | | | |
| Glycine | 75.0 | 30.0 | 0.4 |
| L-Alalanyl L Glutamine | 217.0 | 862.0 | 3.9723501 |
| L-arginine hydrochloride | 211.0 | 84.0 | 0.39810428 |
| L-Cystine 2HCl | 313.0 | 63.0 | 0.20127796 |
| L-Histidine hydrochloride-H2O | 210.0 | 42.0 | 0.2 |
| L-Isoleucine | 131.0 | 105.0 | 0.8015267 |
| L-Leucine | 131.0 | 105.0 | 0.8015267 |
| L-Lysine hydrochloride | 183.0 | 146.0 | 0.7978142 |
| L-Methionine | 149.0 | 30.0 | 0.20134228 |
| L-Phenylalanine | 165.0 | 66.0 | 0.4 |
| L-Serine | 105.0 | 42.0 | 0.4 |
| L-Threonine | 119.0 | 95.0 | 0.79831934 |
| L-Tryptophan | 204.0 | 16.0 | 0.078431375 |
| L-Tyrosine | 181.0 | 72.0 | 0.39779004 |
| L-Valine | 117.0 | 94.0 | 0.8034188 |
| *Vitamins* | | | |
| Choline chloride | 140.0 | 4.0 | 0.028571429 |
| D-Calcium pantothenate | 477.0 | 4.0 | 0.008385744 |
| Folic Acid | 441.0 | 4.0 | 0.009070295 |
| Niacinamide | 122.0 | 4.0 | 0.032786883 |
| Pyridoxine hydrochloride | 206.0 | 4.0 | 0.019417476 |
| Riboflavin | 376.0 | 0.4 | 0.0010638298 |
| Thiamine hydrochloride | 337.0 | 4.0 | 0.011869436 |
| i-Inositol | 180.0 | 7.2 | 0.04 |
| *Inorganic Salts* | | | |
| Calcium Chloride (CaCl2-2H2O) | 147.0 | 264.0 | 1.7959183 |
| Ferric Nitrate (Fe(NO3)3"9H2O) | 404.0 | 0.1 | 2.4752476E-4 |
| Magnesium Sulfate (MgSO4-7H2O) | 246.0 | 200.0 | 0.8130081 |
| Potassium Chloride (KCl) | 75.0 | 400.0 | 5.3333335 |
| Sodium Bicarbonate (NaHCO3) | 84.0 | 3700.0 | 44.04762 |
| Sodium Chloride (NaCl) | 6400.0 | 6400.0 | 110.344826 |
| Sodium Phosphate monobasic (NaH2PO4-2H2O) | 154.0 | 141.0 | 0.91558444 |
| *Other Components* | | | |
| D-Glucose (Dextrose) | 180.0 | 4500.0 | 25.0 |
| Phenol Red | 376.4 | 15.0 | 0.039851222 |

# Oral and Poster Communications

## Oral Communications

Stephanie Simonet*, Marie Therese Aloy, Emma Armandy, Marc Janier, Olivier Tillement, Francois Lux, Michael Beuve, Jean Luc Ravanat, Walid Rachidi, Claire Rodriguez-Lafrasse, Dominique Ardail. The use of gadolinium-based nanoparticles to improve radiation therapy efficacy in HNSCC. 15th International Congress of Radiation Research (ICRR 2015). May 25-29, 2015. Kyoto, Japan.

Stephanie Simonet*, MT Aloy, E Armandy, O Tillement, F Lux, JL Ravanat, W Rachidi, C Rodriguez-Lafrasse, D Ardail. Les nanoparticules à base de gadolinium associées à la radiothérapie : intérêt dans le traitement des cancers des Voies Aérodigestives Supérieures. SIRLaF CIRFA 13- 13ème Colloque International de Radiobiologie Fondamentale et Appliquée. November 8-12, 2015. Obernai, France.

Stephanie Simonet*, Dominique Ardail, Walid Rachidi. The use of gadolinium-based nanoparticles to improve radiation therapy in HNSCC. Journée LabEx. October 10$^{th}$, 2016. Villeurbanne, France.

Stephanie Simonet*, Dominique Ardail, Walid Rachidi. The use of gadolinium-based nanoparticles to improve radiation therapy in HNSCC. Journée EDISS. October 13$^{th}$, 2016. Villeurbanne, France.

Stephanie Simonet*, Dominique Ardail, Walid Rachidi. The use of gadolinium-based nanoparticles to improve radiation therapy in HNSCC. February 20$^{th}$, 2017. Grenoble, France.

Stephanie Simonet, Dominique Ardail, Walid Rachidi. Modulation of the proteomic profile in SQ20B HNSCC cell line after Gd-nanoparticles radiosensitization. Nanohybrides 14- May 29$^{th}$-June 2$^{nd}$, 2017. Bastia, Corsica, France.

## Poster

Stephanie Simonet*, E Armandy, C Malesys, D Beal, S Gerbaud, O Tillement, F Lux, JL Ravanat, W Rachidi, C Rodriguez-Lafrasse, D Ardail. The use of the gadolinium-based AGuIX nanoparticles to improve radiation therapy efficacy in Head and Neck Squamous Cell Carcinoma (HNSCC). LabEx presentation, December 2016. Lyon, France.

**Submitted**; Simonet *et al*.

# The use of gadolinium-based nanoparticles (AGuIX®) to counteract the radioresistance of HNSCC: from cellular uptake to subcellular damage

S. Simonet[a,b], C. Rodriguez-Lafrasse[a,c], D. Beal[b], S. Gerbaud[d], C. Malesys[a], O. Tillement[e], F. Lux[e], W. Rachidi[b,f]* and D. Ardail[a]*

[a] Institut de Physique Nucléaire de Lyon, Laboratoire de Radiobiologie Cellulaire et Moléculaire, CNRS UMR 5822, Université de Lyon, Faculté de Médecine Lyon-Sud, Pierre Bénite, France.

[b] Commissariat à l'énergie atomique et aux énergies alternatives (CEA)/Institut Nanosciences et Cryogénie (INAC)/Systèmes Moléculaires et nanoMatériaux pour l'Energie et la Santé (SyMMES)/Chimie Interface Biologie pour l'Environnement, la Santé, et la Toxicologie (CIBEST). 17 avenue des martyrs, F-38054 Grenoble CEDEX.

[c] Unité Médicale d'Oncologie Moléculaire et Transfert, Hospices Civils de Lyon, Laboratoire de Biochimie et Biologie Moléculaire, Centre Hospitalier Lyon-Sud, Pierre Bénite, France

[d] Laboratoire BGE U1038- Biomics, Bioscience and Biotechnology Institute of Grenoble. CEA-DRF. Grenoble, France.

[e] Institut Lumière Matière, UMR 5306 CNRS, Université de Lyon, Université Lyon 1, Villeurbanne cedex, France.

[f] Université Grenoble Alpes, F-38000 Grenoble, France.

*: co-corresponding authors

Authors to whom correspondence should be addressed are Dr. Dominique Ardail (dominique.ardail@univ-lyon1.fr) and Dr Walid Rachidi (walid.rachidi@univ-grenoble-alpes.fr)

Abstract: 148 words

Manuscript: 4839 words

Number of references : 58

**Competing interests**: F. Lux, and O. Tillement have to disclose the patent WO2011/135101. O. Tillement has to disclose the patent WO2009/053644. These patents protect the AGuIX® nanoparticles described in this publication.

This work was supported by France Hadron (ANR-11-INBS-0007) and Labex Primes (ANR-11-LABX-0063). Stéphanie Simonet was supported by a grant from Labex Primes

**Submitted**; Simonet *et al*.

**Abstract**

Resistance of tumor cells to radiation therapy remains a serious concern, therefore the study of radiosensitizers has emerged as a persistent hotspot in radiation oncology, particularly in head and neck carcinoma. Considering the drawbacks of conventional chemo-radiotherapy, the use of gadolinium-based nanoparticles as radiosensitizers has shown great promise in pre-clinical research. However, the translation to clinics is hindered by disparities in observed *in vitro* biological responses, with sometimes contradictory results. This study was aimed to determine the radiosensitizing potential of AGuIX® after cellular uptake, and the resulting subcellular events in a radioresistant HNSCC cellular model. Our results demonstrated that once taken up, AGuIX® accumulated in lysosomes. After photons exposure, AGuIX® increased intracellular oxidative stress leading to complex DNA damage. Although radiation triggered late apoptosis and mitochondrial impairment, pre-treatment with AGuIX® radiosensitized cells by specifically increasing autophagic cell death. Collectively, these results provide insights into the complexity of nanomedicine.

**Keywords**: Radiotherapy, Head and Neck Cancer, radiosensitization, gadolinium-based nanoparticles (AGuIX®), Lysosomes, DNA damage

**Background**

Head and neck squamous cell carcinoma (HNSCC) is the sixth-most common cancer, accounting for over 600,000 new cases and 350,000 deaths worldwide per year[1]. Despite advances in new radiotherapeutic or chemoradiation strategies for the treatment of HNSCC, patient prognosis has not improved[2,3] as the development of radioresistance, in particular in recurrent tumors, remains a major clinically unresolved problem. Thus, for an effective patient management, there is still an urgent need to identify and develop novel agents to radiosensitize HNSCC tumors. Despite its critical role in cancer therapy, there are additional challenges associated with radiotherapy. Firstly, the toxicity to surrounding normal tissues often limits the maximum dose of irradiation (IR) that can be delivered to tumors[4]. In addition, tumors include a high degree of heterogeneity in their genotype, phenotype, and microenvironment, leading to variability in radiation sensitivity and responses in different tumor cell populations[5,6,7].

For over a decade, nanomedicine has been proposed as a new strategy to improve radiotherapy treatments. Studies have been devoted to the development of tumor-targeting nanodrugs with the aim to improve the radiation effects in the tumor, while diminishing the exposure of healthy tissues to cytotoxic, and genotoxic effects[8,9,10]. High-Z atoms, such as metallic (gold, platinum), and oxide (hafnium, gadolinium) nanoparticles (NPs), have been proposed as potential nanodrugs to amplify radiation-based therapies[11,12,13]. The activation of these nanoparticles by radiation should lead to an electron burst and consequently to oxidative stress which will in turn

lead to damages to biomolecules. Among these, gadolinium-based nanoparticles (GBNs) have been shown to hold significant potential as theranostic agents[14], the presence of gadolinium allowing them to be used as contrast agents for magnetic resonance imaging (MRI)[15]. Among these, AGuIX® (Activation and Guidance of Irradiation by X-ray) are ultrasmall (< 5 nm) gadolinium-based nanoparticles which have been characterized by a safe behavior[14,16], a renal clearance[13], and a preferential accumulation in tumors[17] by the enhanced permeability and retention (EPR) effect. Therefore, owing to their physicochemical properties, AGuIX® exposed to radiation are expected to produce extra radical oxygen species (ROS) in addition to the primary water radiolysis products.

Up to now, a significant *in vitro* radiosensitizing effect of GBNs has been reported following different experimental conditions such as varying the energy of the irradiation from keV to MeV, different concentrations of nanoparticles (from 0.1 to 1 mM), and times of incubation (from 1h to 24h), as well as different types of tumor cell lines, or the nature of irradiation (photons, neutrons or ions)[14]. Indeed, several *in vitro* studies have demonstrated the radiosensitizing effect of GBNs nanoparticles combined to photon irradiation in glioblastoma cells[18,19], cervical carcinoma HeLa cells[20], HNSCC[21], and prostate cancer cells (K. Butterworth, personal communication). Apart from the work of Miladi *et al.*, where the involvement of mitotic catastrophe and late apoptosis was demonstrated[21] in HNSCC, little is known about the subcellular effects of GBNs, the organelles involved in their radiosensitizing effect, and the connection between the physical, chemical, and biological effects of GBNs. Moreover, although GBNs were never found to be localized within nuclei[22], γ-H2AX or 53BP1 foci have been generally quantified to reflect DNA double strand breaks (DSBs) and contradictory results have been reported with the same GBNs in different cell lines. While an increase of residual DSBs have been demonstrated in HNSCC, 1h after treatment with GBNs combined to radiation[21], opposite results have been reported with AGuIX® in glioblastoma[19].

Given the variety of experimental conditions and cells involved in the studies mentioned above, as well as for other high-Z NPs, it seems impossible that all induce the same cellular response. Moreover, in the direction of a better understanding of the radiosensitization process, the clonogenic survival curve assay cannot be the only way to probe the cellular responses which therefore should be investigated in more details. This work has been undertaken with AGuIX® which contain DOTAGA as a macrocyclic $Gd^{3+}$ chelate which is a more stable and better chelator[15] compared to the acyclic ligand DTPA that could release toxic gadolinium[23].

Despite AGuIX®'s potential to induce radiosensitization in cancer cells, the complexity of the phenomenon in the current state justifies that only a few clinical trials have been undertaken (NCT02820454: NANO-RAD and NCT03308607: NANOCOL) to date. The objective of this work was therefore to better understand the mechanisms of action mediating the biological effects of

this new formulation of AGuIX® and the subcellular targets in cells in order to move towards clinical applications in a more robust way.

## Methods

Cellular Culture

The SQ20B J.L. cell line was derived from a human larynx radioresistant carcinoma obtained from the John Little Laboratory (Harvard School of Public Health, Boston, USA) with an $SF_{2Gy}$ of 72%. Cells were cultured as previously reported[24].

AGuIX® treatment and irradiation

AGuIX® nanoparticles[14] are resuspended in $dH_2O$ and further diluted to the appropriate concentration in DMEM alone.

SQ20B J.L. cells were seeded at a density of 40 000 cells/$cm^2$ 16 hours prior to AGuIX® treatment and incubated with 0.8mM Gd for 24 hours in DMEM-Glutamax. Nanoparticles were removed by washing with PBS before irradiation with an X-Rad 320 irradiator (Precision X-ray Inc., North Branford, CT): Energy: 250 kV, intensity: 15 mA, and 2Gy/min dose rate.

*DMF/BSO treatment*

After treatment with AGuIX® and washing with PBS, cells were incubated for 4 hours prior to irradiation with 100 µM dimethylfumarate (DMF), a GSH-depleting agent, and 100 µM L-buthionine sulfoximine (BSO), a GSH biosynthesis inhibitor.

Clonogenic Cell Survival Assay

After treatment with or without AGuIX® and irradiation, clonogenic cell survival curves were performed as previously described[25]. After coloration with Giemsa, clones with 64 cells or more were counted using COLCOUNT™ (Oxford Optronix). Clonogenic survival curves were fitted according to the linear quadratic equation ($SF= e^{-[\alpha \bullet D + \beta \bullet D \bullet D]}$) where SF is the surviving fraction, α represents the probability of lethal events and β the sublethal events; and D the irradiation dose. The survival fraction at 4Gy ($SF_{4Gy}$) was first used to assess the radiosensitizing concentration of AGuIX® nanoparticles (AGuIX® treatment of 1 hour).

Inductively Coupled Plasma-Optical Emission Spectrometry (ICP-OES)

After treatment with 0.8mM AGuIX® for 1, 4, 12, and 24 hours and trypsination, cells were centrifuged, rinsed with PBS before adding ultrapure water and 4-5 mL of aqua regia (mix of nitric acid and hydrochloric acid (1:3)). The samples were kept at 80°C for three hours, filtered through a 0.2 µm filter and analyzed with a Varian 710-ES (Varian, Les Ullis, France).

Toxicity Assays

*Trypan blue toxicity assay*

After treatment with AGuIX®, cells were trypsinized (for incubation times over 24h) and re-plated as to not exceed an 80% confluency. After addition of 10 µL of trypan blue solution to 10 µL of the cell suspension, viability was measured using the Countess automated cell counter (Invitrogen).

*MTT toxicity assay*

After trypsination and re-plating, 200 µL of a 0.5 g/ml of MTT solution (Sigma, St-Quentin-Fallavier, France) was added to each well. The plate was incubated for two hours at 37°C and 5% $CO_2$ and rinsed with PBS. 100 µL of DMSO were added to each well and left for 30 minutes under agitation before reading at 560 nm using the SpectraMax M2 spectrophotometer (Molecular Devices).

*Proliferation assay: confluency percentage measurements by Incucyte*

After treatment with AGuIX®, cells were trypsinized and re-seeded in a 96-well plate at a density of 5 000 cells per well. Pictures were taken in phase contrast by the Incucyte (Essen Biosciences, Ann Arbor, MI, U.S.A.) every two hours for 7 days.

Comet Assay +/- FPG

Alkaline single-cell gel electrophoresis (Comet Assay) was performed as described by De Rosa *et al.*[26] and Forestier *et al*.[27]. The study of the damage's extent was done for time after irradiation 0, 30, and 120 minutes and was evaluated as the average of the triplicate values of the percent tail intensity.

γH2Ax Immunofluorescence Assay

The method used was described by Wozny *et al*[24]. Each slide was counted for a minimum of 300 nuclei per slide using the Metafer (MetaSystems™, Heidelberg, Germany) analysis system which uses the size and intensity as parameters to distinguish a foci under a 63X objective.

Fluorescence Confocal Microscopy

Cells were plated in two-chambers LabTek®II Chambered #1.5 German Coverglass System (Dutscher, Brumath, France) and AGuIX®-Cya5.5 were used.

For co-localization studies with the nucleus, cells were fixed in 4% PFA for 20 minutes, and exposed to DAPI (1µM) for 15 minutes. The cells were kept in 1 mL of PBS for observation under the confocal spinning disk microscope. For the co-localization studies with the mitochondria or lysosomes, live-cell imaging was performed. SQ20B J.L. cells were incubated with either 200 nM Mitotracker-Green (ThermoFischer, Saint-Aubin, France) or 75 nM Lysotracker-green (ThermoFischer) for 45 minutes in culture medium prior to AGuIX®-Cya5.5 treatment. The probes were then washed out with PBS before treatment with AGuIX®-Cya5.5 for 24 hours, cells were observed using the confocal spinning disk. AGuIX®-Cya5.5 were excited with a laser at 642 nm,

while Lysotracker and Mitotracker-Green were excited at 491 nm. Images were taken in 60X oil objective on a z-width of 15 µm with step-sizes of 0,5 µm.

Autophagy was visualized under the microscope using the LC3B primary antibody diluted at 1/500 (BioTechne, Lille, France) and the secondary antibody, rabbit IgG-Alexa Fluor 488 (1/500 dilution). Images were taken using the Isis software under the 10X objective.

Study of the cellular death pathways

The CaspACE™ FITC-VAD-FMK in situ Marker (Promega, Charbonnières Les Bains, France) was used to quantify total caspase activity by flow cytometry, as previously described by Gilormini *et al*[28].

Necrosis was studied using the Annexin V/P.I. assay (Life Technologies, Courtaboeuf, France). The cells were trypsinized and marked for 15 minutes with annexin and P.I. per tube in 1X buffer. After centrifugation, cells were re-suspended in PBS and analyzed using the FACSCalibur (Becton Dickinson). The excitation/emission wavelength were 488/530 for Annexin FITC and 585/45 for P.I.

For autophagy, LC3B protein expression was studied via Western Blot analysis using the LC3B primary antibody at 1:2000 (BioTechne, Lille, France) and the secondary antibody, rabbit IgG HRP-conjugated at 1:20 000. 20µg of proteins was deposited on a 12% polyacrylamide gel.

Reactive oxygen species assay

MitoSOX™ (Life Technologies) and CM-$H_2$DCFDA (Thermo Fischer) were used to detect mitochondrial and cellular ROS respectively. MitoSOX™ was used at 5µM, while CM-$H_2$DCFDA was used at 2.5µM in HBSS for 10 minutes. The fluorescence intensity was measured by flow cytometry at an excitation/emission wavelength of 488/575 nm (Mitosox™) and 488/525 nm (CM-$H_2$DCFDA).

Mitochondrial membrane potential

The mitochondrial membrane potential was measured using the JC-1 dye (Sigma) as previously reported[28].

Measurement of the common mitochondrial DNA (mtDNA) deletion

mtDNA extraction was done without DNA purification as described in Peinnequin *et al.*[29]. qPRC was done using three primers: total mtDNA, deleted mtDNA, and GAPDH.

Statistical analysis

Each experiment was done in triplicates. Statistical analysis was realized with the Student's *t* test. Significant results have a *p* value < 0.05 (*), < 0.01 (**) or < 0.001 (***).

## Results

### *AGuIX® treatment and subcellular localization*

Preliminary experiments aimed to assess the best experimental conditions (AGuIX® concentration, time of incubation) to radiosensitize SQ20B J.L. cells. As summarized in Supplemental Figure 1, a concentration of 0.8 mM AGuIX® after 24h of treatment was selected for further investigations. AGuIX® uptake was linear with time (Supplemental Figure 1B) with an intracellular amount of 0.11pg Gd internalized by SQ20B cells, 24h after treatment. Without radiation, AGuIX® nanoparticles are not cytotoxic at the cellular (Supplemental Figure 2A and 2B) nor at the mitochondrial level (Supplemental Fig 2C). Confocal microscopy showed that AGuIX® co-localized in large quantities with lysosomal structures throughout the cytoplasm. AGuIX® were not visualized in mitochondria nor in the nucleus (Figure 1).

### *In vitro assessment of AGuIX®'s radiosensitization in SQ20B J.L. cells*

As depicted in Figure 2A, the survival curve of SQ20B cells demonstrates an enhanced sensitivity to radiation in the presence of AGuIX®. The sensitivity enhancement ratio (SER) was 1.4 at 4Gy (Figure 2B) and the dose enhancement factor (DEF) was 1.3. The α-parameter (reflecting direct lethal damage) was increased from 0.1593 to 0.2357 with AGuIX® whereas the β-parameter (sub-lethal damage) did not change. As shown in Figure 3, no differences were observed in the single-strand breaks (SSBs) at all time points (Figure 3 A-D) whereas an increase of oxidized purines (8-oxo-G) was observed right after a 4 Gy irradiation (t=0), following AGuIX® treatment (Figure 3A). Considering the initial peak of γH2Ax foci (t=30 min), there were no significant differences between untreated and treated cells (Figure 3E). For the residual γH2Ax foci (t=24h), Figure 3G shows that the number of cells displaying more than 50 foci/nucleus is significantly increased after AGuIX® treatment compared to radiation alone (45 nuclei with 50 or more foci/nucleus versus 23 nuclei with 50 or more foci/nucleus thus confirming that the treatment with AGuIX® results in the persistence of more complex and lethal DSBs compared to radiation alone.

### *Cellular death pathways induced by AGuIX® treatment*

As demonstrated by the clonogenic survival curve, AGuIX® combined to radiation increased SQ20B cell death. But one question remains: what kind of death? When considering apoptosis and necrosis, no significant differences were obtained between AGuIX® treated and untreated SQ20B cells, even 192h post-irradiation (Supplemental Figure 3). Mitotic catastrophe and senescence were also investigated but no differences between AGuIX®-treated cells compared to radiation alone were obtained (data not shown). Autophagy was then studied using LC3B as a specific autophagosomes' antibody. Although no differences in LC3B protein expression occurred up to 72 hours after irradiation, an increase was obtained starting 120h up to 192h (Figure 4A

and B). Interestingly, a more important increase was obtained after treatment with AGuIX® compared to radiation alone: +62.5% at 120 h and +114%, 192h after the combined treatment, respectively. This result was confirmed by confocal microscopy using the same LC3B antibody (Fig 4C). Collectively, these results demonstrated that the treatment of SQ20B cells with AGuIX® before irradiation significantly strengthened autophagy and/or autophagic cell death in SQ20B.

***Involvement of oxidative stress in the radiosensitizing effect of AGuIX®***

A kinetic study of ROS production was performed up to 4 hours post-irradiation either at the cytosolic (cROS) or the mitochondrial level (mROS). As can be seen in Figure 5A and 5B, we were not able to highlight any significant differences in mROS nor cROS between AGuIX®-treated cells and irradiated cells, a result that seemed surprising considering the radiosensitizing effect obtained. SQ20B J.L. cells are known to be highly radioresistant and we previously demonstrated that these cells are over-protected against oxidative stress due to their high endogenous glutathione (GSH) content[30]. We therefore depleted SQ20B cells from their GSH content using DMF + BSO[30] after AGuIX® treatment but prior to irradiation. Under these experimental conditions, flow cytometry studies with ROS specific probes allowed us to show a burst of mROS immediately after irradiation, which is not maintained over time, and without any significant differences between irradiated cells and irradiated cells treated with AGuIX® (Figure 5C). This result is consistent with the fact that we did not obtain any co-localization of AGuIX® with mitochondria (Figure 1). This initial burst of mROS was probably solely related to the consequences of water radiolysis after irradiation. At the whole cellular level, the initial burst of ROS, immediately after irradiation (Figure 5D), was much more important quantitatively compared to that obtained for mROS, and was significantly reinforced by AGuIX®. This burst of ROS then dropped at 15 and 30 min after irradiation until a second increase in cROS started after one hour and peaked four hours post- irradiation. In both cases, the pretreatment of SQ20B cells with AGuIX® led to a significant enhancement of cROS compared to radiation alone. Since the amount of ROS was increased, the consequences in terms of radiosensitization were ascertained by the clonogenic survival curve depicted in Figure 5E. Under these experimental conditions, *i.e* after GSH depletion, the 50% EBR increased from 1.281 to 1.571 and the α parameter from 0.113 to 0.299 (see Table 1). Collectively, these results strongly suggest that the initial effect of AGuIX® was somewhat subdued by the endogenous high level of antioxidant defenses.

***Mitochondrial subcellular damage induced by the addition of AGuIX® nanoparticles***

**I**n addition to nuclear damage (Figure 3), we further focused on the potential mitochondrial damage after the combined treatment. As can be observed on Figure 6A, we started observing a decrease of the mitochondrial membrane potential 72h after irradiation. This trend increased with time to reach - 30% (irradiated-only cells) versus - 36% (AGuIX® treated cells) 240h post irradiation which was not significant. These results demonstrated that AGuIX® had no influence on the decrease of the ΔΨm obtained after radiation.

Figures 6B represents the ratio of deleted mtDNA/total mtDNA 24h and 72h post-irradiation. As shown, no significant differences are observed 24 hours post-irradiation while at 72h post-

irradiation, there is no effect after a 4Gy irradiation alone (deleted mtDNA/total mtDNA ratio = 1.16) while we can observe an increase in the amount of deleted mitochondrial DNA with a ratio of deleted mtDNA/total mtDNA of 2.93 which is statistically significant compared to irradiated only cells.

## Discussion

Radiation therapy plays an essential role in the treatment of HNSCC, yet the therapeutic efficacy is hindered by the treatment-associated toxicity and tumor recurrence. Recent radiosensitization research has focused on therapeutic strategies involving, among others, nanoparticles to enhance radiation damage to cancer cells while limiting the radiation effects on normal tissues. Despite promising results obtained in terms of radiosensitization by high-Z nanoparticles, the absence of the precise cellular targets and connection between the physical, chemical, and biological effects is slowing down the translation to more clinical trials.

AGuIX® are gadolinium-based nanoparticles developed mainly for imaging due to their magnetic resonance contrast properties, but also have a potential role in radiation therapy as a radiosensitizer[9,12-15,17-19,21]. Moving towards the improvement of gadolinium chelators as MRI contrast agents[31], the formulation of AGuIX® has moved towards a macrocyclic chelator (DOTA) instead of a linear gadolinium chelator (DTPA). In the present study, the radiosensitizing potential of this new formulation of AGuIX® in the HNSCC cell model SQ20B J.L. was demonstrated, resulting in a $SF_{4Gy}$ of 1.382 with an Enhanced Biological Factor (EBR) of 1.3 which is similar to what is currently published for studies using AGuIX®, namely in HeLa (cervical cancer)[20], Panc-1 (pancreatic cancer)[32], U87 (glioblastoma)[19,33], and B16F10 (melanoma) cells[17], with DEFs varying from 1.17 to 1.54.

Regarding AGuIX®, and more generally high-Z NPs, an open question remains: is there a preferential localization of AGuIX® for radiosensitization? In accordance with Štefančíková *et al.* in glioblastoma[33], we showed that AGuIX® are not targeted to the nucleus nor the mitochondria but are mostly located in lysosomes, while a few AGuIX® remaining free in the cytosol. Similar results were also obtained in CHO cells for example, where these NPs clusters of sizes between 400-900 nm were observed in the cytoplasm regardless of the concentration used or incubation time [34].

In an effort to understand the effect of AGuIX® at the subcellular level, the results reported above raise the following questions: is there a biological effect and is this effect mandatory to target the nucleus? The debate as to whether the radiosensitizing effect induced by the combined treatment is dependent or not on DNA-damage has been studied by several teams working with AGuIX®, as well as other metal-based NPs. Although similar results were found for initial DSBs, results varied for the number of residual foci, 24 hours after irradiation and AGuIX® treatment. Indeed, an increase of residual DSBs, was reported in a melanoma model[17] or in in a head and neck cell line[35] whereas no increase of DSBs were obtained in glioblastoma cells[19] under the same experimental conditions. Although the residual DSBs, expressed as the number of cells that still

have $\gamma H_2Ax$ foci 24h after the combined treatment was moderately increased in this study, the number of cells displaying more than 50 foci/nucleus was significantly increased after treatment with AGuIX® compared to radiation alone. This observation suggests that the treatment with AGuIX® caused a net increase of more complex and lethal DSBs compared to radiation alone, a result which is in perfect accordance with the increase of the α parameter obtained from the clonogenic survival curve. All these data strongly underline the large variations in the results obtained, depending on the conditions of treatment used, as well as the cellular type studied. For other metal-based NPs, such as gold NPs, similar contradictory results have been reported. As an example, the use of 1.9 nm gold nanoparticles did not enhance radiation-induced DSBs formation nor inhibit DNA repair in MDA-MB-231 breast cancer cells irradiated with MV electrons[36], while the combination of 50 nm citrate-coated gold NPs with 6 MV photons resulted in an increase of DSBs in HeLa cells[37,38].

The next question that needed to be clarified was: which connections exist between the physical and biological effects of AGuIX®? The hypothetical mechanism behind the use of metal-based nanoparticles is based on the over-production of secondary electrons leading to an increase of cellular ROS which in turn would lead to cell death. However, only a few data are up to now available *in vitro*. As pointed out in this work, and despite of radiosensitization, the increase of ROS production following the combined treatment was lower than expected. One possible explanation was that SQ20B cells, as many other radioresistant cancer cells, exhibit upregulated antioxidant systems (see Zhou *et al*., as a review)[39]. Previous work from our lab effectively reported that SQ20B cells display a high endogenous glutathione (GSH) content which largely contributes to their radioresistant properties. Although GSH is a major ROS-scavenging system in cells, the important redox modulating enzymes including the peroxidases, peroxiredoxins, and thiol reductases also rely on the pool of reduced GSH as their source of reducing equivalents[30,40]. In view of these elements, a transient GSH-depleting strategy was previously investigated which resulted in the radiosensitization of the SQ20B cell line used in this study[30]. Using the same experimental approach, *i.e* after GSH depletion, we clearly demonstrated that the pretreatment of cells with AGuIX® resulted in a net increase of ROS after radiation thereby strongly suggesting a ROS-mediated radiosensitizing effect of AGuIX®. This increase of ROS was further evidenced through the clonogenic survival curve by an increase of the EBR from 1.3 to 1.6. Nevertheless, one must keep in mind that it still remains very difficult, if not impossible, to discriminate for sure a direct production of ROS by AGuIX® as a consequence of irradiation, from an overproduction of ROS as a cellular response and therefore to conclude about an additive or a synergetic effect of irradiation and AGuIX®.

Up to now, another recurring question persists: what kind of cell death and/or biological effect is induced after the pre-treatment of cells with AGuIX®? To our knowledge, only one study using DTPA-based gadolinium nanoparticles reported an increase of mitotic catastrophe followed by late apoptosis[21]. Otherwise, many reports were published concerning the effect of other type of NPs in the triggering of apoptosis. In combination with radiotherapy, examples include the effect of gold nanorods on melanoma cells[41], the effect of thio-glucose-bound gold nanoparticles (Glu-GNPs) on lung cancer cells[42], or the effect of silver NPs on glioma cells[43,44]. With AGuIX®, no enhancement of apoptosis nor mitotic catastrophe was obtained after radiation. Autophagy

and/or autophagic cell death was the only cellular event that was significantly enhanced after AGuIX® compared to radiation alone. Although autophagy is predominantly cytoprotective, even in response to radiation[45,46], excessive or persistent autophagy can also be cytotoxic[47,48]. Indeed, many biological responses, among which cell death pathways, are governed by threshold effects, above and below which either no response occurs or a qualitatively different response is initiated. Thus, it is not particularly surprising that excessive autophagy (as obtained after our combined treatment) can promote cell death rather than cell survival. Up to now, many trials were conducted to modulate autophagy to improve the outcome of cancer treatment in combination with radiotherapy[49]. Among these, some studies using nanoparticles combined with radiation presented evidence for a radiosensitizing effect involving autophagy: AgNPS in glioma cells at clinically relevant megavoltage energies[44], copper cysteamine NPs in colorectal carcinoma[50], or selenium NPs in breast cancer cells[51]. In this work, evidence is presented for an enhancement of autophagy with AGuIX® after radiation. As visualized by fluorescence microscopy (see Figure 4C), AGuIX® could trigger autophagic cell death or potentially autosis[52], an autophagy-dependent non-apoptotic form of cell death, characterized by unique morphological changes. However, at this stage of our work, our results do not really allow us to distinguish for sure between cell death accompanied by signs of autophagy (i.e cell death with autophagy) from cell death as a consequence of autophagy (autophagic cell death)[52].

Nevertheless, it has been very recently suggested that one unique and defining aspect of regulated autophagic cell death is the absolute requirement for lysosome membrane permeabilization (LMP)[53]. Although the authors demonstrated the requirement of the Bax/Bak proteins to increase LMP, LMP is known to occur in response to a large variety of stimuli[54], among which ROS[55,56] is one of them. As AGuIX® were found to be mainly localized in lysosomes (Figure 1), the exposure of cells to radiation led to an increase of ROS, most certainly in lysosomes. Because lysosomes are organelles extremely active in redox reaction and contain significant amounts of transition metals, like iron[57], ROS produced after exposure of AGuIX® to radiation may form other reactive species such as $HO^{\cdot}$ through the Fenton reaction[58] which are highly deleterious to lysosomal membranes. Future studies should be designed to address this hypothesis.

Concerning mitochondria, our results show that the pretreatment of cells with AGuIX® did not change the impact of radiation on this organelle, a result that could potentially be explained by the fact that AGuIX® did not get into mitochondria due to inner membrane impermeability.

In this study, we demonstrated that AGuIX® were able to radiosensitize SQ20B, an HNSCC cell line, via the induction of intracellular ROS which strengthened the radiation effect. Once taken up by cells, AGuIX® largely accumulated in lysosomes and resulted in the generation of complex DNA damage. Moreover, autophagy and/or autophagic cell death appeared to mediate the effectiveness of this treatment combination. However, future studies are required to understand the mechanisms linking lysosomes-entrapped AGuIX® with the upregulation of autophagy/autophagic cell death after radiation.

**Submitted**; Simonet *et al*.


## Acknowledgments

We acknowledge the contribution of the flow cytometry platform of the SFR BioSciences-Gerland-Lyon-Sud (UMS3444/US8) and of the CRCL. This work was supported by France Hadron (ANR-11-INBS-0007) and Labex Primes (ANR-11-LABX-0063). We would also like to thank G. Alphonse for irradiation support, and P. Montagne for flow cytometry support.

## Figure Legends

**Figure 1**: Subcellular localization of AGuIX®-Cya5,5 (red) in SQ20B J.L. cells observed in fluorescence confocal microscopy, 60X, with respect to **A.** the nucleus (DAPI: blue); **B**. mitochondria (Mitotracker-Green) and **C**. lysosomes. (Lysotracker-Green). Representative data of 200+ cells.

**Figure 2**: Radio-sensitization of SQ20B J.L. cells with AGuIX® nanoparticles. **A**. Clonogenic cell survival curve 0-10Gy: untreated (0 mM Gd) versus treated cells (0.8mM Gd). The survival at 4Gy was 0.49 (+/- 0.03) for untreated cells and decreased to 0.34 (+/- 0.03) after treatment of cells with 0,8 mM AGuIX® for 24h. Experimental (exp) values are the numbers obtained with ColCount, while the calculated (calc) values are obtained with the linear quadratic formula. Each value represents the mean +/- SD of 3 experiments performed in triplicate (***, p<0,005 vs. irradiated SQ20B cells). **B.** Table with radiation response of SQ20B J.L. cells untreated or treated with AGuIX®.

**Figure 3**: DNA-damage induced by AGuIX® combined to ionizing radiation. **A-D**: Kinetic study of single-strand breaks (+/- FPG) measured by the comet assay following a 4Gy irradiation: **A**. 0 h; **B**. 0.5 h; **C**. 2h; **D**. 24h. **E-G**: Kinetic study of double-strand breaks measured by the γH2Ax assay following a 2Gy irradiation: **E**. 0.5 h; **F**. 6 h; **G**. 24 h. Representative data of 300+ nucleus.

**Figure 4**: Kinetic study of autophagy using LC3B antibody **A**. Western Blot analysis 24-192 h post-irradiation and total proteins. **B**. Quantification of LC3B protein (total proteins were used for the normalization). **C**. Representative images of LC3B expression by fluorescence microscopy: nucleus (blue, DAPI); autophagosomes (green, LC3B antibody) 0, 24, and 192 hours post-irradiation; 10X objective. Representative data of two independent experiments.

**Figure 5**: Study of the mitochondrial and cytosolic oxidative stress induced after AGuIX® + radiation. Values were normalized as a function of the non-treated and non-irradiated cells. **A-B**: Kinetic study of mitochondrial ROS (mROS) (A) and cytosolic ROS (cROS) (B) 0 - 4 hours post-irradiation (10 Gy). **C-D** Kinetic study of mROS (C) and cROS (D) 0 - 4 hours post-irradiation (10 Gy) after glutathione depletion. Mean average intensity measured by flow cytometry in triplicates. **E.** SQ20B J.L. clonogenic survival curve varying treatment conditions (+/- AGuIX® and/or +/- DMF/BSO). Representative data of two independent experiments with biological triplicates.

**Table 1**: Summary of the parameters evaluating the radiosensitizing effect of the addition of AGuIX® and/or DMF + BSO.

**Figure 6:** Functional consequences of the combined treatment on mitochondria. **A.** Kinetic study 24-240h post-irradiation (10 Gy) of the percentage drop in the mitochondrial membrane

potential (ΔΨm). **B**. Deleted mtDNA/total mtDNA ratio for SQ20B J.L. cells following a 4Gy irradiation with or without AGuIX®. Representative data of two independent experiments with biological triplicates.

**Submitted**; Simonet *et al*.

## References


1. Parkin DM, Bray F, Ferlay J, Pisani P. Global cancer statistics, 2002. *CA Cancer J Clin* 2005;**55**:74-108.
2. Haddad RI, Shin DM. Recent advances in head and neck cancer. *N Engl J Med* 2008;**359**:1143-54.
3. Begg AC. Predicting recurrence after radiotherapy in head and neck cancer. *Semin Radiat Oncol* 2012;**22**:108-18.
4. Stone HB, Coleman CN, Anscher MS, McBride WH. Effects of radiation on normal tissue: consequences and mechanisms. *Lancet Oncol* 2003;**4**:529-36.
5. Meacham CE, Morrison SJ. Tumour heterogeneity and cancer cell plasticity. *Nature* 2013;**501**:328-37.
6. Burrell RA, McGranahan N, Bartek J, Swanton C. The causes and consequences of genetic heterogeneity in cancer evolution. *Nature* 2013;**501**:338-45.
7. Junttila MR, de Sauvage FJ. Influence of tumour micro-environment heterogeneity on therapeutic response. *Nature* 2013;**501**:346-54.
8. Excorcia FE, McDevitt MR, Villa CH, Scheinberg DA. Targeted nanomaterials for radiotherapy. *Nanomedicine (Lond)* 2007;**2**:805-15.
9. Le Duc G, Miladi I, Alric C, Mowat P, Brauer-Krisch E, Bouchet A, et al. Toward an image-guided microbeam radiation therapy using gadolinium-based nanoparticles. *ACS Nano* 2011;**5**:9566-74.
10. Yhee JY, Lee S, Kim K. Advances in targeting strategies for nanoparticles in cancer imaging and therapy. *Nanoscale* 2014;**6**:13383-90.
11. Hainfeld JF, Dilmanian FA, Slatkin DN, Smilowitz HM. Radiotherapy enhancement with gold nanoparticles. *J Pharm Pharmacol* 2008;**60**: 977-85.
12. Porcel E, Liehn S, Remita H, Usami N, Kobayashi K, Furusawa Y, et al. Platinum nanoparticles: a promising material for future cancer therapy? *Nanotechnology* 2010;**21**:85103.
13. Le Duc G, Roux S, Paruta-Tuarez A, Dufort S, Brauer E, Marais A, et al. Advantages of gadolinium based ultrasmall nanoparticles vs molecular gadolinium chelates for radiotherapy guided by MRI for glioma treatment. *Cancer Nanotechnol.* 2014;**5**:4.
14. Sancey L, Lux F, Kotb S, Roux S, Dufort S, Bianchi A, et al. The use of theranostic gadolinium-based nanoprobes to improve radiotherapy efficacy. *Br J Radiol* 2014;**87**:20140134.
15. Mignot A, Truillet C, Lux F, Sancey L, Louis C, Denat F, et al. A top-down synthesis route to ultrasmall multifunctional Gd-based silica nanoparticles for theranostic applications. *Chemistry* 2013;**19:**6122-36.

16. Bianchi A, Dufort S, Lux F, Courtois A, Tillement O, Coll JL, et al. Quantitative biodistribution and pharmacokinetics of multimodal gadolinium-based nanoparticles for lungs using ultrashort TE MRI. *MAGMA* 2014;**27**:303-16.
17. Kotb S, Detappe A, Lux F, Appaix F, Barbier EL, Tran VL, et al. Gadolinium-Based Nanoparticles and Radiation Therapy for Multiple Brain Melanoma Metastases: Proof of Concept before Phase I Trial. *Theranostics* 2016;**6**:418-27.
18. Mowat P, Mignot A, Rima W, Lux F, Tillement O, Roulin C, et al. In Vitro radiosensitizing effects of ultrasmall gadolinium based particles on tumour cells. *J Nanosci Nanotechnol* 2011;**11**:7833-9.
19. Štefančíková L, Lacombe S, Salado D, Porcel E, Pagáčová E, Tillement O, et al. Effect of gadolinium-based nanoparticles on nuclear DNA damage and repair in glioblastoma tumor cells. *J Nanobiotechnology* 2016;**14**:63.
20. Luchette M, Korideck H, Makrigiorgos M, Tillement O, Berbeco R. Radiation dose enhancement of gadolinium-based AGuIX nanoparticles on HeLa cells. *Nanomedicine* 2014;**10**:1751-5.
21. Miladi I, Aloy MT, Armandy E, Mowat P, Kryza D, Magne N, et al. Combining ultrasmall gadolinium-based nanoparticles with photon irradiation overcomes radioresistance of head neck squamous cell carcinoma. *Nanomedicine* 2015;**11**:247-57.
22. Rima W, Sancey L, Aloy MT, Armandy E, Alcantara GB, Epicier T, et al. Internalization pathways into cancer cells of gadolinium-based radiosensitizing nanoparticles. *Biomaterials* 2013;**34**:181-95
23. Rogosnitzky M, Branch S. Gadolinium-based contrast agent toxicity: a review of known and proposed mechanisms. *Biometals* 2016;**29**:365-76.
24. Wozny A-S, Alphonse G, Battiston-Montagne P, Simonet S, Poncet D, Testa E, et al. Influence of Dose Rate on the Cellular Response to Low- and High-LET Radiations. *Front Oncol* 2016; **6**:58.
25. Beuve M, Alphonse G, Maalouf M, Colliaux A, Battiston-Montagne P, Jalade P, et al. Radiobiologic parameters and local effect model predictions for head-and-neck squamous cell carcinomas exposed to high linear energy transfer ions. *Int J Radiat Oncol Biol Phys* 2008;**71**:635-42.
26. De Rosa V, Lu PE, Forestier A, Favier A, Hincal F, Dimaond AM, et al. Low doses of selenium specifically stimulate the repair of oxidative DNA damage in LNCaP prostate cancer cells. *Free Radic Res* 2012;**46**:105-16.
27. Forestier A, Douki T, Sauvaigo S, Do Rosa V, Demeilliers C, Rachidi W. Alzheimer's disease-associated neurotoxic peptide amyloid-β impairs base excision repair in human neuroblastoma cells. *Int J Mol Sci* 2012;**13**:14766-87.

28. Gilormini M, Malesys C, Armandy E, Manas P, Guy JB, Magné N, et al. Preferential targeting of cancer stem cells in the radiosensitizing effect of ABT-737 on HNSCC. *Oncotarget* 2016;**7**:16731-44.
29. Peinnequin A, Poyot T, Dib A, Aubourg A, Mouret C, Demeilliers C. Direct quantification of mitochondrial DNA and its 4.9-kb common deletion without DNA purification. *Anal Biochem* 2011;**409**:298-300.
30. Boivin A, Hanot M, Malesys C, Maalouf M, Rousson R, Rodriguez-Lafrasse C, et al. Transient alteration of cellular redox buffering before irradiation triggers apoptosis in head and neck carcinoma stem and non-stem cells. *Plos One* 2011;**6**;e1455.
31. Frullano L, Caravan P. Strategies for the preparation of bifunctional gadolinium(III) chelators. *Curr Org Synth* 2011;**8**:535-65.
32. Detappe A, Kunjachan S, Rottmann J, Robar J, Tsiamas P, Korideck H, et al. AGuIX nanoparticles as a promising platform for image-guided radiation therapy. *Cancer Nanotechnol* 2015;**6**:4.
33. Štefančíková L, Porcel E, Eustache P, Li S, Salado D, Marco S, et al. Cell localization of gadolinium-based nanoparticles and related radiosensitizing efficacy in glioblastoma cells. *Cancer Nanotechnol* 2014;**5**:6.
34. Porcel E, Tillement O, Lux F, Mowat P, Usami N, Kobayashi K, et al. Gadolinium-based nanoparticles to improve the hadrontherapy performances. *Nanomedicine* 2014;**10**:1601-8.
35. Wozny AS, Aloy MT, Alphonse G, Magné N, Janier M, Tillement O, et al. Gadolinium-based nanoparticles as sensitizing agents to carbon ions in head and neck tumor cells. *Nanomedicine* 2017;**13**:2655-60.
36. Jain S, Coulter JA, Hounsell AR, Butterworth KT, McMahon SJ, Hyland WB, et al. Cell-specific radiosensitization by gold nanoparticles at megavoltage radiation energies. *Int J Radiat Oncol Biol Phys* 2011;**79**:531-39.
37. Chithrani DB, Jelveh S, Jalali F, van Prooijen M, Allen C, Bristow RG, et al. Gold nanoparticles as radiation sensitizers in cancer therapy. *Radiat Res* 2010;**173**:719-28.
38. Berbeco RI, Korideck H, Ngwa W, Kumar R, Patel J, Sridhar S, et al. DNA damage enhancement from gold nanoparticles for clinical MV photon beams. *Radiat Res* 2012;**178**:604-8.
39. Zhou S, Ye W, Shao Q, Zhang M, Liang J. Nrf2 is a potential therapeutic target radioresistance in human cancer. *Crit Rev Oncol Hematol* 2013;**88**:706-15.
40. Forman HJ, Zhang H, Rinna A. Glutathione: overview of its protective roles, measurement, and biosynthesis. *Mol Aspects Med* 2009;**30**:1-12.
41. Xu W, Luo T, Li P, Zhou C, Cui D, Pang B, et al. RGD-conjugated gold nanorods induce radiosensitization in melanoma cancer cells by downregulating $\alpha(v)\beta_3$ expression. *Int J Nanomedicine* 2012;**7**:915-24. (43)

42. Wang C, Li X, Wang Y, Liu Z, Fu L, Hu L. Enhancement of radiation effect and increase of apoptosis in lung cancer cells by thio-glucose-bound gold nanoparticles at megavoltage radiation energies. *J Nanopart Res* 2013; **15**:1642.
43. Liu P, Huang Z, Chen Z, Xu R, Wu H, Zang F, et al. Silver nanoparticles : a novel radiation sensitizer for glioma ? *Nanoscale* 2013;**5**:11829-36.
44. Liu P, Jin H, Guo Z, Ma J, Zhao J, Li D, et al. Silver nanoparticles outperform gold nanoparticles in radiosensitizing U251 cells in vitro and in an intracranial mouse model of glioma. *Int J Nanomedicine* 2016;**11**:5003-14.
45. Lomonaco SL, Finniss S, Xiang C, Decarvalho A, Umansky F, Kalkanis SN, et al. The induction of autophagy by gamma-radiation contributes to the radioresistance of glioma stem cells. *Int J Cancer* 2009;**125**:717–22.
46. Ko A, Kanehisa A, Martins I, Senovilla L, Chargari C, Dugue D, et al. Autophagy inhibition radiosensitizes in vitro, yet reduces radioresponses in vivo due to deficient immunogenic signalling. *Cell Death Differ* 2014;**21**:92–9.
47. Daido S, Yamamoto A, Fujiwara K, Sawaya R, Kondo S, Yondo Y. Inhibition of the DNA-dependent protein kinase catalytic subunit radiosensitizes malignant glioma cells by inducing autophagy. *Cancer Res* 2005;**65**:4368-75.
48. Jo GH, Bögler O, Chwae Y-J, Yoo H, Lee SH, Park JB, et al. Radiation-induced autophagy contributes to cell death and induces apoptosis partly in malignant glioma cells. Cancer *Res and Treat* 2015;**47**:221-41.
49. Tam SY, Wu VW, Law HK. Influence of autophagy on the efficacy of radiotherapy. *Radiat Oncol* 2017;**12**:57.
50. Liu Z, Xiong Lk, Ouyang G, Ma L, Sahi S, Wang K, et al. Investigation of copper cysteamine nanoparticles as a new type of radiosensitiers for colorectal carcinoma treatment. *Sci Rep* 2017; **7**:9290.
51. Chen F, Zhang XH, Hu XD, Liu PD, Zhang HQ. The effects of combined selenium nanoparticles and radiation therapy on breast cancer cells in vitro. *Artif Cells Nanomed Biotechnol* 2017;**7**:1-12.
52. Liu Y, Levine B. Autosis and autophagic cell death: the dark side of autophagy. *Cell Death Differ* 2015;**22**:367–376.
53. Karch J, Schips TG, Maliken BD, Brody MJ, Sargent MA, Kanisicak O, et al. Autophagic cell death is dependent on lysosomal membrane permeability through Bax and Bak. *eLife* 2017; **6**. Pii: e30543.
54. Johansson AC, Appelqvist H, Nilsson C, Kågedal K, Roberg K, Öllinger K. Regulation of apoptosis-associated lysosomal membrane permeabilization. *Apoptosis* 2010;**15**:527-40.
55. Denamur S, Tyteca D, Marchand-Brynaert J, Van Bambeke F, Tulkens PM, Courtoy PJ, et al. Role of oxidative stress in lysosomal membrane permeabilization and apoptosis

induced by gentamicin, an aminoglycoside antibiotic. *Free Radic Biol Med* 2011;**51**:1656–65.

56. Oku Y, Murakami K, Irie K, Hoseki J, Sakai Y. Synthesized Aβ42 Caused Intracellular Oxidative Damage, Leading to Cell Death, via Lysosome Rupture. *Cell Struct Funct* 2017;**42**:71-79.
57. Yu Z., Persson HL, Eaton JW, Brunk UT. Intralysosomal iron: a major determinant of oxidant-induced cell death. *Free Radic Biol Med* 2003;**34**:1243–52.
58. Baird SK, Kurz T, Brunk UT. Metallothionein protects against oxidative stress induced lysosomal destabilization. *Biochem J* 2006;**394**:275–83.

**Figure 1**

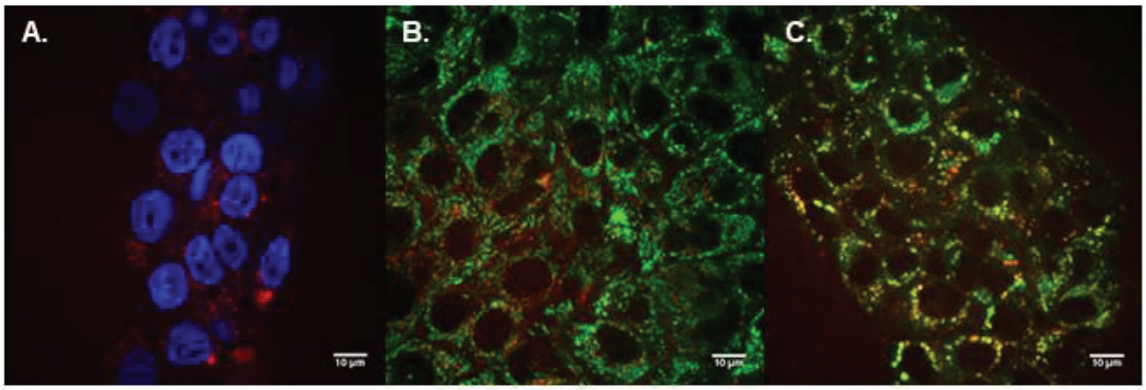

**Figure 2**

**A.**

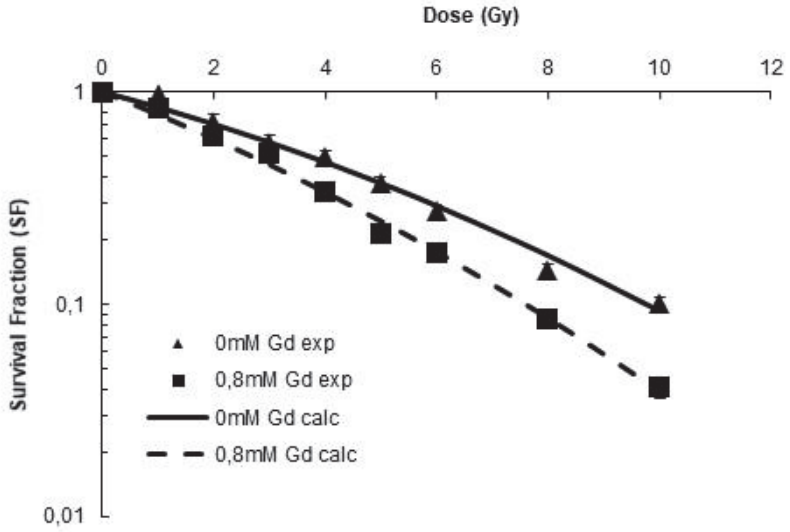


**B.**

| [Gd] (mM) | α | β | 10% | 50% | EBR-10% | EBR-50% |
|---|---|---|---|---|---|---|
| 0 | 0,1593 | 0,0079 | 9,75 | 3,65 | 1,281 | 1,377 |
| 0,8 | 0,2357 | 0,0088 | 7,61 | 2,65 | | |

**Figure 3**

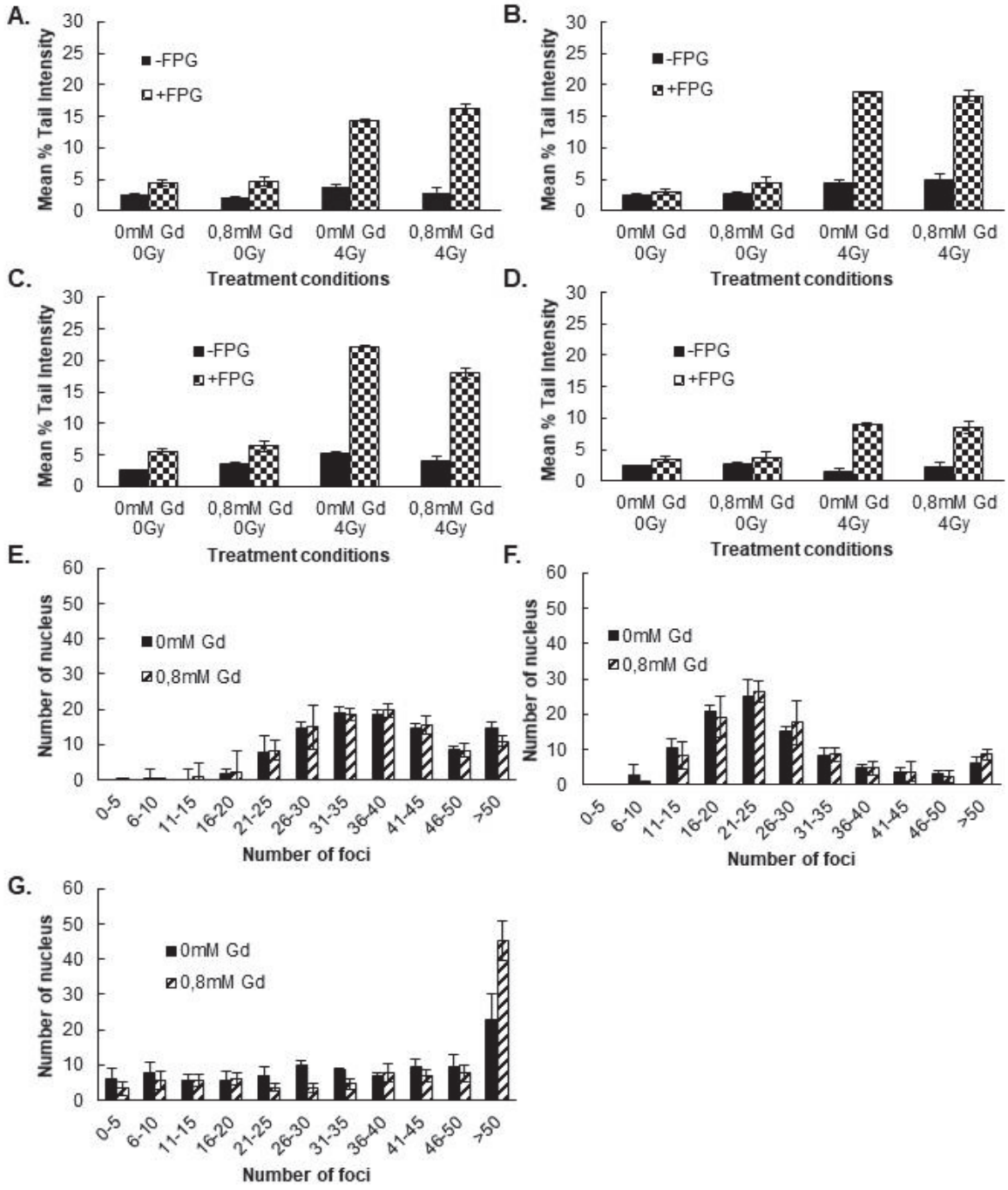
A.
Mean % Tail Intensity
-FPG
+FPG
0mM Gd 0Gy
0,8mM Gd 0Gy
0mM Gd 4Gy
0,8mM Gd 4Gy
Treatment conditions
B.
Mean % Tail Intensity
-FPG
+FPG
0mM Gd 0Gy
0,8mM Gd 0Gy
0mM Gd 4Gy
0,8mM Gd 4Gy
Treatment conditions
C.
Mean % Tail Intensity
-FPG
+FPG
0mM Gd 0Gy
0,8mM Gd 0Gy
0mM Gd 4Gy
0,8mM Gd 4Gy
Treatment conditions
D.
Mean % Tail Intensity
-FPG
+FPG
0mM Gd 0Gy
0,8mM Gd 0Gy
0mM Gd 4Gy
0,8mM Gd 4Gy
Treatment conditions
E.
Number of nucleus
0mM Gd
0,8mM Gd
0-5
6-10
11-15
16-20
21-25
26-30
31-35
36-40
41-45
46-50
>50
Number of foci
F.
Number of nucleus
0mM Gd
0,8mM Gd
0-5
6-10
11-15
16-20
21-25
26-30
31-35
36-40
41-45
46-50
>50
Number of foci
G.
Number of nucleus
0mM Gd
0,8mM Gd
0-5
6-10
11-15
16-20
21-25
26-30
31-35
36-40
41-45
46-50
>50
Number of foci

**Submitted**; Simonet *et al*.

## Figure 4

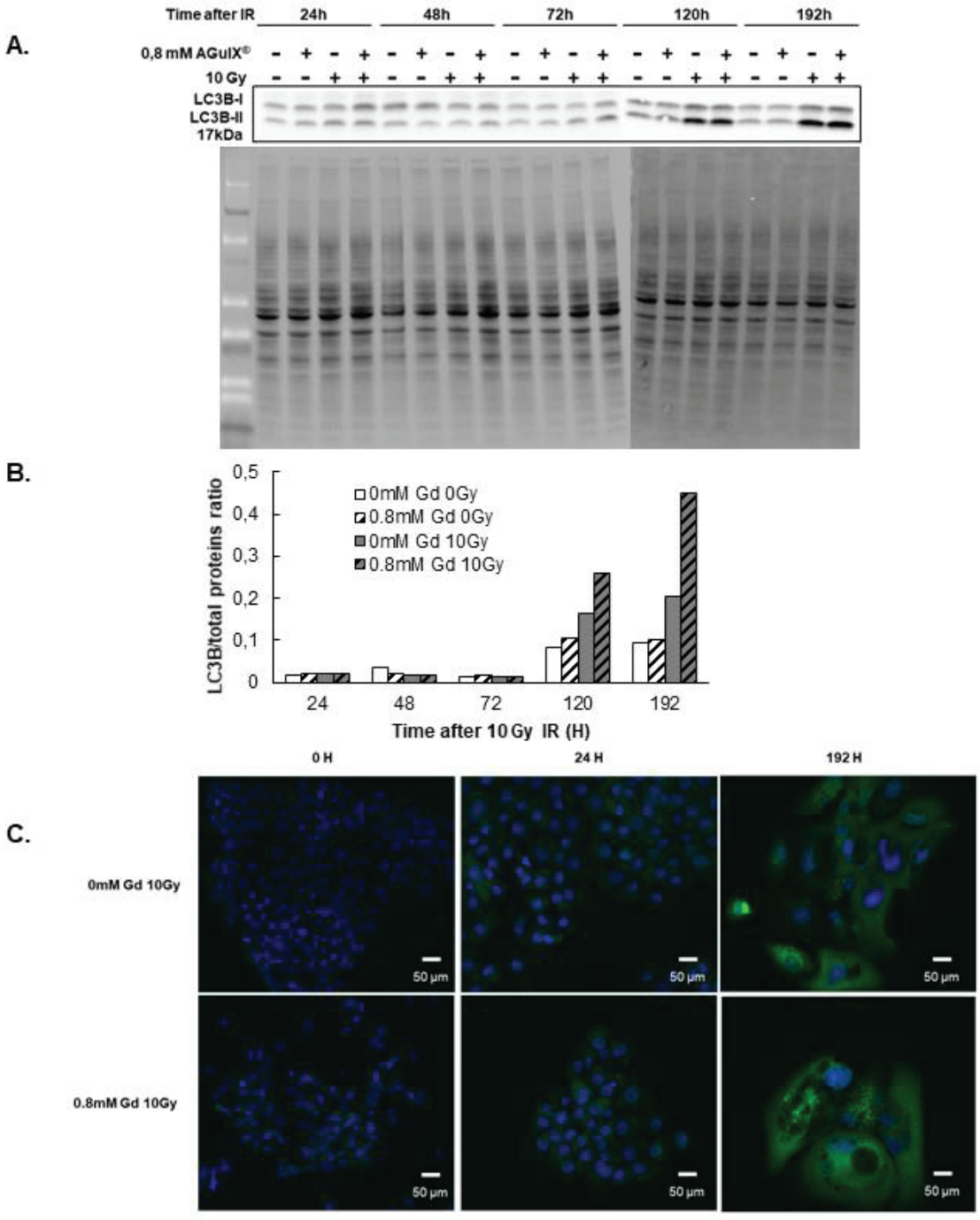

**Figure 5**

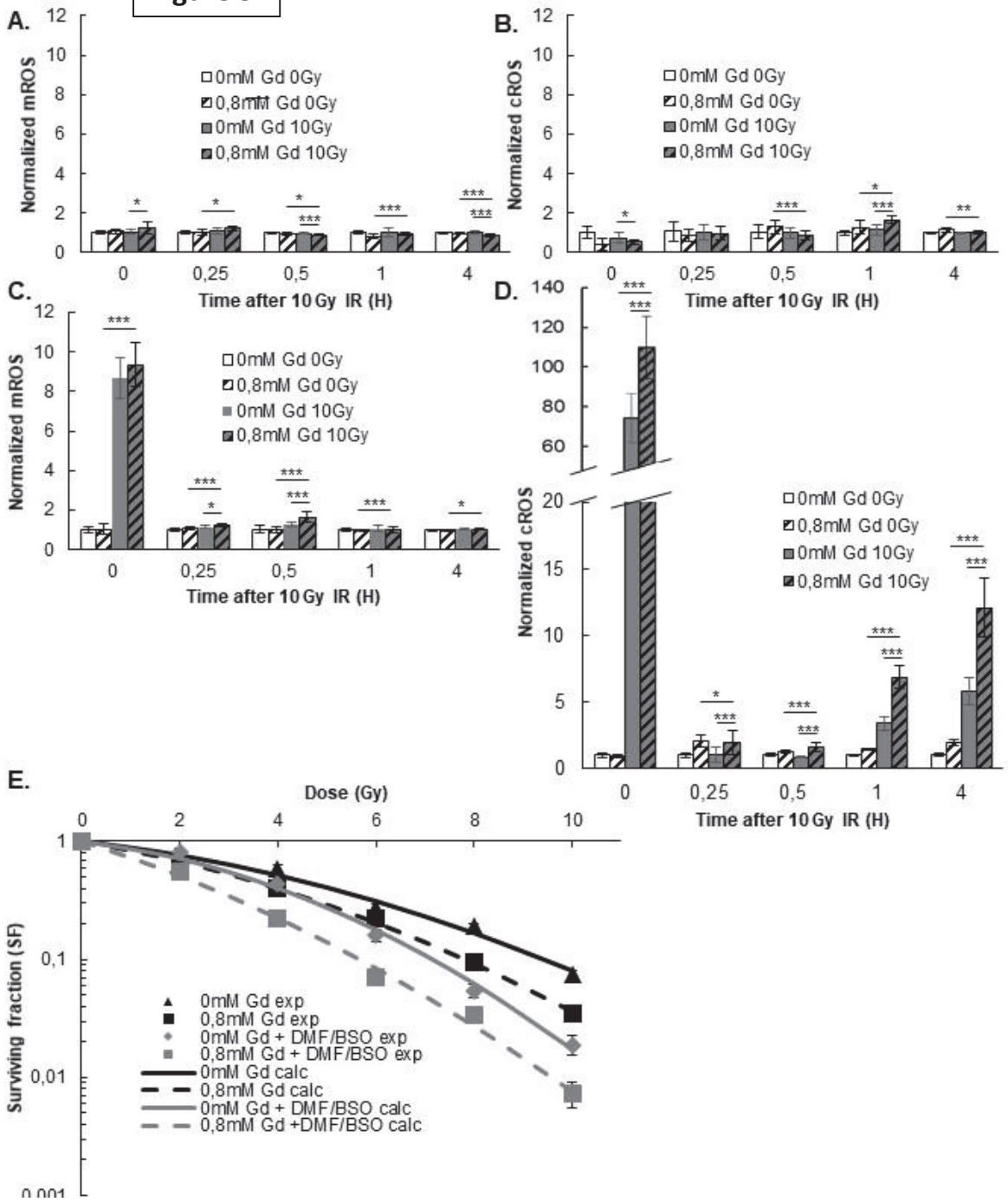
A.
Normalized mROS
0mM Gd 0Gy
0,8mM Gd 0Gy
0mM Gd 10Gy
0,8mM Gd 10Gy
Time after 10 Gy IR (H)
B.
Normalized cROS
Time after 10 Gy IR (H)
C.
Normalized mROS
Time after 10 Gy IR (H)
D.
Normalized cROS
Time after 10 Gy IR (H)
E.
Dose (Gy)
Surviving fraction (SF)
0mM Gd exp
0,8mM Gd exp
0mM Gd + DMF/BSO exp
0,8mM Gd + DMF/BSO exp
0mM Gd calc
0,8mM Gd calc
0mM Gd + DMF/BSO calc
0,8mM Gd +DMF/BSO calc

**Figure 6**

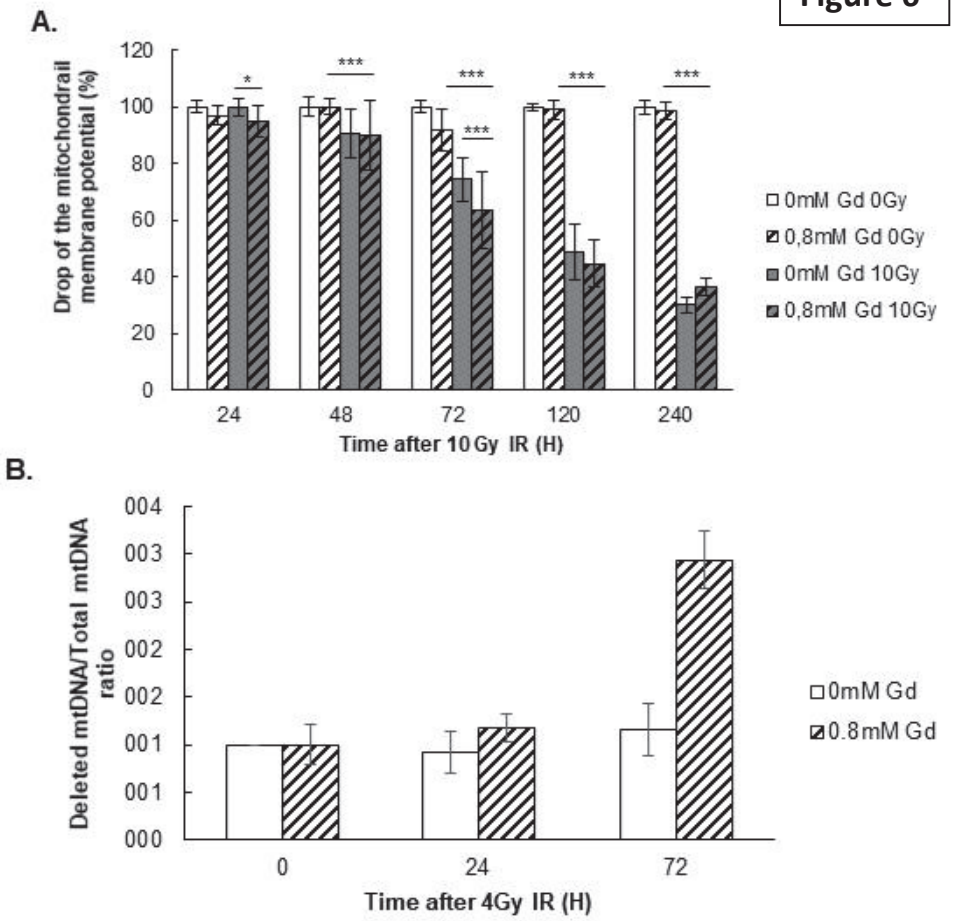
A.
Drop of the mitochondrail membrane potential (%)
120
100
80
60
40
20
0
*
***
***
***
***
***
24
48
72
120
240
Time after 10 Gy IR (H)
0mM Gd 0Gy
0,8mM Gd 0Gy
0mM Gd 10Gy
0,8mM Gd 10Gy
B.
Deleted mtDNA/Total mtDNA ratio
004
003
003
002
002
001
001
000
0
24
72
Time after 4Gy IR (H)
0mM Gd
0.8mM Gd

**Submitted**; Simonet *et al*.

| DMF/BSO | WITHOUT | | WITH | |
|---|---|---|---|---|
| [Gd] (mM) | 0 | 0,8 | 0 | 0,8 |
| α | 0.11 | 0.164 | 0.1134 | 0.2995 |
| β | 0.0143 | 0.168 | 0.0293 | 0.0187 |
| 10% | 9.3 | 7.8 | 7.1 | 5.7 |
| 50% | 4.1 | 3.2 | 3.3 | 2.1 |
| EBR-10% | 1.192 | | 1.246 | |
| EBR-50% | 1.281 | | 1.571 | |

## Legends for Supplemental Figures

**Supplemental Figure 1:** Determination of the radiosensitizing conditions. A. Survival fraction at 4Gy with varying AGuIX concentration from 0 to 3 mM in DMEM without fetal bovine serum. B. Quantity of gadolinium internalized by SQ20B J.L. cells as a function of treatment time (1-4-12-24 hours of exposure to AGuIX® treatment) in serum-free DMEM-Glutamax (0.8mM Gd) quantified by ICP-AES. The three wavelengths of gadolinium are represented (342, 336, and 332 nm). This is a mean of 2 independent experiments with 3 flasks for each, and 3 separate readings from the ICP.

**Supplemental Figure 2:** Toxicity assays. A. Proliferation assay measuring the percentage confluency using the IncuCyte Live Cell Analysis. B. Percentage viability using the blue trypan assay. C. Percent (%) proliferation measured by the MTT assay. Representative data of two independent experiments with biological triplicates.

**Supplemental Figure 3:** Study of cellular deaths pathways. A. Caspase activation 24-240 h post-irradiation using the CaspACE™ FITC-VAD-FMK *in situ* Marker (Promega) and measured by flow cytometry. Representative data of three independent experiments with biological triplicates. B. Study of necrosis 24-192h post-irradiation using the Annexin V/P.I. assay measured by flow cytometry.

## Supplemental Figure 1

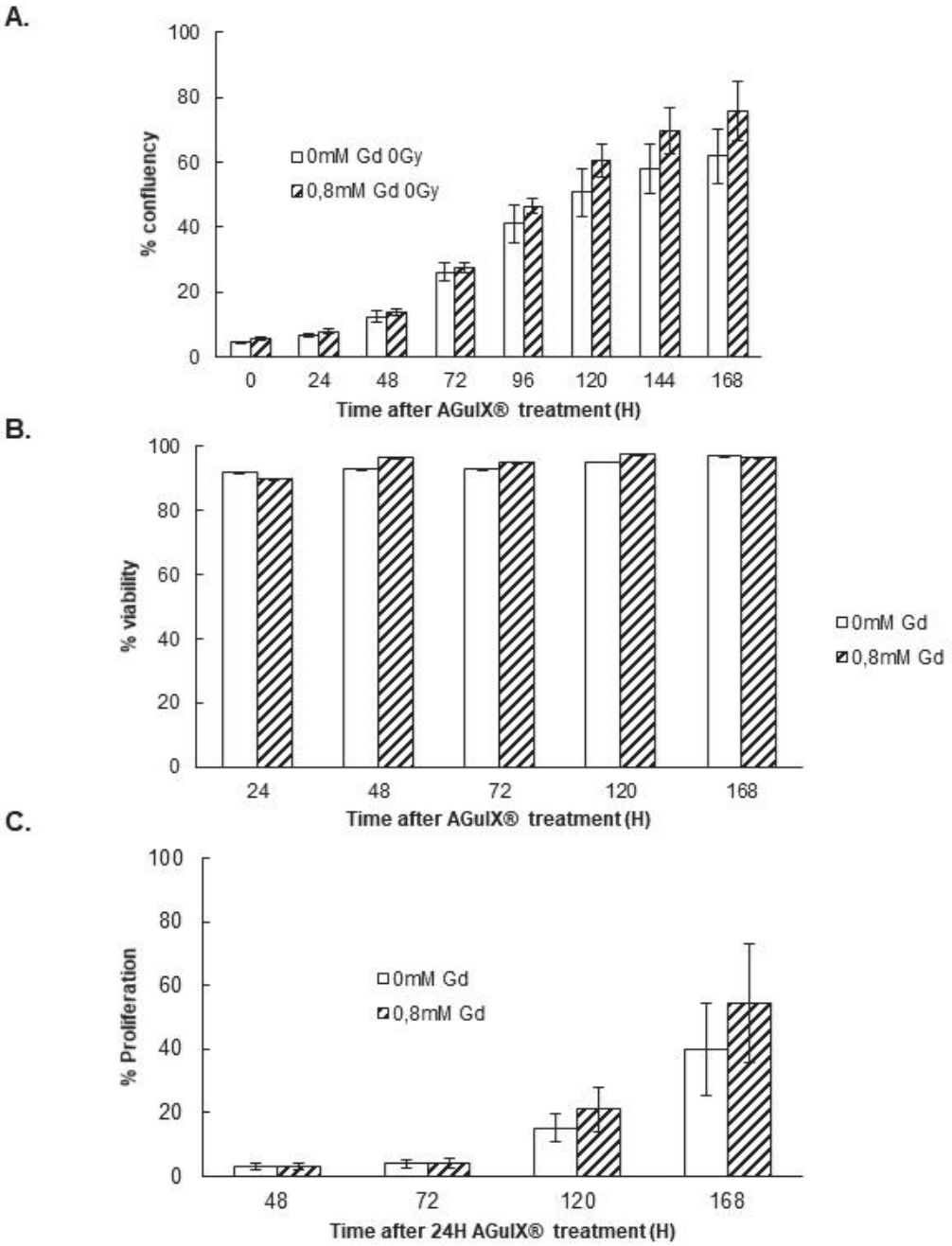

**Submitted**; Simonet *et al*.

**Supplemental Figure 2**

A.

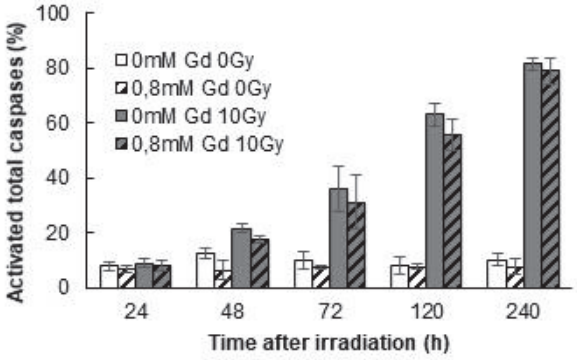


B.

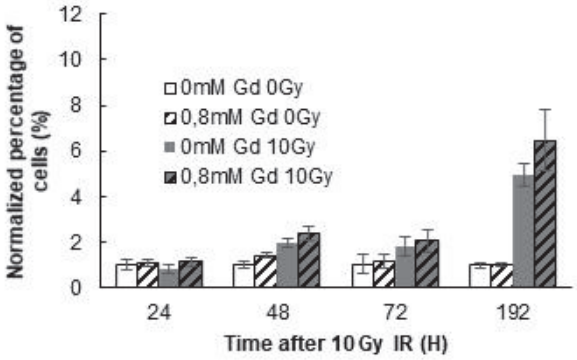

**Supplemental Figure 3**

A.

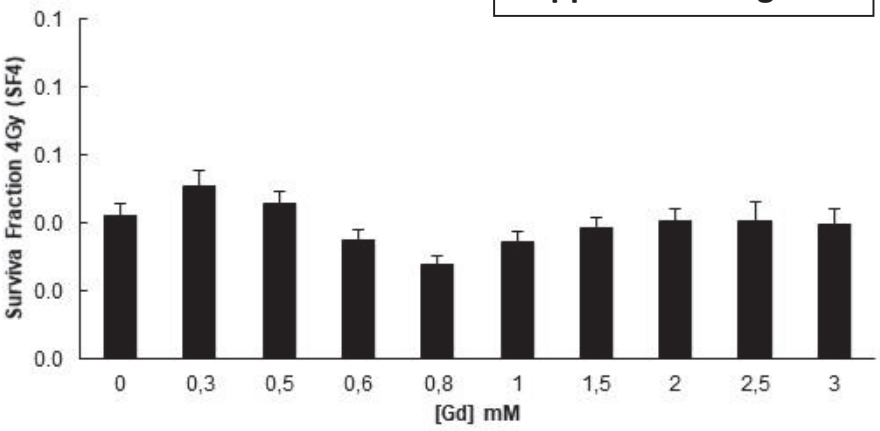


B.

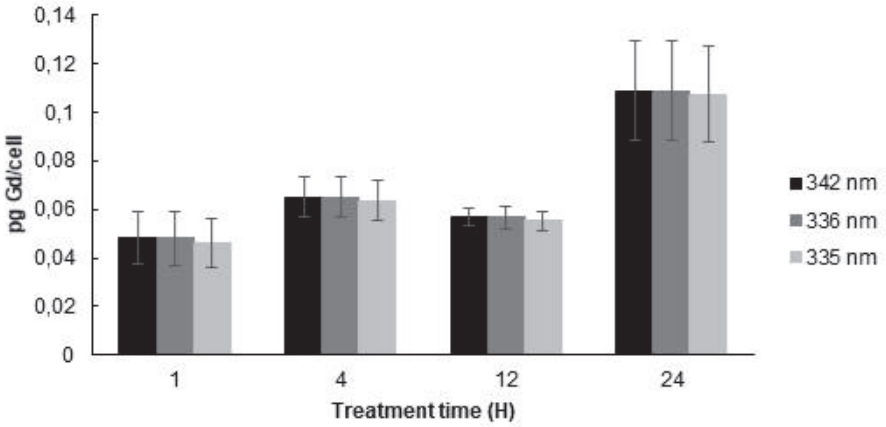

## Abstract

Head and Neck Squamous Cell Carcinoma is ranked among the top ten deadliest cancers due to its high radioresistance and recurrence. One radiosensitizing strategy is the use of high-Z metal nanoparticles. In this study, ultrasmall gadolinium-based nanoparticles, AGuIX®, were used for their potential as a radiosensitizing agent. The objectives of this work were to determine the radiosensitizing conditions of AGuIX® in an HNSCC cell model, their localization after uptake, and the biological consequences generated at the subcellular level after the combined treatment. A preliminary proteomic approach was initiated in order to identify potential molecular targets involved in radiosensitization.

The treatment of SQ20B cells with 0.8mM Gd for 24h resulted in a dose enhancement factor (DEF) of 1.3. AGuIX® were predominantly localized in lysosomes. The overproduction of radical oxygen species following AGuIX® + radiation was intimately involved in the radiosensitization, although largely subdued by the high level of endogenous antioxidant defenses. Autophagy was specifically triggered after the combined treatment, while other irradiation-induced cell deaths remained unchanged. The number of complex, residual double strand breaks (DSBs) was specifically increased with AGuIX® combined to radiation. Lastly, our preliminary proteomic analysis allowed the isolation of potential molecular targets with great promise. Collectively, it seems that the radiosensitizing effect observed in this work may result from a combination of events.

Future work is required to understand the mechanisms linking lysosomes-entrapped AGuIX® with the upregulation of autophagic cell death after radiation.

**Keywords**: Head and Neck Squamous Cell Carcinoma (HNSCC); ionizing radiation; nanomedicine; radiosensitizing strategies; nanoparticles; AGuIX®; Radical Oxygen Species (ROS)

## Résumé

Les cancers des Voies Aérodigestives Supérieures sont classés parmi les dix cancers les plus agressifs du fait de leur radioresistance intrinsèque et leur forte probabilité de récurrence. L'objectif de ce travail a été d'étudier le potentiel radiosensibilisant de nanoparticules à base de gadolinium, AGuIX®, sur un modèle cellulaire de cancer des VADS. Après avoir déterminé et validé les conditions optimales de radiosensibilisation de notre modèle par les AGuIX®, leur localisation après internalisation ainsi que les conséquences biologiques générées à l'échelle subcellulaire ont été successivement étudiées. Enfin, une approche préliminaire protéomique a été initiée afin d'identifier des cibles moléculaires potentielles impliquées dans cette radiosensibilisation.

Le traitement des cellules SQ20B avec 0.8mM Gd pendant 24h se sont révélées être optimales avec un DEF (dose enhancement factor) de 1.3. Les AGuIX® sont localisées presque exclusivement dans les lysosomes après internalisation. La radiosensibilisation est liée à une surproduction de radicaux libres oxygénés, minimisée toutefois par des défenses antioxydantes endogènes élevées. Le traitement combiné (AGuIX®+ irradiation) déclenche spécifiquement la mort cellulaire autophagique et s'accompagne d'une augmentation significative du nombre de cassures double brins résiduelles complexes. L'étude protéomique préliminaire a permis d'identifier une cible moléculaire potentiellement impliquée dans cette radiosensibilisation (la ribonucléotide réductase), cible qui fera l'objet d'une suite à ce travail. De plus, la prochaine étape sera de comprendre les mécanismes qui relient les AGuIX® internalisées dans les lysosomes avec l'augmentation de la mort cellulaire autophagique après irradiation.

**Mots clés**: Cancers des Voies Aéro-Digestives Supérieurs (VADS); irradiation ionisante; nanomédicine; stratégie radiosensibilisante; nanoparticules; AGuIX®; Radicaux Libres Oxygénés (RLO)